Advancing the Synthetic and Analytical Techniques of Inverse Vulcanisation

A thesis submitted in accordance with the requirements of The University of Liverpool for the degree of Doctor of Philosophy

Authored by one

Liam James Dodd

Who was thusly supervised by one

Dr Tom Hasell

Submitted upon the month of

November 2023

"Fortune finds those who tread not the same path twice."

Liam James Dodd

Preface

Abstract

Inverse vulcanisation is a diverse and versatile polymerisation reaction that reacts elemental sulfur with an olefinic organic compound to generate polymers that can contain large amounts of sulfur by mass. Such reactions usually entail a bulk polymerisation where sulfur is heated beyond its melting point, to temperatures where radical capped sulfur chains form. Upon cooling these chains are unstable, but they can be reacted with carbon – carbon double bonds to create inverse vulcanised polymers: organic units interconnected by chains of sulfur atoms. Normally the organic component would contain multiple olefinic moieties, such that the product is crosslinked, which is generally more stable than the less common examples of linear inverse vulcanised polymers. Inverse vulcanised polymers have a great many applications that make them attractive next generation materials, and many of these properties can be tuned by controlling how much sulfur is used in the synthesis. Even more exciting is the wide library of reactive olefins that are amenable to inverse vulcanisation, each bringing a new product polymer with a different complement of properties. What makes inverse vulcanisation so much more attractive, is that sulfur is an industrial by-product that is produced in vast excesses with supply greatly outweighing demand. Thus, elemental sulfur is remarkably cheap, and since the olefinic reactant can come from a renewable source, inverse vulcanisation can meet the principles of green chemistry. However, inverse vulcanisation suffers from a poorly understood mechanism, little to no regimentation in how syntheses are conducted, and severe issues in the analysis and understanding of the structure of the product polymers, which are issues that the work carried out in contribution to this thesis aimed to remedy with three topics. The first topic examine in this thesis is the catalysis of inverse vulcanisation, which can improve the yield and reaction time of inverse vulcanisation whilst inducing reaction in otherwise unreactive comonomers, and giving product polymers of better properties. By varying the catalyst structure, conclusions were drawn about what makes an effective catalyst and how such catalysts might work. As a follow on from the first, the second topic investigates metal free amine catalysts, which circumvent sustainability concerns of metal containing catalysts as well as metal contamination of the environment. As a natural branch to this project, previously under-investigated alkyne crosslinkers were studied, as well as a dispersion polymerisation method, useful for highly reactive crosslinkers. The final topic is the use of Raman spectroscopic analysis for characterisation of inverse vulcanised polymer structure, something near impossible by other means and which carries of wealth of critical but otherwise hard to obtain information, such as the sulfur chain length, the homogeneity, and the unpolymerized elemental sulfur content of the product polymer.

Declaration

The research contained in this thesis document was undertaken within the Department of Chemistry at the University of Liverpool between September 2019 and July 2023. The research presented herein is entirely my own work, unless otherwise stated in the preface or indicated in the text. I have read the PGR Code of Practice and declare that this document adheres to the academic standards defined in Appendix 4. This thesis does not exceed the specified maximum word count and complies with the requirements as set out by the Faculty of Science & Engineering.

Liam J. Dodd

November 2023

Liam James Dodd

Foreword

Note, this foreword is reduced for the public facing version of this thesis. See the personal copy of this thesis for the complete foreword.

My PhD. That was a thing that happened. And now as I type the end of it, remembering all the bad times, I can't help but feel like I don't want it to end, because the good tremendously outweighed the bad. I realise that I didn't respect what I had as much as I should have, and at times took it for granted. But given the problems I faced, I can say realistically that I did the best I could, and I'm happy about that.

I will have to make some acknowledgements of the fantastic people I worked with and met on my journey:

- We worked together, we got to know one another, we learned each other's quirks. There is perhaps no one who knows me better, as I shared with you some of my deepest secrets in those long hours in the lab, and I know there is no one who knows you more deeply than I. We fought side by side and sometimes head to head: disagreeing, pushing each other's buttons, and leaving with burns from our conflicts. But looking back on it my friend, I can say with no doubt in my heart: Khan, you were the best hotplate a man could hope for.
- To Tom Hasell, you are an astounding supervisor and an all-round fantastic person. I cannot conceive of a more able, diligent, and empathetic supervisor. You always knew how to move forward, work with uncertainty, and tackle the problems that arose. Your unbelievable guidance has brought me to a better standard of work, and your grounded and realistic approach to life has improved me as a person. I would not have survived this PhD if not for your understanding nature that never made me feel punished for problems like my endless insomnia. I cannot express the sheer respect I have for you, and I wish you the very best that life could bring your way. It was an absolute pleasure to work under you, and I aspire to be like you moving forward.
- To Haoran Wang, you have been my closest friend in the Hasell group. You have looked out for me, been there to talk to, and have been so much fun to be around. I hope that I have been as good to you as you have been to me. You are a true friend, and even if we end up on different sides of planet, I'll stay in contact.
- To Xi Deng, getting to know you has been fun and rewarding. I will never forget the hike; out of nowhere seeing you running down the hill screaming and scaring the bejesus out of two full herds of sheep. You're a great guy and I hope you find everything you're looking for.
- To Peiyao Yan, Xinxin, and Xiaofeng Wu, thank you for making my trip to China possible. I have made memories there that will last a lifetime, and it could never have happened without you.
- To all the new friends I met in China: Jinhong, Xunxingwei, Haidong, Xuguangli, Zhi-Bin, Cuiyunfei, and Lixiaohu; thank you for welcoming me so warmly to your wonderful country, and thank you for making my time there truly memorable.
- To Justin Chalker, Harshal Patel, Alfrets Tikoalu, Sam Tonkin, Lynn Lisboa, Jasmine Pople, Tom Nicholls, Jiaoyu Wang, Asja Kroeger, and Daniel Lewis, thank you so much for making my time at Flinders University memorable. Thank you for your help, your welcome, and for including in all the shenanigans that made my time in Australia so colourful.
- To George Fleming, I know you will likely never see this, but I missed you after the pandemic forced you to move on from our group. You laughed at all my jokes, and that meant a lot. I will never forget your review of my very first paper draft, wherein you referred to my writing style as that of a "pretentious thespian git". I still laugh aloud at that.

Liam James Dodd

- To William Sandy, what an undergraduate student you were. Your amazing effort and enthusiasm were nothing short of stellar. You will go far mate.
- To Bowen Zhang, you got me blind drunk at the Christmas party, resulting in me vomiting on a table in front of Tom, who I had just asked for a PhD position. You then got me blind drunk at your wedding, leading to Haoran and Wei having to carry me home. Vengeance will come at my Viva party.
- To Douglas Parker, you are a man who can tell entertaining stories for hours, and I am a man who struggles to know what to say to make conversation. It's not hard to see why I value your company.
- To Joseph Dale, Lynx Africa is good.
- To Samuel Petcher, I once told you that when I pictured a good PhD student, you are what came to mind. I stand by that statement.
- To Alexander Cowan, it was your early influences that led to me reaching this point, so I owe you a great deal of thanks.
- To Edward Powell and Ian Whale, there's not really much point in me writing a lot here, since I can't put into words what you mean to me. Instead, I'll just say, you don't have to read beyond this point.
- To my Mum, I am forever a mummy's boy, and I will scream that proudly from the rooftops.
- To "You Know Who You Are", see the personal copy of the thesis.

It is now quite surreal, to think that once this is submitted, I will have to move on to the next stage in my life. I have experienced this at every major step of my education, but it never gets any less bizarre. I look forward now, bewildered despite having some plans for where to go next, and what I might do. Maybe you have already experienced this yourself and get where I am coming from, or maybe one day you will experience it for the first time and think "huh".

Liam James Dodd

Table of Contents

Liam James Dodd

Liam James Dodd

Liam James Dodd

List of Abbreviations

2-MBT: 2-mercaptobenzothiazole

CFU: colony forming units

DAA: diallylamine

DABCO: 1,4-diazabicyclo[2.2.2]octane

DBDC: di-n-butyldithiocarbamate

DCM: dichloromethane

DCPD: dicyclopentadiene

DEB: 1,3-diethynylbenzene

DEDC: diethyldithiocarbamate

DFT: density functional theory

DIB: 1,3-diisopropenylbenzene

DMA: dynamic mechanical analysis

DMDC: dimethyldithiodicarbamate

DMF: dimethylformamide

DNBD: dinorbornadiene

DODC: di-n-octyldithiocarbamate

DSC: differential scanning calorimetry

DT ring: 1,2-dithiol-3-thione ring

DVB: divinylbenzene

EGDMA: ethylene glycol dimethacrylate

ENB: ethylene norbornene

FTIR: Fourier transform infra-red

GPC: gel permeation chromatography

HOMO: highest occupied molecular orbital

HPLC: high performance liquid chromatography

ICP-OES: inductively coupled plasma optical emission spectroscopy

KEtX potassium ethyl xanthogenate

K^{i}PrX potassium isopropyl xanthogenate

LUMO: lowest unoccupied molecular orbital

LWIR: long wave infra-red

MPA: monopropargylamine

MWIR: mid wave infra-red

NBD: norbornadiene

NMR: nuclear magnetic resonance spectroscopy

NON: 1,8-nonadiyne

PXRD: powder x-ray diffraction

RAFT: reversible addition fragmentation chain transfer

SEC: size exclusion chromatography

SERS: surface enhanced Raman scattering

SWIR: short wave infra-red

TAA: triallylamine

TAPAT: triallylphosphate

TAPIN: triallylphosphine

TAPIT: triallylphosphite

T_d: decomposition temperature

T_g: glass transition temperature

TGA: thermogravimetric analysis

TLC: thin layer chromatography

TNE: Trommsdorff-Norrish effect

TPA: tripropargylamine

XRF: X-ray fluorescence

Liam James Dodd

List of Publications

First Author Publications

Investigating the Role and Scope of Catalysts in Inverse Vulcanization; L. J. Dodd, Ö. Omar, X. Wu, T. Hasell; ACS Catalysis, 2021, 11, 4441-4455.

Raman Analysis of Inverse Vulcanised Polymers; L. J. Dodd, C. Lima, D. Costa-Milan, A. R. Neale, B. Saunders, B. Zhang, A. Sarua, R. Goodacre, L. J. Hardwick, M. Kuball, T. Hasell; Polymer Chemistry, 2023, 14, 1369-1386.

Inverse Vulcanisation of Self-Activating Amine and Alkyne Crosslinkers; L. J. Dodd, W. Sandy, R. A. Dop, B. Zhang, A. Lunt, D. R. Neill, T. Hasell; Polymer Chemistry, 2023, 14, 4064-4078.

Other Publications

Fabrication of TiN-Based Superhydrophobic Anti-Corrosion Coating by Inverse Vulcanization; C. Maio, P. Yan, H. Liu, S. Cai, L. J. Dodd, H. Wang, X. Deng, J. Li, X. Wang, X. Hu, X. Wu, T. Hasell, Z. Quan; Bulletin of the Chemical Society of Japan, 2022, 95, 1253-1262.

Inverse vulcanised sulfur polymer nanoparticles prepared by antisolvent precipitation; B. Zhang, S. Petcher, R. A. Dop, P. Yan, W. Zhao, H. Wang, L. J. Dodd, T. McDonald, T. Hasell; Journal of Materials Chemistry A, 2022, 10, 13704-13710.

Inverse Vulcanization with SiO2-Embedded Elemental Sulfur for Superhydrophobic, Anticorrosion, and Antibacterial Coatings; C. Miao, X. Xun, L. J. Dodd, S. Niu, H. Wang, P. Yan, X. Wang, J. Li, X. Wu, T. Hasell, Z. Quan; ACS Applied Polymer Materials, 2022, 4, 4901-4911.

Mercury capture with an inverse vulcanized polymer formed from garlic oil, a bioderived comonomer; B. Zhang, L. J. Dodd, P. Yan, T. Hasell; Reactive & Functional Polymers, 2021, 161.

Sulfur-rich polymers with heating/UV light-responsive shape memory and temperature-modulated self-healing; Z. Yang, P. Yan, X. Li, C. Miao, S. Cai, W. Ji, M. Song, L. J. Dodd, X. Wu, T. Hasell, P. Song; Polymer Chemistry, 2023, 14, 3686-3694.

Liam James Dodd

Chapter 1: Introduction

This chapter aims to introduce the concept of inverse vulcanisation in the broad scale, in order to place the work detailed in later chapters into the wider context of the field. As such this chapter will largely focus upon literature review, introducing noteworthy publications and generally setting the scene for the rest of this thesis. Other chapters may start with shorter, more refined literature review sections, which will provide the relevant information for those specific chapters.

1.1. Properties of Elemental Sulfur

More than 60 million tonnes of elemental sulfur is produced annually by the refinement of petrochemical feedstocks.[1.1] In order to reduce acid rain, fuels must be purified of sulfurous contaminant compounds, which would combust to form sulfur dioxide, which then goes on to dissolve in atmospheric rainwater to form sulfuric acid. As such crude fuels are subjected to hydrodesulfurisation and the Claus process, which convert sulfurous contaminant compounds to elemental sulfur.[1.2-1.4]

Although this sulfur has several applications, such as being used to create fertilisers and sulfuric acid, the supply greatly outweighs the demand, resulting in the excess sulfur being stored on the megaton scale in open to air stockpiles, with unexplored environmental consequences (Figure 1.1).[1.4,1.5] Sulfur is known to have some antibacterial properties, which could mean that megaton scale sulfur stockpiles could be harmful to microbiological ecosystems.[1.6] There is also the consideration that elemental sulfur can be ignited, and burns to form sulfur dioxide, so if a sulfur stockpile were to be struck by lightning, there is a possibility of a large, hazardous fire that liberates toxic sulfur dioxide into the atmosphere, thereby undoing the efforts to mitigate acid rain.[1.7] These stockpiles are expected to expand more rapidly in coming years as the depletion of fossil fuels forces the usage of previously avoided petrochemical resources of higher levels of sulfur contamination.
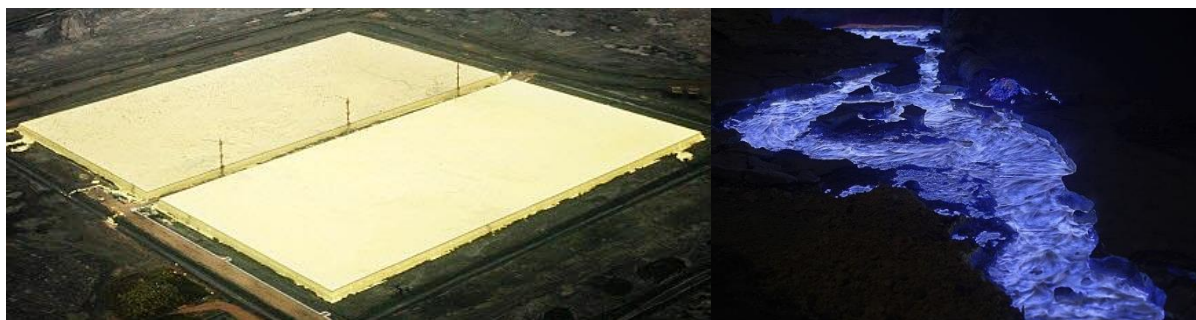
Figure 1.1: Left: a sulfur stockpile at Syncrude near fort McMurray, 2007, Alberta, Canada. Right: the characteristic blue fire of burning molten sulfur, Kawah Ijen volcano, Indonesia.

Because of the excess production of elemental sulfur, and the desire of landowners to decrease their stockpile sizes, elemental sulfur is a cheap and abundant resource that is widely available, and often purchasable for close to the cost of shipping (£1.05 for 1 kg).[1.8] One potential way in which the excess of elemental sulfur could be utilised, is in the field of materials chemistry. At room temperature, elemental sulfur exists primarily as the α-sulfur allotrope, a crown shaped eight membered ring in an orthorhombic crystal structure, with traces of the less stable cyclo-heptasulfur allotrope present.[1.5,1.9,1.10] At 95.3 °C α-sulfur converts to β-sulfur, another eight membered ring of sulfur atoms, this time in a monoclinic crystal structure.[1.9,1.11] Continued heating results in the melting of elemental in the range of 114 °C to 120 °C, which is broad due to the interconversion of β-sulfur into various other forms of sulfur, all with different melting points.[1.11,1.12]

Liam James Dodd

Through the molten phase to 159 °C or above, sulfur – sulfur bonds enter into an equilibrium where they homolytically cleave into thiyl radicals, though the exact temperature where this process becomes non-negligible is debated.[1.5,1.10,1.13] Thus, the rings of sulfur are cleft to form radical capped chains of sulfur atoms, termed thiyl radicals. These thiyl radicals can attack upon one another and other sulfur rings to extend their chains forming sulfur oligomers and polymers, which are the predominant species when elemental sulfur forms a clear red solid at temperatures of 190 °C or above (Figure 1.2).[1.5] This polymeric solid is not stable to depolymerisation, and upon cooling, depolymerises back to cyclo-sulfur, prohibiting its use in any long term application.[1.5,1.10,1.13] Thus, in order to utilise elemental sulfur, the resultant material must be stable to depolymerisation.
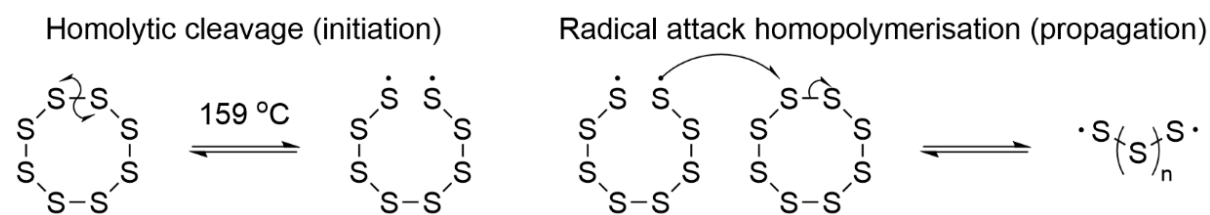
Figure 1.2: The homolytic cleavage of cyclo-octasulfur to form thiyl radicals and subsequently, their homopolymerisation to form a sulfur polymer.[1.5]

1.2. Inverse Vulcanisation

For decades elemental sulfur has been used in conventional vulcanisation for the modification of the properties of polymers. By means of reaction between the thiyl radicals formed from the homolytic cleavage of elemental sulfur, and carbon – carbon double bonds, organic polymer chains can be crosslinked with sulfur bridges.[1.13-1.15] An example of this is shown in Figure 1.3a, which is adapted from the scheme proposed by Coleman *et al.* who suggested that thiyl radicals abstract a proton from the carbon alpha to the double bond, forming a resonance stabilised radical, which then attacks on other sulfur chains to crosslink.[1.14] It should however be noted that it has not been proven beyond reasonable doubt that thiyl radicals are responsible for this crosslinking, and that an alternate theorem is that elemental sulfur cleaves heterolytically to form a zwitterion, though there is less evidence of this.[1.14] Other theories suggest mechanisms closer to that of thiol-ene click chemistry.[1.16] Regardless, conventional vulcanisation does not use large amounts of sulfur, and so cannot be the solution to the ever-increasing excess sulfur problem.

In 2013, the landmark discovery of inverse vulcanisation was made: a bulk polymerisation of molten sulfur with an organic small molecule crosslinker that contains at least two carbon – carbon double bonds (Figure 1.3b).[1.17] This reaction is capable of forming inverse vulcanised polymers of high sulfur content that can be stable to depolymerisation, and the variety of reactive crosslinkers gives rise to a plethora of unique materials with differing properties. The reaction itself requires no solvent, though one can be applied if desired to modify the properties of the product, and has a theoretical atom economy of 100 %.[1.17] Figure 1.3c shows the structures of some representative small organic molecules that can be used in inverse vulcanisation reactions. Note that there are several examples of crosslinker molecules derived from renewable sources, for example limonene, and that the scope of inverse vulcanisation has been expanded to include molecules with one double bond, more than two double bonds, and even triple bonds.[1.18-1.23]

Note that in the literature, there is some lack of clarity regarding what constitutes an inverse vulcanised polymer. Some define an inverse vulcanised polymer, as a polymer with more than 50 % by mass sulfur content, and those polymers of less than 50 % sulfur content by mass are considered

Liam James Dodd

to be conventionally vulcanised polymers. This distinction may not be so valuable in terms of categorising the polymers, and also places a polymer of 51 % sulfur by mass into a different category than one of 49 % sulfur content by mass, despite these polymers likely having very similar properties. As such, the definition that shall be used from here on, is that a conventionally vulcanised polymer is one where sulfur chains crosslink a macromonomer, and that an inverse vulcanised polymer is one where sulfur chains crosslink small organic molecules.
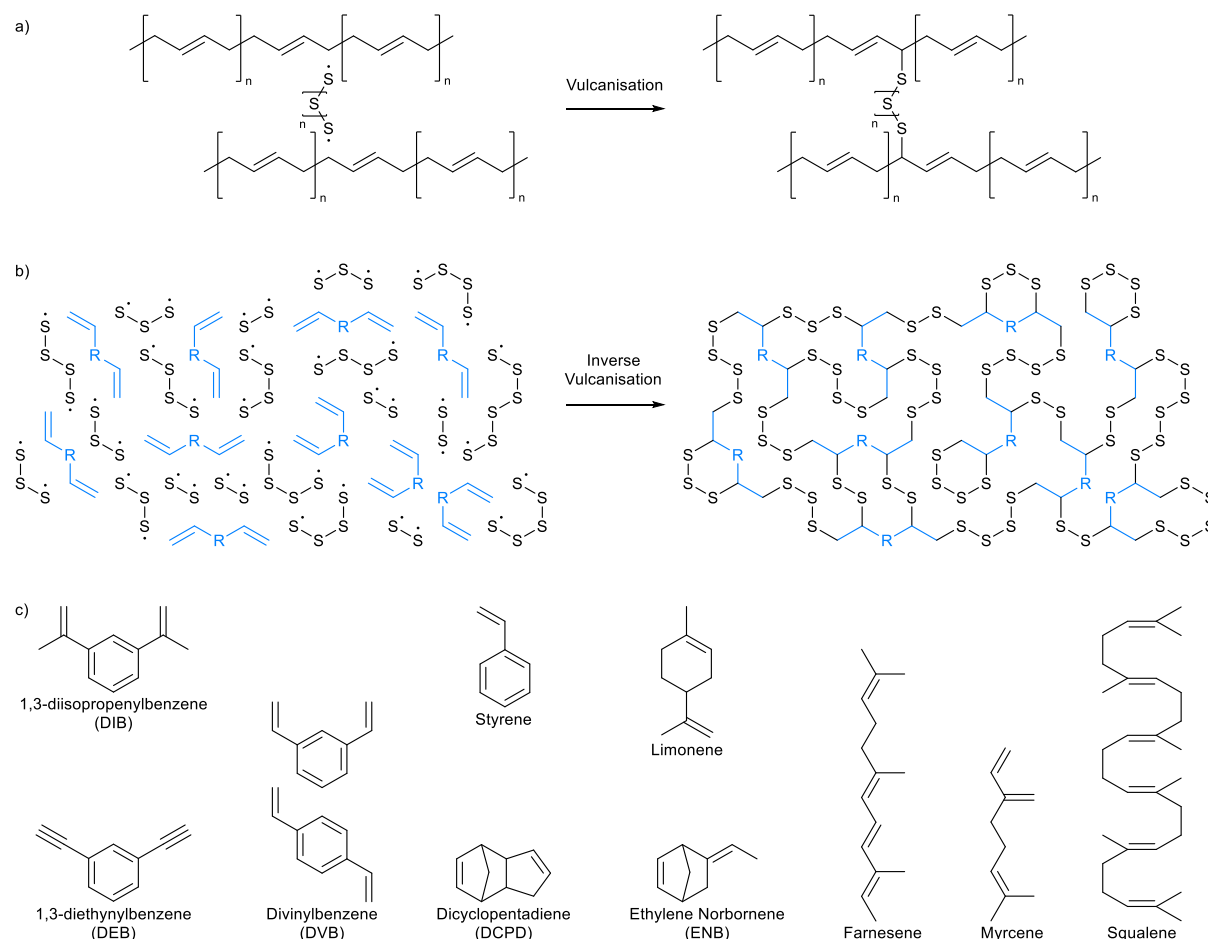
Figure 1.3: a) A simplified reaction scheme for conventional vulcanisation. Note that the carbon – carbon double bonds may be incorporated into the macromonomer chains as part of the backbone or as pendant groups. b) A simplified reaction scheme for inverse vulcanisation. c) Names, abbreviations and structures of representative examples of small organic molecules that are active in inverse vulcanisation.[1.18-1.23] Note that divinylbenzene is usually supplied as a mixture of the ortho and para isomers as shown.

In the seminal publication, 1,3-diisopropenylbenzene (DIB) was reacted with molten elemental sulfur in a bulk polymerisation method, at 185 °C using between 50 and 90 % by mass in the reaction feed.[1.17] Within five minutes a glass red solid formed, which was then cooled to room temperature, revealing that it was stable to depolymerisation over the course of months, shape-persistent, and showed no signs of crystalline elemental sulfur contained within its structure. Powder x-ray diffraction (PXRD) revealed only amorphous scattering with no peaks corresponding to crystalline elemental sulfur, and differential scanning calorimetry (DSC) indicated glass transition temperatures (T_g's) which are diagnostic of a polymer structure, and showed no peaks corresponding to the melting of either α-sulfur or β-sulfur (95 °C and 115 °C respectively) when the sulfur feed ratio was 80 % by mass or less.[1.9-]

Liam James Dodd

[1.12,1.17] It is worth noting that more recent research has pointed out that both PXRD and DSC rely on elemental sulfur being in a crystalline state in order to detect it, and newly applied analysis techniques have detected amorphous elemental sulfur where PXRD and DSC have failed to detect any elemental sulfur at all.[1.24,1.25] Therefore it may be that many inverse vulcanised polymers that were previously assumed to be free of elemental sulfur, may in fact contain this impurity, though this will be discussed in great detail in later chapters.

It was also found that the polymers' T_g's were tuneable with sulfur content; highest with more DIB, and lowest with more sulfur.[1.17] This trend is explained by two principles. Firstly, as more crosslinker is added, the crosslink density of the polymers is increased, which makes the chain more immobile. Therefore, they require more input thermal energy to allow them to move more freely. The second principle is that adding more crosslinker results in shorter crosslinking chains of sulfur, as fewer sulfur atoms are distributed across more reactive carbon – carbon double bonds. It has been shown in the literature, that longer chains of sulfur atoms contain weaker central sulfur – sulfur bonds, which are easier to break.[1.25,1.26] Therefore, with more crosslinker, there are fewer of these weaker bonds, making it harder to break enough sulfur – sulfur bonds that the chains can move over one another.

When the prepolymer was poured into a hot mould towards the end of the five-minute reaction time, it was found that the prepolymer would take on the shape of the mould before forming into a shape persistent red glass, thereby allowing for melt processability.[1.17] To conclude the seminal publication, the electrochemical behaviour of DIB inverse vulcanised polymers as the cathode material of lithium ion batteries was examined. It was found that the cyclic voltammogram of the polymer cathode batteries were similar to those of elemental sulfur, but in contrast to other lithium sulfur batteries, demonstrated good capacity retention with extensive discharge and recharge cycles.[1.17]

1.3. Applications of Inverse Vulcanised Polymers

It was demonstrated in the initial publication that inverse vulcanised polymers could find application in the field of energy storage materials, however in the years since, numerous potential applications for inverse vulcanised polymers have become apparent as their properties have been explored.[1.17] In addition to their low-cost reagents, simple and facile synthesis, and potential for recyclability, inverse vulcanised polymers can sometimes display self-healing properties. These self-healing properties, as well as their combination of thermoplastic and thermoset properties, and recyclability and remoulding potential, are all resultant from the reversible breakage and formation of the sulfur – sulfur bonds within their structures.[1.4] It is worth bearing in mind during the following discussion of the potential applications of inverse vulcanised polymers, that many inverse vulcanised polymers possess these properties innately, making them attractive candidates for next generation materials. It is on account of these properties and the discussions that follow, that inverse vulcanised polymers are beginning to see uptake in industry.

1.3.1. Remediation of Water

Elemental sulfur itself can be used to sequester chemically soft metals from water, which are a significant health concern in many parts of the world. However, sulfur has relatively low affinity for these metals in comparison to specialised metal uptake materials, and it is difficult to process into effective devices due to its high crystallinity and powdered morphology.[1.1,1.5] Inverse vulcanised polymers are a potential alternative as they have been shown to have high affinities for soft metals like palladium, and mercury, and are often melt processable into useful shape persistent devices.

Chalker *et al.* were among the first to report inverse vulcanised polymers with application of water remediation as the target.[1.22] Reported was a material produced by a modified inverse vulcanisation

Liam James Dodd

method, comprised of elemental sulfur and limonene (Figure 1.4). The reaction was performed with an active vacuum distillation attached to the reaction vessel, which drew off p-cymene, volatile thiols and sulfides as the distillate. It was noted that the formation of aromatic p-cymene from limonene in the presence of sulfur had been reported in the literature previously, but it does hint to the conclusion that the mechanism of inverse vulcanisation is likely more complex than simple radical attack, and can have unexpected branches to its reaction pathways.[1.27] The product of the reaction was too low molecular weight to be considered a true polymer, but rather an oligomer which was otherwise easy to synthesize, scalable to 100 g in its synthesis, and had an affinity for aqueous mercury (II) and palladium (II). The waxy material was capable of taking up 55 % of mercury (II) from a $HgCl_2$ solution (10 mL, 2000 parts per billion) in water, and that the mercury (II) could not dissociate from the material back into water once bound. Though 55 % uptake is relatively poor compared to some materials, sulfur - limonene polysulfide's remarkably low cost and ease of processing could make it an attractive material. What makes it more attractive is the fact that the material undergoes a colour change upon absorbing mercury (II) which may provide a simple means of assessing the material's lifetime.[1.22]
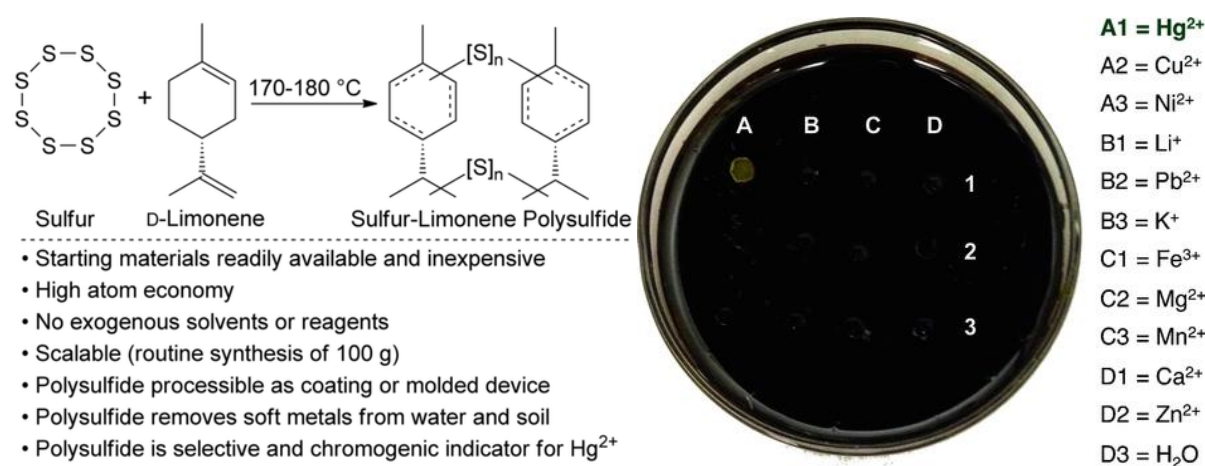
Figure 1.4: The synthetic scheme and advantages of the sulfur – limonene polysulfide material synthesized by Chalker *et al.*, as well as a photograph that demonstrates the colour change in the material when it is exposed to aqueous mercury (II). Reproduced from Angewandte Chemie International Edition.[1.22]

Since the report of sulfur – limonene polysulfide, several other inverse vulcanised polymers have been demonstrated to uptake mercury and other harmful metals from water, with greater efficiency than sulfur – limonene polysulfide, and better investigated absorption thermodynamics and kinetics. It has become apparent that several factors that can be influenced by the choice of the organic comonomer strongly influences metal uptake, such as the wettability, as more hydrophilic comonomers promote interaction with water, allowing for better adsorption kinetics of the metal ions.[1.28] It is generally accepted that the soft sulfur atoms form the binding sites for soft metal ions, but the sulfurous component of the inverse vulcanised polymers is inherently hydrophobic, so a commonly employed countermeasure is to maximise the surface area of the polymers, thus improving the number of binding sites and allowing for better adsorption kinetics. By this logic, one method which coated sulfur – limonene polysulfide onto silica gel improved its uptake capacity of mercury (II) from water, from 55 % to 99 %.[1.29] When organomercury compounds are the uptake target, longer carbon chains in the organic comonomer have been shown to be assistive, by providing lipophilic sites that the organomercury has an affinity for.[1.28]

Liam James Dodd

Inverse vulcanised polymers have also been demonstrated to show different affinities for different metal ions, depending on the organic comonomer: castor oil as a comonomer is capable of removing cadmium (II), although is not effective enough to be viable as a commercially applied material; canola oil is effective at removing gold (III), as is limonene when coated on silica, and it has also been shown that a quaternary amine containing comonomer was effective in removing gold (III) as well as many other metal ions; and iron (III) is removed effectively by inverse vulcanised polymers of canola oil.[1.28] It is important to remember that the adsorbed metals can sometimes chemically react with inverse vulcanised polymers, which can actually be advantageous: mercury (II) can be reduced to the inert and non-toxic mineral, cinnabar (mercury sulfide), and gold (III) can be reduced to its metallic state, assisting recovery.[1.28]

The work conducted for this thesis did not interact heavily with the heavy metal remediation application of inverse vulcanised polymers, so a detailed account of these advanced polymers will not be given. For this, an excellent review article titled "Inverse Vulcanized Polymers for Sustainable Metal Remediation" is recommended.[1.28] Rather, what is interesting to the work in this thesis, is the way in which the polymers can be modified with processing techniques. The morphology and microscopic structure of inverse vulcanised polymers play critical roles in several factors regarding metal uptake. It has also been shown that modifications to the polymer structure, both during and post synthesis can have a large impact on the mercury uptake of inverse vulcanised polymers, and this aligns well to focus of this thesis, in that it is a modification of the synthetic method.

The mercury uptake of an inverse vulcanised polymer of DIB was shown to be enhanced by a supercritical CO_2 foaming process (Figure 1.5).[1.30] With appropriate tuning of the conditions, it was found that supercritical CO_2 could penetrate well into a DIB inverse vulcanised polymer, and that when the pressure was rapidly released, the CO_2 quickly returned to the gas phase and foamed the polymer, introducing pores of sizes in the range of 5 and 100 μm, with most pores being between 10 and 20 μm. This foaming process slightly increased the T_g of the polymers, thought to be the result of the removal of low molecular weight oligomers that acted as plasticisers, by the supercritical CO_2 in which they were solubilised and extracted from the polymer matrix. When tested for mercury (II) uptake, it was found that the foamed DIB inverse vulcanised polymer removed approximately 95 % of mercury from the solution, whereas the equivalent un-foamed polymer removed only 45 %.[1.30]

One example of where a polymer was modified during its synthesis, was in the work performed by Petcher *et al.* who were able to produce a sodium chloride porogen with some degree of control of the salt crystal size by means of recrystallisation.[1.31] The porogen was then heated in an oven whilst the inverse vulcanised polymer was synthesized separately upon a hotplate. During inverse vulcanisation, the sulfur and organic phases are initially immiscible, but gradually merge into a single phase as the reaction proceeds and forms more inverse vulcanised oligomers that act as an emulsifier. Left to react for longer, these oligomers will form a crosslinked matrix. After the inverse vulcanisation reaction mixture became monophasic, it was poured onto the hot sodium chloride porogen, which was returned to the oven, allowing the mixture to penetrate into the porogen and finish reacting to form a salt templated, highly crosslinked network polymer. The sodium chloride was then removed by Soxhlet extraction, and the porous polymer was tested for mercury uptake. It was found that this process was amenable to a variety of different organic crosslinkers although some failed to penetrate into the porogen well due to high viscosity or resulted in polymers with too poor mechanical strength to maintain the templated structure. Nevertheless, it was found that higher temperatures of synthesis resulted in inverse vulcanised polymers of greater mercury uptake capacities, the highest reported for any salt templated inverse vulcanised polymer at that time.[1.31] However, salt templated inverse vulcanised polymers still have relatively low uptake capacities, 2.27 mg g^{-1} from a Langmuir isotherm

fitting for the case of Petcher *et al.*'s work, compared to 836.7 mg g^{-1} for a metal organic framework reported elsewhere.[1.31,1.32]
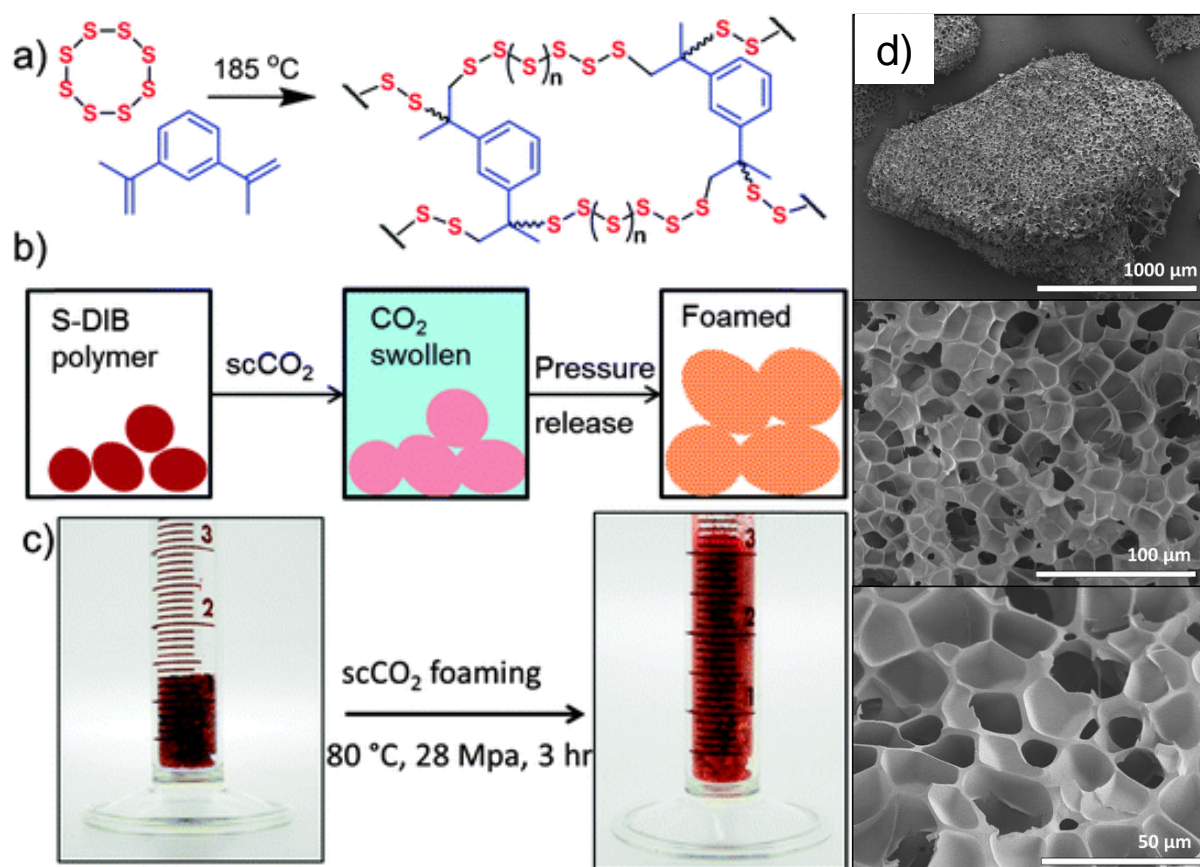
Figure 1.5: a) Reaction scheme of elemental sulfur and DIB, b) supercritical CO_2 processing method to foam the polymer, c) photographs of an inverse vulcanised polymer made from 50 % by mass sulfur and 50 % by mass DIB, before and after supercritical CO_2 foaming, and d) SEM imaging of the supercritical CO_2 foamed sulfur-DIB inverse vulcanised polymer. Reproduced from Chemical Communications.[1.30]

The primary advantage of salt templating inverse vulcanised polymers is the low cost of the reagents and materials involved as well as the relative safety of the process which requires no significantly hazardous chemicals or techniques, meaning the process may be quite amenable to industrialisation. There are however other techniques for processing inverse vulcanised polymers besides salt templating that can yield notably higher uptake capacities. Some examples include electrospinning (uptake capacity: 327.7 mg g^{-1}), carbonisation (uptake capacity: 850 mg g^{-1}), and coating onto microporous supports (716 mg g^{-1}).[1.30-1.34]

1.3.2. Antimicrobial Materials

Elemental sulfur itself has antimicrobial properties, but is limited in its applications due to its powdered form.[1.35] Inverse vulcanised polymers are a potential means to provide sulfur as a continuous solid with sufficiently robust mechanical properties that they can be applied in a wider range of antimicrobial materials, for example, thin coatings.[1.17] Despite this, the antimicrobial properties of inverse vulcanised polymers have received little research attention.

One publication by Smith *et al.* examined the antimicrobial properties of the inverse vulcanised polymers of two organic crosslinkers, DIB and dicyclopentadiene (DCPD).[1.36] In the initial testing, it was

Liam James Dodd

found that inverse vulcanised polymers of both organic crosslinkers prevented exponential growth and biofilm (a surface film made up of adhered bacteria) formation of *E. coli* bacteria on their surfaces. Further, more controlled characterisation of the surface bactericidal effects of these inverse vulcanised polymers, showed that the DIB inverse vulcanised polymer caused a 99.9 % reduction in the survival of two different species of bacteria on its surface, *E. coli* and *S. aureus*. The DCPD inverse vulcanised polymer did indeed show reductions in the number of surviving *E. coli* bacteria on its surface, though not nearly as significantly as the DIB inverse vulcanised polymer, and showed little reduction in the population of *S. aureus* surviving on its surface. From these results, it is clear that the choice of organic crosslinker has significant influence over the extent to which, and over the species of which an inverse vulcanised polymer can kill bacteria.[1.36]

Attempting to uncover the way in which their inverse vulcanised polymers were killing bacteria, it was hypothesized that sulfur, which has antibacterial properties in and of itself, could be leaching out of the polymers, however evidence against this was found in that direct contact between the polymer and the bacteria was required for killing of the bacteria.[1.36] Should a leaching mechanism be the case, it would be expected to see a reduction in living bacteria not only on the surface, but nearby to it, as bactericidal materials leave the polymer surface and diffuse into the surrounding medium. Further evidence against a leaching mechanism was found in that no crystalline sulfur could be detected in or around the polymer, before or after bactericidal studies. This may be advantageous since antibacterial materials that use leaching mechanisms gradually lose their antibacterial properties as over time the antibacterial species they contain are gradually depleted.[1.36]

An alternative theory was that the reversible sulfur – sulfur bonds were cleaving open to form species toxic to bacteria. This theory would seem to have some merit as similar species have already been proven to be toxic to bacteria and it would explain the observation that inverse vulcanised polymers required contact to kill bacteria.[1.36] Additionally, it has been proven elsewhere, that the central sulfur – sulfur bond of a polysulfide chain becomes progressively weaker, the longer that polysulfide chain is.[1.26] This may provide some explanation as to why DIB gave an inverse vulcanised polymer that was more bactericidal than DCPD. DCPD has a lower molecular mass than DIB, therefore when the same mass of these crosslinkers are used in polymer synthesis, as was the case in this particular publication, there are more moles of DCPD present than DIB in their respective syntheses. With more moles of DCPD would come a greater crosslinking density which would reduce the average length of polysulfide bridges between organic units, thus resulting in fewer weak sulfur – sulfur bonds which can readily cleave to form bactericidal chemical species.[1.36]

Another important publication in the field of antibacterial studies was that of Dop *et al.*, who used more in depth methods to characterise the bactericidal effects of a range of different inverse vulcanised polymers made from a wider range different crosslinkers.[1.37] The crosslinkers employed were DVB, DIB, DCPD, perillyl alcohol, rapeseed oil, and linseed oil, and it was found that not only does the bactericidal effects depend on the identity of the organic crosslinker, but also upon the T_g of the polymer (Figure 1.6). Of exceptional importance, it was discovered that inverse vulcanised polymers showed little or no bactericidal effects when tested at temperatures below their T_g, but showed significantly greater bactericidal effects when tested at temperatures exceeding their T_g. This not only informs future research, but also suggests that it could be that the reversible sulfur – sulfur bond formation may have a role to play in the antibacterial properties of inverse vulcanised polymers, as it is above the T_g where homolytic bond cleavage becomes more significant, presenting a greater presence of thiyl radicals, and it was noted that other studies have shown that such sulfur radicals can be toxic to bacteria. Also tested was whether the hydrophobicity of the polymers had an effect on their bactericidal effect but no correlation was found.[1.37]

Liam James Dodd

Because Dop *et al.* observed a reduction in viable cells in solutions treated with inverse vulcanised polymers, a leaching study was conducted, despite the fact that Smith *et al.*'s worked had steered away from the conclusion of leaching effects.[1.36,1.37] Perillyl alcohol polymers showed more rapid reductions in viable cells when tested above their T_g which could be because when the polymer is above its T_g it has greater chain mobility, permitting easier diffusion of bactericidal species out of its structure and into the surroundings. Additionally, yellow precipitates formed in the test containers by the end of the tests, which DSC confirmed to be elemental sulfur. [1]H nuclear magnetic resonance spectroscopy (NMR) was conducted on the solution that had been treated with the inverse vulcanised polymer, and no signals were detected, suggesting that the leachate contained no hydrogen containing species such as inverse vulcanised oligomers. However, inductively coupled plasma optical emission spectroscopy (ICP-OES) revealed that the solution did contain elemental sulfur.[1.37]

It was noted that further studies should be conducted to determine with greater certainty, what species leach out of the polymer, such as H_2S, especially considering that a following publication showed that inverse vulcanised polymers generate hydrogen sulfide gas over long periods of contact with water.[1.24] Regardless, Dop *et al.*'s study inadvertently highlighted that analysis of the presence of crystalline elemental sulfur alone in inverse vulcanised polymers is not sufficient, as none of their polymers contained crystalline elemental sulfur, yet either amorphous sulfur leached out and crystallised, or the polymers depolymerised to form it.[1.37]
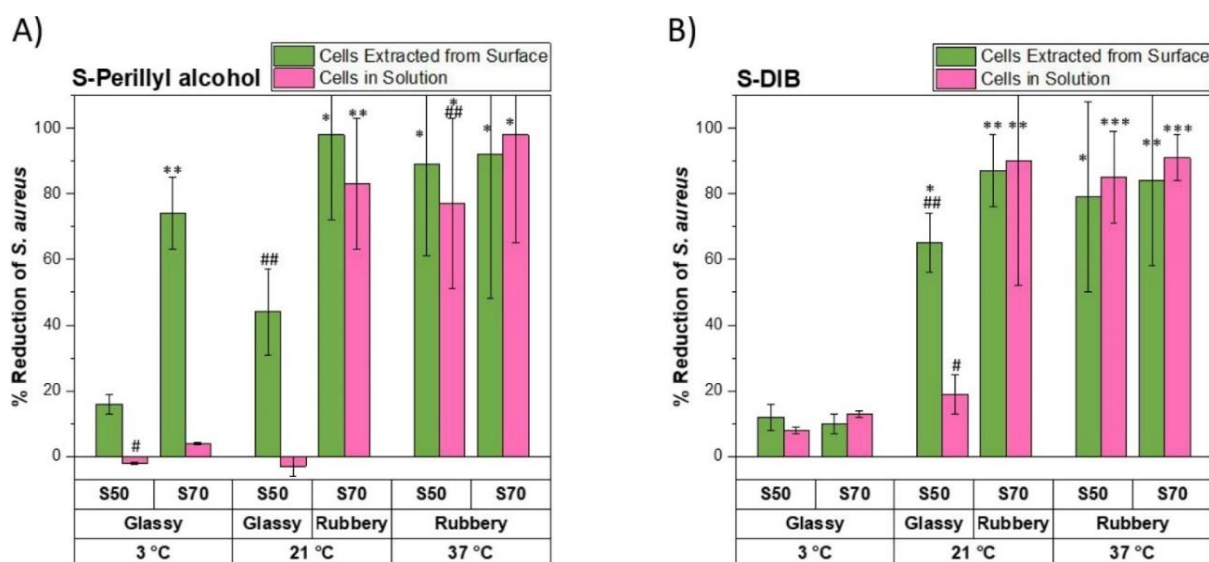
Figure 1.6: Summary of the percentage reduction in viable *S. aureus* cells extracted from the surface and from solution compared to polypropylene for (A) inverse vulcanised polymers of perillyl alcohol and (B) inverse vulcanised polymers of DIB, at varying test temperatures and sulfur/comonomer ratios. *p < 0.05 relative to polypropylene, **p < 0.01 relative to polypropylene, ***p < 0.001, #p < 0.05 relative to polypropylene, and ##p < 0.01 for 50 % by mass sulfur compared to 70 % by mass sulfur polymers at the same test conditions. Reproduced from Biomacromolecules.[1.37]

1.3.3. Infra-red Optical Components

Since inverse vulcanised polymers are comprised of chemical bonds with very low polarity, mostly sulfur – sulfur bonds and carbon - sulfur bonds, (note that carbon and sulfur have the same Pauling electronegativity) they often have low infra-red absorbances, as their stretching modes either do not, or very weakly, satisfy the selection rule for infra-red spectroscopy, that being, infra-red vibrational modes must cause a change in dipole moment.[1.38] In addition to this sulfur is a highly polarisable atom,

Liam James Dodd

and a high proportion of polarisable atoms within a material's structure gives rise to high refractive index.[1.39] As such, inverse vulcanised polymers are potential next generation materials for infra-red optics, which are applied in thermal imaging devices. The high refractive index means that lenses can be made thinner and still achieve the same lens power, which is important to minimise costs, though inverse vulcanised polymers are far cheaper than the current industry standard chalcogenide glasses and crystalline semi-conductors.[1.39] Thinner lenses are also important to minimise the weight of the lens, which can be important to the application, but is also important to the lifetime of the lens, as it can be that heavier lenses are gradually deformed by their own weight, which pulls them out of shape and of course the precise shaping of a lens is vital to its function.

Crystalline semiconductors such as silicon, germanium, and zinc selenide give high performance components, but can be hard to refine to a sufficient purity, difficult to appropriately shape, and have poor scalability to their synthesis and purification raising the cost as a result.[1.39] Chalcogenide glasses are defined as compounds of a chalcogen (either sulfur, selenium, and tellurium) with a group fourteen or fifteen element, and are accepting of a wide range of ratios of chalcogen to group fourteen or fifteen element, with the only requirement being that the product must not crystallise (it must be a glass). Heavier chalcogens tend to give greater transparency but lower T_g, and poorer mechanical properties, so there is a trade-off between performance and mechanical and thermal shape persistence. Chalcogenide glasses are chemically stable, non-hygroscopic, highly refractive, and almost as transparent to infra-red light as crystalline semiconductors, with the additional advantage that they are solution processable under inert atmosphere and melt processable. However, the raw materials needed to make them can be rare, must be very pure, and need multiple high temperature processes to fabricate materials, all of which raises the cost. Worse, the end-of-life products of these materials can be toxic, and so require special disposal or they pose the risk of serious environmental and health consequences.[1.39]

Since inverse vulcanised polymers remedy many of the drawbacks of chalcogenide glasses and crystalline semiconductors, in that they can be mechanically robust, melt processable, and highly infra-red transparent and refractive, as well as being cheap, easy to make, scalable, and often have no need for purification, they could be ideal replacements for chalcogenide glasses and crystalline semi-conductors.[1.39] As such, several publications have centred around this application.

It was recognised that if DIB contained a third olefin moiety, then the crosslinking potential of a single molecule could be increased, thereby resulting in a higher crosslink density which would give higher T_g and mechanical robustness.[1.39] It would also allow for more sulfur stabilisation, raising the percentage of sulfur in the polymer, which has a twofold effect: it raises the proportion of highly polarisable sulfur atoms for greater refractive index, and it reduces the percentage content of organic units, which are the main cause for infra-red absorption, thereby yielding higher infra-red transparency. As such, 1,3,5-triisopropenylbenzene was synthesized and inverse vulcanised to yield materials' whose T_g was tuneable with sulfur content, was more resistant to laser damage than its DIB analogue, and showed self-healing when exposed to heat, which is a large advantage over the current industry standard materials, as they become useless if damaged and must be discarded, whereas this material could be repaired.[1.39]

A seemingly sensible advancement to the use of inverse vulcanised polymers as infra-red optical components would be the substitution of sulfur for selenium, which as a heavier element, is more polarisable and therefore would instil a higher refractive index to the resultant material.[1.39] Selenium would also offer the advantage of NMR analysis as sulfur does not have NMR active isotopes for which spectrometers are easily accessible, and these isotopes are heavily quadrupolar.[1.40] Selenium on the other hand bypasses this limitation, however in the ten years since inverse vulcanisation's discovery,

Liam James Dodd

no successful attempts to substitute elemental sulfur for elemental selenium have been reported. This is likely due to the fact that selenium is harder to work with, with an inconveniently high melting temperature of 221 °C (31 °C higher than the temperature where sulfur forms a polymeric solid), with multiple accessible allotropes with raising temperature, each with very differently properties, resulting in poorly defined products.[1.40] Selenium also lacks parallel chemistry with sulfur, and so it may be wrong to assume that an analogue of inverse vulcanisation with selenium is possible. Finally, for sulfur inverse vulcanisation, hydrogen sulfide gas can be formed as a by-product, which is toxic (comparable to carbon monoxide) and offensive to the sense of smell, by the description of the odour of rotten eggs, though an added risk is that at hydrogen sulfide levels that are verging on toxicity, humans become nose-blind to the stench.[1.41] Hydrogen sulfide's selenium analogue is gaseous hydrogen selenide, which is more toxic and more repulsive to olfactory systems.[1.42] As such it may be unacceptably hazardous to substitute elemental selenium into an inverse vulcanisation type reaction.

To circumvent these issues with selenium two methods have been employed.[1.39] One method dopes elemental sulfur with selenium, to replace some sulfur atoms in cyclo-octasulfur with selenium, leading to a precursor material: $S_{90}Se_{10}$, and although the sulfur loading was limited, it was successfully employed in inverse vulcanisation with DIB to generate a polymer with higher refractive index than the selenium free DIB inverse vulcanised polymer analogue.[1.39] The second method employed achieved higher loadings of selenium: rather than heating elemental selenium, incurring its many allotropic phase transitions, elemental sulfur was heated to the molten state, and then grey selenium (an allotrope of elemental selenium) was introduced to the molten elemental sulfur (Figure 1.7). The thiyl radicals of the molten sulfur cracked the chains of selenium atoms, creating an in-situ mixed chalcogen, which was then used to crosslink DIB. The resultant material showed higher loadings of selenium than the products of the first method, as well as exhibiting refractive indices as high as 2.1, with high mid wave infra-red (MWIR) transparency.[1.39]
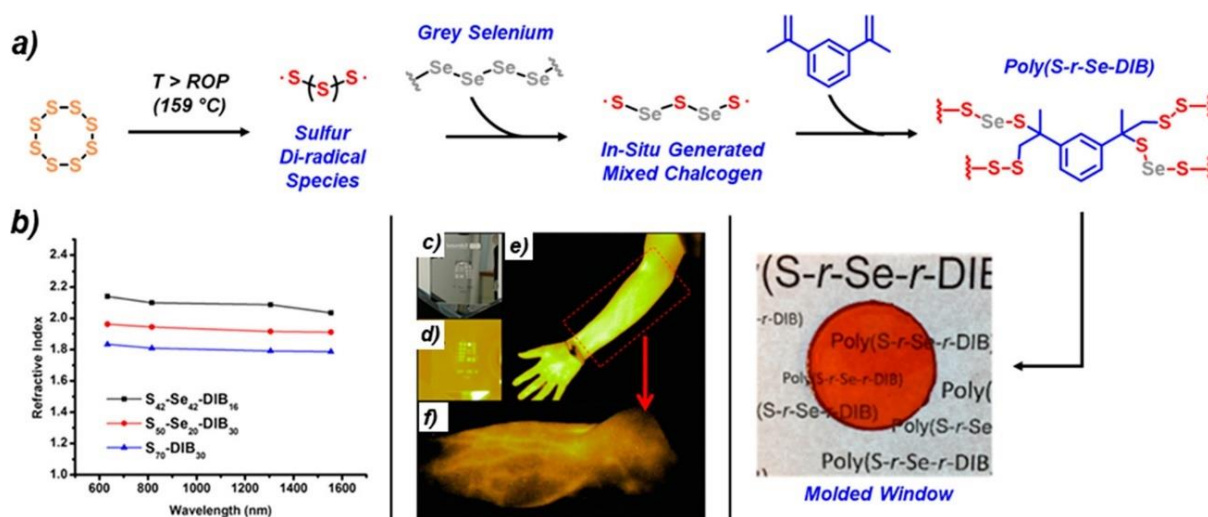
Figure 1.7: a) Scheme for the synthesis of a selenium and sulfur containing inverse vulcanised polymer of DIB, b) refractive indices of such terpolymers of varying composition vs wavelength, c) digital image of a USAF target, images captured with a mid-IR camera, operating at 3–5 µm, through a 1 mm thick panel of sulfur and selenium containing DIB inverse vulcanised polymer, of d) a USAF target, transparent at 3–4 µm, e) IR thermal image of human arm, and f) higher resolution image of human forearm. Reproduced from ACS Macro Letters.[1.39]

It is worth noting that the regions of the infra-red spectrum in regards to optical applications, are defined by atmospheric absorptions and blackbody emission as follows: short wave infra-red (SWIR)

has wavelengths from 1 to 3 μm; MWIR has wavelengths from 3 to 5 μm, below atmospheric water absorptions, and mostly results from blackbody radiation; 5 to 7 μm is mostly unused in imaging due to strong H_2O absorptions; long wave infra-red (LWIR) has wavelengths from 7 to 14 μm, above atmospheric water absorptions, and mostly results from blackbody radiation; and wavelengths longer than 14 μm are rarely used due to atmospheric CO_2 absorptions.[1.39] Blackbody radiation is the result of heat, with hotter sources producing a wider range of wavelengths and shorter wavelengths of peak emission (the higher the temperature, the more the emission moves from LWIR to MWIR), and this is what allows thermal imaging. Inverse vulcanised polymers are exciting in the field of infra-red optics, in part due to their MWIR and LWIR transparency.[1.39]

In another publication, it was recognised that because most of the infra-red absorbance of inverse vulcanised polymers stems from their organic monomer units, that with appropriate choice of organic comonomer, being one with low infra-red absorbance, inverse vulcanised polymers of minimal infra-red absorbance could be prepared.[1.43] Several organic comonomers: DIB, norbornadiene (NBD) and dinorbornadiene (DNBD), were selected for the study (Figure 1.8). DIB has an aromatic ring its structure which gives rise to some infra-red absorbance. Both NBD and DNBD are purely aliphatic and thus have lower infra-red absorbance. They also have rigid poly-cyclic structures, which is associated with increased rigidity in the product inverse vulcanised polymers.[1.44]

Computational chemistry was used to model the infra-red spectra of the inverse vulcanised polymers that would result from organic crosslinkers, though several simplifications to their structures had to be made as modelling an entire crosslinked network of billions of atoms is not practical or feasible.[1.43] As predicted, DIB provided a calculated spectrum of higher absorbance due to its aromatic ring. The NBD inverse vulcanised provided a spectrum of very low IR absorbance, however, NBD boils at temperatures too far below that of inverse vulcanisation, and at the time, no methods existed to circumvent this limitation.[1.43]

DNBD is sufficiently high boiling to be used in inverse vulcanisation and provided a calculated spectrum of relatively low infra-red absorbance, albeit higher than that of NBD due to the greater content of carbon – hydrogen bonds.[1.43] Thus, an inverse vulcanised polymer of DNBD was synthesized, showing a good match between the experimental and calculated IR spectra. The DNBD inverse vulcanised polymer was then applied as a thin film in several simple imaging tests in which is it was compared to a thin film of a DIB inverse vulcanised polymer. It was found that an infra-red image could be developed by an infra-red camera, when a plate of their DNBD inverse vulcanised polymer was placed in front of the camera's lens, whereas an image could not be developed under the same conditions when a film of DIB inverse vulcanised polymer was used.[1.43]

Though the image developed when the DNBD inverse vulcanised polymer was in place had some loss of quality, the result was still promising as this material was synthesized in a laboratory setting as a proof of concept.[1.43] Production of industry standard optical components is a very delicate and precise technique that can only be achieved with specialist equipment, which suggests that if a DNBD inverse vulcanised polymer was synthesized and developed into a component by use of these methods, it may indeed be satisfactory as an optical component.
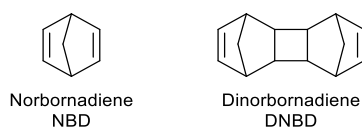
Norbornadiene
NBD

Dinorbornadiene
DNBD

Figure 1.8: Names, abbreviations, and chemical structures of norbornadiene and dinorbornadiene.

Liam James Dodd

1.3.4. Cathodes in Lithium Sulfur Batteries

Lithium sulfur batteries are an attractive class of next generation energy storage devices due to the low cost of the sulfur cathode and the relatively high specific capacities they can provide.[1.45] However, the poor processability of elemental sulfur can make fabrication of effective cathodes difficult, and the discrete molecular nature of sulfur promotes the loss of electrochemical intermediates into the electrolyte, and away from the cathode where they are useful, (referred to as the shuttling effect) which limits the retention of specific capacity and ultimately decreases the cycle life of the battery.[1.46] Inverse vulcanised polymers may be able to remedy these drawbacks as they can provide sulfur source in the form of a melt or solution processable solid, that contains sulfur bonded into and therefore trapped as part of, a crosslinked matrix, which may be able to prevent the shuttling effect.[1.17,1.45,1.46]

To this end, the electrochemical properties of a DIB inverse vulcanised polymer were investigated in a standardised testing cell known as a coin cell.[1.17] Cyclic voltammetry experiments, used to analyse the redox behaviour of electrochemical species at varying potentials, revealed coin cells of sulfur and coin cells of DIB inverse vulcanised polymers behaved similarly. The reduction peaks between 2.3 V and 2.4 V in both cyclic voltammograms were assigned to the initial reduction of sulfur to linear lithium polysulfides ($Li^+ S^- - S_n - S^- Li^+$) and the reduction peaks between 2.0 V and 2.1 V were assigned to further reduction of these linear lithium polysulfides to shorter chain linear lithium polysulfides, though cyclic voltammetry experiments alone cannot confirm these assignments. More in depth studies of the battery cycling behaviour revealed high specific capacity and long cycling lives of the coin cells of DIB inverse vulcanised polymers. The specific capacities obtained were in the range of other cutting edge cathode composites for lithium sulfur batteries, and at the time, were the best for a polymer-based cathode in such batteries, outperforming those of more expensive and difficult fabrication.[1.17]

Because of these initial results, lithium sulfur batteries that utilise inverse vulcanised polymers in the cathode have become one of the most popular research focuses of articles published within the inverse vulcanisation domain. Many aim to create batteries with even more favourable characteristics by changing the choice of organic crosslinker or the synthetic and processing conditions. Thus, there is far too much content to give any viable discussion of it here. Alternatively, something of key importance to the study of lithium sulfur batteries with inverse vulcanised cathode materials is their mechanism of electrochemical cycling and the shuttling effect. Though these concepts are vital to the intelligent design of superior batteries, the difficultly in their study has led to a limited literature precedent. One prominent literature article details the use of solid state NMR to uncover aspects of the mechanism of electrochemical cycling in lithium sulfur batteries with inverse vulcanised cathode materials.[1.46] Several inverse vulcanised polymers of DIB were synthesized at different feed ratios of DIB to sulfur. These polymers were then subjected to $^{13}C\{^1H\}$ cross polarisation magic angle spinning NMR to elucidate the structural environments of the organic units (Figure 1.9). Upon analysis of the resultant spectra, it was found that the chemical shifts of the non-aromatic quaternary carbon and the aromatic tertiary carbons changed depending on the feed ratio used to make the polymer. It was theorised this was to be due to different sulfur chain lengths placing these carbons in slightly different environments. With more DIB in the feed ratio comes a higher crosslinking density and therefore a shorter average sulfur chain length. Using this logic, assignments for these peaks were given and it was suggested that the peaks which are present with low mass ratios of DIB but absent at high mass ratios of DIB belong to carbons in the presence of long chains of sulfur, and that those peaks that intensify as more DIB is present, belong to carbons in the presence of short sulfur chains. Relaxation time experiments and computational chemistry helped justify the assignments.[1.46]

The effect of the sulfur chain length on the electrochemistry of the DIB inverse vulcanised polymers was placed under scrutiny.[1.46] Inverse vulcanised polymers with DIB feed ratios of 50 % by mass (DIB50-

Liam James Dodd

S50) and 10 % by mass (DIB10-S90) were used in these experiments to work with polymers with significantly different sulfur chain lengths. Cyclic voltammetry experiments provided similar results to those in the prior literature: two progressive reduction peaks, the higher potential one assigned to formation of long chain polysulfides and the lower potential one being assigned to short chain polysulfides.[1.17,1.46] These assignments are sensible in that it has been proven elsewhere that longer sulfur bridges sport progressively weaker sulfur – sulfur bonds toward the centre of the sulfur bridge. This weaker sulfur – sulfur bond should require less forcing conditions to be broken and therefore need less reducing conditions (less negative potential) in order to undergo reduction.[1.26]

However, there were some differences between the cyclic voltammograms of DIB10-S90 and DIB50-S50.[1.46] For DIB50-S50, which contains fewer short sulfur bridges, the reduction peak assigned to the formation of longer linear lithium polysulfides, was smaller than in comparison to that of DIB10-S90. This result was expected in that DIB10-S90 contains a greater number of long sulfur chains within its structure which are capable of being reduced to form long linear lithium polysulfides. DIB50-S50 on the other hand, contains fewer long sulfur bridges and so cannot form as many long linear lithium polysulfides, leading to a lower peak current in the cyclic voltammogram. It was also noted that for both inverse vulcanised polymers, the reduction peak associated with the formation of short linear lithium polysulfides, diminished with progressive cycles of cyclic voltammetry whereas the peak associated with long linear lithium polysulfides remained relatively unaffected. This suggests that the formation of long linear lithium polysulfides is more reversible, and that short linear lithium polysulfides are less reversible in their electrochemistry, which may be explained by their small size making them more prone to the shuttle effect and loss into the electrolyte.[1.46]
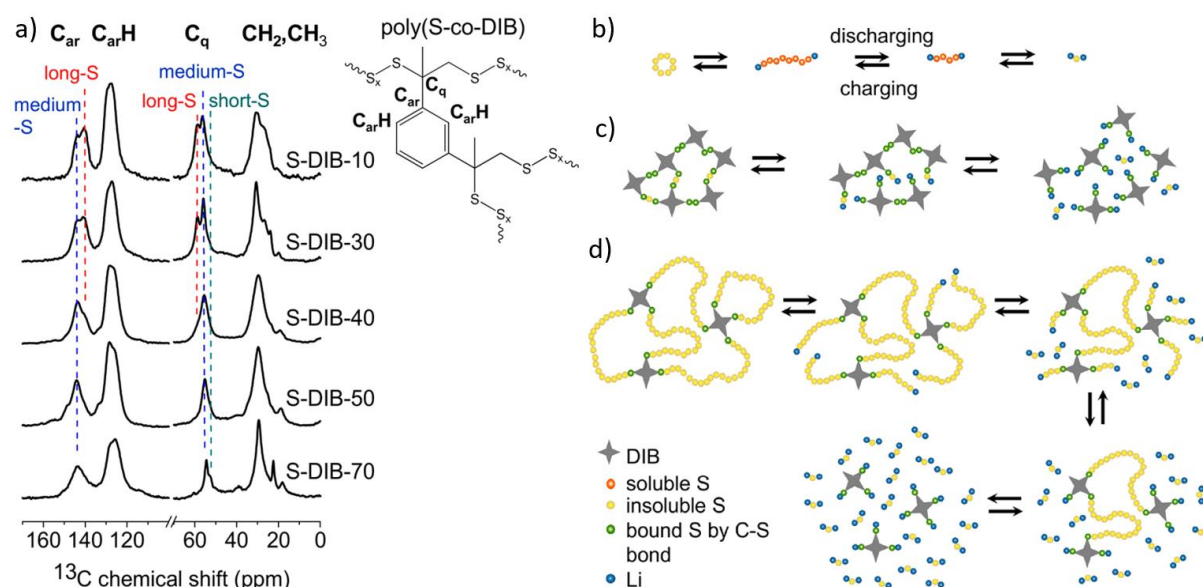
Figure 1.9: a) $^{13}C\{^{1}H\}$ CP MAS NMR spectra of inverse vulcanised polymers of DIB, with varying ratio of DIB to sulfur (the samples are denoted as S-DIB-X where X is the weight percentage of DIB), as well as a schematic representation of the reaction mechanisms during the discharge/charge cycle, where b) shows elemental sulfur forming soluble long-chain polysulfides from the initial stage of discharge, which diffuse into the electrolyte, c) shows S-DIB-50 at the cathode, where Li_2S formation is minimal and the hyperbranched structure can be easily fragmented into the monomeric units due to the short sulfide chains, and d) shows S-DIB-10 at the cathode, where long chain lithium polysulfides are anchored to the polymeric network, preventing dissolution into the electrolyte. Reproduced from Chemistry of Materials.[1.46]

Liam James Dodd

The discharge/charge profiles of DIB10-S90 and DIB50-S50 were then compared.[1.46] Typically an initial smaller discharge plateau in lithium sulfur batteries is associated with short linear lithium polysulfides, and then a later, longer discharge plateau is observed that is associated with long linear lithium polysulfides. DIB50-S50 exhibited only one discharge plateau, suggesting a relative absence of long linear polysulfides, supporting prior conclusions.[1.46]

Additionally, DIB50-S50 exhibited greater loss of current capacity with progressive cycles of charging and discharging, which may be explained by the loss of short linear lithium polysulfides by the shuttle effect, which DIB50-S50 would be more prone to given that it has fewer long linear lithium polysulfides which would be resistant to this shuttling effect because their greater length makes it more difficult for them to escape the polymer network. In contrast, DIB10-S90 showed discharge plateaus associated with short and long linear lithium polysulfides and exhibited much less loss of current capacity with progressive charge/discharge cycles, the explanation of which is the inverse of that for DIB50-S50.[1.46]

[7]Li cross polarisation magic angle spinning NMR was used to better understand the behaviour of lithium polysulfides during the cycling of the batteries.[1.46] Cells with DIB50-S50 and DIB10-S90 cathodes were discharged to various extents and NMR was performed upon the cathodes, which were not washed such that any soluble species would remain in the cathode and would be seen in the spectra. The identification of the different chain lengths of the lithium polysulfides from these spectra was not successful, but the differences between DIB50-S50 and DIB10-S90 were noted. In the case of DIB50-S50, a broad signal at about –0.4 ppm appears from the beginning of the discharge, and grows in intensity as the discharge process advances. This signal was assigned to a C-S-Li unit, which was postulated to be a major reduction product of DIB50-S50. For DIB10-S90, two distinct signals, the intensity of which varied with the degree of discharge, were observed at 1.0 ppm and 2.3 ppm.[1.46]

The 1.0 ppm signal appeared when the state of discharge was 25 % and grew in intensity as the discharge proceeded, though it was eventually swamped by the 2.3 ppm signal which first appeared at 30 % discharge and grew in intensity as discharge proceeded.[1.46] Using other literature sources, the peak at 1.0 ppm was assigned to longer C-S_x-Li units and the peak at 2.3 ppm was assigned to Li_2S, which argued against other literature sources that suggested by X-ray diffraction studies that Li_2S does not form.[1.47]

Hoefling *et al.* suggested that due to the constraining polymer structure, the Li_2S would be unable to crystallise and give long range order, thereby rendering it invisible to X-ray diffraction. Additional ^{7}Li NMR experiments were performed on the cathodes once they were washed. This resulted in a loss of the residual electrolyte peak, however the discharge products were largely unaffected by this washing, suggesting that they are either bound to or trapped within the polymeric structure, providing further evidence for this being the reasoning why inverse vulcanised cathodes outperform cathodes containing free sulfur.[1.46]

Finally [13]C{[1]H} cross polarisation magic angle spinning NMR was utilised to study exclusively those lithium polysulfides bound to organic units, at different degrees of discharge.[1.46] This was advantageous as it had already been seen to some degree that the chain length of the polysulfide affects the chemical shift of the carbons under study, so here it was expected that some information would be gained on the chain lengths of lithium polysulfides at different degrees of discharge. DIB50-S50 showed a gradual reduction in intensity of the peak assigned to medium linear lithium polysulfides, while the peak assigned to short linear lithium polysulfides gained intensity as the discharge proceeded, suggesting that medium linear lithium polysulfides are converted to shorter ones as discharge progresses. A similar conclusion was drawn for DIB10-S90 in that long was converted to medium and then to short linear lithium polysulfides as discharge progressed. The fact that short,

Liam James Dodd

medium and long linear lithium polysulfides were all detectable by $^{13}C\{^1H\}$ NMR suggests that the chains remain bound to the organic units while they shorten, which is a conclusion consistent with the lack of effect of washing in both the ^7Li and ^{13}C NMR experiments.

1.4. Alternative Routes of Synthesis and Modification

As Inverse vulcanisation has progressed, numerous off-shoots and variations of the synthetic route have emerged, that produce product polymers that appear to be inverse vulcanised polymers, but were not synthesized by means of thermally induced polymerisation, or do not use classic olefinic comonomers. Others have synthesized inverse vulcanised polymers by the traditional route, and then utilised other chemistries to modify the polymer structure. What follows is an account of some of the most prominent literature articles regarding such strategies.

1.4.1. Synthesis by Aqueous Polysulfide Anions

Polymer nanoparticles were synthesized in a route that avoided aggressive heating and the use of thiyl radicals, in a synthesis conducted entirely in water, which is impressive because in a standard inverse vulcanisation both the sulfur and the organic comonomer are hydrophobic.[1.48] Sodium sulfide was added to elemental sulfur in water, which caused the elemental sulfur to react with the sodium sulfide, forming anion capped sulfur chains: polysulfide anions. These anions could be of controlled length by simply controlling the ratio of elemental sulfur to sodium sulfide, though whether this control translated to a controlled sulfur rank (the number of sulfur atoms in a chain within the polymeric structure) in the product polymers that were obtained when a divinylic comonomer was added to the solution, is uncertain.[1.48]

Added to the polysulfide anion solution, was divinyl sulfone (Figure 1.10a), which has electron deficient alkene groups due to the electron withdrawing sulfone group, and though divinyl sulfone has not been tested in a classical inverse vulcanisation, it polymerised within minutes as the negatively charged polysulfide anions were able to easily react with the electron deficient alkenes.[1.48] With a steric stabiliser and appropriate surfactant, this synthesis yielded spherical polymer nanoparticles which would disperse in aqueous media.[1.48]

When tested for mercury uptake, the material showed good adherence to the Langmuir isotherm, with a maximum uptake of 1064 mg g^{-1} from aqueous HgCl$_2$.[1.48] To improve the mercury uptake further, the polymer nanoparticles were functionalised with thiols via reduction by tris(2-carboxyethyl) phosphine, resulting in a measured uptake of nearly 9200 mg g^{-1} even under acidic conditions which usually hinders binding. Using the thiol functionalised polymer material, an aqueous mercury ion concentration was reduced from 11.5 ppm to 0.005 ppm, well below the world health organisation guidelines for safe drinking water.[1.48] Many other detailed characterisations of the mercury uptake were carried out, but are not mentioned here, as the focus for this discussion was the fact that a polymer that bears a structure analogous to that of an inverse vulcanised polymer, was in fact made under conditions that would be considered alien to inverse vulcanisation: near room temperature synthesis; aqueous media; and anions over radicals.[1.48]

1.4.2. Synthesis from a Non-Olefinic Crosslinker

Another reaction that strongly resembled inverse vulcanisation in terms of the products, but started from unusual reagents, was the use of para-diidobenzene (Figure 1.10a), which does not contain any olefinic moieties, yet still reacted with elemental sulfur, and even more surprisingly, formed a crosslinked network, where only a linear polymer would be expected since para-diiodobenzene contains only two functional groups.[1.49] This crosslinking was attributed to the reaction of aromatic hydrogens at the high reaction temperature of 230 °C, with attack upon the hydrogen assisted by the

Liam James Dodd

electronic effects of the iodine atoms upon the benzene ring. Active vacuum was required in the synthesis to draw off the elemental iodine by-product, though sometimes this was not sufficient to satisfactorily purify the product polymers of iodine, and Soxhlet extraction was employed.[1.49]

The resultant materials ranged between 33 % and 76 % by mass sulfur, as determined by combustion microanalysis, which displayed decreasing T_g and decomposition temperature (T_d) with increasing sulfur content.[1.49] These materials could achieve a combination of high extensibility of 300 %, and complete strain performance recovery within 2 hours at room temperature. The materials were also scratch-healable under ultraviolet or thermal treatment, and had refractive indices higher than 1.8.[1.49]
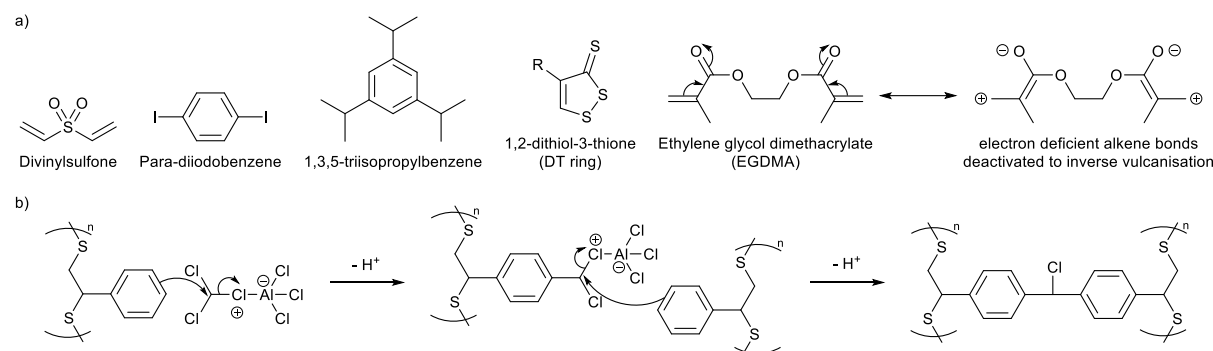
Figure 1.10: a) Names, abbreviations, and chemical structures of relevant molecules and fragments, as well as an illustration of how resonance decreases the electron density of ethylene glycol dimethacrylate's alkene bonds, and b) a mechanism for crosslinking a styrene inverse vulcanised linear polymer by Friedel Crafts alkylation using dichloromethane and aluminium trichloride.

Another example of where a non-olefinic monomer was applied, was the polymerisation of 1,3,5-triisopropylbenzene (Figure 1.10a).[1.50] That is, an organic comonomer with only alkyl groups as functionalities. Reactions were performed by normal bulk polymerisation inverse vulcanisation methods, with the rather forcing temperature of 180 °C, and required a full 24 hours to achieve a homogenous polymer, from sulfur percentages between 50 and 90 percent by mass. The polymers showed some solubility, suggesting highly branched rather than fully crosslinked polymers, but with the exception of the polymer made from 90 % by mass sulfur, all the polymers showed no elemental crystalline sulfur which is evidence towards consumption of sulfur in the reaction.[1.50]

The polymers showed increasing T_g with increasing sulfur content, which is explained by remembering that it is more difficult for the isopropyl groups to react and crosslink than a normal alkene bond in classical inverse, and thus, more sulfur leads to more crosslinking in these reactions, giving a more crosslinked structure that has a higher T_g.[1.50] In general this is true of inverse vulcanisation in that adding more sulfur leads to more crosslinks, giving a more crosslinked, higher T_g structure, until the structure is fully crosslinked at which point the sulfur crosslinks start to get longer, yielding weaker, more easily broken crosslinks that result in a decreasing T_g as more sulfur is added.[1.50]

What is not general about this reaction is the formation of hydrogen sulfide.[1.50] In classical inverse vulcanisation, hydrogen sulfide evolution occurs as a byproduct of a minor competing pathway, which is hydrogen abstraction by thiyl radicals to give thiols, which can go on to form hydrogen sulfide gas. In this work, hydrogen abstraction is the main pathway, where instead of attacking a double bond (because none are present) thiyl radicals abstract a hydrogen from 1,3,5-triisopropylbenzene's propyl groups, resulting in a carbon radical that can attack on sulfur chains to form an inverse vulcanised polymer network. The evidence of this hydrogen abstraction was obvious in the combustion

Liam James Dodd

microanalysis data as the sulfur to carbon and hydrogen to carbon ratios were lower than that of the combined input reagents, indicating that hydrogen sulfide had formed.[1.50]

NMR revealed that all hydrogens of the isopropyl groups could be abstracted: both the tertiary hydrogen which results in a resonance stabilised radical, and the six primary hydrogens which are more abundant so are kinetically easier to abstract but generate a less stable radical.[1.50] Further evidence of hydrogen abstraction came in the form of thiol signals in the NMR, suggesting polysulfide chains capped with thiols were present in the structure. What is even more interesting is that the NMR detected the presence of 1,2-dithiol-3-thione rings (DT rings) (Figure 1.10a), bound to the aryl group at the 4 position, an important reaction by-product that will be discussed in detail in a Section 1.5.4 as it was of great interest in this thesis work. As a closing remark, evidence of oxidation by means of S-O bond formation was found.[1.50]

1.4.3. Modification by Friedel-Crafts

Friedel Crafts chemistry was used to convert a normally unstable polymer, inverse vulcanised styrene, into a crosslinked network.[1.51] A linear polymer of inverse vulcanised styrene will dissolved in chloroform; said solubility owing to the linearity of the polymer. Under nitrogen, aluminium trichloride was added to the chloroform at room temperature, and after 2 hours a suspension had formed. The aluminium trichloride acted as a Lewis acid catalyst, and promoted reaction of the styrene units' benzene ring with chloroform, thereby alkylating the benzene ring. A further Friedel-Crafts reaction upon the alkylated unit with another styrene unit crosslinks two polymer chains together (Figure 1.10b). As this crosslinking process continued the polymer eventually became high enough in molecular weight and crosslink density that it was rendered insoluble, resulting in the observed suspension. This polymer was used for the application of water remediation, however this will not be discussed here, as the purpose of reviewing this publication was to point out how the choice of organic comonomer in inverse vulcanisation can open up opportunities to further the modify the product polymer, which in this case yielded a product of radically different properties.[1.51]

1.4.4. Mechanochemical Synthesis

A mechanochemical synthesis route was employed to generate inverse vulcanised polymers by means of ball milling the reagents for the relatively short time of 3 hours.[1.52] This provided several advantages, including: reactions at room temperature; reduced H_2S by-product production; avoiding the Trommsdorff-Norrish effect (TNE); and a broader monomer range that is not limited by their boiling point. Ten organic comonomers were studied, eight of which were previously reported in inverse vulcanisation, and two never before reported in inverse vulcanisation on account of their prohibitively low boiling points. All ten successfully formed polymers when reacted by mechanochemical synthesis in a ball mill, as indicated by the appearance of a T_g in their DSC thermograms. PXRD revealed that in some cases crystalline elemental sulfur was present in the product polymers, but when Soxhlet extraction was employed to remove the impurity, the exposure to heat caused changes to the polymers by means of thermally induced reaction; undesirable as a purely mechanochemically synthesized polymer was the target. Excitingly, it was demonstrated that these mechanochemically synthesized polymers were effective at removing aqueous mercury from solution, were healable by both application of heat or ultra-violet light, and had superior mechanical properties (Figure 1.11).[1.52]

Surprisingly, some of the polymers made by mechanochemical synthesis showed T_g's lower than their thermally synthesized counterparts, whilst showing lower solubility.[1.52] Typically, a lower T_g is indicative of lower crosslink density, which results in higher solubility, so these results indicate something unexpected is occurring with the mechanochemically synthesized polymers. Additionally, combustion microanalysis revealed decreases in the carbon to hydrogen ratios and the carbon to

Liam James Dodd

sulfur ratios. Normally an increase in these ratios is expected, as generation of hydrogen sulfide by-product (hypothesized to stem from hydrogen abstraction in the thermal synthesis route) removes hydrogen and sulfur atoms from the system. Energy dispersive spectroscopy detected an iron content in the polymers (up to 20 % by mass indicated by ICP-OES) with traces of chromium, both elements found in the stainless steel container and balls of the ball mill used in the synthesis, and it was hypothesized that chemical binding of the polymer to these elements was the explanation of the raised crosslink density that provided the insolubility, and the decreases in the aforementioned elemental ratios. Evidence of C-O, C=O, S-O, and S=O bonds was also found.[1.52]
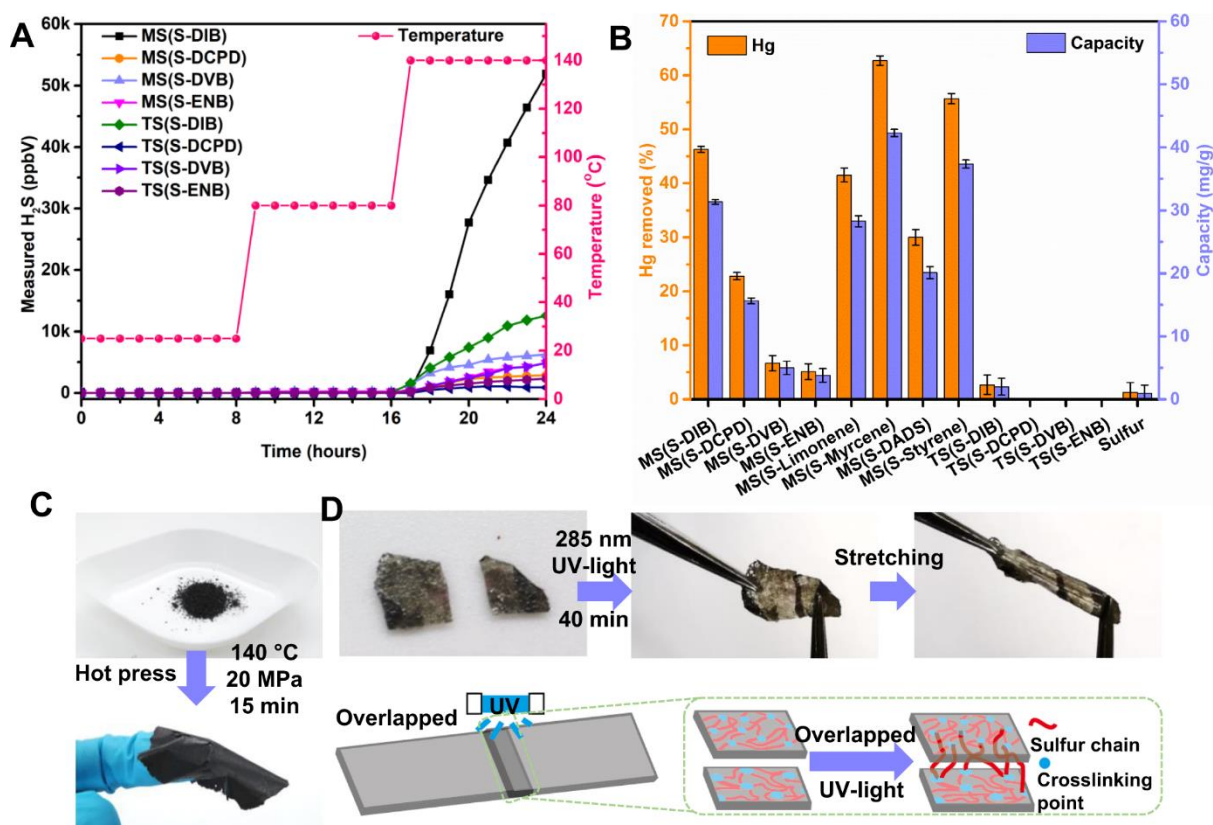
Figure 1.11: a) H_2S measurements on selected mechanochemically synthesized and thermally synthesized polymers with ramping temperature at room temperature, 80 °C and 140 °C, b) the percentage mercury removed from 138 ppm $HgCl_2$ solution after 24 h exposure to each of the materials listed, and the capacity of mercury removing of each of the materials listed, c) a mechanochemically synthesized polymer of sulfur and DIB as an example to show the polymer film is able to be made from polymer powder, and d) a film of mechanochemically synthesized polymer of sulfur and DIB as an example to show the UV-induced self-healing ability of the mechanochemically synthesized polymer. Reproduced from Nature Communications.[1.52]

1.4.5. Photochemical Synthesis

Jia *et al.* quoted many of the same limitations of thermally induced inverse vulcanisation as was mentioned in the mechanochemical synthesis publication, but provided a different remedy to these problems, by the discovery of a method for photoinduced inverse vulcanisation using light of either 380 nm or 435 nm (10 W power) at room temperature, which was used to polymerise a variety of previously established crosslinkers as well as new ones like examples of alkynes which have previously received little research attention.[1.52,1.53] Where photoinduced polymerisation was applied to a crosslinker that had been previously reported to polymerise by thermal means, the products of

Liam James Dodd

thermally induced and photochemically induced polymerisation had comparable characterisations by several methods, suggesting the products were of similar nature. PXRD indicated that there was no crystalline elemental sulfur in the product polymers of photoinduced polymerisation, and white lead (II) acetate did not turn into black lead (II) sulfide when left in the presence of an in-progress photoinduced polymerisation, indicating that no hydrogen sulfide gas evolved. Another advantage of the photoinduced reaction route is that thermal polymerisations usually require a curing period, where a polymer is left in a high temperature environment for an extended period of time in order to complete the reaction: this step is not necessary and provides no benefit for a photopolymerised product. The photoinduced reaction route was even capable of reacting gaseous crosslinkers with elemental sulfur, something not reported before in the literature.[1.53]

In attempting to learn about the mechanism of photoinduced inverse vulcanisation, several observations were made.[1.53] Firstly, because elemental sulfur absorbs up to 520 nm wavelength with the strongest absorption between 380 and 435 nm, and the crosslinker absorptions are mainly located below 320 nm, irradiation with 520 nm light provoked no reaction. Interestingly, it was found that reactions with higher energy 380 nm photons, proceeds more slowly than reactions using 435 nm photons, which was supposed to be because 380 nm light has sufficient energy to excite competing reversible reaction pathways, such as the formation and extension of radical capped polysulfide chains, a conclusion that was supported by the observation of sulfur homopolymerisation under 325 nm Raman spectroscopy.[1.53]

An alternative explanation is that 380 nm excitation was sufficiently energetic to excite the shorter-lived triplet state, which does not provide sufficient time for reaction.[1.53] From further investigations, the likely rate determining step was ring-opening of cyclo-octasulfur. It was noted that cyclo-octasulfur has two photo-electronic transitions resulting a narrow indirect bandgap (phonon dependent and requires sufficient temperature to permit generation of this phonon) and a wide direct band gap (a phonon independent process). In photoinduced inverse vulcanisation, efficient electronic transitions only occurred in the ultra-violet excited direct band gap, indicating that cleavage of S–S bonds requires activation by ultra-violet light.[1.53]

Ethylene glycol dimethylacrylate (EGDMA) does not react well in thermally induced inverse vulcanisation, requiring a catalyst to form a stable polymer, and this difficulty carried over to photoinduced inverse vulcanisation, where EGDMA required a photosensitizer or dye to achieve reaction.[1.53] The difficulty in reacting EGDMA will be discussed in a later chapter. Further evidence of a photoinduced radical mechanism was found by electron paramagnetic resonance, which detected radicals in ultra-violet irradiated elemental sulfur. Computational chemistry was employed to further investigate the mechanistic pathway. A plausible reaction pathway for the formation of a DIB inverse vulcanised polymer from cyclo-octasulfur with DIB under three different conditions was calculated. In the absence of a co-catalyst and light irradiation, it was found that the ring-opening of cyclo-octasulfur had an activation barrier of 0.55 eV to form the active sulfur species. This barrier was reduced to 0.22 eV in the presence of the co-catalyst. The calculations suggested that sulfur ring-opening occurs by light irradiation only under its excited state, which would result in excited sulfur radicals which can attack the photo-activated carbon atoms in the C=C bonds of DIB to generate the polymer, and this reaction is exothermic by about 4.90 eV.[1.53]

Another relevant publication to photoinduced inverse vulcanisation is a computational study of how elemental sulfur can be photoexcited, and what states it can relax to that result in ring opening.[1.54] Therein, a gap in the literature was identified in that previous studies of photoexcitation of elemental sulfur had only ever been done by a very simplistic method, that being to calculate the electronic energies of the ground state, then transfer an electron from the highest occupied molecular orbital

Liam James Dodd

(HOMO) to the lowest unoccupied molecular orbital (LUMO) without changing the spin angular momentum. This simplistic approach prohibits comprehensive exploration of the various electronic states that can exist, and ignores the potential for non-radiative decay transitions that could precede a de-excitation event.[1.54] To remedy this, time dependent density functional theory (DFT) was applied with the B3LYP functional and 6-31+G* basis set, which is a relatively weak level of theory, but was likely the best compromise for the highly computationally demanding timed dependent DFT technique, which carries a much higher computational cost than DFT.[1.54] This was used to find the excited states of the ground state, and similarity transformed equation of motion - coupled cluster singles doubles was employed to scan across the states that these excited states could be excited to (cc-pVDZ basis set was employed).[1.54]

Unsurprisingly, the results of the trivial ground state calculations mirrored the literature closely, however, the more advanced calculations of the excited states were able to provide Jablonski diagrams to map the available excited states (Figure 1.12a and Figure 1.12c).[1.54] Ground state sulfur is a singlet state, and so photoexcitation can only yield a singlet excited state, since the selection rule for electronic excitations prohibits changes in spin angular momentum from a photoexcitation. Intersystem crossing is a non-radiative process, and as such is not bound by this selection rule, and so can interconvert singlet and triplet states. It was found that the lowest energy, most easily accessible singlet state with a non-negligible oscillator strength (a higher oscillator strength results in greater photo-absorption: a more allowed transition) was termed the S6 state, which was not the lowest energy excited singlet state; this would be the S1 state, which is not easily reached by photo-excitation (poor absorption, poor oscillator strength). It was found that comparing the results to experimental absorption spectra gave good agreement.[1.54]

Further results from the computations suggested that the S6 state could rapidly relax by internal conversion to the S1 state, which has a poor oscillator strength, and so is a poor emitter, meaning non-radiative decay would be the preferred mode of de-excitation for the S1 state.[1.54] This S1 state can also undergo intersystem crossing to a triplet state. The spin orbit coupling values associated with this transition were calculated, and were found to be large, indicating that the routes by which spin angular momentum could be converted were easy, resulting in rapid intersystem crossing to triplet states that are quite optically active. Because this intersystem crossing was found to be so rapid, it appears it would be the kinetically dominant process. The pathway of this process was from a symmetrical S1 state in the classic puckered crown cyclo-octasulfur conformation, to a triplet state where the cyclo-octasulfur distorts into more of an oval shaped ring, before finally progressing to a triplet state where the ring breaks open a sulfur – sulfur bond to yield a chain capped with diradicals: such diradicals being the active species in photoinduced inverse vulcanisation (Figure 1.12b).[1.53,1.54]

To complete the study, a closer examination of this diradical was carried out. The diradical was allowed to relax to its lowest energy state, and then calculated its electronic energies and spin densities. They found the diradical adopted a helical structure with some variation of the bond lengths that were indicative of their strengths, however the most important finding of this study was that the spin densities on terminal atoms was high, but the penultimate atoms in the chain also had somewhat high spin density, indicating radical character on the terminal atoms and electronic interaction with the penultimate atoms' orbitals to delocalise and stabilise the radicals (Figure 1.12d and Figure 1.12e). The four mid chain sulfur atoms were found to have no significant spin density, indicating negligible radical character. Attempts to repeat this analysis after forcing the triplet diradical into a singlet state were attempted, but as soon as the constraints were removed, the singlet diradical underwent intersystem crossing to reach the triplet state.[1.54]

Liam James Dodd
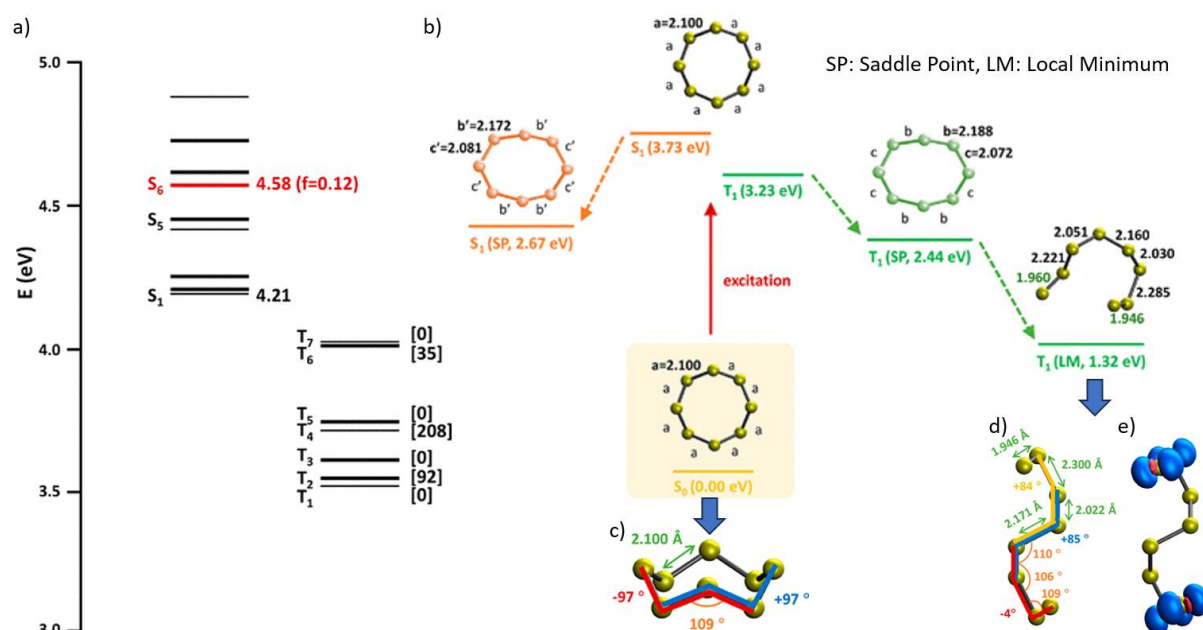
Figure 1.12: a) Jablonsky diagram of the excited states of the S_8 ring, obtained at the STEOM-CCSD/cc-pVDZ level of theory. Thicker lines represent doubly degenerate excited states while a red line indicates the singlet state with the largest oscillator strength (f). The values between square brackets represent the spin–orbit couplings between the S1 state and T_n states (in cm^{-1}). b) diagram of the S_8 ring relaxation pathways in the lowest singlet and triplet states obtained by means of excited-state geometry optimizations at the TDDFT/B3LYP/6-31+G* level of theory. The a, b, and c labels and the associated numbers indicate the S–S bond lengths (in Å). c) The geometric structure of the S_8 ring, as optimized at the B3LYP/6-31+G* level of theory. d) The geometric structure and e) spin density of the S_8 chain in its triplet configuration, as optimized at the B3LYP/6-31+G* level of theory. Reproduced from ACS Materials Letters.[1.54]

1.4.6. Electrochemical Synthesis

Another alternative synthetic route to inverse vulcanised polymers is an electrochemical synthesis, wherein reducing potentials induce ring opening polymerisation in specially synthesized cyclic trisulfides.[1.55] Inverse vulcanisation by thermal induction suffers problems such as: high temperatures increasing the cost of the reaction; immiscibility between the sulfur and organic reactant phases leading to inhomogeneous products; the serious scale-up hazard of the TNE; liberation of toxic H_2S gas as a by-product; limited control over sulfur rank; and hard to control C-S stereochemistry. The electrochemical synthesis route circumvents many of these issues.[1.55]

The first stage of the electrochemical synthesis was to synthesize specialised monomers by a literature method of reacting elemental sulfur with an alkene bond in DMF at 120 °C for 16 hours in the presence of a [Ni(NH$_3$)$_6$]Cl$_2$ catalyst, yielding the products seen in Figure 1.13.[1.55] R1 was chosen because of the symmetry and simplicity of the predicted product P1, though P2 was produced as a by-product and removed by vacuum distillation or column chromatography. It was found later that P2 underwent much more complex electrochemistry than the other products, and could even convert to P1 during polymer synthesis, and so P2 was not studied further. One disadvantage to the electrochemical synthesis is the fact that a synthetic step is required prior to the polymerisation reaction, which requires prolonged heating at temperatures somewhat lower than inverse vulcanisation, but for a similar timescale, which lessens the advantage of the polymerisation itself requiring no heating. This

Liam James Dodd

also complicates the synthetic procedure, which is one major advantage of thermal inverse vulcanisation: it merely requires mixing and heating of reagents.[1.55]

Cyclic voltammetry of the products shown in Figure 1.13 was performed in the potential window of -3.0 V to +1.5 V versus the ferrocene/ferrocenium couple.[1.55] P1, P3, and P4 exhibited two irreversible redox peaks, one at reducing potential between −2.5 and −2.2 V and one at oxidising potential between 1.0 and 1.4 V. As an aside DFT was used to predict the reduction potential of P1, P3, and P4, and a method was found that gave good agreement between the experimental and simulated values, as well as suggesting structures for the reduced species. It was suggested that the irreversibility of these redox peaks might be due to a rapid chemical conversion immediately after oxidation or reduction of P1, P3, or P4 into a new species with entirely different electrochemistry. Chronoamperometry was performed on P1, P3, and P4, at oxidising and reducing potentials, and it was found that a new product precipitated at reducing potential, but not oxidising potential.[1.55]
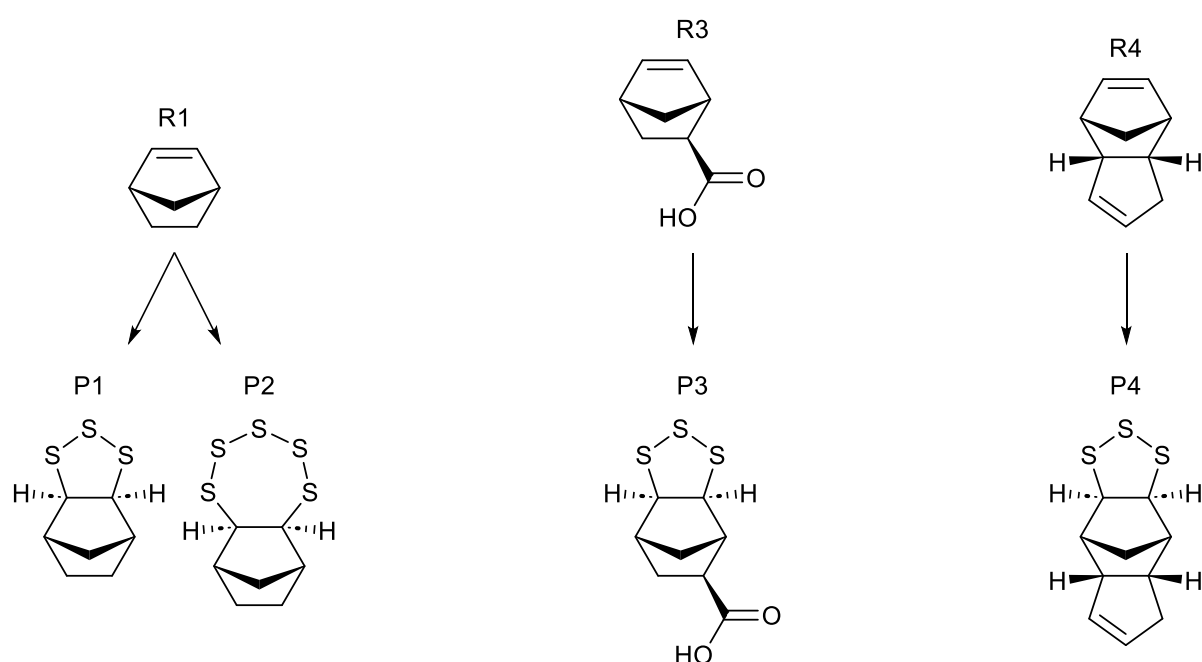
Reaction conditions: elemental sulfur reagent; [Ni(NH$_3$)$_6$]Cl$_2$ catalyst; DMF solvent; 120 °C for 16 hours

Figure 1.13: Reaction schemes for the electrochemical synthesis of inverse vulcanised polymers.[1.55]

It was hypothesized that under reducing conditions, P1, P3, and P4 can form polymers by means of electrochemically induced ring opening polymerisation.[1.55] P4 was focused upon to prove polymerisation by means of characterisation of the polymerisation products of P4, which was convenient because P4's ^{1}H NMR signals did not overlap with those of the electrolytes used in the electrochemical experiments. Characterisation of the precipitate after purification by recrystallisation from chloroform with an acetonitrile antisolvent, indicated the formation of a ring-opened linear polymer product of P4, which was soluble in THF and chloroform, and had a molecular weight of 3900 g mol^{-1} with 1.91 polydispersity from GPC. It was found that the alkene bonds shown in P4 were maintained and unaffected by the electrochemical polymerisation. When the polymer product of P4 was reduced by LiAlH$_4$ to destroy the polymer structure, the obtained product was characterised and found to be P4 but instead of a cyclic trisulfide, there were only two sulfur atoms, each as a thiol, with

Liam James Dodd

the C-S bonds maintained. This was used as evidence to suggest that a polymer structure was the precursor to the LiAlH₄ reduced product.[1.55]

Method optimisation was carried out, monitoring the effects of the method changes upon the polydispersity and molecular weight.[1.55] The results of this method optimisation are too broad to discuss in depth here, but some key conclusions included that the polymerisation does not need an inert atmosphere, and that the polymer product becomes increasingly insoluble as the chain grows and the molecular weight increases until it reaches a critical value where the product precipitates, and this limits the molecular weight but also keeps it consistent and protects the polymer product itself from a destructive reduction at the electrode from which it moves away from upon precipitation.[1.55]

The polymerisation kinetics were studied by taking aliquots of the reaction solution and analysing them by GPC and ^{1}H NMR.[1.55] From this study it was found that: the reaction proceeds by pseudo first order kinetics; the polymerisation was accepting of the presence of the carboxylic acid functional group of P3; and the molecular weight barely changed over the course of two hours, which was explained by the polymerisation itself being too rapid to see on the minutes timescale, rapidly resulting in fully polymerised products, and that the kinetics instead was probing the rate of formation of polymer chains rather than the rate of growth of the chains.[1.55]

The mechanism of the polymerisation was studied by DFT.[1.55] It was found that initiation of the electrochemical polymerisation occurred at -2.29 V. After the reduction, it was found that there was a very small energy barrier to a slightly thermodynamically favourable reversible cleavage of an S-S bond. The calculations showed that the radical anion had its negative charge and spin spread across the three sulfur atoms. The lone sulfur atom carried the greatest negative charge and barely any spin, so it was primarily anionic with little radical character. The terminal sulfur atom of the di-sulfur side showed half as much negative charge as the lone sulfur atom. This sulfur atom showed much more spin, but this spin was also shared with the neighbouring sulfur atom, much in concurrence with the findings of Cho et al..[1.54,1.55] The DFT study then revealed how the radical anion propagates by attacking another monomer that is not reduced, which was found to give a "self-correcting" mechanism; that is, the mechanism exclusively yielded sulfur rank 3, and when rank 2 and rank 4 form, they cannot propagate and revert back to a previous intermediate that goes on to form rank 3 chains. In other words, it was found that attack of the anionic lone sulfur upon the central sulfur of another monomer was the only attack that was thermodynamically feasible, kinetically viable, and yielded a product capable of a thermodynamically feasible and kinetically viable propagation. All other forms of attack were either kinetically unviable or thermodynamically unfeasible, or yielded a product that could not propagate in a thermodynamically feasible or kinetically viable manner, leaving the only statistically possible pathway to be undergoing the reverse of the reaction back to a species that would be capable of lone sulfur anionic attack upon the central sulfur of another monomer.[1.55]

After the mechanistic study, it was considered that because the formation of S-S bonds should be reversible regardless of whether they are formed via electrochemical polymerisation or thermal polymerisation, if the electrochemically synthesized polymers were heated, then the S-S bonds should reverse in their formation and backbite to yield P1, P3, and P4 from their respective polymer products. This was attempted, and to shift the equilibrium towards the monomers, a vacuum distillation was applied to the heated polymers in order to vaporise the monomer and remove it from the polymer mixture. This process was followed by TGA-GC-MS, and found: from the TGA, the mass of polymer decreases at higher temperature; from the GC, that the monomer signal evolves at higher temperatures and longer times; and from the MS, that the distilled product had the correct molecular weight to be the appropriate monomer. The ^{1}H NMR analysis agreed with the conclusions, and

Liam James Dodd

ultimately a yield of 72 % of the monomer was obtained, which could then be recycled into another electrochemical synthesis to form the polymer again.[1.55]

A study on the metal capture capability of the electrochemically synthesized polymers was conducted, which will not be discussed here as it is not so relevant to the work detailed later in this thesis.[1.55] Another aspect which is interesting is the fact that P4 is formed from DCPD, a commonly thermally polymerised crosslinker, but in the electrochemical synthesis, the cyclopentene alkene was preserved and remained P4's polymer product. Through this remaining alkene, it was rationalised that the polymer product of P4 could be crosslinked by curing. This was found to be successful in forming a crosslinked polymer from P4's polymer product, which was of comparable properties to thermally inverse vulcanised DCPD polymers, though the electrochemical route has the advantage that the TNE is significantly less likely, making the reaction much safer.[1.55] The publication was concluded by comparing the electrochemical route to the thermal route of synthesis, pointing out that it is a good complementary technique to work alongside thermally induced inverse vulcanisation, but one that will not necessarily replace it.[1.55] While the electrochemical synthesis remedies many issues with the thermal synthesis, it has some drawbacks and caveats in that: it produces only low molecular weight linear polymers, though these can be crosslinked by other means; it requires an initial chemical synthesis to acquire a monomer capable of undergoing the electrochemical synthesis; and that electrochemical polymerisations can sometimes have practical issues with scale up.[1.55]

1.5. Controlling and Understanding Inverse Vulcanisation

One theme that pervades the work carried out in this thesis is an effort to characterise the fundamental chemistry of inverse vulcanisation; to control and understand the reaction in order to open up avenues for further research to exploit. In that regard, the work of this thesis is somewhat distanced from the applications of inverse vulcanisation, but instead tries to set the scene for those applications by providing a better foundation of knowledge for those applications to be built upon. Because of this, it is valuable to observe other aspects of the literature that have similar goals.

1.5.1. Divinylbenzene and Method Control

DVB will be near ubiquitous in the project work of this thesis, so a review of DVB itself is prudent. Conveniently, DVB has been the subject of method studies in some previous publication, so it is possible to simultaneously review both DVB and the methods of inverse vulcanisation. DVB was selected as a model crosslinker many times in the work of thesis because of its high boiling point (195 °C), capacity to react easily and cleanly, and the fact that it forms convenient, easy to handle products, which are likely reasons that DVB was chosen for method studies in the past.[1.20,1.29,1.56-1.60] The common practice for forming DVB inverse vulcanised polymers is to heat an amount of sulfur until it is molten and then add the DVB with stirring.[1.20,1.29,1.56-1.60] The amount of DVB in the reaction mixture is typically between 30 % and 70 % by mass, as loadings outside this range either do not react well or provide polymers that are unstable to depolymerisation. There are many variations to the method, each adapting to the circumstances of the research. The reaction temperature can be as low as 135 °C or as high as 185 °C in the case of Gomez *et al.* who wished to drive the reaction as quickly as possible. For particularly high temperature reactions, the reaction may be carried out in a pressurised container and under inert atmosphere, to prevent the loss of crosslinker by vaporisation. The methodology employed here used lower reaction temperatures to avoid these methodological complications and the unexplored effects of increased pressure upon the reaction and its products.[1.20,1.29,1.56-1.60]

Once the reaction mixture vitrifies (the solution becomes so viscous the stirrer bar can no longer rotate), it is common practice to leave the reaction mixture in a high temperature environment for an extended period of time.[1.20,1.29,1.56-1.60] This is known as curing and promotes the reaction of any

Liam James Dodd

remaining carbon-carbon double bonds. Curing also allows the reversible formation of sulfur – sulfur bonds to generate an equilibrium structure. Typical curing times range between 1 hour and 1 day, but do not typically involve temperature higher than 140 °C, especially if the reaction was performed at higher temperatures than this, because this runs the risk of the TNE, to which DVB will become prone to at high temperatures especially without stirring.[1.20,1.29,1.56-1.60] DVB reacts particularly quickly in comparison to many other crosslinkers, though reaction times vary heavily depending on the temperature of the reaction and the amount of DVB present. Reaction times as short as 5 minutes with low DVB content, and up to 15 minutes with higher DVB loadings have been reported, though it is worth remembering that the conditions involved in such experiments were quite forcing. Comparatively, reaction times as long as 3 hours at a reaction temperature of 135 °C and an equal mass of elemental sulfur and DVB have been reported. The products of these reactions vary in their physical properties, based on a great many factors including reaction temperature and DVB loading. Generally, red-brown plastics with T_g's below 0 °C are obtained with low DVB loading (30 % by mass), and hard, brittle, dark brown glasses are obtained with high DVB loading (70 % by mass), with T_g's of around 80 °C. It is worth noting that the vast majority of commercial sources sell DVB in 80 % purity, with the majority of the impurity being ethylstyrene with the alkyl group situated on the benzene ring. Furthermore, DVB is usually sold as a mixture of its meta and para isomers, though the ortho isomer does not occur, because it intramolecularly reacts to form a bicyclic structure that easily oxidises to naphthalene, and this is purified out of commercial sources before retail.[1.20,1.29,1.57-1.60]

DVB was used as the model crosslinker in a publication focused on defining the effects of modifying the inverse vulcanisation method to achieve different results.[1.60] Four different methods were used in the synthesis of DVB polymers at 185 °C, which are defined as follows. One step was where DVB and sulfur were mixed together and then heated to the reaction temperature where they remained with stirring for 30 min to 6 hours; two step was where sulfur was heated to the reaction temperature and then DVB was added and left with stirring for 30 min to 6 hours; ramp was where sulfur was heated at 160 °C until red in colour before DVB was added, which was then left to stir for 30 min, after which time the temperature was raised to 200 °C and held there for 30 min to 2 hours; cure was where sulfur was heated at 185 °C until red in colour, at which point DVB was added, and the contents were stirred at 185 °C for 5 to 30 min before being plunged into liquid nitrogen, after which the resulting mixture was cured in an oven at 120 °C for 3 hours. For one step, two step, and ramp, the reactions were quenched by either plunging into liquid nitrogen or by allowing to cool to room temperature. Reactions were tested on scales between 1 g and 10 g, as well as by varying the sulfur content from between 10 % and 90 % by mass. The one step procedure was conducted under inert atmosphere (nitrogen) as well as in air, and low temperature experiments were conducted using the one step procedure, with sulfur and DVB stirred at 135 °C for 24 hours. Some of these reactions were also performed with DIB for comparison.[1.60] It was found that the one step procedure provided the highest solubility of the products in dichloromethane (DCM), followed by ramp, followed two step, followed by cure which had the lowest solubility, though they were all below 30 %.[1.60] Using the one step method, as the scale of the reaction was increased, the solubility increased dramatically from roughly 25 % at 0.5 g to nearly 90 % at 2 g, but then back down to 55 % at a 10 g scale. It was also found that the reaction time had an enormous effect on the solubility, from 25 % at 30 min to essentially 100 % at 6 hours. Polymers made by the ramp method showed similar trends in solubility, however polymers made by the cure method had little solubility (less than 10 %) indicating a well crosslinked structure. When subjected to the low-temperature synthesis, the DVB polymer was completely insoluble and had the highest T_g of any polymer made in this paper, and the DIB polymer displayed limited solubility indicating that, regardless of monomer, this method likely produces a more cross-linked structure.[1.60]

Liam James Dodd

It was also found that the higher the sulfur content, the less of an impact the reaction time and scale made, and that quenching the polymers in liquid nitrogen reduced the solubility across all reaction methods.[1.60] Generally, gel permeation chromatography (GPC) mirrored the results of the solubility studies, showing that less soluble samples had higher molecular weight. Inert gas atmospheres upon the reactions had no notable effect on solubility or molecular weight. The T_g can also be indicative of molecular weight and crosslinking, and it was found that generally the T_g results mirrored the GPC and solubility with the exception of the cure method provided lower molecular weights but comparable T_g's to the one step and two step methods, suggesting that cure method gives higher degrees of crosslinking which renders the polymer of low molecular weight and low solubility while one step and two step give more linear polymers, which can be of higher molecular weight but still have higher solubility. Many more useful deductions were made from this in-depth study, but they are too numerous to mention here without reproducing the entire publication within the flow of this text.[1.60]

1.5.2. Crosslinker Control

One particularly valuable publication demonstrates that blends of two crosslinkers can be used to reliably tune properties of the product polymer, such as T_g, molecular weight, solubility, mechanical properties, and colour, all by controlling the ratio of the polymers to one another (Figure 1.14).[1.44] In this publication, an inverse vulcanised polymer of limonene, which is normally not shape persistent and is of low molecular weight, was shown to have its properties enhanced: raising the molecular weight, T_g, and shape persistency with all a small amount of DCPD in the reaction feed. The T_g increased linearly with increasing DCPD content in the blend. This relationship was found to extend to blends of DCPD with other crosslinkers and multiple weight percentages of sulfur. When DCPD was blended with canola oil to form an inverse vulcanised terpolymer, there was a decrease in compression modulus following a logarithmic trend. Data on the flexural moduli of various polymers were also obtained, but because the mechanical properties of inverse vulcanised polymers were not called into scrutiny by the work in this thesis, an account of these findings will not be given here.
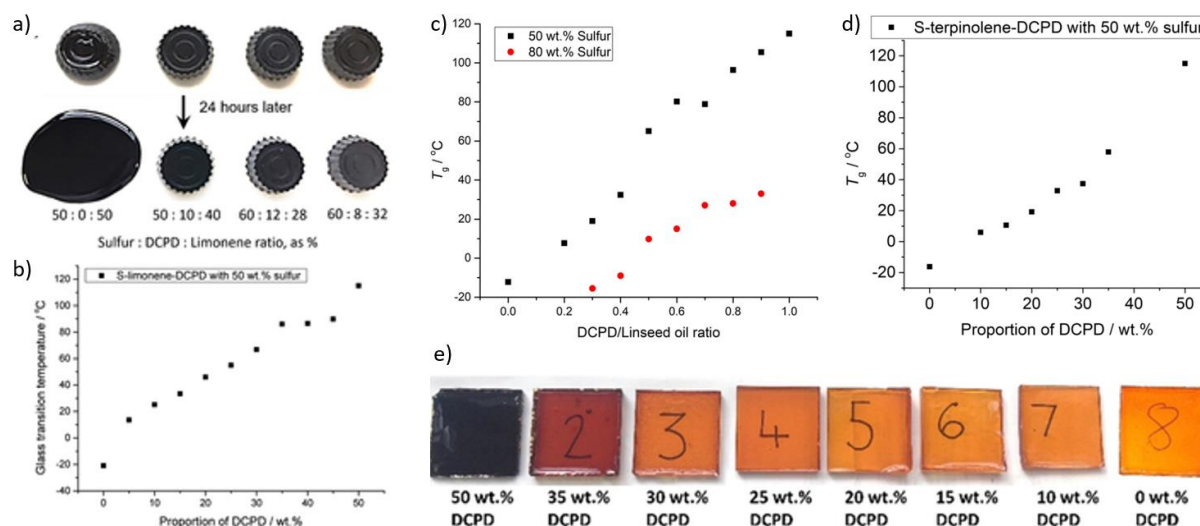
Figure 1.14: a) Photographs of moulded objects produced from sulfur, DCPD, and terpinolene. The top row shows the objects as made, and below after 24 hours. The T_g's of inverse vulcanised polymers with varying proportions of DCPD and either b) limonene, c) linseed oil, or d) terpinolene. e) Photographs of 5 mm thick blocks of polymers made from 50 % by mass sulfur with the remaining 50 % being a blend of DCPD and terpinolene. Reproduced from Chemistry A European Journal.[1.44]

Liam James Dodd

Incredibly, a polymerisation of ethylene glycol dimethacrylate (EGDMA), a crosslinker that is normally unreactive to inverse vulcanisation, was induced by blending it with DCPD. In general, it is observed that electron rich alkenes react readily in inverse vulcanisation, whereas electron deficient ones, particularly by resonance like EGDMA, are unreactive (Figure 1.10b). This is not well understood, since methacrylates are normally reactive in classic chain growth polymerisations. It could be speculated that the thiyl radical of inverse vulcanisation is not reactive enough to attack upon a low electron density alkenes like those of α,β-unsaturated ketones, but this seems contradictory to the fact the sulfur based radicals are common chain transfer agents for such monomers. Finally, terpinolene alone forms a transparent but non-shape persistent polymer when inverse vulcanised alone, rendering it inconvenient for applications, but when DCPD was blended in alongside it, the resultant polymer was shape persistent, but became increasingly opaque with higher proportions of DCPD in the blend.[1.44]

1.5.3. Ageing and Dark Sulfur

A crucial study that examined the effects of aging upon inverse vulcanised polymers was performed, discovering what became termed as "dark sulfur", that being elemental sulfur trapped within an inverse vulcanised polymer, that is not part of the polymer structure by chemical bonds, and is not detectable by PXRD or DSC because it is not crystalline, but amorphous.[1.24] It was observed that when an inverse vulcanised polymer was left undisturbed for a period of time, the T_g of the polymer increased. Since it can sometimes be observed that polymers depolymerise and exhibit "sulfur bloom" (where obvious elemental sulfur crystals form in and on the polymer), it was concluded that this increase in T_g was due to the shortening of the sulfur rank. Closer investigation revealed no loss of mass, nor an increase in the crystalline elemental sulfur that could be observed by DSC. Nor did the solubility or Fourier transform infra-red (FTIR) spectra, which suggested that the organic units were not changing and no thiols were forming.[1.24] Thin layer chromatography (TLC) revealed that elemental sulfur was indeed present in these polymers even though it was not observable by DSC and PXRD.[1.24] No organic species were detected by TLC nor high performance liquid chromatography (HPLC) which was used to quantify the content of dark sulfur. It was shown that dark sulfur, forming from the age induced depolymerisation of the inverse vulcanised polymers, could be re-uptaken into the polymeric chemical structure by heating the polymers up, re-polymerising the dark sulfur which thereby restored the T_g to its value before ageing occurred. It was also found that disulfide linkages are far less likely to depolymerise, or do not do so at all. Also observed was that a water signal accrued intensity in the polymer DSC thermograms as ageing proceeded, and that T_g's below room temperature were more conducive to uptake of water, as it is at these temperatures where the polymer chains are more mobile, and therefore better able to allow atmospheric water into the polymer structure.[1.24]

1.5.4. Colour From Side Reactions

One aspect of inverse vulcanised polymers that was mentioned by the seminal publication as "under investigation", but has evaded explanation in the ten years since, is their colour. A publication was produced with the intention of assisting practitioners of inverse vulcanisation in selecting monomers, also shed light on one potential source of colour from within the polymers.[1.61] It was rationalised that if the mechanism of inverse vulcanisation propagates by radical attack only, then the only products that can form are thioethers and polysulfides, and these are known not to be chromophores in the visible light spectrum.[1.61] Thus, there had to be some by-product forming that gave rise to this colouration that is ubiquitously observed in inverse vulcanised polymers, and Onose *et al.* set out to discover what the identity of this by-product was and determine what aspects of the monomer structure influence its formation.[1.61] It was noted that inverse vulcanisation studies generally focus around crosslinked polymer products, but these are difficult to characterise due to their insolubility,

Liam James Dodd

and because of this, only mono-olefinic monomers were used in the study, thereby generating linear polymers that were soluble, and thus subject to intensive NMR analysis.[1.61]

Monomers were carefully selected for use in this study: two terminal olefins; one cis and one trans olefin, collectively termed inner olefins; and two exo-olefins.[1.61] Of the two members of each of these classes, one was conjugated to a benzene ring, and the other sported only aliphatic chains. Trivially, it was found that terminal olefins provided the highest yields, particularly styrene, and this likely due to the fact that terminal olefins are kinetically easy to attack, and styrene has the additional advantage of resonance stabilisation. The other groups of olefin provided lower yields and multiple different products that had to be separated by column chromatography before analysis.[1.61]

It was found that β-methyl styrene mirrored the chemistry of β-alkyl styrenes in typical chain growth polymerisations, in that it was less reactive.[1.61] There is a steric effect from the alkyl group that slows the reaction, but more important is a resonance effect. Radical attack upon the alpha carbon generates a beta carbon radical. Rather than propagate, this radical ends the growth of its polymer chain by abstracting a gamma hydrogen from the alkyl group. The resultant gamma radical then resonates into the benzene ring and is deactivated by the particularly stable resonance form of a radical at the para position. This explained the exceptionally poor results of polymerisation of β-methyl styrene and is a cautionary note to inverse vulcanisation chemists, to be aware of this deactivating chemistry where an alpha unsaturated carbon is bonded to an aromatic group while the beta unsaturated carbon is neighboured by a saturated gamma carbon.[1.61]

The study then went on to explain their most interesting results, those of the exo-olefins which reacted poorly and provided multiple products, with a particular by-product of interest being DT rings. Though no precise mechanism of how DT rings would form was provided, they were detected by NMR exclusively in the spectra of exo-olefins.[1.61] Additional evidence that DT rings can form came from hydrogen sulfide sensing by silver nitrate upon the reaction outgas. Silver sulfide forms, and by weighing it, it was found that exo-olefins produced substantially more hydrogen sulfide than the other olefins, which is consistent with the fact that DT rings require four instances of hydrogen abstraction, thereby yielding two molecules of hydrogen sulfide. Literature sources demonstrated that DT rings are chromophores which could result in the observed colour in inverse vulcanised polymers, as well as the gradual darkening of inverse vulcanised polymers that are cured, as it was shown that curing results in an increase of DT ring formation.[1.61]

1.6. Mechanistic Studies of Polymerisations with Sulfur

Because much of the work in this thesis occurred at a more fundamental level than the applications, and often related to how the inverse vulcanisation reaction occurs, it is prudent to have an understanding of the current literature precedent for its mechanism. Despite great research effort, the mechanisms of both conventional vulcanisation and inverse vulcanisation have remained elusive. Conventional vulcanisation has been known for over a century and yet it is only recently that research efforts have begun to prove aspects of its mechanism in any confidence. Inverse vulcanisation has only been known since 2013, and so has not seen such extensive mechanistic studies.[1.17]

It is however predicted that progress in uncovering the mechanism of inverse vulcanisation will be challenging, due to the difficulty in characterisation of the product polymers and the complicating facet that any sulfur – sulfur bond can undergo scission at any time during the reaction, to break a growing polymer chain in two and generate two new thiyl radicals that are capable of propagation.[1.5,1.17] Indeed, at the current time there is no mathematical polymerisation model, like the Carother's equation, that has been developed to take into account growing polymer chains that can

Liam James Dodd

spontaneously divide and generate new initiator radicals at the same time.[1.62] Nevertheless, what follows is a brief discussion of some of the investigations carried out upon both kinds of vulcanisation.

1.6.1. Mechanism of Conventional Vulcanisation

One proposed mechanism for conventional vulcanisation detailed a complex radical mechanism, beginning with homolytic fission of cyclo-sulfur to give a linear diradical, though this mechanism was debated with alternatives proposing ionic mechanisms based on heterolytic cleavage of S_8 rings.[1.63] These ionic mechanism theories were substantiated by the fact that vulcanisation reactions were unhindered by the presence of radical acceptors in the reaction, though this could be explained by the fact that any sulfur – sulfur bond is capable of undergoing scission, thus two radical traps would be required for every sulfur – sulfur bond present in order to cause a complete quench of the reaction.[1.64] Attempts to disprove the presence of radicals via a different method: electron paramagnetic resonance, lead to conflicting conclusions, as G. Blokh was not able to detect radicals, but Dondi *et al.* were, though it may be worth noting that the publication by Dondi *et al.* is 56 years more modern than Blokh's and was likely performed with technology half a century more advanced.[1.65,1.66] A more recent study proposes a mechanism that involves both radicals and ions, which may explain the controversy in previous arguments.[1.13] In model reactions, it was found that the lowest temperature that could be used to achieve reaction was 160 °C. This onset temperature was consistent with the temperature found in DSC for homolytic cleavage of cyclo-sulfur. Using FTIR spectroscopy, it was confirmed that the thermal event in the DSC thermogram of sulfur at 159 °C corresponds to homolytic cleavage of cyclo-sulfur, and with a similar method it was possible to identify that the thermal event in the DSC thermogram of sulfur at 230 °C corresponded to heterolytic cleavage of cyclo-sulfur, though this onset temperature shifts to 200 °C in the presence of an activator.[1.13]

Both temperatures for heterolytic fission of cyclo-sulfur, 230 °C and 200 °C far exceed those of the industrial conditions that are routinely used for the vulcanisation of rubber, so a purely ionic mechanism was therefore ruled out.[1.13] Having confirmed that radicals are involved in the reaction mechanism, it was proposed that vulcanisation proceeds via α-allyl-hydrogen abstraction from a polymer chain by a thiyl radical, as it has been proven that thiyl radicals are capable of this abstraction.[1.66,1.67] The radicalised polymer can then proceed to attack upon cyclo-sulfur and polymerise. In addition to this, the thiyl radical involved in the initial hydrogen abstraction forms a thiol, which at elevated temperatures (above 160 °C without an activator and above 80 °C with an activator) can cleave to form a thiolate anion. This thiolate anion can also take part in vulcanising the polymer chains and its presence is a possible explanation as to why previous research came to conflicting conclusions in regards to whether the reaction was based on radical or ionic intermediates.[1.13] A possible mechanism, consistent with Lian *et al.*'s finding is shown in Figure 1.15a.

1.6.2. Mechanism of Inverse Vulcanisation

With regards to inverse vulcanisation, many theorise that the reaction proceeds via a similar mechanism to conventional vulcanisation. That being said, α-allyl-hydrogen abstraction cannot be the dominant mechanism, because such a hydrogen abstraction leads to hydrogen sulfide as a by-product, and given that because these reactions contain so much sulfur, large amounts of H_2S gas would be given off, which is not the case.[1.17] Even further evidence that α-allyl-hydrogen abstraction cannot be the primary mechanism comes in the form of DVB, which is one of the most rapidly polymerising inverse vulcanisation crosslinkers documented, yet it entirely lacks α-allyl-hydrogens.[1.20,1.29,1.56-1.60] Many current postulates involve the generation of thiyl radicals via homolytic fission of cyclo-sulfur in a manner similar to conventional vulcanisation.[1.68,1.69] The thiyl radicals then add across the carbon – carbon double bonds of the crosslinker, placing a radical upon the carbon skeleton, which can then continue propagation by attacking on other sulfur rings and polymers.[1.17,1.68] An alternative to this

theory is that the thiyl radicals abstract an α-allyl-proton, thus radicalising the crosslinker molecule.[1.70,1.71] The latter theory provides an explanation as to why some inverse vulcanisation reactions produce hydrogen sulfide gas, which could form from the thiols formed from hydrogen abstraction. However, not all inverse vulcanisations produce hydrogen sulfide gas, and the production of hydrogen sulfide has been found to vary with temperature, sulfur concentration and crosslinker structure, which points to the conclusion that both radical addition and proton abstraction occur to different extents in different reactions.[1.72] It is also worth noting that if thiols are formed by proton abstraction, then there is the possibility of an anionic mechanism of polymerisation, which utilises thiolates in a similar manner to the mechanism put forward by Lian *et al.*[1.13] A possible mechanism for inverse vulcanisation is shown in Figure 1.15b.
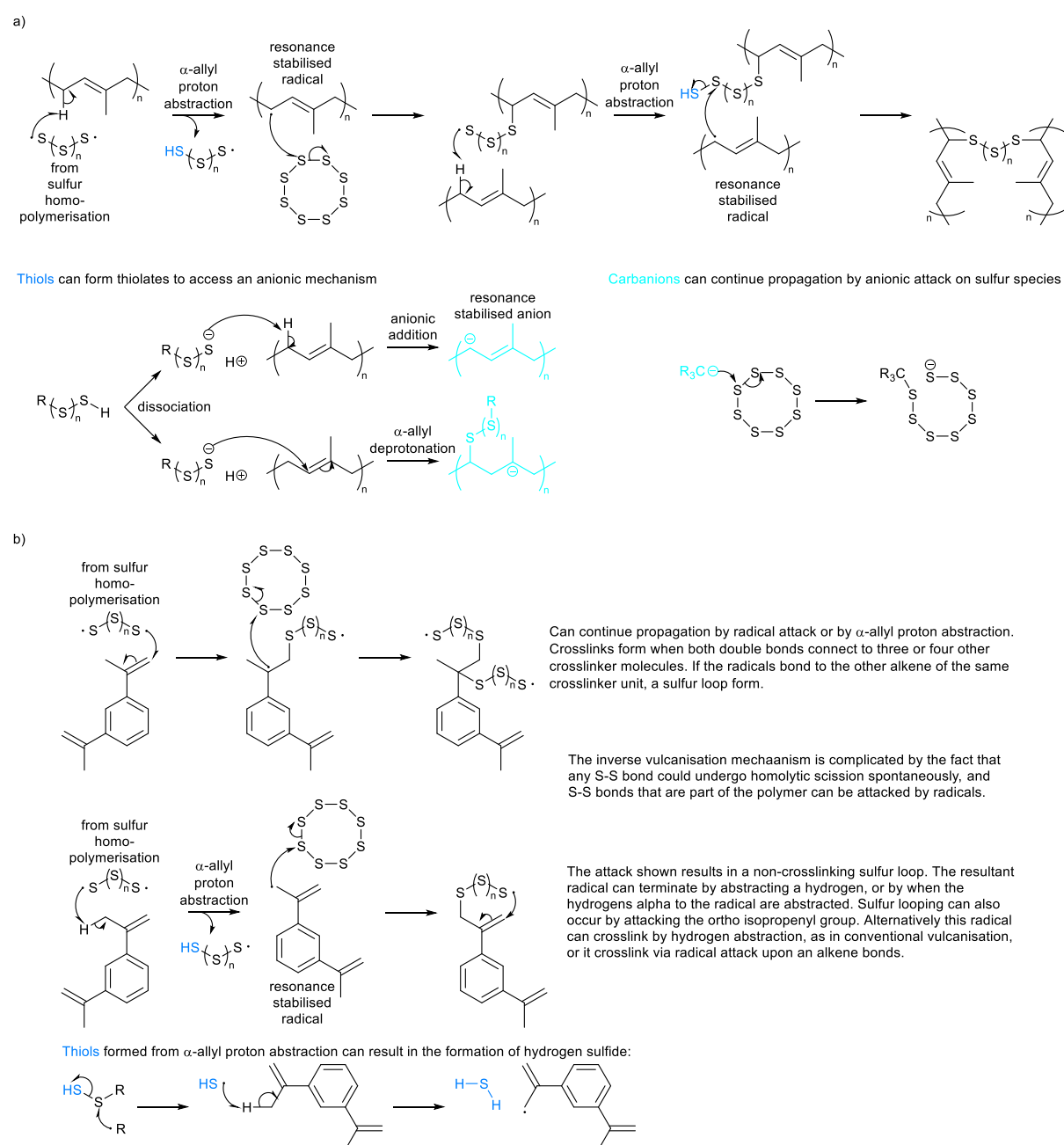

Figure 1.15: a) A possible mechanism for the vulcanisation of polyisoprene, and b) key points of a possible mechanism for the inverse vulcanisation of DIB.

Liam James Dodd

Inverse vulcanisation has received no dedicated mechanistic studies, or at least none that have been satisfactorily conclusive to result in publication to this date. Great difficulty lies in the analysis of these polymers, which shall be discussed in detail in a later chapter. It seems however that comparing inverse vulcanisation and conventional vulcanisation mechanistically may not be appropriate, as the two share marked differences. One such difference is that conventional vulcanisation appears not to consume the double bonds involved whereas inverse vulcanisation has been proven beyond reasonable to consume the double bonds of the crosslinker molecules (Figure 1.15).[1.17] This points to some measure of fundamental difference between the two reactions that may preclude the idea that the two are mechanistically similar, but unfortunately the majority of the research community have avoided any focused effort to discern inverse vulcanisation's mechanism on the grounds that the polymers can be functional in their application without precise knowledge of how they form, and that conventional vulcanisation is still debated after one hundred years, so research projects dedicated to inverse vulcanisation's mechanism may carry the risk of being time consuming and ultimately fruitless.

It is worth considering that in the seminal publication, a speculative mechanism was put forward, however, newer articles began to overstate the certainty of this initially proposed mechanism, leading to a number of following publications stating that radical attack is certain to be the mechanism, when this has not been proven beyond doubt.[1.17] Regarding this, a recently released publication addresses some of the previous assumptions and sheds new light on aspects of the mechanism.[1.73] The analysis of the inverse vulcanised polymer of DIB was revisited; produced by the original method, from which the previously suggested the structure would be crosslinked as shown in Figure 1.3b, though this has been disputed because if the original DIB inverse vulcanised polymers were indeed crosslinked, they should not have shown the solubility that they did.[1.17]

Cross polarised magic angle spinning ^{13}C NMR was used to investigate inverse vulcanised polymers of DIB, supported by computationally predicted NMR chemical shifts.[1.73] It was found that the experimental spectra did not completely agree with the predicted chemical shifts: there were only trace amounts of methylene tertiary carbons, which would be expected to common in the original structure, and instead there was twice the intensity of methyl group carbons. Longitudinal relaxation time experiments also supported these conclusions. As such, it was rationalised that crosslinking bis-sulfurated units cannot be the common microstructure in a DIB inverse vulcanised polymers and instead, it was hypothesized that a thiocumyl unit (Figure 1.16) was forming as the predominant microstructure; that is, a linear unit, explaining the polymers solubility. Formation of the usual crosslinking units is not impossible, and do seem to occur, but the overall structure of the polymer seemed closer to that of a branched polymer rather than a fully crosslinked polymer.[1.73]

To support these conclusions further, the DIB inverse vulcanised polymers were reduced with $LiAlH_4$ to destroy the sulfur chains and cap the organic units with thiols.[1.73] This yielded a soluble product which was analysed by solution phase NMR, revealing three types of structure in the mixture, which can be seen in Figure 1.16. Observed was DIB units with: two thiocumyl thiols, indicative of linear units in the polymer; one thiocumyl thiol and one unreacted double bond, indicative of a terminal units in the polymer; and one thiocumyl thiol with two thiols on the other moiety that would correspond to a bis-sulfurated moiety as expected from the original postulate, indicative of a branching unit in the polymer. What was not detected in a measurable concentration, was reduced units containing the four thiols that would indicate a crosslinking unit. Even still, the branching unit was quite uncommon by comparison to the linear unit, suggesting that DIB inverse vulcanised polymers synthesized in this way are predominantly linear. To help confirm the assignments, chemical syntheses were performed to produce model compounds that mirrored the reductive degradation products of the linear and terminal polymer units.[1.73]

Liam James Dodd
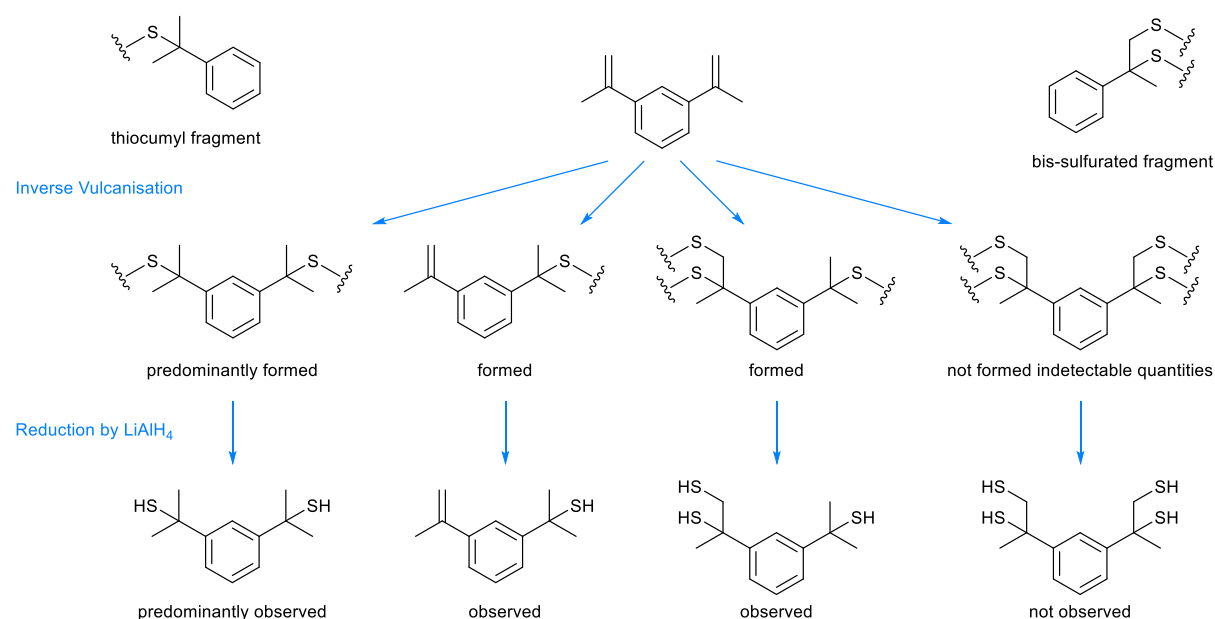
Figure 1.16: Structures from the study of the mechanism of DIB inverse vulcanised polymer formation.

Computational chemistry was then employed to assist in finding a mechanism that could lead to the observed products of the thiocumyl fragments.[1.73] The Gibbs free energies of the intermediates and transition states were calculated to find a kinetically viable and thermodynamically feasible pathway. It was found that hydrogen abstraction to yield an allyl radical was the most kinetically demanding pathway, though it was still accessible, and led to a thermodynamically feasible intermediate. More interestingly, it was found that radical attack at the less substituted end of the double bond to yield a primary radical was both less kinetically viable and less thermodynamically feasible than radical attack at the less substituted end of the double bond to yield a tertiary radical, though both pathways are still accessible. This was all surprising, because these reaction pathways would seem to suggest that the originally assumed structure of a bis-sulfurated alkene bond is accessible and expected, but it is not observed experimentally, so some other factor must prevent its formation. Analysis of the tertiary radical revealed that its tendency to undergo elimination depolymerisation is too rapid to allow it to be a viable intermediate in the polymerisation pathway. Thus, formation of the primary radical is the only route towards polymerisation. The calculations showed that termination of the primary radical by hydrogen abstraction is thermodynamically favourable and kinetically easy, provided the hydrogen is abstracted from a H-S bond, though abstraction from an allylic fragment is not kinetically impossible.[1.73]

To complete the study, tetrasulfides capped with cumyl groups, and chemically synthesized linear polymers of cumyl tetrasulfides were synthetically prepared in a well-controlled manner.[1.73] The ^{13}C NMR spectra of these well-defined products closely corresponded to those of polymers made from DIB in an inverse vulcanisation method, thereby further confirming the structure. As such, it was concluded that inverse vulcanisation of DIB proceeds by thiyl radical attack upon the alkene bonds of DIB to form primary radicals which terminate by hydrogen abstraction to form a cumyl unit in a linear polymer. These cumyl units are the major component of the DIB inverse vulcanised polymer, and a minor component has branching bis-sulfurated groups.[1.73]

Liam James Dodd

1.6.3. Thiol-ene and Thiol-yne Click Chemistry

Although thiols have not been proven beyond reasonable doubt in inverse vulcanisation chemistry, it is intuitive to draw comparisons between the chemistry of thiols, and the matching results of inverse vulcanisation. Thiols see common use in chain growth polymerisations as chain transfer agents, with the relatively weakly bound thiol hydrogen being abstracted, thus terminating the growth of one chain whilst the newly formed sulfur centred radical goes off to initiate a new chain growth.[1.74]

Another important field which utilises thiols is thiol-ene click chemistry, which is a vast and diverse field with numerous applications.[1.16,1.75-1.77] It is prudent to give a summary of this field here on two grounds: as mentioned before, there are comparisons to be drawn between thiol-ene click chemistry products and inverse vulcanisation leading to speculation that their could be mechanistic similarities; and thiol-ene click chemistry has been shown to be capable of generating polymers. Thiol-ene click chemistry is too vast a field to fully explore within this thesis, so here, only a brief account of the reaction and some aspects of its mechanism will be given, not the numerous inventive applications that have arisen from the field.

Click chemistry is defined as chemical reactions with the following properties: high yield with little to no by-products, or ones that are easily purified without the need for chromatography; accepting of a wide scope of chemical substrates; is stereospecific; is tolerant of air and water; uses readily available materials; and can be performed without a solvent, or in an environmentally benign solvent.[1.78] These stipulations are made on the basis that it allows such reactions to be performed easily and at low cost, facilitating their uptake into useful roles within industry and society, whilst also being closer to sustainability. The reaction of thiols and alkenes can satisfy the stipulations of click chemistry if the high reactivity of the thiols can be controlled to give selectivity in the reaction.[1.75] Under appropriate conditions, such reactions can occur on the seconds timescale with another advantage being that they can be triggered via a photolatent base.

The most basic scheme of thiol-ene click chemistry can be seen in Figure 1.17. Typically, thiol-ene reactions occur via a radical process complete with classic initiation, propagation and termination steps, though dependent on the thiol and the alkene it is to be combined with, nucleophilic variants resembling Michael addition are also possible.[1.76] Note that the chain growth propagation by attack of a carbon radical upon an alkene is undesirable, and it is in fact thiol chain transfer that is the desired reaction, to the extent that ideally, chain transfer should occur at a degree of polymerisation of one in thiol-ene click chemistry. That is, one a carbon radical is formed by thiol radical attack upon an alkene, chain transfer should be the next and only reaction, thus terminating what could have otherwise been a polymer chain, to generate a new thiol radical.

Generally, for radical thiol-ene click chemistry, bond strain about the alkene bond and increasing electron richness of the alkene bond, promotes reactivity, much in the same way as is observed in inverse vulcanisation: electron poor alkenes like EGDMA do not react well, and the strained norbornene alkene of DCPD reacts at a lower temperature than its cyclopentene alkene.[1.18,1.29,1.44] It is also observed that excessive substitution levels about the alkene can also reduce reactivity in thiol-ene click chemistry.

Liam James Dodd
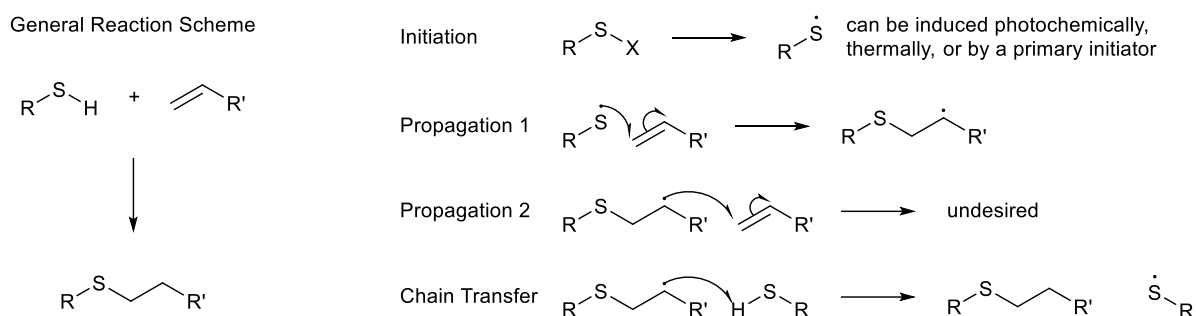
Figure 1.17: Reaction scheme and basic mechanism for thiol-ene click chemistry.

Note that there are other related fields of thiol focused click chemistry, such thiol-maleimide click chemistry, which is not discussed here due to its tangential relevance to inverse vulcanisation.[1.16,1.75-1.77] More relevant is thiol-yne click chemistry, as inverse vulcanisation can utilise alkynes.[1.19,1.79,1.80] Whereas alkynes do not react as cleanly in inverse vulcanisation, they are effective in thiol click chemistry. Thiol-yne click chemistry is much analogous in its mechanism to thiol-ene click chemistry, with the exception that alkynes can react twice sequentially, whereas alkenes react only once with thiols. When thiol-yne click chemistry is capable of forming products such as that shown in Figure 1.18, it is not hard to see why a comparison to inverse vulcanisation is so attractive.[1.79] Comparable hyperbranched polymers could also be formed if thiol-ene click chemistry was applied with a thiol and a compound containing two alkene bonds, just like the comonomers of inverse vulcanisation. With that being the case it is attractive to consider they may have similar mechanisms, though it is worth noting that thiol-ene and thiol-yne click chemistry can only form thioether linkages, whereas inverse vulcanisation can form disulfide, trisulfide, and longer linkages.
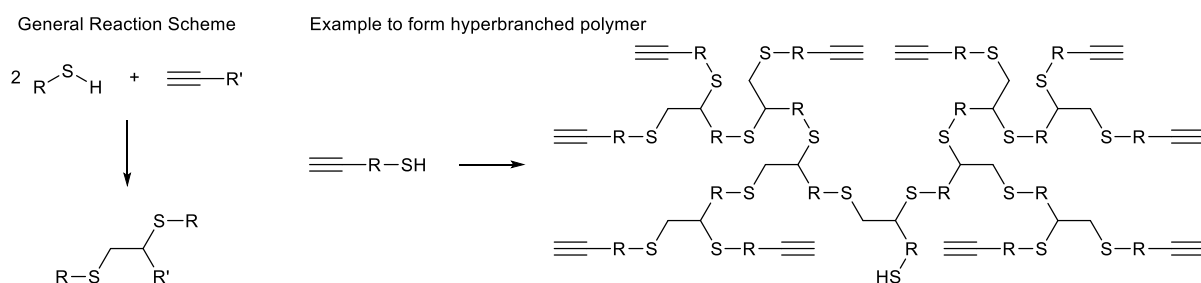
Figure 1.18: Reaction scheme for thiol-yne click chemistry and an illustrative example for how a hyperbranched polymer with resemblance to an inverse vulcanised polymer might form.[1.79]

1.6.4. Chemistry of Organic Sulfide Compounds

Organic sulfide linkages are expected to be a major component of inverse vulcanised polymers' molecular structure. As such, a discussion of the general behaviour of organic sulfide compounds is prudent, as much of this behaviour may carry through to inverse vulcanised polymers. Three classes of sulfides will be considered here: thioethers, disulfides, and trisulfides; corresponding to sulfur ranks of one, two, and three, in inverse vulcanised polymers (Figure 1.19).

 Tetrasulfides and pentasulfides do also exist, and are thought to exist in inverse vulcanised polymers, but examples of discrete organic molecular tetrasulfides and longer, that are well characterised in the literature are uncommon (Figure 1.19).[1.55] Note that inorganic sulfides will not be discussed here due to a lack of applicability to inverse vulcanised polymers.

Liam James Dodd

Sulfur Rank = 1   Sulfur Rank = 2   Sulfur Rank = 3   Sulfur Rank = 4   Sulfur Rank = 5

Thioether   Sulfoxide   Sulfone   Disulfide   Thiosulfinate   Thiosulfonate   Trisulfide   Tetrasulfide   Pentasulfide

Figure 1.19: General structures of some sulfur containing organic molecules.

Thioethers are the shortest sulfur rank sulfide, and do not contain a sulfur – sulfur bond, thus making them exempt from the dynamic chemistry associated with reversible sulfur – sulfur bond formation that gives inverse vulcanised polymers many of their properties.[1.4] As such they might be considered something of a "dead-end" in inverse vulcanised polymers, due to their irreversibility, but this does not mean they have no important impact upon the structure and behaviour of inverse vulcanised polymers. Because they do not contain a relatively weak sulfur – sulfur bond, they may form the strongest crosslinks in inverse vulcanised polymers, and increase their T_g's. In general, thioethers can be synthesized by simple S_N2 reactions of a thiol or thiolate with an electrophile, though this synthetic route is not so important for inverse vulcanisation.[1.81] What is important to note, is that thioethers can be susceptible to oxidation to sulfones and sulfoxides, and that this reaction does not generally require particularly forcing conditions.[1.82-1.86] Many synthetic strategies towards sulfones and sulfoxides apply catalysts and oxidising agents like hydrogen peroxide, but these are applied for the purposes of selectivity and complete conversion (Figure 1.19).[1.82-1.86] Otherwise, thioethers can oxidise in air, and when heated to inverse vulcanisation temperatures, this reaction may be very feasible.[1.82-1.86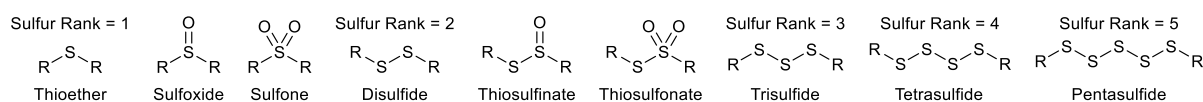] However, it is important to not that while some sources have reported differences between inverse vulcanisation reactions performed in air and under nitrogen, oxidation in the structures of inverse vulcanised polymers is not widely reported.[1.25,1.60]

Disulfides are most commonly synthesized by oxidation of thiols with relatively gentle oxidisers, so it is not inconceivable that they could form this way in an inverse vulcanisation exposed to air, though this would certainly be a minor process in comparison to the much more dominant scission of longer sulfur chains that is believed to be predominant in inverse vulcanisation.[1.87-1.89] Disulfides are also readily oxidised in the human body, where the product disulfide bridges connect together two cysteine amino acid units in a protein. Like this, the disulfide bridges can control the shape of proteins by anchoring together two different parts of a protein chain. This is somewhat reminisce of how disulfide bridges form crosslinks in inverse vulcanised polymers, though the contexts are vastly different.[1.90] Disulfides are also prone to oxidation to thiosulfonates and thiosulfinates, though these species can also be formed from thiols under oxidising conditions (Figure 1.19).[1.82] Disulfides are generally less stable than thioethers on account of the fact that disulfides contain the relatively weak sulfur – sulfur bond. Trisulfides are somewhat more challenging to produce synthetically than disulfides, and as a result, their oxidation has been less explored in the literature, though it is expected that because of their structural similarities, disulfides and trisulfides would share much of the same behaviour in terms of oxidation.[1.91-1.94] One key difference is that trisulfides have weaker sulfur – sulfur bonds than disulfides, and so a re more reactive, as was demonstrated in the literature where it was identified that disulfide linkages in inverse vulcanised polymers have less dynamic chemistry than trisulfides, and that it is the trisulfides that are responsible for the self-healing of inverse vulcanised polymers.[1.26,1.95]

1.7. Aims and Objectives

It has been identified that inverse vulcanisation has numerous attractive potential applications, but in order for inverse vulcanised polymers to reach their maximum potential, they must first be optimised and understood. There is a plethora of valuable literature contributions that focus on the applications of inverse vulcanisation, but there are comparatively fewer publications that concentrate upon the

Liam James Dodd

more fundamental aspects of this field of polymer chemistry. As such, understanding of the reaction itself is limited, and the methods by which polymerisations are performed are somewhat dysregulated. This leads to a gap in the literature where the focus of research is more towards the end goal of applying the polymers, whilst the methods and chemistry are lesser focused on, and there is little consistency between how different research groups perform inverse vulcanisation. Thus, one of the core themes of this thesis will be a step back from the polymerisation applications, and a greater focus on how inverse vulcanisation is performed and understood. The goal of this thesis was to introduce more rigorous methodology to the inverse vulcanisation reaction which has a two-fold advantage: it can allow for greater consistency in the wider field as the capacity to gain more reproducible results is demonstrated through stricter reaction methods; and it provides a more well defined, consistent, and robust platform to begin exploring the more fundamental aspects of the chemistry of inverse vulcanisation. The research performed in contribution to this thesis was aimed at providing synthetic and analytical techniques that can be useful to the research of others, thereby improving the efficacy and scope of inverse vulcanised polymers in those aforementioned applications. Toward this end, the research conducted in contribution to this thesis falls into three chapters, each with its own particular goals that align with the overall objectives of the thesis.

The second chapter, dedicated to catalysis of inverse vulcanisation, aimed to provide a robust and consistent methodology to the bulk polymerisation inverse vulcanisation method, whilst remedying some of the key drawbacks of inverse vulcanisation, such as high reaction temperatures prohibiting the use of low boiling comonomers, and raising the energy cost of synthesis to name a few. It also had the objective of laying the groundwork for building a fundamental understanding of how the catalysts of inverse vulcanisation work, potentially allowing future rational design of catalysts towards the desired applications of the polymers. One last key objective of the catalysis chapter was to assist researchers interested in inverse vulcanisation, in choosing the right catalyst for their work by creating a library of catalysts to compare between.

The third chapter follows on from the second and addresses concerns regarding the extraction of the catalyst from the polymer network, and the concern of heavy metal contamination through trace residues of catalyst left within the polymer. These concerns were circumvented by using organocatalysts that are intentionally and irreversibly incorporated into the polymer network. As part of this research, a dispersion polymerisation method for the polymerisation was investigated that allows the use of low boiling comonomers, beneficial to any researchers who aim to use such crosslinkers in inverse vulcanisation. This chapter had the objective of exploring such self-catalysing comonomers in terms of the method by which they are polymerised, the behaviour of the products, and the mechanism of catalysis, such that these self-catalysing comonomers can be more confidently applied in the research community.

The fourth research chapter had the aim of introducing a new analysis technique to inverse vulcanisation so that these hard to analyse polymers can be better understood at the molecular level, which is critical in establishing structure property relationships that would be critical to the rational design of future polymers and the optimisation of currently existing ones. More precisely, the aim of this chapter was to find Raman spectroscopic analysis techniques that can circumvent the issues with autofluorescent backgrounds that normally preclude such analysis, thereby enabling what should be an information rich and applicable analysis technique for inverse vulcanised polymers. Naturally, this chapter aimed to fully explore the capabilities of Raman spectroscopy in inverse vulcanisation, but one objective that was key from the start of the study, was the determination of the number of sulfur atoms in a chain, within the structure of an inverse vulcanised polymer. Such information can only be inferred by other analysis techniques at this time, yet this information is crucial to the applications of

Liam James Dodd

inverse vulcanised polymers. Finally, the objective of this research into Raman spectroscopy as applied to inverse vulcanised polymers, was to create a comprehensive and accessible guide for using Raman spectroscopy to characterise inverse vulcanised polymers, such that the analysis technique could see easier uptake amongst the research community.

1.8. References

1.1 Sulfur and Its Role In Modern Materials Science; D. A. Boyd; Angewandte Chemie International Edition, 2016, 55, 15486-15502.

1.2 Heterogeneous catalysis of the hydrodesulfurization of thiophenes in petroleum: an organometallic perspective of the mechanism; R. J. Angelici; Accounts of Chemical Research, 1988, 21, 387-394.

1.3 Sulfur Recovery Processes In Gas Purification, 5th edition; A. L. Kohl, R. B. Nielsen; Gulf Publishing, Houston, Texas, 1997, 670-730.

1.4 Polymerizations with elemental sulfur: A novel route to high sulfur content polymers for sustainability, energy and defense; J. J. Griebel, R. S. Glass, K. Char, J. Pyun; Progress in Polymer Science, 2016, 58, 90-125.

1.5 Elemental Sulfur; B. Meyer; Chemical Reviews, 1976, 76, 367-388.

1.6 Sustainable Polysulfides for Oil Spill Remediation: Repurposing Industrial Waste for Environmental Benefit; M. J. H. Worthington, C. J. Shearer, L. J. Esdaile, J. A. Campbell, C. T. Gibson, S. K. Legg, Y. Yin, N. A. Lundquist, J. R. Gascooke, I. S. Albuquerque, J. G. Shapter, G. G. Andersson, D. A. Lewis, G. J. L. Bernardes, J. M. Chalker; Advanced Sustainable Systems, 2018, 2.

1.7 Lavoisier: Chemist, Biologist, Economist; J. P. Poirier; University of Pennsylvania Press, Philadelphia, Pennsylvania, 1998, 107-108.

1.8 https://www.agrigem.co.uk/nutrigrow-elemental-sulphur-25kg (date accessed: 21/07/2022)

1.9 Chemistry of the Elements, 2nd edition; N. N. Greenwood, A. Earnshaw; Butterworth-Heinemann, Oxford, 1997, 654-656.

1.10 Elemental Sulfur and Sulfur-Rich Compounds I; R. Steudel; Springer-Verlag Berlin, Berlin, 2003, 1-79.

1.11 Handbook of Chemistry and Physics, 97th edition; I. H. Bell, L. I. Berger, P. E. Bradley, T. J. Bruno, C. E. Carraher, J. Cheng, R. D. Chirico, I. Cibulka, C. J. Cramer, V. Diky, M. Frenkel, J. R. Fuhr, R. N. Goldberg, T. W. Grove, A. H. Harvey, S. R. Heller, N. E. Holden, M. L. Huber, A. Kazakov, D. E. Kelleher, C. A. Koh, E. W. Lemmon, D. R. Lide, F. J. Lovas, Y. Luo, S. N. Lvov, M. Mantina, A. D. McNaught, T. M. Miller, N. Moazzen-Ahmadi, P. J. Mohr, C. D. Muzny, D. B. Newell, I. Ozier, L. I. Podobedova, C. J. Powell, R. Radebaugh, J. Reader, A. J. Remijan, E. D. Sloan, L. E. Snyder, P. D. N. Svoronos, B. N. Taylor, D. G. Truhlar, R. Valero, W. L. Wiese, C. Wohlfarth, D. Zwillinger; CRC Press, Boca Raton, Florida, 2017, 117.

1.12 Inorganic Chemistry; E. Wilberg, A. F. Holleman; Academic Press, De Gruyter, 2001.

1.13 Insights into the Vulcanization Mechanism through a Simple and Facile Approach to the Sulfur Cleavage Behavior; Q. S. Lian, Y. Li, K. Li, J. Cheng, J. Y. Zhang; Macromolecules, 2017, 50, 803-810.

1.14 Sulfur Vulcanization of Hydrocarbon Diene Elastomers; M. M. Coleman, J. R. Shelton, J. L. Koenig; Industrial & Engineering Chemistry Product Research and Development, 1974, 13, 154-165.

1.15 Elemental sulfur: chemistry and physics; N. Kharasch; Interscience Publishers, New York, 1965.

1.16 Thiol-Ene Click Chemistry; C. E. Hoyle, C. N. Bowman; Angewandte Chemie International Edition, 2010, 49, 1540-1573.

1.17 The use of elemental sulfur as an alternative feedstock for polymeric materials; W. J. Chung, J. J. Griebel, E. T. Kim, H. Yoon, A. G. Simmonds, H. J. Ji, P. T. Dirlam, R. S. Glass, J. J. Wie, N. A. Nguyen, B. W. Guralnick, J. Park, A. Somogyi, P. Theato, M. E. Mackay, Y. E. Sung, K. Char, J. Pyun; Nature Chemistry, 2013, 5, 518-524.

Liam James Dodd

1.18 Low cost and renewable sulfur-polymers by inverse vulcanisation, and their potential for mercury capture; D. J. Parker; H. A. Jones; S. Petcher; L. Cervini; J. M. Griffin, R. Akhtarb, T. Hasell; Journal of Materials Chemistry A, 2017, 5, 11682-11692.

1.19 Inverse vulcanization of elemental sulfur with 1,4-diphenylbutadiyne for cathode materials in Li–S batteries; P. T. Dirlam, A. G. Simmonds, T. S. Kleine, N. A. Nguyen, L. E. Anderson, A. O. Klever, A. Florian, P. J. Costanzo, P. Theato, M. E. Mackay, R. S. Glass, K. Char, J. Pyun; RSC Advances, 2015, 5, 24718–24722.

1.20 Inverse vulcanization of sulfur with divinylbenzene: Stable and easy processable cathode material for lithium-sulfur batteries; I. Gomez, D. Mecerreyes, J. A. Blazquez, O. Leonet, H. B. Youcef, C. Li, J. L. Gómez-Cámer, O. Bondarchuk, L. Rodriguez-Martinez; Journal of Power Sources, 2016, 329, 72-78.

1.21 Nucleophilic Activation of Elemental Sulfur for Inverse Vulcanization and Dynamic Covalent Polymerizations; Y. Zhang, N. G. Pavlopoulos, T. S. Kleine, M. Karayilan, R. S. Glass, K. Char, J. Pyun; Journal of Materials Chemistry A, 2019, 57, 7-12.

1.22 Sulfur-Limonene Polysulfide: A Material Synthesized Entirely from Industrial By-Products and Its Use in Removing Toxic Metals from Water and Soil; M. P. Crockett, A. M. Evans, M. J. H. Worthington, I. S. Albuquerque, A. D. Slattery, C. T. Gibson, J. A. Campbell, D. A. Lewis, G. J. L. Bernardes, J. M. Chalker; Angewandte Chemie International Edition, 2015, 127, 1–6.

1.23 Squalene-derived sulfur-rich copolymer@ 3D graphene-carbon nanotube network cathode for high-performance lithium-sulfur batteries; T. S. Sahu, S. Choi, P. Jaumaux, J. Zhang, C. Wang, D. Zhou, G. Wang; Polyhedron, 2019, 162, 147-154.

1.24 Dark Sulfur: Quantifying Unpolymerized Sulfur in Inverse Vulcanized Polymers; J. J. Dale, S. Petcher, T. Hasell; ACS Applied Polymer Materials, 2022, 4, 3169-3173.

1.25 Raman Analysis of Inverse Vulcanised Polymers; L. J. Dodd, C. Lima, D. Costa-Milan, A. R. Neale, B. Saunders, B. Zhang, A. Sarua, R. Goodacre, L. J. Hardwick, M. Kuball, T. Hasell; Polymer Chemistry, 2023, 14, 1369-1386.

1.26 Polysulfides as Biologically Active Ingredients of Garlic; U. Münchberg, A. Anwar, S. Mecklenburg, C. Jacob; Organic and Biomolecular Chemistry, 2007, 5, 1505–1518.

1.27 Practical and Highly Selective Sulfur Ylide-Mediated Asymmetric Epoxidations and Aziridinations Using a Cheap and Readily Available Chiral Sulfide: Extensive Studies To Map Out Scope, Limitations, and Rationalization of Diastereo- and Enantioselectivities; O. Illa, M. Namutebi, C. Saha, M. Ostovar, C. C. Chen, M. F. Haddow, S. Nocquet-Thibault, M. Lusi, E. M. McGarrigle, V. K. Aggarwal; Journal American Chemical Society, 2013, 135, 11951–11966.

1.28 Inverse Vulcanized Polymers for Sustainable Metal Remediation; F. G. Müller, L. S. Lisboa, J. M. Chalker; Advanced Sustainable Systems, 2023, 7, 2300010.

1.29 Catalytic Inverse Vulcanization; X. Wu, J. A. Smith, S. Petcher, B. Zhang, D. J. Parker, J. M. Griffin, T. Hasell; Nature Communications, 2019, 10, 647.

1.30 Porous inverse vulcanised polymers for mercury capture; T. Hasell, D. J. Parker, H. A. Jones, T. McAllister, S. M. Howdle; Chemical Communications, 2016, 52, 5383-5386.

1.31 Macroporous sulfur polymers from a sodium chloride porogen—a low cost, versatile remediation material; S. Petcher, D. J. Parker, T. Hasell; Environmental Science: Water Research & Technology 2019, 5, 2142-2149.

1.32 Determination of Hg (II) in tea and mushroom samples based on metal-organic frameworks as solid phase extraction sorbents; Y. Wu, G. Xu, F. Wei, Q. Song, T. Tang, X. Wang, Q. Hu; Microporous Mesoporous Materials, 2016, 235, 204–210.

1.33 Rapid Mercury(II) Removal by Electrospun Sulfur Copolymers; M. Thielke, L. Bultema, D. Brauer, B. Richter, M. Fischer, P. Theato, M. W. Thielke, L. A. Bultema, D. D. Brauer, B. Richter, M. Fischer, P. Theato; Polymers, 2016, 8, 266.

Liam James Dodd

1.34 High Surface Area Sulfur-Doped Microporous Carbons From Inverse Vulcanised Polymers; J. S. M. Lee, D. J. Parker, A. I. Cooper, T. Hasell; Journal of Materials Chemistry A, 2017, 5, 18603–18609.

1.35 Influences of Phosphorus and Sulphur on Ductility Dip Cracking Susceptibility in Multipass Weld Metal of Alloy 690; K. Saida, Y. Nomoto, H. Okauchi, H. Ogiwara, K. Nishimoto; Science and Technology of Welding and Joining, 2012, 17, 1–8.

1.36 Investigating the Antibacterial Properties of Inverse Vulcanized Sulfur Polymers; J. A. Smith, R. Mulhall, S. Goodman, G. Fleming, H. Allison, R. Raval, T. Hasell; ACS Omega, 2020, 5, 5229–5234.

1.37 Antibacterial Activity of Inverse Vulcanized Polymers; R. A. Dop, D. R. Neill, T. Hasell; Biomacromolecules, 2021, 22, 5223–5233.

1.38 Atkins' Physical Chemistry, 10th edition; P. W. Atkins, J. De Paula; Oxford University Press, Oxford, 2014.

1.39 100th Anniversary of Macromolecular Science Viewpoint: High Refractive Index Polymers from Elemental Sulfur for Infrared Thermal Imaging and Optics; T. S. Kleine, R. S. Glass, D. L. Lichtenberger, M. E. Mackey, K. Char, R. A. Norwood, J. Pyun; ACS Macro Letters, 2020, 9, 245-259.

1.40 Handbook of Chemistry and Physics, 97th edition; I. H. Bell, L. I. Berger, P. E. Bradley, T. J. Bruno, C. E. Carraher, J. Cheng, R. D. Chirico, I. Cibulka, C. J. Cramer, V. Diky, M. Frenkel, J. R. Fuhr, R. N. Goldberg, T. W. Grove, A. H. Harvey, S. R. Heller, N. E. Holden, M. L. Huber, A. Kazakov, D. E. Kelleher, C. A. Koh, E. W. Lemmon, D. R. Lide, F. J. Lovas, Y. Luo, S. N. Lvov, M. Mantina, A. D. McNaught, T. M. Miller, N. Moazzen-Ahmadi, P. J. Mohr, C. D. Muzny, D. B. Newell, I. Ozier, L. I. Podobedova, C. J. Powell, R. Radebaugh, J. Reader, A. J. Remijan, E. D. Sloan, L. E. Snyder, P. D. N. Svoronos, B. N. Taylor, D. G. Truhlar, R. Valero, W. L. Wiese, C. Wohlfarth, D. Zwillinger; CRC Press, Boca Raton, Florida, 2017, 751-754.

1.41 Severe hydrogen sulphide poisoning treated with 4-dimethylaminophenol and hyperbaric oxygen; J. Lindenmann, V. Matzi, N. Neuboeck, B. Ratzenhofer-Komenda, A. Maier, F. M. Smolle-Juettner; Diving and Hyperbaric Medicine, 2010, 40, 213–217.

1.42 Hydrogen Selenide Poisoning: An Illustrative Case with Review of the Literature; L. C. Alderman, J. J. Bergin; Archives of Environmental Health: An International Journal, 1986, 41, 354-358.

1.43 Infrared Fingerprint Engineering: A Molecular-Design Approach to Long-Wave Infrared Transparency with Polymeric Materials; T. S. Kleine, T. Lee, K. J. Carothers, M. O. Hamilton, L. E. Anderson, L. R. Diaz, N. P. Lyons, K. R. Coasey, W. O. Parker, L. Borghi, M. E. Mackay, K. Char, R. S. Glass, D. L. Lichtenberger, R. A. Norwood, J. Pyun; Angewandte Chemie International Edition, 2019, 58, 17656-17660.

1.44 Crosslinker Copolymerization for Property Control in Inverse Vulcanization; J. A. Smith, S. J. Green, S. Petcher, D. J. Parker, B. Zhang, M. J. H. Worthington, X. F. Wu, C. A. Kelly, T. Baker, C. T. Gibson, J. A. Campbell, D. A. Lewis, M. J. Jenkins, H. Willcock, J. M. Chalker, T. Hasell; Chemistry - A European Journal, 2019, 25, 10433 –10440.

1.45 Sulfur composite cathode materials for rechargeable lithium batteries; J. L. Wang, J. Yang, C. R. Wan, K. Du, J. Y. Xie, N. X. Xu; Advanced Functional Materials, 2003, 13, 487-492.

1.46 Mechanism for the Stable Performance of Sulfur-Copolymer Cathode in Lithium-Sulfur Battery Studied by Solid-State NMR Spectroscopy; A. Hoefling, D. T. Nguyen, P. Partovi-Azar, D. Sebastiani, P. Theato, S. W. Song, Y. J. Lee; Chemistry of Materials, 2018, 30, 2915–292.

1.47 In Operando X-Ray Diffraction and Transmission X-Ray Microscopy of Lithium Sulfur Batteries; J. Nelson, S. Misra, Y. Yang, A. Jackson, Y. Liu, H. Wang, H. Dai, J. C. Andrews, Y. Cui, M. F. Toney; Journal of the American Chemical Society; 2012, 134, 6337–6343.

1.48 Aqueous "polysulfide-ene" polymerisation for sulfur-rich nanoparticles and their use in heavy metal remediation; H. Shin, J. Kim, D. Kim, V. H. Nguyen, S. Lee, S. Han, J. Lim, K. Char; Journal of Materials Chemistry A, 2018, 6, 23542–23549.

Liam James Dodd

1.49 Synthesis of Poly(phenylene polysulfide) Networks from Elemental Sulfur and p-Diiodobenzene for Stretchable, Healable, and Reprocessable Infrared Optical Applications; J. M. Lee, G. Y. Noh, B. G. Kim, Y. Yoo, W. J. Choi, D. Kim, H. G. Yoon, Y. S. Kim; ACS Macro Letters, 2019, 8, 912–916.

1.50 Reaction between 1,3,5-Triisopropylbenzene and Elemental Sulfur Extending the Scope of Reagents in Inverse Vulcanization; Y. Lai, Y. Liu; Macromolecular Rapid Communications, 2023.

1.51 Mesoporous knitted inverse vulcanised polymers; S. Petcher, B. Zhang, T. Hasell; Chemical Communications, 2021, 57, 5059-5062.

1.52 Mechanochemical synthesis of inverse vulcanized polymers; P. Yan, W. Zhao, F. McBride, D. Cai, J. Dale, V. Hanna, T. Hasell; Nature Communications, 2022, 13.

1.53 Photoinduced inverse vulcanization; J. Jia, J. Liu, Z. Wang, T. Liu, P. Yan, X. Gong, C. Zhao, L. Chen, C. Miao, W. Zhao, S. Cai, X. Wang, A. I. Cooper, X. Wu, T. Hasell, Z. Quan; Nature Chemistry, 2022, 14, 1249–1257.

1.54 Ring-to-Chain Structural Relaxation of Elemental Sulfur upon Photoexcitation; E. Cho, S. M. Pratik, J. Pyun, V. Coropceanu, J. Brédas; ACS Materials Letters, 2022, 4, 2362-2367.

1.55 Electrochemical Synthesis of Poly(trisulfides); J. M. M. Pople, T. P. Nicholls, L. N. Pham, W. M. Bloch, L. S. Lisboa, M. V. Perkins, C. T. Gibson, M. L. Coote, Z. Jia, J. M. Chalker; Journal of the American Chemical Society, 2023, 145, 11798–11810.

1.56 https://www.sigmaaldrich.com/GB/en/product/aldrich/414565?, (date accessed: 29/03/2023)

1.57 Mechanical and Electrical Properties of Sulfur-Containing Polymeric Materials Prepared via Inverse Vulcanization; S. Diez, A. Hoefling, P. Theato, W. Pauer; Polymers, 2017, 9, 16.

1.58 Inverse vulcanization of bismaleimide and divinylbenzene by elemental sulfur for lithium sulfur batteries; M. Arslan, B. Kiskan, E. C. Cengiz, R. Demir-Cakan, Y. Yagci; European Polymer Journal, 2016, 80, 70-77.

1.59 Elemental Sulfur as a Reactive Medium for Gold Nanoparticles and Nanocomposite Materials; W. J. Chung, A. G. Simmonds, J. J. Griebel, E. T. Kim, H. S. Suh, I. B. Shim, R. S. Glass, D. A. Loy, P. Theato, Y. E. Sung, K. Char, J. Pyun; Angewandte Chemie International Edition, 2011, 50, 11409-11412.

1.60 Tailoring Polysulfide Properties through Variations of Inverse Vulcanization; K. Orme, A. H. Fistrovich, C. L. Jenkins; Macromolecules, 2020, 53, 9353–9361.

1.61 Tracking side reactions of the inverse vulcanization process and developing monomer selection guidelines; Y. Onose, Y. Ito, J. Kubawara, T. Kanbara; Polymer Chemistry, 2022, 13, 5486-5493.

1.62 Introduction to Polymers, 3rd edition; R. J. Young, P. A. Lovell; CRC Press, Boca Raton, Florida, 2011.

1.63 Principles of polymer chemistry; P. J. Flory; Cornell University Press, Ithaca, New York, 1953.

1.64 Rubber Chemistry and Technology; J. R. Shelton, E. T. McDonel; 1960, 33, 342-356.

1.65 Investigation of Rubber Vulcanization Process by Means of Electron Paramagnetic Resonance (Radiospectroscopy); G. A. Blokh; Doklady Akademii Nauk Sssr 1959, 129, 361-364.

1.66 The mechanisms of the sulphur-only and catalytic vulcanization of polybutadiene: An EPR and DFT study; D. Dondi, A. Buttafava, A. Zeffiro, C. Palamini, A. Lostritto, L. Giannini, A. Faucitano; European Polymer Journal 2015, 62, 222-235.

1.67 Study on the dual-curing mechanism of epoxy/allyl compound/sulfur system; Q. S. Lian, Y. Li, T. Yang, K. Li, Y. F. Xu, L. Liu, J. B. Zhao, J. Y. Zhang, J. Cheng; Journal of Materials Science, 2016, 51, 7887-7898.

1.68 Green Chemistry and Polymers Made From Sulfur; M. J. H. Worthington, R. L. Kucera, J. M. Chalker; Green Chemistry, 2017, 19, 2748-2761.

1.69 Inverse vulcanization of elemental sulfur and styrene for polymeric cathodes in Li-S batteries; Y. Y. Zhang, J. J. Griebel, P. T. Dirlam, N. A. Nguyen, R. S. Glass, M. E. Mackay, K. Char, J. Pyun; Journal of Polymer Science Part A: Polymer Chemistry, 2017, 55, 107-116.

Liam James Dodd

1.70 Benzoxazine-Based Thermosets with Autonomous Self-Healing Ability; M. Arslan, B. Kiskan, Y. Yagci; Macromolecules, 2015, 48, 1329-1334.

1.71 NMR and EPR Structural Analysis and Stability Study of Inverse Vulcanized Sulfur Copolymers; V. K. S. Wadi, K. K. Jena, S. Z. Khawaja, K. Yannakopoulou, M. Fardis, G. Mitrikas, M. Karagianni, G. Papavassiliou, S. M. Alhassan; ACS Omega, 2018, 3, 3330-3339.

1.72 High Sulfur Content Polymers: The Effect of Crosslinker Structure on Inverse Vulcanization; J. A. Smith, X. F. Wu, N. G. Berry, T. Hasell; Journal of Polymer Science Part A: Polymer Chemistry, 2018, 56, 1777-1781.

1.73 On the Mechanism of the Inverse Vulcanization of Elemental Sulfur: Structural Characterization of Poly(sulfur-random-(1,3-diisopropenylbenzene)); J. Bao, K. P. Martin, E. Cho, K. Kang, R. S. Glass, V. Coropceanu, J. Bredas, W. Parker, J. T. Njardarson, J. Pyun; Journal of the American Chemical Society, 2023, 145, 12386–12397.

1.74 Thiols as chain transfer agents in free radical polymerization in aqueous solution; C. Henríquez, C. Bueno, E.A. Lissi, M.V. Encinas; Polymer, 2003, 44, 5559-5561.

1.75 Thiol-click chemistry: a multifaceted toolbox for small molecule and polymer synthesis; C. E. Hoyle, A. B. Lowe, C. N. Bowman; Chemical Society Reviews, 2010, 39, 1355-1387.

1.76 Thiol-ene ''click'' reactions and recent applications in polymer and materials synthesis; A. B. Lowe; Polymer Chemistry, 2010, 1, 17-36.

1.77 The Power of Thiol-ene Chemistry; M. J. Kade, D. J. Burke, C. J. Hawker; Journal of Polymer Science Part A: Polymer Chemistry, 2010, 48, 743-750.

1.78 Click Chemistry: Diverse Chemical Function from a Few Good Reactions; H. C. Kolb, M. G. Finn, K. B. Sharpless; Angewandte Chemie International Edition, 2001, 40, 2004–2021.

1.79 Thiol–Yne Chemistry: A Powerful Tool for Creating Highly Functional Materials; R. Hoogenboom; Angewandte Chemie International Edition, 2010, 49, 3415-3417.

1.80 Thiol-yne click chemistry: A powerful and versatile methodology for materials synthesis; A. B. Lowe, C. E. Hoyle, C. N. Bowman, Journal of Materials Chemistry, 2010, 20, 4745–4750.

1.81 Organic Chemistry, 2nd edition; J. Clayden, N. Greeves, S. Warren; Oxford University Press, Oxford, 2012.

1.82 Switchable Synthesis of Sulfoxides, Sulfones and Thiosulfonates through Selectfluor-Promoted Oxidation with H2O as O-Source; X. Guo, X. Sun, M. Jiang, Y. Zhao; Synthesis, 2022, 54, 1996-2004.

1.83 Switchable Synthesis of Aryl Sulfones and Sulfoxides through Solvent-Promoted Oxidation of Sulfides with O2/Air; Z. Cheng, P. Sun, A. Tang, W. Jin, C. Liu; Organic Letters, 2019, 21, 8925-8929.

1.84 TAPC-promoted oxidation of sulfides and deoxygenation of sulfoxides; K. Bahrami, M. M. Khodaei, M. S. Arabi; Journal of Organic Chemistry, 2010, 75, 6208-6213.

1.85 An Efficient Oxidation of Sulfides to Sulfones with Urea-Hydrogen Peroxide in the Presence of Phthalic Anhydride in Ethyl Acetate; M. Lutz, M. Wenzler, I. Likthotvorik; Synthesis, 2018, 50, 2231-2234.

1.86 Green Organocatalytic Oxidation of Sulfides to Sulfoxides and Sulfones; E. Voutyritsa, I. Triandafillidi, C. G. Kokotos; Synthesis, 2017, 49, 917-924.

1.87 A Mild and Environmentally Benign Oxidation of Thiols to Disulfides; M. Kirihara, Y. Asai, S. Ogawa, T. Noguchi, A. Hatano, Y. Hirai; Synthesis, 2007, 3286-3289.

1.88 Simple and Selective Oxidation of Thiols to Disulfides with Dimethylsulfoxide Catalyzed by Dichlorodioxomolybdenum(VI); R. Sanz, R. Aguado, M. R. Pedrosa, F. Arnáiz; Synthesis, 2002, 856-858.

1.89 1,3-Dibromo-5,5-Dimethylhydantoin [DBDMH] as an Efficient and Selective Agent for the Oxidation of Thiols to Disulfides in Solution or under Solvent-Free Conditions; A. Khazaei, M. A. Zolfigol, A. Rostami; Synthesis, 2004, 2959-2961.

1.90 Formation and transfer of disulphide bonds in living cells; C. S. Sevier, C. A. Kaiser; Nature Reviews Molecular Cell Biology, 2002, 3, 836–847.

Liam James Dodd

1.91 Synthesis of Unsymmetric Trisulfides from 9-Fluorenylmethyl Disulfides; S. Xu, Y. Wang, M. N. Radford, A. J. Ferrell, M. Xian; Organic Letters, 2018, 20, 465-468.

1.92 Unsymmetrical Organotrisulfide Formation via Low-Temperature Disulfanyl Anion Transfer to an Organothiosulfonate; D. Ali, R. Hunter, C. H. Kaschula, S. De Doncker, S. C. M. Rees-Jones; Journal of Organic Chemistry, 2019, 84, 2862-2869.

1.93 Novel and Efficient Synthesis of Unsymmetrical Trisulfides; S. Lach, M. Sliwka-Kaszynska, D. Witt; Synlett, 2010, 2857-2860.

1.94 Novel and Efficient Methods for the Synthesis of Symmetrical Trisulfides; A. Kertmen, S. Lach, J. Rachon, D. Witt; Synthesis, 2009, 1459-1462.

1.95 Stretchable and Durable Inverse Vulcanized Polymers with Chemical and Thermal Recycling; P. Yan, W. Zhao, S. J. Tonkin, J. M. Chalker, T. L. Schiller, T. Hasell; Chemistry of Materials, 2022, 34, 1167–1178.

Liam James Dodd

Chapter 2: Catalysis of Inverse Vulcanisation

Whilst inverse vulcanisation can be a remarkable polymerisation for the production of next generation polymers, it still has drawbacks, such as a relatively high reaction temperature that is energy expensive, a limited range of reactive comonomers, and the production of the toxic by-product hydrogen sulfide. Catalysis was shown to remedy these drawbacks to a good extent while introducing advantages such as shorter reaction times, increased yields, and improved polymer properties. This discovery was of exceptional value, and the work performed in this chapter adds to it by looking more deeply at the catalysts. A rigorously controlled reaction method was developed to ensure minimal variability in the reaction results before more than twenty-five unique catalysts were tested in inverse vulcanisation. By observing the differences in catalyst structure and the subsequent differences in the results of the reaction, conclusions about how the catalyst structure affects the efficacy of the catalyst were drawn, and in doing so postulates about the catalytic mechanism were made, and a library of catalysts was assembled, to allow easy selection of catalysts by practitioners of inverse vulcanisation.

2.1. Catalytic Inverse Vulcanisation

In 2019, it was discovered that several activators (activators are rate enhancing species that are not regenerated catalytically) used in conventional vulcanisation were also active as catalysts in inverse vulcanisation.[2.1] Although purely inorganic activators like ZnO were found to have no effect, metal diethyldithiocarbamates (Figure 2.1a) were found to have numerous benefits in inverse vulcanisation, such as decreasing the reaction time, decreasing the amount of toxic hydrogen sulfide by-product that is given off, improving the yield of reaction, increasing the T_g of the product polymers, allowing otherwise unreactive crosslinkers to be used in inverse vulcanisation (a key example being EGDMA) and permitting the usage of lower reaction temperatures which has several benefits in and of itself. Higher temperatures in inverse vulcanisation prohibit the use of low boiling point crosslinkers and have also been shown to promote the formation of hydrogen sulfide as a by-product, and increase the risk of the hazardous TNE, both of which must be avoided in an industrial synthesis plant on the grounds of air pollution and catastrophic disasters, respectively.[2.1]
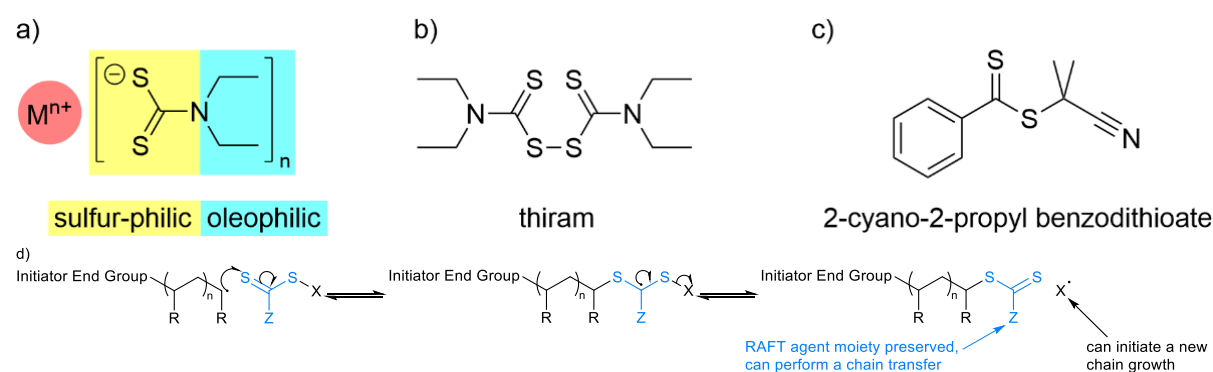
Figure 2.1: Molecular structures of a) a general metal diethyldithiocarbamate, with the potential lyophilicities of its moieties indicated, b) thiram and c) 2-cyano-2-propyl benzodithioate, as well as d) a general mechanism for the action of a RAFT agent.[2.2]

It was found that Thiram (Figure 2.1b), a metal free catalyst was of poor activity, and that 2-cyano-2-propyl benzodithioate (Figure 2.1c), a common reversible addition fragmentation chain transfer (RAFT) polymerisation agent had no activity, thus eliminating RAFT as the mode of action of catalytic inverse vulcanisation.[2.1] RAFT itself is a broad and exciting field of polymer chemistry that has inspired many theses, so it is clear that inclusive discussion of RAFT cannot be included here, but a representative mechanism is shown in Figure 2.1d.[2.2] Briefly, RAFT is a controlled polymerisation

Liam James Dodd

where a specialised chain transfer agent is used, normally a dithioester of trithiocarbonate, because when these chain transfer agents react with a polymer chain end, they give a polymer end group that is itself, a chain transfer agent. Like this, the chain transfer agent does not get used up, as each chain transfer event produces a new chain transfer moiety, and this has numerous benefits that are well discussed in the literature.[2.2]

From the aforementioned observations, it was rationalised that a sulfur – metal or sulfur – sulfur bond needs to be present in the catalyst molecule, with the prior being the more effective. From their experimental observations, Wu *et al.* proposed the mechanism shown in Figure 2.2. Several metal diethyldithiocarbamate (DEDC) compounds were screened as catalysts in inverse vulcanisation and with the exception of sodium (I) DEDC, which was uncharacteristically effective at enhancing the rate of reaction, the identity of the metal (II) cations made little difference to the rate of reaction.[2.1] Firstly, it was found that metal free molecules were poor catalysts, or non-catalytic, suggesting that a metal cation may be important for sulfur or comonomer binding.[2.1] Secondly, catalytic inverse vulcanisation permits lower reaction temperatures, which may be explained by the weakening of sulfur – sulfur bonds by coordination to the metal centre, as the high temperatures of uncatalyzed inverse vulcanisation are theorised to be necessary for homolytic sulfur – sulfur bond cleavage. Thirdly, that catalytic inverse vulcanisation allows unreactive comonomers to be polymerised, which can be explained by coordination of the cation to the carbon – carbon double bonds of the comonomer, thereby providing a lower energy reaction pathway. It was also proposed that the DEDC ligand may assist in the cleavage of sulfur – sulfur bonds and carbon – carbon double bonds by behaving as a nucleophile, further explaining why catalytic inverse vulcanisation permits lower reaction temperatures. Finally, it was suggested that the metal DEDC's may act as phase transfer agents between the immiscible sulfur and organic phases, as the sulfur containing dithiocarbamate group may have an affinity for the sulfur phase whilst the alkyl chains may have an affinity for the organic phase.[2.1] Wu *et al.* were unable to propose a route by which the catalyst may be regenerated, which is not surprising since in such complex reactions, regeneration of the catalyst often occurs after the rate limiting step and is particularly difficult to study. Since a potential route to the regeneration of the catalyst has not yet been identified, the conclusions that metal DEDC's act as initiators or activators, rather than catalysts, are not ruled out.[2.1]

Sulfur coordinates to the metal centre, which withdraws electron density from the S-S bond, weakening it and priming it for assisted cleavage by the DEDC ligand. This step may be repeated several times before progression to the next step.

An alkene coordinates to the metal centre, which withdraws electron density from the C=C bond, weakening it and priming it for assisted cleavage by the DEDC ligand.

As in the first step, the metal DEDC assists in the cleavage of the S-S bond

The comonomer has been incorporated into a sulfur chain. Reaction of the remaining alkene bond by catalysis or otherwise, will result in a crosslinking unit. Meanwhile the metal centre can incorporate more comonomer units into the polymer.

Figure 2.2: A proposed mechanism for catalytic inverse vulcanisation.[2.1] The alkene bonds highlighted in dark blue are still reactive and the sulfur chains highlighted in light blue may still be prone to scission and further polymerisation. The sulfur rings in the mechanism above may be replaced with growing sulfur homopolymer chains or growing inverse vulcanised oligomers. The second DEDC ligand may also act as a nucleophile at any point in the mechanism. The mechanism has been portrayed here as anionic but, could in fact be a radical mechanism or a mixture of both.

Liam James Dodd

It should be remembered that the mechanism of inverse vulcanisation and conventional vulcanisation are both still unknown at this time, so it is too much to demand that the work of Wu *et al.* decipher the mechanism of catalytic inverse vulcanisation in the first publication. An alternative however, is to look to activated conventional vulcanisation using metal DEDC's, which received some attention in a publication founded on computational chemistry.[2.3] in this work, the vulcanisation process was divided into three steps: firstly was induction 1, where sulfurating agents form from sulfur reacting with the activator; induction 2, where the sulfurating agent forms a crosslink precursor by sulfurating the carbon polymer chain; and finally crosslinking, where the sulfurated polymer crosslinks with other polymer chains, either on its own or with help from the activator.[2.3] It was found that stage 1 had six fundamental steps wherein two molecules of activator at a time, cooperate to break apart a cyclo-octasulfur molecule, with one molecule of activator removing two atoms at a time, as shown in Figure 2.3.[2.3] The rate limiting step was found to be the first insertion of zinc dimethyldithiocarbamate (DMDC) into the cyclo-octasulfur ring.[2.3] In stage 2 of the mechanism for activated conventional vulcanisation, the polymer inserts into the sulfurating agent via alpha allyl proton position, after which, the activator molecule detaches from the now sulfurated polymer, to leave behind a perthiol (Figure 2.4).[2.3] Also detailed was another pathway by which a perthiol could generated upon a polymer chain with the assistance of another molecule of cyclo-octasulfur, and this leads to a slightly different sulfurated polymer, but this pathway is unlikely due to the low concentrations of sulfur in conventional vulcanisation.[2.3] In stage 3, the perthiol crosslink precursor can crosslink to other polymer chains with or without the assistance of an activator molecule, though assistance is energetically preferred (Figure 2.5).[2.3] To conclude this work, the activator structure was varied and observed were the effects on the electron density at the zinc metal centre and DEDC sulfur atoms, as well as the activator activity.[2.3] It was found that a less electron dense zinc provided better activation, and so the alkyl groups should be kept short to minimise their electron donation, or be replaced with an electron withdrawing moiety.[2.3]
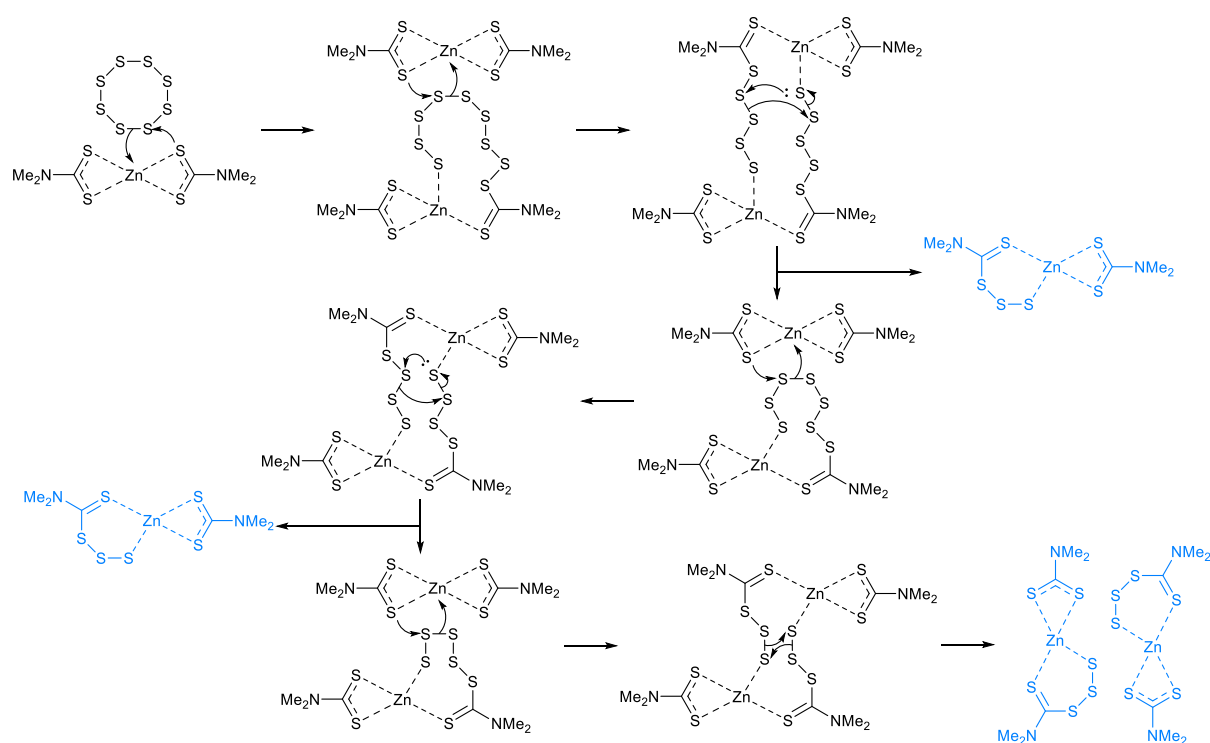

Figure 2.3: A mechanism for stage 1 of Shi *et al.*'s work. Molecules highlighted in blue are termed active sulfurating agents, which are important in stage 2.
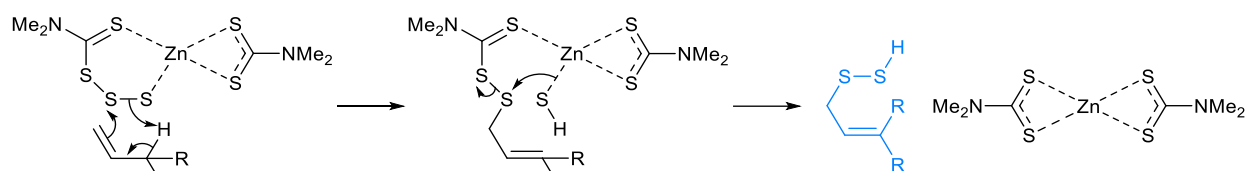
Liam James Dodd

Figure 2.4: A mechanism for stage 2 of Shi *et al.*'s work. The molecules highlighted in blue is termed a crosslink precursor, and is important in stage 3.
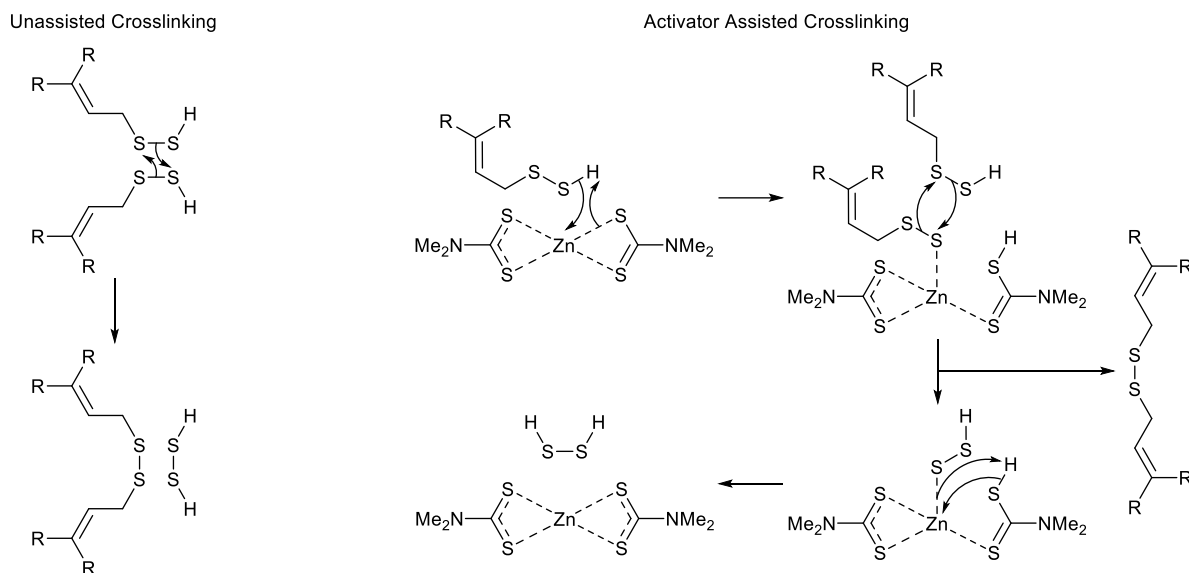
Figure 2.5: A mechanism for stage 3 of Shi *et al.*'s work.

2.2. Project Outline

Since catalytic inverse vulcanisation was such a recent discovery, little was known about the mechanism. Though a sensible mechanism was proposed from the experimental observations, no mechanistic aspect had been proven beyond reasonable doubt.[2.1] An increased understanding of the mechanism of catalytic inverse vulcanisation would allow rational design of better catalyst molecules. Therefore, this project had the aim of elucidating the role of catalysts in inverse vulcanisation. By observing the previously proposed mechanism, predictions were made about what parts of the catalyst molecule's structure would be important to those mechanistic aspects. Those parts of the catalyst molecule's structure were then varied to provide alternative catalysts with superior or inferior catalytic activity to the initial structure. If the theoretical predictions of the catalyst's activity were found to be accurate experimentally, this was taken as evidence for the existence of that aspect of the mechanism. In doing so a preliminary understanding of the catalytic mechanism has been built up along with a basic understanding of what factors make a good catalyst. In addition to this the scope of different catalysts was expanded, broadening the variety of molecules known to give a rate enhancement to inverse vulcanisation, including several metal free catalyst molecules. In doing so, a library of benchmarked catalytic molecules was compiled to allow easy comparison and selection of the catalysts tested here. Also studied was the versatility of catalytic inverse vulcanisation to varied reaction conditions and different organic comonomers.

2.3. General Considerations

All chemicals were used as received. Ground sulfur sublimed powder reagent grade ≥99.5 % was obtained from Brenntag UK & Ireland. Sodium disulfide nonahydrate 98 %+ extra pure was obtained

Liam James Dodd

from Acros Organics. Sodium diethyldithiocarbamate was obtained from Alfa Aesar. Zinc (II) dibutyldithiocarbamate >98 %, diethyldithiocarbamic acid ferric salt >95 %, copper (II) diethyldithiocarbamate >97 % Dicyclopentadiene (stabilized with BHT) [precursor to Cyclopentadiene] >97%, and 1,3-Diisopropenylbenzene (stabilized with TBC) >97% and nickel (II) diethyldithiocarbamate >97 % were obtained from Tokyo Chemicals Industry. Dioctylamine 97 %, Ntert-butylbenzenesulfenamide 97 %, potassium ethyl xanthogenate 96 %, O-isopropylxanthic acid potassium salt 98 %, guanidine hydrochloride ≥99 %, thiourea ACS reagent ≥99.0 %, 2-mercaptobenzothiazole 97 %, silver diethyldithiocarbamate ACS reagent 99 %, carbon disulfide anhydrous ≥99 %, divinylbenzene technical grade 80 %, zinc (II) diethyldithiocarbamate 97 %, zinc (II) dimethyldithiocarbamate 97 %, ammonium diethyldithiocarbamate, aluminium trichloride anhydrous powder 99.99 % trace metals basis, calcium chloride anhydrous free-flowing Redi-Dri™ ACS reagent ≥96 %, 15-crown-5 98 %, 18-crown-6 99 %, lead (ii) acetate trihydrate ACS reagent grade >99 %, magnesium chloride hexahydrate BioXtra ≥99.0 %, ferrocene 98 % and tetrabutylammonium hexafluorophosphate ≥99.0% were all obtained from Sigma Aldrich. Iron (II) diethyldithiocarbamate and cobalt (II) diethyldithiocarbamate were sourced from Wu *et al.* and were the exact same samples used in their previous research. All FTIR spectra were recorded on a Bruker Vertex 70 FTIR diamond crystal platinum ATR. All DSC data were obtained using a TA instruments discovery series DSC25 equipped with an RCS coolant system and Tzero aluminium hermetic pans and lids, using a heating rate of 10 °C min^{-1} and a cooling rate of 5 °C min^{-1} in the range of 0 °C to 150 °C, except where a polymer had a low glass transition temperature, in which case the lower limit of the heating range was extended to -80 °C. NMR spectra were acquired on the University of Liverpool Bruker DEPT400 NMR, with exception of the NMR kinetics study which was performed on University of Liverpool Bruker DPX400. PXRD data were collected in transmission mode on a Panalytical X'Pert PRO MPD equipped with a high throughput screening (HTS) XYZ stage, X-ray focusing mirror and PIXcel detector, using Cu Kα radiation. Data were measured on loose powder samples held on thin Mylar film in aluminium well plates, over the range 4 to 40° in approximately 0.013° steps over 60 minutes.

2.4. General Method and Research Strategy

In order to begin this project, a rigorous method for the inverse vulcanisation of sulfur and DVB was developed to create consistent reaction conditions that would allow comparison of the results between reactions. In the literature it had been found that inverse vulcanisation reactions involving DVB were sensitive to their conditions, reinforcing that control over reaction variables is crucial.[2.4] It has been found that inverse vulcanisation reactions are particularly sensitive to their reaction conditions, so in this project great care was taken to ensure consistency in the reaction method.

All reactions, unless otherwise specified, were run in triplicate to allow averaging of the data and calculation of a standard deviation. The same hotplate and thermocouple were used for every reaction. The hotplate was equipped with an aluminium heating pan and block which were found to be crucial for obtaining consistent data as they allowed consistent positioning of the reaction vials upon the hotplate, which affected stirring, and it allowed for better heat distribution from the hotplate, minimizing the effect of hotspots. To protect the reaction vials from the variable conditions in the laboratory, the heating pan, heating block and reaction vials were wrapped tightly in an excess of aluminium foil. The general reaction method was as follows: 5.00 ± 0.01 g (0.0195 mol) of sulfur (ground sulfur sublimed powder, reagent grade, ≥99.5 % purity, obtained from Brenntag UK & Ireland) was melted at 135 °C in a 40 mL reaction vial, without a lid, in the presence of 0.28 mmol of a selected catalyst (± 0.9 mg about the target mass was permitted), with 200 rpm stirring from a 14 mm cross shaped PTFE stirrer. The system was left for 10 to 20 mins to allow thermal equilibration. 5.00 ± 0.01 g (0.0384 mol) of DVB (divinylbenzene, technical grade, 80 % purity, obtained from Sigma Aldrich) was

Liam James Dodd

poured into the reaction vial and the stirring rate was immediately increased to 900 rpm, at which point a timer was started. Upon addition of DVB, a 1 °C to 3 °C temperature drop was noted on the thermocouple due to the addition of cold DVB, however the reaction temperature always recovered to the set temperature within three minutes. Once the solution became so viscous that the stirrer fully stopped rotating, the timer was stopped, giving the vitrification time. The polymers were then cured for a minimum of five hours (usually overnight) on the hotplate as it was found that curing them in the oven provided different results, potentially due to the different mechanisms of heating (conduction versus convection). The justification for the minimum five-hour curing time is supported by the fact that polymers cured for different lengths of time showed little change in their T_g and soluble fractions after about four hours of curing (Figure 2.6a). All polymers were analysed by DSC and FTIR. Loadings of catalyst greater than 0.28 mmol were trialled, however this frequently resulted in the TNE, which detrimentally affected the polymer's properties in an inconsistent and unpredictable manner, preventing comparison between different polymers. To give confidence in the reaction set up's capacity to give consistent results, the uncatalyzed inverse vulcanization of DVB and sulfur was performed multiple times throughout the project, in intervals of several months. Said reactions always yielded results statistically indistinct from one another.
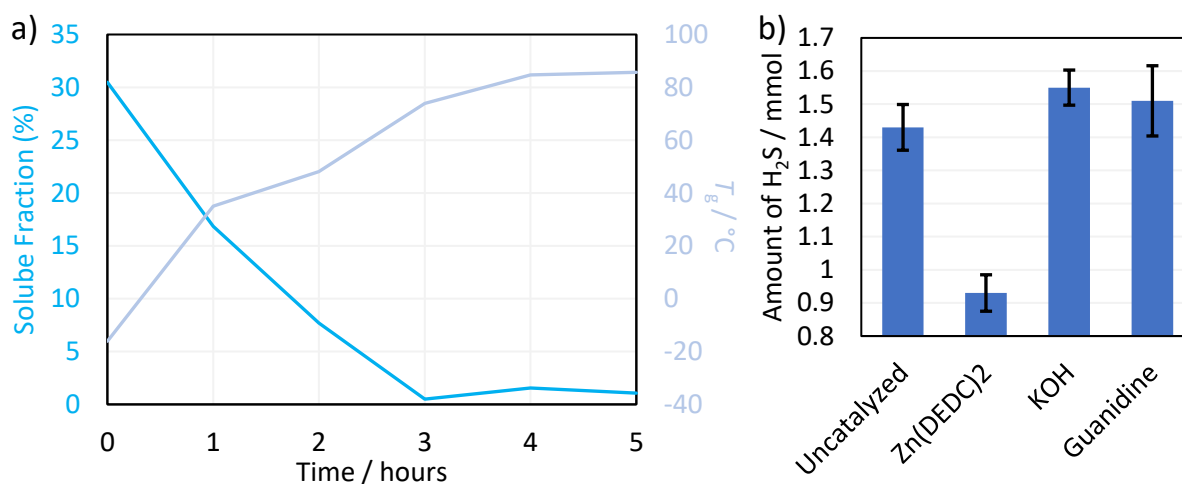
Figure 2.6: a) the soluble fraction and T_g of DVB inverse vulcanised polymers as a function of curing time, and b) the amount of hydrogen sulfide given off by inverse vulcanisations at 135 °C, using 5 g of DVB and 5 g of elemental sulfur, with different catalysts.

DVB was chosen as the model organic comonomer because it is inexpensive, can undergo inverse vulcanisation without a catalyst (useful for benchmarking), and may have negligible loss from evaporation at the temperatures used. To quantify the volatility, neat DVB was heated without sulfur at 135 °C for 1 h (a typical vitrification time). The remaining mass of DVB which had homopolymerized into a white solid, was found to be 93.7 ± 0.3%, suggesting that a significant amount of DVB evaporates over the course of inverse vulcanisation reactions and that yields may be increased in reactions with short vitrification times since there is less time for DVB to evaporate before being incorporated into a polymer. The yield of uncatalyzed inverse vulcanisation was found to be 91.7 ± 1.2%, lower than the DVB evaporation experiment, which suggests there is some other loss to the yield. This loss cannot be from the volatilization of sulfur because, after sulfur was heated for 1 h at 135 °C, the remaining mass was found to be 99.9 ± 0.0%, unsurprising given that the boiling point of sulfur is 445 °C.[2.5]

The loss to the yield was instead attributed to hydrogen sulfide formation. Several reactions were repeated under gas capture conditions where the amount of hydrogen sulfide given off was quantified

Liam James Dodd

by bubbling the exhaust gases of the reactions via Dreschel bottle, through a solution of lead (II) acetate, which precipitates lead sulfide when it is exposed to hydrogen sulfide.[2.6] These reactions were performed as described in the general method for inverse vulcanisation, but the reaction vials were sealed with a septum. A gentle inlet flow of compressed air was introduced to the reaction vials via needle and the exhaust gas was outlet through a second needle into thin walled orange tubing. This tubing was immersed in a dry ice and water bath, the temperature of which remained at 4 °C. This cold trap condensed any volatilized crosslinker given off by the reaction, but was not sufficiently cold to condense hydrogen sulfide. The exhaust gas exited the tubing into a Dreschel bottle where it was bubbled through an aqueous solution of lead (II) acetate trihydrate (50 g in 200 cm^3). After the overnight curing stage, the precipitate was filtered off over pre-weighed filter paper and desiccated for a week before its mass was measured again. These reactions were carried out in triplicate to allow averaging of the masses of lead sulfide, and calculation of standard deviations. Note that some hydrogen sulfide may have become trapped within bubbles inside the polymer structure after it vitrified, preventing it from reaching the lead (II) acetate solution. It is also probable that the exhaust gases of the reactions bubbled through the lead (II) acetate solutions too quickly to allow all of the hydrogen sulfide to react. Additionally, not all the precipitate could be collected from the Dreschel bottles, as some remained firmly stuck to the container or trapped within the glass inlet tube of the Dreschel head. Because of these factors it is predicted that the amount of hydrogen sulfide given off by these reactions is higher than what has been represented here. This is supported by the fact that the quantity of hydrogen sulfide given off, as indicated here, is approximately 50 mg, which is not enough to account for the total losses in the yield. Regardless, a qualitative comparison between the catalysed and uncatalyzed gas capture reactions gave statistically significant results. It was found that a reaction catalysed by Zn(DEDC)$_2$ gives off less hydrogen sulfide (0.93 mmol, 32 mg) than the equivalent uncatalyzed reaction, providing confidence that hydrogen sulfide formation is a loss to the yield and that catalysis minimizes this loss (Figure 2.6b).

Once a robust method was established, the inverse vulcanisation of DVB and sulfur was repeated numerous times with 0.28 mmol of various catalysts. A standard catalyst loading of 0.28 mmol was chosen, because it corresponds to a 1 % weight loading (100 mg) of the previously most reported catalyst, Zn(DEDC)$_2$, in a 10 g scale reaction. The equivalent molar loading of all catalysts used corresponds to a molar ratio of approximately 137 : 70 : 1 in terms of DVB : S$_8$: catalyst.

For each reaction three main variables were used to judge the efficacy of a catalyst. The first of which was the vitrification time, defined as the time elapsed between the addition of the DVB to the molten sulfur and the moment at which the reaction solution became too viscous for the stirrer to rotate. A shorter vitrification time is indicative of a greater rate of reaction and a greater rate enhancement provided by the catalyst in question.

The second variable used to judge the efficacy of the catalysts was the yield of the reaction. Naturally, a higher yield is desirable, but this is even more so here, as an increased yield may mean fewer toxic hydrogen sulfide emissions. A higher yield may also be indicative of a facet of the mechanism, as it has been suggested that the formation of hydrogen sulfide is the result of hydrogen abstraction from the organic comonomer molecule; thus, a higher yield may indicate a catalyst that is more effective at suppressing hydrogen abstraction by providing a faster competing kinetic pathway for inverse vulcanisation to occur by.[2.7]

The third variable by which the catalysts' efficacies were judged was the T_g of the product polymers, obtained by DSC. A more cross-linked polymer, with a more uniformly crosslinked structure, should have a higher T_g value. This is because the polymer structure increases in rigidity with increasing crosslinking, making it harder for the polymer chains to move over one another. Thus, more thermal

Liam James Dodd

energy is required to overcome this immobilization, giving a higher T_g value. Therefore, in this study, the T_g value is used as an indication of how crosslinked a polymer is and therefore how effective the catalyst is. A more effective catalyst may drive a reaction further toward completion and increase double bond consumption, thereby increasing the crosslinking density and the T_g value. A more effective catalyst may also promote more uniform crosslinking if it acts as a phase transfer catalyst, as the reaction will no longer be constrained to the phase boundaries, thus preventing microscopic regions of high crosslinking and regions of less crosslinking. Typical DSC thermograms of inverse vulcanised polymers that were synthesized in this work can be found Figure 2.7. All DSC data were obtained using a TA instruments discovery series DSC25 equipped with an RCS coolant system and Tzero aluminium hermetic pans and lids, using a heating rate of 10 °C min^{-1} and a cooling rate of 5 °C min^{-1} in the range of 0 °C to 150 °C, except where a polymer had a low glass transition temperature, in which case the lower limit of the heating range was extended to -80 °C. Note that none of the obtained DSC thermograms indicated the presence of unreacted crystalline elemental sulfur when DVB was the organic comonomer, which would be evident from the melting transitions of crystalline S_8 at 95 and 115 °C.[2.5,2.8-2.11]
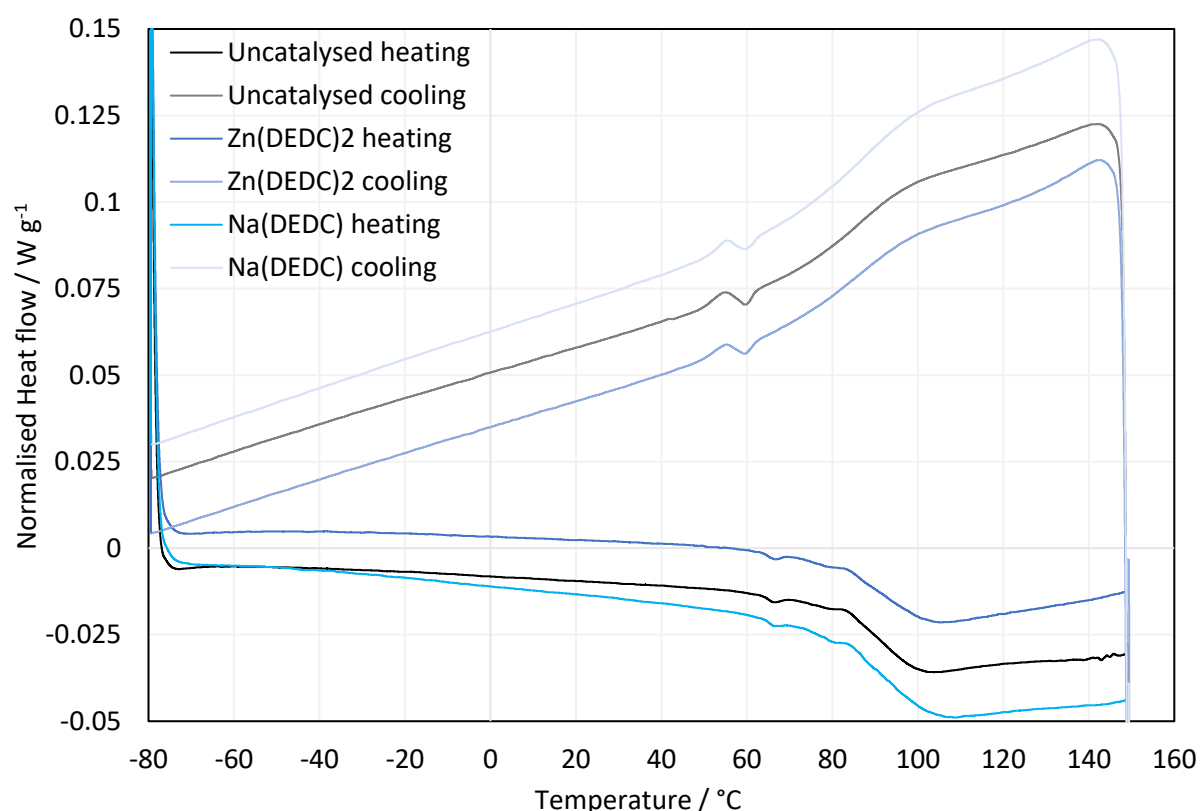
Figure 2.7: Representative DSC thermograms of several product polymers of catalytic inverse vulcanisations. The feature in the cooling curves at about 60 °C is an artefact.

Additionally, the FTIR spectra (all recorded on a Bruker Vertex 70 FTIR diamond crystal platinum ATR) of all polymers were recorded and compared to that of the neat organic comonomer used in their synthesis, usually DVB, to identify any characteristic peaks of unpolymerized vinyl bonds. Representative FTIR spectra are shown in Figure 2.8 and Figure 2.9. Most polymer spectra contained extremely weak signals that could be ambiguously assigned to those of unpolymerized vinyl bonds, but due to the weak nature of these signals and the fact that all polymer spectra were nearly identical for a given organic comonomer, the FTIR analysis holds little diagnostic value in the judgment of each catalyst's efficacy. The insolubility of the resultant polymers prohibited solution NMR.

Liam James Dodd
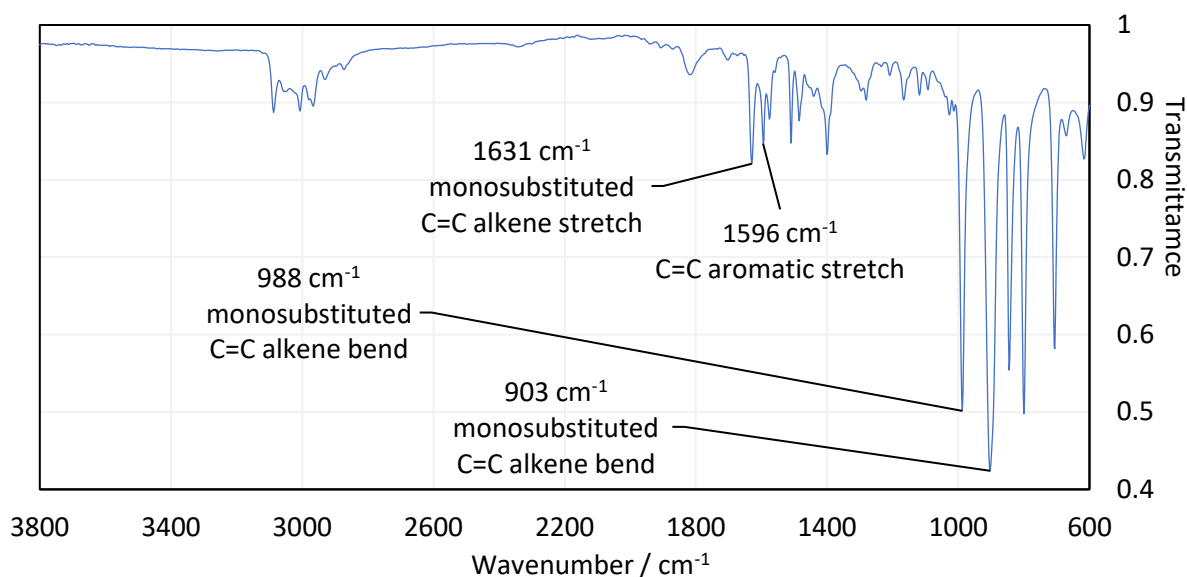
Figure 2.8: The FTIR spectrum and assignments of neat DVB.
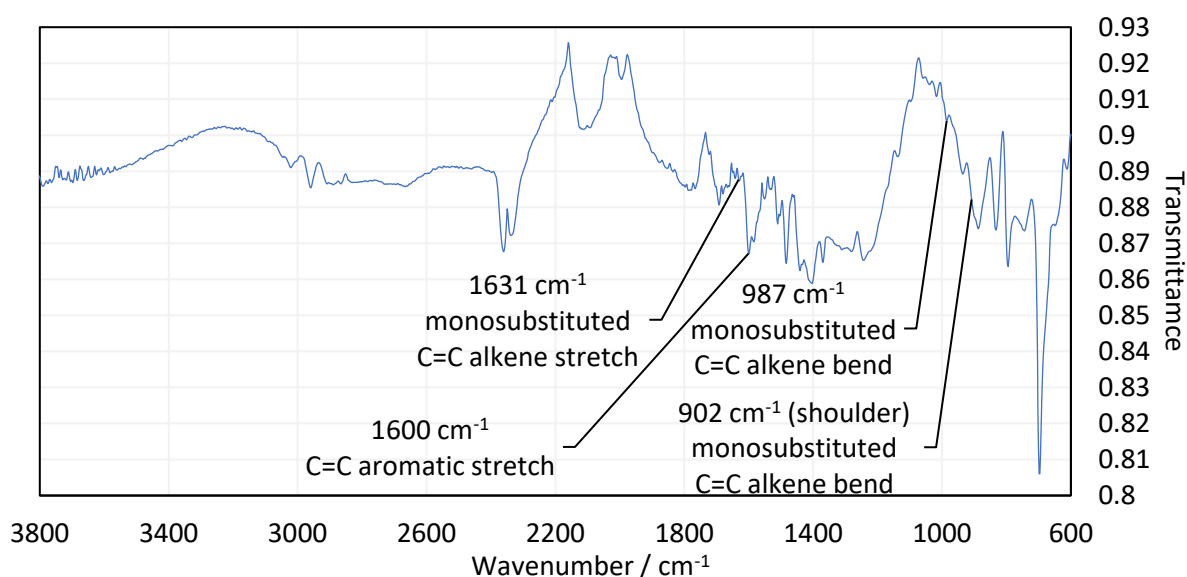
Figure 2.9: FTIR spectrum and assignments of a DVB inverse vulcanised polymer formed by catalytic inverse vulcanisation using 0.28 mmol Na(DEDC) as a catalyst.

Solubility studies were also initially conducted as a measure of the crosslinking of the polymers. While a fully crosslinked network is insoluble, an incomplete reaction can leave a soluble fraction of shorter chain oligomers that are not a part of the crosslinked network. A good catalyst can promote complete reaction, incorporating such soluble oligomers into the crosslinked network, thereby reducing the solubility. The solubility study method, which was used to obtain the data seen in Figure 2.6, was as follows. The polymers were ground to powder and 500 mg (± 0.9 mg) of this powder was immersed in 10 mL of chloroform in pre-weighed vial 1 ($mass_{V1pre}$). Vial 1 was sealed tightly and left for 24 hours, after which time, the chloroform solution was withdrawn (leaving the undissolved solid behind) using pre-weighed glass pipette 1 ($mass_{P1pre}$) and filtered through a second pre-weighed glass pipette equipped with cotton wool ($mass_{P2pre}$) into pre-weighed vial 2 ($mass_{V2pre}$). The chloroform was left to fully evaporate (typically two to three days) after which time the new masses of vial 1 ($mass_{V1new}$), vial 2 ($mass_{V2new}$), pipette 1 ($mass_{P1new}$) and pipette 2 ($mass_{P2new}$) were measured. The soluble and insoluble fractions were calculated by use of the following equations:

Liam James Dodd

$$Soluble\ fraction\ (\%) = \frac{mass_{V2new} - mass_{V2pre}}{500\ mg} \times 100$$

$$
\begin{aligned}
&Insoluble\ fraction\ (\%) \\
&= \frac{mass_{V1new} + mass_{P1new} + mass_{P2new} - mass_{V1pre} - mass_{P1pre} - mass_{P2pre}}{500\ mg} \times 100
\end{aligned}
$$

It was predicted that the soluble and insoluble fractions should summate to the initial mass of polymer powder used, however this was never the case as the soluble and insoluble fractions usually summated to greater than the initial mass of polymer. This is theorised to be the result of chloroform becoming entrapped within the polymer matrix and contributing to its mass. This would predominantly affect the insoluble fraction's mass. The solubility studies conducted on various polymer samples with the exception of the data shown in Figure 2.6, showed there was no inherent trend that could be established, thought to be the result of a large margin of error in the data which made it impossible to measure such small values accurately (the soluble fraction was almost always less than 1 %), thus the time-consuming solubility studies were discontinued.

2.5. Benchmarks for the Catalytic Trials

The uncatalyzed inverse vulcanisation of DVB was used as a control reaction, followed by catalytic inverse vulcanisations using $Zn(DEDC)_2$ and $Na(DEDC)$ as benchmarks, since these are the two most detailed catalysts in the previous work. Consistent with previous findings, both $Zn(DEDC)_2$ and $Na(DEDC)$ decreased the vitrification time, improved the yield, and enhanced the T_g value of the product polymers (Figure 2.10). Further consistent with previous findings, $Na(DEDC)$ was found to be the more effective catalyst, and this conclusion has been further reinforced in this work, as all the catalysts have been tested in equal molar quantities.[2.1]

The finding that $Na(DEDC)$ gives a greater rate enhancement than $Zn(DEDC)_2$, despite having one fewer ligand, hints at the importance of the identity of the cation in the catalyst. There is, however, no certainty that these catalysts use the same mechanism, which may explain the significant difference in vitrification times between these two metal DEDC's. In fact, later experiments further suggested that $Na(DEDC)$ does in fact use a different mechanism.

To increase confidence that the vitrification time is a good measure of the rate of the reaction, an NMR kinetics experiment was performed upon the aforementioned inverse vulcanisation experiments with no catalyst and $Zn(DEDC)_2$ and $Na(DEDC)$ as catalysts. The method for these experiments is as follows. Dimethylformamide (DMF) was added to $CDCl_3$ to obtain a $CDCl_3$ NMR solvent with 10 mg/mL of DMF as an internal standard. Three reactions were run as described in the general method for inverse vulcanisation, using no catalyst, $Zn(DEDC)_2$ and $Na(DEDC)$ respectively each in a single iteration. Over the course of the reactions, aliquots were removed from each reaction mixture, and were quenched in a pre-weighed glass vial cooled by liquid nitrogen. The vials were weighed again and an appropriate volume of $CDCl_3$ solution with DMF internal standard was added to the now known mass of aliquots, such that the aliquot solutions were approximately 10 mg/mL with respect to the reaction aliquot, suitable for NMR spectroscopy. The exact concentration of the aliquots was calculated for each case since the volume of solvent added and the mass of the aliquots were known. These aliquot solutions were then analysed by ^{1}H NMR on the University of Liverpool DPX400 instrument. All spectra were calibrated by the DMF formamide peak to 8.02 ppm. The ratio of the integrations of the DMF formamide peak (integration between 7.94 ppm and 8.10 ppm in all cases) and the alkene region peaks (integration between 5.00 ppm and 6.00 ppm in all cases) was calculated for each aliquot. Then, these ratios were divided by the concentration of the aliquot, in order to take into account the varying aliquot masses and solvent volumes used to make up the samples. These

Liam James Dodd

integration ratios per unit concentration (given the letter I) were used to track the disappearance of DVB comonomer from the reaction as time progressed. This allowed calculation of the rate constants of the reaction, which was done for both first order and second order kinetic models, with second order kinetics giving the better fit. In order to simulate an aliquot taken at zero minutes into the reaction, 16.5 mg/mL of DVB in $CDCl_3$ solution with DMF internal standard was analysed by ^{1}H NMR. The integration ratio per unit concentration for this sample was called I_0. To take into account that the aliquot samples would be 50 % by mass sulfur and 50 % by mass DVB, but the I_0 sample consisted of 100 % by mass DVB, the concentration of this sample was treated as though it was half its true value: that is 8.25 mg/mL rather than 16.5 mg/mL.

The following mathematical considerations define why the ratios of the inverse of the vitrification times should be equal to the ratios of the second order rate constants. Note that a similar justification for first order kinetics can be rationalized. The integrated rate law for second order kinetics is:

$$\frac{1}{[A]_t} = kt - \frac{1}{[A]_0}$$

Where t = time, k = the second order rate constant, $[A]_t$ is the concentration at a given time and $[A]_0$ is the initial concentration. In the context of this NMR kinetics study, the aforementioned integration ratio per unit concentration is being used as a measure of the concentration, such that $[A]_0$ is replaced with $[I]_0$ and $[A]_t$ is replaced with $[I]_t$, which are the initial integration ratio per unit concentration, and the integration ratio per unit concentration at a given time, respectively.

$$\frac{1}{[I]_t} = kt - \frac{1}{[I]_0}$$

If it is assumed that the reaction mixture vitrifies at a certain degree of double bond consumption, corresponding to a particular degree of crosslinking that is sufficiently high to render the mixture immobile, and that this particular level of double bond consumption does not vary between different reactions with the same mass loading of DVB, (assuming no net influences of DVB homopolymerisation and that, even with potentially differing mechanisms, the degree of crosslinking needed to immobilize the reaction is the same) then the vitrification time can be defined as t_{vit} and the $[I]_t$ that vitrification occurs at can be defined as $[I]_{vit}$. Thus, the equation becomes:

$$\frac{1}{[I]_{vit}} = kt_{vit} - \frac{1}{[I]_0}$$

Consider then, two reactions, reaction a and reaction b. Each will have its own integrated rate law:

$$\frac{1}{[I]_{vit}} = k_a t_{vit,a} - \frac{1}{[I]_0} \text{ and } \frac{1}{[I]_{vit}} = k_b t_{vit,b} - \frac{1}{[I]_0}$$

Remembering that $[I]_{vit,a} = [I]_{vit,b}$ because it is assumed that the vitrification point depends on the degree of consumption of double bonds. If the integrated rate law for reaction a is divided by the integrated rate law for reaction b, then what remains is:

$$k_a t_{vit,a} = k_b t_{vit,b}$$

This rearranges to give:

$$\frac{k_a}{k_b} = \frac{t_{vit,a}^{-1}}{t_{vit,b}^{-1}}$$

Liam James Dodd

Thus, the ratio of two reactions' rate constants should equal the ratio of the inverse of their vitrification times. It would be possible to calculate the rate constants of all reactions performed in this work using the above relationship, though this was not done due to concerns in the magnitude of the errors. If reaction a is a known standard, with known vitrification time and a known rate constant, and reaction b is a reaction of interest with an experimentally determined vitrification time then:

$$k_{standard}\frac{t_{vit,interest}}{t_{vit,standard}} = k_{interest}$$

The results in Figure 2.10 and Table 2.1 show that the ratios of the second-order rate constants of loss of the alkene region peaks, corresponding to the reaction of DVB vinyl bonds, are comparable to the ratios of the inverse of vitrification times for the selected reactions. This suggests that the vitrification time is a good indicator of the rate of the reaction, which is simple and easy to measure.
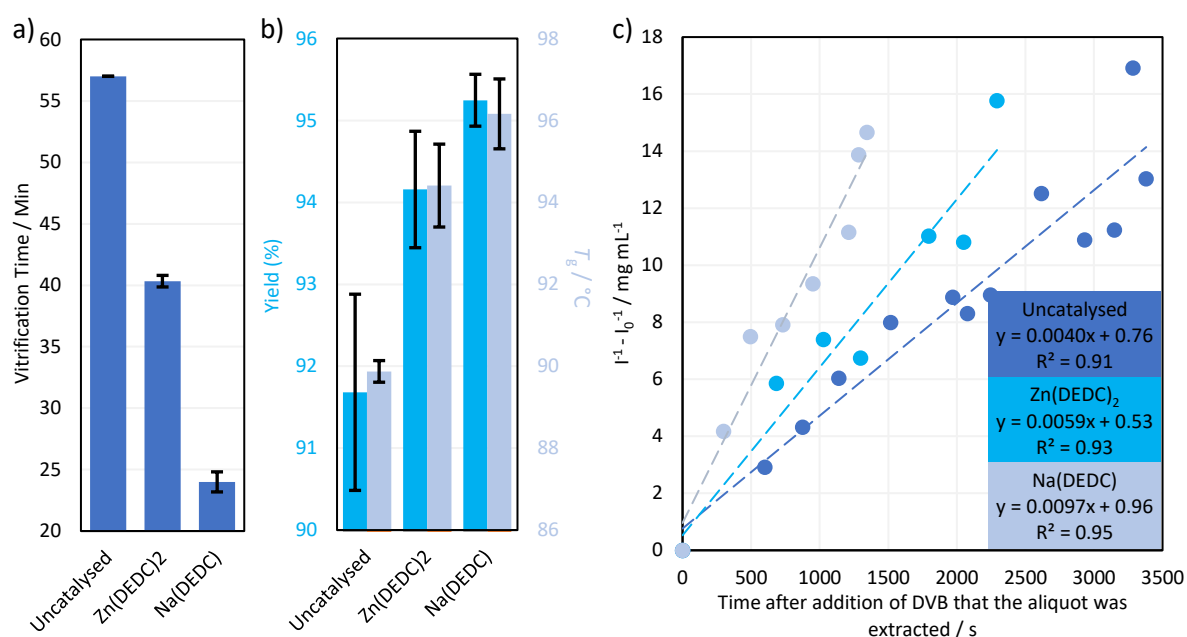
Figure 2.10: a) vitrification times, b) yields and T_g's and c) NMR kinetics plots for an uncatalyzed inverse vulcanisation and catalytic inverse vulcanisations using Zn(DEDC)$_2$ and Na(DEDC).

Table 2.1: Data from the NMR kinetics experiments.

Reaction	Uncatalyzed	Zn(DEDC)$_2$	Na(DEDC)
Vitrification time^{-1} / min^{-1}	0.0175	0.0248	0.0417
Ratio of vitrification time^{-1}	1	1.41	2.38
NMR kinetics 2nd order rate constant ± standard error / mg mL^{-1} s^{-1}	3.96×10^{-3} ± 0.38×10^{-3}	5.89×10^{-3} ± 0.74×10^{-3}	9.65×10^{-3} ± 0.87×10^{-4}
Ratio of the 2nd order rate constants	1	1.49	2.44

2.6. Effects of Catalyst Cation Identity

Following on from the conclusion that the identity of the cation is of importance in the mechanism of catalytic inverse vulcanisation, several catalysts were tested for their alternative cations: Ag(DEDC), a monovalent cation, Fe(DEDC)$_3$, a trivalent cation, and NH$_4$(DEDC), a non-metallic cation, the last of which was tested in both a 0.28 mmol loading and a 0.56 mmol loading (Figure 2.11). NH$_4$(DEDC) was amenable to being tested in different mass loadings, as it was sufficiently poor as a catalyst that a higher loading did not induce the TNE.

Liam James Dodd

It is challenging to draw conclusions from the data regarding Ag(DEDC) and Fe(DEDC)$_3$, since it is impossible to vary the valence of the cation without changing the number of ligands. Nevertheless, the results of these tests further indicate that catalysts need not be limited to divalent cations, as both Ag(DEDC) and particularly Fe(DEDC)$_3$ surpassed Zn(DEDC)$_2$ in terms of their rate enhancements. It is worth noting that the case of Fe(DEDC)$_3$ highlights the fact that a catalyst which provides a greater rate enhancement is not necessarily the best choice from a practical perspective: after the stirrer stopped rotating, the Fe(DEDC)$_3$ reactions underwent the TNE, which is known to cause rapid and inhomogeneous polymerisations that detrimentally affect the properties of the product polymers, explaining the poor T_g value (41.8 ± 0.4 °C) for this catalyst's product polymer. The vitrification time data for Fe(DEDC)$_3$ should still be valid and be unaffected by the TNE, as the auto-acceleration occurred after the stirrer had ceased to rotate. If a smaller loading of Fe(DEDC)$_3$ were to be used, then the TNE could likely be avoided. Interestingly, as reported in a review article, polysulfide anions, a potential reactive intermediate in catalytic inverse vulcanisation, preferentially complexed to iron (III) over iron (II).[2.12] If polysulfide anions are present in catalytic inverse vulcanisation, then this affinity for iron (III) may give some explanation as to why Fe(DEDC)$_3$ was such a powerful catalyst and why it was superior to Fe(DEDC)$_2$ in terms of vitrification time, the results for which will be discussed later.
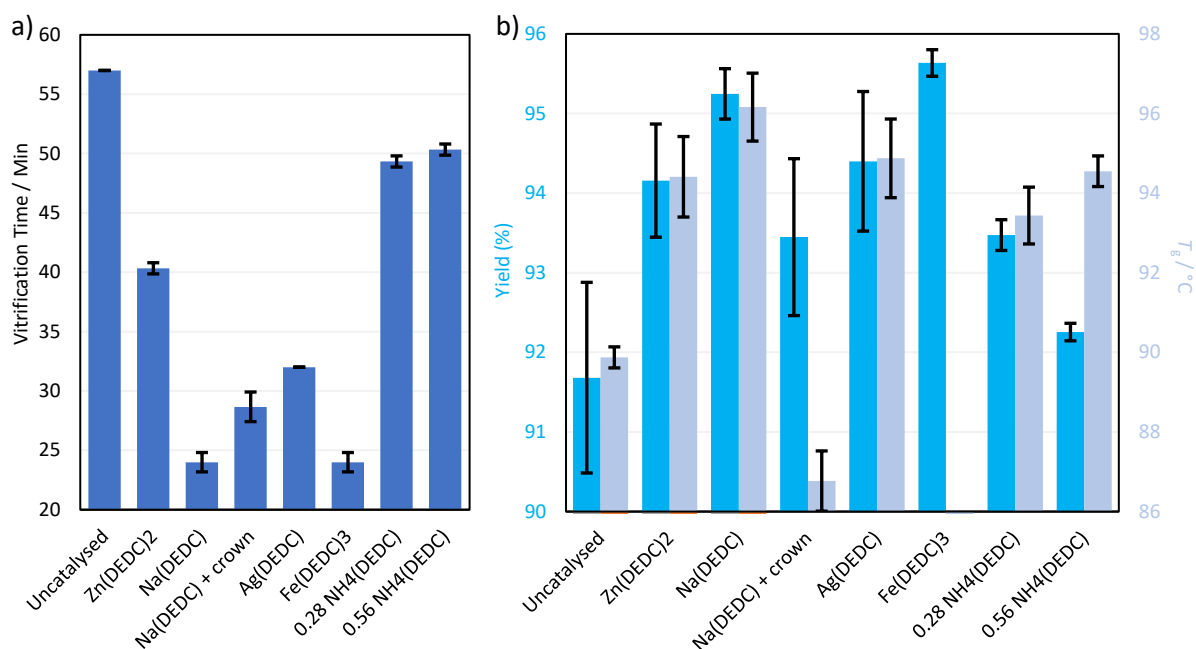
Figure 2.11: a) vitrification times and b) yields and T_g's of inverse vulcanisation and catalytic inverse vulcanisations using Zn(DEDC)$_2$, Na(DEDC), Na(DEDC) + 15-crown-5, Ag(DEDC), Fe(DEDC)$_3$, 0.28 mmol NH$_4$(DEDC) and 0.56 mmol NH$_4$(DEDC). The T_g of Fe(DEDC)$_3$ is 41.8 ± 0.4 °C and is low due to the TNE.

In contrast, NH$_4$(DEDC) provided relatively poor rate enhancements in both its 0.28 and 0.56 mmol loadings. This may be because NH$_4$(DEDC) has a non-metallic cation which should lack the capability of monomer binding that metallic cations are capable of, suggesting that monomer complexation is an important part of the mechanism. An alternative explanation of NH$_4$(DEDC)'s poor rate enhancement, which also explains why the 0.56 mmol loading of NH$_4$(DEDC) provided a smaller rate enhancement than the 0.28 mmol loading, is that the ammonium cation acidifies the reaction, potentially deactivating any nucleophiles, such as polysulfide anions, that may be present in the reaction.[2.12,2.13] Though poor, NH$_4$(DEDC) still provided some rate enhancement, which suggests that, even if the cation is not capable of binding a monomer, the ligand will still have importance in the mechanism. This is also a reflection of the proposed mechanism that the ligand in the catalyst might

Liam James Dodd

aid sulfur – ring opening. As a final note on $NH_4(DEDC)$, the yield data are complicated by the loss of ammonia from the catalyst during the reaction, and a further complication is that amines, including ammonia, can break sulfur – sulfur bonds and so may participate in the mechanism.[2.14,2.15]

To determine whether the sodium ion has importance in the mechanism of catalytic inverse vulcanisation, 15-crown-5, which is a crown ether that is well-known to complex and capture the sodium ion, was used in an equimolar quantity with Na(DEDC). When a catalytic inverse vulcanisation using Na(DEDC) was performed in the presence of an equimolar quantity of 15-crown-5, it was found that the vitrification time was longer than that when the 15-crown-5 was absent. This may be explained by the need for the sodium ion to be exposed to enable interaction with the monomers: when they are complexed to the sodium ions, 15-crown-5 ligands are likely to inhibit any interaction of the monomers. The reaction in the presence of 15-crown-5 was still significantly faster than that of the uncatalyzed inverse vulcanisation of DVB, which suggests several possibilities: that there may still have been some free sodium ions; that interaction of the monomers to the sodium ions is not completely prohibited; or that the sodium ion is not essential in the mechanism but is assistive in achieving faster rates. How exactly the sodium ion interacts with the monomers and accelerates the reaction is unclear, since Lewis acidity in the sodium ion's behaviour would be surprising, and this dissuades from the conclusion that the sodium ion is binding the monomers, and may instead have an interaction that is not as yet identified. As such, Na(DEDC) may present some mechanistic differences from that proposed in Figure 2.2. Further confidence in the importance of monomer binding as a mechanistic step can be found in the work presented by Draganjac *et al.*, which details a variety of metal – ligand complexes that have polysulfide anions as ligands. Such complexes stabilize the formation of polysulfide anions while maintaining their reactivity.[2.15]

The aforementioned results strongly suggest that the identity of the metal cation is of importance in the mechanism of catalytic inverse vulcanisation. Therefore, a series of period 4 d-block cation based catalysts, $Mn(DEDC)_2$, $Fe(DEDC)_2$, $Co(DEDC)_2$, $Ni(DEDC)_2$, $Cu(DEDC)_2$, and $Zn(DEDC)_2$, were tested in inverse vulcanisation reactions to investigate the effect of changing the metal ion itself while keeping the ligands and the conditions constant. It was expected that the softness of the metal cation would affect the strength of coordination of the monomers, although several other factors, such as orbital vacancies and complex geometry, may also influence the results. Unfortunately, the syntheses of $Mg(DEDC)_2$ and $Ca(DEDC)_2$, two catalysts that would provide a more straightforward probe of the softness, were failures.[2.16,2.17] $Mn(DEDC)_2$ was synthesized successfully by a literature method, the details of which can be found in Section 2.15.1 along with the characterisation data.[2.16] This literature method follows the following general reaction scheme: $x\ Na(DEDC) + M^xCl_x \rightarrow M^x(DEDC)_x + x\ NaCl$.[2.16] This may explain why the synthesis of $Mn(DEDC)_2$ was successful but the syntheses of $Mg(DEDC)_2$ and $Ca(DEDC)_2$ were failures: The reaction is enthalpically driven by the thermodynamic favourability of forming sodium chloride over the metal chloride reagent. This is successful in the case of $Mn(DEDC)_2$, but is not successful for $Mg(DEDC)_2$ and $Ca(DEDC)_2$ because the formation of sodium chloride over magnesium chloride or calcium chloride is not sufficiently favourable to drive the reaction.

Regardless, observing Figure 2.12a, the vitrification time rises and then falls from left to right across the periodic table, finally increasing again upon reaching zinc, which could be a result of zinc (II) having a complete d subshell. When the vitrification time is plotted against the $\Delta G°_{f,m2+}$(aq) value, which may be used as a natural index of the softness of the cation, that is a more positive value indicates a softer cation, a tentative trend emerges.[2.18] Figure 2.12c indicates that, to some extent, a softer cation gives a faster vitrification time, with manganese (II) and cobalt (II) being outliers to this trend. One potential reason for $Mn(DEDC)_2$'s deviation from the trend may be due to decomposition of the catalyst during the reaction, as it was found that, when $Mn(DEDC)_2$ was heated to 100 °C for 1 h, it had decomposed

Liam James Dodd

from a burgundy powder to a brown sludge, which had an FTIR spectrum significantly different from that of Mn(DEDC)$_2$ (Figure 2.25 in Section 2.15.1). Additionally it was found that Mn(DEDC)$_2$ decomposed from a burgundy powder to a pale brown powder over the course of months under ambient conditions. The other first-row transition-metal catalysts, including Fe(DEDC)$_3$, did not thermally decompose. No explanation as to why Co(DEDC)$_2$ deviates from the trend can be given at this time. It is possible that Mn(DEDC)$_2$ and Co(DEDC)$_2$ use alternative mechanisms in comparison to the other metal centres, but no evidence or explanation for this can be found. Regardless, given that two of the six reactions' vitrification times must be ignored to acquire this trend, it cannot be stated with any confidence that the vitrification time is linked to the cation softness, and it may be that the trend in Figure 2.12c is a coincidence. However, it can be noted that copper (II) diethyldithiocarbamate provided the best performance of all of the tested catalysts, if equal weighting is given to the three factors of rate, yield, and T_g. This could well be related to copper being the softest of the cations tested, giving rise to preferential interactions with sulfur.
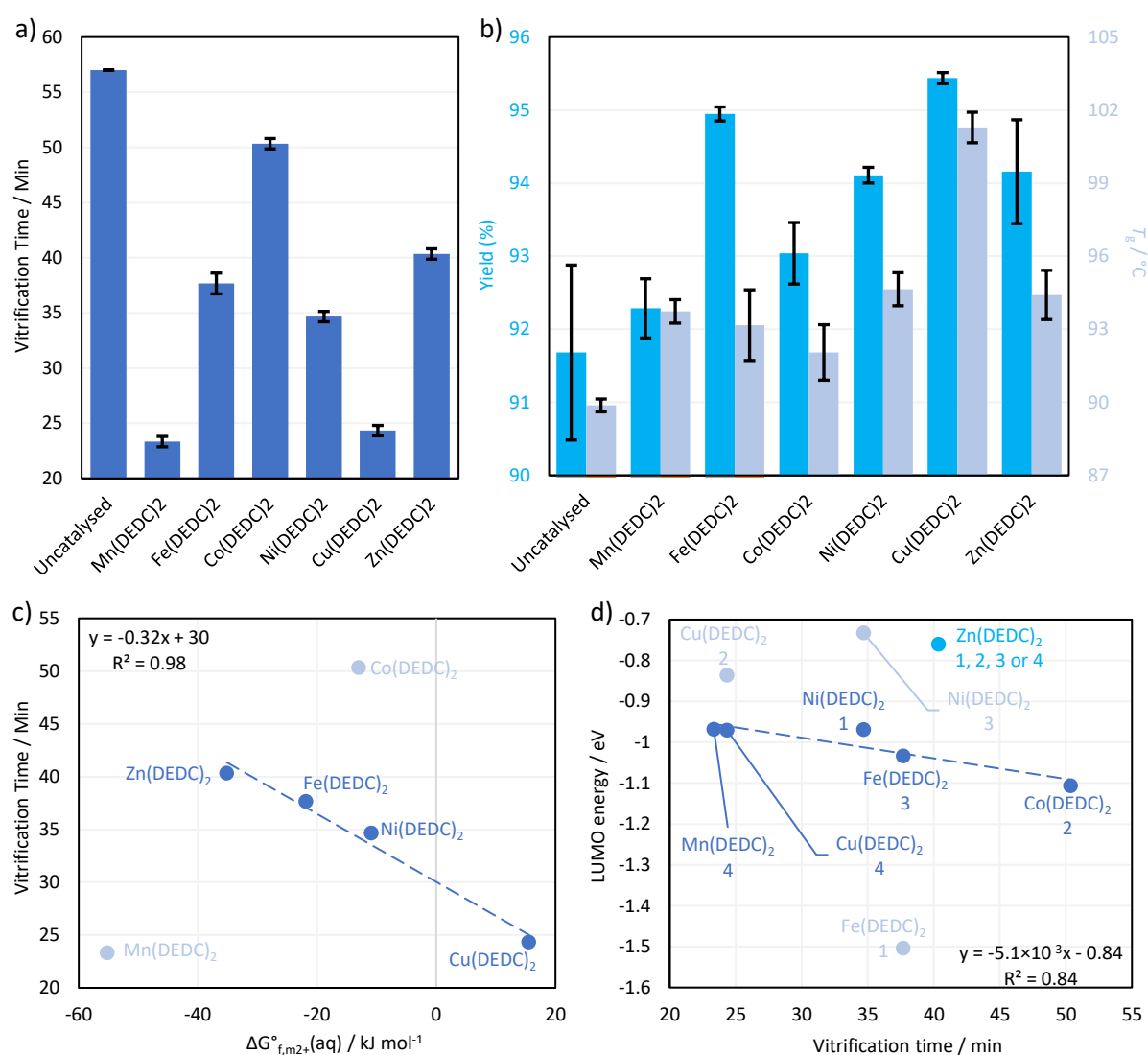
Figure 2.12: a) vitrification times and b) yields and T_g's of inverse vulcanisation and catalytic inverse vulcanisations using Mn(DEDC)$_2$, Fe(DEDC)$_2$, Co(DEDC)$_2$, Ni(DEDC)$_2$, Cu(DEDC)$_2$ and Zn(DEDC)$_2$. c) Vitrification times against the $\Delta G°_{f,m2+}$(aq) for the d-block metal cation DEDC's.[2.18] d) Vitrification times against the calculated LUMO energy for the d-block metal cation DEDC's, with the multiplicities specified. Note that for Zn(DEDC)$_2$ the HOMO and LUMO energies were the same for each multiplicity.

Liam James Dodd

Since no definite trend could be established with confidence regarding the cation softness, other potential trending factors were investigated that were not linked to the cation softness. The efficacies of the catalysts above may depend on their orbital energies, such as the HOMO energy, LUMO energy, or HOMO–LUMO gap, and it was hoped that these factors would give a clearer trend with the vitrification times. Attempts to determine the HOMO and LUMO energies experimentally by means of cyclic voltammetry provided no clear trend with the vitrification time. The detailed electrochemistry data is reported in Section 2.15.2. Instead, the HOMO and LUMO energies were calculated using DFT by the following method: the SMILES strings of $[(C_2H_5)_2NCS_2]_2M$ (M = Zn, Fe, Ni, Mn, Cu, Co), were first constructed using the MarvinSketch software.[2.19] Rough 3D geometries were then constructed using OpenBabel, which were preliminarily optimized at the molecular mechanics level (Universal Force Field) prior to optimisation using DFT at the B3LYP/6-31G+(d,p) level of theory, using the Gaussian 16 software.[2.20,2.21] The corresponding orbital energies were evaluated on these optimized structures.

As shown in Figure 2.12d, a plausible trend was found between the vitrification time and the LUMO energy, if the value for Zn(DEDC)$_2$ was ignored. Zn(DEDC)$_2$ may deviate from this trend on account of its complete d subshell, and so its LUMO will not be a d orbital, providing a valid reason for it not to adhere to the trend. This suggests that the LUMO energy influences the vitrification time of the metal d block catalysts. However, this trend is not without its theoretical weaknesses. Several of the metal DEDC's converged to unexpected geometries, namely square planar, which cannot be explained. Furthermore, several multiplicities provided computational results for the HOMO and LUMO energies; which multiplicity the complexes adopt in reality is difficult to determine. Other factors affecting the efficacy of the catalyst could include the metal – sulfur binding energy, which may influence the association and dissociation energies. It should be noted that evidence of organic comonomer binding by several different catalysts could not be detected by NMR (using the University of Liverpool Bruker DEPT400 NMR instrument) for various catalyst to comonomer molarity ratios, aligning with the conclusion that first – row transition metals do not usually coordinate alkenes and that the mechanism in Figure 2.2 may adhere to a concerted pathway. All orbital energy data can be found in Table 2.2.

Table 2.2: Orbital energies from computational chemistry for the 1st row transition metal DEDC's.

Name	Multiplicity	HOMO-1 / eV	HOMO / eV	LUMO / eV	LUMO+1 / eV	HOMO-LUMO gap / eV
Mn(DEDC)$_2$	4	-5.75902	-5.56908	-0.96791	-0.69879	4.60117
Fe(DEDC)$_2$	1	-5.12581	-4.58349	-1.50397	-0.94723	3.07951
Fe(DEDC)$_2$	3	-5.64038	-5.55058	-1.03322	-0.92219	4.51736
Co(DEDC)$_2$	2	-5.77589	-5.28227	-1.10641	-0.92301	4.17586
Ni(DEDC)$_2$	1	-4.86948	-4.74975	-0.96927	-0.89036	3.78048
Ni(DEDC)$_2$	3	-5.70242	-5.46105	-0.73226	-0.71675	4.72879
Cu(DEDC)$_2$	2	-5.93752	-4.92880	-0.83621	-0.59348	4.09259
Cu(DEDC)$_2$	4	-5.28744	-3.95000	-0.97063	0.361639	2.97937
Zn(DEDC)$_2$	1	-5.97263	-5.90378	-0.76056	-0.72437	5.14322
Zn(DEDC)$_2$	2	-5.97263	-5.90378	-0.76056	-0.72437	5.14322
Zn(DEDC)$_2$	3	-5.97263	-5.90378	-0.76056	-0.72437	5.14322
Zn(DEDC)$_2$	4	-5.97263	-5.90378	-0.76056	-0.72437	5.14322

Computational calculations provided further evidence that the metal centres do not bind the organic comonomer via the carbon – carbon double bond π orbital. Zn(DEDC)$_2$ and Cu(DEDC)$_2$, the latter being the most powerful of the metal DEDC catalysts, were modelled with DVB coordinated to the metal centre through the π orbital of a nonaromatic carbon – carbon double bond. These calculations converged to structures where DVB was totally dissociated from the metal centre, even when the

Liam James Dodd

starting structure had the DVB molecule explicitly bound as a ligand. The computational chemistry data revealed that there was no energy minimum at all where DVB was coordinated to the metal complex. This suggests that the metal centre does not bind the organic comonomer through the reactive carbon – carbon double bond and that the mechanism of catalytic inverse vulcanisation does not include such a binding as a step.

2.7. Hydropolysulfides and Polysulfide Anions in Catalysis

In addition to the metal DEDC's themselves and their identities, there are several other potential aspects to the mechanism of catalytic inverse vulcanisation. One such aspect may be hydropolysulfides, polysulfide anions, and their related metal polysulfide complexes. Hydropolysulfides and their deprotonation products are reactive species which could be intermediates in catalytic inverse vulcanisation. The IUPAC gold book defines a hydropolysulfide as "compounds having the structures RS_2H, RS_3H… RS_nH, in which S_n is a chain of sulfur atoms, and R is hydrocarbyl".[2.22] Thus a polysulfide anion is any such deprotonation product of a hydropolysulfide. The literature precedent on hydropolysulfides is limited and finely dispersed, as they have received no dedicated research efforts because they are difficult to store.[2.12]

One review reports that hydropolysulfides are most easily generated from deprotonated hydrogen sulfide (HS^-) or thiolates, both of which exist in appreciable quantities in solution due to their pK_a values of 6.8 and 8 to 9, respectively.[2.12] These deprotonated species attack on other sulfur – containing species, like RSSR, to extend their chain length. In terms of catalytic inverse vulcanisation, a metal DEDC could assist in the production of precursors to hydropolysulfides or even replace the precursors entirely and directly generate the hydropolysulfides themselves by attacking on sulfur. The review goes on to describe that hydropolysulfides are more acidic than their single – sulfur counterparts and readily form polysulfide anions.[2.12] These polysulfide anions have enhanced nucleophilicity in comparison to their analogous thiolates, which would give them enhanced reactivity as intermediates in catalytic inverse vulcanisation. Furthermore, these polysulfide anions are better one-electron donors in comparison to their single – sulfur analogues and so would be better able to promote a radical mechanism as well as an anionic mechanism, in line with the proposed theory that conventional vulcanisation may have both anionic and radical pathways.[2.23]

Additionally, polysulfide anions are good ligands to a wide range of metal centres.[2.12,2.13] The review by showed evidence that polysulfide anions preferentially complexed to iron (III) over iron (II), which may explain the superior rate enhancement provided by $Fe(DEDC)_3$ over $Fe(DEDC)_2$. Another review details a wide range of metal polysulfide complexes, almost all of which had enhanced stability in comparison to the free polysulfide anion but still maintained their reactivity, suggesting that they would be accessible and reactive intermediates in catalytic inverse vulcanisation.[2.13]

Elsewhere, the nucleophilic behaviour of polysulfide anions was demonstrated by showing their reactions α,β-unsaturated carbonyl compounds that in some cases, generated polymer products.[2.24] It was shown that polysulfide anions were amenable to phase transfer catalysis, which may provide confidence in the phase transfer action of metal DEDCs in catalytic inverse vulcanisation.[2.24] More recently, it has been demonstrated that polysulfide anions could easily be generated by the reaction of sulfur and Na_2S and that the aqueous polysulfide anions were reactive toward a divinyl compound, divinyl sulfone.[2.25] Though divinyl sulfone is a vinylic compound, the intensely electron withdrawing sulfone group activates the carbon – carbon bonds to nucleophilic attack in a conjugate addition manner. Therefore, drawing comparisons between this and the classic vinyl compounds of inverse vulcanisation, which are typically non-electrophilic, may not be appropriate.[2.25]

Liam James Dodd

Several literature sources detail methods for the synthesis of metal polysulfide complexes, many of which require only elemental sulfur and a metal complex to be mixed together, sometimes even at room temperature.[2.26–2.31] Molybdenum complexes with dithiocarbamate ligands, the same ligands as the metal DEDCs, have been used to synthesize molybdenum polysulfide complexes, using only elemental sulfur in refluxing acetone.[2.31] This provides confidence that metal polysulfide complexes may form from the metal DEDC catalysts under inverse vulcanisation conditions, giving a plausible route to the generation of reactive polysulfide anions in catalytic inverse vulcanisation, which would benefit from the aforementioned enhanced stability and maintained reactivity.

Finally, direct evidence that metal DEDC's can coordinate nucleophiles such as amines was found, which suggests that the hypothesis of polysulfide anion complexation to a metal centre could indeed stretch to metal DEDC's.[2.16] Metal DEDC catalysts may therefore form metal polysulfide complexes under inverse vulcanisation conditions, and these complexes may be reactive intermediates in the catalytic pathway.

Proving the formation of such metal polysulfide complexes under inverse vulcanisation conditions is challenging. To provide evidence for the theory that metal polysulfide complexes form under inverse vulcanisation conditions, it was attempted to synthesize several metal polysulfide complexes from metal DEDC's. 0.5 g of selected transition metal DEDC's were heated at 135 °C in the presence of 10 g of sulfur, a large excess which was an attempt to drive the equilibrium of the reaction towards the products, for one hour under nitrogen. The sulfur was then washed upon filter paper with chloroform. The chloroform was collected and removed by rotary evaporator, leaving behind the products as powders. It was then attempted to recrystallize the products from various solvents, but it was found that when the products were concentrated in solution, sulfur precipitated. This was also observed in the rotary evaporation step, though to a lesser extent as the products spent less time in concentrated solutions. It is proposed here that the precipitation of sulfur is caused by the intermolecular recombination of polysulfide ligands to form elemental sulfur. This recombination reaction would proceed more quickly in concentrated solutions, but may also proceed in dilute solutions, albeit more slowly. Nevertheless, the instability of the complexes in solution prohibited purification.

To gather further evidence of the formation of metal polysulfide complexes, the reaction of molten sulfur with several metal DEDC's was repeated. After one hour, an aliquot of the molten reaction mixture was poured into a separate container and was allowed to cool to room temperature. This aliquot was not washed with chloroform. The remaining reaction mixture was treated as before, obtaining product powders from the chloroform washes after rotary evaporation. The washed and unwashed products, along with the reagent metal DEDC's and elemental sulfur were submitted for PXRD. PXRD data were collected in transmission mode on a Panalytical X'Pert PRO MPD equipped with a high throughput screening (HTS) XYZ stage, X-ray focusing mirror and PIXcel detector, using Cu Kα radiation. Data were measured on loose powder samples held on thin Mylar film in aluminium well plates, over the range 4 to 40° in approximately 0.013° steps over 60 minutes.

As can be seen in Figures 2.13 to 2.19, several of the product powders show new peaks that are not present in the diffractograms of elemental sulfur or their respective metal DEDC reagent. While this does not prove beyond reasonable doubt that metal polysulfides have formed, it does suggest that some new species has formed from these reactions and that metal polysulfides as intermediates in catalytic inverse vulcanisation is an area that should receive further scrutiny by future research.

The presence of peaks in the diffractograms of the washed and unwashed products, that were not present in the diffractograms of the reagents were taken as evidence of the formation of a new species from the reagents, possibly a metal polysulfide. In the following diffractograms of Figures 2.13 to 2.19,

Liam James Dodd

such peaks are labelled with an asterisk. The disappearance or attenuation of some reagent peaks from the washed and unwashed product spectra may also be taken as evidence of chemical alteration, but this is more ambiguous as the peaks may simply not be sufficiently intense to be seen, amongst the other more intense peaks.

Several peaks in the product diffractograms overlap with peaks in the sulfur diffractogram, but seem too intense to be the result of sulfur. These peaks could be due to the products, or it could be that the unexpected intensities observed could be due to relatively large crystals of sulfur in the particular orientations that gives rise to that particular peak. Specifically, Co(DEDC)$_2$ gave rise to these unexpectedly intense peaks. There is also the possibility that new peaks associated with the products may not be visible due to overlapping peaks from the reagents. Particularly it is expected that the metal polysulfides will have relatively similar structures to their parent metal DEDC's and so may give similar diffractograms.

It is worth noting that all product diffractograms contain peaks from both reagents: the parent metal DEDC and sulfur. For the washed products, the solution phase decomposition of the complexes yields elemental sulfur, which is why sulfur peaks are present, despite washing, and this decomposition will likely have decreased the intensity of any peaks associated with the products. Fe(DEDC)$_3$ shows the greatest evidence of forming a new species which is in good agreement with the literature, which states that polysulfide anions have a high affinity for Fe^{3+}.[2.12]

In contrast, Ni(DEDC)$_2$ showed little evidence of chemical change. The diffractograms were also compared against a simulated diffractogram of gamma sulfur, generated in the CCDC Mercury software, from deposited data, using the same parameters as the real diffractograms.[2.35] In some cases the new peaks in the products aligned to an extent with those of gamma sulfur, but several new peaks did not. Furthermore, several very intense peaks of gamma sulfur were absent in all diffractograms, suggesting the absence of gamma sulfur.

Figure 2.13: PXRD diffractograms of elemental sulfur, Fe(DEDC)$_2$ and the washed and unwashed products of mixing molten sulfur and Fe(DEDC)$_2$.

Liam James Dodd

Figure 2.14: PXRD diffractograms of elemental sulfur, Fe(DEDC)$_3$ and the washed and unwashed products of mixing molten sulfur and Fe(DEDC)$_3$.
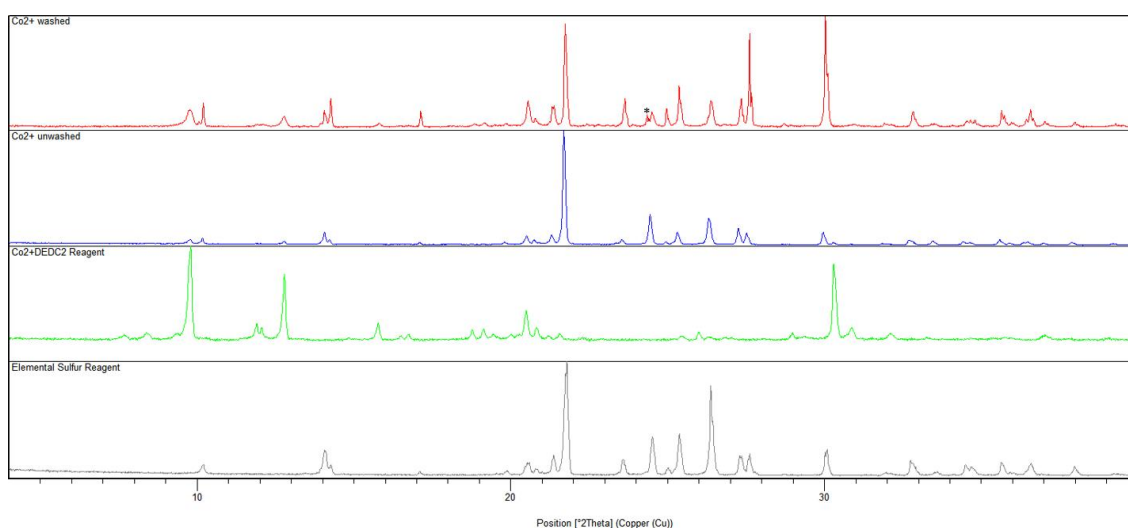
Figure 2.15: PXRD diffractograms of elemental sulfur, Co(DEDC)$_2$ and the washed and unwashed products of mixing molten sulfur and Co(DEDC)$_2$.
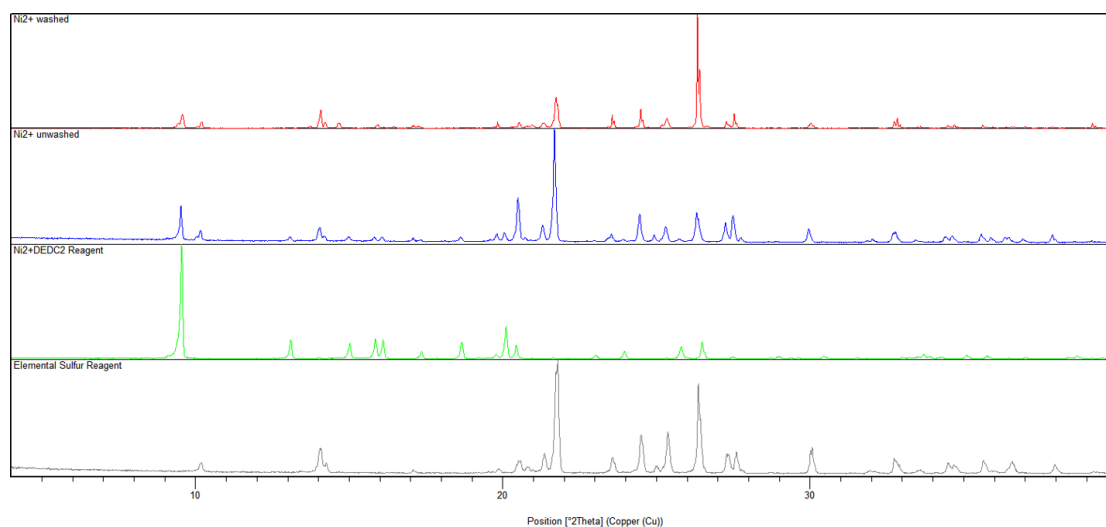
Figure 2.16: PXRD diffractograms of elemental sulfur, Ni(DEDC)$_2$ and the washed and unwashed products of mixing molten sulfur and Ni(DEDC)$_2$.

Liam James Dodd
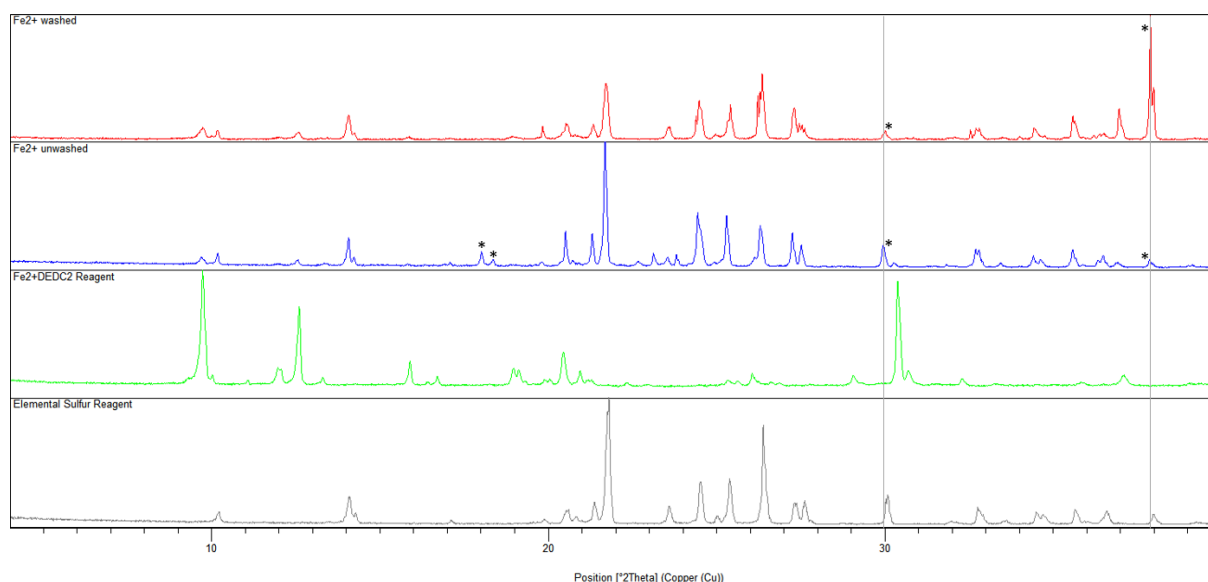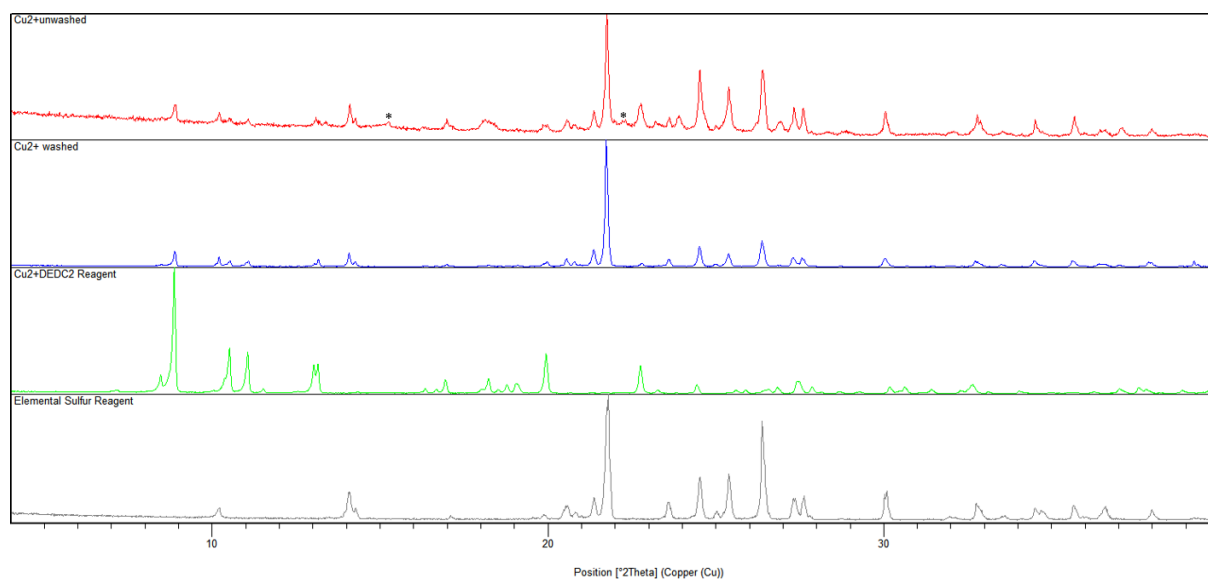
Figure 2.17: PXRD diffractograms of elemental sulfur, Cu(DEDC)$_2$ and the washed and unwashed products of mixing molten sulfur and Cu(DEDC)$_2$.
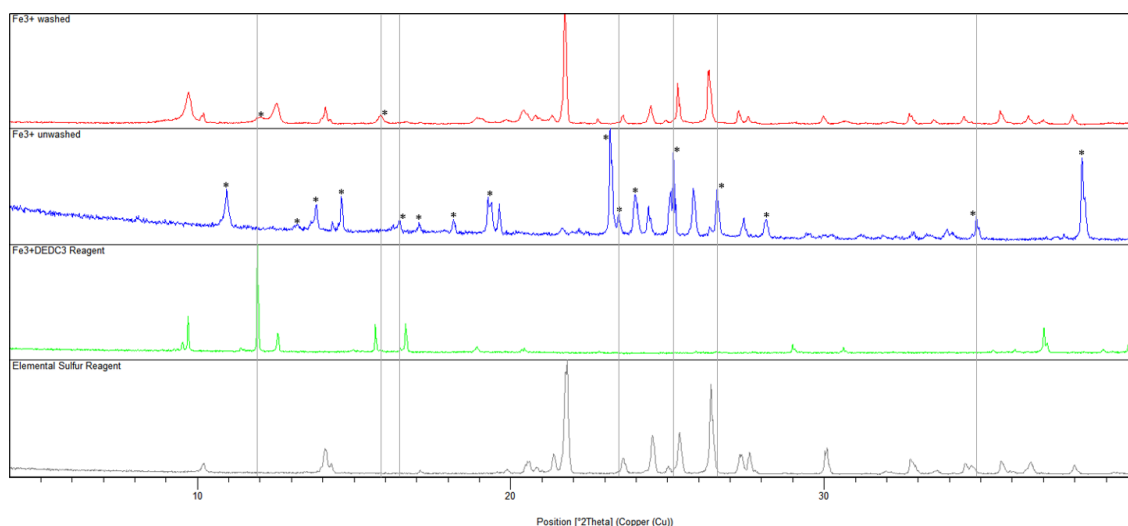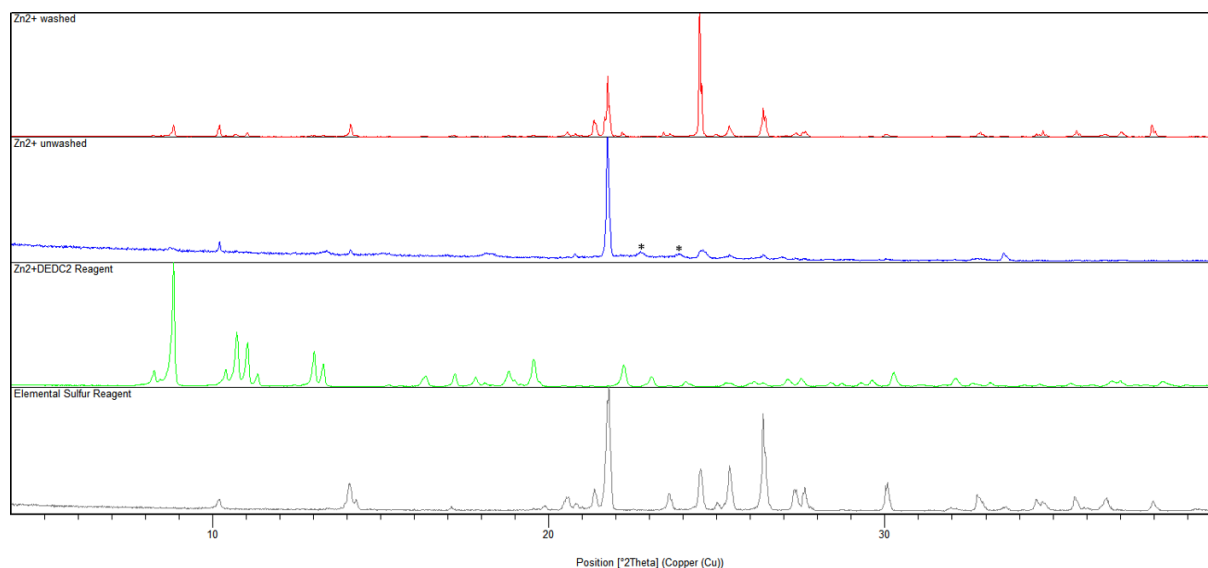

Figure 2.18: PXRD diffractograms of elemental sulfur, Zn(DEDC)$_2$ and the washed and unwashed products of mixing molten sulfur and Zn(DEDC)$_2$.

Liam James Dodd
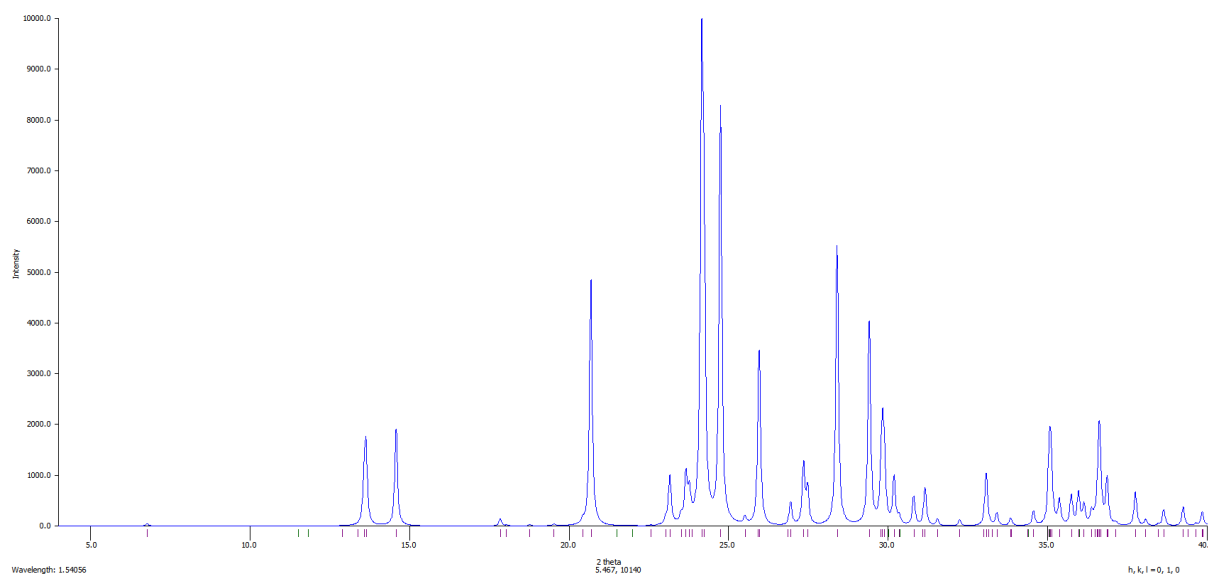
Figure 2.19: Simulated PXRD diffractogram of gamma sulfur, generated using the following parameters in the CCDC Mercury software: wavelength 1 (Angstroms): 1.54056, start (degrees 2 theta): 4, stop (degrees 2 theta): 40, step (degrees 2 theta): 0.013.

To provide some confidence that polysulfide anions could attack the organic comonomers of inverse vulcanisation, computational chemistry was employed. The nucleophilic attack of S_4^{2-} on two organic comonomers was modelled, using the nudged elastic band method at the B3LYP/DEF2-TZVP level of theory with Grimme DFT-D4 dispersion correction, on optimized reactant and product geometries was used to calculate the reaction coordinates for the nucleophilic attack of the S_4^{2-} anion upon methyl methacrylate (a simplified and less computationally demanding version of EGDMA) and separately DVB. EGDMA was of interest here because its double bond is in conjugation to an electron – withdrawing ester group and so should be primed to accept nucleophilic attack in a conjugate addition manner. The second organic comonomer of choice was DVB, because it is electron – rich and therefore may be less prone to acting as an electrophile. Additionally, nucleophilic attack on DVB would yield a carbanion. Carbanions are typically high – energy species that are not stable, even though the negative charge could delocalise into the aromatic ring in the case of DVB. This argument can be offset by the fact that this species is a catalytic intermediate and needs to have a somewhat high energy, otherwise it would be unreactive and poorly active in a catalytic pathway.

The computational experiments yielded total electronic energies for the attack of S_4^{2-} on methyl methacrylate and separately DVB. These total electronic energies do not take into account several thermodynamic factors such as entropic contributions but may be able to give some qualitative indication of the activation energies for nucleophilic attack. Nevertheless, these calculations provided electronic activation energies of 8.4 kcal mol^{-1} for methyl methacrylate and 1.5 kcal mol^{-1} for DVB, with transition state geometries that were confirmed by result of a negative frequency (imaginary mode) associated with the motion of bond – forming (Figure 2.20). These values are comparatively small for activation energy values, which further reinforces the need to evaluate them qualitatively. The result of these calculations suggest that, when it is modelled under a vacuum, S_4^{2-} should readily bind to EGDMA and DVB, when the electronic energies are considered. DVB has the lower electronic activation energy, suggesting it would bind most readily, which is a surprising result that could stem from resonance stabilization of the negative charge. Further optimizations, such as the inclusion of solvent molecules in the calculations, would likely achieve more reliable values for the true activation energies but would require intensive computational work.

Liam James Dodd
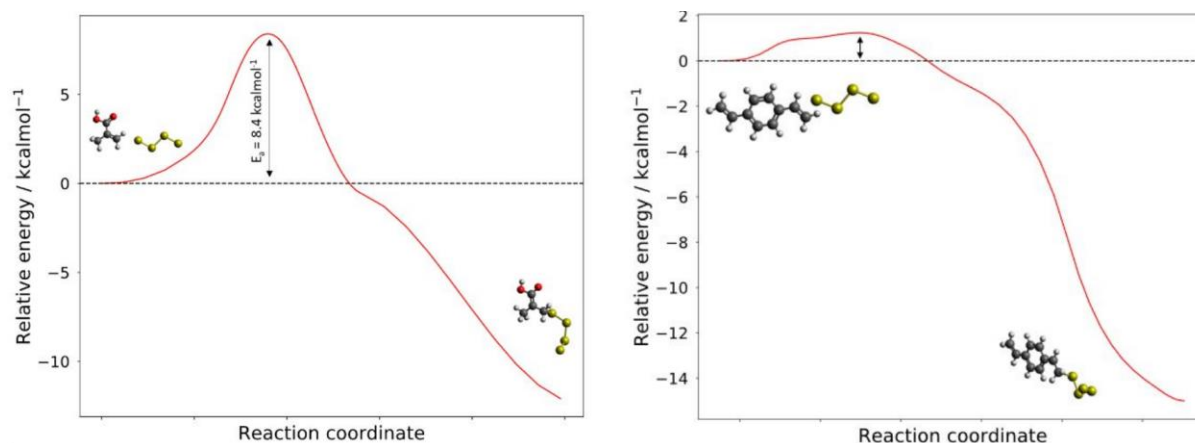
Figure 2.20: The reaction coordinates for the nucleophilic attack of the S42- anion upon methyl methacrylate (left) and DVB (right).

2.8. Phase Transfer Catalysis

To investigate the effect of the structure of the ligand upon the reaction, metal DEDC's with different alkyl chain lengths were trialled. It was previously theorised that the metal DEDC catalysts were behaving as phase transfer agents, using their dithiocarbamate moiety, which may interact favourably with the sulfur phase, to react with and bind sulfur.[2.1] This could give rise to a metal polysulfide catalytic intermediate.[2.26-2.31] Then, via the oleophilic alkyl chains on the DEDC ligand unit, the catalytic intermediate could draw the bound sulfur into the organic phase, where it can react with crosslinker molecules more readily.[2.1] Previously demonstrated was the enhanced nucleophilicity of polysulfide anions with various α,β-unsaturated carbonyl compounds and showed that polysulfide anions were amenable to phase transfer catalysis.[2.24] Furthermore, the sulfur and organic phases of inverse vulcanisations normally show poor miscibility, and initially the reactions can be seen to be in two phases (Figure 2.21). The duration of this biphasic stage varies with comonomer identity, reaction temperature, and catalysis and lasted around twenty minutes for the benchmark reaction with no catalyst in this work. When catalysis was present, the biphasic stage could be as short as five minutes. In higher temperature reactions, or reactions involving other crosslinkers, such as DCPD, the biphasic stage was also drastically shortened.
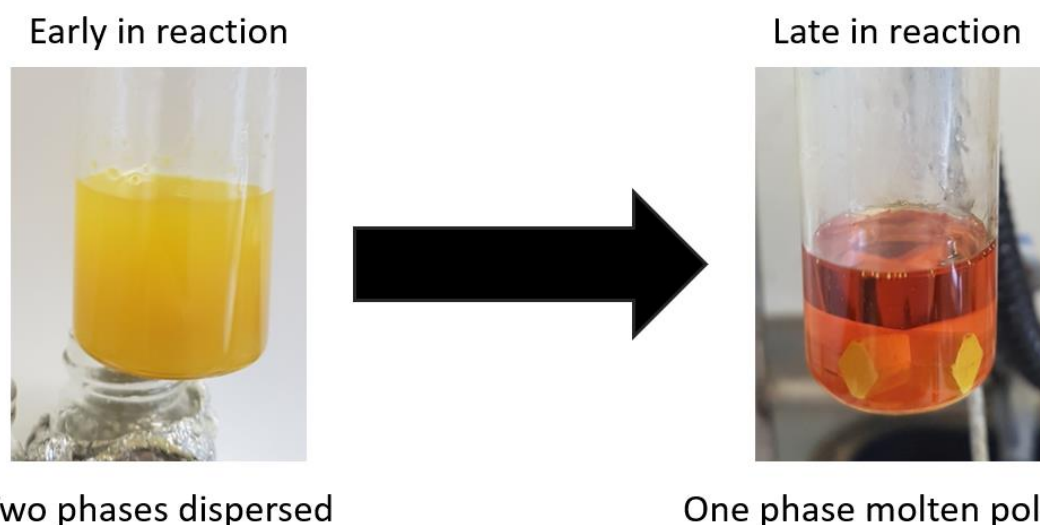
Figure 2.21: Pictures showing the biphasic and monophasic stages that occur early and late, respectively, in an inverse vulcanisation of DVB.

Liam James Dodd

Without a catalyst, it is likely that a reaction only occurs at the phase boundaries during the biphasic stage. As the reaction proceeds, organo-sulfur copolymer oligomers are formed, which increase the miscibility of the two phases until they become a single phase, which is observed in the later stages of the reaction (Figure 2.21). An amphiphilic catalyst may accelerate this process of enhancing phase miscibility. If this is indeed the case, then the length of the alkyl chains, and resultant oleophilicity of the catalyst, would be expected to influence the partitioning and therefore the reaction rate. To test this hypothesis, $Zn(DMDC)_2$, $Zn(DEDC)_2$, zinc di-n-butyldithiocarbamate ($Zn(DBDC)_2$) and zinc di-n-octyldithiocarbamate ($Zn(DODC)_2$) were trialled in inverse vulcanisation reactions (Figure 2.22). Note that $Zn(DODC)_2$ was not commercially available and had to be synthesized, the method and characterisation of which can be found in Section 2.15.3.
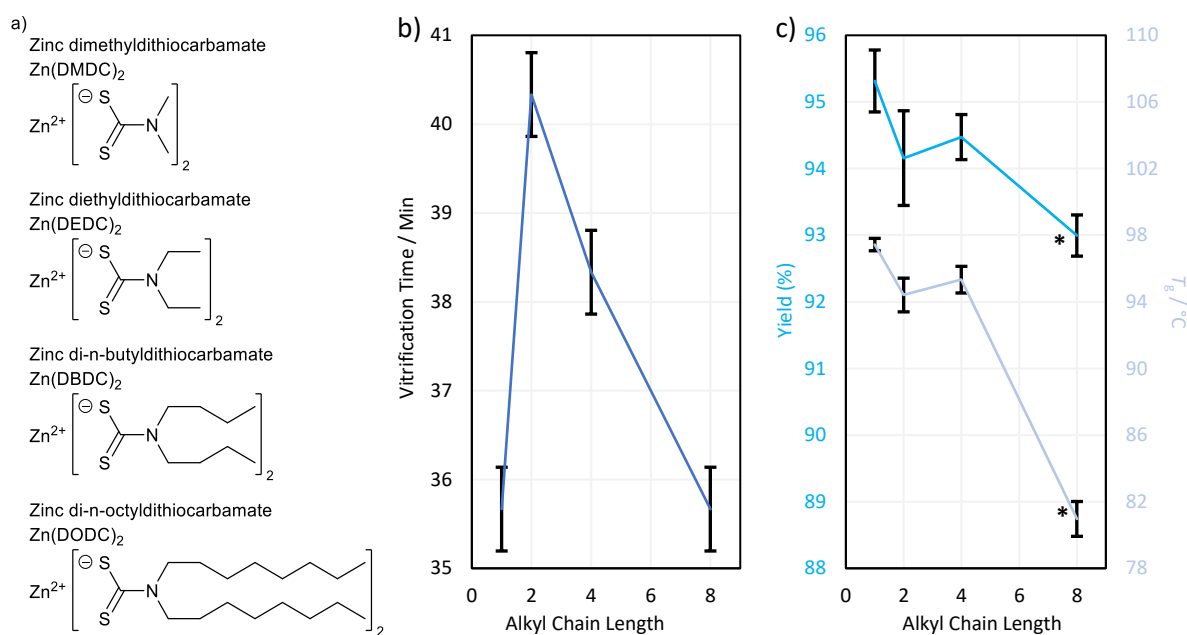
Figure 2.22: a) molecular structures of $Zn(DMDC)_2$, $Zn(DEDC)_2$, $Zn(DBDC)_2$ and $Zn(DODC)_2$, b) vitrification times and c) yields and T_g's of inverse vulcanisation and catalytic inverse vulcanisations using $Zn(DMDC)_2$, $Zn(DEDC)_2$, $Zn(DBDC)_2$ and $Zn(DODC)_2$. Data points marked with an asterisk have been detrimentally affected by the TNE.

The results seen in Figure 2.22 show there is indeed a difference in vitrification time as a function of ligand alkyl chain length, though it is not straightforward. For a chain length of two, four, or eight carbon atoms, the vitrification time decreases with increasing alkyl chain length. This increase in rate would be consistent with an increase in oleophilicity leading to improved phase transfer or compatibilization. The rapid inverse vulcanisation in the presence of $Zn(DMDC)_2$ does not follow this trend but could potentially be related to its short alkyl chains allowing more rapid diffusion. It could also be explained by the finding that less electron dense zinc dialkyldithiocarbamates were more effective catalysts in conventional vulcanisation, and thus, short chain catalysts like $Zn(DMDC)_2$ would be expected to be the most rapid.[2,3] It is important to remember that conventional vulcanisation is not amenable to phase transfer catalysis because of its overwhelming majority of the organic phase: very little sulfur is used in conventional vulcanisation. Therefore, there is no obvious reason why long chain catalysts that have been shown here to be effective in inverse vulcanisation, would also be effective in conventional vulcanisation. It is unknown why $Zn(DODC)_2$ induced the TNE during the curing step, rendering its yield and T_g data invalid, as several other catalysts had significantly shorter vitrification times and showed no evidence of the TNE. A weak explanation could be that the long

Liam James Dodd

chains of Zn(DODC)$_2$ made the reaction mixture more viscous, thereby hampering stirring and effective heat dumping, leading to the TNE, but it is hard to imagine 0.1956 g of a substance (the catalytic loading of 0.28 mmol of Zn(DODC)$_2$) being sufficiently present in a 10 g scale reaction to have that much of an effect on the reaction mixture viscosity. Indeed, Zn(DODC)$_2$ was only present as 1.9 % by mass in its reactions, which seems too small an amount to have such a great effect on the viscosity, especially when the reaction naturally forms longer and longer chain polymers as the reaction progresses, which certainly have a much higher viscosity than Zn(DODC)$_2$ and a much greater proportional presence as well. As a final note, the effect of changing the alkyl chain length is relatively small in comparison to the effect of some of the other aspects of the catalyst that have been varied. This may be because the alkyl chain length is only important in the initial biphasic stage of the reaction.

2.9. Alternatives to Classic Dithiocarbamate Catalysts

Potassium ethyl xanthogenate (KEtX) and potassium isopropyl xanthogenate (K^{i}PrX) have structural similarities to the dithiocarbamates (Figure 2.23a). KEtX can be used as an alternative to Na(DEDC) to generate carbamoyl radicals.[2.32]
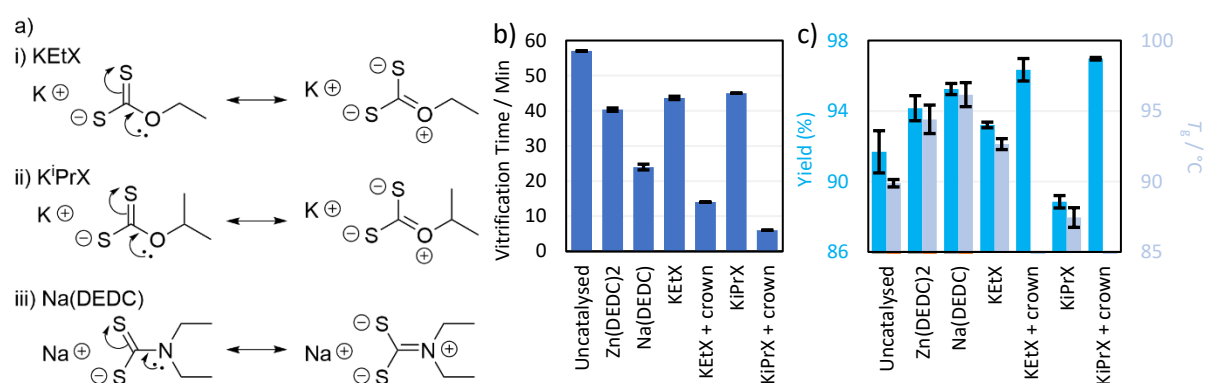
Figure 2.23: a) molecular structures and alternative resonance forms of i) potassium ethyl xanthogenate, ii) potassium isopropyl xanthogenate, and iii) sodium diethyldithiocarbamate. b) vitrification times and c) yields and T_g's of inverse vulcanisation and catalytic inverse vulcanisations using Zn(DEDC)$_2$, Na(DEDC), KEtX, KEtX in the presence of an equimolar quantity of 18-crown-6, K^{i}PrX and K^{i}PrX in the presence of an equimolar quantity of 18-crown-6. The T_g's for KEtX in the presence of an equimolar quantity of 18-crown-6 and K^{i}PrX in the presence of an equimolar quantity of 18-crown-6 are 41.7 ± 1.9 °C, and 40.9 ± 2.6 °C, respectively, and are low due to the TNE.

Figure 2.23b shows that both KEtX and K^{i}PrX provided nominal rate enhancements in comparison with Zn(DEDC)$_2$ but were significantly slower than Na(DEDC). Although a comparison is complicated by the difference in cations between Na(DEDC) and the two xanthogenates, the lower rate enhancement provided by the xanthogenates may be attributed to the fact that they each possess one fewer alkyl chain than Na(DEDC), hampering their ability to act as phase transfer agents. An alternative explanation may relate to the electron-donating power of oxygen and nitrogen. Since nitrogen is widely considered to be more effective in donating its lone pair in comparison to oxygen, the dithiocarbamate nitrogen may donate more electron density to the sulfur atoms than the corresponding oxygen of a xanthogenate (Figure 2.23a). The slightly longer vitrification time of K^{i}PrX in comparison to KEtX could be attributed to the bulkier isopropyl group causing slightly more steric hindrance, though this conclusion is made cautiously, considering how close the vitrification times are, despite being statistically significant. Interestingly, when KEtX and K^{i}PrX were used as catalysts in the presence of an equimolar quantity of 18-crown-6 (which provided a negligible rate enhancement when it was used as a catalyst alone), their vitrification times were drastically shortened, to the point

Liam James Dodd

where the TNE occurred, suggesting that complexation of the potassium ion by the crown ether activates the xanthogenate. This result is in stark contrast to the result obtained when Na(DEDC) was reacted in the presence of 15-crown-5, which hindered the reaction. This suggests that the dithiocarbamates and the xanthogenates operate by different mechanisms, indicating that the identity of the non-sulfur heteroatom is more important than anticipated. The work performed by Jung *et al.* may give some explanation for this, as their work suggests several mechanistic pathways where the dithiocarbamate carbon is directly attacked and is involved in molecular transformations.[2.16] Since the non-sulfur heteroatom of the dithiocarbamates and the xanthogenates is bonded to this carbon, it would be expected to influence its behaviour. It was also indicated that steric hindrance plays a significant role in the attack upon this centre, providing some backing to the theory that increased steric hindrance about K^iPrX is responsible for its slightly slower rate.[2.16]

2.10. Inorganic Catalysts

It was found that Na_2S could react with sulfur to produce polysulfide anions that are then capable of polymerising with alkenes in aqueous media, though it is worth remembering that a very electron deficient alkene was used in contrast to the usually electron rich alkenes that are typically used in inverse vulcanisation, and that usually, electron deficient alkenes like EGDMA are typically of low reactivity in inverse vulcanisation.[2.1,2.25] Nevertheless, Na_2S was trialled here as a comparison to the metal DEDC catalysts. It is worth noting that, since the structure of Na_2S is significantly different from those of the metal DEDC catalysts, they likely function according to different mechanisms. Na_2S, by comparison to metal DEDC catalysts, was found to be quite a poor catalyst in inverse vulcanisation, providing a vitrification time of 49.3 ± 0.3 min, only a few minutes shorter than that for the uncatalyzed inverse vulcanisation of DVB, and a yield and T_g value of 92.8 ± 0.4 % and 91.9 ± 0.1 °C, respectively, marginally higher than those for the uncatalyzed reaction.

Because it is hypothesized that the DEDC ligand of classic inverse vulcanisation catalysts acts a nucleophile and assists in cleaving sulfur – sulfur bonds, it was thought that a stronger nucleophile could make for a more active catalyst. Unfortunately, the nucleophilicity of the metal DEDC's is difficult to quantify, so as a substitute three more inorganic species, LiOH, NaOH, and KOH, were tested to allow an assessment of the effects of basicity, the results of which can be seen in Figure 2.24.[2.33]
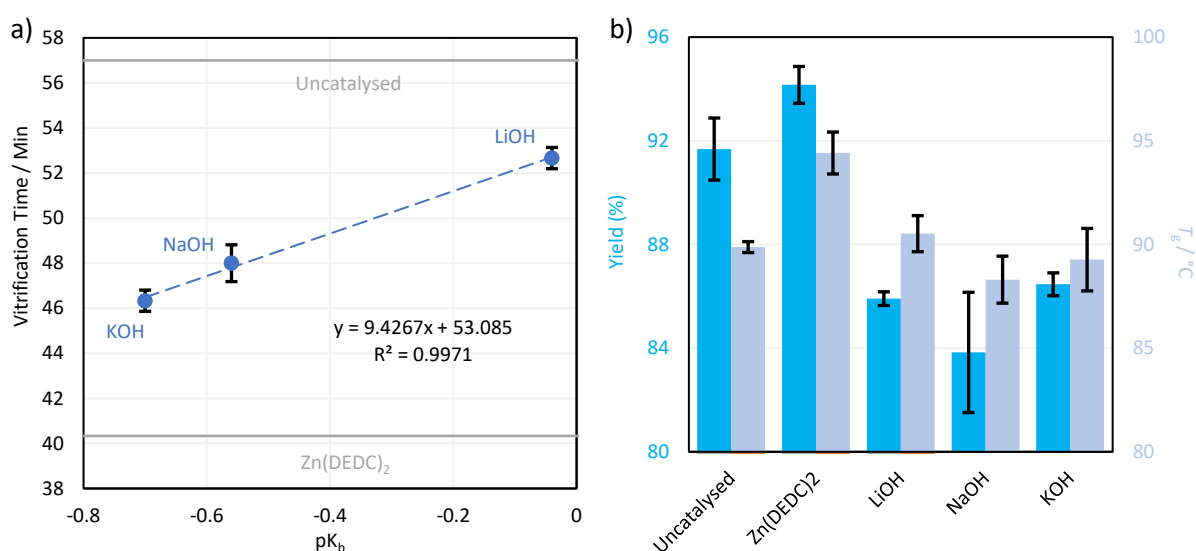
Figure 2.24: a) pK_b vs vitrification time for three alkali metal hydroxides and b) the yield and T_g of product polymers of inverse vulcanisation and catalytic inverse vulcanisations using $Zn(DEDC)_2$, Na(DEDC), LiOH, NaOH and KOH.[2.33]

Liam James Dodd

Figure 2.24 shows that with decreasing pK$_b$ comes a greater rate enhancement, suggesting that stronger bases can accelerate the inverse vulcanisation process more, possibly by the formation of polysulfide anions.[2.12,2.13] This finding is consistent with the conclusion that NH$_4$(DEDC) was acidifying the reaction when it was present in greater quantities, thus slowing the reaction. Where LiOH, NaOH, and KOH were used as catalysts, the yield of the reaction in all cases was found to be lower than the yield of uncatalyzed inverse vulcanisation, possibly explained by increased generation of H$_2$S gas in comparison to the uncatalyzed inverse vulcanisation reaction. Evidence of this was found when the KOH reaction was repeated under gas capture conditions and was found to produce more hydrogen sulfide in comparison to the uncatalyzed inverse vulcanisation of DVB, 1.55 mmol vs 1.44 mmol of H$_2$S (Figure 2.6b).

2.11. Metal Free Catalysts

Encouraged by the catalytically active organic species in the reaction, including DXDC (X = M, E, B, O), EtX, ^{i}PrX, and hydropolysulfides, a series of organo-catalysts were examined for activity in the inverse vulcanisation reaction. Metal free catalysts for inverse vulcanisation would be beneficial because they avoid metal contamination of the product polymers, which may raise concerns about toxicity. Additionally, they may offer cost savings and pose fewer issues with renewability, as there are concerns that supplies of some metals may be depleted. Thus, the metal free catalysts shown in Figure 2.25a were trialled in inverse vulcanisation reactions, the results of which can be seen in Figure 2.25b and Figure 2.25c.
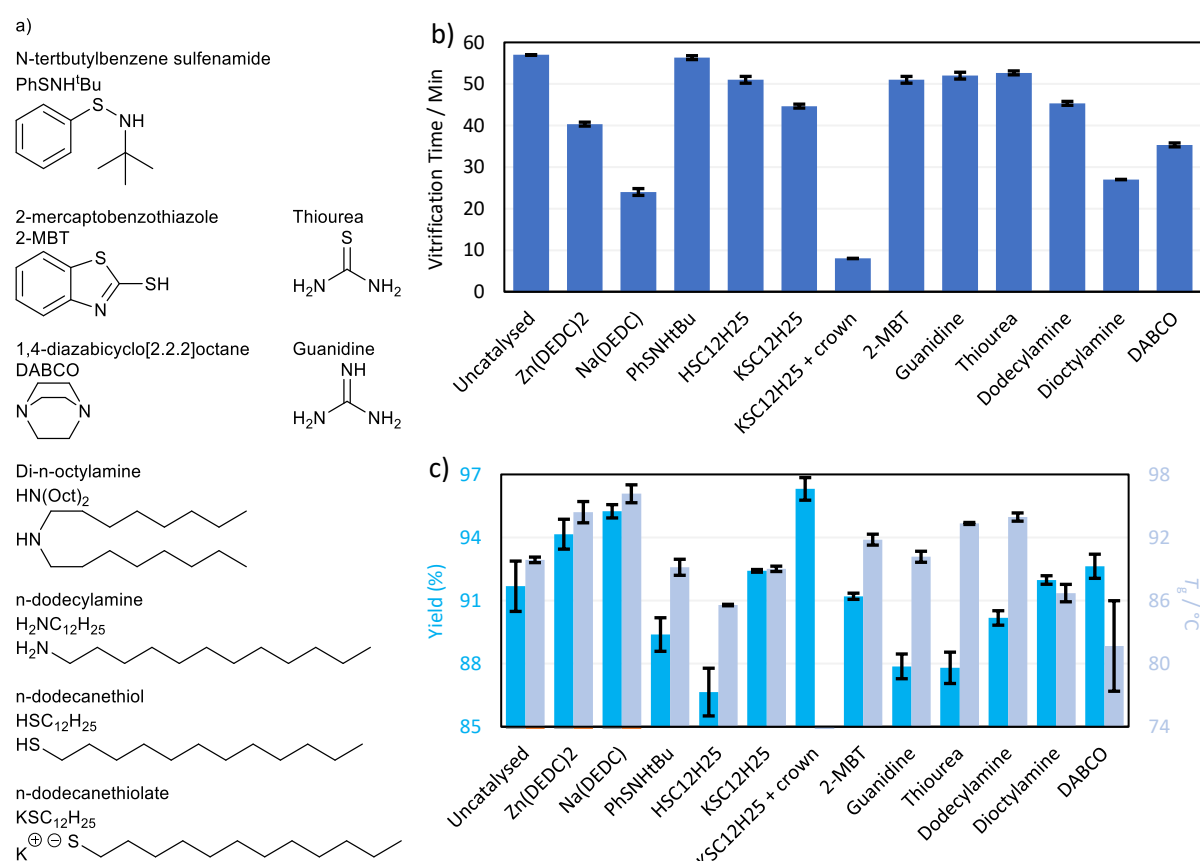
Figure 2.25: a) molecular structures of the organo-catalysts, b) vitrification times and c) yields and T_g's of inverse vulcanisation and catalytic inverse vulcanisations using Zn(DEDC)$_2$, Na(DEDC), and the organo-catalysts. The T_g for potassium dodecane thiolate in the presence of an equimolar quantity of 18-crown-6 is 41.1 ± 1.6 °C, and is low due to the TNE.

Liam James Dodd

Many of the organo-catalysts were ineffective at decreasing the vitrification time. Of note, N-tert-butylbenzene sulfenamide (PhSNH^{t}Bu), a radical initiator, provided essentially no rate enhancement at all, resulting from its boiling point of 60 °C, causing it to near instantly vaporise and leave the reaction mixture (PhSNH^{t}Bu was added to the reaction alongside DVB, which differs from the standard method where the catalyst is added to and heated up with, the sulfur).

Dodecanethiol has a solubilising alkyl chain and contains sulfur, even though its functional group is different from that of a dithiocarbamate. Thiols are widely regarded as good nucleophiles that can be further enhanced in nucleophilicity by deprotonation to the thiolate form. However, dodecanethiol was found to be quite a poor catalyst, as it provided a small but significant rate enhancement, perhaps through phase compatibilization alone. Thiolates are regarded to be even better nucleophiles than their thiol counterparts.

Potassium dodecane thiolate was used as a catalyst in inverse vulcanisation by a slightly different method than usual. KOH (104.5 mg, 1.862 mmol) was dissolved in 2 mL of EtOH. The vial was briefly purged with nitrogen and sealed with a septum, before injecting an equimolar quantity of dodecanethiol (379.9 mg, 0.4469 mL). 0.368 mL of this solution (constituting 0.28 mmol of potassium dodecanethiolate) was added to each reaction vial immediately before the addition of DVB. The EtOH is expected to have boiled off near instantly at the reaction temperature, leaving behind the potassium dodecane thiolate catalyst. See Section 2.15.4 for evidence of potassium dodecanethiolate formation.

Potassium dodecanethiolate was found to be a significantly better catalyst in comparison to dodecanethiol, which may be a result of the enhanced nucleophilicity of the sulfur atom in its anionic state. Potassium dodecanethiolate, however, is not a metal free catalyst and it is unproven if the potassium cation that accompanies the thiolate has a coordinating effect as is suspected for the other metal dithiocarbamates. Nevertheless, it seems that, where a sulfur atom is the nucleophilic centre of the catalyst, an anion is superior to a neutral sulfur.

This conclusion is supported by the relatively poor catalytic activity of 2-mercaptobenzothiazole (2-MBT), which was tested because its functional group resembles a dithiocarbamate but lacks a metallic cation. An additional reason that may explain 2-MBT's poor catalytic activity is its lack of an anionic charge, rendering it a weaker nucleophile. Such a conclusion is supported by the faster rate of reaction in the case of potassium dodecanethiolate over dodecanethiol. Interestingly, dodecanethiol provided a polymer with a poor yield and low T_g value in comparison to the uncatalyzed reaction, despite the rate enhancement, and potassium dodecanethiolate provided a polymer with high T_g and good yield. This may suggest that an anionic mechanistic pathway is what suppresses hydrogen sulfide evolution and provides polymers with high T_g values, consistent with the proposed theory that conventional vulcanisation proceeds by a radical and an anionic pathway that run simultaneously.[2.23] The yield and T_g provided by 2-MBT, which was non-ionic, were not statistically significant from those of the uncatalyzed inverse vulcanisation of DVB.

When potassium dodecanethiolate thiolate was used as a catalyst in the presence of an equimolar quantity of 18-crown-6, the reaction was accelerated to the point of the TNE, similarly to those reactions of KEtX and K^{i}PrX in the presence of 18-crown-6. Here this can be simply explained as the crown ether enhancing the nucleophilicity of the thiolate by complexing the potassium counterion.

Guanidine and thiourea lack alkyl chains entirely but still consist of a central carbon atom singly bonded to two heteroatoms and double-bonded to one heteroatom, analogous to the dithiocarbamate group. Both provided rate enhancements, attributed to some nucleophilic behaviour, but the rate enhancements were statistically insignificant from one another, indicating that

Liam James Dodd

the presence of a single non-ionic sulfur atom did not have a significant effect upon the rate enhancement of the catalyst. Interestingly, it has been reported that thioureas can be thermal decomposition products of metal DEDC's.[2.16] Because of the poor rate enhancement provided by thiourea itself and the superior rate enhancements provided by all metal DEDC's, it seems unlikely that a decomposition to thioureas is an important pathway in enhancing the rate of inverse vulcanisation. It should be noted that the guanidine was used as a hydrochloride salt, and this work has already highlighted that acidification of the reaction may deactivate catalysis.

The poor activity of these two catalysts is attributed to their lack of anionic moieties and their lack of solubilising moieties, hampering their nucleophilicity and any phase transfer agent behaviour. Consistent with dodecanethiol, which was non-ionic, both guanidine and thiourea, which are also non-ionic, provided yields lower than that of uncatalyzed inverse vulcanisation, suggesting that they too are promoting hydrogen sulfide formation. Because of this, the reaction using guanidine as a catalyst was repeated under gas capture conditions (Figure 2.6b). Although the amount of hydrogen sulfide given off was found to be higher than that for the uncatalyzed inverse vulcanisation of DVB, (1.51 vs 1.44 mmol of H_2S), the standard deviation in the result for the guanidine-catalysed reaction is too large to say for certain that guanidine promotes the formation of hydrogen sulfide (Figure 2.6b).

Moreover, a complement of amines were tested in this work to benchmark them against other catalysts, since nucleophilic activation of inverse vulcanisation by means of amines has been reported, and amines have been shown to cleave sulfur – sulfur bonds.[2.14,2.15] Dodecylamine, dioctylamine, and 1,4-diazabicyclo[2.2.2]octane (DABCO) were chosen as representative examples of primary, secondary, and tertiary amines, respectively. Conveniently, dodecylamine has an alkyl chain of length equivalent to that of dodecanethiol; thus, a comparison of the two is appropriate.

Of the two, dodecylamine was the superior catalyst in terms of vitrification time, yield, and T_g, indicating that a sulfur atom is not necessary to provide nucleophilic activation. This is perhaps because as dodecylamine is a more powerful nucleophile than dodecanethiol it saw a greater rate enhancement. The greater reactivity of dodecylamine may have allowed the catalytic pathway to better compete with the pathway responsible for hydrogen sulfide formation, leading to the higher yield observed. It is, however, worth noting that dodecylamine provided a yield lower than that of uncatalyzed inverse vulcanisation, so while it may be better at suppressing hydrogen sulfide formation in comparison dodecanethiol, it is still promoting hydrogen sulfide formation.

Of the amine catalysts/nucleophilic activators tested, dioctylamine was particularly effective in giving rapid reactions and maintained a yield comparable to that of uncatalyzed inverse vulcanisation but fell short in providing high T_g values. Similarly, DABCO provided a good rate enhancement and a yield that was statistically insignificant from that of uncatalyzed inverse vulcanisation, though the T_g value of the product polymer was more than 8 °C lower than that of an uncatalyzed polymer. These low T_g values are attributed to the relatively large molecular profile of the catalysts, particularly DABCO, which is rigid and bulky in all three dimensions and lacks the ability to unravel and extend its hydrocarbon units, unlike the other catalysts. This may disrupt the structure of the polymers and decrease the number of interchain interactions that would normally hold them together, leading to a lower T_g value.

It should be noted that the use of amines as catalysts in inverse vulcanisation is complicated by the fact that they have the potential to form thioamide groups.[2.34] It has been reported that primary amines can react directly with sulfur, to form thioamides, and that primary and secondary amines can react with sulfur and an alkyne to form thioamides, all of which can occur at temperatures lower than
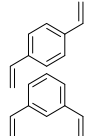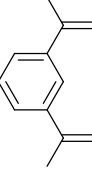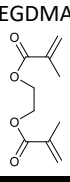
that of inverse vulcanisation. Whether thioamides are forming here as a result of the presence of amines, and their effect upon the product polymers if they are forming, is unclear.

2.12. Versatility of Catalytic Inverse Vulcanisation

To test the resilience of catalytic inverse vulcanisation to variation under the reaction conditions, and its flexibility across different kinds of crosslinkers, a small selection of catalysts was assessed against reactions of several different organic comonomers. DIB was selected for its similarity to DVB. DCPD was selected because it is not aromatic and is structurally dissimilar to DVB. EGDMA was selected because it is a representative example of a comonomer that contains heteroatoms which are in conjugation with the carbon – carbon double bond and because it has poor reactivity without a catalyst.[2.1] These experiments were performed to determine whether the conclusions of the catalytic trials upon the inverse vulcanisation of DVB were applicable to other crosslinkers.

Table 2.3 shows that in almost all cases the addition of a catalyst enhanced the vitrification time, yield, and T_g values and that the results mirrored those of the catalytic trials in terms of which catalysts were better and worse. The only exception to this was Na(DEDC), which was less effective than $Zn(DMDC)_2$ when it was used with the alternative crosslinkers, which is in agreement with the previous findings that Na(DEDC) was not be compatible with all organic comonomers.[2.1] This is also suggestive that Na(DEDC) uses a different mechanism than the transition metal DEDC's.

Table 2.3: Vitrification times, yields and T_g's of inverse vulcanisations and catalytic inverse vulcanisations with different catalysts, feed ratios, alternative crosslinkers and varied temperatures. Where standard deviations are not provided the reaction was not performed in triplicate.

Crosslinker	Sulfur : crosslinker mass ratio	Temperature of reaction and curing stage / °C	Catalyst (0.28 mmol used)	Vitrification time ± standard deviation / min	Yield ± standard deviation (%)	T_g ± standard deviation / °C
DVB	50 : 50	135	none	57.0 ± 0.0	91.7 ± 1.2	89.9 ± 0.3
			$Zn(DEDC)_2$	40.3 ± 0.5	94.1 ± 0.7	94.4 ± 1.0
	70 : 30	135	none	33.0 ± 0.8	93.9 ± 0.2	46.2 ± 1.1
			$Zn(DEDC)_2$	21.7 ± 0.5	95.3 ± 0.1	34.8 ± 0.3
	30 : 70	135	none	109.0 ± 0.0	80.5 ± 0.3	83.3 ± 0.9
			$Zn(DEDC)_2$	98.0 ± 0.8	84.7 ± 0.5	82.4 ± 0.7
DIB	50 : 50	160	none	32 ± 0.0	92.1 ± 0.3	4.99 ± 0.63
			$Zn(DEDC)_2$	16 ± 0.0	92.5 ± 0.1	2.30 ± 1.17
	50 : 50	135	none	158	79.0	21.6
			$Zn(DMDC)_2$	70	85.1	26.6
			Na(DEDC)	126	77.9	14.9
			KEtX	129	75.4	18.6
			2-MBT	154	82.6	29.3
			Dioctylamine	146	86.4	29.4
DCPD	50 : 50	135	none	220	60.0	45.2
			$Zn(DMDC)_2$	58	94.7	111.6
			Na(DEDC)	155	88.7	79.2
			KEtX	175	66.2	57.0
			2-MBT	194	68.9	68.3
			Dioctylamine	164	76.3	77.4
EGDMA	50 : 50	160	none	134	82.8	unclear
			$Zn(DMDC)_2$	74	90.1	10.6
			Na(DEDC)	103	86.9	5.5
			KEtX	94	84.6	5.5
			2-MBT	135	82.3	7.6
			Dioctylamine	121	81.7	6.9

Liam James Dodd

In the literature, reactions with EGDMA took long times to reach completion at 135 °C, so the EGDMA reactions here were performed at 160 °C, to provide shorter vitrification times that were feasible to measure. At 160 °C the sulfur – EGDMA reaction mixture vitrified without a catalyst, but the resultant polymer was unstable to depolymerisation upon cooling. Only the inverse vulcanisation of EGDMA with $Zn(DMDC)_2$ as a catalyst formed a stable polymer with a homogeneous structure. All of the EGDMA inverse vulcanised polymers, except that which was synthesized with the $Zn(DMDC)_2$ catalyst, showed numerous irregular features in their DSC thermograms alluding to an inhomogeneous and poorly formed polymer structure, as well as characteristic peaks of elemental sulfur, and sulfur cold crystallisations. The reaction using $Zn(DMDC)_2$ as a catalyst provided a DSC thermogram with only a T_g transition, indicating that it is the only completely successful catalyst for EGDMA.

The inverse vulcanisation of DVB was performed at varied mass ratios of DVB to sulfur. In almost all cases, the addition of 0.28 mmol of $Zn(DEDC)_2$ to a 135 °C reaction provided the benefits of lower vitrification times, higher yields, and higher T_g values, as can be seen in Table 2.3. To further demonstrate the versatility of catalytic inverse vulcanisation, the inverse vulcanisation of DVB and sulfur at a 50 : 50 mass ratio was tested at 160 °C; however, this led to the TNE.

It was noted that, with a greater amount of DVB, the vitrification time was longer; therefore, the inverse vulcanisation of DVB and sulfur in a 70 : 30 mass ratio was carried out. The reaction did not exhibit the TNE; however, when the reaction was repeated with 0.28 mmol of $Zn(DEDC)_2$, the TNE was observed. This indicates that introducing a catalyst into a reaction which is expected to be rapid (due to a highly reactive crosslinker and/or high temperature) is not beneficial, as it accelerates the reaction too much.

To demonstrate that catalytic inverse vulcanisation can be beneficial at higher temperatures when a less reactive crosslinker is used, the inverse vulcanisation of DIB, which is less reactive than DVB, and sulfur at a 50 : 50 mass ratio was tested at 160 °C with and without 0.28 mmol of $Zn(DEDC)_2$. The results shown in Table 2.3 indicate that catalysis is indeed beneficial at higher temperatures with this crosslinker. This emphasizes the need for the thoughtful application of catalysis in inverse vulcanisations, as adding too much catalyst or adding a catalyst to an already rapid reaction has been demonstrated here to be detrimental. Note that, over the course of the overnight curing at 160 °C, the DIB polymers degraded from a solid to a liquid, indicating a drop in T_g. This degradation appears to have affected the catalysed reaction more significantly, explaining its slightly lower T_g. The degradation could likely be avoided with optimisation of the curing process.

2.13. Library of Tested Catalysts

One of the main advantages to the work performed here is that numerous catalysts were trialled by a method that allows comparison between them. Table 2.4 compiles all the results of the catalytic trials into a library of tested catalysts to allow easy comparison and selection of catalysts by those interested in applying catalytic inverse vulcanisation.

Liam James Dodd

Table 2.4: Vitrification times (Vit. Time), yields, and T_g values of catalytic inverse vulcanisations relative to the corresponding uncatalyzed inverse vulcanisation, as well as absolute values with standard deviations.

Catalyst Entry	Relative Vit. Time	Relative Yield	Relative T_g	Vit. Time / min	Yield (%)	T_g / °C
Classic Catalyst Benchmarks						
Uncatalyzed	1.00	1.00	1.00	57 ± 0	92 ± 1	90 ± 0
Zn(DEDC)$_2$	0.71	1.03	1.05	40 ± 1	94 ± 1	94 ± 1
Na(DEDC)	0.42	1.04	1.07	24 ± 1	95 ± 0	96 ± 1
Na(DEDC) + 15-crown-5	0.50	1.02	0.97	29 ± 1	93 ± 1	87 ± 1
Classic Catalysts with Varied Valence Cations and Non-Metallic Cations						
Ag(DEDC)	0.56	1.03	1.06	32 ± 0	94 ± 1	95 ± 1
Fe(DEDC)$_3$	0.42	1.04	0.47	24 ± 1	96 ± 0	42 ± 0
0.28 NH$_4$(DEDC)	0.87	1.02	1.04	49 ± 1	94 ± 0	93 ± 1
0.56 NH$_4$(DEDC)	0.88	1.01	1.05	50 ± 1	92 ± 0	95 ± 0
Classic Catalysts with Different Alkyl Chain Lengths						
Zn(DMDC)$_2$	0.63	1.04	1.08	36 ± 1	95 ± 1	97 ± 0
Zn(DBDC)$_2$	0.67	1.03	1.06	38 ± 1	95 ± 0	95 ± 1
Zn(DODC)$_2$	0.63	1.01	0.90	36 ± 1	93 ± 0	81 ± 1
Classic Catalysts with Alternate 1st Row Transition Metal Cations						
Mn(DEDC)$_2$	0.41	1.01	1.04	23 ± 1	92 ± 0	94 ± 1
Fe(DEDC)$_2$	0.66	1.04	1.04	38 ± 1	95 ± 0	93 ± 2
Co(DEDC)$_2$	0.88	1.01	1.02	50 ± 1	93 ± 0	92 ± 1
Ni(DEDC)$_2$	0.61	1.03	1.05	35 ± 1	94 ± 0	95 ± 1
Cu(DEDC)$_2$	0.43	1.04	1.13	24 ± 1	95 ± 0	101 ± 1
Inorganic Bases						
LiOH	0.92	0.94	1.01	53 ± 1	86 ± 0	91 ± 1
NaOH	0.84	0.91	0.98	48 ± 1	84 ± 2	88 ± 1
KOH	0.81	0.94	0.99	46 ± 1	87 ± 0	89 ± 2
Xanthogenates as Alternatives to Classic Catalysts						
KEtX	0.77	1.02	1.03	44 ± 1	93 ± 0	93 ± 0
KEtX + 18-crown-6	0.25	1.05	0.46	14 ± 0	96 ± 1	42 ± 2
K^{i}PrX	0.79	0.97	0.97	45 ± 0	89 ± 0	87 ± 1
K^{i}PrX + 18-crown-6	0.11	1.06	0.45	6 ± 0	97 ± 0	41 ± 3
Organocatalysts						
PhSNH^{t}Bu	0.99	0.97	0.99	56 ± 1	89 ± 1	89 ± 1
HSC$_{12}$H$_{25}$	0.89	0.95	0.95	51 ± 1	87 ± 1	86 ± 0
KSC$_{12}$H$_{25}$	0.78	1.01	0.99	45 ± 1	92 ± 0	89 ± 0
KSC$_{12}$H$_{25}$ + 18-crown-6	0.14	1.05	0.46	8 ± 0	96 ± 1	41 ± 2
18-crown-6	0.98	1.01	1.01	56 ± 1	93 ± 0	91 ± 1
2-MBT	0.89	0.99	1.01	51 ± 1	91 ± 0	92 ± 2
Guanidine	0.91	0.96	1.00	52 ± 1	88 ± 1	90 ± 2
Thiourea	0.92	0.96	1.04	53 ± 1	88 ± 1	93 ± 0
Amine Activators						
Dodecylamine	0.80	0.98	1.05	45 ± 1	90 ± 0	94 ± 0
Dioctylamine	0.47	1.00	0.96	27 ± 0	92 ± 0	87 ± 1
DABCO	0.62	1.01	0.91	35 ± 1	93 ± 1	82 ± 4

Liam James Dodd

2.14. Conclusions

In conclusion, it has been demonstrated here that catalytic inverse vulcanisation is a versatile and beneficial technique in terms of producing higher quality inverse vulcanised polymers, in less time and in higher yield. Catalytic inverse vulcanisation has been demonstrated with a variety of representative crosslinkers and catalysts. A wide range of metal diethyldithiocarbamates were shown to be reliable catalysts, as they provided increases in rate, yield, and glass transition temperature. Several other organic and organometallic species have also been shown to enhance the rate, yield, and T_g. More significantly, a library of catalysts for inverse vulcanisation has been explored which allows easy comparison and selection of the catalysts, on the basis of several variables that were tested here. Copper(II) diethyldithiocarbamate provided the greatest performance of all of the tested catalysts, if equal weighting is given to the three factors of rate, yield, and T_g. If only the time required to reach vitrification is considered, then potassium isopropyl xanthogenate or potassium dodecanethiol, both in the presence of 18-crown-6 ether, provided the greatest enhancement. However, in commercial terms the relative cost of each catalyst will be a consideration, and excessively rapid rates may cause processing challenges, and so the choice of catalyst will be a compromise of several factors. Zinc (II) dimethyldithiocarbamate is as an ideal candidate for catalytic inverse vulcanisation, on account of its better than average rate enhancement, yield, and T_g, while also being remarkably cost effective at the same time, and compatible to different comonomers; therefore it is recommended by the authors.

In the compilation of this library of catalysts, several tentative conclusions about the mechanism of catalytic inverse vulcanisation have been drawn. Sulfur monomer binding by the catalyst may be an important step in the reaction but is not inherently necessary to achieve a rate enhancement. Where sulfur monomer binding is present as a mechanistic step, it is plausible that the ion softness and LUMO energy may influence the behaviour of catalysts with a metal cation. Conversely, it seems that coordination of the organic comonomers by their alkene π orbitals is not present as a mechanistic step, as no evidence could be found by NMR (using the University of Liverpool Bruker DEPT400 NMR instrument) or computational studies. It was found that the catalysts may behave as nucleophiles, lowering the bond dissociation energy of the initial cleavage of S−S bonds in the reaction, and this action can be hampered if the reaction mixture is acidified. It was found that catalysts which may be prone to acting as bases could promote hydrogen sulfide formation, explaining the lower yields in these cases. Evidence has been found that the catalysts may act as phase transfer agents, as longer alkyl chains make them more soluble in the organic phase and enhance the rate of the reaction. This may better allow them to draw bound sulfur chains out of the molten sulfur phase and into the comonomer phase. Additionally, metal polysulfide complexes as catalytic intermediates have been further confirmed as a useful avenue of research in the mechanism of catalytic inverse vulcanisation.

To determine the exact mechanistic nature of catalytic inverse vulcanisation is challenging, especially because of the insolubility of the products and difficulty in characterising their exact structure. This is not unlike the similar challenges of determining the nature of the catalysis/acceleration of conventional vulcanisation, a matter still under debate despite its long history and widespread industrial use. Rather, this work aimed to provide additional data and expand the previously small library of reported cases and to identify potential mechanistic steps for future study, while highlighting what factors affect catalyst efficiency.

Liam James Dodd

2.15. Appendices

2.15.1. Synthesis and Characterisation of Mn(DEDC)$_2$

Mn(DEDC)$_2$ was synthesized by a literature method.[2.16] Na(DEDC) (4.9832 g, 0.0221 mol) was dissolved in 40 cm^3 of deionised water and mixed with MnCl$_2$.4H2O (1.9965 g, 0.0101 mol) dissolved in 20 cm^3 of deionised water. A burgundy precipitate formed instantly upon mixing. The mixture was left stirring for 1 hour, after which time the precipitate was filtered off and washed with 1 litre of deionised water. The burgundy powder was left in a vacuum desiccator for one week. Yield: 3.2178 g, 90.6 %. The product was found to be soluble in methanol, ethanol, chloroform and acetone. CHNS calculated: C 34.17 %, H 5.74 %, N 7.97 %, S 36.49 %; actual: C 32.28 %, H 5.49 %, N 7.46 %, S 34.89 %. NMR spectra could not be obtained due to paramagnetic line broadening. The synthesis of Ca(DEDC)$_2$, Mg(DEDC)$_2$ and Al(DEDC)$_3$ were attempted by this method and that detailed by Hasegawa *et al.* but were unsuccessful.[2.17] FTIR analysis was performed using recorded a Bruker Vertex 70 FTIR diamond crystal platinum ATR, on the fresh Mn(DEDC)$_2$ product as well as the Mn(DEDC)$_2$ product after thermal decomposition (heating at 100 °C for 1 hour), with the results shown in Figure 2.25 and Table 2.5. Electrospray mass spectrometry in positive ion mode was performed for the fresh product, with the results shown in Table 2.6 and Figure 2.26.
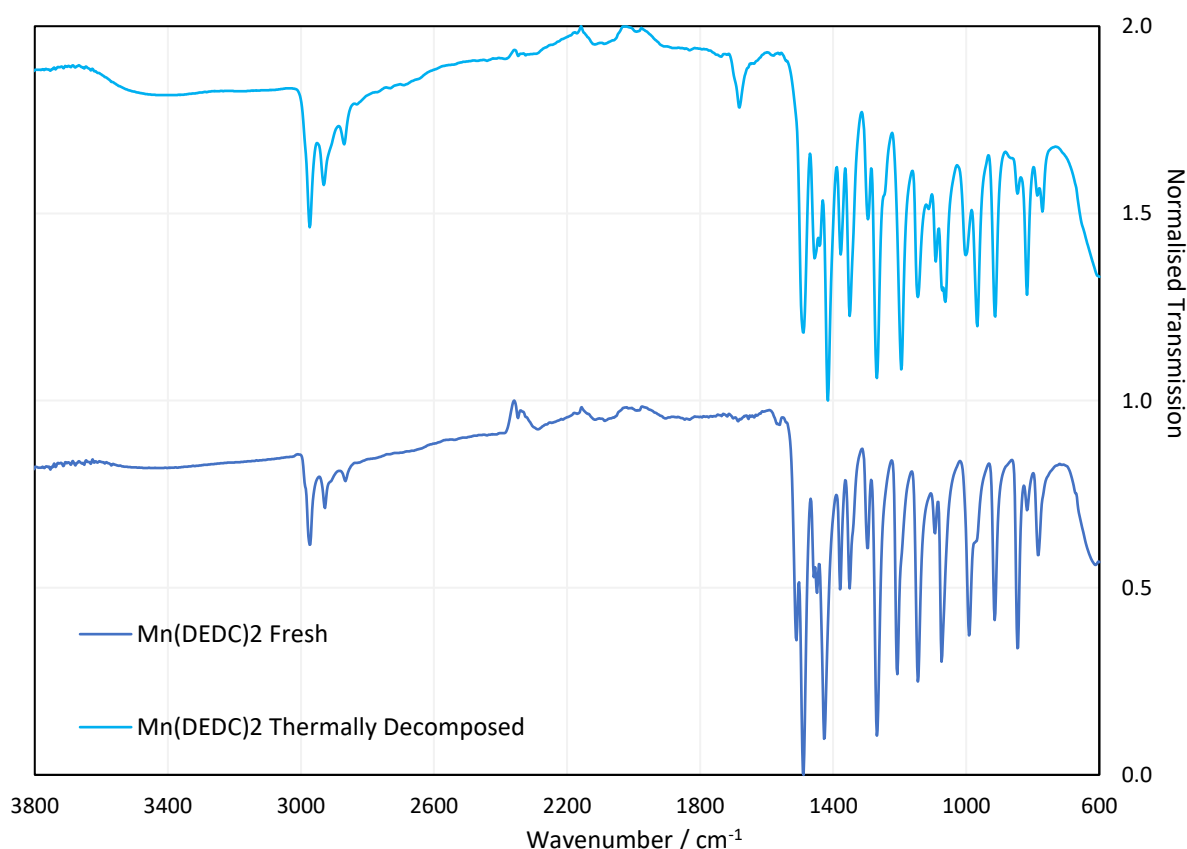
Figure 2.25: FTIR spectra of Mn(DEDC)$_2$ before and after thermal decomposition.

Table 2.5: FTIR assignments for Mn(DEDC)$_2$.

Wavenumber / cm^{-1}	Assignment
2974.0, 2927.8, 2806.1	C-H stretch
1488.9	C-N [2.15]
1448.4	C-H bend
991.3	C-S [2.15]

Liam James Dodd
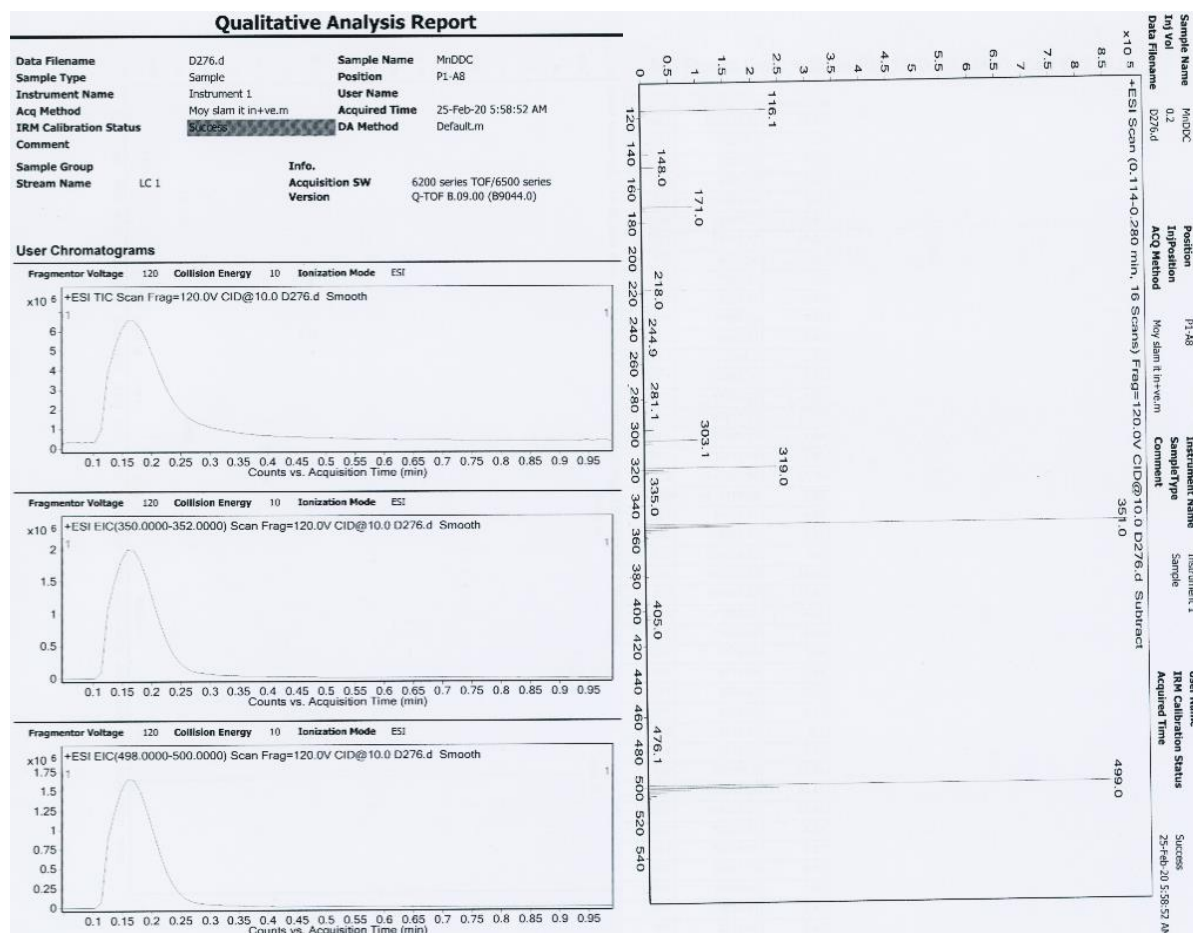
Figure 2.26: Mass spectra and accompanying technical information for Mn(DEDC)$_2$.

Table 2.6: Mass spectrometry electrospray positive ion mode assignments for Mn(DEDC)$_2$. Theoretical M_R = 351.46.

Peak	Assignments
351.0 (base peak)	
148.0 (weak)	
499.0 (molecular ion)	
335.0	- CH$_3$ - H
319.0	- 2 CH$_3$ - 2 H
303.1	- 3 CH$_3$ - 3 H
281.1	+ 2 H - N(CH$_2$CH$_3$)$_2$
116.1	- 2 CH$_3$ - 2 H
171.0	- 2 CH$_3$ - 2 H

Liam James Dodd

2.15.2. Electrochemistry of Metal DEDC's

Cyclic voltammetry data was obtained using a glassy carbon working electrode, platinum mesh counter electrode and a silver wire reference electrode. Experiments were performed upon solutions of a selected catalyst in 0.002 M concentration, with 0.1 M tetrabutylammonium hexafluorophosphate (≥99.0% purity, obtained from Sigma Aldrich) as a base electrolyte in acetonitrile. The solutions were purged with nitrogen before use for approximately half an hour. After the measurements were completed, a large excess of ferrocene (98 % purity, obtained from Sigma Aldrich) was added to the cell, and another cyclic voltammogram (scan rate 0.2 V s^{-1}) was performed, which was used to determine the potential of the ferrocene/ferrocenium couple against which the previous experiments were referenced. One final cyclic voltammetry was performed on a fresh solution of a selected catalyst, without purging with nitrogen, to determine the effect of the presence of oxygen.

Several sources of error in these experiments that may prevented the determination of a trend between the potentials of redox with the vitrification time include potential drift over the course of different experiments; electrochemical irreversibility giving rise to skewed potentials; poorly resolved peaks giving rise to inaccurate potential measurements; resistance across the cell giving rise to inaccurate potential measurements; limited solubility of the metal DEDC's in acetonitrile resulting in weak signals; and the fact that the potentials of redox in cyclic voltammetry do not depend solely upon the HOMO and LUMO energies, but also have contributions from the energy needed to rearrange the molecule, leading to an overpotential with respect to the orbital energy.
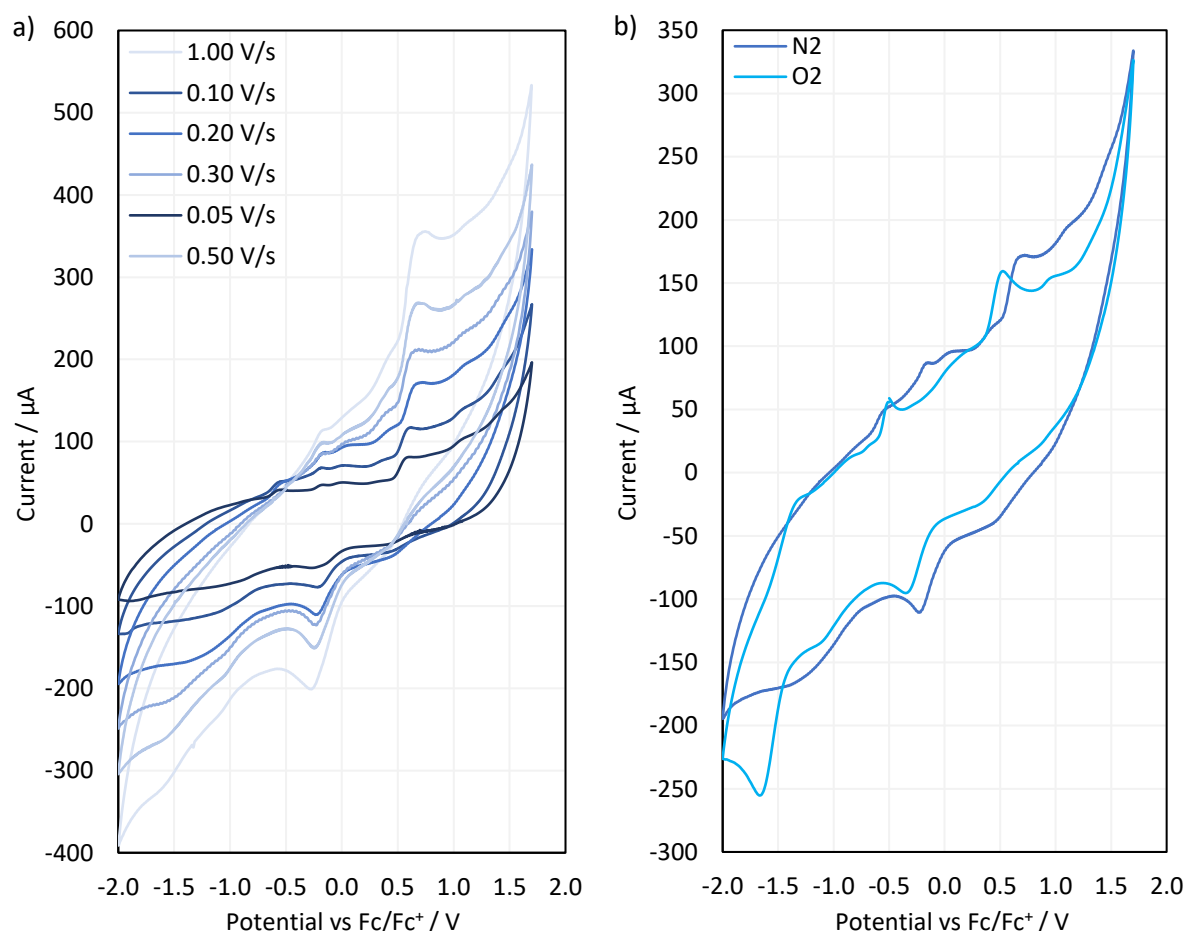
Figure 2.27: Cyclic voltammograms of a) Mn(DEDC)$_2$ at different scan rates under nitrogen, and b) cyclic voltammograms of Mn(DEDC)$_2$ at a scan rate of 0.2 V s^{-1} under N$_2$ and air.

Liam James Dodd
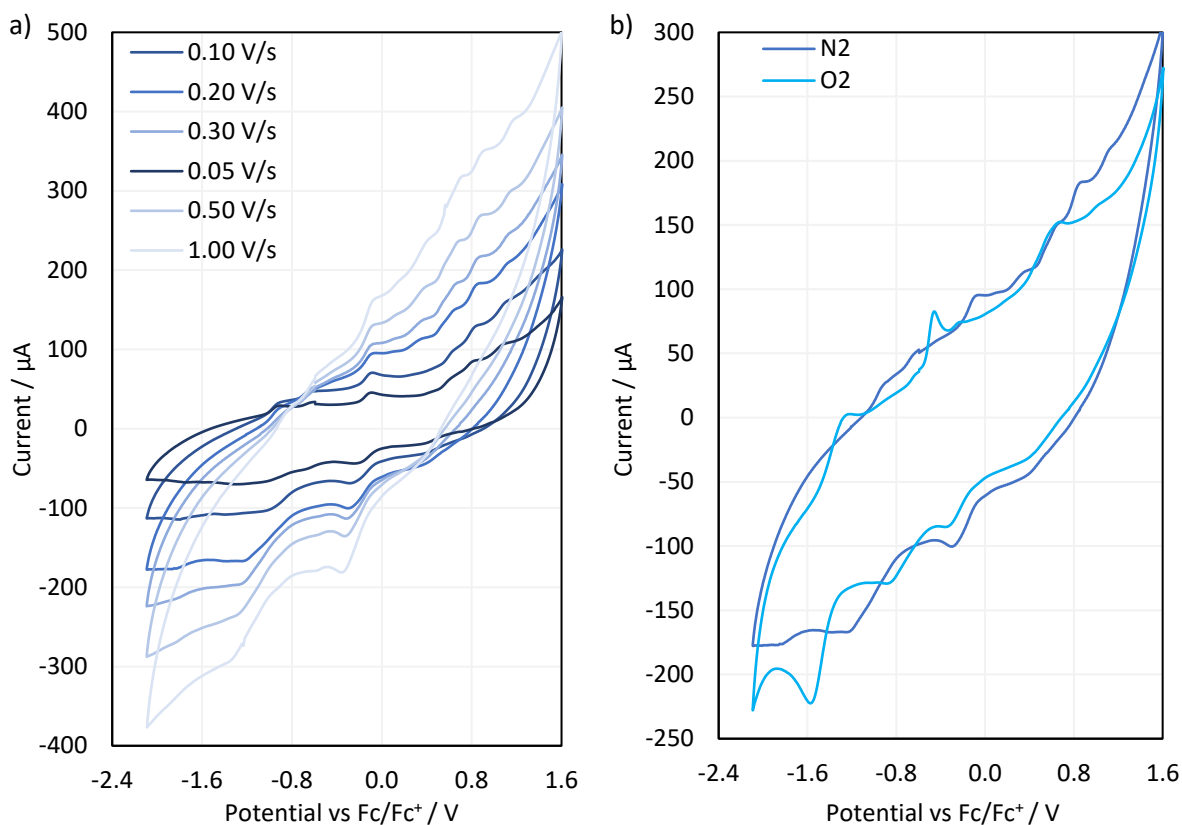
Figure 2.28: Cyclic voltammograms of a) Fe(DEDC)$_2$ at different scan rates under nitrogen, and b) cyclic voltammograms of Fe(DEDC)$_2$ at a scan rate of 0.2 V s^{-1} under N$_2$ and air.
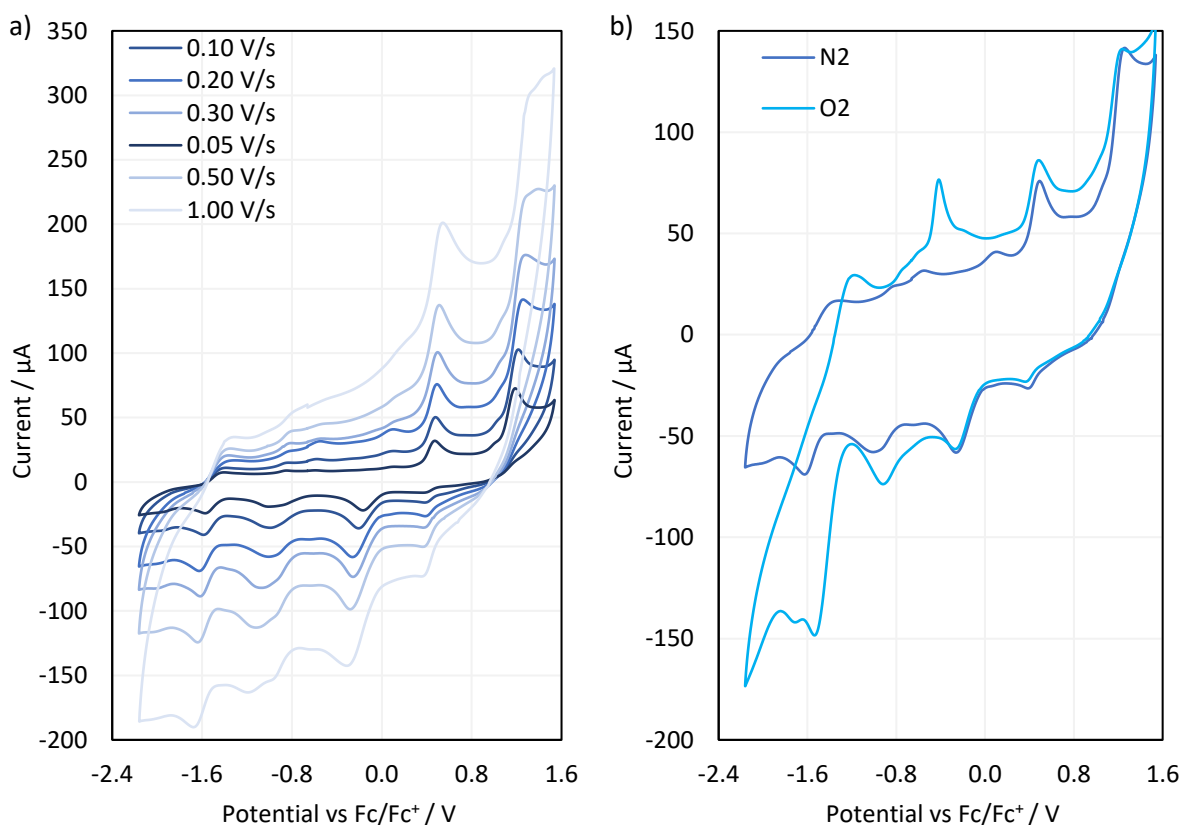
Figure 2.29: Cyclic voltammograms of a) Co(DEDC)$_2$ at different scan rates under nitrogen, and b) cyclic voltammograms of Co(DEDC)$_2$ at a scan rate of 0.2 V s^{-1} under N$_2$ and air.

Liam James Dodd
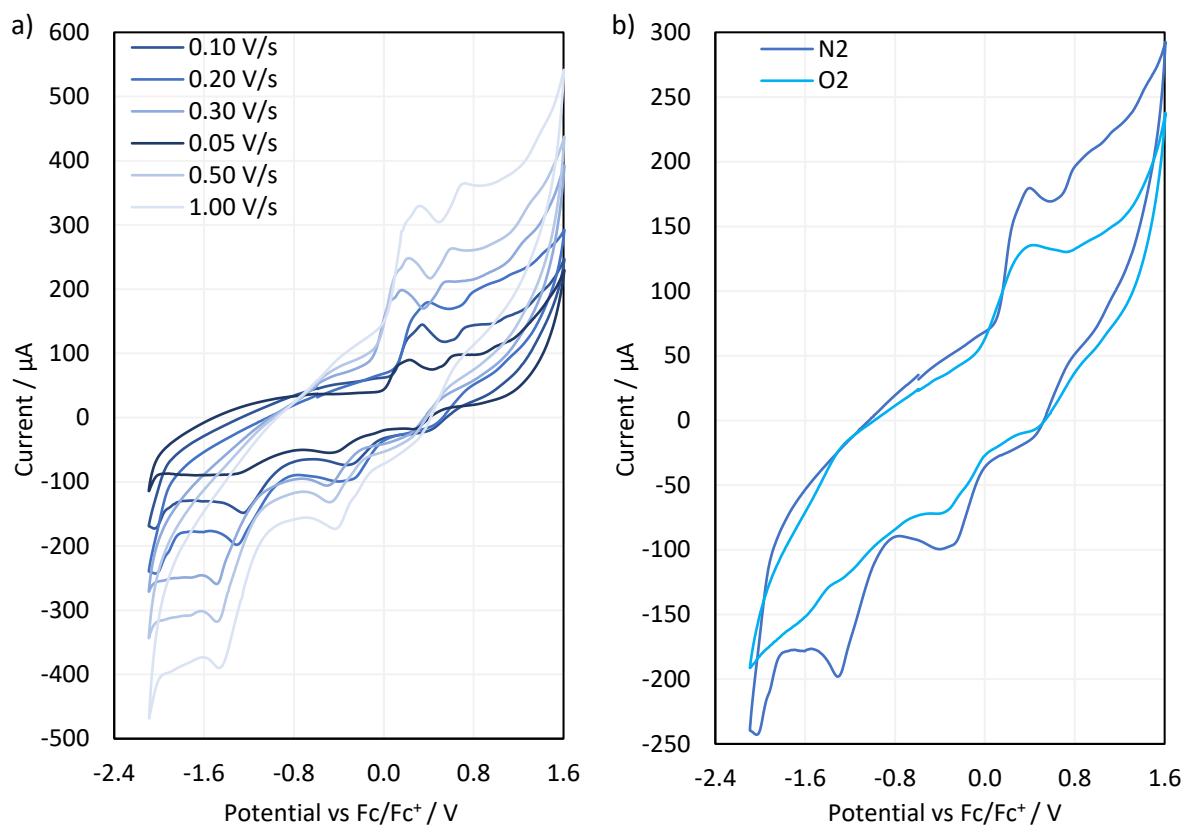
Figure 2.30: Cyclic voltammograms of a) Ni(DEDC)$_2$ at different scan rates under nitrogen, and b) cyclic voltammograms of Ni(DEDC)$_2$ at a scan rate of 0.2 V s^{-1} under N$_2$ and air.
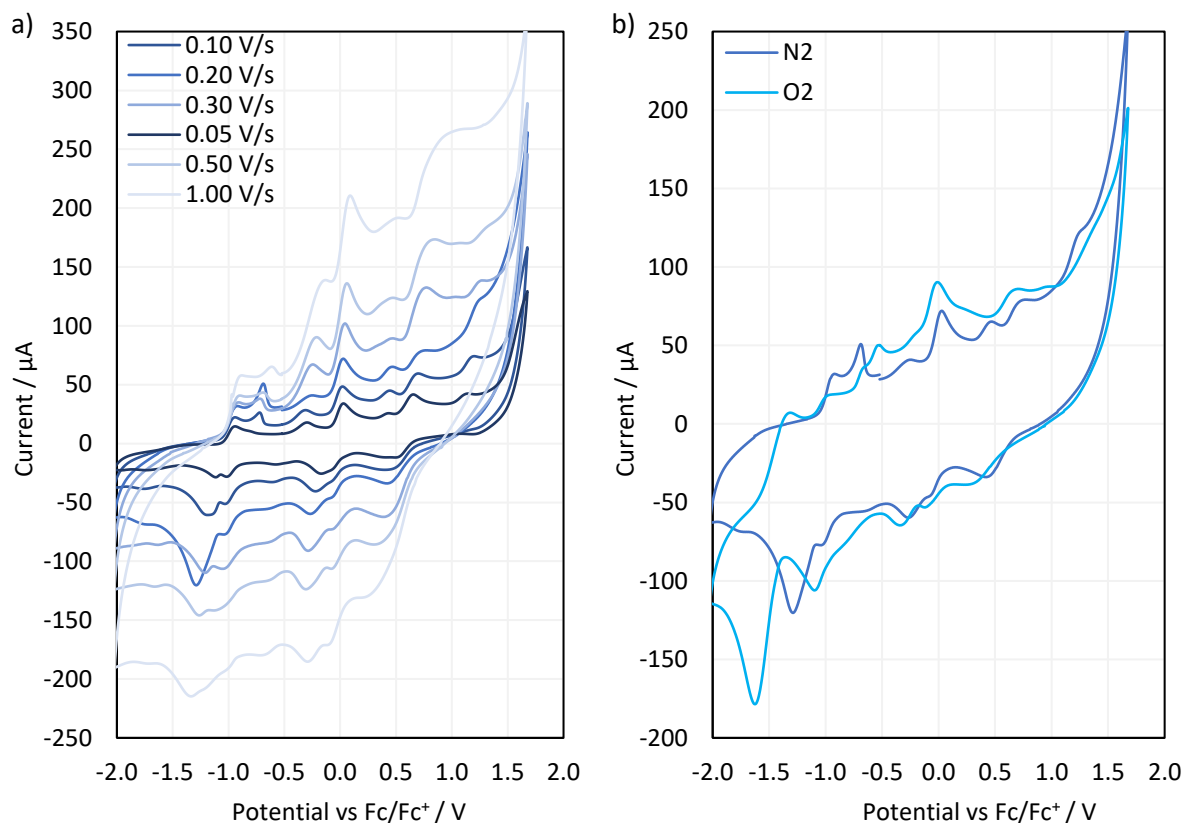
Figure 2.31: Cyclic voltammograms of a) Cu(DEDC)$_2$ at different scan rates under nitrogen, and b) cyclic voltammograms of Cu(DEDC)$_2$ at a scan rate of 0.2 V s^{-1} under N$_2$ and air.

Liam James Dodd
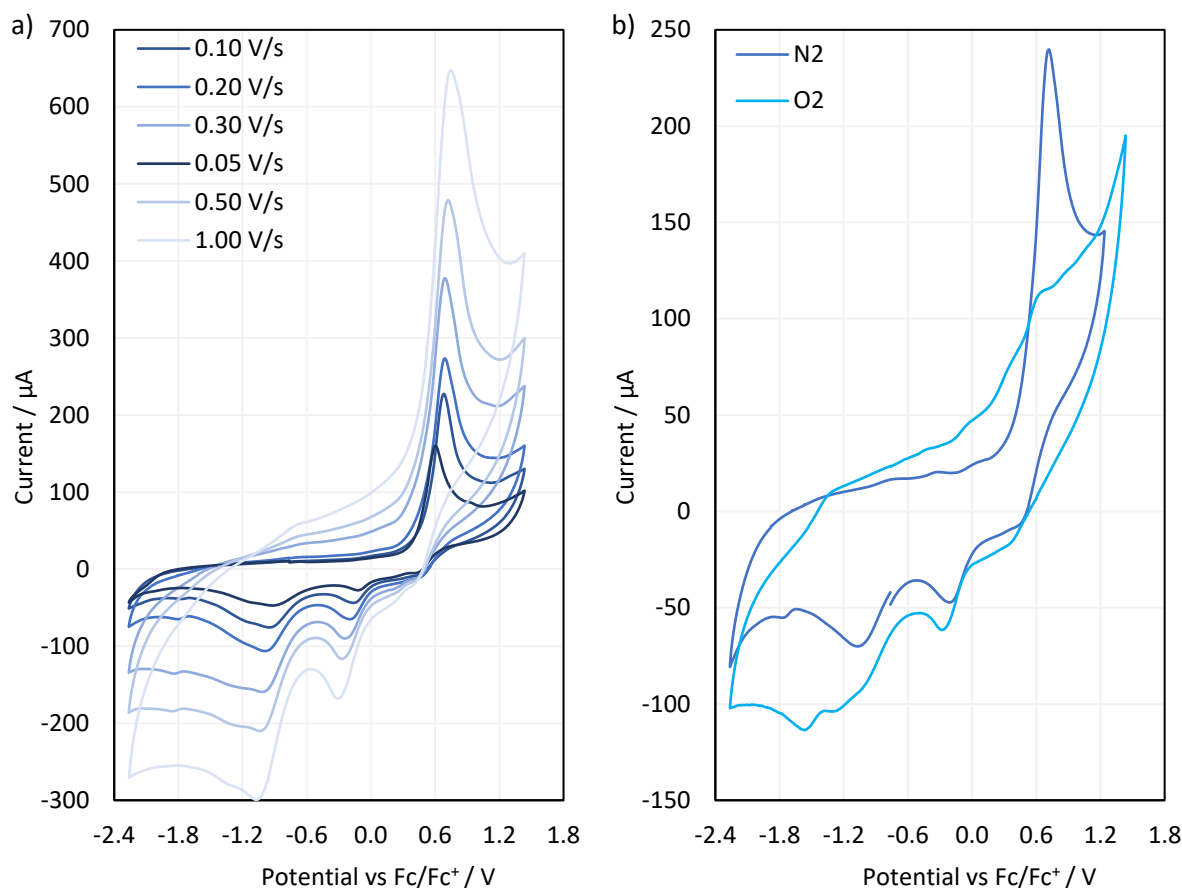
Figure 2.32: Cyclic voltammograms of a) Zn(DEDC)$_2$ at different scan rates under nitrogen, and b) cyclic voltammograms of Zn(DEDC)$_2$ at a scan rate of 0.2 V s^{-1} under N$_2$ and air.

2.15.3. Synthesis and Characterisation of Zn(DODC)$_2$

Zinc di-n-octyldithiocarbamate was synthesized by literature methods.[2.35] All glassware was oven dried at 95 °C for one day before use. Reaction vessels were purged with nitrogen for half an hour before use. Carbon disulfide (5.370 g, 0.070 mol) was added dropwise from a pressure equalising dropping funnel into a round bottom flask containing dioctylamine (16.3535 g, 0.0677 mol) and zinc oxide (2.7091 g, 0.0333 mol) at room temperature. Upon addition of carbon disulfide, the reaction mixture became yellow. The mixture was left to stir for 30 minutes under active nitrogen purge, after which time the temperature was increased to 70 °C, followed by another two hours of stirring, then a second temperature increase to 90 °C, followed by a further two hours of stirring, and a final temperature increase to 130 °C. At this time the pressure equalising dropping funnel was replaced with a reflux condenser connected to a vacuum adaptor and a round bottom flask. The reaction was left under vacuum distillation conditions overnight to remove the by-product water. The oil product was filtered on hot celite to remove leftover zinc oxide, by use of a heat gun, which was needed to heat the oil as it was too viscous to be poured or filtered when cold. 8.9856 g of a clear yellow oil was obtained. 2D TLC using chloroform as an eluent with a potassium permanganate stain indicated that the product (Rf$_x$ 0.9, Rf$_y$ 0.9) was impure with dioctylamine (Rf$_x$ 0, Rf$_y$ 0) (identities were confirmed by 1D TLC). 2.56 g of the product was dissolved in 10 cm^3 of chloroform, and filtered on a silica plug, using additional chloroform to wash the product through. TLC of the filtrate showed no spot at Rf 0, but still maintained a spot at Rf 0.9. The filtrate was rotary evaporated to dryness at 60 °C for 7 hours, yielding 1.32 g of a dark brown clear oil which became a soft, light brown solid when cool (Figure 2.35). CHNS calculated: C 58.46 %, H 9.81 %, N 4.01 %, S 18.36 %; actual: C 58.81 %, H 9.81 %, N 3.96 %, S 18.01. ^{1}H NMR and

Liam James Dodd

^{13}C NMR were obtained in CDCl$_3$, using the University of Liverpool Bruker DEPT400 NMR instrument, the spectra of which are shown in Figure 2.33 and Figure 2.34 respectively. FTIR analysis was performed using a Bruker Vertex 70 FTIR diamond crystal platinum ATR on the Zn(DODC)$_2$ with the results shown in Figure 2.35 and Table 2.7. Electrospray mass spectrometry in positive ion mode was performed for the fresh product, with the results shown in Table 2.8 and Figure 2.36.
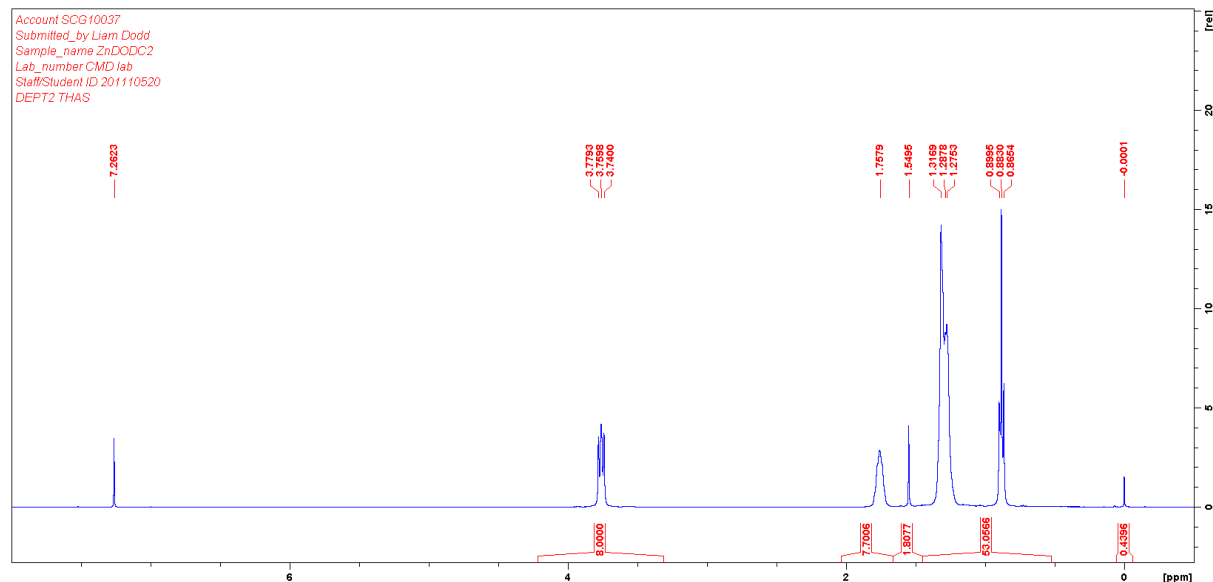

Figure 2.33: ^{1}H NMR spectrum of Zn(DODC)$_2$ in CDCl$_3$.

The triplet at 3.76 ppm in Figure 2.33 is assigned to the CH$_2$ groups bonded to the nitrogen atoms. There are four of these in the molecule, giving a total of 8 hydrogens. This is the only environment which would experience coupling to a single CH$_2$ group, giving a distinguishable coupling pattern. The remaining proton environments are all part of the alkyl chains, which would experience coupling to the adjacent environments, giving rise to complex coupling patterns which would overlap to give the broad peaks seen in the spectrum. This prevents exact assignments. The total number of hydrogen atoms in this environment is 60. When compared to the peak at 3.76 ppm, and ignoring the integration of the water peak at 1.81 ppm the number of hydrogens in these environments is found to be 60.8, close to the expected value. Ignoring the integration of water peak is difficult to do precisely and may have contributed to the discrepancy seen between the experimental and expected values.

Liam James Dodd
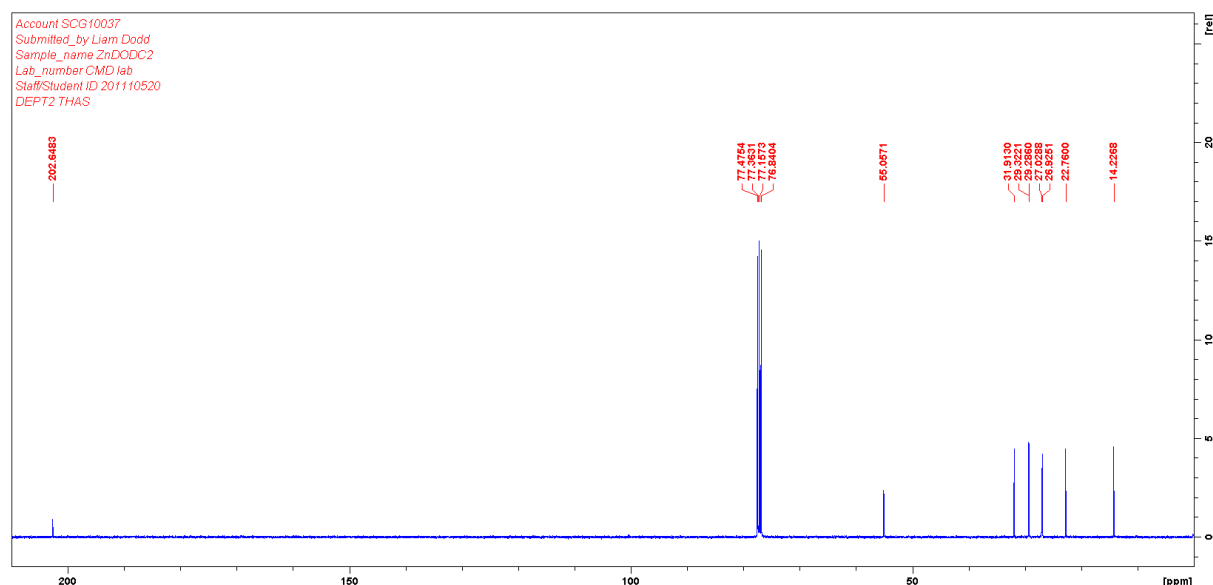
Figure 2.34: ^{13}C NMR spectrum of Zn(DODC)$_2$ in CDCl$_3$.

The peak at 202.65 ppm in Figure 2.35 is assigned to the dithiocarbamate carbon. Besides the dithiocarbamate carbon, the CDCl$_3$ triplet and the chloroform peak within the CDCl$_3$ triplet, there are 8 resonances, which is expected as there are 8 carbons in each alkyl chain of the molecule. The progressively higher chemical shift resonances are assigned to the carbons that are progressively closer to the nitrogen atom, thus the peak at 55.06 ppm is assigned to the carbon directly bonded to the nitrogen and the peak at 14.23 ppm is assigned to the terminal methyl group of the alkyl chains.
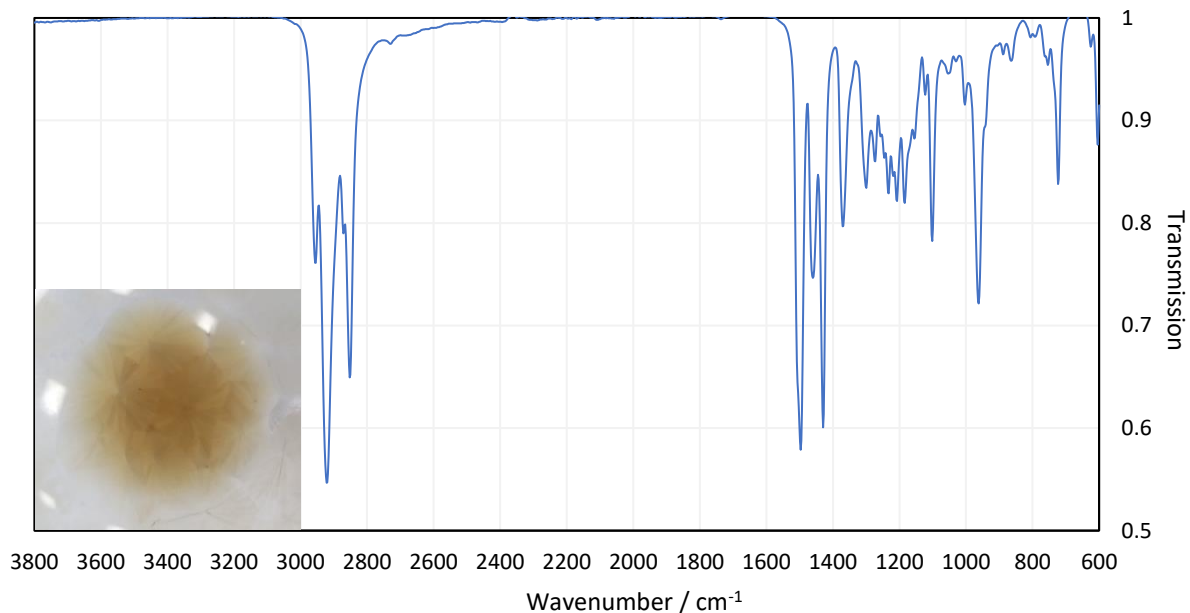
Figure 2.35: FTIR spectrum of Zn(DODC)$_2$ with an inset image of Zn(DODC)$_2$ in a round bottom flask.

Table 2.7: FTIR assignments for Zn(DODC)$_2$.

Wavenumber / cm^{-1}	Assignment
2956.5, 2921.9, 2871.8, 2852.5	C-H stretch, intense due to large alkyl chains
1496.6	C-N [2.16]
1460.0	C-H bend
1002.9	C-S [2.16]

Liam James Dodd
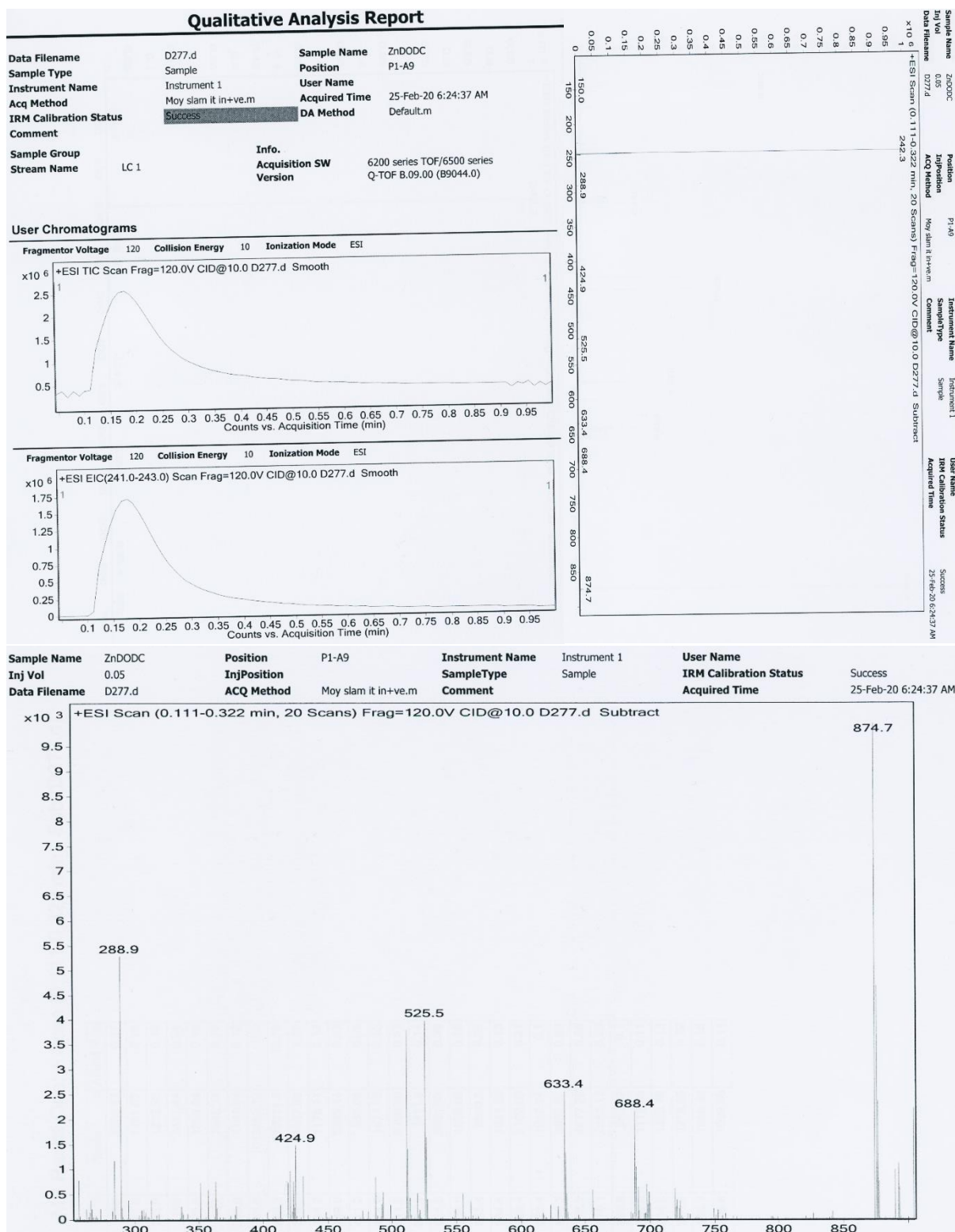
Figure 2.36: Mass spectra and accompanying technical information for Zn(DODC)₂.

Liam James Dodd

Table 2.8: Mass spectrometry assignments for Zn(DODC)$_2$. Theoretical M_R = 698.55.

Peak	Assignment
Cluster below 700, most intense peak at 688.4, peak at 698 consistent with M_R	
Peak cluster at 382	
906.6 or 905.7 (molecular ion)	- C$_7$H$_{25}$
688.4	- 3 C$_7$H$_{25}$
150	+ 4 H - 2 Oct
242.3 base peak	+ 2 H
288.9	+ 2 H - 2 CH$_3$
876.14	- C$_7$H$_{25}$ - 2 CH$_3$ - 2 H
633.4	- 4 CH$_3$ – 4 H
525.5	- C$_7$H$_{25}$ - 4 CH$_3$ - 4 H

2.15.4. Evidence of Potassium Dodecane Thiolate Formation

To prove that potassium dodecane thiolate had successfully formed from KOH and dodecanethiol ^{1}H NMR and ^{13}C NMR (using the University of Liverpool Bruker DEPT400 NMR instrument) were employed upon dodecanethiol alone and separately, equimolar dodecanethiol and KOH, all dissolved in a 50 : 50 volume mix of CD$_3$OD and CDCl$_3$. From here onwards, the sample containing only dodecanethiol will be referred to as HSR, and the sample containing dodecanethiol and KOH will be referred to as KSR.

The peaks below 8 ppm are near identical between Figure 2.37 (the HSR ^{1}H NMR spectrum) and Figure 2.38 (the KSR ^{1}H NMR spectrum), accepting the unexplained poorer resolution of the HSR spectrum. These peaks are assigned to the protons of the alkyl chain that are distant from the sulfur functional group and would be unaffected by changes to it, though to make exact assignments is extremely difficult due to the similarity of the environments and the complex coupling. A peak has been significantly shifted between the two spectra, 8.16 ppm in the HSR spectrum and 8.50 ppm in the KSR spectrum. This peak is significantly more intense in the HSR spectrum suggesting it may be caused by several overlapping peaks. In the KSR spectrum these peaks may have been separated out due to the significantly differing environments that come with closer proximity to the thiolate anion. Additionally, this difference in intensity could be explained by the protons responsible for the 8.50 ppm peak being in close proximity to the quadrupolar potassium cation, which could modify the relaxation time, potentially causing lower signal intensity. Another peak has been significantly shifted between the two spectra, 11.36 ppm in the HSR spectrum and 11.47 ppm in the KSR spectrum. It is not surprising that the thiol proton resonance is not visible in either spectrum. In the HSR spectrum the thiol proton will undergo exchange with the CD$_3$OD alcohol deuteron, and in the KSR spectrum, the thiol proton would be deprotonated by the KOH, regardless of exchange.

Liam James Dodd

The HSR ^{13}C NMR spectrum (Figure 2.39) exhibits 12 singlet resonances (excluding the CDCl$_3$ triplet at 77.16 ppm and the CD$_3$OD septet at 48.52 ppm) which are assigned to the 12 carbons in the chain of dodecanethiol, with the progressively higher chemical shift resonances being assigned to the carbons progressively closer to the sulfur atom. The KSR ^{13}C NMR spectrum (Figure 2.40) also shows 12 resonances (excluding the CDCl$_3$ triplet at 77.16 ppm and the CD$_3$OD septet at 48.52 ppm) which are assigned to the 12 carbons in the chain of potassium dodecanethiolate, with the progressively higher chemical shift resonances being assigned to the carbons progressively closer to the sulfur atom. The differences in chemical shifts of the carbons are taken as evidence for the formation of potassium dodecanethiolate in the presence of KOH. None of the resonances between the HSR and KSR spectra have precisely the same chemical shift but this could be due to difficulties in calibrating the spectra, a result of the non-standard solvent system used. It is not possible for calibration difficulties to be the explanation for the large differences in chemical shift between assignments 1 to 4 in Table 2.9.

Table 2.9: Chemical shifts and assignments for ^{13}C NMR spectra of HSR and KSR.

Carbon in chain (sulfur is defined as position 0)	HSR chemical shift / ppm	KSR chemical shift / ppm	Chemical shift difference / ppm
1	33.81	77.35	43.54
2	31.70	35.69	3.99
3	29.41	31.52	2.11
4	29.37	30.76	1.39
5	29.30	29.26	-0.04
6	29.12	29.10	-0.02
7	28.86	28.95	0.09
8	28.16	28.78	0.62
9	24.34	28.45	4.11
10	24.20	24.35	0.15
11	22.45	22.24	-0.21
12	13.73	13.41	-0.32
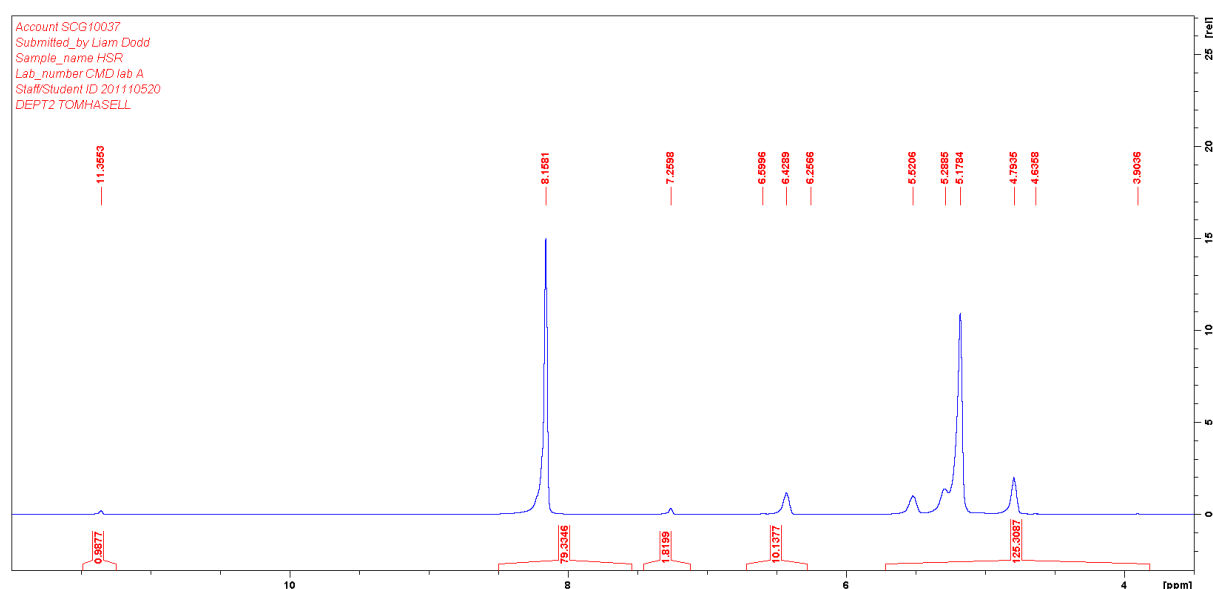
Figure 2.37: ^{1}H NMR of HSR.

Liam James Dodd
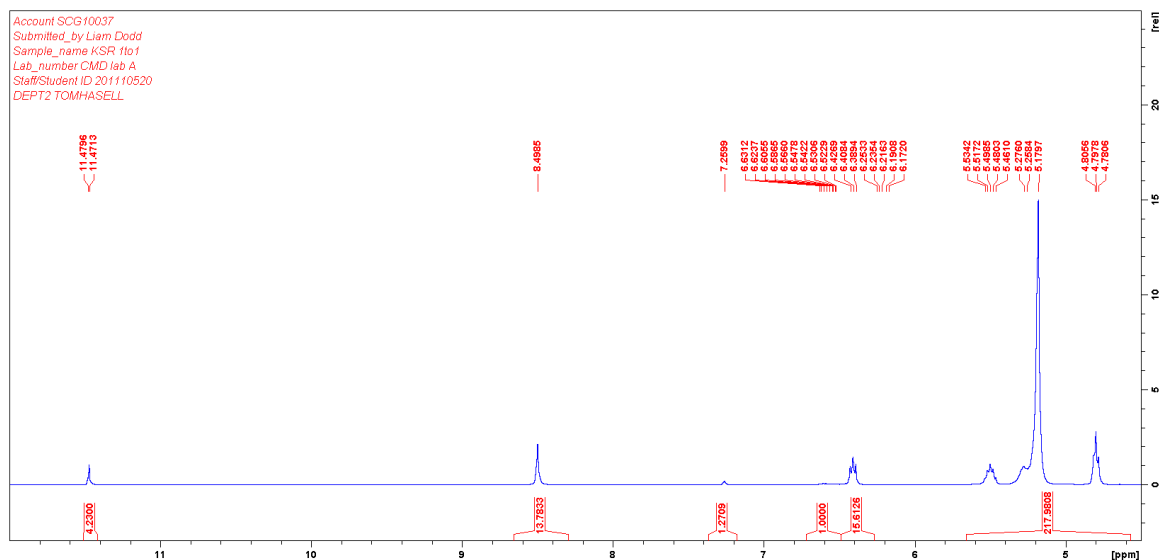
Figure 2.38: ¹H NMR of KSR.
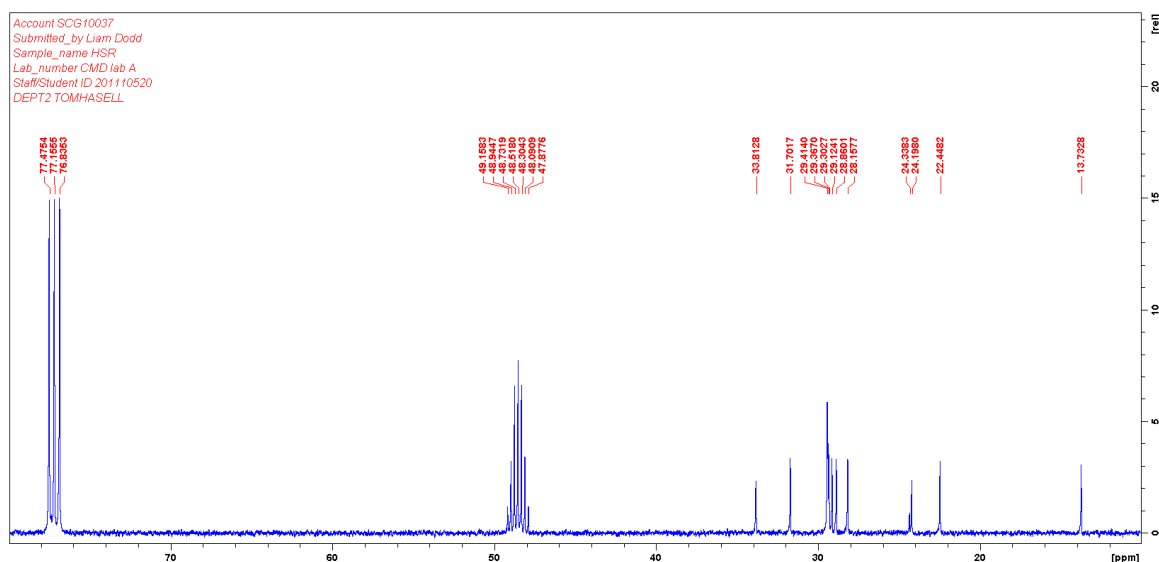
Figure 2.39: ¹³C NMR of HSR.
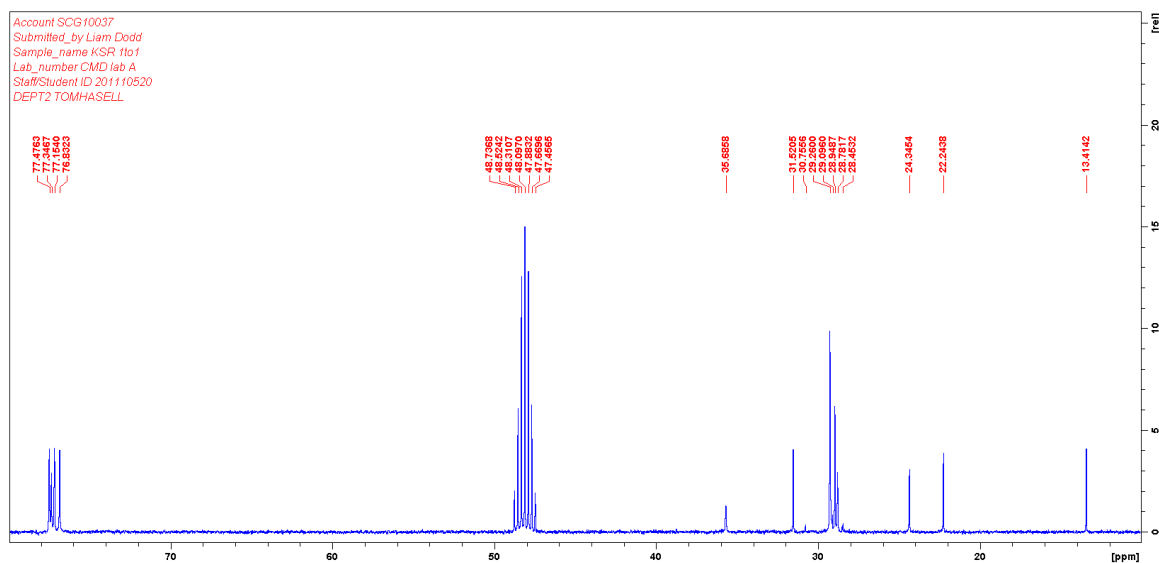
Figure 2.40: ¹³C NMR of KSR.

Liam James Dodd

2.16. References

2.1 Catalytic Inverse Vulcanization; X. Wu, J. A. Smith, S. Petcher, B. Zhang, D. J. Parker, J. M. Griffin, T. Hasell; Nature Communications, 2019, 10, 647.

2.2 End group removal and modification of RAFT polymers; H. Willcock, R. K. O'Reilly; Polymer Chemistry, 2010, 1, 149–157.

2.3 Mechanism of the Zinc Dithiocarbamate-Activated Rubber Vulcanization Process: A Density Functional Theory Study; F. Shi, X. Li, Y. Bai, L. Li, M. Pu, L. Liu, M. Lei; ACS Applied Polymer Materials, 2021, 3, 5188-5196.

2.4 Tailoring Polysulfide Properties through Variations of Inverse Vulcanization; K. Orme, A. H. Fistrovich, C. L. Jenkins; Macromolecules, 2020, 53, 9353–9361.

2.5 Handbook of Chemistry and Physics, 97th edition; I. H. Bell, L. I. Berger, P. E. Bradley, T. J. Bruno, C. E. Carraher, J. Cheng, R. D. Chirico, I. Cibulka, C. J. Cramer, V. Diky, M. Frenkel, J. R. Fuhr, R. N. Goldberg, T. W. Grove, A. H. Harvey, S. R. Heller, N. E. Holden, M. L. Huber, A. Kazakov, D. E. Kelleher, C. A. Koh, E. W. Lemmon, D. R. Lide, F. J. Lovas, Y. Luo, S. N. Lvov, M. Mantina, A. D. McNaught, T. M. Miller, N. Moazzen-Ahmadi, P. J. Mohr, C. D. Muzny, D. B. Newell, I. Ozier, L. I. Podobedova, C. J. Powell, R. Radebaugh, J. Reader, A. J. Remijan, E. D. Sloan, L. E. Snyder, P. D. N. Svoronos, B. N. Taylor, D. G. Truhlar, R. Valero, W. L. Wiese, C. Wohlfarth, D. Zwillinger; CRC Press, Boca Raton, Florida, 2017, 117.

2.6 Sub-surface H2S detection by a Surface Acoustic Wave passive wireless sensor interrogated with a ground penetrating radar; D. Rabus, J. M. Friedt, L. Arapan, S. Lamare, M. Baque, G. Audouin, F. Cherioux; ACS sensors. 2020, 5, 1075–1081.

2.7 High Sulfur Content Polymers: The Effect of Crosslinker Structure on Inverse Vulcanization; J. A. Smith, X. F. Wu, N. G. Berry, T. Hasell; Journal of Polymer Science Part A: Polymer Chemistry, 2018, 56, 1777-1781.

2.8 Elemental Sulfur; B. Meyer; Chemical Reviews, 1976, 76, 367-388.

2.9 Chemistry of the Elements, 2nd edition; N. N. Greenwood, A. Earnshaw; Butterworth-Heinemann, Oxford, 1997, 654-656.

2.10 Elemental Sulfur and Sulfur-Rich Compounds I; R. Steudel; Springer-Verlag Berlin, Berlin, 2003, 1-79.

2.11 Inorganic Chemistry; E. Wilberg, A. F. Holleman; Academic Press, De Gruyter, 2001.

2.12 Small Molecule Signalling Agents: The Integrated Chemistry and Biochemistry of Nitrogen Oxides, Oxides of Carbon, Dioxygen, Hydrogen Sulfide, and Their Derived Species; J. M. Fukuto, S. J. Carrington, D. J. Tantillo, J. G. Harrison, L. J. Ignarro, B. A. Freeman, A. Chen, D. A. Wink; Chemical Research in Toxicology, 2012, 25, 769–793.

2.13 Transition-Metal Polysulfides - Coordination-Compounds with Purely Inorganic Chelate Ligands; M. Draganjac, T. B. Rauchfuss; Angewandte Chemie International Edition, 1985, 24, 742–757.

2.14 Nucleophilic Activation of Elemental Sulfur for Inverse Vulcanization and Dynamic Covalent Polymerizations; Y. Zhang, N. G. Pavlopoulos, T. S. Kleine, M. Karayilan, R. S. Glass, K. Char, J. Pyun; Journal of Polymer Science Part A: Polymer Chemistry, 2019, 57, 7–12.

2.15 Chemically induced repair, adhesion, and recycling of polymers made by inverse vulcanization; S. J. Tonkin, C. T. Gibson, J. A. Campbell, D. A. Lewis, A. Karton, T. Hasell, J. M. Chalker; Chemical Science, 2020, 11, 5537–5546.

2.16 Thermal Decomposition Mechanism of Single-Molecule Precursors Forming Metal Sulfide Nanoparticles; Y. K. Jung, J. I. Kim, J. Lee; Journal of the American Chemical Society, 2010, 132, 178–184.

Liam James Dodd

2.17 Effective Optical Faraday Rotations of Semiconductor EuS Nanocrystals with Paramagnetic Transition-Metal Ions; Y. Hasegawa, M. Maeda, T. Nakanishi, Y. Doi, Y. Hinatsu, K. Fujita, K. Tanaka, H. Koizumi, K. Fushimi; Journal of the American Chemical Society, 2013, 135, 2659– 2666.

2.18 Natural Indices for the Chemical Hardness/Softness of Metal Cations and Ligands; H. Xu, D. C. Xu, Y. Wang; ACS Omega, 2017, 2, 7185–7193.

2.19 ChemAxon. MarvinSketch. 2019.

2.20 Open Babel: An Open Chemical Toolbox; N. M. O. Boyle, M. Banck, C. A. James, C. Morley, T. Vandermeersch, G. R. Hutchison; Journal of Cheminformatics, 2011, 3, 33. https://doi.org/10.1186/1758-2946-3-33.

2.21 Gaussian16 Revision B.01; M. J. Frisch, G. W. Trucks, H. B. Schlegel, G. E. Scuseria, M. A. Robb, J. R. Cheeseman, G. Scalmani, V. Barone, G. A. Petersson, H. Nakatsuji; 2016.

2.22 IUPAC Compendium of Chemical Terminology, 2nd edition; A. D. McNaught, A. Wilkinson; Blackwell Scientific Publications, Oxford, 1997. Online version (2019) created by S. J. Chalk. DOI: 10.1351/goldbook.

2.23 Insights into the Vulcanization Mechanism through a Simple and Facile Approach to the Sulfur Cleavage Behavior; Q. S. Lian, Y. Li, K. Li, J. Cheng, J. Y. Zhang; Macromolecules, 2017, 50, 803-810.

2.24 Phase Transfer-Catalyzed Reactions between Polysulfide Anions and α,β-Unsaturated Carbonyl Compounds; E. B. Krein, Z. Aizenshtat; Journal or Organic Chemistry, 1993, 58, 6103–6108.

2.25 Aqueous "polysulfide-ene" polymerisation for sulfur-rich nanoparticles and their use in heavy metal remediation; H. Shin, J. Kim, D. Kim, V. H. Nguyen, S. Lee, S. Han, J. Lim, K. Char; Journal of Materials Chemistry A, 2018, 6, 23542–23549.

2.26 Photoinduced Reaction of Sulfur with Cyclopentadienyliron Dicarbonyl Dimer and Crystal Structure of Bis(Cyclopentadienyliron) Monocarbonyl Tetrasulfide; C. Giannotti, A. M. Ducourant, H. Chanaud, A. Chiaroni, C. Riche; Journal of Organometallic Chemistry, 1977, 140, 289–295.

2.27 Sulfur Chelates IV. Sulfur Addition to Dithiolato Complexes of Nickel (II); D. Coucouvanis, J. P. Fackler; Journal of the American Chemical Society, 1967, 89, 1346–1351.

2.28 Organometallic Chalcogen Complexes. XVI. Preparation and Structural Characterization of Co4(π-C5H5)4S6. A New Mode of Transition Metal Bonding for a Disulfide Group; V. A. Uchtman, L. F. Dahl; Journal of the American Chemical Society, 1969, 91, 3756–3763.

2.29 Synthesis and Reactions of Binary Metal Sulfides. Structural Characterization of the [(S4)2Zn]2- , [(S4)2Ni]2- , [(S5)Mn- (S6)]2- , and [(CS4)2Ni]2- Anions; D. Coucouvanis, P. R. Patil, M. G. Kanatzidis, B. Detering, N. C. Baenziger; Inorganic Chemistry; 1985, 24, 24–31.

2.30 Synthesis, Characterization, and Reactions of Iron-Sulfur Clusters Containing the S2 Ligand: [Cp2Fe2(S2)(SR)2]0,1+, [Cp4Fe4S5]0,1+,2+, and [Cp4Fe4S6]; G. J. Kubas, P. J. Vergamini; Inorganic Chemistry, 1981, 20, 2667–2676.

2.31 Oxidation of Molybdenum Dithiocarbamate Complexes with Elemental Sulfur; J. W. Mcdonald, W. E. Newton; Inorganica Chimica Acta, 1980, 44, 81–83.

2.32 Dithiocarbamate group transfer cyclization reactions of carbamoyl radicals under "Tin Free" conditions; R. S. Grainger, P. Innocenti; Angewandte Chemie International Edition, 2004, 43, 3445–3448.

2.33 Li-7, Na-23, K-39 and Cs-133 NMR comparative equilibrium study of alkali metal cation hydroxide complexes in aqueous solutions. First numerical value for CsOH formation; K. Popov, L. H. J. Lajunen, A. Popov, H. Rönkkömäki, M. Hannu-Kuure, A. Vendilo; Inorganic Chemistry Communications, 2002, 5, 223–225.

2.34 Hyperbranched multiple polythioamides made from elemental sulfur for mercury adsorption; A. Yasin, Y. Chen, Y. Liu, L. Zhang, X. Zan, Y. Zhang; Polymer Chemistry, 2020, 11, 810–819.

2.35 CCDC 1555240: Experimental Crystal Structure Determination [Data set]. Cambridge Crystallographic Data Centre. A. Batsanov, 2017, https://doi.org/10.5517/CCDC.CSD.CC1P6C19

Liam James Dodd

2.36 Zinc Dithiocarbamate Lubricating Oil Additives; G. A. Aguilar, F. S. Cheng, K. J. Chase; U.S. Patent 0258896, 11/09/2012.

Liam James Dodd

Chapter 3: Self-Activating Crosslinkers

Whilst catalysis brings several benefits to inverse vulcanisation, it also draws some concerns, such as the sustainability of metal containing catalysts when there are limited supplies of metals available. There is also the potential for contamination of the environment with metal residues from the polymers, if those polymers are not purified of their catalyst. In some cases catalyst extraction from the polymers may not be possible, or it could be an extra energy expenditure in their synthesis which hinders the sustainability of the polymers. These concerns can be circumvented with non-metallic catalysts, namely amines.

This chapter explores research into the use of amines as catalysts in inverse vulcanisation, as well as functionalised amines which are intentionally incorporated into the polymer structure, thus making them activators. This led to the investigation of alkyne containing amines, and a study of how they polymerise, which is interesting because to date, alkynes have been under-investigated in inverse vulcanisation, despite their potential to crosslink twice per moiety, potentially leading to a polymer where more sulfur can be stabilised. Such activators with crosslinking moieties were also investigated as lone comonomers in addition to being included in catalytic quantities alongside a primary comonomer. In the prior case, a dispersion polymerisation method was developed to work with the high rate of an inverse vulcanisation with such large quantities of activator.

3.1. Project Outline

Whilst catalysis is versatile in the crosslinkers it positively affects, there are some remaining concerns regarding its application.[3.1] First is whether the catalyst can or should be extracted from the polymer, and what consequences such a post synthetic step might have on the polymers and their production cost. This concern could be eliminated if the catalytic molecule was intentionally incorporated into the polymer structure. Though it would no longer be a true catalyst due to its consumption in the reaction, the 'catalyst' molecule would then contribute to the polymer's properties as a crosslinker, rather than an impurity. Thus the 'catalyst' would be considered an activator, and this term will be used henceforth when referring to this work.

The second concern is that many established catalysts are derived from metal dialkyldithiocarbamates, leaving a trace metal residue in the polymers, raising environmental concerns.[3.1] If the metallic catalyst could be replaced by a fully organic molecule, which has been demonstrated with amines, then this issue would also be circumvented.[3.1,3.2] It has previously been reported that DCPD can be used as a second organic comonomer in an inverse vulcanisation reaction that mainly consists of some other organic comonomer, and it was found that this was beneficial to the properties and allowed tuning of the T_g. Thus, it is not difficult to imagine an amine containing crosslinker taking up a similar role as DCPD.[3.3]

In line with these ideas, this work focused upon the inverse vulcanisation of self-activating amine crosslinkers: molecules that contain both an activating amine moiety and crosslinker moieties. In doing so, alkyne crosslinkers, which have thus far seen limited research attention in inverse vulcanisation, were also explored as a natural branch of this research avenue.[3.4] Alkynes have the potential to react with sulfur twice, forming twice as many crosslinks as an alkene would, and this could lead to a higher crosslink density (Figure 3.1). As such, it was thought that alkynes may permit a smaller load of crosslinker to be capable of stabilising more sulfur, leading to even higher sulfur contents in the resultant polymers, which could be valuable to the electrochemical applications, and the antimicrobial applications of inverse vulcanised polymers.

Liam James Dodd

That being said, recent developments in the field of inverse vulcanisation show that there could be complications to this statement. Pyun *et al.* recently found evidence that polymers of DIB do not react as was initially thought; rather than radical addition across the double bond to create two new C-S bonds, a more complex mechanism dominates, resulting primarily in a linear polymer unit where each double bond produces one new C-S bond.[3.5] Whether reactions with alkynes could be subject to the same sort of mechanism is unknown, but because Pyun's new findings centre around the formation of thiocumyl moieties and there seems there is no intuitive way such a moiety could form from an inverse vulcanised polymer of an alkyne, it will be initially assumed that radical addition as traditionally expected of inverse vulcanisation occurs here.[3.5] Furthermore, it cannot be that all comonomers in inverse vulcanisation are subject to this new mechanism proposed by Pyun, because if that were the case, styrene would not be able to form an inverse vulcanised polymer, but it is documented that it can.[3.6]

Several self-activating crosslinkers to be used in inverse vulcanisation reactions were identified (Figure 3.1). Tripropargylamine (TPA) is an example of an alkyne and an amine containing crosslinker, comparable to the already published alkene analogue triallylamine (TAA) which was used here as a direct comparison to TPA to examine the differences between alkyne and alkene comonomers.[3.7] 1,8-nonadiyne (NON), although not directly comparable to TPA in terms of structure, was used as the best available comparison to TPA in terms of an alkyne crosslinker without a self-activating amine moiety. Additionally, diallylamine (DAA) and monopropargylamine (MPA) were also successfully polymerised, which is particularly exciting since they can be polymerised at below the melting temperature of sulfur, and MPA has only a single alkyne moiety. Finally, TPA and TAA were shown to successfully blend with DCPD and linseed oil in inverse vulcanisations, showing their value as trace presence activators.

$$\kappa = \text{(Number of Double Bonds * 1000) / Molecular Weight}$$
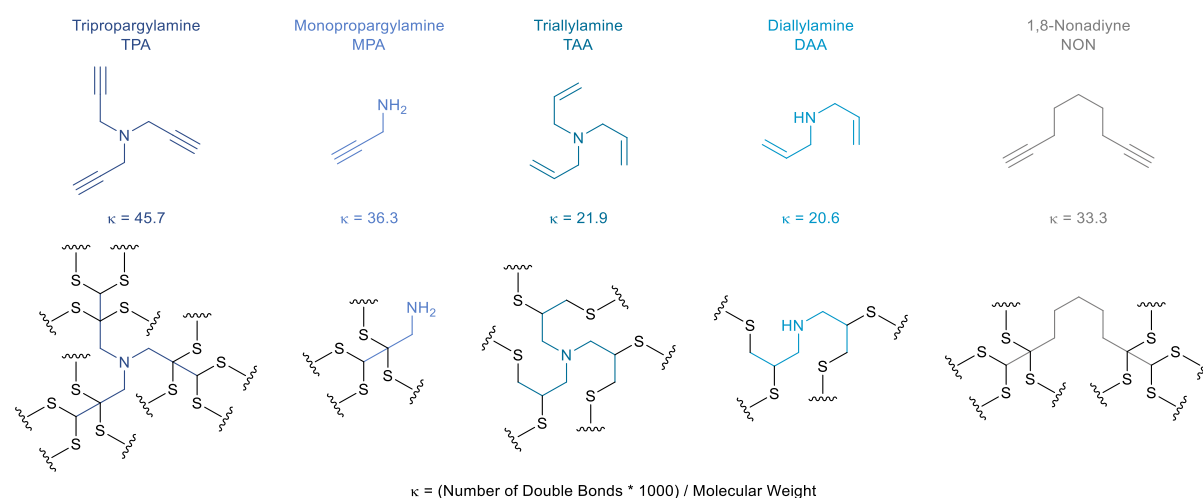
Figure 3.1: Names, abbreviations, molecular structures, and potential for crosslinking (κ) values, for the crosslinkers used in this study, as well as schematics illustrating their potential to crosslink chains of sulfur. For comparison, DVB has κ = 15.

3.2. General Considerations

All chemicals were used as received. All Chemicals were obtained from Sigma Aldrich unless otherwise specified. Ground sulfur sublimed powder reagent grade ≥99.5 % was obtained from Brenntag UK & Ireland. Triallylphosphine 97+% and triallylphosphite were obtained from thermo scientific. Triallylphosphate >96%, Dicyclopentadiene (stabilised with BHT) [precursor to Cyclopentadiene] >97%, and 1,3-Diisopropenylbenzene (stabilised with TBC) >97% were obtained from Tokyo Chemicals Industry. Prop-2-yn-1-amine 98% was obtained from Manchester organics. CHNS combustion

Liam James Dodd

microanalyses were performed on an elementar Vario Micro cube, with a first analysis performed to acquire rough data that was then used to calibrate the instrument for a second, more accurate analysis. Differential scanning calorimetry was performed on a TA instruments DSC25 discovery series equipped with an RCS90 and using Tzero aluminium hermetic pans and aluminium lids, in the heating range -90 °C to 150 °C, at a heating rate of 15 °C min^{-1} and a cooling rate of 7.5 °C min^{-1}. PXRD data were collected in transmission mode on a Panalytical X'Pert PRO MPD equipped with a high throughput screening (HTS) XYZ stage, X-ray focusing mirror and PIXcel detector, using Cu Kα radiation. Data were measured on loose powder samples held on thin Mylar film in stainless steel well plates, over the range 4 to 40 ° in approximately 0.013 ° steps over 60 minutes. FT-IR spectra were obtained on a Bruker vertex 70 diamond ATR. All TGA data was obtained on a TA instruments TGA550, operating under nitrogen with a ramp rate of 20 °C min^{-1} using platinum pans equipped with disposable aluminium cups. For the battery testing, samples were held isothermal at 350 °C for 1 hour.

3.3. Method

To begin this study, the aforementioned crosslinkers were used as the sole comonomer in inverse vulcanisation reactions, providing a simpler starting point compared to reactions where they would be used in conjunction with another crosslinker. Initial attempts to synthesize inverse vulcanised polymers of TPA, TAA, and NON via bulk polymerisation were unsuccessful. NON formed an unacceptably inhomogeneous polymer, whereas TPA and TAA violently underwent the TNE, not surprising given that in a 50 % by mass sulfur reaction, the remaining 50 % of the mass is all activator.

Bulk polymerisations are prone to the TNE due to their poor heat dissipation, however the addition of a solvent to the polymerisation can significantly decrease the risk by diluting the heat production over a larger volume. As such a dispersion polymerisation method was employed, which after optimisation, came to the following general method: mass X ± 0.0050 g of sulfur and mass Y ± 0.0050 g of a chosen crosslinker (X plus Y always equalled 10 g in every reaction) were reacted overnight in 50 cm^3 refluxing xylene with 1400 rpm stirring. This afforded two products: one that was insoluble in the xylene, and one that remained soluble in the xylene.

The two were separated by filtration, though the xylene-insoluble product often remained adhered to the round bottom reaction flask, and was removed by embrittlement via direct addition of liquid nitrogen and scraping with a spatula. The xylene-soluble product was evaporated to dryness, and then cured overnight in an oven at 140 °C. The resultant xylene-soluble product after curing was termed, the Sol product, of which it is important to note, may no longer be soluble in xylene and other solvents due to reacting and crosslinking further upon curing. That is, the Sol product is the material given from reaction that was soluble in xylene immediately after the reaction, but may no longer be soluble due to being cured overnight to form a more crosslinked structure.

On the other hand, the xylene-insoluble material obtained from the reaction was purified by Soxhlet extraction on toluene overnight, after which it was cured in an oven at 140 °C to give what was termed, the Insol product. In summary, the Sol product is the material that, after purification and curing, was obtained from the xylene solution of the reaction. It is important to remember that although the Sol product originated from a soluble species, it may no longer be soluble after the processing. Meanwhile, the Insol product was obtained by purifying and curing the material that naturally precipitated out of the xylene reaction solution. The products of these reactions will be referred to by the following naming convention: NAMEα-Sβ-X, where NAME is the abbreviation of the crosslinker in use, α is the feed ratio of that crosslinker in the reaction, β is the feed ratio of sulfur in that reaction, and X is replaced with either Sol to refer to the Sol product, or Insol for the Insol product.

Liam James Dodd

The above optimised method was reached after several iterations where several variables were modified. It was found that reaction volumes of 25, 50, and 100 mL of xylene had negligible effect, and so 50 mL was chosen as the best compromise between convenient extraction and efficient use of solvent. With a 50 mL reaction volume, sodium dodecyl sulfate as a surfactant was tested, in weights of 0.01, 0.1, and 1 gram in a reaction, which was found to have negligible effect on the reaction.

The method for polymerising MPA and DAA had to be modified because these crosslinkers boil below the melting temperature of sulfur (83 °C for MPA and 111 °C for DAA). To account for this, MPA and DAA were reacted as above, but at the initial temperatures of 70 °C and 100 °C, respectively. After 24 hours, a pre-polymer had formed. Attempting to cure this pre-polymer in the oven resulted in the TNE. Instead, the reaction was continued in the round bottom reaction flask by increasing the temperature to reflux and leaving it overnight. Other than this modification, the method remained the same as the general method.

Interestingly, MPA and DAA reacted with sulfur despite the sulfur not having sufficient thermal energy to melt or undergo ring-opening, which is the generally accepted route for initiation of the polymerisation. This suggests that amine containing crosslinkers may offer an alternative route for initiation, perhaps by direct nucleophilic attack of the nitrogen upon the sulfur rings. This would cleave open the sulfur rings to yield reactive sulfide anions, which would open up an anionic polymerisation pathway. Such anionic polymerisations with an electron rich alkene might be unexpected, especially because it yields a carbanion, which is generally accepted to be unreactive, however, the mechanism proposed in Figure 3.2 avoids this intermediate via a concerted transition state.

This conclusion of an amine initiated anionic pathway is supported by the fact that when 1,7-octadiene (boiling point 114 to 121 °C, initial reaction temperature 100 °C), which was thought to be a good comparison to NON, was used in such a reaction, no changes were observed. 1,7-octadiene has no amine moiety, and since it was exposed to temperatures insufficient to ring open sulfur, there were no sulfur radicals to initiate the polymerisation, so without an alternate source of initiation, no reaction occurred. The lack of reaction was confirmed by the fact that after the reaction period, yellow sulfur powder in a clear and colourless solvent was observed, exactly the appearance of the reagents. ^{1}H NMR of the xylene solvent revealed unreacted 1,7-octadiene was the only impurity.
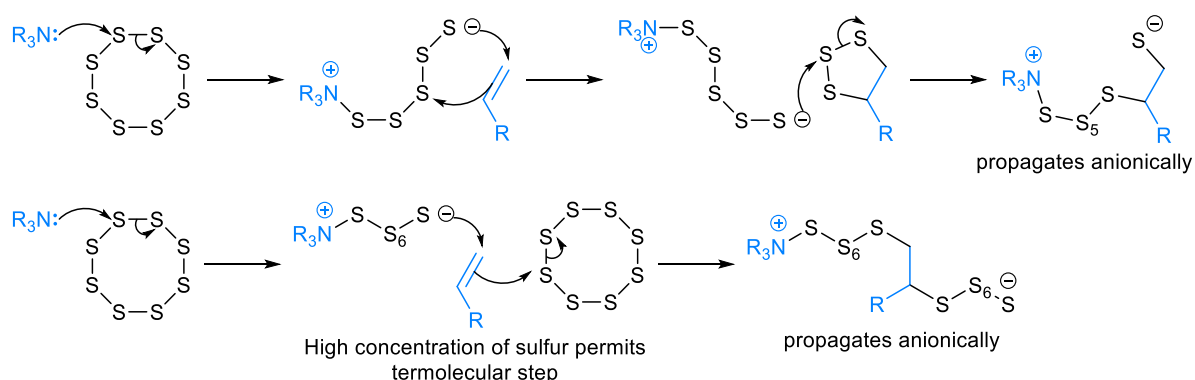
Figure 3.2: Proposed mechanism for anionic initiation of an inverse vulcanisation reaction by nucleophilic activation via amine activator.

Liam James Dodd

3.4. Yields

Figure 3.3 shows the yields of the Sol and Insol products of dispersion polymerisation inverse vulcanisations of TPA, TAA, NON, DAA, and MPA. As the mass loading of TPA was increased, the yield of the TPA Insol product also increased, up to a maximum at 50 % mass loading, after which it began to decrease. An explanation for this is that as more crosslinker is added, more sulfur is able to be incorporated into the polymer, giving a greater yield, until it reaches the point where there is so much crosslinker that there is then not enough sulfur to react with all the crosslinker, resulting in wastage of crosslinker and thus a lower yield.

Figure 3.3: The yields of the Sol and Insol products at different weight percentages of crosslinker in the reaction feed for a) TPA and MPA, b) TAA and DAA, c) NON.

The yield of the Sol product remained relatively constant for different mass loadings of TPA, with a significant dip at 50 % mass loading. An explanation for this is that as more crosslinker is added, there is the potential to form more products overall, both Sol and Insol. However, because there is a limited supply of reagents, the Sol and Insol products are in competition with one another. Higher crosslinker loads would favour the more highly crosslinked Insol product. This would explain why the yield of the Sol remains relatively constant, even though there is more crosslinker available to form products, and it would also explain the dip in yield for the sol product when the Insol product was at its highest yield; where the Insol product was taking up the majority of the reagents, leaving few to form the Sol product. At high crosslinker loadings of TPA (70 %) the yield of the Sol product went up whilst the yield of the Insol went down. This could be due to an insufficient supply of sulfur to fully incorporate all of the crosslinker molecules into a network, instead yielding more of the less crosslinked Sol product.

In comparison to TPA, MPA shows a relatively similar behaviour, but with some minor differences that likely arise due to the difference in potential for crosslinking between them. Overall, the Insol yields for MPA were lower than those for TPA, which is reasonable because MPA contains fewer double bonds and so has less capacity to crosslink chains of sulfur. Thus, it would be expected that MPA would not be able to stabilise as much sulfur as TPA. It is an interesting result that MPA, which contains only a single alkyne unit, was able to produce polymers sufficiently crosslinked that they became insoluble in the reaction solution, which provides evidence that both double bonds of the alkyne react. Conversely, at high loadings of sulfur, MPA provided greater yields of the Sol product than TPA, again explained as MPA having less crosslinking capacity, and being more prone to forming lower molecular

Liam James Dodd

weight, less crosslinked products. Just as for TPA, at high loadings of MPA, the yield of the Insol product increased at the expense of the Sol product, explained with the same reasoning as for TPA.

The trends observed for TPA are also observed in the yield trends of NON, suggesting that these two alkyne crosslinkers behave relatively similarly, despite the presence or absence of an activating amine moiety. That being said, the absolute values for the yields of NON are higher for its Sol product and lower for its Insol product. This could be due to the fact that NON has one fewer alkyne groups to react and form a polymer, and thus NON has less crosslinking capacity per molecular weight unit, which would make it favour the less crosslinked Sol product over the more crosslinked Insol product.

TAA shows different trends in its yield data than TPA or NON, however TAA's trends could still be explained by the same principles. In this case the Sol products' yields were higher than the Insol products. This could be because TAA is an alkene, so it can only react once per alkene moiety, whereas its alkyne analogue, TPA could potentially react twice. As a result, TAA would only be able to react half as many times, and would therefore favour the less crosslinked Sol product over the more crosslinked Insol product. In this case TAA favours the Sol product sufficiently that the Sol product has a higher yield than the Insol product. This yield of Sol product rises as the loading of TAA in the reaction increases. This could be explained by a greater incorporation of sulfur into the polymer with more crosslinker being available to react with it. Otherwise, the TAA Insol products follow the same rise and fall in yield as the TAA loading is increased, likely for the same reason as TPA and NON's Insol products.

Surprisingly, DAA does not behave similarly to TAA, and instead DAA's yields much more closely match those trends seen in TPA and NON. This difference in behaviour between TAA and DAA is ascribed to the fact that TAA is a tertiary amine, whereas DAA is a secondary amine, and so has an N-H bond, which might show unexpected chemistry. Another surprising difference is that DAA overall shows higher absolute yields than TAA, despite having one fewer double bond to react with sulfur, which is suggested to be the effect of unexpected chemistry involving the N-H bond.

It can be seen in several cases in the yield data, that the Sol and Insol yields for a particular polymer at a particular feed percentage of crosslinker, sums to less than 100 %. This could be due to the loss of hydrogen sulfide gas. Another likely loss to the yields was the formation of a volatile fraction, as it was noted that solvent condensed during the rotary evaporation stage of the reaction processing, was frequently coloured yellow. Since this solvent was discarded, any volatised oligomers of polymer contained therein would not contribute to the yield.

3.5. Solubility Studies

Figure 3.4 shows the soluble fractions of the Sol and Insol products of dispersion polymerisation inverse vulcanisations of TPA, TAA, NON, MPA, and DAA. It is important to remember that during the post-reaction processing, the Sol and Insol products are made by curing their precursors after extracting them from the reaction. This curing leads to increased crosslinking, and so the Sol and Insol products will have decreased in solubility during this curing. As such, just because the Sol product originated from the xylene-soluble product of the reaction, it may not be soluble after this processing.

For each solubility study, approximately 50 mg (within 2 mg) of polymer was left in 2 cm^3 of chloroform for 24 hours. After this time the chloroform was filtered off into a pre-weighed vial. The chloroform was left for 3 days to fully evaporate, after which time the vial was reweighed to determine the mass of the soluble fraction, which was then taken as a percentage of the initial 50 mg of polymer.

Liam James Dodd

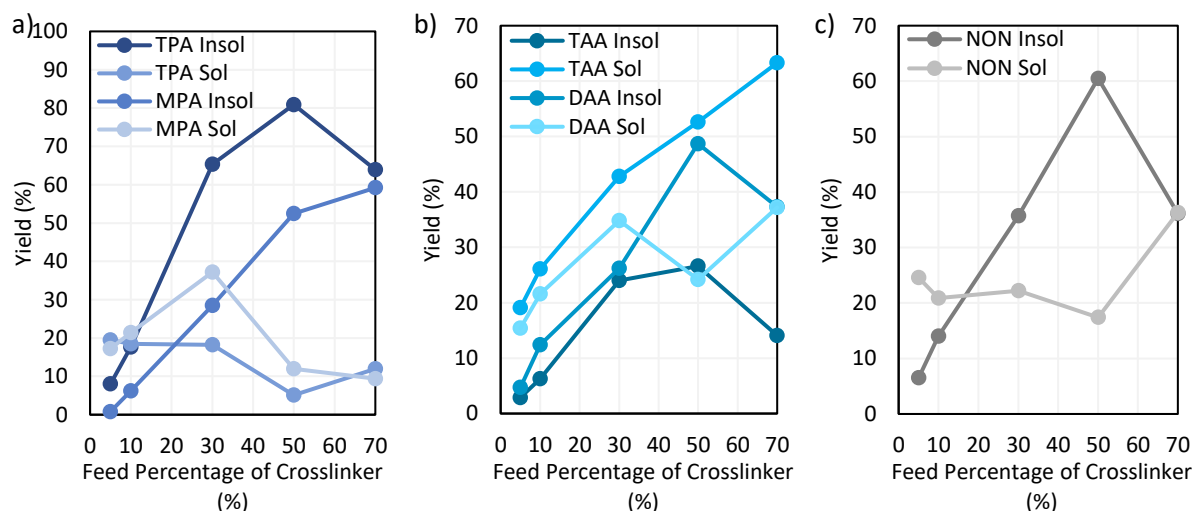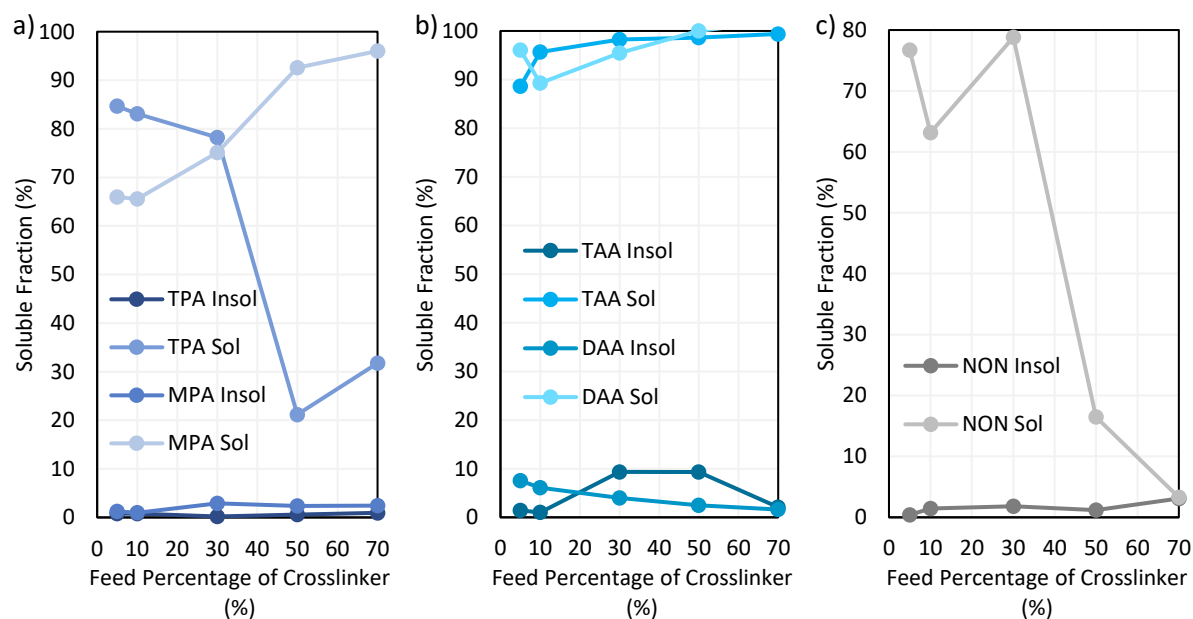Figure 3.4: The soluble fractions of the Sol and Insol products at different weight percentages of crosslinker in the reaction feed for a) TPA and MPA, b) TAA and DAA, c) NON.

The Insol products of all the different crosslinkers in all cases showed very low to no soluble fraction, indicating a highly crosslinked and therefore insoluble structure for the Insol products. In line with the conclusions from the yield data, the TAA Sol products all showed very high soluble fractions, indicating low crosslink density and low molecular weight in the TAA Sol products, similarly observed for DAA. The Sol products of NON and TPA show a similar trend in that they show a high soluble fraction for crosslinker loadings of 30 % or lower, and a lower soluble fraction for crosslinker loadings of 50 % and higher. This could be because at such high crosslinker loadings for the alkynes, there is sufficient crosslinking upon curing, that even the Sol product is quite crosslinked and of high molecular weight.

It is worth noting that polymers of NON do not contain a nitrogen atom, whereas polymers of TPA, MPA, TAA, and DAA do, and it cannot be known from this study, whether the nitrogen atom has an effect on the solubility of the polymers in chloroform, or whether the soluble fraction is solely influenced by the crosslink density and molecular weight. Both the solubility study and the yield data suggest that polymers of NON and TPA, which are both alkyne crosslinkers, behave similarly to each other and differently to polymers of TAA, which is an alkyne crosslinker. This is observed in spite of the fact that NON does not contain a nitrogen atom, and so is not self-activating, but TPA does contain a nitrogen atom and is self-activating. This does not mean that TPA's self-activation is not beneficial, as polymers of TPA typically showed yields higher than those of NON, but instead points to the conclusion that the alkyne moiety's capacity to react multiple times is the dominant factor in terms of the crosslink density. Why the Sol products of MPA become increasingly soluble with rising crosslinker loading cannot be explained at this time.

3.6. Differential Scanning Calorimetry

Note that for Figure 3.5, the bars do not show the error in the measurement but instead show the onset and end temperatures of the T_g. Observing Figure 3.5, it can be seen that the T_g's obtained from the second heating cycle of DSC for TAA follow an expected trend. For both the Sol and Insol products, as the mass loading of TAA was increased, the T_g increased too, explained by the increasing amount of TAA giving more crosslinking in the product polymers. The T_g's of the Sol products of TAA inverse vulcanisations were always lower that the corresponding Insol products, which provides evidence to

Liam James Dodd

the conclusion that the Insol products are more crosslinked than the Sol products. The Sol products for DAA show a similar trend to those of TAA, however for the DAA Insol products, unexpectedly the T_g decreases as the loading of crosslinker increases (accepting that the T_g for DAA50-S50-Insol could not be identified). A possible explanation is that as the quantity of crosslinker is increased, there becomes insufficient sulfur to form a well crosslinked network, leaving more and more double bonds unreacted at higher crosslinker loadings. This would give the polymer more linear character, resulting in a lower T_g.

However, if this was the case then a raise in the solubility of DAA Insol polymers with increasing crosslinker loading would be expected, which is not observed, and furthermore, polymers of TPA and TAA would be expected to show the same trend, as they have even more double bonds to react, and so should suffer from this effect more so than DAA, which is not the case. As such, the best explanation that can be postulated here is that the unexpected behaviour of DAA is due to its N-H bond which could introduce unexpected chemistry, whereas TAA and TPA are both tertiary amines and contain no N-H bonds. Sol polymers of NON show a similar trend to that of TAA, however the Insol products of NON, MPA, and TPA showed an interesting result in that the Insol polymers often did not show a T_g at all, except at very low crosslinker loadings.
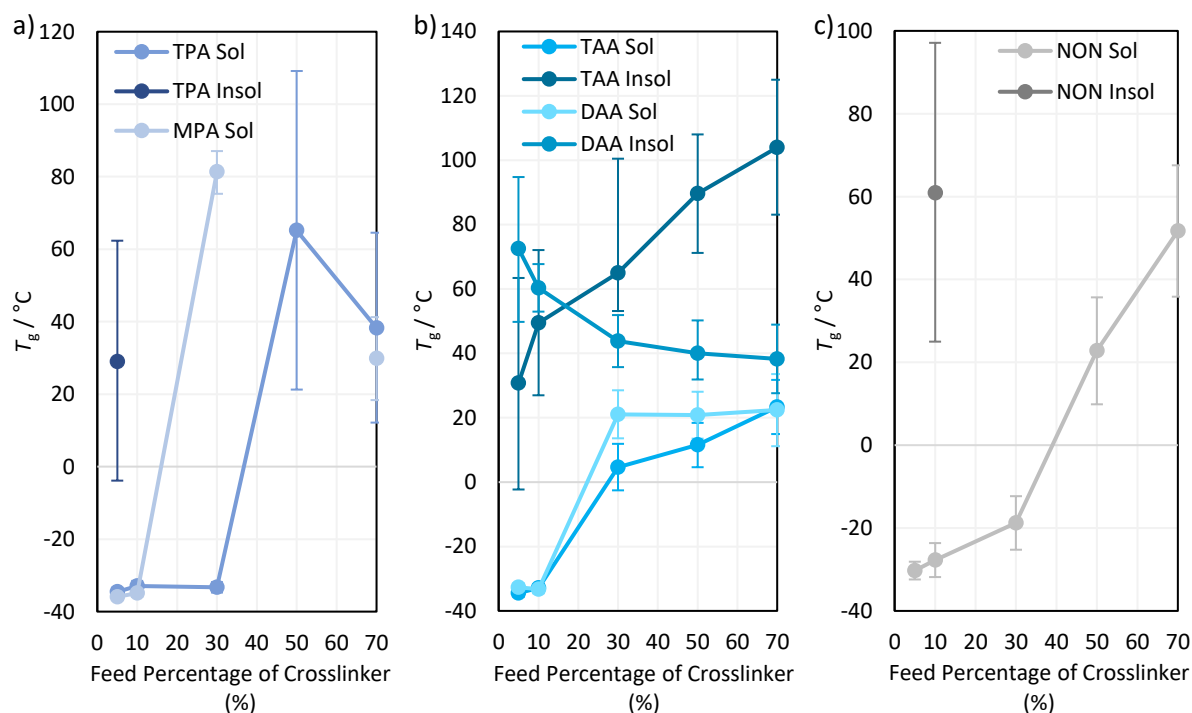
Figure 3.5: The T_g's, obtained from the second heating cycle of DSC, of the Sol and Insol products at different weight percentages of crosslinker in the reaction feed for a) TPA and MPA, b) TAA and DAA, c) NON. Note that the bars indicate the onset and end temperatures of the T_g.

TGA analysis provided no meaningful trends between the polymers' decomposition temperatures, and it was inaccurate to determine the mass losses as the steps were drawn out. Additionally, TGA experiments were particularly detrimental to the instrument, and so only a few select samples were run, with the protocol chosen to minimise the maintenance load on the TGA. TGA analysis did show that the polymers' decomposition temperatures are all above 190 °C, yet they show no T_g below this temperature (Figure 3.6). This suggests that the alkyne crosslinkers have such a high crosslink density, that their T_g is higher than their decomposition temperature; the polymer will decompose before becoming a melt or flexible material, which cannot be said of any other inverse vulcanised polymer at

Liam James Dodd

this time. To confirm this, the Insol polymers of TPA and NON were heated upon a hotplate to 170 °C and then agitated with spatula, revealing that they were still glass-like and brittle.

Note that an explanation for the change in T_g of TPA and MPA's Sol products with increasing mass loading of TPA cannot be given at this time, though they appear to have a similar trend, with the exception that MPA is staggered to the left. Additionally, MPA Insol products showed an endothermic peak in their heating cycles, at -48 °C, and a corresponding exothermic peak in their cooling cycles at −52 °C. These peaks were weaker in samples with less sulfur, implying that they are a melt transition linked to either free sulfur species, or the sulfurous component of the polymer. In some cases, particularly for the Insol products, the onset to end range of the polymers' T_g's are quite broad, which may indicate a microscopically inhomogeneous polymer with many different environments for the polymer chains, each with different degrees of immobilisation, and this could result in a more drawn out T_g.

Polymer	Insol T_d / °C	Sol T_d / °C
TPA70-S30	209.8	227.0
TPA50-S50	210.3	196.2
TPA30-S70	214.9	211.4
TPA10-S90	213.9	221.0
TPA5-S95	209.6	223.4
TAA70-S30	206.7	218.8
TAA50-S50	198.5	214.3
TAA30-S70	194.2	215.3
TAA10-S90	194.3	215.6
TAA5-S95	210.2	222.1
NON70-S30	217.5	209.8
NON50-S50	218.3	204.9
NON30-S70	213.4	212.2
NON10-S90	217.0	220.0
NON5-S95	219.8	224.4
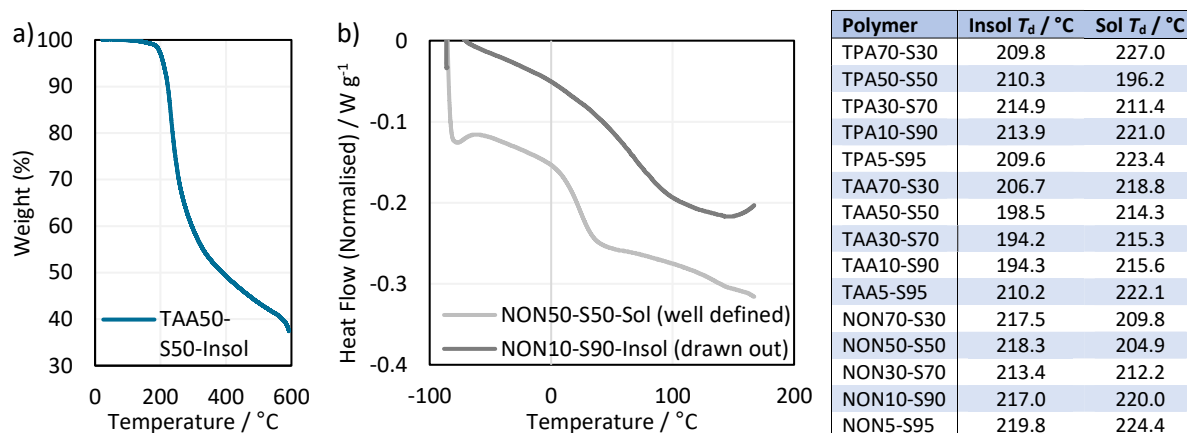
Figure 3.6: a) a representative TGA thermogram, b) a representative DSC thermogram, as well as a table listing some decomposition temperatures for certain polymers obtained from TGA.

DSC was able to detect the presence of crystalline elemental sulfur in the polymers (endothermic peaks in the heating cycles, corresponding to the melt transitions of elemental sulfur at 110 to 120 °C), with a corroborating technique being PXRD, which can detect the crystalline scattering peaks amongst the polymers' amorphous scattering signal. In general, as seen in Table 3.1, there was good agreement between DSC and PXRD in terms of detecting elemental sulfur in the polymers. DSC and PXRD found that Sol products of 30 % or less crosslinker feed ratio, regardless of crosslinker identity, contained crystalline elemental sulfur. This suggests that these polymers do not have sufficient crosslinking to stabilise all of their sulfur, and either some left over sulfur reactant remains as an impurity, or some polymerised sulfur is depolymerising to give the crystalline elemental sulfur contaminant. DSC suggested that none of the Insol products contained elemental sulfur, which for TPA, TAA, and NON, PXRD agreed with. This suggests that these products are sufficiently crosslinked to stabilise all their sulfur, at the various sulfur loadings used here, though it is worth remembering that the Soxhlet extraction used to purify the Insol products, may also have purified the Insol products of elemental sulfur too. In the cases of MPA50-S50-Insol, MPA30-S70-Insol, MPA10-S90-Insol, MPA5-S95-Insol, DAA50-S50-Insol, and DAA30-S70-Insol, PXRD detected crystalline elemental sulfur where DSC did not. For MPA Insol products, it is perhaps not surprising that they contain some elemental sulfur, as MPA contains only two double bonds by which it can crosslink, in the form of an alkyne, and so it lacks the crosslinking potential of the other crosslinkers. As such it seems that the PXRD results are trustworthy, even though they are in contradiction with the DSC; it may be that DSC was not sufficiently sensitive to detect the crystalline elemental sulfur.

Liam James Dodd

Table 3.1: Detection of elemental sulfur in Sol and Insol polymers by DSC and PXRD.

Polymer	Elemental Sulfur by DSC		Elemental Sulfur by PXRD	
	Insol	Sol	Insol	Sol
TPA70-S30	No	No	No	No
TPA50-S50	No	No	No	No
TPA30-S70	No	Yes	No	Yes
TPA10-S90	No	Yes	No	Yes
TPA5-S95	No	Yes	No	Yes
TAA70-S30	No	No	No	No
TAA50-S50	No	No	No	No
TAA30-S70	No	Yes	No	Yes
TAA10-S90	No	Yes	No	Yes
TAA5-S95	No	Yes	No	Yes
NON70-S30	No	No	No	No
NON50-S50	No	No	No	No
NON30-S70	No	Yes	No	Yes
NON10-S90	No	Yes	No	Yes
NON5-S95	No	Yes	No	Yes
MPA70-S30	No	No	No	Yes
MPA50-S50	No	Yes	Yes	Yes
MPA30-S70	No	Yes	Yes	Yes
MPA10-S90	No	Yes	Yes	Yes
MPA5-S95	No	Yes	Yes	Yes
DAA70-S30	No	No	No	No
DAA50-S50	No	No	Yes	No
DAA30-S70	No	Yes	Yes	No
DAA10-S90	No	Yes	No	Yes
DAA5-S95	No	Yes	No	Yes

For the DAA Insols that contain elemental sulfur by PXRD, it is hard to explain the results, given that polymers with a greater loading of sulfur reactant, did not display elemental sulfur presence by PXRD or DSC. One potential explanation for the unexpected results could be the time difference between taking the DSC and PXRD measurements. It has been shown that over time, elemental sulfur can crystallise from inverse vulcanised polymers. As such, the DSC measurements, taken shortly after the polymers were synthesized may not show elemental sulfur signals, whereas the PXRD measurements, which were taken as soon as the instrument was available sometime after the polymer synthesis, do show elemental sulfur signals. To help corroborate this, the DSC experiments were repeated after the PXRD experiments, and in this case, DSC was able to detect some elemental sulfur in agreement with the PXRD results. It is hard to know exactly when a polymer will begin to display elemental sulfur signals due to ageing, and it may be that given long enough, all polymers synthesized here will begin to develop sulfur crystals that can be detected by DSC and PXRD. Raman spectroscopy was also attempted for the detection of elemental sulfur, but was unsuccessful due to the intense fluorescence of the dark coloured samples.[3.8] TLC was also unsuccessful at detecting elemental sulfur where PXRD and DSC could not, perhaps because there was no elemental sulfur, or perhaps because the samples were sufficiently crosslinked that elemental sulfur remained entrapped and immobilised in the polymer structure, preventing its extraction into the TLC eluent.

3.7. Fourier Transform Infra-red Spectroscopy

Because of the high IR transparency of the polymers, FTIR spectroscopy was of limited use in characterisation. There was little difference in the spectra of the same polymer with different sulfur

Liam James Dodd

loadings. Because of this, even though FTIR spectra were obtained for all products, only the spectra of the neat crosslinkers, and the Sol and Insol products at 50 % crosslinker loading are shown in Figure 3.7, though all spectra are available in Section 3.12.1.
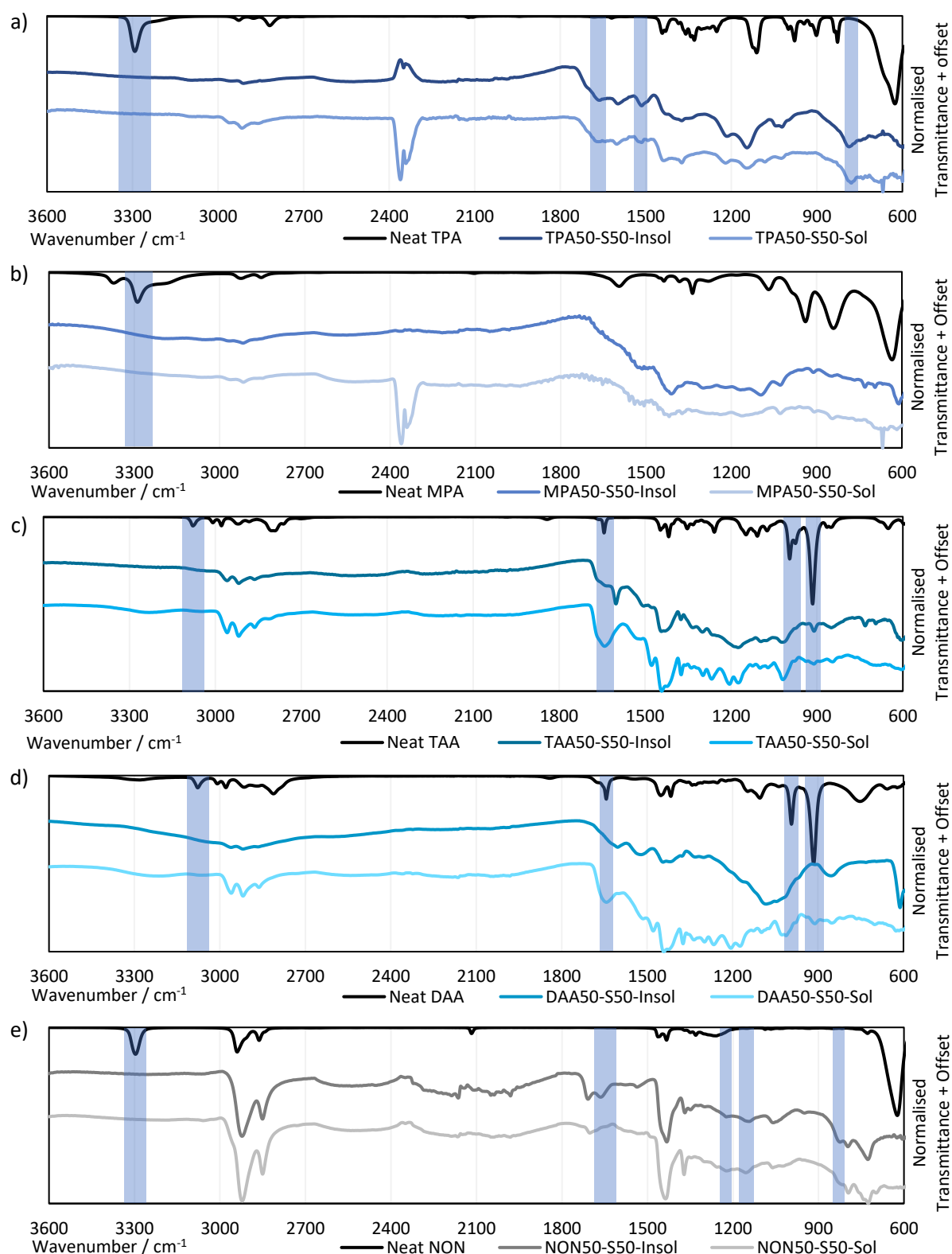
Figure 3.7: FTIR spectra of a) Neat TPA, TPA50-S50-Insol, and TPA50-S50-Sol; b) Neat MPA, MPA50-S50-Insol, and MPA50-S50-Sol; c) Neat TAA, TAA50-S50-Insol, and TAA50-S50-Sol; d) Neat DAA, DAA50-S50-Insol, and DAA50-S50-Sol; e) Neat NON, NON50-S50-Insol, and NON50-S50-Sol.

Liam James Dodd

To assist with the assignment of the spectra, density functional theory was used to predict the IR spectra of abbreviated models of the polymers (Figure 3.8). The spectral data for these polymer models are shown in Table 3.2. Calculations were performed according to pre-established literature methods found to be successful for inverse vulcanised polymers: an initial energy minimisation with MMFF94s molecular mechanics, followed by geometry optimisation and energy calculation using the BP86 functional, the def2-TZVPP basis set, and a GD3(BJ) empirical dispersion correction, all using the Gaussian 09 code.[3.8]
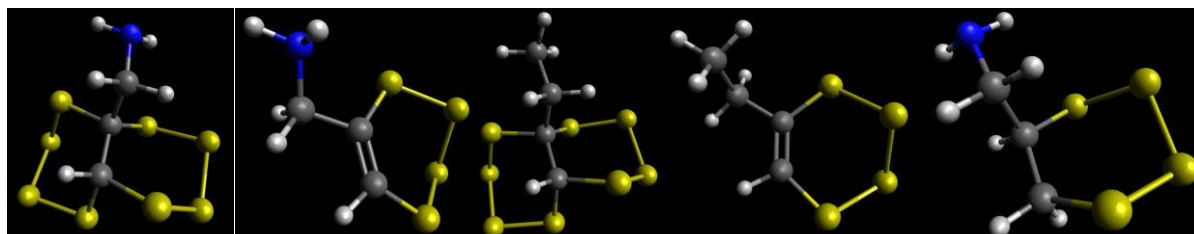
Figure 3.8: Geometry optimised structures for the models of the polymers. From left to right the identities are MPAfullreact (used in comparison to TPA and MPA polymers), MPApartreact (used in comparison to TPA and MPA polymers), NONfullreact (used in comparison to NON polymers), NONpartreact (used in comparison to NON polymers), TAAfullreact (used in comparison to TAA and DAA polymers). White atoms are hydrogen, grey atoms are carbon, yellow atoms are sulfur, and blue atoms are nitrogen.

Table 3.2: Calculated IR data for the models of the polymers.

Model	Wavenumber / cm^{-1}	Assignment
MPAfullreact	653.659	1,2 - C-S asymmetric stretch, with skeletal vibrations
	692.846	1,1 - C-S asymmetric stretch, with skeletal vibrations
	718.928	1,1 - C-S symmetric stretch, with skeletal vibrations
	806.712	NH_2 vibration
	884.233	Carbon skeleton vibration with C-S asymmetric stretch
	936.638	C-C-C asymmetric stretch
	971.676	N-C-C-C asymmetric stretch
	1072.88	S_2C-H wag
	1100.89	N-C stretch
	1146.45	C-H and N-H wags
	1194.03	C-H and N-H wags
	1313.59	CH_2 wag
	1348.31	NH_2-CH_2 symmetric wag
	1417.62	CH_2 scissor
	1611.02	NH_2 scissor
	2966.67	CH_2 and C-H asymmetric stretch
	2972.10	CH_2 and C-H symmetric stretch
	3025.85	CH_2 asymmetric stretch
	3399.34	NH_2 symmetric stretch
	3482.25	NH_2 asymmetric stretch
MPApartreact	615.327	C-S stretch
	734.513	C-H, CH_2, NH_2 wags and rocks
	779.500	NH_2 vibration
	806.274	S-C=C-S asymmetric vibration
	913.527	C-C stretch with CH_2, NH_2 wags and rocks
	1026.36	C-N stretch
	1085.66	N-C-C asymmetric stretch

Liam James Dodd

		1133.15	Skeletal vibration
		1235.64	C-H wag
		1280.10	C-H wag
		1353.66	CH_2 rock
		1441.48	CH_2 scissor
		1530.68	C=C stretch
		1599.81	NH_2 scissor
		2878.99	CH_2 asymmetric stretch
		2957.03	CH_2 asymmetric stretch
		3047.98	C-H stretch
		3414.73	NH_2 symmetric stretch
		3505.29	NH_2 asymmetric stretch
NONfullreact		643.226	1,2 - C-S asymmetric stretch, with skeletal vibrations
		685.627	1,1 - C-S asymmetric stretch, with skeletal vibrations
		724.624	C-S stretch with skeletal vibrations
		794.024	Carbon skeleton wag
		892.147	Carbon skeleton breathing
		953.569	C-C-C-C asymmetric stretch
		1032.35	CH_3-CH_2-CS2- asymmetric stretch of carbon bonds
		1065.63	CH wag with CH_3 rocking
		1074.46	Carbon skeletal vibration
		1082.87	Carbon skeletal vibration
		1183.42	CH wag
		1266.29	CH_2 rock
		1308.42	CH_2 rock
		1363.66	CH_3 vibration
		1419.88	CH_2 scissor
		1443.19	CH_3 vibration
		1452.41	CH_3 scissor
		2953.30	CH_2 symmetric stretch
		2972.56	All CH bonds breathing
		2976.19	CH_3 breathing
		3013.59	CH vibrations
		3044.29	CH_3 asymmetric stretch
		3051.51	CH vibrations
NONpartreact		603.739	C-S stretch
		735.193	C-S stretch with carbon skeleton vibrations
		753.278	Carbon skeleton rocking
		813.427	S-C=C-S asymmetric stretch
		907.745	C-C-C symmetric stretch with C-S stretch
		1025.29	C-C-C asymmetric stretch with C-S stretch
		1053.10	C=C stretch with carbon skeleton vibrations
		1090.41	C-C-C=C central bond stretch
		1222.32	C=C stretch with carbon skeleton vibrations
		1270.10	C-S stretch with carbon skeleton vibrations
		1291.48	CH_2 rock
		1358.33	CH_3 vibration
		1429.13	CH_2 scissor
		1444.29	CH_3 vibration
		1455.89	CH_3 scissor
		1543.23	C=C stretch

Liam James Dodd

		2942.55	CH_2 symmetric stretch
		2966.23	CH_3 breathing
		2988.42	CH_2 asymmetric stretch
		3037.72	CH_3 asymmetric stretch
		3042.52	CH_3 asymmetric stretch
		3053.32	C=C-H stretch
TAAfullreact		655.125	C-S stretch
		791.242	C-S stretch with carbon skeleton + NH_2 vibrations
		839.355	Carbon skeleton rocking + NH_2 vibrations
		871.885	Carbon skeleton rocking + NH_2 vibrations
		956.764	S-C-C-S stretch
		1004.36	C-C-C asymmetric stretch
		1075.13	N-H stretch
		1107.25	Carbon skeleton stretches + NH_2 vibrations
		1163.14	Carbon skeleton stretches
		1184.16	C-H wags with C-S stretch
		1240.40	Carbon skeleton wag + NH_2 wag
		1260.50	C-H wags with C-S stretch
		1325.13	C-H and N-H wags
		1346.23	NH_2-CH_2 symmetric wag
		1381.29	S-CH_2 scissoring
		1430.28	N-CH_2 scissoring
		1612.34	NH_2 scissoring
		2931.91	C-H vibrations
		2949.52	CH_2 symmetric stretches
		2960.86	C-H breathing
		3012.98	CH_2 asymmetric stretches
		3022.48	S-CH_2 asymmetric stretch
		3388.41	NH_2 symmetric stretch
		3466.67	NH_2 asymmetric stretch

Regarding TPA, MPA, and NON, the alkyne C-H vibration at approximately 3300 cm^{-1} in the neat crosslinker spectra, does not appear in the spectra of the Sol or Insol products, indicating that the alkyne bond has been consumed in the inverse vulcanisation reaction as expected. Unfortunately, the carbon – carbon triple bond vibration was too weak in the neat spectra to be diagnostic in the polymer spectra, which were always of high raw transmittance.

Regarding TAA and DAA, the FTIR spectra suggest a nearly complete reaction. The alkene C-H mode at about 3100 cm^{-1} in the neat crosslinker spectra is absent in the spectra of the Sol and Insol products. The C=C mode at about 1650 cm^{-1} in the neat crosslinker spectra is plausibly present in the spectra of the Sol and Insol products of TAA and DAA, as there is a peak in the polymer spectra that could be assigned to the C=C bond, but it seems too broad and too intense to be solely the result of the C=C mode. The C=C peak at 990 cm^{-1} is also plausibly absent in the spectra of the Sol and Insol products versus the neat crosslinker.

The C=C peak at approximately 910 cm^{-1} is much more diagnostic however as it is significantly more intense in the neat crosslinker spectra. TAA50-S50-Sol, TAA50-S50-Insol, and DAA50-S50-Sol all show a weak peak that can be attributed to the C=C mode at 910 cm^{-1}. DAA50-S50-Insol does not show any evidence of this peak, nor does it show evidence of the 1650 cm^{-1} peak, suggesting that of the alkene crosslinkers, DAA sees the greatest consumption of its double bonds, which is reasonable, because DAA starts with the fewest double bonds, and the Insol product is expected to be the most thoroughly

Liam James Dodd

reacted. Even so, all the aforementioned conclusions drawn from the FTIR data are somewhat ambiguous due to the weak signal strength of the polymers which makes it hard to assign peaks with certainty.

Where the alkyne crosslinkers are concerned, the FTIR spectra may be indicative of a facet of the mechanism, as at about 1670 cm^{-1} there are weak peaks in the spectra of TPA50-S50-Sol, TPA50-S50-Insol, and NON50-S50-Insol, which could be assigned to trisubstituted C=C bonds. This would suggest that the inverse vulcanisation of alkynes occurs progressively, from C≡C to C=C to C-C. There is a peak at 1530 cm^{-1} in the Sol and Insol spectra of TPA, which the computational data suggest could also be assigned to the presence of a C=C mode, and similarly the Sol and Insol spectra of NON show a peak at 1030 cm^{-1} and 1220 cm^{-1} both of which the computational chemistry suggests could result from a C=C bond.

The NON polymer spectra also show a weak peak at 815 cm^{-1}, whilst TPA polymers show a peak at 790 cm^{-1}, both of which could be tentatively assigned to trisubstituted C=C modes, which provides a little more evidence to the conclusion of a progressive reaction. C=C bond modes are not observed in the spectra of MPA polymers, which could be explained by the fact that MPA has fewer double bonds per molecule, and so sees greater consumption of its double bonds in comparison to TPA and NON, which have enough double bonds that some are left over in the product polymers as C=C. As a final note, the FTIR spectra indicate that the organic backbone of the crosslinkers is left intact upon polymerisation, which is supported by the results of the computationally predicted IR data.

3.8. Sulfur Content

Since each dispersion polymerisation produced two products simultaneously, the Sol and Insol, it was not possible to predict how much sulfur was incorporated into each product. Combustion microanalysis was attempted upon the polymers, but provided results that may be untrustworthy, especially since the total of all elements present added up to greater than 100 % total mass (Table 3.3). Combustion microanalysis struggles to accurately determine the sulfur content of inverse vulcanised polymers due to a large extrapolation error in the calibration curve of the instrument.

Typically, combustion microanalysis instruments combust a sample completely in oxygen, and then perform gas chromatography on the gaseous products. The gas chromatography signal intensities can be related to the elemental content of the sample through the use of a calibration curve, which is constructed by performing combustion microanalysis on samples of known elemental content and relating these elemental contents to the signal intensities provided by the gas chromatography.

This requires calibration standards of precisely known elemental contents, and unfortunately in the case of sulfur, there are no suitable and easily obtainable calibration standards with precisely known sulfur contents higher than around one to ten percent. This results in tremendous extrapolation errors when a calibration curve set up between one and ten percent sulfur content, is used to analyse inverse vulcanised polymers of sulfur contents that are typically between fifty and ninety percent.

Additionally, analysis of the polymers in combustion microanalysis was unacceptably detrimental to the instrument. As such, an alternative method to determine the sulfur content was sought out. X-Ray Fluorescence (XRF) was identified as a potential route to the analysis of the elemental sulfur content, which has not been applied in the field of inverse vulcanisation thus far.

Liam James Dodd

Table 3.3: Unreliable combustion microanalysis data for TPA, TAA, and NON polymers.

Polymer Name	Expected				Combustion Microanalyses			
	%C	%H	%N	%S	%C	%H	%N	%S
TPA70-S30-sol	57.7	4.8	7.5	30.0	62.6	5.5	7.7	23.4
TPA70-S30-insol					46.3	3.4	5.4	36.3
TPA50-S50-sol	41.2	3.5	5.3	50.0	58.3	5.2	7.0	28.9
TPA50-S50-insol					41.2	2.9	4.9	45.2
TPA30-S70-sol	24.7	2.1	3.2	70.0	15.3	1.6	1.3	82.2
TPA30-S70-insol					37.5	2.7	4.4	55.3
TPA10-S90-sol	8.2	0.7	1.1	90.0	4.4	0.8	0.0	97.3
TPA10-S90-insol					38.8	2.2	4.4	53.4
TPA05-S95-sol	4.1	0.4	0.5	95.0	4.0	0.7	0.0	97.5
TPA05-S95-insol					39.3	2.2	4.2	53.7
TAA70-S30-sol	55.1	7.7	7.2	30.0	53.8	6.8	6.4	32.0
TAA70-S30-insol					46.3	3.4	5.4	36.3
TAA50-S50-sol	39.4	5.5	5.1	50.0	45.8	3.8	5.1	43.1
TAA50-S50-insol					41.2	2.9	4.9	45.2
TAA30-S70-sol	23.6	3.3	3.1	70.0	24.2	2.8	2.8	69.8
TAA30-S70-insol					37.5	2.7	4.4	55.3
TAA10-S90-sol	7.9	1.1	1.0	90.0	11.3	1.6	0.1	88.8
TAA10-S90-insol					38.8	2.2	4.4	53.4
TAA05-S95-sol	3.9	0.6	0.5	95.0	7.1	1.2	0.4	93.9
TAA05-S95-insol					39.3	2.2	4.2	53.7
NON30-S70-sol	27.0	3.0	0.0	70.0	8.2	1.3	0.0	94.0
NON30-S70-insol					39.4	3.9	0.0	55.8
NON10-S90-sol	9.0	1.0	0.0	90.0	3.3	0.7	0.0	99.2
NON10-S90-insol					44.1	4.5	0.0	50.5

To test this analysis technique, a series of easier to characterise DVB based polymers were made by the following bulk polymerisation method. All reactions were performed upon a hotplate equipped with an aluminium heating pan and an aluminium heating block, which ensured consistent positioning of the reaction vials upon the hotplate, giving consistent stirring. To a 40 mL reaction vial, a 14 mm cross-shaped stirrer was added. The mass was then recorded. A desired amount of elemental sulfur, weighed out to within 0.0099 g of the target mass, was then added to the reaction vial. The reaction vial was heated to 135 °C, such that the sulfur melted. At least ten minutes for thermal equilibration was then allowed, with 200 rpm stirring during. Then, an amount of DVB sufficient to bring the total mass of reagents to 10 g was weighed out to within 0.0099 g in a vial. The mass of this vial and DVB was then tared, and the contents of the vial were added to the 40 mL reaction vial. The stirring was then increased to 800 rpm and a septum with an air balloon was affixed to the reaction vial to minimise crosslinker evaporation. The tared vial was the re-weighed to find the exact mass of DVB added to the reaction vial. The reaction vials were then left on the hotplate at 135 °C overnight to cure. The septum and balloon were then removed, and the reaction vial was re-weighed to determine the yield, after which the glass vial was cooled with liquid nitrogen to detach the polymer from the vial. The vial was then shattered to retrieve the polymer. The polymer was then shattered to retrieve the stirrer. The polymer was then powderised and analysed by combustion microanalysis and XRF (Table 3.4). Expected CHNS values were calculated by assuming that all losses to the yield were the result of crosslinker evaporation.

Liam James Dodd

Table 3.4: Comparison of combustion microanalysis and XRF data for some standard DVB polymers.

Polymer	Reactant masses / g	Yield	Expected			Combustion Microanalyses			XRF
			%C	%H	%S	%C	%H	%S	%S
DVB70-S30	DVB: 6.9785 g S$_8$: 3.0062 g	9.4947 g 95.08 %	63.05	5.29	31.67	62.80	5.37	31.39	34.82
DVB50-S50-A	DVB: 4.9885 g S$_8$: 5.0064 g	9.6995 g 97.05 %	44.64	3.75	51.61	44.16	3.75	51.81	62.42
DVB50-S50-B	DVB: 4.9888 g S$_8$: 5.0058 g	9.7355 g 97.40 %	44.82	3.76	51.42	43.98	3.74	51.82	60.62
DVB30-S70	DVB: 2.9944 g S$_8$: 7.0075 g	9.8924 g 98.91 %	26.91	2.26	70.83	25.96	2.33	72.13	85.39

Table 3.4 shows that combustion microanalysis can be remarkably accurate when the polymerisation is carefully controlled, and the volatilisation of crosslinker is accounted for. The XRF over-estimates the quantity of sulfur, and it is found that this is because of the one hour exposure time used in these initial XRF experiments. Later experiments with very short exposure times underestimated the amount of sulfur, and the longer the exposure time was, the more the sulfur content was less underestimated and became more over estimated. This is presumed to be due to the carbon content being burned off by the X-rays. This indicates that inverse vulcanised polymers must be analysed as rapidly as possible, with the minimum energy directed on them as possible, in order to minimise sample degradation, and if repeat measurements are desired, one must analyse a different sample of the same polymer rather than analysing the same sample multiple times. This could also have ramifications for other mainstream analysis techniques of inverse vulcanised polymers that use X-rays, for example PXRD. Great effort was made to find a method of XRF analysis that produced trustworthy results, but these efforts were ultimately fruitless. No suitable baseline could be created for the measurements which could've been due to a combination of matrix effects (which cannot easily be taken into account in the largely unstudied structures of inverse vulcanised polymers), and the lack of stability in the baseline between measurements. Numerous other issues were encountered, such as inconsistent and complex shaped calibration curves which could've been a result of changing sample density. For high density samples, the XRF response tends to come from a hemisphere of the sample under the irradiation point, but in higher density samples, the X-rays penetrate deeper in and give a response from deeper in the sample, resulting in a tear drop shaped response zone. Since sulfur polymers vary in density as their sulfur loading changes, it was believed that the response zone was changing shape from a hemi-sphere for high density samples, to a tear-drop at lower density samples, and that this could have resulted in a change in the signal response with sulfur loading, however attempts to take this into account were not successful in yielding sensible calibration curves, meaning that either this hypothesis is untrue, or there are more unaccounted for effects. Regardless, even though XRF was unsuccessful in analysing the polymers, further research attention may be warranted as it presents a rapid and convenient technique to analyse the sulfur content of the polymers.

3.9. NMR Characterisation

In order to better understand the structure of these polymer, an NMR characterisation using literature methods was attempted.[3.5] In short, this method involves breaking down the polymer with LiAlH$_4$ and analysing the degradation products, which in the literature case, were monomeric units of the polymer.

Approximately 100 mg of polymer was added to an oven dried 14 mL glass vial containing a PTFE stirrer, all of which was sealed with a septum and purged with nitrogen for a few minutes. Afterward

Liam James Dodd

5 mL of 1 M LiAlH$_4$ in THF was injected into the vial, and the reaction was left stirring overnight with a nitrogen balloon affixed. The next day it was noted that there was still remaining solid in the reaction solution, indicating that the LiAlH$_4$ reaction had not gone to completion in terms of degrading the polymer structure. The reaction solution was quenched by the dropwise addition of deionised water until addition of more water caused no further fizzing, at which point 1 M HCl in deionised water was added to make the reaction solution up to 10 mL. During the quench, vigorous fizzing was noted, indicating that there was plentiful LiAlH$_4$ remaining. The reaction mixture was transferred into a 20 mL vial, where in the aqueous phase was extracted three times with EtOAc. The EtOAc, usually clear yellow, clear orange, or clear brown in colour, was washed with brine and dried over MgSO$_4$, before it was evaporated to dryness, leaving a solid residue. The residue was analysed by ^{1}H NMR, ^{13}C NMR, ^{13}C DEPT135 NMR, ^{1}H ^{1}H COSY NMR, and ^{1}H ^{13}C HSQC NMR. This process was performed on the Sol and Insol products of TPA50-S50, TAA50-S50, NON50-S50, MPPA50-S50, and DAA50-S50, though it is important to note that the EtOAc extracts from the TPA50-S50-Insol and NNON50-S50-Insol were clear and colourless, and yielded no residue when evaporated to dryness.

Here this analysis method seems not to have worked so effectively. This may be because these polymers are crosslinked, whereas the polymer analysed in the literature was largely linear with few branching units. Thus, it may be that highly crosslinked polymers are less amenable to this analysis technique, which is supported by the fact that TPA50-S50-Insol and NON50-S50-Insol yielded no degradation product at all after the reaction with LiAlH$_4$, and it is predicted that these would be the most crosslinked of the polymers. Nevertheless, the other eight polymers yielded degradation products which were analysed by ^{1}H NMR, ^{13}C NMR, ^{13}C DEPT135 NMR, ^{1}H ^{1}H COSY NMR, and ^{1}H ^{13}C HSQC NMR. See Section 3.13.2 for the NMR spectra. In line with the idea that the LiAlH$_4$ degradation was not going to completion, the NMR shown in Section 3.13.2 does not seem to show the spectra of a clean monomeric unit cut from the polymer, and instead seems to show the NMR of an oligomer, with broadened peaks that are characteristic of the many similar environments of an oligomer. Despite the challenge in analysing these spectra, they still provided useful information.

The NMR spectra of the polymers indicated that the structure mostly consisted of alkyl groups, consistent with the expected structure, and where the crosslinker structure was more simple, the NMR spectra of the degradation products was more simple as well. Alkene region resonances were observed, concurrent with the results of the FTIR analyses, suggesting that the reactions do leave some leftover alkene resonances and that the alkynes react progressively from alkyne to alkene to sp3 hybridised centres. The spectra showed similarities and consistencies between the degradation products suggesting that the reaction pathways are largely the same between the different crosslinkers, and thus yield related products. The Sol products gave spectra with a greater population of broad resonances whereas the Insol products generally gave less cluttered spectra with less broad peaks, suggesting that the Insol products are more well defined compared to the Sol products, and that the Sol products have a greater variety of different molecular substructures. Lesser amounts of aromatic byproduct fragment were detected in the spectra which are tentatively attributed to benzenes, thiophenols, and thiophenes, the latter of which have been shown in the literature to form from intramolecular reactions under inverse vulcanisation conditions when multiple alkynes are present.[3,4] The polymer products of inverse vulcanisations with alkynes are the only ones where thiophenol and benzene resonances could be detected, suggesting that only alkynes can form these moieties. Additionally, NON50-S50-Sol has weaker aromatic resonances than the other amine containing polymers, suggesting that the reaction pathway to form the aromatic structures is kinetically assisted by an amine activated pathway. However, in all cases, the aromatic signals were much weaker than the alkyl signals, so it seems likely that the aromatic components are a small population substructural by-product.

Liam James Dodd

3.10. Phosphorus Containing Crosslinkers

An interesting comparison to the aforementioned amine crosslinkers, are analogues with a phosphorus atom. Trivalent phosphorus is widely considered to be a stronger nucleophile than trivalent nitrogen, as phosphorus has a lower electronegativity, and higher principal quantum number for its outermost electrons, making its lone pair more readily donated. The phosphorus containing crosslinkers used here are shown in Figure 3.9. Triallylphosphine (TAPIN) is directly comparable to TAA, whereas triallylphosphite (TAPIT) and triallylphosphate (TAPAT) are an interesting comparison to TAPIN for the increasing number of oxygens bonded to the phosphorus. For TAPIT, it would be expected that the phosphorus would be less electron rich than TAPIN, and for TAPAT, the phosphorus no longer has a lone pair and instead has an oxygen atom. What effect these factors had on the catalytic properties, or whether indeed these molecules where catalytic at all was a point of interest. Unfortunately, due to the cost of these crosslinkers, they could not all be tested in the full range of feed ratios as the aforementioned crosslinkers. This cost would likely prevent widespread use of such phosphorus containing crosslinkers, except in specialty applications, but they are still a useful comparison to the already tested nitrogen crosslinkers.

| Triallylphosphine | Triallylphosphite | Triallylphosphate |
| TAPIN | TAPIT | TAPAT |
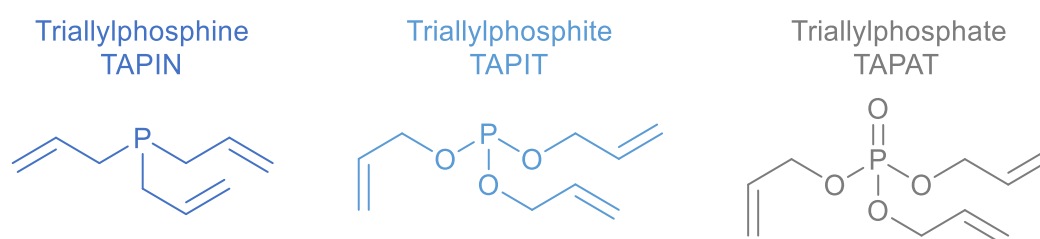
Figure 3.9: Names, abbreviations, and chemical structures of the phosphorus containing crosslinkers.

Interestingly, both TAPIT and TAPIN required week-long reaction times to reach completion (they were also cured for two days to ensure complete reaction), which in comparison to TAA, indicates that they might not possess any rate enhancing moieties within the crosslinker structure. Recently reported was the formation of phosphine sulfides from phosphines in an inverse vulcanisation reaction, so it seems sensible that an analogous reaction pathway could be occurring here, which would deactivate the phosphorus atoms' lone pair, and replace it with an inactive sulfide, explaining the longer reaction time for TAPIN and TAPIT.[3.11] The formation of these phosphine sulfides is hypothesized to be driven by the formation of the strong phosphorus – sulfur double bond. The analogous nitrogen – sulfur double bond is not strong and so is not exergonic to form, which would explain why amines are not subject to this reaction and do provide rate enhancements.

Observing Figure 3.10a it can be seen that the yields of TAPIN, TAPIT, and TAPAT largely follow the same trends as that of TAA, excepting that TAPIT and TAPIN are missing the data points for 50 and 70 % sulfur loading. As expected, the Insol products of TAPIN, TAPIT, and TAPAT all had negligible soluble fractions. Meanwhile, as expected, the Sol products showed decreasing solubility as the feed percentage of crosslinker was increased, indicating a more crosslinked Sol product. As before, DSC and PXRD indicated that the Insol products contained no crystalline elemental sulfur, whereas Sol products at higher feed percentages of sulfur did contain crystalline elemental sulfur, with explanations mirroring those for TPA, TAA, and NON. Observing Figure 3.10c, the Sol products show rising T_g values with increasing crosslinker loading, in a fashion similar to TPA, TAA, and NON. The Insol products are more difficult to explain with regards to their T_g's. From the results of TAA, it would be expected that Insol products of alkene crosslinkers should show T_g's, but this was not the case for TAPIT, which might suggest that TAPIT Insols are like the alkyne crosslinker Insol products, in that they are sufficiently

Liam James Dodd

crosslinked to not show a T_g, though this is a surprising result. It is also hard to explain why for TAPAT and TAPIN Insols, their T_g's decrease and then increase with rising crosslinker loading.
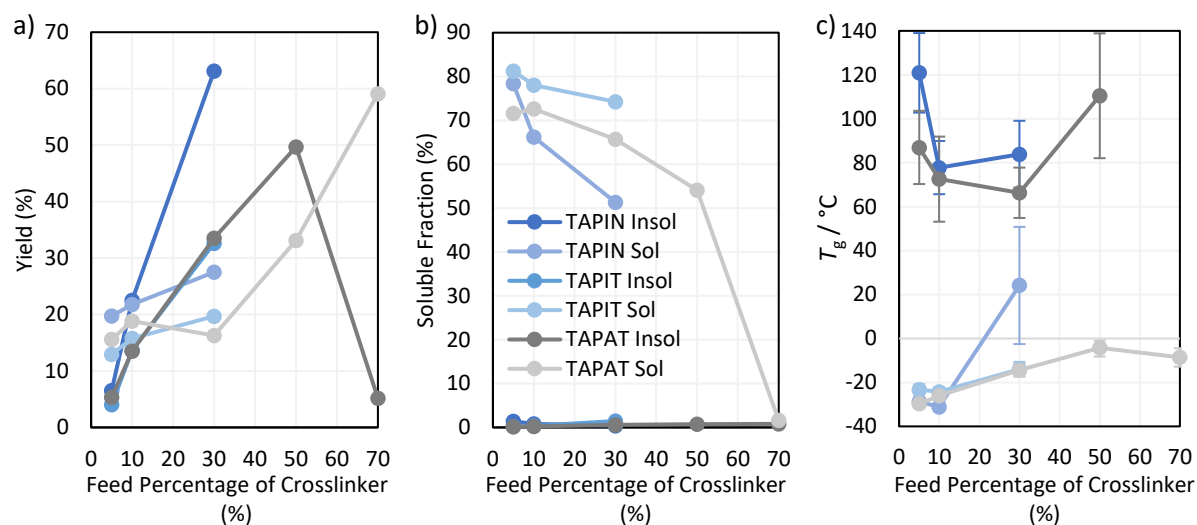
Polymer		TAPAT70-S30	TAPAT50-S50	TAPAT30-S70	TAPAT10-S90	TAPAT5-S95	TAPIT30-S70	TAPIT10-S90	TAPIT5-S95	TAPIN30-S70	TAPIN10-S90	TAPIN5-S95
Elemental Sulfur by DSC	Insol	No	No	No	No	No	No	No	No	No	No	No
	Sol	No	No	No	Yes	Yes	No	No	Yes	No	Yes	Yes
Elemental Sulfur by PXRD	Insol	No	No	No	No	No	No	No	No	No	No	No
	Sol	No	No	Yes	Yes	Yes	No	No	Yes	No	Yes	Yes

Figure 3.10: a) the yields, b) the soluble fractions and, c) the T_g's obtained from the second heating cycle of DSC, of the Sol and Insol products at different weight percentages of crosslinker in the reaction feed for TAPIN, TAPIT, and TAPAT. Note that in c) the bars indicate the onset and end temperatures of the T_g. Where data points are missing, no T_g could be identified in the thermogram. Also included is a table indicating whether elemental sulfur could be detected in the polymers by DSC or PXRD.

One interesting observation from Figure 3.10, is that TAPIT Insol and TAPAT Insol show very similar results for their yields, soluble fractions and T_g's, which might imply that they are in fact, the same product. This seems plausible because if TAPIT were to be oxidised, the product would be TAPAT. Attempts to prove such a transformation by ^{31}P NMR were unsuccessful, as even the most soluble polymers were not sufficiently soluble to provide a signal.

3.11. Crosslinker Blends

One potential benefit of crosslinkers like TPA and TAA, is that they could be blended with other crosslinkers, to act as an activator to the inverse vulcanisation reaction. TPA and TAA as activators would be intentionally incorporated into the polymer structure, eliminating concerns about extracting the catalyst, whilst also raising no issues with heavy metal contamination as do catalysts like Zn(DMDC)$_2$.[3.1] To demonstrate this, TPA and TAA were blended with DCPD and linseed oil in bulk polymerisations by the following method.

All reactions were performed in triplicate upon a hotplate equipped with an aluminium heating pan and an aluminium heating block, which ensured consistent positioning of the reaction vials upon the hotplate, giving consistent stirring. To a 40 mL reaction vial, a 14 mm cross-shaped stirrer was added.

Liam James Dodd

The mass was then recorded. A desired amount of elemental sulfur (5.0000 g for a reaction with DCPD, and 3.0000 g for a reaction with linseed oil), weighed out to within 0.0050 g of the target mass, was then added to the reaction vial. The reaction vial was heated to 135 °C, such that the sulfur melted. At least ten minutes for thermal equilibration was then allowed, with 200 rpm stirring during. Then, approximately 17 g of DCPD or 23 g of linseed oil (the exact masses were recorded) were added to a vial. Note that 17 g of DCPD was sufficient for three reactions each containing 5 g of DCPD, and that 23 g of linseed oil was sufficient for three reactions each containing 7 g of linseed oil. Using the exact mass of crosslinker recorded, the appropriate mass of either TAA or TPA was added to the crosslinker and thoroughly mixed to make a stock solution that would constitute the appropriate concentration of TAA or TPA to give the following mass percentages when added to the molten sulfur: 49 % DCPD and 1 % TAA or TPA, 47 % DCPD and 3 % TAA or TPA, 69 % linseed oil and 1 % TAA or TPA, 67 % linseed oil and 3 % TAA or TPA. For a DCPD reaction 5.0000 g ± 0.0050 g of the chosen stock solution was added to a new vial. This vial was then tared, and its contents added to the molten sulfur in the reaction vial, then re-weighing the empty vial to find the exact amount of stock solution added to the reaction by means of weighing by difference. For a linseed oil reaction 7.0000 g ± 0.0050 g of the chosen stock solution was added to a new vial. This vial was then tared, and its contents added to the molten sulfur in the reaction vial, then re-weighing the empty vial to find the exact amount of stock solution added to the reaction by means of weighing by difference. Once the stock solutions were added to the reaction vials, the reaction vials were immediately sealed with a septum with an affixed air balloon, and the stirring was increased to 800 rpm (any faster resulted in flicking of droplets the reaction mixture to the top of the vial). The time of the addition of the stock solution was noted. The air balloon was for pressure regulation, but also prevented volatilised crosslinker from escaping, thereby minimising crosslinker evaporation as volatilised crosslinker was unable to escape. The reactions were monitored closely, and the time at which the reaction mixture became so viscous that the stirrer could no longer rotate was noted. The time elapsed between addition of the stock solution and the ceasing of stirring was noted as the vitrification time. The reaction vials were then left on the hotplate at 135 °C for two days to cure. The septum and balloon were then removed, and the reaction vial was re-weighed to determine the yield, after which the glass vial was cooled with liquid nitrogen to detach the polymer from the vial. The vial was then shattered to retrieve the polymer. The polymer was then shattered to retrieve the stirrer.

Of note, blends were also attempted with DVB, which is a more reactive crosslinker, but these proved to react too quickly, resulting in the TNE. This reinforces the conclusion that catalysis and activation should be applied with due care and consideration in these reactions, and should not be attempted where a reaction is already reasonably quick.

Initial attempts to polymerise linseed oil by the method above resulted in the polymer product bubbling up the reaction vial in a manner that appeared similar to the TNE, which was unexpected for linseed oil. Linseed oil showed reaction times much longer than would be expected to produce the TNE. Regardless, the proportion of linseed oil in the reactions was increased to seventy percent by mass, to slow the reaction down and mitigate the TNE. For some of the catalysed reactions with seventy percent linseed, the reaction mixture bubbled up, still at reaction times too long for the TNE to be expected. Closer inspection suggested this bubbling up of the reaction may not have been due to the TNE. Such TNE's would likely occur when the reaction is still stirring, or most likely, very soon after the stirrer ceases to rotate, which is when heat transfer to the surroundings becomes poorest but there is still sufficient reactive material in the mixture for the TNE to occur. In these linseed oil reactions, the bubbling up did not occur immediately after the stirring ceased, and occurred sometime during the overnight cure when the reaction was not being observed. This suggests that the bubbling up of the reaction might not be due to a TNE, but instead, a much slower release of a gaseous side-

Liam James Dodd

product during the curing step. This suggests that reactions with a fifty percent mass loading of linseed oil could be viable, but since the reactions with a seventy percent mass loading of linseed oil gave results that were convenient to measure, reactions with a fifty percent mass loading of linseed oil were not attempted.

The results shown in Figure 3.11 indicate that both TAA and TPA are effective activators for both DCPD and linseed oil, as the vitrification times (the time between adding the crosslinker into the reaction, and the point where the reaction mixture was sufficiently viscous that the stirrer could no longer rotate) were decreased when TA and TPA were present. The yield of DCPD reactions were improved when TAA and TPA were included in activator quantities, which suggests that either hydrogen sulfide generation is suppressed by the activated pathway that outcompetes it, or more likely, that because the reaction takes less time to reach completion, there is less crosslinker evaporation. It should be noted that, as an improvement to the method used previously in the literature, the method employed here used a sealed reaction vessel with an air balloon for pressure regulation, with the intention of minimising crosslinker evaporation.[3.1] Reactions with DVB followed by CHNS analysis showed this method to be highly effective for this purpose, giving sulfur and carbon contents very close to the predicted values.
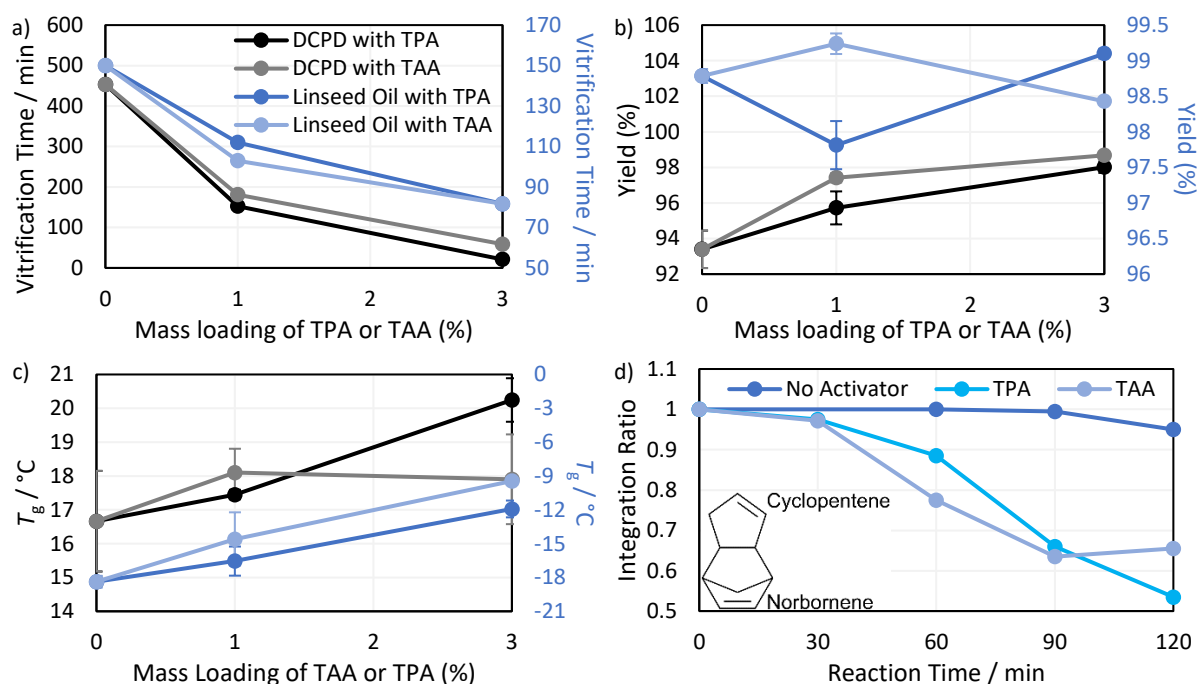
Figure 3.11: a) vitrification times, b) yields and c) T_g's of DCPD and linseed oil polymers blended with either 0, 1 or 3 % by mass TAA or TPA in the feed ratio. Note that the DCPD polymers were 50 % by mass sulfur in the feed ratio, and the linseed oil polymers were 30 % by mass sulfur. The error bars show the standard deviation, and are too small to be seen a). d) the integration ratio of the norbornene region and the cyclopentene region from ^{1}H NMR spectra taken at different reaction times of a DCPD reaction with 50 % by mass sulfur and either 0 % or 1 % by mass TPA or TAA.

There are no clear trends in the linseed oil reaction yields, which may be because the linseed oil reaction achieves such a high yield without activation that it is hard to enhance it further. It can be noted that TPA was a stronger activator than TAA in terms of the vitrification time. It was considered that because TPA is a lighter molecule than TAA, 0.1 g or 0.3 g (a 1% or 3% mass loading respectively) of TPA constitutes more moles of activator than TAA. However, 0.1 g of TAA is 0.72 mmol, and 0.1 g

Liam James Dodd

of TPA is 0.76 mmol which is a small difference. Thus, it is not surprising that when a reaction was performed with 0.76 mmol of TAA, the results were only marginally different to a 0.72 mmol loading. Both DCPD and linseed oil reactions benefitted from the presence of TAA and TPA in terms of the glass transition temperatures of the products, suggesting that these activators help to achieve a more crosslinked, fully reacted, final structure. Overall, there is not much difference between TAA and TPA in terms of their benefits as activators.

For DCPD, the molecule has its two alkene bonds in different environments, resulting in different activation energies, and as described in the literature at low temperatures, only one bond reacts in inverse vulcanisation, giving more linear character to the resultant polymer.[3.3,3.12] It was theorised here that TAA and TPA might encourage both bonds to react by lowering the reaction energy, or producing sufficiently reactive sulfur species, capable of attacking both double bonds. To answer this, reactions of fifty percent by weight sulfur, and either 50 % DCPD, 49 % DCPD + 1 % TPA, or 49 % DCPD + 1 % TAA were conducted as described above, with aliquots of the reaction taken at 30, 60, 90 and 120 minutes reaction times. ^{1}H NMR was performed on these aliquots to observe the changes in the integration ratios of the norbornene alkene hydrogens as compared to the cyclopentene alkene hydrogens, the results of which can be seen in Figure 3.11d.

The first note to make is that the ^{1}H NMR signals were not straightforward to analyse as would be expected of pristine DCPD. This is because of several reasons, including the different ways DCPD can react (as described in the literature, like retro Diels Alder before polymerisation) and the fact that when one alkene bond reacts, the other alkene bond is no longer in a molecule of DCPD, but is instead in a DCPD unit within a polymer, and therefore its chemical shift is no longer the same.[3.3,3.12] These factors result in small complications to the signals meaning they were no longer well defined multiplets and were instead rough regions which corresponded to either the norbornene alkene hydrogens of the cyclopentene alkene hydrogens. Such complications may explain why the two environments for the two cyclopentene hydrogens did not always have equal integrations. Note that in all NMR spectra the regions that were integrated over were always kept consistently to 6.09 to 5.85 ppm for the norbornene region and 5.58 to 5.4 ppm for the cyclopentene region. Note that an aliquot of the activator free reaction could not be taken at 30 minutes due to the inhomogeneity of the reaction mixture. Integration ratios at longer reaction times may be less accurate to the decreased intensity of the signals, particularly for the activated reactions.

From Figure 3.11d it can be observed that with no activator, the norbornene and cyclopentene alkenes react at similar rates in the early stage of the reaction, when there is plentiful unreacted high energy sulfur species. However, as the reaction progresses, the integration ratio begins to decrease, indicating that the norbornene alkene is being consumed more quickly than the cyclopentene alkene. For the reactions where TPA or TAA is present, this decrease in the integration ratio occurs much sooner and is more pronounced. Because Figure 3.11d does not provide information on the overall rate of reaction, but only indicates whether the cyclopentene or norbornene alkene has a greater population at a given time, this observation could mean either of two things: that the addition of an activator accelerates consumption of the norbornene alkene more than the cyclopentene alkene, or that the addition of an activator accelerates consumption of both alkenes proportionally, thus the reaction reaches completion sooner, and the naturally higher rate of consumption of the norbornene alkene occurs sooner in time. Regardless, it appears that activation with TPA and TAA does not seem to favour promotion of reaction upon the less reactive cyclopentene.

It is worth noting that this nucleophilic activation by including an amine containing crosslinker is likely to be amenable to other comonomers in inverse vulcanisation. Previous publications have already demonstrated that several comonomers can benefit from amine activation, including divinylbenzene,

DIB, styrene, 4-amino styrene, methyl methacrylate, and ethylene glycol dimethacrylate.[3.1,3.2] As such it is expected that nucleophilic activation by amines should work on a broad scope of comonomers in inverse vulcanisation, and that the extent of this scope warrants further investigation beyond this proof of concept example with DCPD.

3.12. Conclusions

It has been shown here that previously unreported amine containing alkyne crosslinkers can be polymerised successfully in inverse vulcanisation, provided measures are in place to manage their high reactivity, yielding polymers with T_g's higher than their T_d. By using a dispersion polymerisation, highly reactive crosslinkers can reliably be polymerised whilst avoiding hazardous TNE's, giving two products which can have different applications. Amine containing crosslinkers have also been polymerised by this method to harness the advantages of amine activation without concerns of metallic contamination of the polymers, nor the need to extract the catalyst from the polymer in post-synthesis. It has been found that amines provide an alternate route of activation for inverse vulcanisation polymerisations, and that this permits inverse vulcanisation of low boiling crosslinkers, at temperatures where sulfur is in the solid state. By this method, propargylamine was polymerised, which is of note because it contains only a single alkyne bond, and yet was still able to form a crosslinked polymer. FTIR revealed that it is likely that alkynes react progressively in inverse vulcanisation, first converting to alkene, before reacting again to form a saturated system, and that these resultant polymers are reasonably effective at inhibiting antimicrobial growth. The phosphorus containing analogues of amine containing crosslinkers were found to have no activating effects which may be due to the formation of phosphorus-sulfur bonds, which deactivate the phosphorus. Finally, it was shown that amine containing crosslinkers can be used as a secondary crosslinker, present in catalytic quantities, in an inverse vulcanisation of a primary comonomer, and this brings several benefits, such as improved yield, decreased reaction time, and increased T_g.

3.13. Appendices

3.13.1. FTIR Spectra of the Polymers
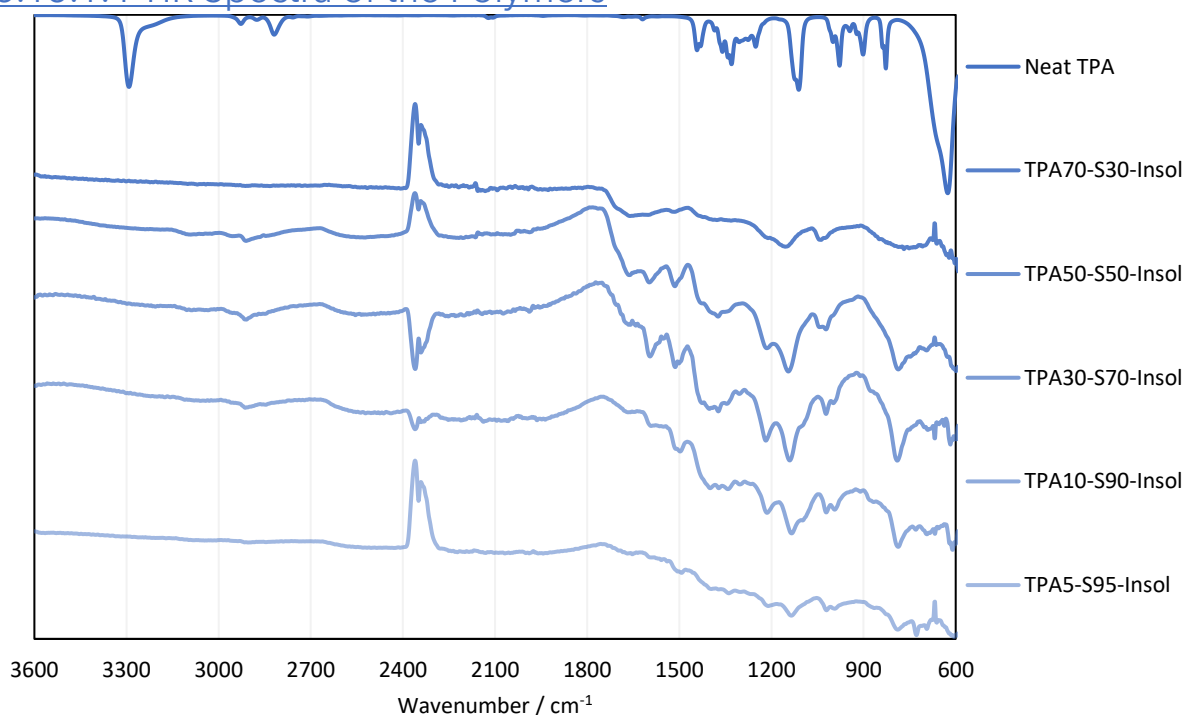
Figure 3.12: FTIR spectra of Insol polymers of TPA.

Liam James Dodd
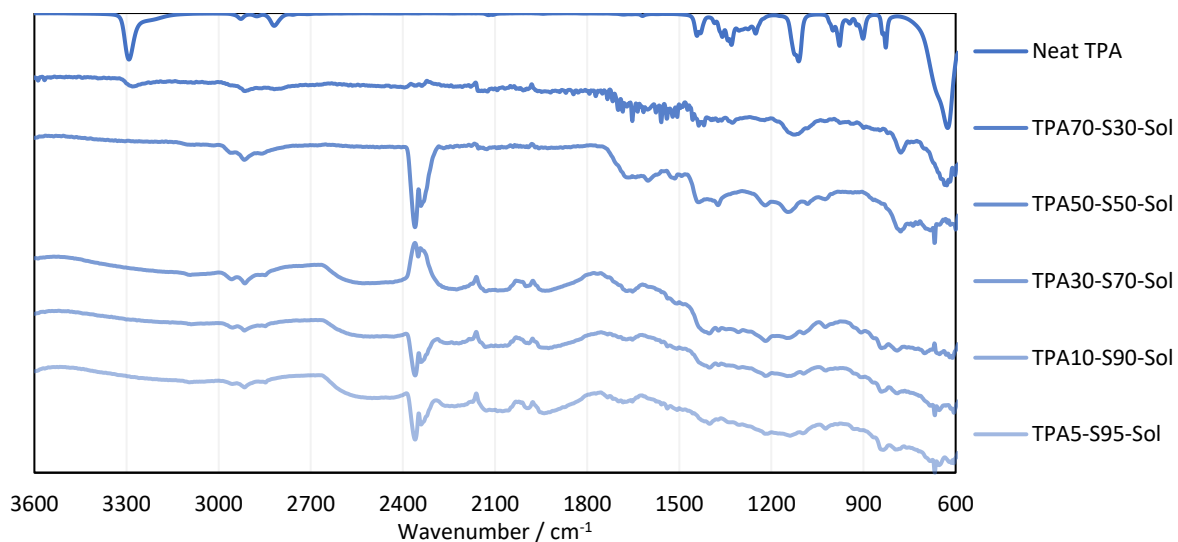
Figure 3.13: FTIR spectra of Sol polymers of TPA.
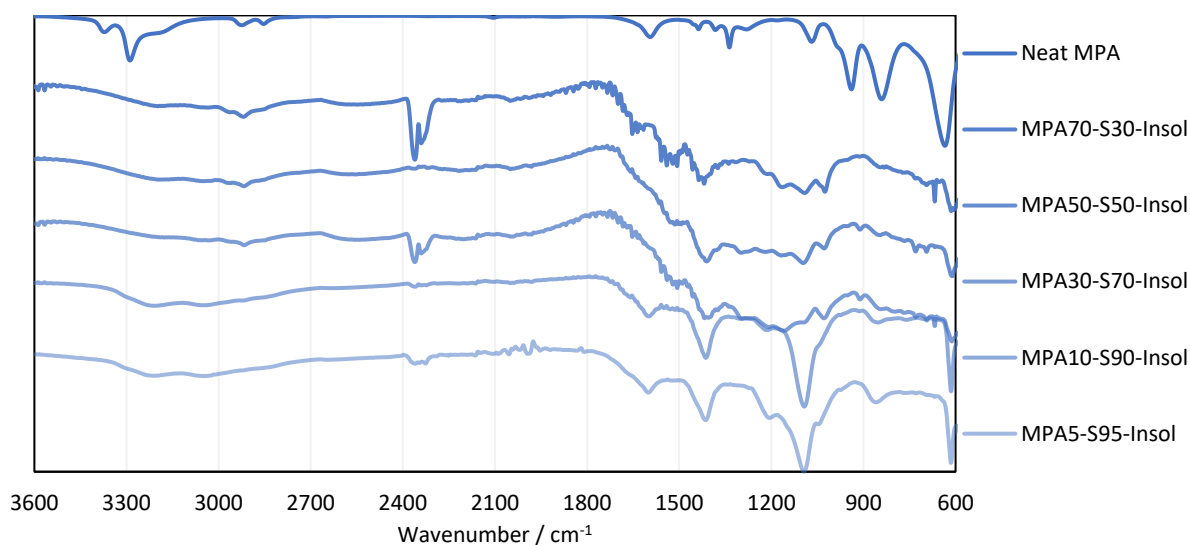
Figure 3.14: FTIR spectra of Insol polymers of MPA.
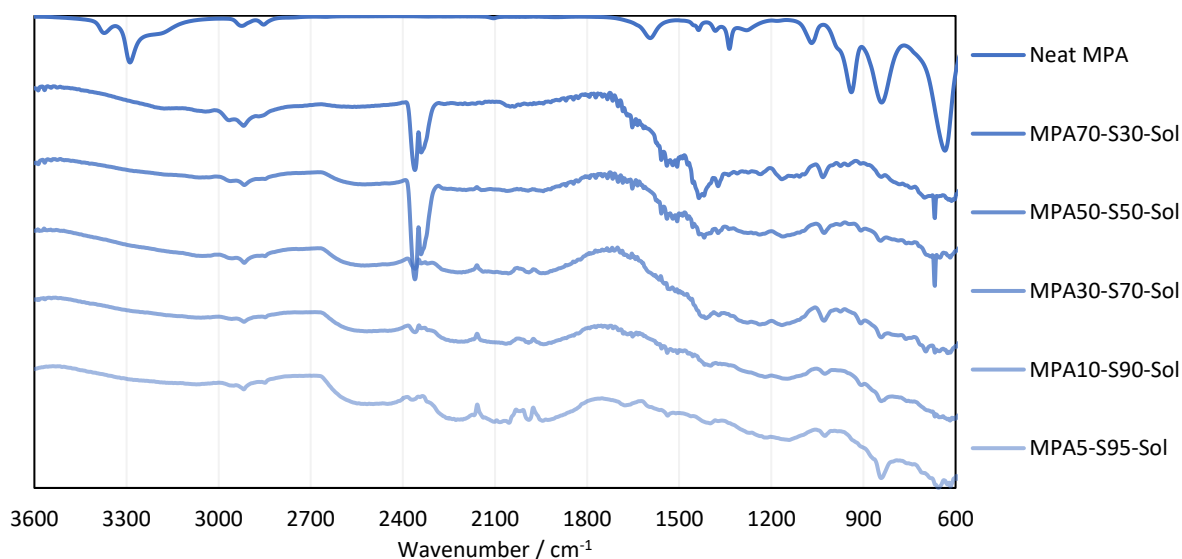
Figure 3.15: FTIR spectra of Sol polymers of MPA.

Liam James Dodd
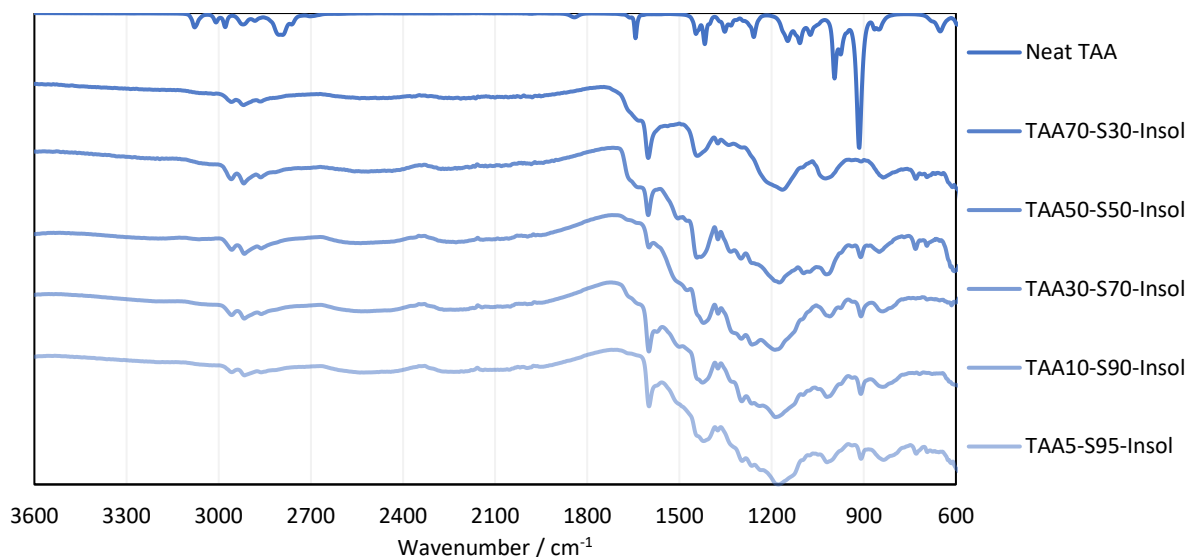
Figure 3.16: FTIR spectra of Insol polymers of TAA.
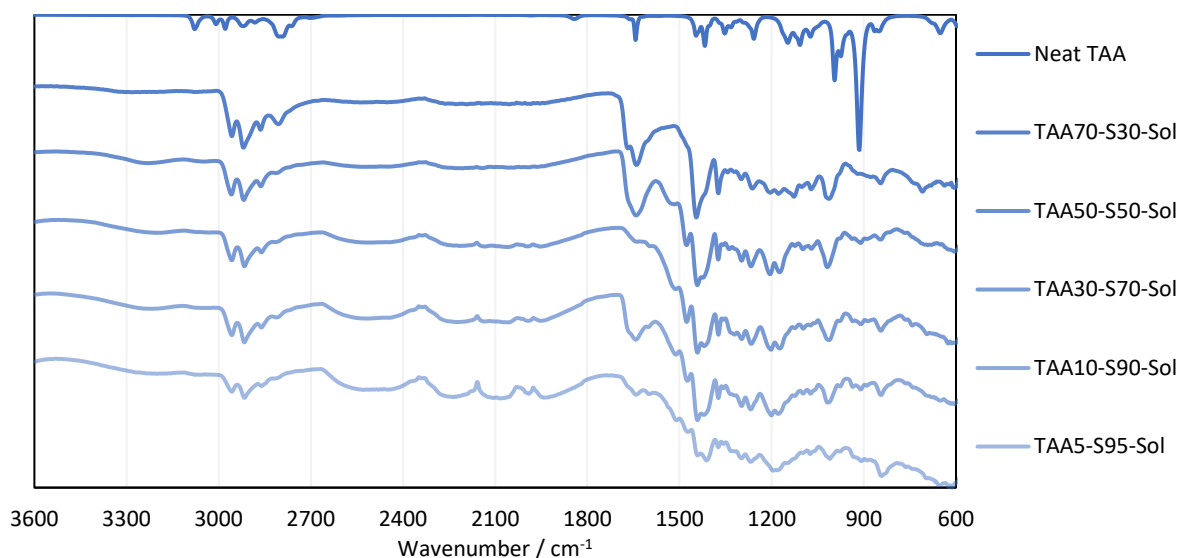
Figure 3.17: FTIR spectra of Sol polymers of TAA.
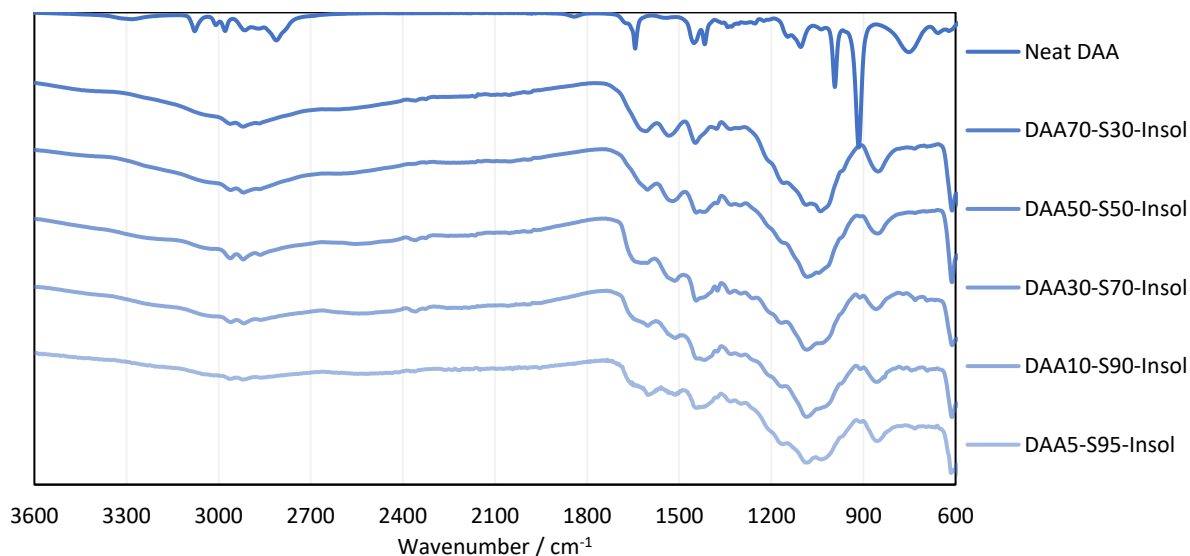
Figure 3.18: FTIR spectra of Insol polymers of DAA.

Liam James Dodd
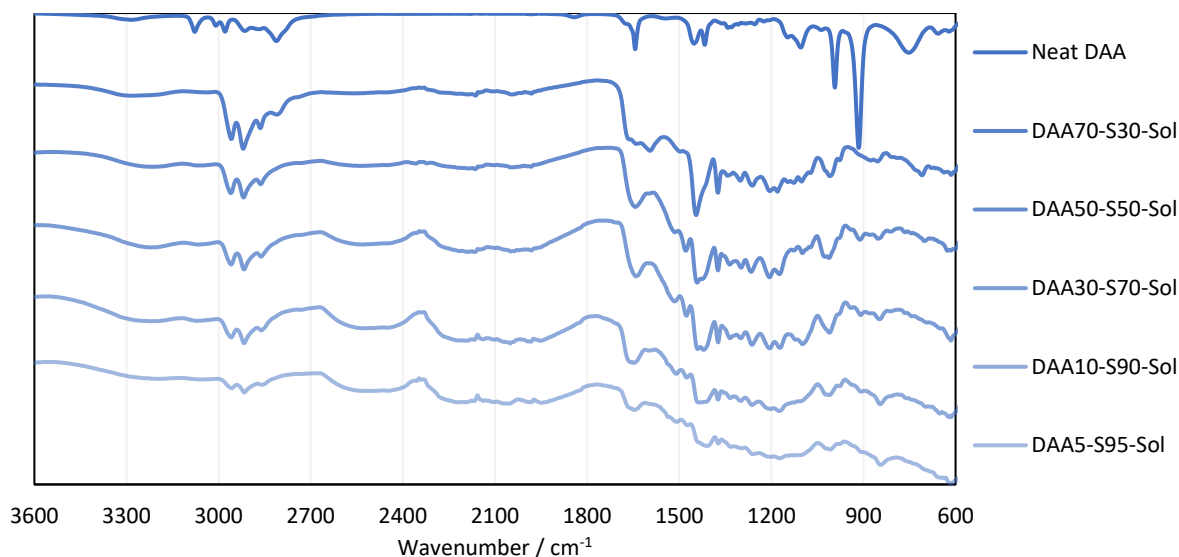
Figure 3.19: FTIR spectra of Sol polymers of DAA.
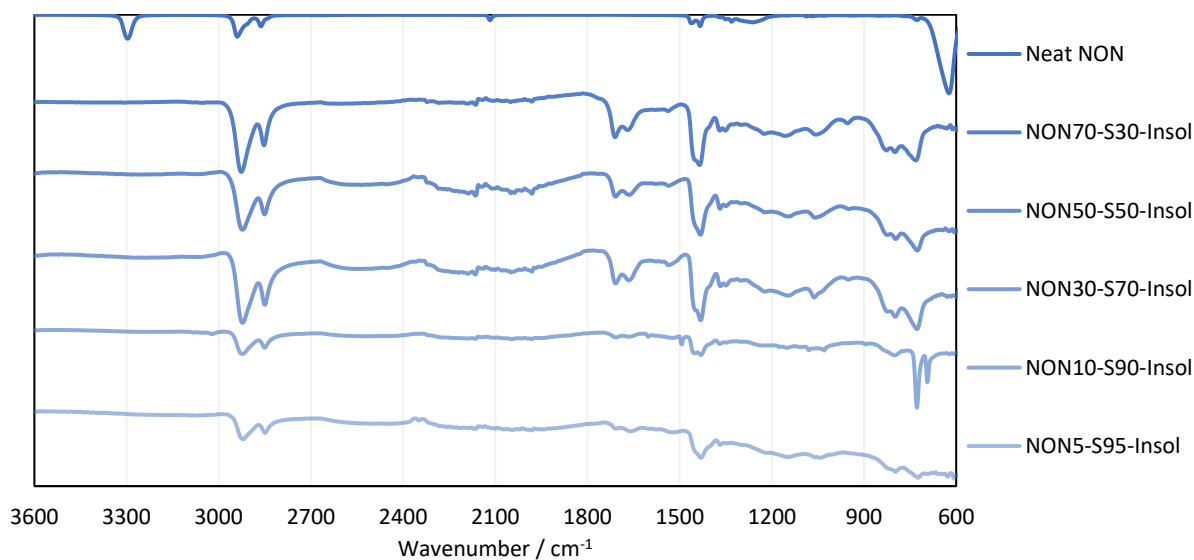
Figure 3.20: FTIR spectra of Insol polymers of NON.
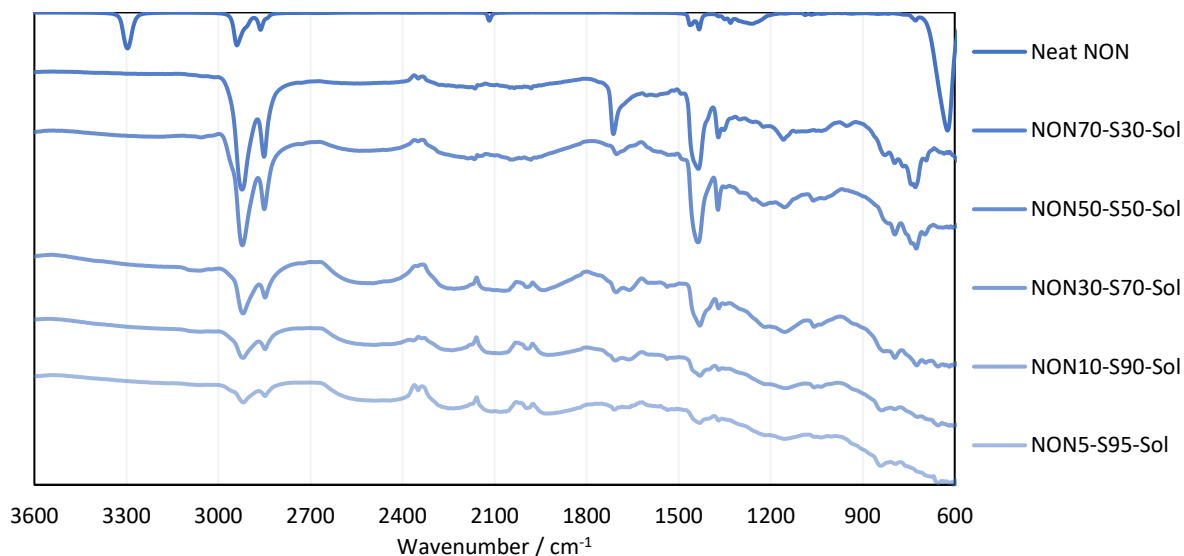
Figure 3.21: FTIR spectra of Sol polymers of NON.

Liam James Dodd

3.13.2. NMR of the Degradation Products

Firstly, approximately 100 mg of polymer was added to an oven dried 14 mL glass vial containing a PTFE stirrer, all of which was sealed with a septum and purged with nitrogen for a few minutes. Afterward 5 mL of 1 M $LiAlH_4$ in THF was injected into the vial, and the reaction was left stirring overnight with a nitrogen balloon affixed. The next day it was noted that there was still remaining solid in the reaction solution, indicating that the $LiAlH_4$ the reaction had not gone to completion in terms of degrading the polymer structure. The reaction solution was quenched by the dropwise addition of deionised water until addition of more water caused no further fizzing, at which point 1 M HCl in deionised water was added to make the reaction solution up to 10 mL. During the quench, vigorous fizzing was noted, indicating that there was plentiful $LiAlH_4$ remaining. The reaction mixture was transferred into a 20 mL vial, where in the aqueous phase was extracted three times with EtOAc. The EtOAc, usually clear yellow, clear orange, or clear brown in colour, was washed with brine and dried over $MgSO_4$, before it was evaporated to dryness, leaving a solid residue. The residue was analysed by ^{1}H NMR, ^{13}C NMR, ^{13}C DEPT135 NMR, ^{1}H ^{1}H COSY NMR, and ^{1}H ^{13}C HSQC NMR. This process was performed on the Sol and Insol products of TPA50-S50, TAA50-S50, NON50-S50, MPPA50-S50, and DAA50-S50, though it is important to note that the EtOAc extracts from the TPA50-S50-Insol and NNON50-S50-Insol were clear and colourless, and yielded no residue when evaporated to dryness.

Figure 3.22: The ^{1}H NMR spectrum of the degradation products of TPA50-S50-Sol. Note that in the figure the title suggests the sample is that of an Insol. This is a mistake in the naming, but sample is indeed TPA50-S50-Sol.

Liam James Dodd
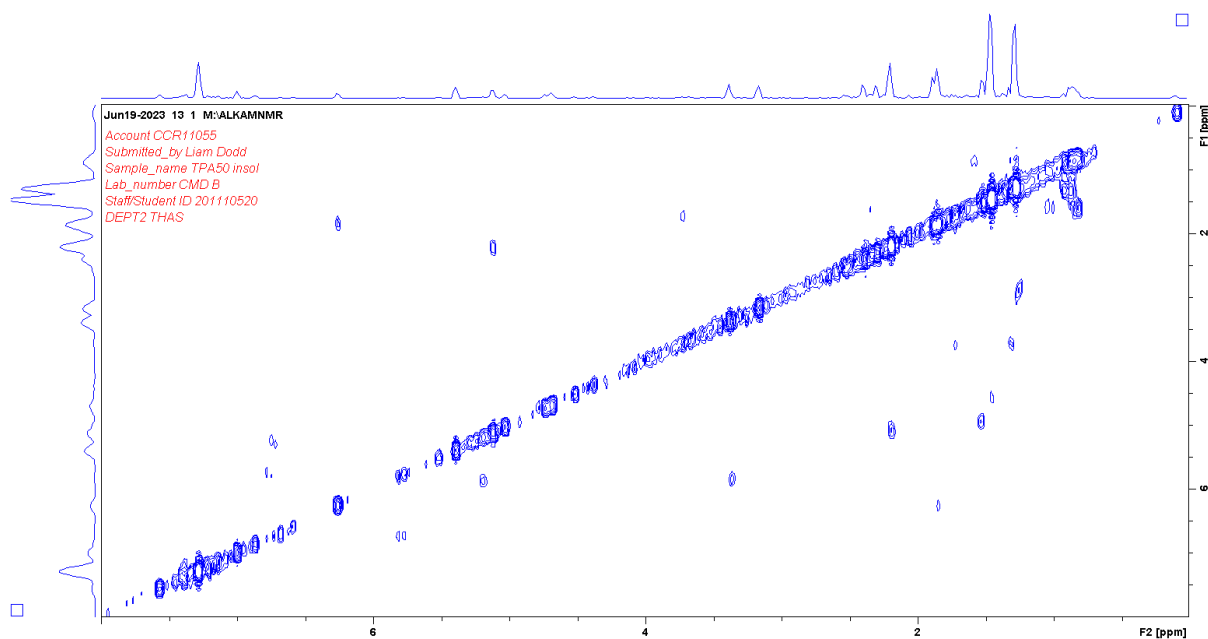
Figure 3.23: The ^{1}H ^{1}H COSY NMR spectrum of the degradation products of TPA50-S50-Sol. Note that in the figure the title suggests the sample is that of an Insol. This is a mistake in the naming, but sample is indeed TPA50-S50-Sol.
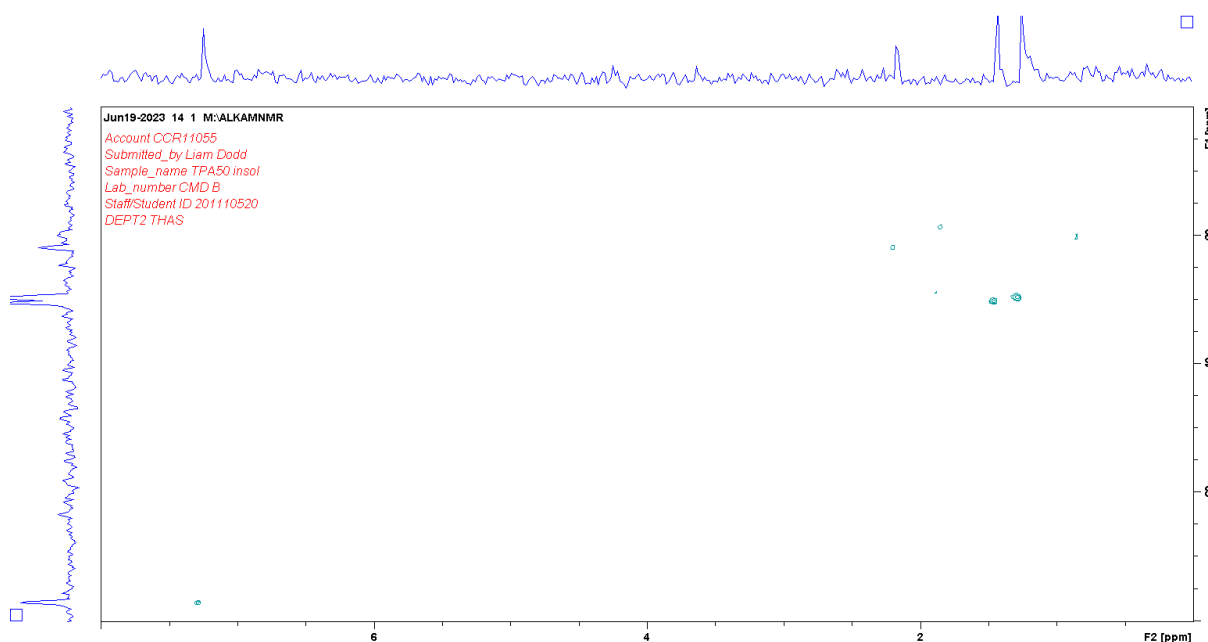
Figure 3.24: The ^{1}H ^{13}C HSQC NMR spectrum of the degradation products of TPA50-S50-Sol. Note that in the figure the title suggests the sample is that of an Insol. This is a mistake in the naming, but sample is indeed TPA50-S50-Sol.

Figure 3.22 contains numerous broad peaks over wide chemical shift ranges, suggesting that the degradation products are oligomeric in nature, rather than clean cut monomer units. Figure 3.22 does however provide some insights. First of all, though they are of low integration, there appears to aromatic hydrogens between 7.5 ppm and 6.5 ppm. These have been attributed to thiophenes, as the signals seem to be for the most party singlets, which would be explained by the formation of a thiophene structure. However, thiophene resonances would be expected below 7 ppm, so it also proposed that there is some formation of benzene rings and thiophenol rings, which would explain

Liam James Dodd

the dense multiplet above 7 ppm, as well as the peaks as high as 7.5 ppm. Figure 3.23 shows that the thiophene resonances are not coupled to the benzene resonances, supporting the conclusion that these resonances belong to separate types of fragment. Figure 3.23 also shows that there is coupling between the supposed thiophene resonance at 6.24 and the resonance at 1.85 which could be an alkyl fragment bound to the thiophene ring. The peak at 3.35 ppm is dubiously attributed to a thiophenol thiol, because it occurs in the expected range, but is not broad as would be expected. Importantly, these aromatic peaks are much weaker than the alkyl region, which may suggest that these aromatic fragments are by-products rather than the predominant species. Another minority by-product appears to be alkenes, as there are resonances in the region of 5.5 to 5 ppm, which is in agreement with the results of the FTIR spectroscopy that the alkynes may react to form alkenes first, before reacting onward. Below 2.5 ppm is where the majority of the signals are, but it is too complex to analyse in detail. There are several broad peaks in this range which could be attributed to the thiol hydrogens that would be expected of this degradation product. There seems to be numerous alkyl resonances scattered throughout the region, which Figure 3.23 shows are intercoupled in a complex manner, again suggesting an oligomeric structure for the degradation product. The ^{13}C NMR and DEPT135 ^{13}C NMR failed to give any signals, despite being placed on a long NMR experiment to enhance their signal to noise ratios. Strangely, Figure 3.24 shows that the ^{1}H ^{13}C HSQC NMR did manage to acquire ^{13}C signals, but overall Figure 3.24 does not provide much diagnostic information.

Figure 3.25: The ^{1}H NMR spectrum of the degradation products of TAA50-S50-Insol.

Liam James Dodd

Figure 3.26: The ^{1}H ^{1}H COSY NMR spectrum of the degradation products of TAA50-S50-Insol.

Figure 3.27: The ^{1}H ^{13}C HSQC NMR spectrum of the degradation products of TAA50-S50-Insol.

Figure 3.25 shows that much like TPA50-S50-Sol, TAA50-S50-Insol shows some aromatic signals, many of them matching closely to those of TPA50-S50-Sol, with the exception of the broad peak at about 7.25 ppm that appears in the TPA50-S50-Sol spectrum, but not in the TAA50-S50-Insol spectrum, suggesting that TAA50-S50-Insol cannot form all the aromatic species that TPA50-S50-Sol can. Based on the assignments from the TPA50-S50-Sol spectrum, it may be that TAA50-S50-Sol cannot form benzenes or thiophenols but still can form thiophenes. The peaks that appear in Figure 3.22 between 4.75 ppm and 3.5 ppm do not appear in Figure 3.25 though it is hard to assign these peaks with any certainty. This does point to the fact that TAA50-S50-Insol may have fewer reaction pathways in its formation as compared to TPA50-S50-Sol. This might be expected since the alkyne functional group adds another pi bond in comparison to the alkene group, and TPA derived polymers could be expected to be more complex than TAA derived polymers. What else supports this conclusion in that for TAA50-

Liam James Dodd

S50-Insol, the lower chemical shift region of the spectrum is notably less dense with signals than the analogous region in the TPA50-S50-Sol region. That being said, several signals in this region directly match between the two polymers, namely those a t 0.85 ppm, 1.25 ppm and 1.45 ppm. This suggests that there is a significant degree of similarity between the polymers which may imply that TPA can react via similar pathways to TAA, thus generating somewhat similar polymers. This may also imply that alkyne bonds can react in a similar way to alkene bonds, thus producing products that are similar; in other words, this may be evidence that alkynes do react as expected in inverse vulcanisation. Note that Figure 3.25 does show signals for ethyl acetate. Once again, the ^{13}C NMR and DEPT135 ^{13}C NMR did not yield any signals through the noise for TAA50-S50-Insol, though the ^{1}H ^{13}C HSQC did manage to produce a very weak ^{13}C NMR spectrum, though the HSQC itself is not of particular utility in understanding the polymer structure.

Figure 3.28: The ^{1}H NMR spectrum of the degradation products of TAA50-S50-Sol.

Figure 3.29: The ^{1}H ^{1}H COSY NMR spectrum of the degradation products of TAA50-S50-Sol.

Liam James Dodd

Figure 3.30: The ^{1}H ^{13}C HSQC NMR spectrum of the degradation products of TAA50-S50-Sol.

Observing Figure 3.28, many of the same conclusions that were drawn from TPA50-S50-Sol and TAA50-S50-Insol can be made about TAA50-S50-Sol. One thing that is clear, is that the NMR spectra of TAA50-S50-Sol is more complex than the spectra of TAA50-S50-Insol. In addition to this, TAA50-S50-Sol shows some broad peaks in its spectra, which are absent int the spectrum of TAA50-S50-Insol, but have analogous peaks in the spectra of TPA50-S50-Sol. This implies that the Sol products have a tendency to display more broad peaks, which points toward the conclusion that the Sol products are less well defined than the Insol products, and have more by-product fragments in their structure. Once again, the ^{13}C NMR and DEPT135 ^{13}C NMR did not yield any signals through the noise for TAA50-S50-Sol, though the ^{1}H ^{13}C HSQC did manage to produce a very weak ^{13}C NMR spectrum, though the HSQC itself is not of particular utility in understanding the polymer structure.
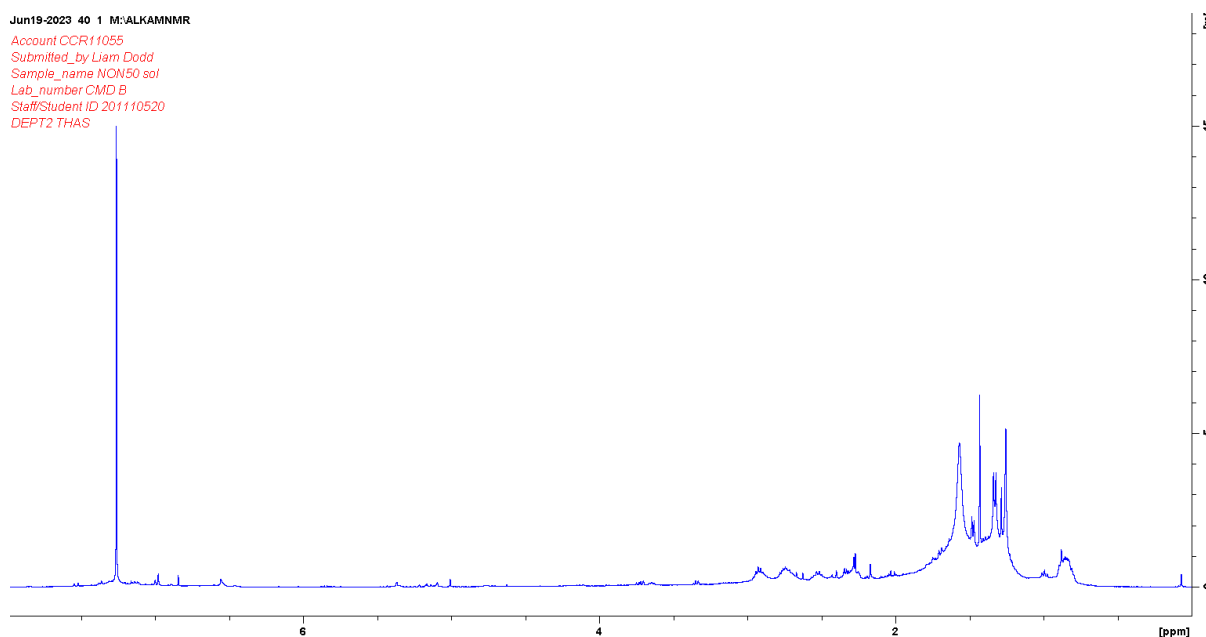
Figure 3.31: The ^{1}H NMR spectrum of the degradation products of NON50-S50-Sol.

Liam James Dodd
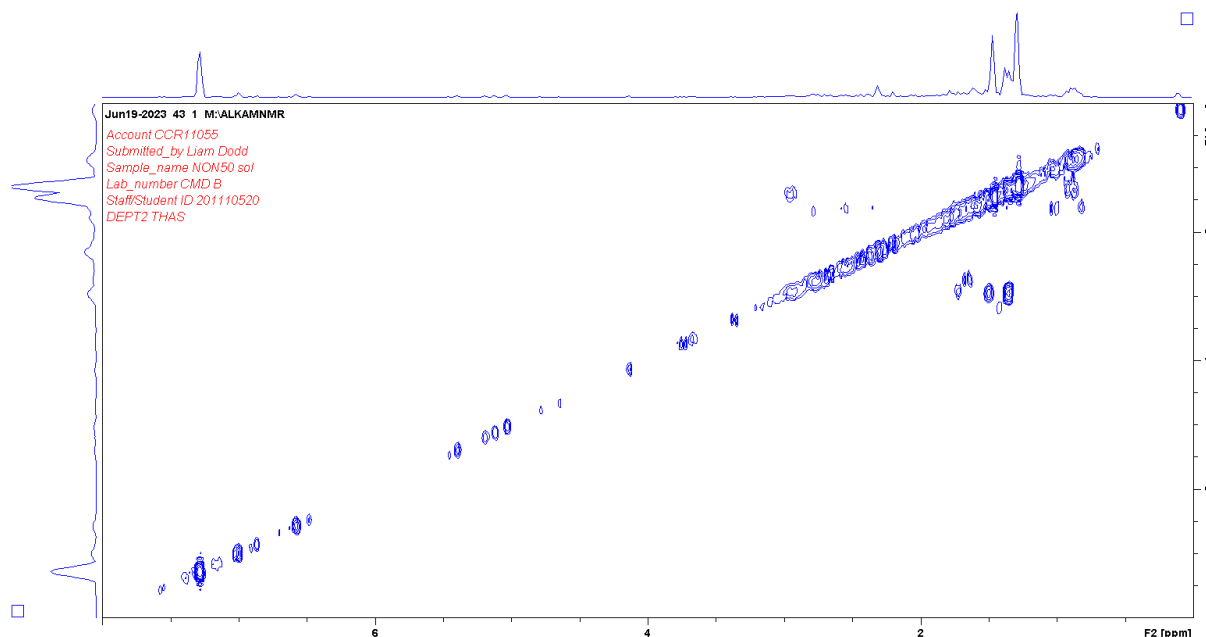
Figure 3.32: The ^{1}H ^{1}H COSY NMR spectrum of the degradation products of NON50-S50-Sol.
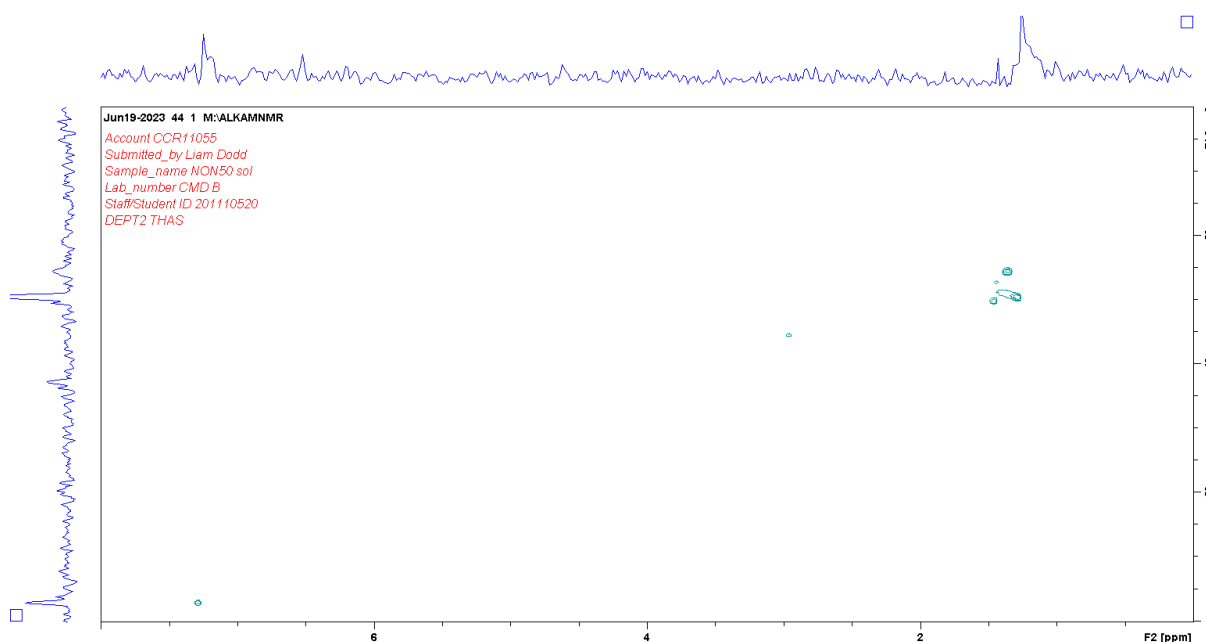
Figure 3.33: The ^{1}H ^{13}C HSQC NMR spectrum of the degradation products of NON50-S50-Sol.

Figure 3.31 shows that the ^{1}H NMR spectrum for NON50-S50-Sol is notably different to those of TAA or TPA polymers, likely due to the significant structural dissimilarity, and the higher predominance of aliphatic protons (NON has five CH_2 groups, in three separate environments, whereas TAA and TPA have three CH_2 groups, all in the same environment). What is interesting is that NON50-S50-Sol shows significantly weaker aromatic resonances than TAA or TPA, which suggests that the route to form these aromatic structures may rely on an amine activated reaction pathway, which NON does not have access to, and thus must use a kinetically slower route. NON50-S50-Sol also shows some alkene resonances, though they are comparatively weaker than those observed for TPA50-S50-Sol. These could be because that, as with TPA, NON's alkynes react progressively to an alkene and then to sp3 hybridised groups, but unlike TPA, because NON contains one fewer alkyne group, it a more complete reaction is observed due to there being proportionally less pi bonds for sulfur to react with in NON as

Liam James Dodd

compared to TPA. Much like the other Sol products, NON50-S50-Sol displays several broad peaks, reinforcing that the Sol products have a tendency to be less well defined than the Insols, and contain a wider variety of hydrogen environments. There are still some peaks present in Figure 3.31 that are analogous to those shown in the spectra of TPA and TAA polymers, for example the peak at 0.85 ppm which recurs in all the other ^{1}H NMR spectra. This indicates that despite the structural differences between TPA, TAA, and NON, they are all forming related products, which implies they are all accessing relatively similar reaction pathways. Once again, the ^{13}C NMR and DEPT135 ^{13}C NMR did not yield any signals through the noise for NON50-S50-Sol, though the ^{1}H ^{13}C HSQC did manage to produce a very weak ^{13}C NMR spectrum, though the HSQC itself is not of particular utility in understanding the polymer structure.
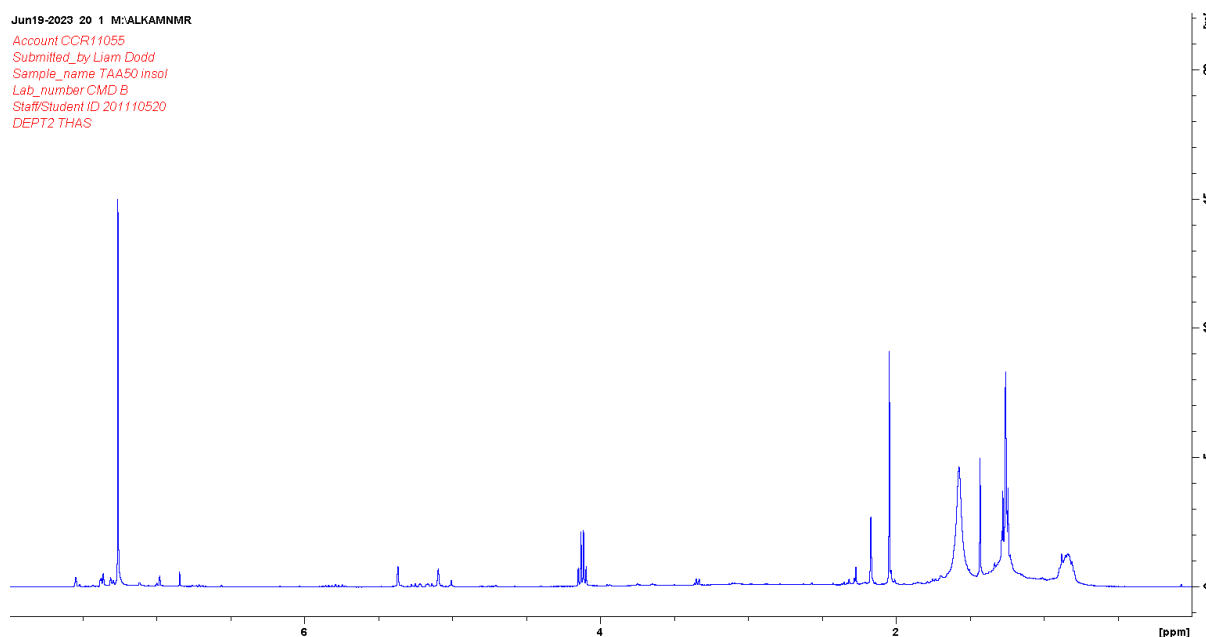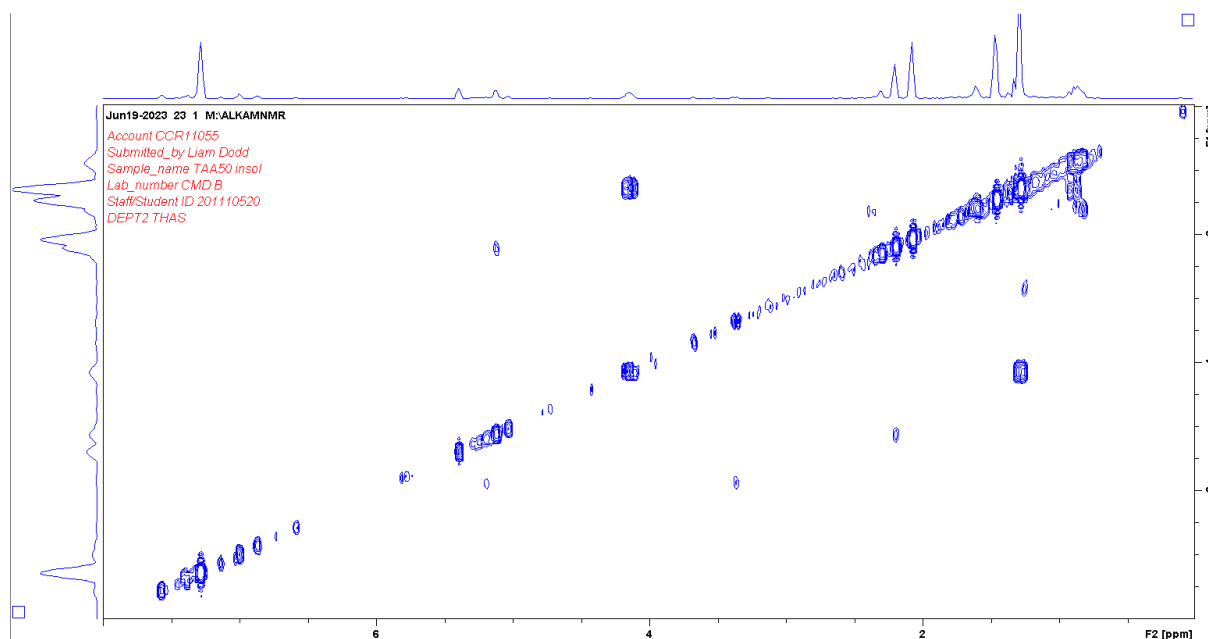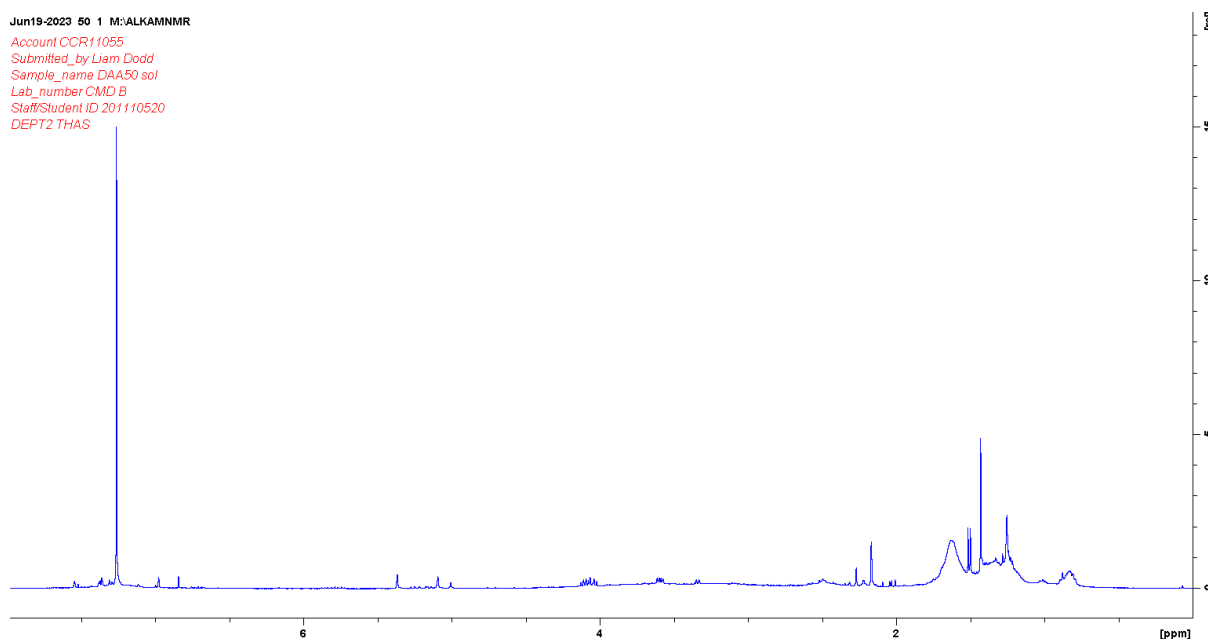

Figure 3.34: The ^{1}H NMR spectrum of the degradation products of DAA50-S50-Sol.
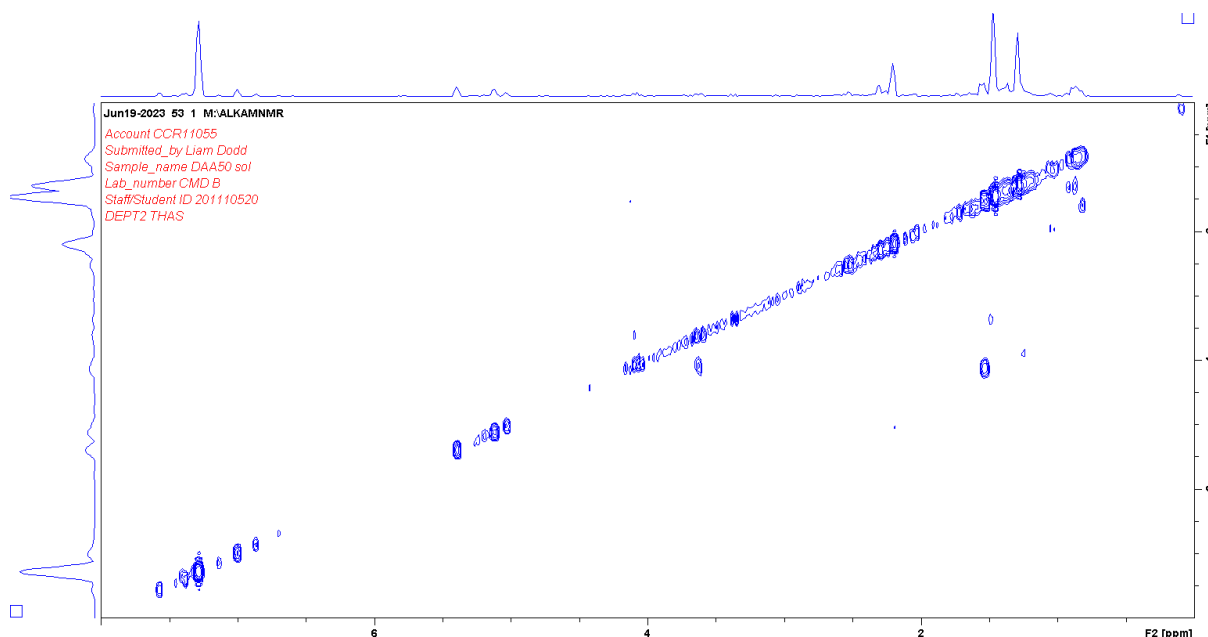
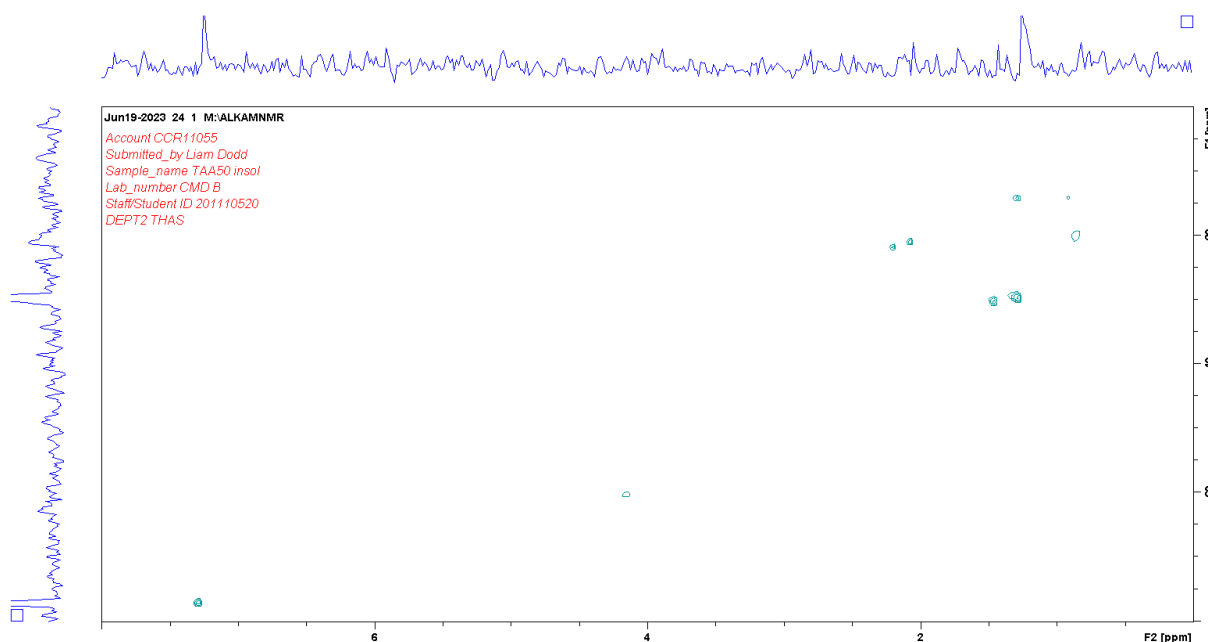Figure 3.35: The ^{1}H ^{1}H COSY NMR spectrum of the degradation products of DAA50-S50-Sol.

Liam James Dodd

The NMR spectra for DAA50-S50-Sol largely reinforce the conclusions drawn from the other spectra. Again, there is evidence of incomplete consumption of alkene bonds, suggesting that the Sol products are less well reacted and less well crosslinked in comparison to the Insol products. These alkene peaks are however quite weak, suggesting that for the most part, the reaction was close to completion. DAA50-S50-Sol displays no evidence of benzenes or phenols, much like TAA50-S50-Sol and TAA50-S50-Insol, again suggesting that alkenes are less effective at forming the aromatics by-products. Again, the intensity for the aromatic resonances are quite weak in comparison to the predominant sp3 region of the spectrum. As a Sol product DAA50-S50-Sol shows more numerous broad peaks, reinforcing the conclusion that the Sol products are less well defined. Nevertheless, DAA50-S50-Sol does show similarities in its spectra as compared to the other polymers, such as the 0.85 ppm peak, again reinforcing that these polymers are utilising similar reaction pathways to form similar products. The ^{13}C NMR, DEPT135 ^{13}C NMR, and the ^{1}H ^{13}C HSQC NMR did not yield any signals through the noise for DAA50-S50-Sol.
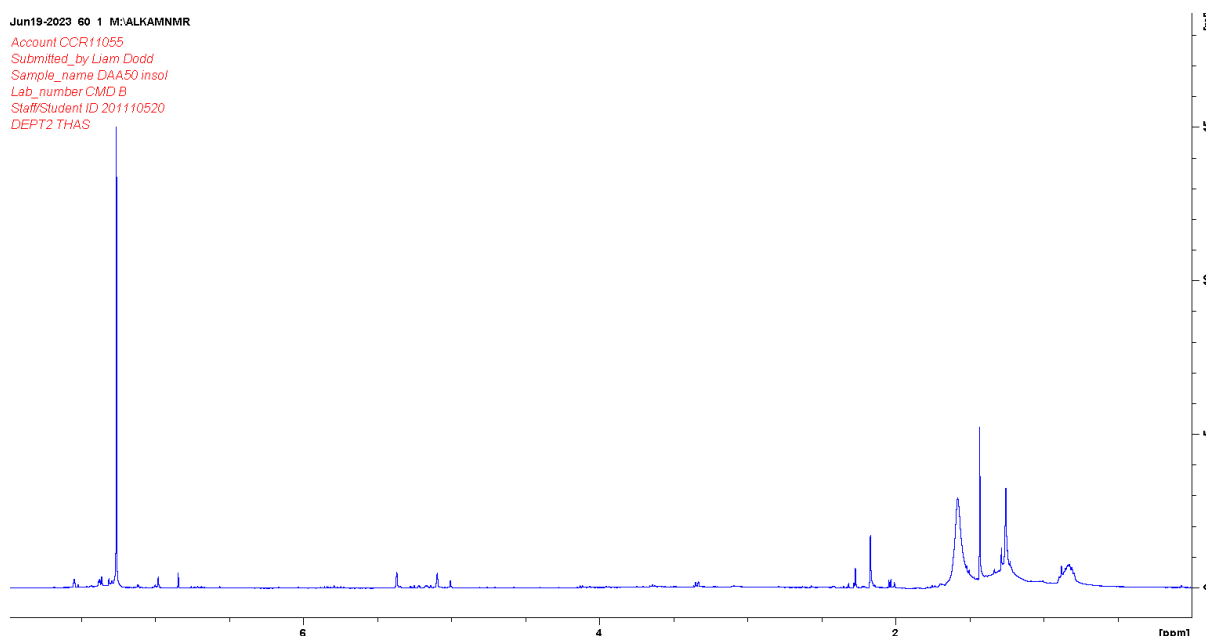
Figure 3.36: The ^{1}H NMR spectrum of the degradation products of DAA50-S50-Insol.

Liam James Dodd
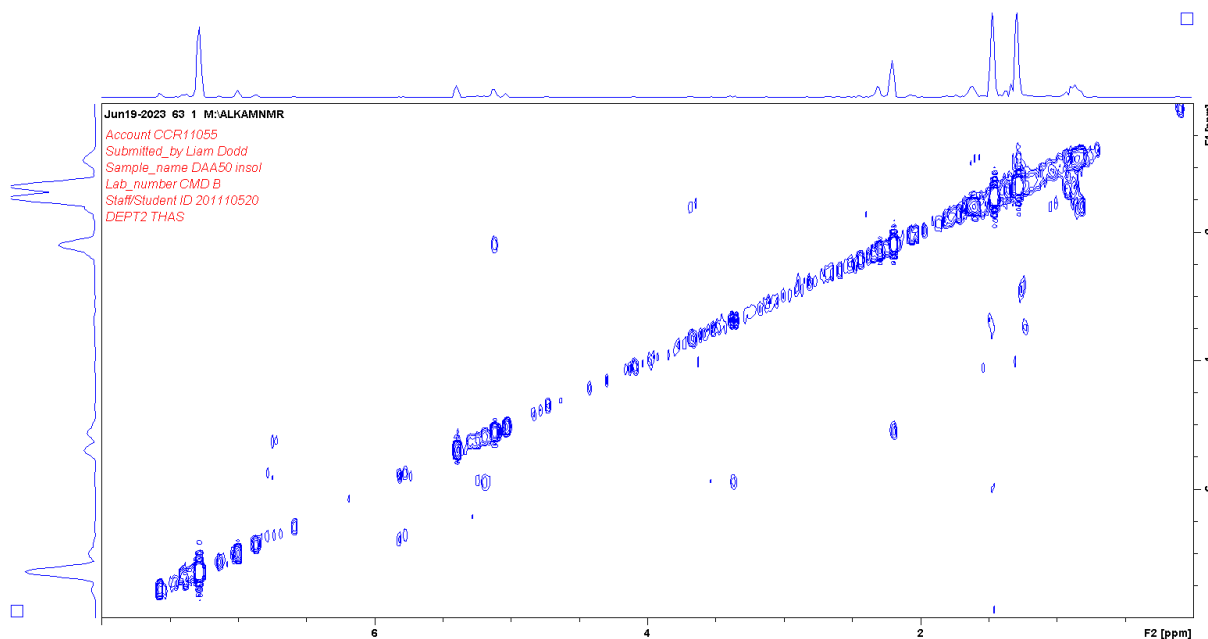
Figure 3.37: The ^{1}H ^{1}H COSY NMR spectrum of the degradation products of DAA50-S50-Insol.
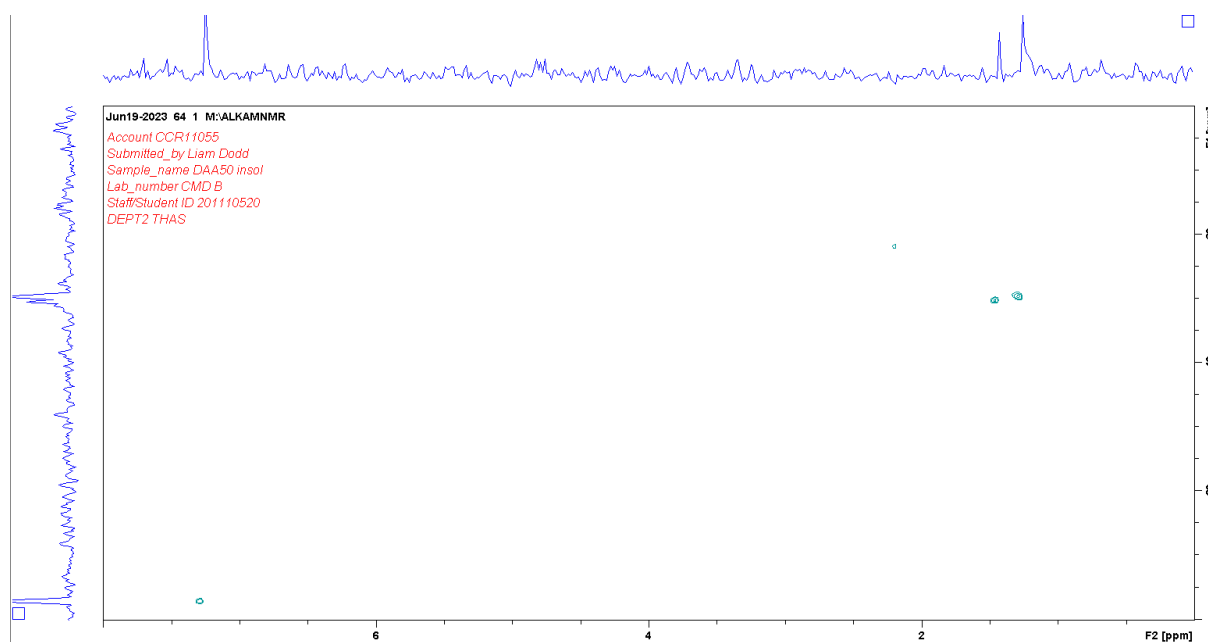
Figure 3.38: The ^{1}H ^{13}C HSQC NMR spectrum of the degradation products of DAA50-S50-Insol.

The spectra of DAA50-S50-Insol only reinforce the previous conclusions and do not add anything of note. Once again, the ^{13}C NMR and DEPT135 ^{13}C NMR did not yield any signals through the noise for DAA50-S50-Insol, though the ^{1}H ^{13}C HSQC did manage to produce a very weak ^{13}C NMR spectrum, though the HSQC itself is not of particular utility in understanding the polymer structure.
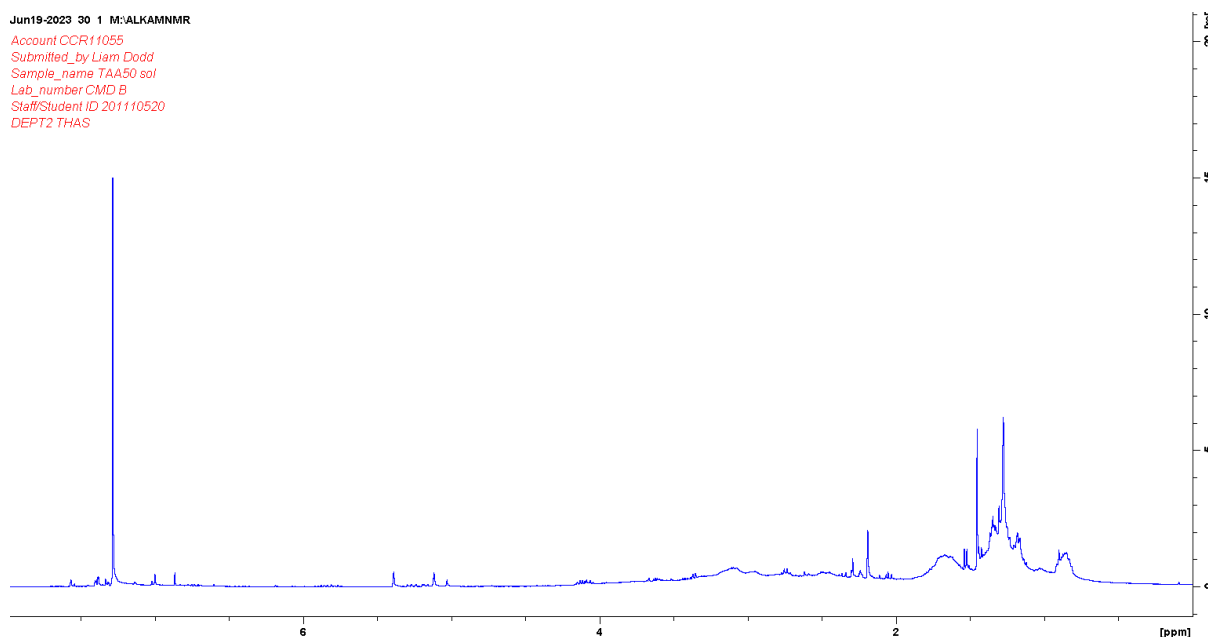
Liam James Dodd
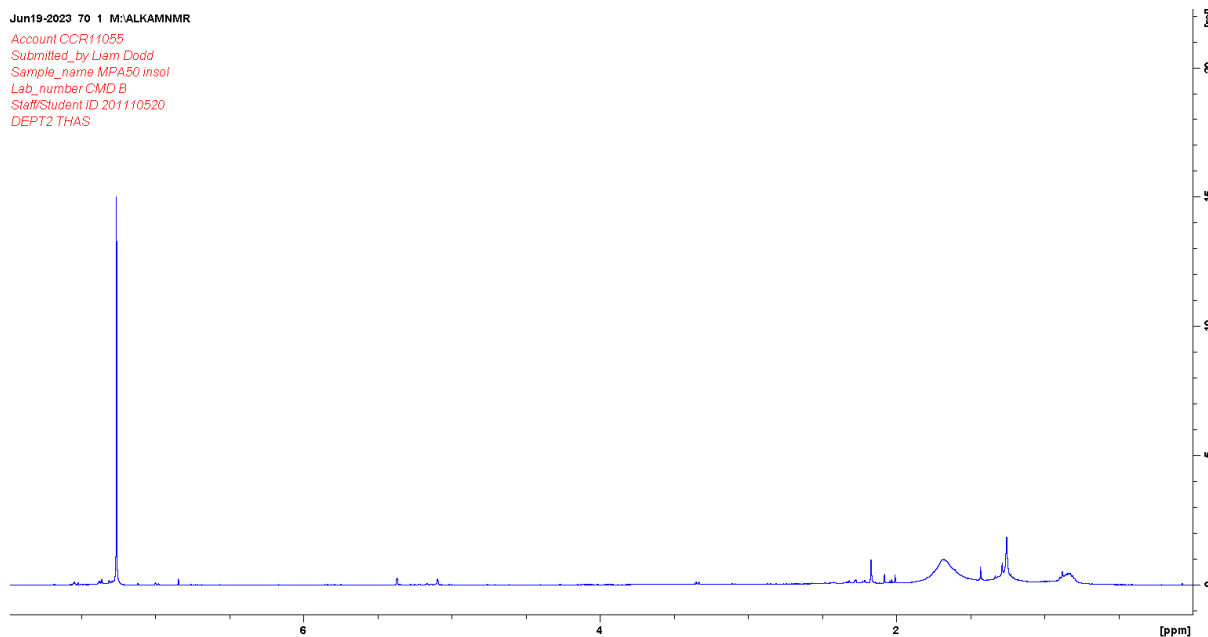
Figure 3.39: The ^{1}H NMR spectrum of the degradation products of MPA50-S50-Insol.
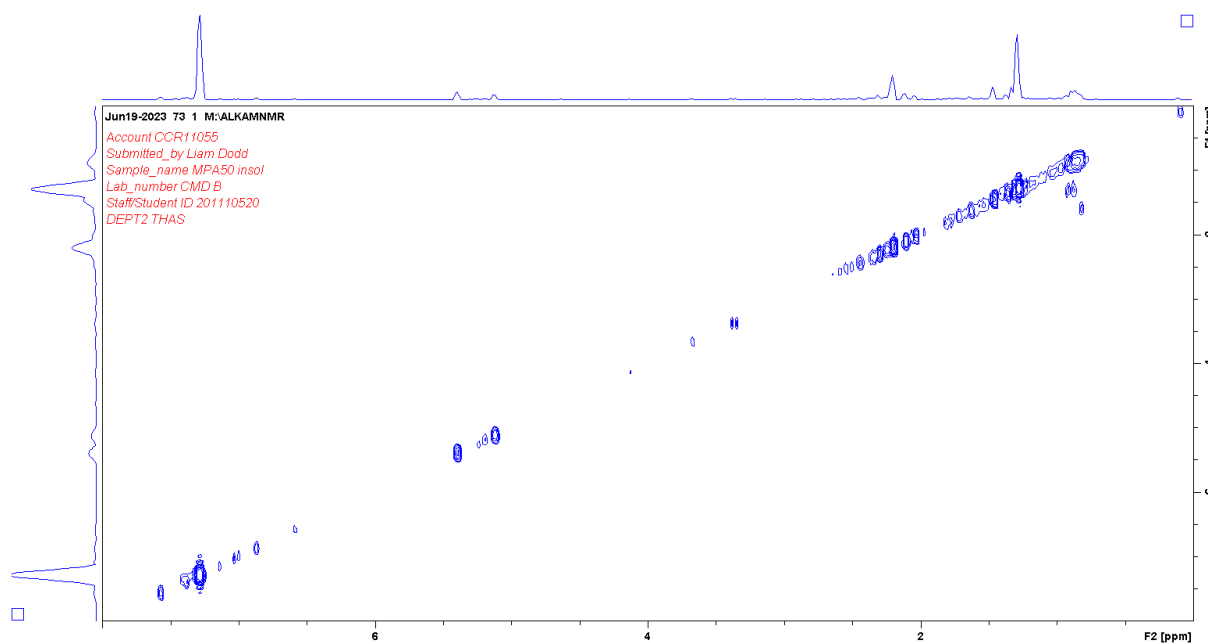
Figure 3.40: The ^{1}H ^{1}H COSY NMR spectrum of the degradation products of MPA50-S50-Insol.

Liam James Dodd
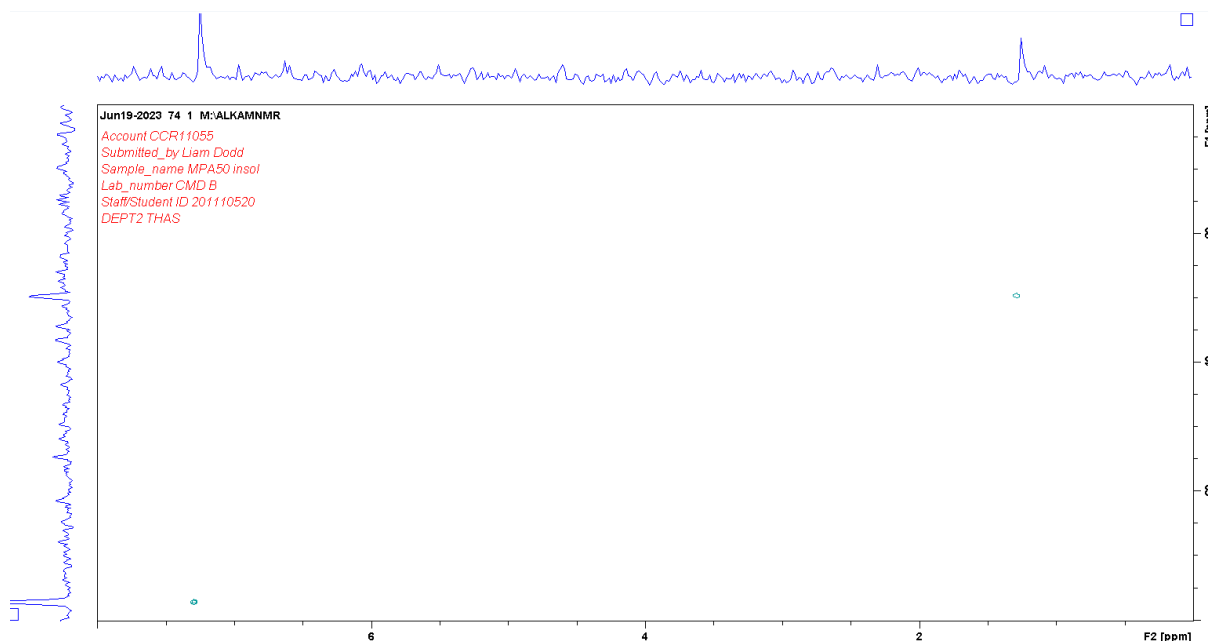
Figure 3.41: The ^1H ^{13}C HSQC NMR spectrum of the degradation products of MPA50-S50-Insol.

The spectra of MPA50-S50-Insol do not add any new conclusions of note, and only reinforce the already established conclusions. The only significant difference between the spectra of MPA50-S50-Insol and the other polymer spectra is that the spectrum is comparatively simple, owing to MPA's simple structure. Once again, the ^{13}C NMR and DEPT135 ^{13}C NMR did not yield any signals through the noise for MPA50-S50-Insol, though the ^1H ^{13}C HSQC did manage to produce a very weak ^{13}C NMR spectrum, though the HSQC itself is not of particular utility in understanding the polymer structure.
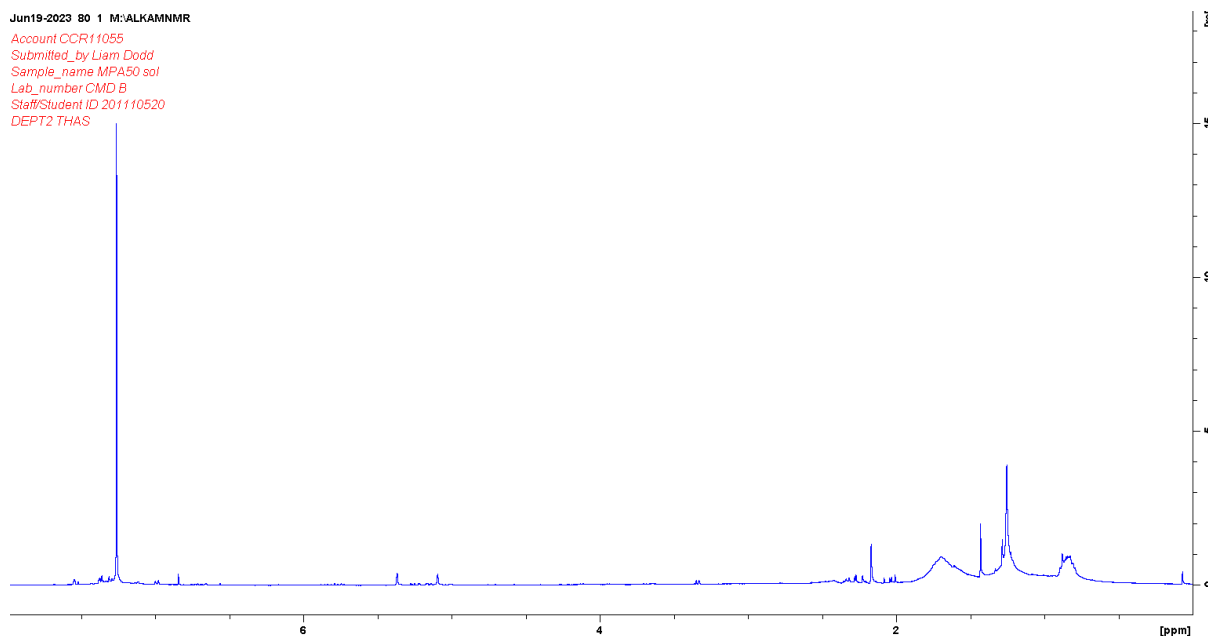
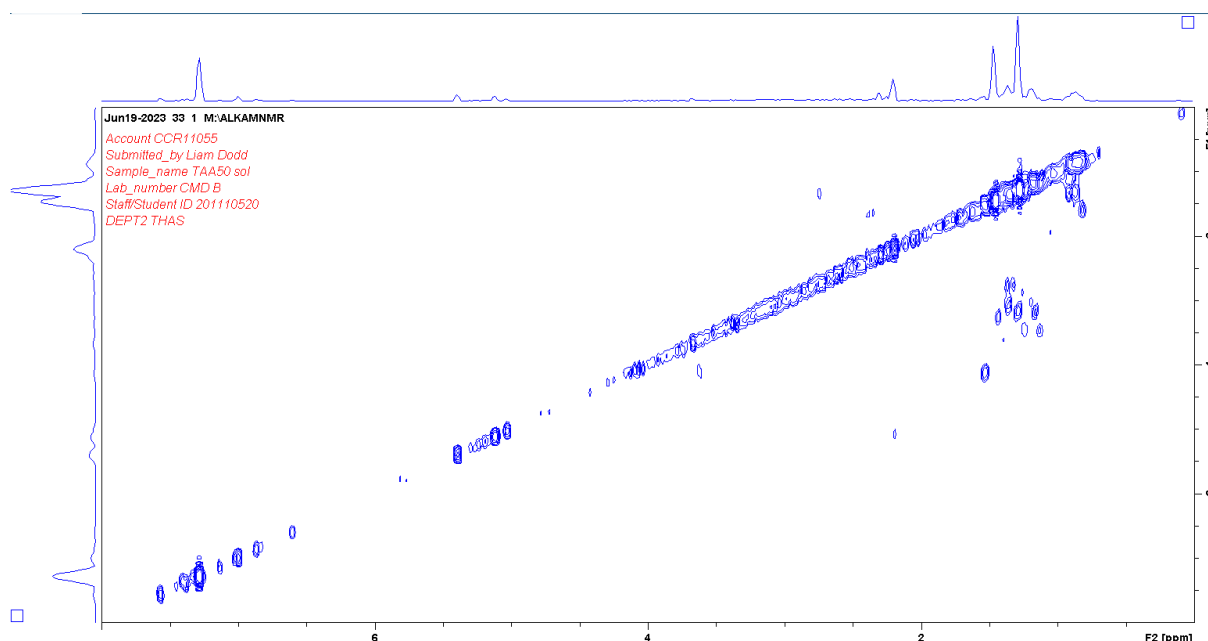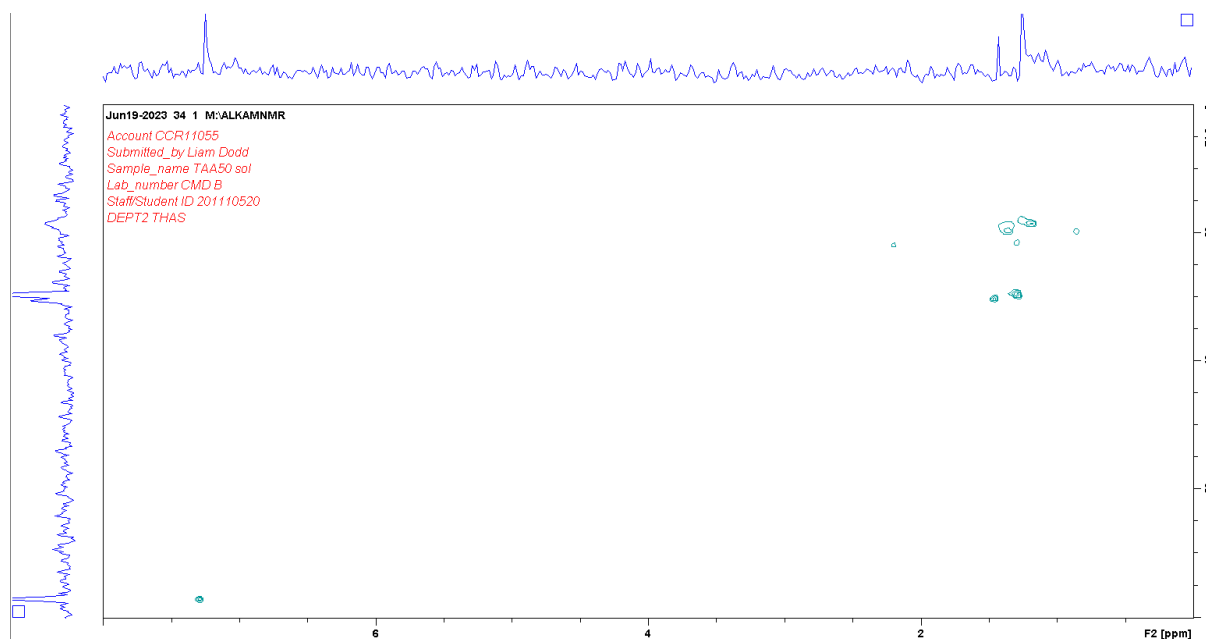Figure 3.42: The ^1H NMR spectrum of the degradation products of MPA50-S50-Sol.

Liam James Dodd
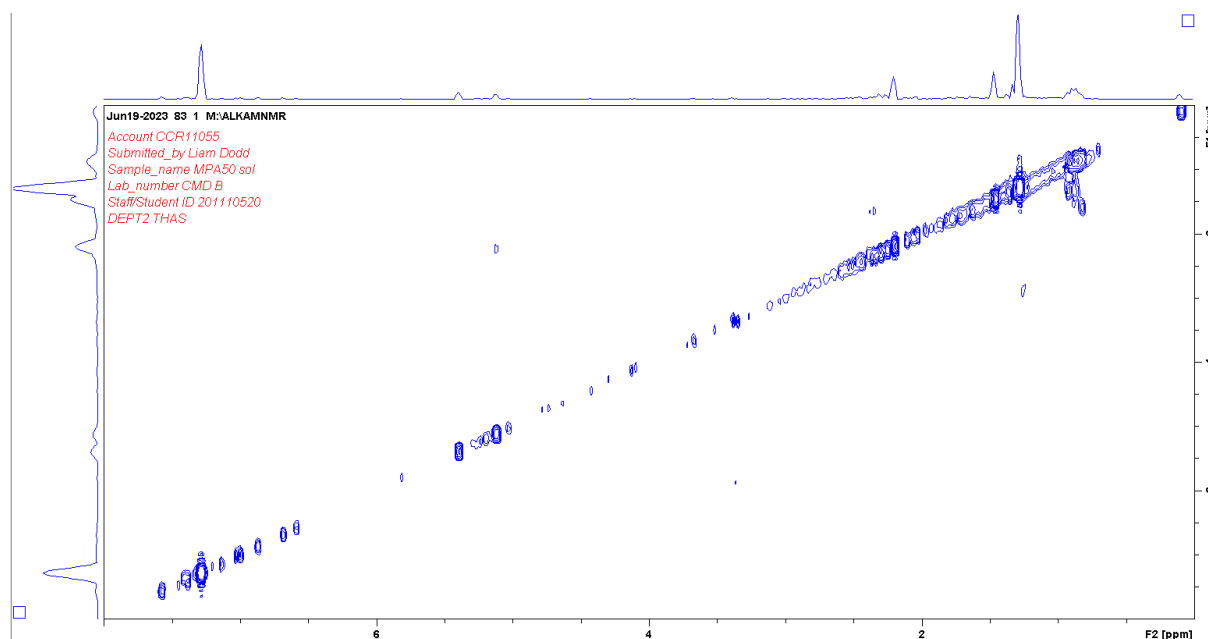
Figure 3.43: The ^{1}H ^{1}H COSY NMR spectrum of the degradation products of MPA50-S50-Sol.
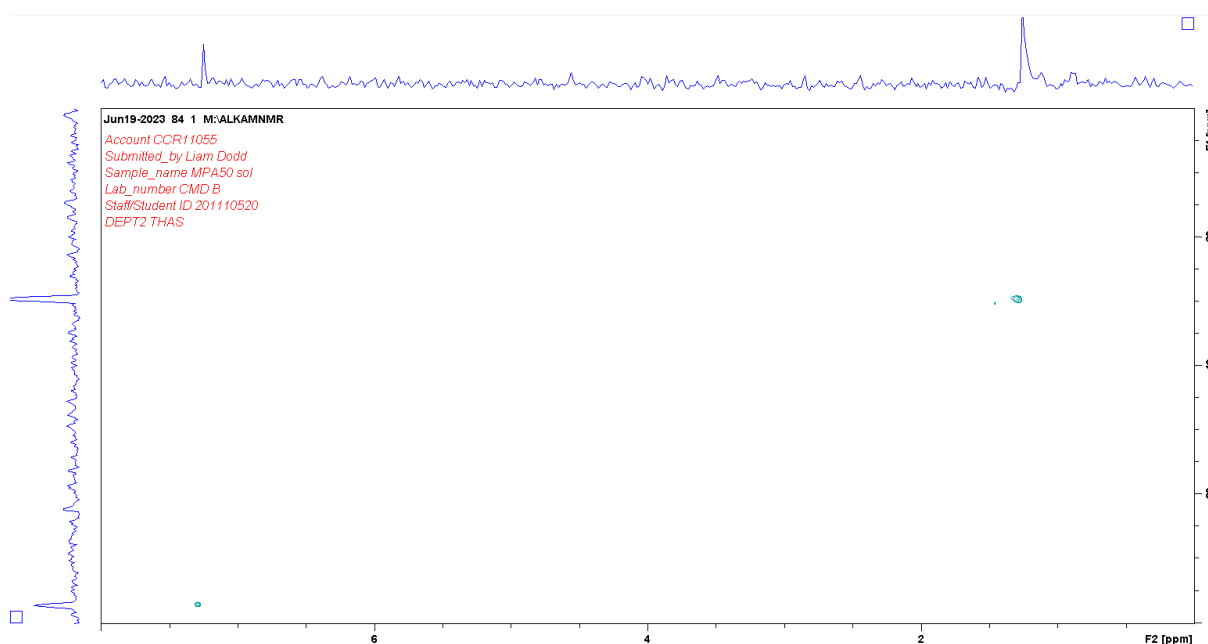
Figure 3.44: The ^{1}H ^{13}C HSQC NMR spectrum of the degradation products of MPA50-S50-Sol.

The spectra of MPA50-S50-Sol do not add any new conclusions of note, and only reinforce the already established conclusions. The only significant difference between the spectra of MPA50-S50-Sol and the other polymer spectra is that the spectrum is comparatively simple, owing to MPA's simple structure. Once again, the ^{13}C NMR and DEPT135 ^{13}C NMR did not yield any signals through the noise for MPA50-S50-Sol, though the ^{1}H ^{13}C HSQC did manage to produce a very weak ^{13}C NMR spectrum, though the HSQC itself is not of particular utility in understanding the polymer structure.

3.14. References

3.1 Investigating the Role and Scope of Catalysts in Inverse Vulcanization; L. J. Dodd, Ö. Omar, X. Wu, T. Hasell; ACS Catalysis, 2021, 11, 4441-4455.

Liam James Dodd

3.2 Nucleophilic Activation of Elemental Sulfur for Inverse Vulcanization and Dynamic Covalent Polymerizations; Y. Zhang, N. G. Pavlopoulos, T. S. Kleine, M. Karayilan, R. S. Glass, K. Char, J. Pyun; Journal of Polymer Science Part A: Polymer Chemistry, 2019, 57, 7–12.

3.3 Crosslinker Copolymerization for Property Control in Inverse Vulcanization; J. A. Smith, S. J. Green, S. Petcher, D. J. Parker, B. Zhang, M. J. H. Worthington, X. F. Wu, C. A. Kelly, T. Baker, C. T. Gibson, J. A. Campbell, D. A. Lewis, M. J. Jenkins, H. Willcock, J. M. Chalker, T. Hasell; Chemistry - A European Journal, 2019, 25, 10433 –10440.

3.4 Inverse vulcanization of elemental sulfur with 1,4-diphenylbutadiyne for cathode materials in Li–S batteries; P. T. Dirlam, A. G. Simmonds, T. S. Kleine, N. A. Nguyen, L. E. Anderson, A. O. Klever, A. Florian, P. J. Costanzo, P. Theato, M. E. Mackay, R. S. Glass, K. Char, J. Pyun; RSC Advances, 2015, 5, 24718–24722.

3.5 On the Mechanism of the Inverse Vulcanization of Elemental Sulfur: Structural Characterization of Poly(sulfur-random-(1,3-diisopropenylbenzene)); J. Bao, K. P. Martin, E. Cho, K. Kang, R. S. Glass, V. Coropceanu, J. Bredas, W. Parker, J. T. Njardarson, J. Pyun; Journal of the American Chemical Society, 2023, 145, 12386–12397.

3.6 Inverse vulcanization of elemental sulfur and styrene for polymeric cathodes in Li-S batteries; Y. Y. Zhang, J. J. Griebel, P. T. Dirlam, N. A. Nguyen, R. S. Glass, M. E. Mackay, K. Char, J. Pyun; Journal of Polymer Science Part A: Polymer Chemistry, 2017, 55, 107-116.

3.7 Organosulfide-plasticized solid-electrolyte interphase layer enables stable lithium metal anodes for long-cycle lithium-sulfur batteries; G. Li, Y. Gao, X. He, Q. Huang, S. Chen, S. H. Kim, D. Wang; Nature Communications, 2017, 8, 850.

3.8 Raman Analysis of Inverse Vulcanised Polymers; L. J. Dodd, C. Lima, D. Costa-Milan, A. R. Neale, B. Saunders, B. Zhang, A. Sarua, R. Goodacre, L. J. Hardwick, M. Kuball, T. Hasell; Polymer Chemistry, 2023, 14, 1369-1386.

3.9 Investigating the Antibacterial Properties of Inverse Vulcanized Sulfur Polymers; J. A. Smith, R. Mulhall, S. Goodman, G. Fleming, H. Allison, R. Raval, T. Hasell; ACS Omega, 2020, 5, 5229–5234.

3.10 Antibacterial Activity of Inverse Vulcanized Polymers; R. A. Dop, D. R. Neill, T. Hasell; Biomacromolecules, 2021, 22, 5223–5233.

3.11 Chemically induced repair, adhesion, and recycling of polymers made by inverse vulcanization; S. J. Tonkin, C. T. Gibson, J. A. Campbell, D. A. Lewis, A. Karton, T. Hasell, J. M. Chalker; RSC Chemical Science, 2020, 11, 5537-5546.

3.12 High Sulfur Content Polymers: The Effect of Crosslinker Structure on Inverse Vulcanization; J. A. Smith, X. F. Wu, N. G. Berry, T. Hasell; Journal of Polymer Science Part A: Polymer Chemistry, 2018, 56, 1777-1781.

Liam James Dodd

Chapter 4: Raman Analysis

Inverse vulcanised polymers have a wide range of advantages, potential applications, sustainability benefits, and methods to tune the polymerisation outputs as desired. However, one persistent issue with the polymers is the difficulty in their analysis. With most mainline characterisation techniques struggling to provide trustworthy data on inverse vulcanised polymers, it can sometimes be challenging to prove that a particular sample is a polymer, never mind extract in-depth information about the polymers themselves. This could prohibit rational design approaches that would improve upon currently existing polymers or result in new polymers with superior properties. As such, new analysis approaches are required to ascertain the most crucial information about the polymers, to which Raman spectroscopy was identified as a potentially information rich technique because it is sensitive to many of the low polarity, high polarizability vibrational modes that should be common to inverse vulcanised polymers: sulfur – sulfur, sulfur – carbon, and carbon skeleton modes. This chapter explores why Raman analysis had not been successfully applied before this project, and then shows how the obstacles to Raman spectroscopy can be overcome, yielding extremely valuable information that is near impossible to obtain by other means: the length of the sulfur chains, the homogeneity of the polymers, and the unpolymerized sulfur content that cannot be detected by many analyses.

4.1. Project Outline

The high weight percentage of sulfur in inverse vulcanised polymers is integral to their unique complement of characteristics.[4.1] However, it is also the high weight percentage of sulfur that makes these materials hard to analyse. The primary techniques used to analyse inverse vulcanised polymers include: DSC, to determine thermal characteristics of the polymer, identify a T_g to confirm a polymeric structure, and identify the presence of unreacted crystalline sulfur in the form of S_8; TGA, to identify the T_d; and PXRD, again to identify unreacted crystalline sulfur as S_8. With these three techniques forming the bulk of the analysis, it is clear that inverse vulcanised polymers are difficult to build a clear picture of at the molecular level. Other complementary techniques can assist in the understanding, but begin to encounter difficulties. Such examples are: dynamic mechanical analysis (DMA), which provides an alternate way to identify the T_g as well as giving a measure of how the mechanical properties vary with temperature when they are relevant to examine; TLC which can identify unreacted elemental sulfur, regardless of its crystallinity which is an advantage over DSC and PXRD, though there can be questions as to whether TLC solvents induce depolymerisation to elemental sulfur; and mass spectrometry though this can be extraordinarily difficult to implement, leading to very limited uptake in the field. Beyond these techniques, several other commonplace analyses encounter significant complications when applied to inverse vulcanised polymers. Combustion microanalysis suffers from a lack of suitable high sulfur content calibration standards and so only estimates the sulfur content. GPC and size exclusion chromatography (SEC) are limited by solubility, which fully crosslinked inverse vulcanised polymers are not, and give dubious results that rely on assuming that the analyte is of similar molecular nature to the comparison standard of known molecular weight; a difficult assumption for inverse vulcanised polymers due to their uniquely high sulfur content and many polysulfide bridges. Solution phase NMR is rarely applicable as these polymers are often insoluble, and solid-state NMR is often not easily accessible. FTIR spectroscopy is easy to perform, but provides limited information, which is unsurprising given that some inverse vulcanised polymers may see application on account of their high IR transparency.[4.2,4.3] FTIR spectroscopy is typically only useful in identifying the consumption of carbon – carbon double bonds, indicating the extent of reaction, and proving or disproving that the organic comonomer skeleton has remained intact. Certainly, FTIR spectroscopy struggles to provide information on the sulfurous

Liam James Dodd

component of inverse vulcanised polymers on account of its selection rule that vibrations must cause a change in dipole moment, and the sulfur – sulfur bond has little to no dipole moment.[4.4]

None of the aforementioned techniques can readily provide information on what is arguably the most crucial component of inverse vulcanised polymers: their bridging sulfur chains. To this end, Raman spectroscopy may be an ideal solution as the sulfur – sulfur bond and the carbon – sulfur bond are both highly Raman active, but in the ten years since inverse vulcanisation's original publication, the technique has seen limited use. If Raman spectroscopy could successfully be performed, it could provide highly desirable information that is otherwise challenging to access, such as the average number of atoms in a sulfur chain and the distribution of chain lengths, which could then be related to the physical properties, providing a better understanding of why they arise. To date, only a few publications have included a Raman study of their inverse vulcanised polymers.[4.5-4.7] One used Raman spectroscopy as a complementary technique to FTIR spectroscopy, but derived little information from the spectra.[4.8] Another used Raman spectroscopy despite the fluorescence of the polymers to identify the presence of unreacted sulfur, which gave sufficiently strong signals to be seen through the fluorescent background. Unfortunately, that same fluorescent background precluded a detailed analysis of the polymer peaks.[4.9]

It was hypothesized here that Raman spectroscopy could have the potential to be remarkably beneficial in the analysis of these otherwise hard to study polymers. Therefore, this project focused upon different Raman spectroscopic techniques (1064 nm Raman spectroscopy, Fourier transform Raman spectroscopy, Kerr-Gated Raman spectroscopy, and UV Raman spectroscopy) that can circumvent fluorescence, comparing and contrasting them in the study of inverse vulcanised polymers. Several different techniques were implemented in the analysis of a representative panel of inverse vulcanised polymers, demonstrating what information can be obtained and how to obtain it. Thus, an account of the advantages and method optimisations for Raman spectroscopic analysis of inverse vulcanised polymers was produced, covering the study of the range and distribution of different sulfur ranks, which is defined as the number of sulfur atoms in a linear sulfur chain, something which cannot easily be measured directly by other techniques at the time of publication, as alternatives such as mass spectrometry are time consuming and troublesome.[4.10] Also included was an assessment of the homogeneity of the polymers, which can be difficult to scrutinise by other means. It has been found that there are several means by which the progress of reactions can be tracked, and a method has been developed to quantify how much sulfur within the polymer remains unreacted, which has the advantage that it does not rely on the sulfur being crystalline, a common drawback of other techniques. This study also presents step by step guides on how to perform these valuable analyses, as well as applying them in some proof of concept examples.

4.2. General Considerations

All chemicals were used as received. Chemicals were obtained from Sigma Aldrich unless otherwise specified. Ground sulfur sublimed powder reagent grade ≥99.5 % was obtained from Brenntag UK & Ireland. DCPD (stabilised with BHT) [precursor to Cyclopentadiene] >97%, and DIB (stabilised with TBC) >97% were obtained from Tokyo Chemicals Industry. Combustion microanalyses were performed on an elementar Vario Micro cube, with a first analysis performed to acquire rough data that was then used to calibrate the instrument for a second, more accurate analysis. DSC was performed from -90 to 150 °C, heating at 10 °C min⁻¹ and cooling at 5 °C min⁻¹ on a TA instruments DSC25 discovery series equipped with an RCS90, using Tzero aluminium hermetic pans and aluminium lids. UV/Vis spectra were obtained using a CARY 5000 UV-Vis-NIR spectrophotometer. Fluorescence measurements were performed on an Edinburgh instruments Fluorescence Lifetime Spectrometer 980, with excitation using a xenon lamp and detection using a photon multiplier tube. Raman spectra were obtained using

Liam James Dodd

one of the following instruments: for handheld 1064 nm Raman, a Snowy Range Instruments model CBex 1064 was used; for all other 1064 nm Raman, a Metrohm i-Raman EX 1064 was used; for 532 nm and 785 nm Raman, an inVia Reflex Qontor Confocal Raman Microscope was used.

4.3. Synthesis

To give an array of polymer samples to analyse by Raman spectroscopy, the inverse vulcanisation of several different organic crosslinkers was performed. These crosslinkers were chosen to be representatives of different broad families of crosslinker, to test the range of applicability of Raman spectroscopy, with their structures shown in Table 4.1. DVB was chosen as the main crosslinker of study, on account of its great success in forming well defined polymers with physical properties that make them straightforward to handle.[4.11,4.12] DIB was chosen on account of its structural similarity to DVB, therefore providing an interesting comparison.[4.1] DCPD was chosen on account of its rigid polycyclic structure, that is not aromatic like DVB or DIB. DCPD is particularly prevalent to be tested because it can be blended with other crosslinkers to modify the final polymer's properties, though such ternary systems were not studied here on account of their complexity in this flagship study.[4.13] Squalene was chosen as a representative of aliphatic crosslinkers with flexible backbones.[4.14,4.15] Although plant oils have flexible backbones and are receiving significant attention on account of their renewability, squalene is a more well defined chemical that was predicted to be easier to analyse by Raman spectroscopy, in contrast to plant oils which normally consist of a complex mixture of related compounds.[4.16] As such, inverse vulcanised polymers of DVB, DIB, DCPD, and squalene were synthesized and then analysed by DSC and combustion microanalysis, as tabulated in Table 4.1.

Table 4.1: Synthetic conditions and analyses of the first batch of inverse vulcanised polymers.

Name	DVB			DIB			DCPD						Squalene		
Chemical structure															
Synthesis at	135 °C			135 °C			135 °C			160 °C			170 °C		
Feed ratio Crosslinker (%)	30	50	70	30	50	70	30	50	70	30	50	70	30	50	70
Sulfur (%)	**70**	**50**	**30**	**70**	**50**	**30**	**70**	**50**	**30**	**70**	**50**	**30**	**70**	**50**	**30**
Microanalysis C expected (%)	27.7	46.1	64.6	27.3	45.5	63.8	27.3	45.4	63.6	27.3	45.4	63.6	26.3	43.9	64.4
C actual (%)	**21.4**	**26.1**	**50.9**	**8.5**	**22.6**	**36.7**	**11.7**	**16.2**	**10.2**	**17.6**	**28.2**	**32.6**	**38.1**	**48.2**	**61.3**
H expected (%)	2.3	3.9	5.4	2.7	4.5	6.2	2.8	4.6	6.4	2.8	4.6	6.4	3.7	6.1	8.6
H actual (%)	**1.7**	**2.1**	**4.1**	**0.9**	**2.2**	**3.3**	**1.5**	**1.7**	**1.5**	**1.8**	**2.6**	**3.1**	**4.8**	**6.3**	**8.3**
S expected (%)	70.0	50.0	30.0	70.0	50.0	30.0	70.0	50.0	30.0	70.0	50.0	30.0	70.0	50.0	30.0
S actual (%)	**76.9**	**71.4**	**44.3**	**90.5**	**75.7**	**59.7**	**88.8**	**82.9**	**88.9**	**82.0**	**69.4**	**64.8**	**56.5**	**45.3**	**29.9**
DSC T_g / °C	39.2	51.0	97.2	4.9	12.6	36.8	20.1	38.4	11.8	47.6	83.5	93.0	18.2	33.2	19.0

The synthesis was performed by standard literature methods. Inverse vulcanisation reactions are particularly sensitive to their reaction conditions, so great care was taken to ensure consistency in the reaction method. The same hotplate and thermocouple were used for every reaction. The hotplate was equipped with an aluminium heating pan and block, and to protect the reaction vials from the variable conditions in the laboratory, the heating pan, heating block and reaction vials were wrapped tightly in an excess of aluminium foil. Sulfur (3, 5, or 7 g ± 0.0099 g) was melted at a desired temperature in a 40 mL reaction vial, without a lid, with 200 rpm stirring from a 14 mm cross shaped

Liam James Dodd

stirrer. The system was left for 10 to 20 mins to allow thermal equilibration. The selected crosslinker (3, 5, or 7 g ± 0.0099 g) was poured into the 40 mL reaction vial, to give a reaction of 10 g scale, and the stirring rate was immediately increased to 900 rpm. The reaction was monitored by dip testing: when an aliquot of the reaction was removed on the end of a spatula, and the aliquot remained a single phase upon cooling, (that is no sulfur precipitated) the reaction solution was poured into a preheated mould and left in the oven at 135 °C overnight to cure. Note that dip testing was not successful for DVB polymers as there was no point at which the aliquot would remain a single phase, but at the same time leave the reaction solution of low enough viscosity to pour. Where necessary, cured polymers were ground to powder. From here on, the polymer samples will be referred to by the following abbreviation system: NAMEα-Sβ, where α is the mass percentage of crosslinker in the feed ratio, and β is the mass percentage of crosslinker in the feed ratio. In the case of DCPD, two different synthesis temperatures were used, so an extra notation, -Tγ, is added to the end of the abbreviation, where γ is the synthesis temperature in °C. For example, a polymer of DCPD and sulfur in a 70 : 30 feed ratio, synthesized at 160 °C would have the abbreviation: DCPD70-S30-T160. Representative DSC thermograms for this first batch of inverse vulcanised polymers are shown in Figure 4.1.
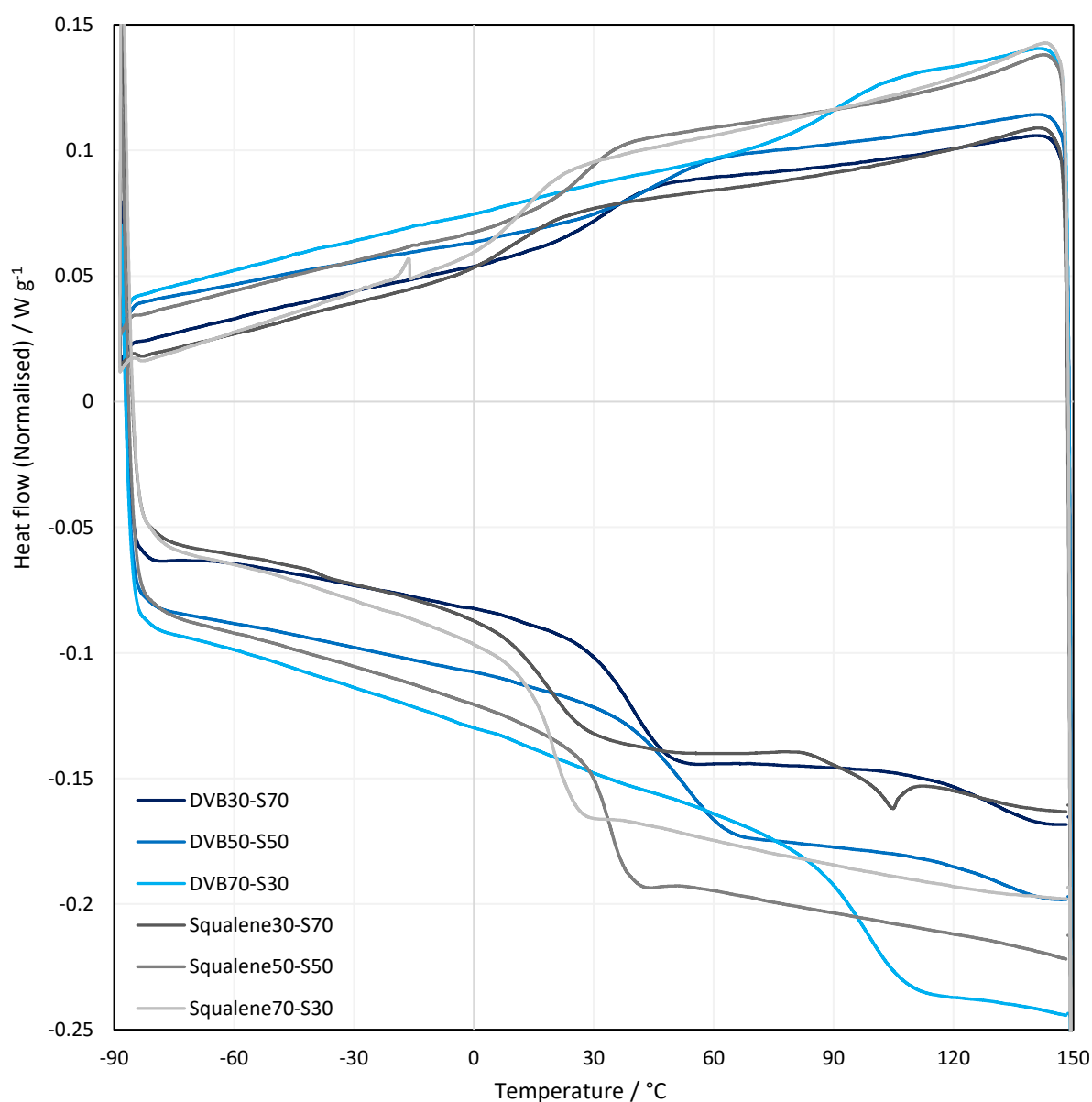
Figure 4.1: Representative DSC thermograms of the first batch of inverse vulcanised polymers.

Liam James Dodd

4.4. Conventional Raman Analysis

Initial attempts at conventional Raman analysis of inverse vulcanised polymers using either a 532 nm laser or a 785 nm laser, displayed fluorescent backgrounds that obscured all Raman signals (Figure 4.2). A 785 nm laser is generally less prone to fluorescence than other shorter laser wavelengths because its lower photon energy is less likely to be sufficiently energetic to excite an electronic transition, which would then allow subsequent fluorescent transitions.
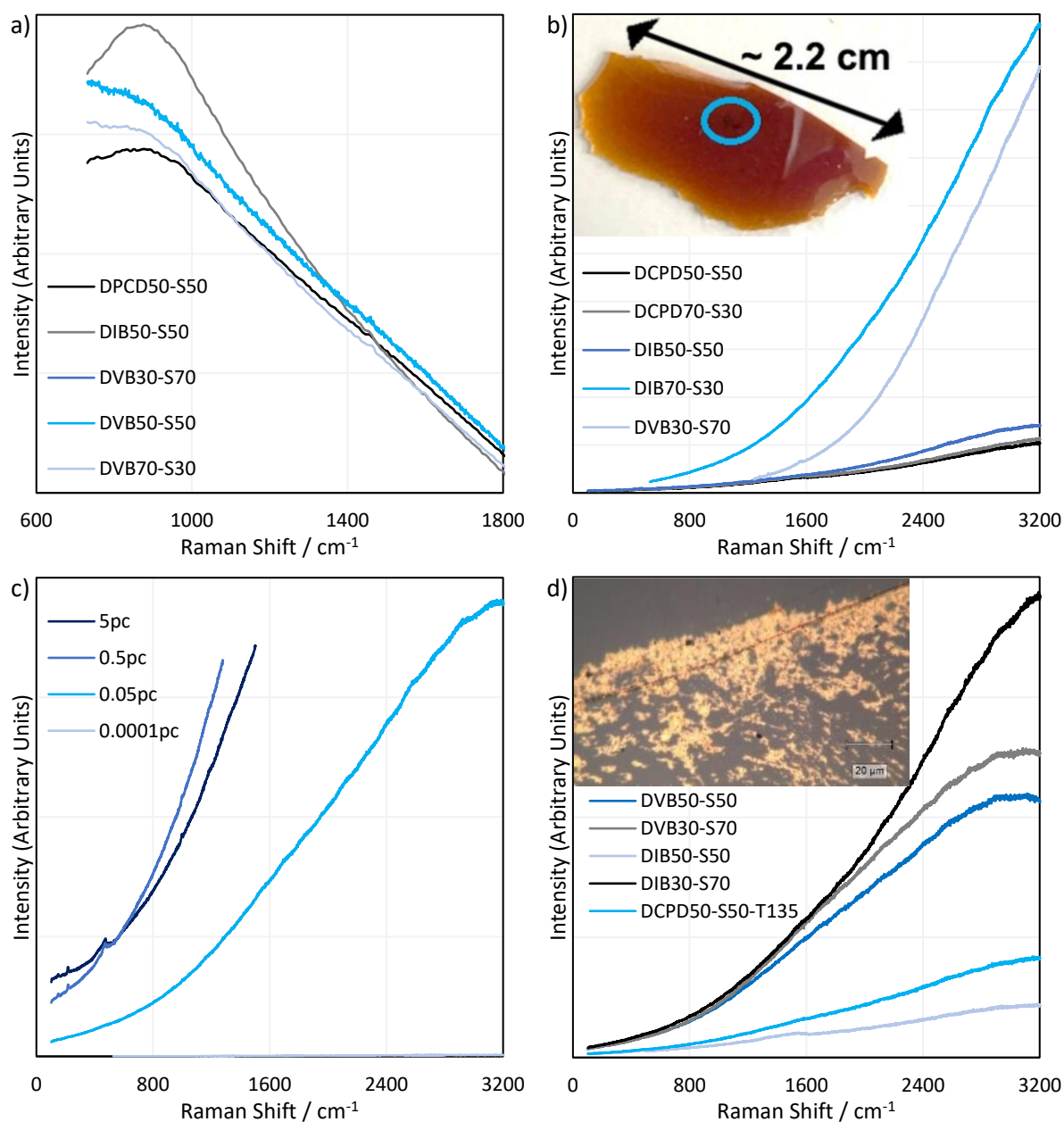
Figure 4.2: Raman spectra of inverse vulcanised polymers obtained with a) a 784 nm, b) a 532 nm excitation laser at 0.1 % power and a 10 s exposure time, c) a 532 nm excitation laser with different laser intensities, analysing DVB50-S50 with a 10 s exposure time, and d) a 532 nm excitation laser, using 0.1 % intensity, with a 10 second exposure time from a 50x objective lens, for different polymers coated with gold nanoparticles. The inset image in b) is of a thin piece of DVB50-S50, displaying visual evidence of laser damage in the form of black spots near its centre. The inset image in d) is of a DVB50-S50 polymer surface coated with gold nanoparticles. Several laser intensities were tried at different focal points with different concentrations of gold nanoparticles, all of which failed to give a spectrum.

Liam James Dodd

In an attempt to enhance the Raman signals, surface enhanced Raman scattering was attempted (SERS) the but unfortunately was not successful in obtaining Raman signals through the fluorescent background (Figure 4.2d). Spherical gold nanoparticles used for the SERS were synthesized by the citrate synthesis method.[4.17] Aqueous sodium citrate (1.4 mL, 38.8 mM) was quickly added to aqueous HAuCl$_4$ (200 mL, 2.53×10^{-4} M) which was already under reflux. The refluxing solution was stirred for 30 min until a clear red solution was obtained. ICP-OES analysis of the solution indicated the purity of the solution: it contained only gold metal in exactly the predicted concentration. The UV/Vis spectrum indicated a plasmon band at 534 nm (Figure 4.3). The nanoparticle solution was concentrated by centrifugation before use in SERS.
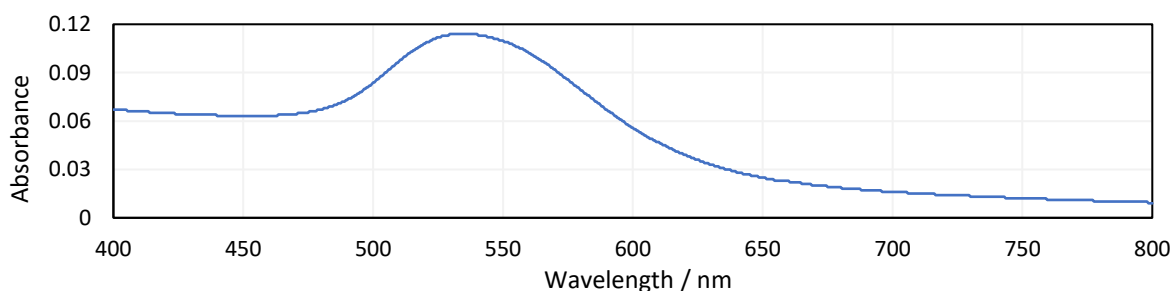
Figure 4.3: UV/Vis spectrum of the spherical gold nanoparticle suspension.

This failure of conventional Raman techniques highlights the necessity for Raman spectroscopy variants that can avoid or significantly reduce fluorescent backgrounds. For the representative panel of polymers, fluorescence was observed in every case, suggesting that the absence of fluorescence, such as that in Berk's work is uncommon, and most inverse vulcanised polymers will require measures to avoid fluorescence.[4.8] As a sidenote, as depicted in Figure 4.2b, it was found that inverse vulcanised polymers can be susceptible to laser damage during Raman spectroscopy, and this should be considered when analysing the polymers: the laser power should be kept as low as possible whilst still acquiring a good signal to noise ratio. In that regard, techniques that minimize the chances of laser damage due to long excitation wavelengths may be particularly valuable.

4.5. UV/Vis and Fluorescence Spectroscopy

It is likely that inverse vulcanisation literature has seen limited contributions from Raman spectroscopy due to the fluorescent background which occurs in several polymer samples. Therefore, it is prudent to characterise this fluorescence; the UV/Vis spectra, and subsequently, the fluorescence spectra of inverse vulcanised polymers were obtained and analysed. Firstly, the UV/Vis of the unreacted crosslinkers showed no absorbance in the visible region; expected since they are clear colourless liquids. All however did show absorbance at UV wavelengths (Figure 4.4)

Crosslinker	Absorption maxima / nm
DVB	242, 254 (shoulder), 264 (shoulder), 282, 295 (shoulder)
DIB	243
DCPD	238 (near detector limit, value may be inaccurate)
Squalene	237 (near detector limit, value may be inaccurate), 264 (shoulder)
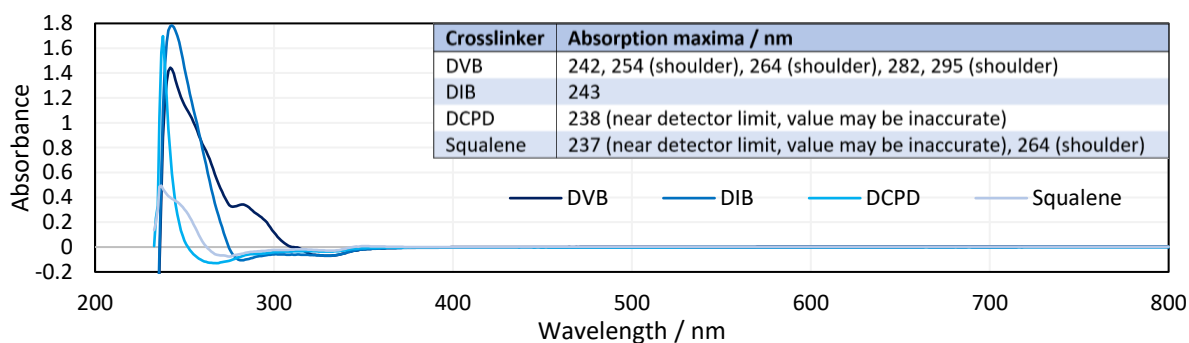
Figure 4.4: UV/Vis spectra of the crosslinkers at the following v/v concentrations in CHCl$_3$: 0.001 % DVB, 0.001 % DIB, 0.5 % DCPD and 0.01 % squalene. Data below 400 nm has an unreliable baseline.

Liam James Dodd

From these UV absorptions, fluorescence spectroscopy was performed, with the results shown in Figure 4.5.

a)

When excited at	Emits at	With relative efficiency
255 nm (4.86 eV)	302 nm (4.11 eV)	0.09
	328 nm (3.78 eV)	1.00
	339 nm (3.66 eV)	0.96
285 nm (4.35 eV)	328 nm (3.78 eV)	0.54
	339 nm (3.66 eV)	0.43
303 nm (4.09 eV)	328 nm (3.78 eV)	0.25
	339 nm (3.66 eV)	0.20
314 nm (3.95 eV)	328 nm (3.78 eV)	0.14
	339 nm (3.66 eV)	0.12

Emission scan with 255 nm excitation
Excitation scan with 302 nm emission
Excitation scan with 328 nm emission
Excitation scan with 339 nm emission

b)

When excited at	Emits at	With relative efficiency
258 nm (4.81 eV)	338 nm (3.67 eV)	1.00

Emission scan with 258 nm excitation
Excitation scan with 338 nm emission

c)

When excited at	Emits at	With relative efficiency
252 nm (4.92 eV)	322 nm (3.85 eV)	1.00
295 nm (4.20 eV)	322 nm (3.85 eV)	0.80
309 nm (4.01 eV)	322 nm (3.85 eV)	0.64

Emission scan with 252 nm excitation
Excitation scan with 322 nm emission

d)

When excited at	Emits at	With relative efficiency
256 nm (4.84 eV)	320 nm (3.87 eV)	1.00
293 nm (4.23 eV)	320 nm (3.87 eV)	0.59

Emission scan with 256 nm excitation
Excitation scan with 320 nm emission

Figure 4.5: Fluorescence spectra of a) 0.00001 % v/v solution of DVB in chloroform, b) 0.0001 % v/v solution of DIB in chloroform, c) 0.1 % v/v solution of DCPD in chloroform, and d) Fluorescence spectra of a 0.1 % v/v solution of squalene in chloroform.

The aromatic crosslinkers, DIB and DVB, were found to be very effective at fluorescence, whereas the aliphatic crosslinkers, DCPD and squalene, were very poor at fluorescence, though they did provide some nominal signal. These results are unsurprising, but the efficiency of aromatic fluorescence is exemplified by the fact that DVB and DIB gave signals roughly ten times stronger than those of DCPD and squalene, despite being in a concentration one thousand times weaker than the aliphatic crosslinkers. It is also worth noting that DVB is a mixture of the para and meta isomers, and is 80 % pure, with most of the impurity being the para and meta isomers of ethyl styrene. This combination of components may explain the complexity of the DVB spectra relative to that of DIB (Figure 4.5). Crucially, all of the crosslinkers only fluoresced when excited with UV wavelengths, and only

Liam James Dodd

fluoresced in the UV region of the spectrum, suggesting that leftover unreacted crosslinker is not responsible for the observed fluorescence of the inverse vulcanised polymers, and it is the polymers themselves that fluoresce when under Raman analysis.

With this conclusion, the polymers were studied by UV/Vis and fluorescence spectroscopy. Because blocks and powders of the polymers gave too strong a signal in UV/Vis, thin films of polymer were created by modifying the synthetic procedure at the pouring and curing stages. Rather than pouring the pre-polymer into a pre-heated mould, it was poured onto a preheated quartz slide. This slide was suspended on silicone blocks at its ends, so that the minimum surface area was in contact with another surface: when the quartz slide was in contact with the oven tray, polymer leaked to the underside, fusing the quartz slide to the tray. A second preheated quartz slide was then lay upon the top of the first, flattening the pre-polymer into a thin film. A gentle pressure was exerted on the top of the assembly by hand using tweezers, in order to squeeze out any air bubbles and thin out the film. This had to be done with care, as if the upper slide shifted over the lower one, the film would be ruined. The assembly was then returned to the oven to cure. This process was difficult to perform, and required perfect timing for the pouring of the polymer: too early, and sulfur would precipitate upon the quartz slide and bubble formation would be promoted by the remaining unreacted crosslinker that could volatilise; too late and the polymer would be too viscous to form a thin film. Pouring had to be done rapidly to prevent excessive cooling of the reaction solution. The perfect quantity of polymer had to be poured onto the quartz plate: too much and the film could be too thick or polymer would obscure the outer faces of the slide, too little and the film could be too thin, or could promote the formation of bubbles. Even with perfect film making technique, some bubbles were usually present in the film. This was unavoidable, and if the bubbles were dispersed in such a way that no sufficiently large area of the film was left unaffected and suitable for analysis, then the sample had to be discarded. Some polymer usually accumulated as hanging drops on the underside of the quartz plate during curing, which were then solidified in place. These could be removed by placing the film into a freezer to embrittle the polymer, after which it could be chiselled off with the flat end of a spatula. Successfully formed thin films can be seen in Figure 4.6.
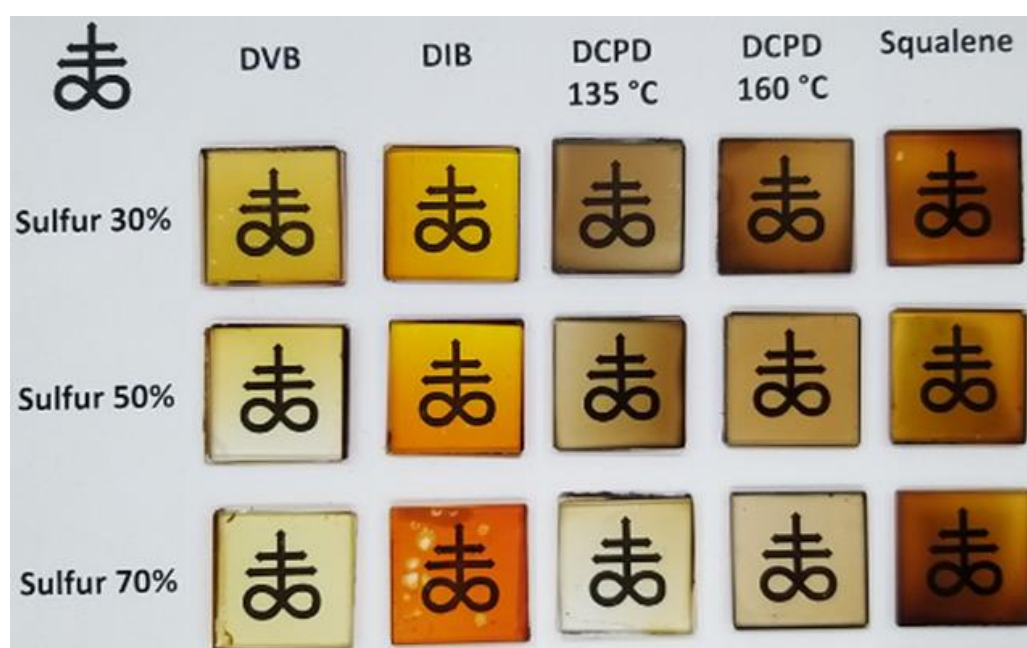
Figure 4.6: A photograph of inverse vulcanised polymer thin films, adhered between two 2.5 cm by 2.5 cm quartz plates, lain on top of a sheet of paper with the alchemical symbol brimstone printed onto the page, indicating the colour and transparency of the films.

Liam James Dodd

UV/Vis spectra of the thin films were obtained in the region of 235 nm to 1100 nm, to cover the range of Raman excitation laser wavelengths that were accessible in this study (Figure 4.7). In general, as shown in Figure 4.7, the polymers showed negligible absorbance at longer wavelengths, but as the wavelength was decreased, the absorbance began to increase, rapidly rising to the detector limit in the UV.

Polymer	Film Thickness / mm	Absorption Coefficient at 1064 nm / cm⁻¹	Wavelength where absorption coefficient becomes > 0.5 cm⁻¹	Tauc plot direct band gap / eV
DVB30-S70	0.06	-1.58×10^{-2}	696 nm	2.91
DVB50-S50	0.05	-2.90×10^{-2}	757 nm	2.92
DVB70-S30	0.04	-0.98×10^{-2}	862 nm	2.72
DIB30-S70	0.04	-5.80×10^{-2}	729 nm	2.45
DIB50-S50	0.06	-5.22×10^{-2}	757 nm	2.48
DIB70-S30	0.03	-10.17×10^{-2}	762 nm	2.99
DCPD30-S70-T135	0.02	-4.49×10^{-2}	956 nm	2.88
DCPD50-S50T-135	0.04	0.13×10^{-2}	1018 nm	2.87
DCPD70-S30-T135	0.02	12.79×10^{-2}	1072 nm	2.91
DCPD30-S70-T160	0.08	0.61×10^{-2}	894 nm	2.89
DCPD50-S50-T160	0.09	3.19×10^{-2}	922 nm	3.03
DCPD70-S30-T160	0.08	5.58×10^{-2}	963 nm	2.93
Squalene30-S70	0.05	6.15×10^{-2}	989 nm	2.21
Squalene50-S50	0.05	0.77×10^{-2}	957 nm	2.63
Squalene70-S30	0.08	2.13×10^{-2}	946 nm	2.30

Figure 4.7: UV/Vis spectra of the polymer thin films, and assorted spectral information. See Section 4.15.1 for the Tauc plots that give the direct band gap values.

DIB and DVB polymers showed no absorbance at wavelengths longer than 850 nm, and very minor absorbance at 785 nm (0.0015 for DVB50-S50 and 0.0018 for DIB50-S50), suggesting they would only poorly absorb that excitation laser wavelength. Since fluorescence was observed during 785 nm Raman analysis, it may be that these polymers are exceptionally efficient at fluorescence, and this small absorption is sufficient to induce fluorescence capable of swamping out the weaker Raman signal. The UV/Vis data in the table of Figure 4.7 suggests that these polymers do not absorb at 1064 nm, and this excitation laser would not suffer from fluorescence.

DCPD polymers showed absorbances at wavelengths as long as 1072 nm, explaining their deeper brown colour (Figure 4.6). Qualitatively, the thin films of DCPD synthesized at 135 °C and 160 °C appear

Liam James Dodd

very similar in their profiles, but the films synthesized at the lower temperature have much more significant absorbance at longer wavelengths. Similarly, squalene polymers also showed absorbance at longer wavelengths, though not with any great efficiency at wavelengths longer than 1000 nm. In general, the UV/Vis spectra suggest that DCPD and squalene polymers would absorb 785 nm laser light, giving rise to fluorescence in the Raman spectrum, and would also absorb 1064 nm light to some degree, suggesting that fluoresce may be possible at this wavelength. Therefore, it is expected that DCPD and squalene polymers may be harder to analyse by 1064 nm Raman spectroscopy than DVB or DIB polymers.

Interestingly, these polymers, even in the form of tens of micrometre thick films, showed tremendous absorbances in the near UV (below 500 nm to the spectrometer limit of 300 nm), suggesting that these polymers could find applications as UV blocking materials, though the degradation seen in the attempts at UV Raman, detailed later on, would need to be studied first.

Using the UV/Vis spectra shown in Figure 4.7, the fluorescence spectra of the polymers thin films were obtained at several excitation wavelengths of interest, the results of which can be found in Section 4.15.2. Unfortunately, the limitations of the equipment prevented studies of the fluorescence under 1064 nm excitation light, but the fluorescence was measured under excitation wavelengths of 784 nm, 532 nm, 266 nm and any others where polymers showed peaks or shoulder peaks in their UV/Vis spectra. The fluorescence spectra were obtained on the same thin films used for the UV/Vis spectrometry. Whereas taking into account the film thickness when comparing the UV/Vis data was simple, for the fluorescence spectrometry such a comparison may be less appropriate. This is because the optimum alignment for each sample cannot be taken into account. Samples were placed into the spectrometer and aligned such that they gave the maximum possible signal. However, this cannot take into account the spot size of the beam on each sample, which may have been different for each set up, skewing any comparison of the results between different samples. It should still be appropriate to compare the intensities of the spectra obtained for the same sample, at different excitation wavelengths, because the alignment of the system was not changed if the sample itself was not changed. In contrast, when comparing the intensities of two different samples' spectra, caution should be taken. Note that the samples did not degrade at any of the tested excitation wavelengths, except 266 nm, thereafter which, the polymer films appeared greyed where they had been irradiated. The 266 nm excitation wavelength spectra were always obtained last, to avoid any potential effects of sample degradation upon other excitation spectra. 266 nm excitation spectra were obtained as quickly as possible, using only one scan, in the hopes of obtaining the polymers' spectra and not the spectra of the degradation products, though again, caution should be exercised when observing these spectra. Besides this, all spectra were averaged over five scans, with emission and detection bandwidths of 2.5 nm, and a dwell time of 0.2 s, with the exception of 784 nm excitation spectra which needed longer dwell times of 1 s. These factors have been taken into account in the intensity scales of Figures 4.29 to 4.33 so accepting the potential issue of the alignment, all spectra should be comparable to one another.

Under 784 nm irradiation, all the polymers gave poor signals that became increasingly weak at emission wavelengths that were further from the excitation wavelength. With 784 nm excitation, the polymers showed nothing more than the background signal at emission wavelengths longer than 850 nm. The polymers showed a shoulder peak at about 825 nm emission. In all cases where 784 nm excitation was applied, the emission intensity was greater at wavelengths closest to the excitation wavelength, which is unfortunate, because this is where the Raman signal occurs in Raman spectroscopy. Even though the fluorescence from the polymers is weak with 784 nm excitation, because it occurs close to the excitation wavelength, it is still capable of obscuring the Raman

spectrum, which is itself, a weak signal. This then illustrates why no Raman signal could be obtained with a 784 nm excitation laser. Between all the polymers excited with 784 nm light, it does not seem as though there is a consistent trend between the sulfur content and the fluorescence intensity, though this could be due to the aforementioned issue with the system alignment. Comparing between the polymers, it appears that polymers of DVB and DIB are the most efficient at fluorescing at 784 nm excitation, potentially due to contributions from their aromatic components. Interestingly, DCPD polymers reacted at 160 °C seem to be less effective at fluorescence than those reacted at 135 °C, suggesting that a more complete reaction may reduce the propensity to fluoresce.

The emission of fluorescence under 532 nm excitation often gave fluorescent signals with what appears to be a Raman signal overlapping with it. It appears that when the polymer contains an aromatic unit (DIB or DVB), the fluorescence is most intense with a high loading of crosslinker, and is least intense with a low loading of crosslinker. For the other crosslinkers used, it seems that the opposite is true; fluorescence is most intense with a high loading of crosslinker. Just like when under 784 nm excitation, DIB and DVB polymers gave more intense fluorescence than DCPD or squalene polymers when under 532 nm excitation. Again, it must be remembered that these results could be skewed by the different alignments used between the different polymers. Fluorescence stemming from 532 nm irradiation usually appeared as a decay in intensity, followed by a rise in intensity in the form of a broad peak. However, this broad peak was not always present, and even when it was, it usually had several smaller peaks super imposed upon it. For DVB's 532 nm excitation fluorescence spectra, DVB30-S70 showed essentially no broad peak, revealing several smaller peaks that are likely to be Raman signals. Interestingly, in the spectrum of DVB70-S30, despite the broad peak, one can see overlapping signals that roughly align with the supposed Raman spectrum seen in DVB30-S70's fluorescence spectrum. There are several other cases of this between the different polymer samples, but there appears to be no clear way to predict the appearance of these Raman signals. In contrast to the aforementioned failure of 532 nm Raman spectroscopy to acquire a Raman signal through the fluorescence, this data might suggest that obtaining a Raman spectrum with a 532 nm laser could be possible where inverse vulcanised polymers are concerned. However, there is a crucial flaw: under 532 nm excitation, the sulfur – sulfur band region would be expected to occur at wavelength between 544 nm and 547 nm, and comparing this wavelength range to the fluorescence spectra, it is obvious that no such signal ever appears with any clarity. Thus it can be concluded that analysis of the sulfur – sulfur band would not be possible with a 532 nm excitation laser, as the signal would always be eclipsed by fluorescence.

The 266 nm excitation spectra are somewhat more dubious to analyse because the polymer films degraded under UV irradiation, so it is hard to know what is the fluorescence of the polymer, and what is the fluorescence of the degradation products. Further confusing would be the attenuation of signal intensities as the polymers became increasingly degraded under the progressively increasing exposure times. Regardless, it is safe to say that no sulfur – sulfur Raman band will be observed in these fluorescence spectra, as this region would be expected to occur at 269 nm when under 266 nm excitation, and the fluorescence spectra were all obtained starting from 275 nm to ensure the photo multiplier tube detector was not over exposed and damaged during the experiment. In general, all 266 nm excitation spectra were more intense than spectra obtained with longer wavelength excitation. All the polymers' spectra appeared fairly similar, with a smaller peak centred at 300 nm, a larger peak centred at around 410 nm, and then a broad shoulder peak at around 480 nm. The data acquired at longer emission wavelengths should be treated with the most scepticism, as it is at these wavelengths where the polymer would have been exposed to 266 nm excitation for the longest and therefore would have been the most degraded. Once again, the polymers show no consistent pattern of fluorescence intensity with sulfur loading, and under this excitation wavelength, the polymers of

Liam James Dodd

different crosslinkers did not show much difference in their fluorescence intensities: no crosslinker gave a polymer that was particularly more efficient at fluorescence than another. Analogous to the 532 nm excitation spectra, there are several cases in the 266 nm excitation where weak peaks appear that could be Raman signals. Particularly peaks appear at 327 nm and 349 nm quite consistently between different spectra. It is plausible to consider that the broad peak at 300 nm could also be a Raman signal, but it is difficult prove whether this is true. For 266 nm excitation, it is important to note that the polymers gave nominal signals all across the measured range. This is in fact true for 532 nm excitation as well, though with weaker intensity. The only time the signal ever fell to background levels, was with 784 nm excitation at emission wavelengths longer than 850 nm. This implies that if one was measuring a Raman spectrum using 532 nm excitation, but the polymer was also exposed to other wavelengths of light, these could additionally cause fluorescence. Therefore, it can be concluded that elimination of background light would be beneficial not only for ambient light background reduction in Raman spectroscopy, but also the elimination of additional fluorescence. This may be a particularly important consideration for 1064 nm Raman spectroscopy, which would not be expected to incite fluorescence on its own, but could be affected by fluorescent transitions induced by shorter wavelengths of light from ambient sources. That is, the polymers may have the potential to absorb wavelengths of light shorter than 1064 nm, and then fluoresce at wavelengths longer than 1064 nm, thereby obscuring the Raman signal.

The main conclusions of this UV/Vis and fluorescence study were: that leftover unreacted crosslinker was not responsible for the fluorescence; that the polymers in films no thicker than 100 μm, show little absorbance at long wavelengths, but show rapidly rising absorbance at shorter wavelengths that quickly reach the detector limit in the UV, making them potentially good UV blocking materials; that despite the very poor absorbance at 785 nm for DVB and DIB polymers, they still showed fluorescence in 785 nm Raman spectroscopy, so inverse vulcanised polymers are likely very efficient at fluorescence; that polymers of DVB and DIB show negligible absorbance at 1064 nm, suggesting this may be an effective probe wavelength for Raman, but polymers of DCPD and squalene may be still be difficult to analyse at this wavelength as they did show nominal absorbance; that the polymers fluoresced under a wide range of wavelengths, though less effectively at long wavelength, and were capable of emitting at wavelengths much longer than the excitation wavelength, and because of this Raman analysis should be carried out in the dark, to prevent stray ambient light from exciting fluorescence; and that the polymers degrade under UV light and so should be stored in the dark. This final conclusion was reinforced when trialling different Raman probe wavelengths, as with deep UV wavelengths (266 and 300 nm) rapid sample decomposition occurred, making them unviable for analysis of inverse vulcanised polymers.

4.6. Screening of Raman Spectroscopies

To establish which Raman spectroscopic techniques were deserving of more in-depth investigation, each was briefly trialled at providing Raman spectra on a panel of representative polymers.

1064 nm Raman spectroscopy is very similar to conventional Raman spectroscopy, with the exception that it uses the less widespread option of a 1064 nm excitation laser. This laser wavelength is usually too low energy to excite an electronic transition, thereby preventing fluorescence. Also a result of the low laser energy, laser burn is uncommon. Unfortunately, the Raman cross section is dependent on λ_{excite}^{-4}, where λ_{excite} is the wavelength of the excitation laser.[4.18] From this dependency it can be shown that when using a 1064 nm laser, the same signal will fall to 30 % of the intensity it would show when using a 784 nm excitation laser, limiting 1064 nm Raman spectroscopy to samples that are strongly Raman active. Since inverse vulcanised polymers contain a high density of highly Raman active modes, it was predicted that 1064 nm Raman spectroscopy would be capable of providing interpretable

Liam James Dodd

signals, and indeed 1064 nm Raman using a handheld instrument was successful in most cases at providing Raman spectra of polymer samples. DVB polymer blocks all gave spectra with the least baseline interference, showing identifiable bands all across the spectral range. DIB also gave interpretable spectra but were more difficult to acquire, and had more substantial baselines. DCPD and squalene showed very substantial baselines that heavily obscured most of the signals, which falls in line with the results of the UV/Vis spectroscopy that indicated these polymers had more substantial absorbances at longer wavelengths. Importantly, it was quite difficult to damage the polymer samples with 1064 nm laser irradiation, a stark advantage over several techniques soon to be discussed.

Fourier transform Raman spectroscopy can largely be considered as an extension of 1064 nm Raman spectroscopy, as they both use the same laser wavelength. However, Fourier transform Raman spectroscopy uses the addition of a Michelson interferometer to allow multiplexing measurements to bring several further advantages, such as shorter acquisition times which minimises the chance of laser burn, better resolution as there are no resolution limiting thin apertures, and an improvement in the background of the signal.[4.18] Samples for Fourier transform Raman spectroscopy were prepared with a hand operated press for preparation of KBr pellets. The well of the 7 mm pellet die was filled with a desired polymer powder with the excess powder being removed. The die set was placed in the hand operated press and the handle was squeezed and held for 15 seconds. The pellet was formed in the centre of the die. The die with the pellet was then placed in the probe laser beam chamber of the Fourier transform Raman spectrometer (Bruker Vertex 70 with a RAM II FT-Raman module). The Fourier transform Raman operated with a Nd-YAG laser of wavelength 1064 nm and a spectral range from 50 to 3600 cm^{-1} with resolution better than 0.4 cm^{-1}. Spectra were averaged over 100 scans (130s total acquisition time) with a laser power between 1 and 100 mW obtaining an excellent rejection ratio. Similar to 1064 nm Raman spectroscopy, Fourier transform Raman spectroscopy was successful in providing spectra of the polymers, with the same observations that DVB and DIB polymer spectra were easier to obtain than DCPD or squalene spectra (Figure 4.8).
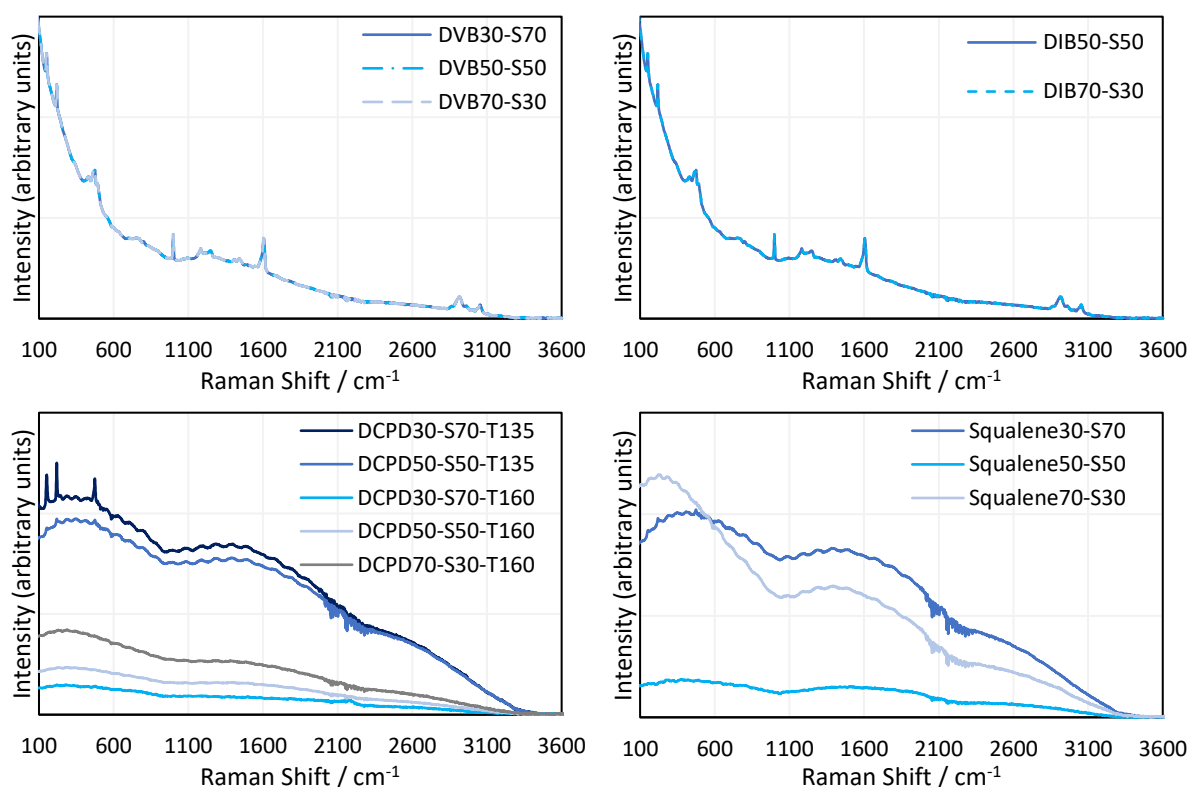
Figure 4.8: Fourier transform Raman spectra of the panel of inverse vulcanised polymers.

Liam James Dodd

UV Raman spectroscopy is also similar to conventional Raman spectroscopy, with the exception that it uses UV wavelengths to excite Raman transitions. This seems counterintuitive, as a shorter laser wavelength will promote auto-fluorescent transitions that would obscure the Raman spectrum. However, even though the laser does promote auto-fluorescence, the energy of the laser shifts the fluorescence to much higher Raman shifts, leaving the lower end of the Raman spectrum free of a fluorescent background. This is because most fluorescent transitions occur at wavelengths longer than 300 nm, which when placed in comparison with a 266 nm excitation laser, equates to a Raman shift of about 4260 cm^{-1}. Very few Raman modes occur at such high shifts, and so the spectrum is left free of fluorescence. An additional advantage of UV Raman is that since the Raman cross section is dependent on λ_{excite}^{-4}, a 266 nm excitation laser gives a signal approximately 75 times stronger than that given by a 784 nm excitation laser.[4.18] However, the shorter laser wavelength of UV Raman spectroscopy promotes laser burn, as it imparts a high amount of thermal energy to the sample, but also carries sufficiently energetic photons to allow photochemical reactions. This proved to be prohibitive to the analysis of inverse vulcanised polymers in UV Raman, as the polymers rapidly degraded and decomposed. Though the spectra showed no signs of fluorescence, they rapidly changed with the duration of laser exposure and therefore the degree of degradation, regardless of method optimisations. Thus, UV Raman is not suitable for the analysis of inverse vulcanised polymers and perhaps indicates that these polymers can be sensitive to UV light. Therefore, inverse vulcanised polymers should be stored in the absence of UV light, and possibly in total darkness. Further studies into the degradation of inverse vulcanised polymers in relation to their storage conditions is a research avenue that should receive attention in the future.

Given that UV Raman spectroscopy was successful in avoiding the fluorescence of the polymers, further attention was paid to the excitation wavelength itself. Whether there was an excitation wavelength at the fringe of visible light and UV light that could avoid auto-fluorescence, without degrading the polymers before a signal can be obtained, was investigated. 366 nm light again, rapidly induced sample degradation, so alongside 266 nm Raman spectroscopy, it is not suitable. On the other hand, a 488 nm laser did show promise. Most samples gave good Raman signals with different sulfur related bands, however not all were free of fluorescence and careful method optimisation was necessary to manage laser absorption and heating damage.

Kerr-Gated Raman spectroscopy is an advanced Raman spectroscopic technique that allows the separation of Raman signals and fluorescent signals based on the time lag between their emissions.[4.19] Because Raman scatter occurs through an intermediate virtual state, relaxation from this virtual state is essentially instantaneous. Fluorescence on the other hand, occurs through an intermediate real state. Because the molecule is excited to a real state, it spends a finite amount of time in that state before relaxing and emitting a fluorescent photon. Thus, fluorescent signals are emitted a short amount of time after a Raman signal. Kerr-Gated Raman spectroscopy uses this short time delay to separate the Raman signal from the fluorescent signal, thereby eliminating fluorescent backgrounds.[4.19]

However, Kerr-Gated Raman spectroscopy is not a widespread technique, and so it is unlikely it will see significant uptake in the field of inverse vulcanised polymers; the analysis performed here was done as a proof of concept. Kerr-Gated Raman spectroscopy was successful in obtaining polymer spectra for all samples, even the ones where other techniques struggled due to fluorescence (Figure 4.9). Though the signals are weaker, Kerr-Gated Raman spectroscopy could be a useful last resort where other techniques fail. The method for preparing samples for Kerr-Gated Raman spectroscopy was the same as the method for Fourier transform Raman Spectroscopy.

Liam James Dodd
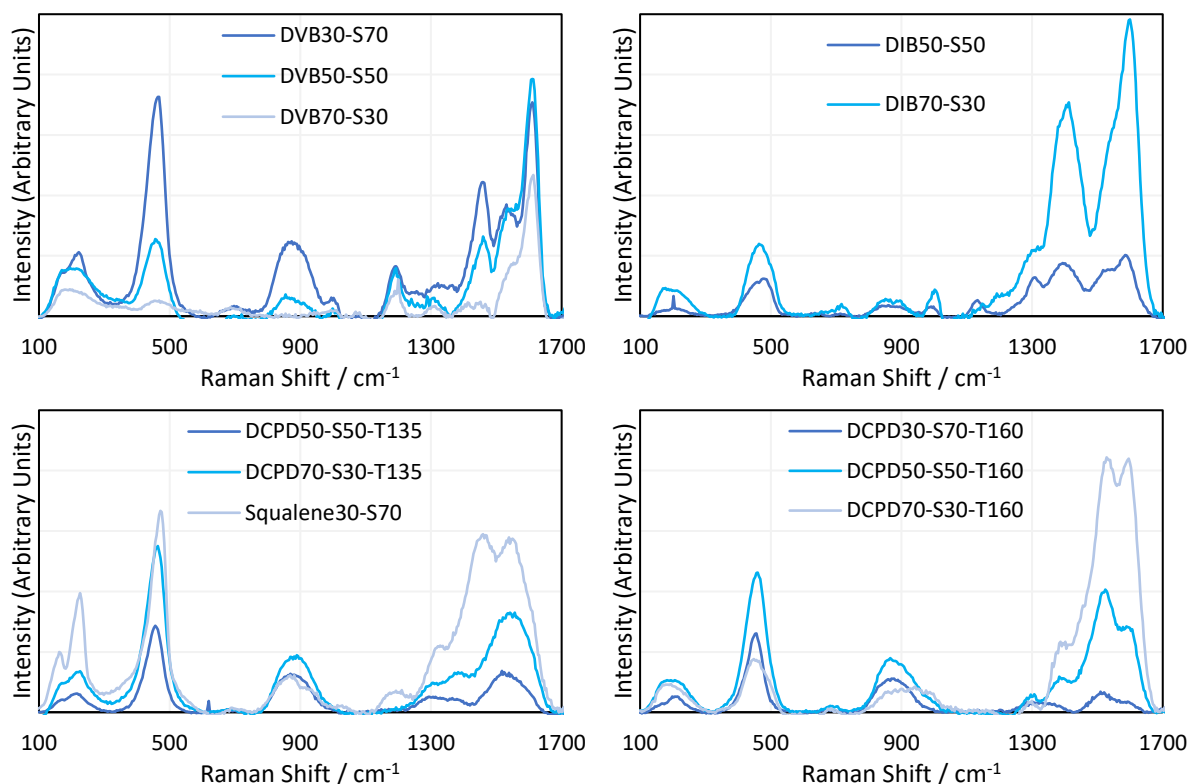
Figure 4.9: Kerr-Gated Raman spectra of the panel of inverse vulcanised polymers.

4.7. 1064 nm Raman Analysis

Since 1064 nm Raman spectroscopy is an accessible technique which showed significant promise, it became the subject of study for further detailed analysis. The instrument used for these initial studies was a handheld instrument (Snowy Range Instruments model CBex 1064), and with baseline correction it was capable of providing easily interpretable spectra that yielded plentiful information (Figure 4.10).
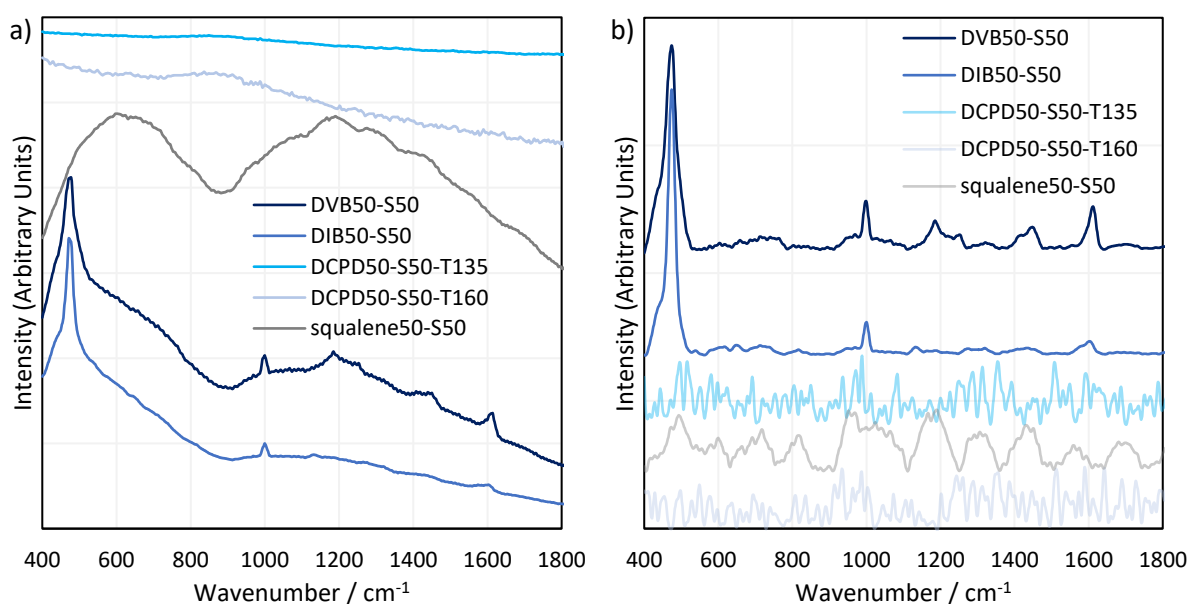
Figure 4.10: a) raw and b) baseline corrected Raman spectra for selected inverse vulcanised polymers. Offsets have been applied to the intensities.

Liam James Dodd

Trivially, for DVB and DIB polymers, aromatic modes appeared at 1000 and 1600 cm^{-1}. Broad peaks between 600 and 800 cm^{-1} have been assigned to the carbon – sulfur bond. Most critically, the sulfur – sulfur bond region (425 cm^{-1} to 550 cm^{-1}) was obvious in the spectra of DVB and DIB, and displayed a peak consisting of several overlapping peaks, all contributing to the band. This alludes to different sulfur – sulfur vibrational modes, as it has been shown that the greater the sulfur rank, the progressively weaker the central sulfur – sulfur bond becomes.[4.20] Band deconvolution was performed upon these compound peaks to elucidate the contributions of the smaller component peaks, however, the analysis of these deconvolutions is far more complex than simply assigning one contributor peak to one sulfur rank. There are numerous complications to take into account when analysing these bands, including, but not limited to: multiple bands arising from the same sulfur rank due to different vibrational modes; overlapping signals from dark sulfur; the accuracy of baseline correction across the sulfur – sulfur band; whether the Raman laser cut off limit is encroaching upon and attenuating the low Raman shift end of the sulfur – sulfur band; and the accuracy of the band deconvolution. Several measures were needed to gain a thorough understanding of this complex, yet information rich band, including the use of model compounds and computational chemistry. Note that dark sulfur is used here as a general term for non-crystalline elemental sulfur, which therefore cannot be detected by DSC or PXRD, as set out in a previous publication.[4.21] Dark sulfur refers to any allotrope, though it is assumed here that dark sulfur comprises primarily of cyclo-octasulfur, the most thermodynamically favourable form of elemental sulfur.

It was thought initially that the bands between 1025 to 1060 cm^{-1} and 1050 to 1210 cm^{-1} could be assigned to sulfonic acids and sulfones respectively, indicating some degree of oxidation. To examine this the syntheses of DVB30-S70, DVB50-S50 and DVB70-S30 were repeated, but this time an inert atmosphere of nitrogen was maintained throughout the polymerisation and curing processes (the polymers had to be cured upon the hotplate rather than in the oven). Due to the affixed septum and gas balloon on the reaction vial, and the curing upon the hotplate which has been shown to give different results to oven curing previously, these new polymers: DVB30-S70-N2, DVB50-S50-N2 and DVB70-S30-N2, were not directly comparable to the previous ones. Therefore, another batch of polymers were synthesized in the same way as DVBα-Sβ-N2, but this time, the balloons and reaction vials were filled with air instead of nitrogen, giving DVB30-S70-Air, DVB50-S50-Air and DVB70-S30-Air. The Raman spectra of these polymers can be found in Figure 4.11.
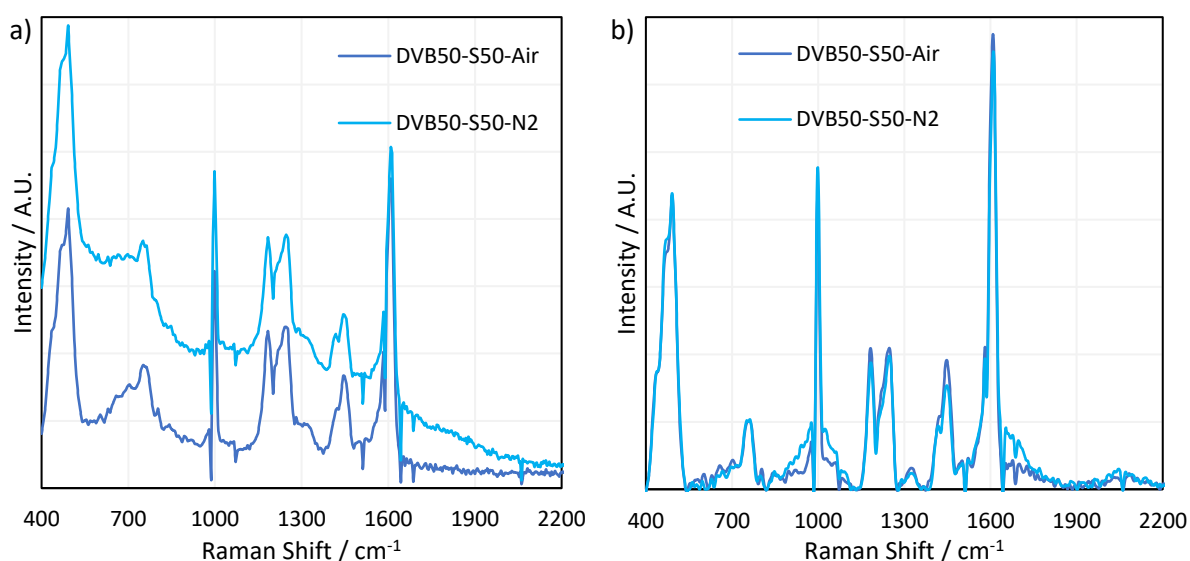
Figure 4.11: Raman spectra, obtained on a handheld instrument, of DVB polymers synthesized under air and nitrogen atmospheres, a) before spectral processing, and b) after spectral processing.

Liam James Dodd

All of the reactions for DVBα-Sβ-N2 and DVBα-Sβ-Air took longer than their unsealed reaction vial counterparts: DVBα-Sβ. This is likely because the presence of the septum prevented the loss of volatilised DVB. It has been shown previously that the greater the quantity of crosslinker in comparison to sulfur, the slower the reaction proceeds; likely due to the decreased proportional presence of initiating sulfur radicals.[4.11] Therefore, if DVB evaporates over the course of the reaction, as it has been proven to do previously, the proportion of sulfur in the reaction is raised, leading to a faster rate.[4.11] Sealing the reaction vial would prevent the loss of DVB and therefore keep the proportion of sulfur lower than if the septum was absent, thereby decreasing the reaction rate. The conclusion that the loss of DVB is prevented by the fixture of a septum is supported by the combustion microanalysis data for DVBα-Sβ-N2 and DVBα-Sβ-Air, where the percentage of sulfur is lower and the percentage of carbon and hydrogen is higher than those values for DVBα-Sβ. In fact, the combustion microanalysis data for DVBα-Sβ-N2 and DVBα-Sβ-Air mirror their predicted values very closely (Table 4.2), unlike DVBα-Sβ, which show significant evidence of crosslinker evaporation. It should be no surprise then, that with such different sulfur compositions between DVBα-Sβ-N2 and DVBα-Sβ-Air compared to DVBα-Sβ, that their T_g's are also very different.

Table 4.2: Analyses of inverse vulcanised polymers synthesized under air or nitrogen.

Polymer	DVB30-S70-N2	DVB30-S70-Air	DVB50-S50-N2	DVB50-S50-Air	DVB70-S30-N2	DVB70-S30-Air
C expected (%)	27.68	27.68	46.13	46.13	64.58	64.58
C actual (%)	22.66	26.69	44.85	43.93	58.96	62.80
H expected (%)	2.32	2.32	3.87	3.87	5.42	5.42
H actual (%)	1.51	2.11	3.70	3.64	4.92	5.31
S expected (%)	70.00	70.00	50.00	50.00	30.00	30.00
S actual (%)	71.97	70.40	51.92	52.53	36.02	30.72
DSC T_g / °C	52.89	55.08	99.27	100.81	79.60	87.88

The data in Table 4.2 indicates that DVBα-Sβ-N2 and DVBα-Sβ-Air are indeed different, though this difference is quite small between DVB50-S50-N2 and DVB50-S50-Air, wherein the combustion microanalysis data values are all within a percent of each other, and the T_g's are very close. For the other four polymers, the differences are pronounced. The T_g is lower when the reaction was done under nitrogen, and the combustion microanalysis values differ by some margin. For DVB30-S70-N2 and DVB70-S30-N2, the %C and %H values are lower than the expected values, whilst the %S value is higher than expected. Contrastingly, DVB30-S70-Air and DVB70-S30-Air adhere much more closely to their expected values, and therefore, their %C and %H values are higher, and their %S values are lower, than their under-nitrogen counterparts. Though it seems that the atmosphere the reaction is performed under affects the resulting polymers, the reasons for these differences cannot be determined here. It was supposed that the DVBα-Sβ-Air polymers may have incorporated some oxygen atoms into their structure, and that any leftover unaccounted-for mass in the combustion microanalysis may be due to oxygen. If this was the case, then the unaccounted-for mass should be higher in the DVBα-Sβ-Air polymers compared to DVBα-Sβ-N2, however this was not consistently the case in the data of Table 4.2. Regardless, the reactions of DVBα-Sβ-N2 took longer than the analogous DVBα-Sβ-Air reaction, suggesting that oxidation does play some role in the reaction mechanism. Furthermore, as depicted in Figure 4.12, the DVBα-Sβ-N2 polymers are visually different to their DVBα-Sβ-Air counterparts, being slightly lighter and more yellow in colour. Unfortunately, 1064 nm Raman spectroscopy could not identify a significant difference between DVBα-Sβ-N2 and DVBα-Sβ-Air, as their spectra appeared the same (Figure 4.11). The peaks that were initially assigned to sulfonic acids and sulfones appeared in both DVBα-Sβ-N2 and DVBα-Sβ-Air spectra, suggesting these peaks are

Liam James Dodd

not related to oxidation products, or that somehow sulfonic acids and sulfones are forming despite the exclusion of oxygen from the reaction; a conclusion that seems highly unlikely, especially since and the computational analyses performed later provided alternative, more convincing assignments. Regardless, even though Raman spectroscopy could not distinguish the polymers formed under nitrogen and under air, the other characterisations suggest that the role of oxidation in the mechanism of inverse vulcanisation merits more dedicated studies.
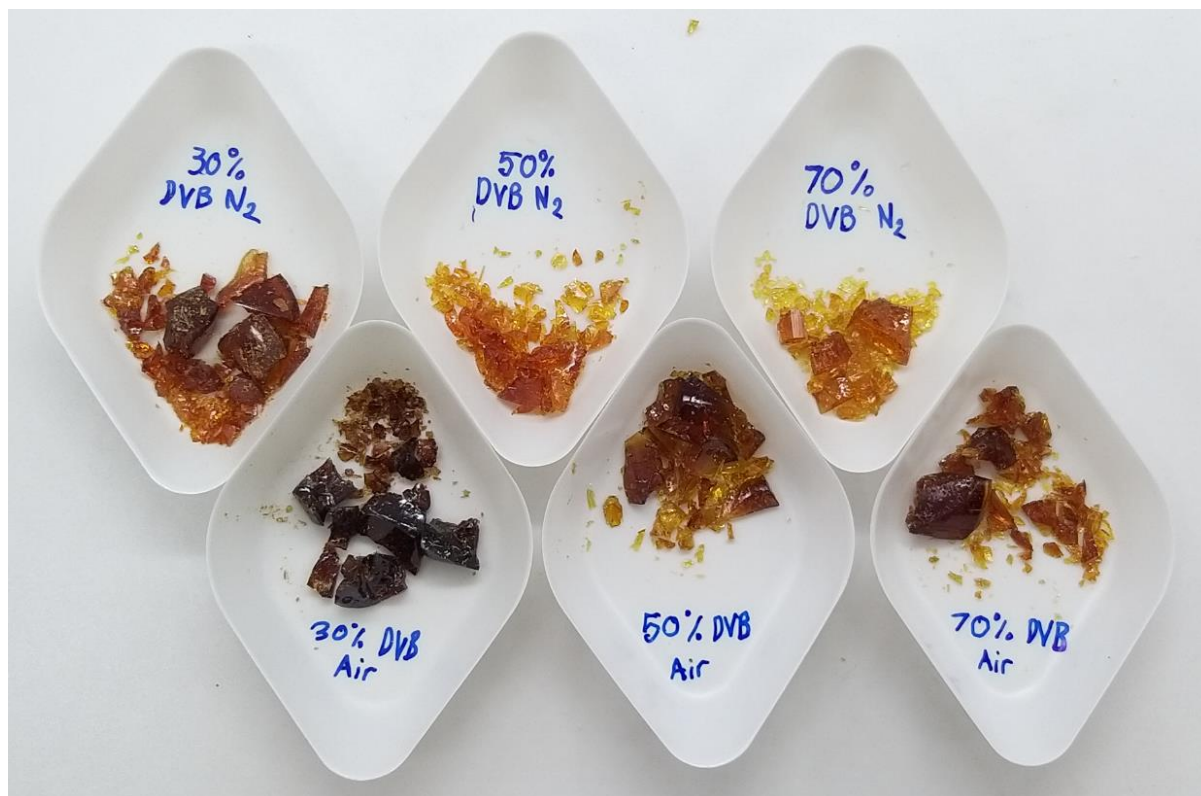
Figure 4.12: A photograph that shows the visual differences between the DVBα-Sβ-N2 and DVBα-Sβ-Air polymers.

4.8. Method Optimisation

As mentioned previously, several complications were identified in the analysis of the Raman spectra of inverse vulcanised polymers. The most easily solved was the cut off limit of the spectrometer employed (400 cm^{-1}). An alternative 1064 nm Raman spectrometer, with a lower cut off limit of 100 cm^{-1}, and generally better performance was used for all following measurements (Metrohm i-Raman EX 1064). Lowering the cut off limit to the spectra had two other advantages. The first was that it allowed for more accurate baseline correction, since the baseline could be identified on either side of the signal, rather than on one side and not the other. The second relates to the presence of dark sulfur. Molecules of sulfur produce several Raman signals, and some of these peaks occur inside the sulfur – sulfur band region. Therefore, dark sulfur contributes to the sulfur – sulfur band (Figure 4.13). However, sulfur molecules also provide signals at much lower Raman shifts, below 400 cm^{-1}, and it was theorised that if one of these signals could be identified, free of any other overlapping signals, then by means of relative intensities, it could be used to calculate the contribution of dark sulfur to the compound peak in the sulfur – sulfur region. This would allow the other peaks to be certified as being related to the polymer, but would also allow the quantification of the proportional presence of

Liam James Dodd

dark sulfur within the polymer, which currently is only possible by extracting the sulfur into a solvent and then applying HPLC.[4.21]

With this more advanced instrument, method optimisation was performed to examine the effect of spectrometer settings, and sample morphology (solid block, powder, or thin film). With regards to spectrometer settings, the greater the laser power, the greater the signal intensity, but the greater the chances of laser damage. The chance of damage can be reduced by reducing the exposure time, which also makes the measurement more convenient, and minimises the contribution of dark noise. For samples such as DVB, their resistance to laser damage was high, and this permitted higher laser intensities (up to 322.5 mW, 75 % laser power). Contrastingly, darker samples, like DCPD and squalene, were very vulnerable to laser damage, and showed significant decomposition at only 20 % laser power (86 mW). This was expected, since these polymers were found to have nominal absorbance of 1064 nm light, and would therefore be more effective at heating up when irradiated at this wavelength. Additionally, DCPD and squalene polymers showed no interpretable signals at any laser power or integration time, regardless of whether the sample was a powder, block, or thin film. It seems that DCPD and squalene polymers are highly effective at fluorescence at 1064 nm excitation wavelengths, since even at 1 % laser power, the detection system could still be swamped with signal unless the integration time was short.
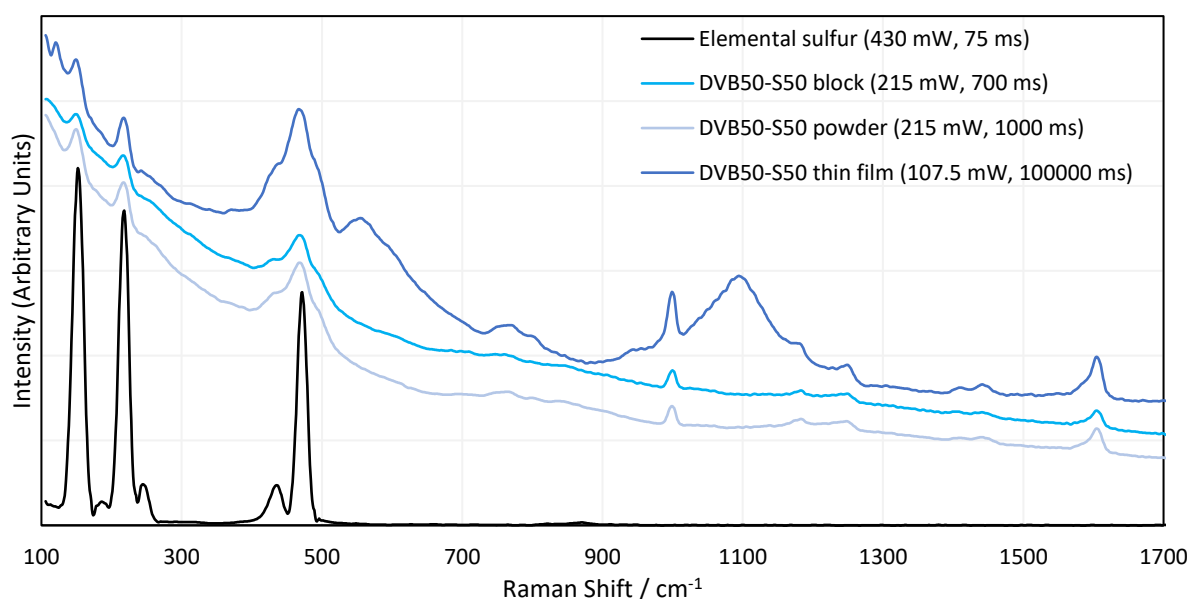
Figure 4.13: Raman spectra of DVB polymers in different morphologies, as well as the Raman spectrum of elemental sulfur, taken on a Metrohm i-Raman EX 1064 nm Raman spectrometer, which has superior specifications to the previously used handheld spectrometer. Offsets have been applied to the intensities. Numbers with the units mW and ms are the laser powers and integration times used to obtain a particular spectrum, respectively.

In terms of morphology, blocks of DVB polymers gave the worst, though still easily interpretable signals (Figure 4.13). Powders gave better signals and thin films of polymer between glass slides gave the best signal intensity in comparison to the background, though concerns can be raised regarding some peaks. New peaks appeared in the spectra of the thin films that were not present in the spectra of either the blocks or the powders (Figure 4.13). The powders and the blocks are the polymer in its pure form, whereas the thin film has the polymer between two glass slides. It is possible that the glass has some contribution to the spectrum, and the new peaks are the result. As a final note, it was

Liam James Dodd

difficult to focus the Raman laser on the thin film sample, and when it was focused, much longer integration times, as well as high laser intensities were required to obtain a signal, which could be explained as a result of the thin sample providing less Raman active material in the laser irradiation zone. Surprisingly, there was no sign of laser damage, which might be explained by the glass slides acting as a heat sink.

With the method optimisation complete, Raman spectra of the panel of representative polymers were required, ready for in depth analysis of the spectral bands. Rather than acquire the spectra of the initial batch of polymers which had been subject to aging, it was decided to synthesize a fresh batch of polymers. Observing Table 4.1, it is clear that the initial batch of polymers suffered from crosslinker evaporation during their syntheses which explains why their sulfur percentages were much higher than expected. This also yielded polymers that were much more similar than desired. For example, DVB30-S70 actually contained 76.9 % sulfur, and DVB50-S50 actually contained 71.4 % sulfur, meaning these two polymers were quite similar by their compositions, and as a result the differences in their Raman spectra may have been less pronounced. Therefore, the method to synthesize this second batch of polymers was modified, to minimise crosslinker evaporation. The method was the same as before, except once the crosslinker was added to the reaction vial, a septum with an air balloon affixed was added to the reaction vial. In this new method, the polymer was not poured into a mould, nor cured in the oven, and instead was cured on the hotplate with the balloon affixed. Unfortunately, squalene was not amenable to this method of synthesis as the reaction underwent the TNE during the curing step despite all method optimisations. The squalene polymers were reacted with the balloon present, but were cured without it. Squalene polymers were also cured at the higher temperature of 145 °C, as this gave polymers with more convenient physical properties. The polymers were then analysed by DSC and combustion microanalysis, as shown in Table 4.3, which indicates that the septum had the desired effect, as the actual values for sulfur, mirror more closely their expected values. DSC traces are provided in Figure 4.14.
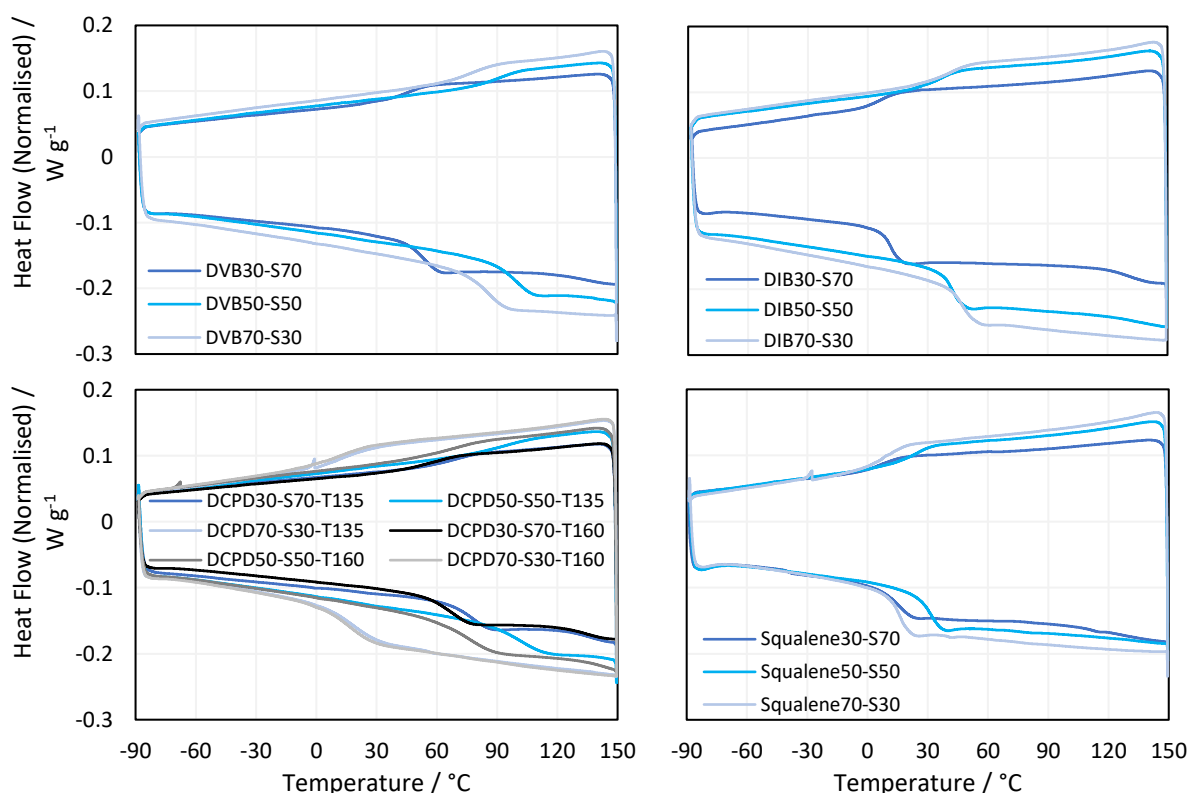
Figure 4.14: DSC thermograms of the second batch of inverse vulcanised polymers.

Liam James Dodd

Table 4.3: Synthetic conditions and analyses of the second batch of inverse vulcanised polymers.

Name	DVB			DIB			DCPD						Squalene		
Chemical structure															
Synthesis at	135 °C			135 °C			135 °C			160 °C			170 °C		
Feed ratio Crosslinker (%)	30	50	70	30	50	70	30	50	70	30	50	70	30	50	70
Sulfur (%)	70	50	30	70	50	30	70	50	30	70	50	30	70	50	30
Microanalysis C expected (%)	27.7	46.1	64.6	27.3	45.5	63.8	27.3	45.4	63.6	27.3	45.4	63.6	26.3	43.9	64.4
C actual (%)	25.4	43.6	60.7	24.9	43.1	60.4	23.3	43.2	59.2	25.7	42.8	59.7	26.5	43.6	60.9
H expected (%)	2.3	3.9	5.4	2.7	4.5	6.2	2.8	4.6	6.4	2.8	4.6	6.4	3.7	6.1	8.6
H actual (%)	2.6	4.0	5.8	2.5	4.2	5.7	2.4	4.3	5.7	2.7	4.3	5.8	3.7	5.9	8.2
S expected (%)	70.0	50.0	30.0	70.0	50.0	30.0	70.0	50.0	30.0	70.0	50.0	30.0	70.0	50.0	30.0
S actual (%)	72.5	52.5	32.9	73.4	52.5	32.3	74.2	52.1	33.7	72.0	52.8	33.4	70.1	50.1	29.8
DSC T_g / °C	53.0	99.0	84.1	11.3	42.2	47.0	76.7	101.3	19.0	66.0	75.9	17.6	14.8	30.6	16.1

This second batch of polymers was analysed by 1064 nm Raman spectroscopy in the form of blocks as this was convenient and minimised the chances of sample contamination, as there was no post-synthetic processing required (Figure 4.15).
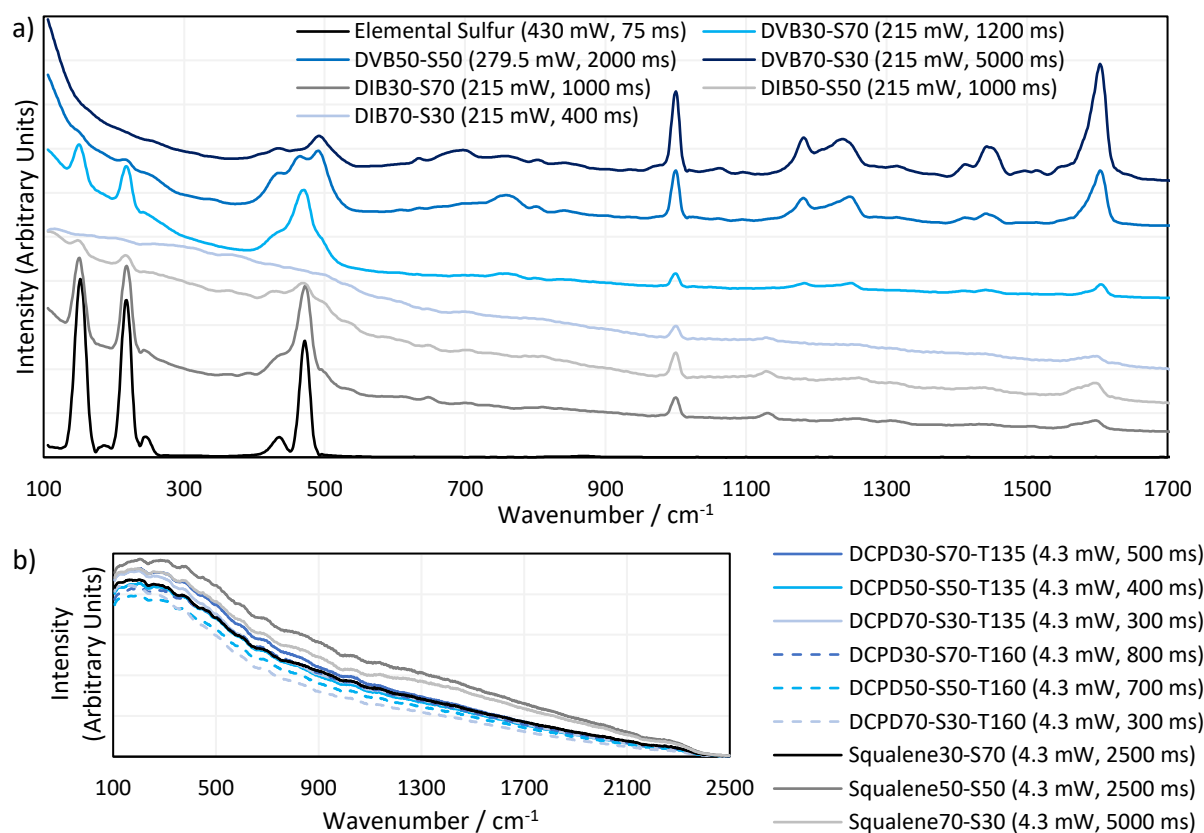
Figure 4.15: The 1064 nm Raman spectra, obtained using the optimised method on the Metrohm i-Raman EX instrument, of inverse vulcanised polymers of a) DVB and DIB, and b) DCPD and squalene. Offsets have been applied to the intensities. Numbers with the units mW and ms are the laser powers and integration times used to obtain a particular spectrum, respectively.

Liam James Dodd

Once again, DVB and DIB polymers gave clear sulfur – sulfur bands and aromatic bands (Figure 4.15a). The intensity and shape of the sulfur – sulfur band in the DVB and DIB polymers varied with sulfur loading, which implies that this band is indeed dependent upon the quantity of sulfur in the polymer. Also, elemental sulfur signals can be observed in the Raman spectra of DVB and DIB polymers, indicating that dark sulfur is present in these polymers. This interesting result suggests many polymers that have previously been assumed to contain no elemental sulfur, may in fact contain undetected elemental sulfur. This further advocates the use of Raman spectroscopy in the field of inverse vulcanisation, as it is a rapid and convenient technique to identify the presence of elemental sulfur in inverse vulcanised polymers, that works where other techniques fail. Further points to note regarding the spectra of DVB and DIB polymers include: that the elemental sulfur signals become weaker when less sulfur is used in the synthesis; that the aromatic signals become more intense in comparison to the sulfur – sulfur band when less sulfur is used in the synthesis; and that the polymers require higher laser powers or integration times in their measurements when less sulfur is used in the synthesis.

Unfortunately, as seen in Figure 4.15b, polymers of DCPD and squalene failed to produce 1064 nm Raman spectra through their fluorescent baselines. As an attempt to remedy this, 1064 nm SERS Raman spectroscopy was performed upon the polymers of DCPD, squalene, and DVB (Figure 4.16). Unfortunately, SERS could not provide a signal for polymers of DCPD and squalene through their fluorescent backgrounds, however, polymers of DVB did show a signal enhancement with SERS.
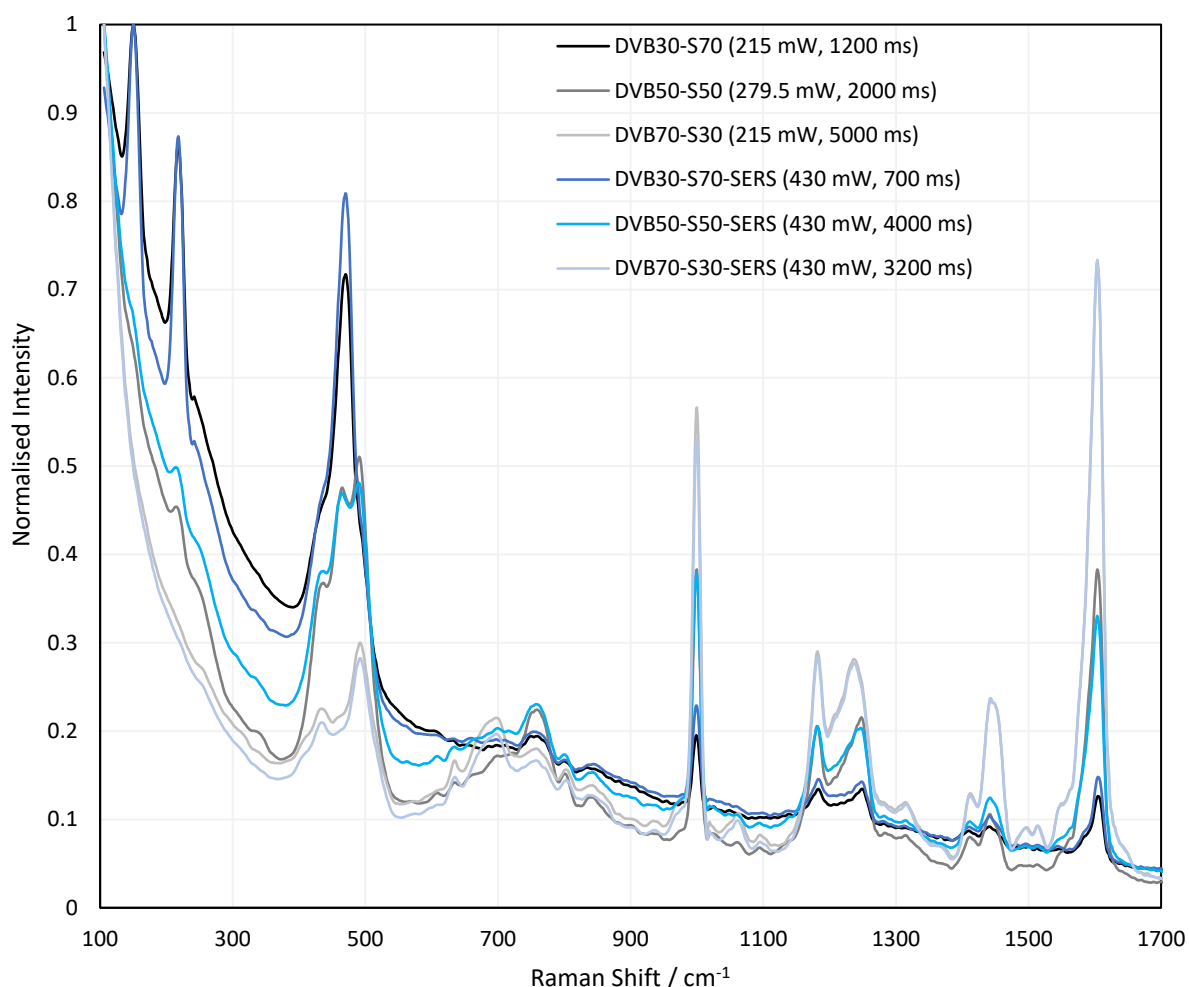
Figure 4.16: The 1064 nm Raman spectra of DVB polymers, with and without gold nanorods on their surface. Numbers with the units mW and ms are the laser powers and integration times used to obtain a particular spectrum, respectively.

Liam James Dodd

Gold nanorods were synthesized by the method described by Vidgerman and Zubarev.[4.22] To 10 mL of a HAuCl$_4$(aq) (5 mM) and hexadecyl trimethylammonium bromide (100 mM) solution, 460 μL of a NaOH(aq) (10 mM) and NaBH$_4$(aq) (10 mM) was added with rapid stirring to make the seed solution. To 10 mL of a HAuCl$_4$(aq) (5 mM) and hexadecyl trimethylammonium bromide (100 mM) solution, 70 μL of an AgNO$_3$(aq) (100 mM) solution, and 700 μL of a hydroquinone (100 mM) solution was added with rapid stirring. To this solution, 160 μL of the seed solution was added with rapid stirring, which continued overnight. ICP-OES analysis of the solution indicated the purity of the solution: it contained only gold metal in just below the expected concentration. The UV/Vis spectrum indicated a plasmon band at 1044 nm (Figure 4.17).
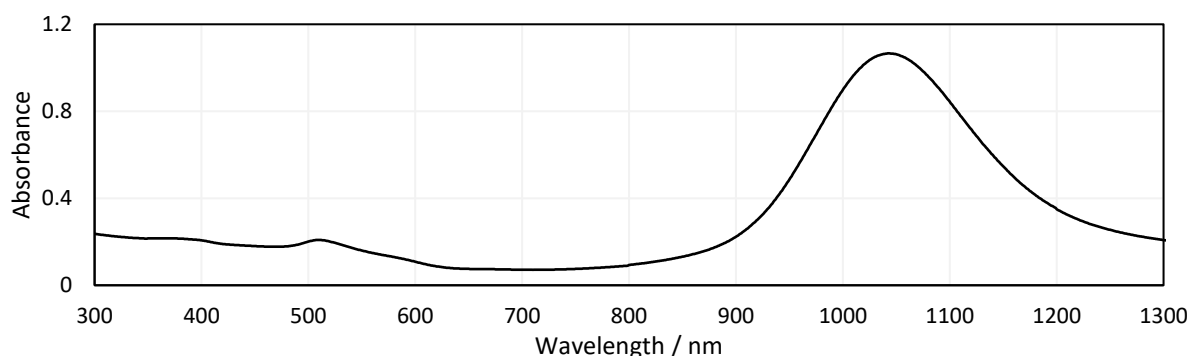
Figure 4.17: the UV/Vis spectrum of the gold nanorod suspension.

4.9. The Sulfur – Sulfur Band

With the aforementioned issues resolved, an attempt to understand the meaning of the different contributor peaks in the sulfur – sulfur band, could be made. To assist in the understanding of this complex spectral region, computational chemistry was employed. Because computational chemistry would be so instrumental to the outcome of the project, great attention was paid to the computational method. To identify a suitable method of predicting Raman spectra, the experimental 1064 nm Raman spectra of six standard molecules were obtained: dimethyldisulfide, dimethyltrisulfide, diallyldisulfide, diallyltrisulfide, diphenyldisulfide, and dibenzyldisulfide; all containing a sulfur – sulfur bond. Next, the Raman spectra of these standard molecules were predicted using DFT in the Gaussian 09 code, using different density functionals with the def2-TZVPP basis set. All spectra were calculated assuming 1064 nm excitation at 298.15 K, in the gas state in a vacuum, after an initial energy minimisation using MMFF molecular mechanics. The four functionals tested were, BP86, HSE06, ωB97XD, and M062X, (all used in conjunction with the def2-TZVPP basis set, with and without Gimme's B3(BJ) empirical dispersion correction) as it was thought that these functionals would provide a good spread of functionals at different levels of theory: for example ωB97XD is a range separated hybrid generalised gradient approximation functional, whereas M062X is a global hybrid meta generalised gradient approximation. B3LYP and EDF2 were also preliminarily tested with a variety of basis sets, but although EDF2 was better than B3LYP, both were quite poor at replicating the Raman spectra. The predicted Raman spectra from these calculations, were then compared to the experimental Raman spectra, and it was found that the spectra calculated by an initial energy minimisation with MMFF molecular mechanics, followed by geometry optimisation and energy calculation with the BP86 functional and the def2-TZVPP basis, with a D3(BJ) empirical dispersion correction, gave the best fit to the experimental data. Grimme *et al.* singled out a charged sulfur ring system, S$_8^{2+}$, as having sulfur – sulfur bonds elongated by DFT-D3, which are then corrected with DFT-D3(BJ) which may explain why this empirical dispersion was advantageous in this case.[4.23] Comparisons of the experimental and computationally predicted spectra for the six standard molecules can be found in Figure 4.18.

Liam James Dodd
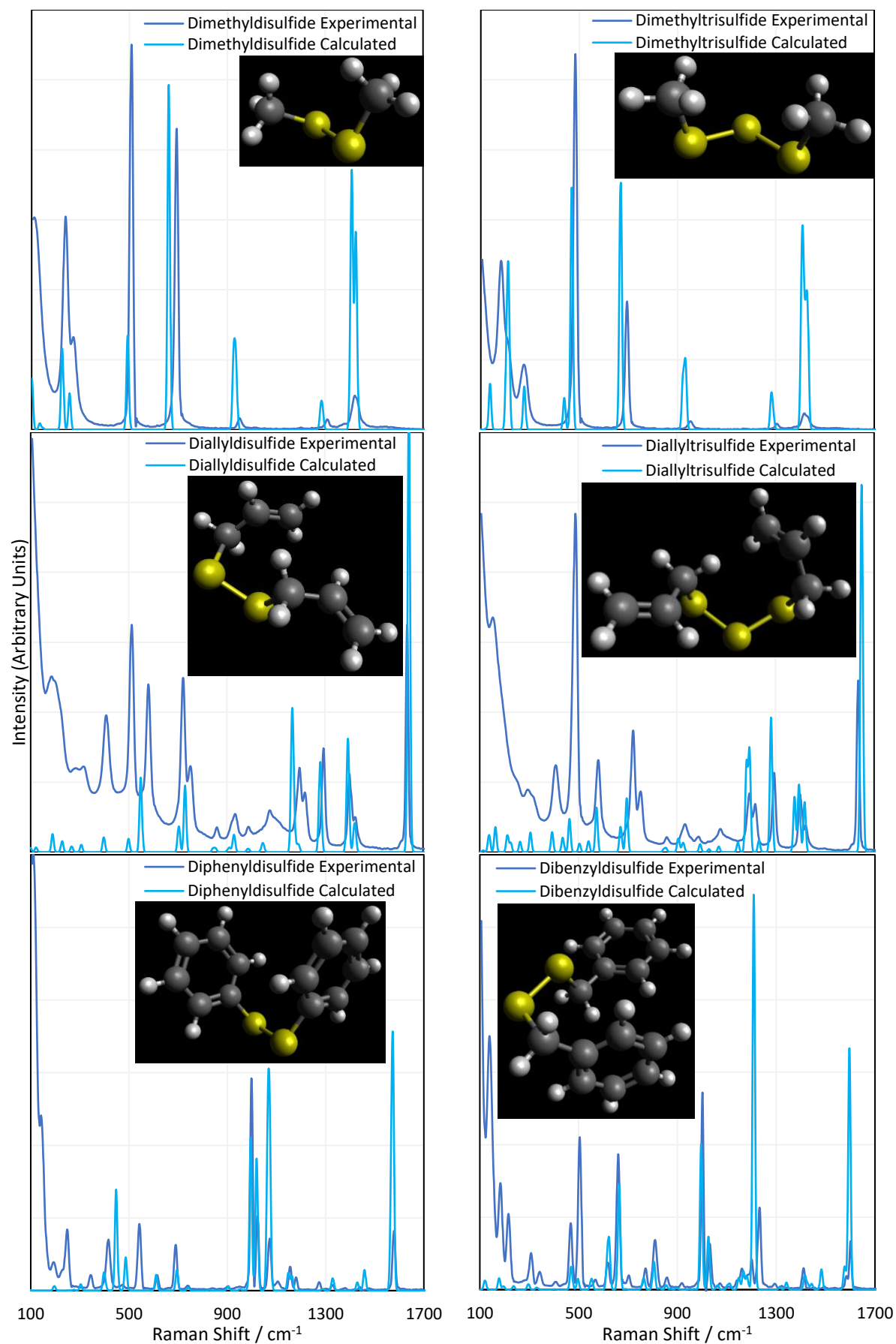
Figure 4.18: Comparison of the experimental and calculated Raman spectra, as well as geometry optimised structures for the six standard molecules.

Liam James Dodd

The spectra shown in Figure 4.18 and all calculated spectra from here on, were all calculated using the optimised calculation method: first, energy minimisation with MMFF molecular mechanics, followed by geometry optimisation and energy calculation using the BP86 functional, with the def2-TZVPP basis set, with a GD3(BJ) empirical dispersion correction.

To improve the fit of the predicted Raman spectra to the experimental spectra, parameterisation was carried out, which entailed using the experimental peak data to correct the predicted data. In terms of parameterising the Raman shifts, it was found that the best improvement in accuracy was given by simply adding 15 cm^{-1} to the predicted values, because on average the calculated spectra underestimated the Raman shifts of sulfur region modes by approximately 15 cm^{-1}. Parameterisation of the intensities of the calculated spectra was a great deal more complicated than the parameterisation of the Raman shifts, but was also more important. In general, the intensity of Raman modes is much more difficult than the peak Raman shifts to predict accurately through computational chemistry. This is because peak Raman shifts are dependent on the bond strength and reduced mass, which influences the frequency of the Raman mode. Meanwhile, the intensity of the Raman scatter is dependent on the polarizability tensor, which is in turn dependent on the three dimensional electron density of the electron clouds about the bond. Electron density is indeed difficult to model by computational methods, due to the many-body problem, which DFT itself was designed to circumvent via assumptions and treating the electrons as a cloud of negative charge with variable density rather than a complex system of interacting point charges. Because of these assumptions and simplifications, and the complex treatment of the data to obtain the Raman intensities, Raman scatter intensities can be challenging to predict accurately, and require careful selection of high levels of theory.

The first obstacle to parameterising the intensities was to overcome the fact that the experimental and calculated spectra of the standard molecules have different units that are not easily interchanged, those being detector counts for the experimental data and Raman Scattering Activity. An additional problem is that the experimental spectra are influenced by experimental parameters such as laser intensity and integration time, which the calculated spectra were not. To circumvent this problem, normalisation and a ratiometric approach was employed. Regardless of any parameters and units, the ratio of two different peak intensities should not vary. Because an aromatic mode at approximately 1600 cm^{-1} exists within the spectra of the DVB polymers as well as two of the standard molecules, diphenyldisulfide and dibenzyldisulfide, the ratio of the intensity of the aromatic mode over the intensity of the sulfur modes was used to apply the corrections. That is, the ratio in the experimental spectra could be used to correct that ratio from the calculated data. Since this correction centres around the aromatic mode, it was sensible to normalise the experimental and calculated spectra to their aromatic modes, thereby eliminating the issue of differing units.

Observing the comparison of the experimental and calculated spectra of the standard molecules (Figure 4.18), and comparing the experimental DVB polymer spectra to the calculated polymer model spectra, it is clear that the calculated spectra consistently underestimate the intensities of the sulfur – sulfur modes in comparison to the aromatic modes. The next complication to the parameterisation was that the degree to which the sulfur modes were underestimated could be dependent on the Raman shift that the modes occurred at. As such, the parameterisation function had to vary with Raman shift, so that the parameterisation value could vary with the Raman shift. The best intensity parameterisation model was found to be a polynomial function which is given in Figure 4.19. Note that the experimental intensity values have been baseline corrected, to eliminate the effects of non-Raman scatter effects, which was found to be crucial. The number of significant figures included in the intensity parameterisation was also found to be crucial. From this parameterisation model, the

Liam James Dodd

polymer model calculated spectra can be parameterised by multiplying the peak intensity of a Raman mode by the appropriate B/A value for that Raman shift.

Polynomial functions receive great criticism because of their capacity to "fit" any "trend" by simply adding more terms, and that because of this they should be treated with scepticism when used to model real – world dependencies and relationships between variables. The use of a polynomial function with many terms is appropriate here because a real – world relationship is not being modelled. No conclusions will be drawn from this fitting, and it does not mean anything in a wider context. It is simply the most accurate way to correct the calculated data to more closely match experimental data, and this is the only goal of a parameterisation function. In reality, there is likely no true trend between the difference in calculated and experimental Raman shifts and Raman intensities, or if there is one, it is likely to be blindingly complex as it arises from the deep complexities of the DFT calculations. But this does not matter to a parameterisation function, as it is not meant to map this trend, nor provide understanding of the root cause of the error. A parameterisation function is merely a method to empirically correct calculated data. It is however noted that because of the way the parameterisation function was applied here, it is not so applicable to other systems, and will be valid for the polymer models that are used later in this chapter. As such, this parameterisation function is a weakness in this method, and limits the scope of the polymers to which it can be applied.

In conclusion, the parameterisation method is to first normalise the calculated spectrum to its 1600 cm^{-1} aromatic mode. Then, for each calculated vibrational mode, the intensity is multiplied by a B/A ratio, read off from Figure 4.19 at a particular Raman shift. Then 15 cm^{-1} is added to the Raman shift of each vibrational frequency. This parameterisation only applies in the region of 300 to 800 cm^{-1}.
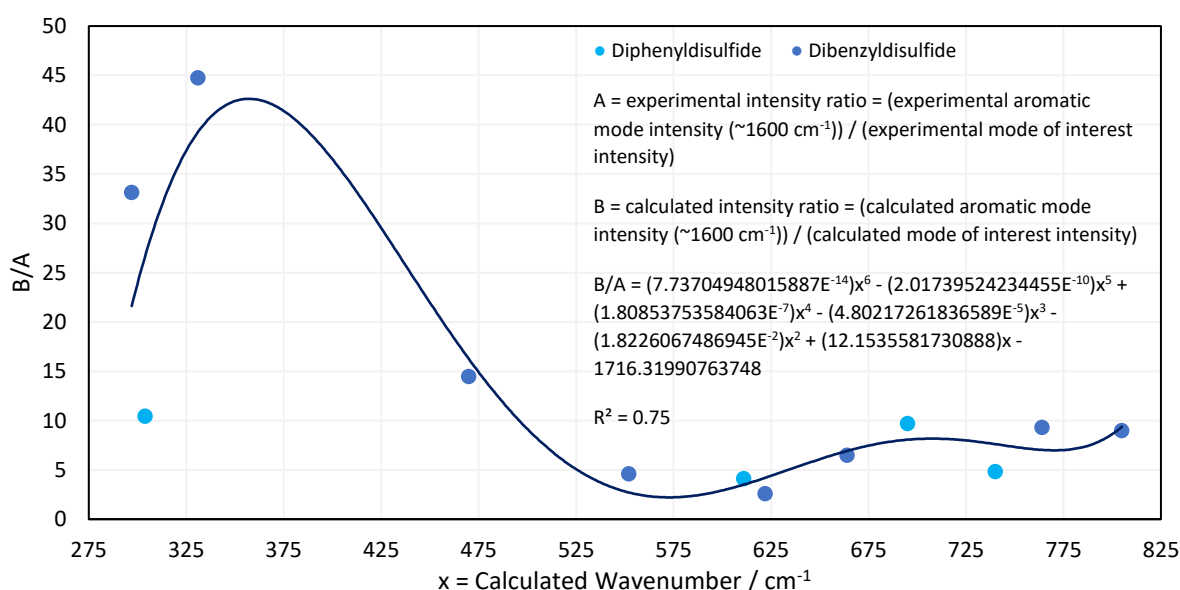
Figure 4.19: Parameterisation model for the intensities of calculated Raman spectra. Black points are for dibenzyldisulfide, red points are for diphenylsulfide.

With an appropriate method for calculating Raman spectra found, the spectra for the polymers could then be calculated. Modelling an entire inverse vulcanised polymer network with DFT is far too computationally expensive to be viable with the current level of technology, therefore a simplified model of the polymer system was needed. Some special DFT systems can apply special assumptions to allow the prediction of polymer properties by faux modelling the entire network, which is done by modelling a repeat unit, and then using assumptions and special methods to extend the results of that

Liam James Dodd

repeat unit to a polymer network. This was not done here for two reasons. Firstly, inverse vulcanised polymers do not have a clear repeat unit due to their complex crosslinking nature. Secondly, excited vibrations are usually localised events occurring in a small system of bonds rather than in an entire polymer network. As such, it was appropriate to create small molecule models that represent small segments of an inverse vulcanised polymer network, and then model those with the aforementioned DFT method. The focus of this system was DVB, because it provided the clearest signals in 1064 nm Raman spectroscopy. To simulate a polymer network, two faux DVB units were connected by sulfur chains as shown in Table 4.4.

Table 4.4: Computational model structures, and their obtained bond lengths for the lowest energy conformer (dark blue – RS isomer, light blue – RR isomer). Rank 6 Trans RS calculation failed due to insufficient memory on the supercomputer.

Sulfur Rank	2	3	4
Cis	2.046 Å / 2.052 Å (top); 2.048 Å / 2.050 Å (bottom)	2.069 Å 2.057 Å / 2.067 Å 2.067 Å (top); 2.068 Å 2.078 Å / 2.066 Å 2.066 Å (bottom)	2.099 Å / 2.115 Å; 2.056 Å / 2.048 Å; 2.050 Å / 2.044 Å (top); 2.051 Å / 2.048 Å; 2.099 Å / 2.111 Å; 2.053 Å / 2.050 Å (bottom)
Trans	2.052 Å / 2.057 Å (top); 2.044 Å / 2.046 Å (bottom)	2.069 Å 2.067 Å / 2.066 Å 2.067 Å (top); 2.067 Å 2.069 Å / 2.067 Å 2.066 Å (bottom)	2.098 Å / 2.115 Å; 2.052 Å / 2.048 Å; 2.052 Å / 2.043 Å (top); 2.048 Å / 2.049 Å; 2.105 Å / 2.111 Å; 2.051 Å / 2.050 Å (bottom)

Sulfur Rank	5	6	Model Applicability
Cis	2.086 Å 2.090 Å / 2.085 Å 2.085 Å; 2.060 Å / 2.047 Å; 2.048 Å / 2.047 Å (top); 2.052 Å / 2.055 Å; 2.059 Å / 2.055 Å; 2.092 Å 2.085 Å / 2.087 Å 2.087 Å (bottom)	2.084 Å 2.080 Å 2.089 Å / 2.078 Å 2.096 Å 2.083 Å; 2.057 Å / 2.061 Å; 2.054 Å / 2.047 Å (top); 2.050 Å / 2.053 Å; 2.053 Å / 2.059 Å; 2.090 Å 2.079 Å 2.086 Å / 2.083 Å 2.080 Å 2.087 Å (bottom)	
Trans	2.092 Å 2.087 Å / 2.086 Å 2.090 Å; 2.058 Å / 2.055 Å; 2.040 Å / 2.045 Å (top); 2.040 Å / 2.045 Å; 2.058 Å / 2.054 Å; 2.087 Å 2.092 Å / 2.086 Å 2.086 Å (bottom)	2.088 Å 2.077 Å 2.092 Å / fail fail fail; 2.052 Å / fail; 2.051 Å / fail (top); 2.051 Å / fail; 2.052 Å / fail; 2.092 Å 2.077 Å 2.087 Å / fail fail fail (bottom)	

Liam James Dodd

This model system left several possible ways to connect up the faux DVB units: each included two chiral carbons, and cis or trans type regiochemistry, as shown in Table 4.4. Thus, every combination of RS or SS stereochemistry with cis or trans regiochemistry had its Raman spectrum predicted, in order to understand the effects of varying these factors upon the calculated spectrum. Additionally, a modification to the calculation method was incorporated to allow determination of the effects of conformation on the calculated spectrum. A conformer search was performed instead of energy minimisation, which was done using MMFF molecular mechanics (the same level as theory as the energy minimisation from before) and this provided the five lowest energy conformations of the RR trans models, allowing determination of how conformation affects the calculated spectrum. Sulfur rank 1 was not modelled because it has no sulfur – sulfur bonds, and it is widely believed that sulfur rank 1 does not form in inverse vulcanised polymers. The cell of Table 4.4 labelled "Model Applicability" shows how the parameterisation model is applicable to the faux DVB system used, as a dibenzyldisulfide unit can be identified in the faux DVB unit of rank 2. This provides some confidence that the applicability issues of the parameterisation function are not important in this example, as one of the molecules used to create it can be identified as closely matching the system to which the parameterisation model was applied. However, this only applies to this system, and the consequences of this lack of applicability will be seen later, as the parameterisation function does not extend to polymers of crosslinkers other than DVB.

The computational chemistry quantified sulfur – sulfur bond lengths as shown in Table 4.4. It has been shown in the literature that the bonds in a sulfur chain become longer and weaker towards the centre of the chain, with this effect increasingly obvious for greater sulfur rank chains.[4.20] The data in Table 4.4 agree with this trend with the exception of the central bond in rank 6 which is shorter than the bonds adjacent to it. In addition, though rank 4 shows the longest sulfur – sulfur bond (the weakest single bond length), rank 5 and rank 6 give weaker overall sulfur chains. This is because, even though rank 5 and rank 6 do not have any single bond that is weaker than the weakest bond of rank 4, they possess a greater population of reasonably weak bonds, and with this greater population, it is statistically more likely to break one of them, which leads to a weaker chain overall.

The computational experiments yielded calculated Raman spectra for each model, as shown in Figure 4.20. As mentioned previously, Raman spectra were predicted for each combination of RR and RS stereochemistry, with cis and trans regiochemistry, for every sulfur rank from 2 to 6. To simplify the presentation of the results, only the rank 2 and rank 6 data will be displayed here. All data is available in Section 4.16.3. For the purposes of studying the sulfur rank of inverse vulcanised polymers, the focus in analysing Figure 4.20 will be the sulfur – sulfur region which is normally taken to be between 425 cm^{-1} to 550 cm^{-1}, though with the computational modes having been calculated here, the vibrational motion of each mode can be visualised, to determine which peaks correspond to a sulfur – sulfur mode, irrespective of whether the peak occurs within the usual sulfur – sulfur region. Table 4.5 shows the analysis of sulfur – sulfur bond vibrations to each vibrational mode.

Encouragingly, Figure 4.20 reveals that in many cases, varying the stereochemistry and regiochemistry does not have a large effect on the spectra though the differences are most pronounced in the sulfur – sulfur region, which suggests that the way in which the atoms are connected up in the polymers has some effect on the sulfur chains, whilst having minimal effect on the organic units. Although it is difficult to suggest reasons why the stereochemistry and regiochemistry affect the spectra, it appears the effects of these structural variations are less pronounced at longer sulfur ranks. Encouragingly, Figure 4.20 suggests that the conformation of the sulfur chains has no significant effect on the spectra. It can be seen in all cases that the spectra of the five lowest energy conformers of each polymer model analysed, are nearly identical, and this was stringently true for every sulfur rank calculated. Close

Liam James Dodd

analysis of the raw data shows that there are very minor differences in the calculated spectral data of each conformer, but these differences have far too small an effect to cause any tangible difference to the analysis, which is encouraging because it suggests that when analysing the sulfur rank, the conformation can be ignored, vastly simplifying the analysis. The fact that inverse vulcanisation reactions are typically cured in order to provide time and energy for the polymers to reach their thermodynamic minimum, provides more confidence that analysis of the lowest energy conformations is the most appropriate method as, during curing, the polymer chains will likely relax toward these minimum energy conformations in the majority of the population.
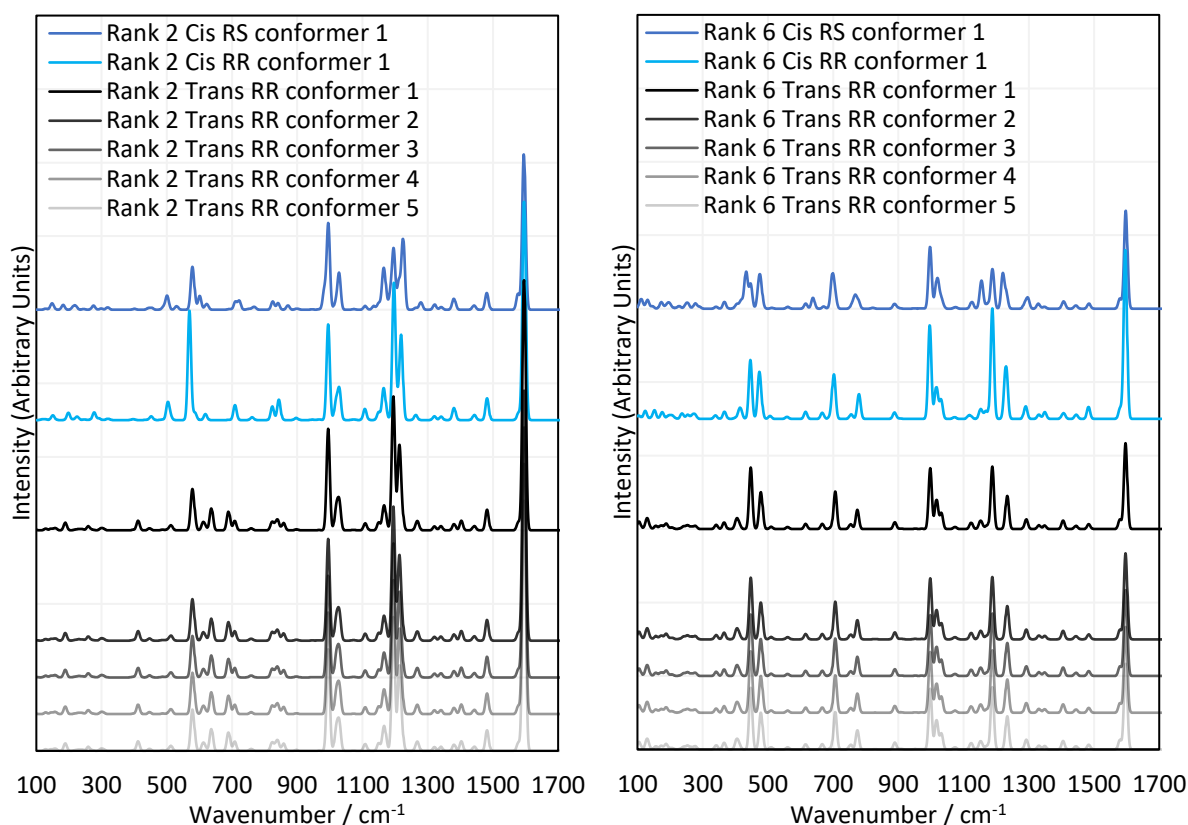
Figure 4.20: Comparisons between selected sets of calculated Raman spectra for the polymer model compounds of rank 2 and rank 6. Offsets have been applied to the intensities.

Table 4.5: Selected calculated Raman data for the lowest energy conformers of the polymer models. The column "S-S mode" indicates whether the vibrational mode had a major, minor, or no contribution from the of S-S bonds. Other information such as the reduced mass, force constants of vibration, and FTIR intensities were also calculated, but there was too much information to represent here.

Rank 2 Cis RR			Rank 2 Cis RS			Rank 2 Trans RR			Rank 2 Trans RS		
Frequency / cm^{-1}	Scatter Activity / A^4 AMU^{-1}	S-S mode	Frequency / cm^{-1}	Scatter Activity / A^4 AMU^{-1}	S-S mode	Frequency / cm^{-1}	Scatter Activity / A^4 AMU^{-1}	S-S mode	Frequency / cm^{-1}	Scatter Activity / A^4 AMU^{-1}	S-S mode
396.7734	1.1792	minor	397.0934	0.2890	none	396.6211	0.1182	minor	396.6569	0.6322	none
396.8257	0.0542	none	401.7281	0.9803	minor	396.9498	0.6624	none	401.8122	0.6162	minor
438.0468	0.3737	none	443.1715	2.1108	none	412.2881	13.0304	major	412.9433	15.8903	major
452.3877	5.0048	major	453.9694	2.5220	major	446.8773	2.8383	major	450.5752	1.0854	major
486.5938	0.7127	major	489.2803	3.6165	major	486.6190	0.8927	major	488.4717	5.7306	major
499.0890	0.2240	none	500.2230	15.9870	major	499.3027	0.4765	minor	503.5418	3.0016	major
503.0579	22.9835	major	504.3268	3.9015	major	507.9172	2.0787	major	508.8794	5.7708	major
511.0024	5.378	major	530.2028	4.7139	major	513.9543	5.7369	major	530.7305	4.6682	major
569.7102	148.9740	minor	578.1634	50.0487	none	577.8815	46.3738	minor	582.1947	1.8686	minor
578.6597	0.4877	none	582.6316	10.0600	minor	581.7208	0.5304	minor	585.5305	9.3374	none
582.5700	0.2415	none	585.5625	3.5184	minor	583.3526	16.0490	minor	600.0292	16.9127	minor
586.2379	9.3881	minor	600.7314	18.8715	major	611.0925	9.9978	none	610.9299	9.8363	minor
618.2633	5.5031	minor	618.6964	3.3914	none	618.6927	3.9480	minor	623.7836	5.2782	minor
619.0075	2.5061	none	624.4643	5.6590	minor	636.7991	29.7872	none	636.4549	31.7562	none
Rank 3 Cis RR			Rank 3 Cis RS			Rank 3 Trans RR			Rank 3 Trans RS		
Frequency / cm^{-1}	Scatter Activity / A^4 AMU^{-1}	S-S mode	Frequency / cm^{-1}	Scatter Activity / A^4 AMU^{-1}	S-S mode	Frequency / cm^{-1}	Scatter Activity / A^4 AMU^{-1}	S-S mode	Frequency / cm^{-1}	Scatter Activity / A^4 AMU^{-1}	S-S mode

Liam James Dodd

Frequency / cm⁻¹	Scatter Activity / A⁴AMU⁻¹	S-S mode	Frequency / cm⁻¹	Scatter Activity / A⁴AMU⁻¹	S-S mode	Frequency / cm⁻¹	Scatter Activity / A⁴AMU⁻¹	S-S mode	Frequency / cm⁻¹	Scatter Activity / A⁴AMU⁻¹	S-S mode
397.9754	0.7157	minor	346.4138	6.3845	none	396.3822	0.1318	none	344.7405	7.4276	none
399.4342	5.4978	major	397.5632	0.2802	minor	398.6430	0.1978	none	397.8191	0.2594	none
401.5072	2.0858	major	397.9396	0.6172	none	403.7601	0.0282	major	397.8228	0.5033	none
425.9122	0.5699	major	399.4569	0.1389	major	416.0992	21.4129	major	400.7163	9.1857	major
443.4569	5.5639	major	408.4074	8.6956	major	427.8158	4.7947	major	408.1557	0.0000	major
453.1230	5.4074	major	436.4734	6.8414	major	445.1553	7.9777	major	437.2184	0.0000	major
476.7709	21.683	major	439.1852	7.1452	major	475.8514	1.0045	major	439.0759	19.5497	major
479.2200	4.3976	major	470.1958	10.2642	major	478.4904	8.3210	major	470.6527	0.0036	major
496.4937	0.9878	major	471.3448	48.8087	major	503.6202	0.6472	minor	470.7327	63.0964	major
511.8940	1.1562	major	505.1372	0.3387	minor	509.0272	0.8359	major	506.2547	1.0994	minor
572.7828	8.2238	major	509.9213	0.9369	minor	579.8395	1.8253	major	509.1209	0.0000	major
585.1860	0.3894	minor	556.0755	1.9256	minor	583.9612	0.7883	none	558.2558	3.0885	minor
590.1864	21.4502	minor	563.4125	1.4975	minor	607.4858	1.2382	none	562.0973	0.0000	minor
611.3447	5.0091	none	614.7741	2.9936	minor	609.8618	18.4340	none	614.8583	9.8098	none
618.3035	3.5940	minor	615.0651	6.1471	minor	626.2799	9.7122	none	615.0056	0.0000	none

Rank 4 Cis RR			Rank 4 Cis RS			Rank 4 Trans RR			Rank 4 Trans RS		
Frequency / cm⁻¹	Scatter Activity / A⁴AMU⁻¹	S-S mode	Frequency / cm⁻¹	Scatter Activity / A⁴AMU⁻¹	S-S mode	Frequency / cm⁻¹	Scatter Activity / A⁴AMU⁻¹	S-S mode	Frequency / cm⁻¹	Scatter Activity / A⁴AMU⁻¹	S-S mode
385.6803	16.1926	major	375.3287	23.1560	major	385.3761	19.4176	major	377.7018	21.4938	major
392.6425	13.0681	major	381.2331	13.2979	major	388.1937	6.8145	major	378.7457	17.6787	major
397.3142	0.2679	minor	397.2987	0.3013	minor	396.7655	0.6364	minor	397.3531	0.2284	minor
397.5269	0.4732	minor	397.7759	0.7115	none	396.9518	0.2172	minor	397.8531	0.6313	none
408.4782	1.1819	major	410.7203	5.8798	major	406.6099	3.6450	major	409.9371	3.9199	major
413.8168	4.0832	major	455.8503	9.1036	major	426.3028	6.5999	major	455.3225	12.0547	major
468.2879	18.6664	major	477.5069	15.9061	major	468.7930	20.0211	major	478.7417	4.4872	major
474.9997	34.6228	major	479.4958	9.8396	major	479.7279	7.5244	major	479.4201	27.8712	major
481.6323	2.9575	major	480.3695	11.7237	major	483.2750	4.7055	major	480.8000	2.7043	major
489.1808	7.3778	major	481.6383	3.9352	major	487.5217	7.8281	major	481.4060	4.7523	major
505.0964	2.1467	minor	501.5078	1.9774	major	500.6426	3.7266	major	500.9025	2.0479	major
506.9684	1.0468	minor	504.8395	0.6294	major	507.1842	0.9360	minor	504.8807	0.6019	major
558.5941	1.3868	minor	560.7124	1.3375	minor	564.5541	0.9934	major	560.2487	1.2156	minor
581.3330	0.8369	minor	578.6194	22.8629	minor	581.5942	1.0552	minor	578.9669	19.8013	minor
607.2743	27.8088	minor	589.3517	48.1509	minor	607.2197	21.1103	minor	589.1034	44.3675	minor
615.2482	4.6518	none	615.1858	4.2310	none	616.1335	3.8956	none	615.1017	4.4169	none
627.6771	34.8107	minor	619.5308	5.5066	minor	628.0747	26.7646	minor	619.3235	4.8540	minor

Rank 5 Cis RR			Rank 5 Cis RS			Rank 5 Trans RR			Rank 5 Trans RS		
Frequency / cm⁻¹	Scatter Activity / A⁴AMU⁻¹	S-S mode	Frequency / cm⁻¹	Scatter Activity / A⁴AMU⁻¹	S-S mode	Frequency / cm⁻¹	Scatter Activity / A⁴AMU⁻¹	S-S mode	Frequency / cm⁻¹	Scatter Activity / A⁴AMU⁻¹	S-S mode
373.1568	2.0738	major	379.1591	0.8852	major	376.2217	1.6138	major	377.3218	1.7794	major
374.0103	12.6668	major	384.2810	0.4372	major	376.3181	1.4264	major	382.4060	0.8858	major
386.0111	1.0977	major	396.2268	2.4616	none	394.7935	5.0400	minor	396.2193	1.5792	minor
396.9780	0.0258	none	396.3314	1.1647	minor	395.2988	1.1243	minor	398.2635	0.0468	none
400.4008	0.1247	minor	400.8521	0.7240	minor	400.0129	4.3785	minor	401.1299	8.7081	major
422.4134	0.7427	minor	401.9240	18.1593	minor	400.1684	30.9256	minor	434.9798	15.9998	major
433.5759	6.5768	major	435.8695	7.1329	major	429.2874	2.7120	major	436.5963	15.0738	major
434.0347	0.5558	major	437.4054	17.7921	major	431.3756	27.9544	major	463.1962	7.4659	major
472.9784	3.0680	major	472.9527	3.0909	major	466.2111	39.1592	major	474.5003	3.4985	major
475.1415	2.9575	major	476.1670	14.7586	major	468.3188	2.2050	major	478.2318	11.3783	major
479.2409	7.9376	major	488.4716	13.7623	major	482.1290	2.6995	major	484.3454	11.5306	major
487.0843	9.9366	major	489.2261	3.6952	major	484.1148	10.9394	major	489.2910	21.2317	major
503.7504	8.0589	minor	508.5128	0.4186	major	495.8502	0.2888	major	491.0064	2.2376	major
521.3032	14.5875	minor	508.6828	3.0981	major	496.6300	33.1536	major	508.2622	1.7121	major
554.8530	0.7785	minor	583.9516	1.8229	minor	582.5476	10.7378	minor	580.9073	55.8488	minor
563.4307	2.7151	minor	584.6623	1.5875	minor	582.5988	9.7604	minor	585.0327	1.3509	minor
614.8432	0.5893	none	609.1934	10.8772	none	596.5802	5.4128	none	585.8608	12.8806	minor
614.8927	0.7130	none	609.4123	14.7636	none	597.7275	27.3935	none	609.2077	12.6544	none
-	-	-	634.4842	2.8787	none	618.7191	4.3863	none	617.1357	4.4570	none
-	-	-	635.1162	40.1094	none	619.2693	10.8661	none	634.0275	20.3170	none

Rank 6 Cis RR			Rank 6 Cis RS			Rank 6 Trans RR			Rank 6 Trans RS		
Frequency / cm⁻¹	Scatter Activity / A⁴AMU⁻¹	S-S mode	Frequency / cm⁻¹	Scatter Activity / A⁴AMU⁻¹	S-S mode	Frequency / cm⁻¹	Scatter Activity / A⁴AMU⁻¹	S-S mode	Frequency / cm⁻¹	Scatter Activity / A⁴AMU⁻¹	S-S mode
398.0592	0.3842	none	395.3790	0.4809	minor	398.1307	0.5993	minor			
398.9942	0.8599	minor	399.5565	0.3116	minor	398.9541	0.2826	minor			
410.2346	3.6185	major	404.9620	5.8561	minor	403.3518	1.9911	minor			
413.5001	6.8671	major	415.6481	5.0474	major	404.2801	10.4538	minor			
416.8919	3.5887	major	420.3812	7.7042	major	412.1293	5.4925	major			
419.2325	4.3811	minor	432.9821	49.5638	major	412.2573	0.7286	major			
445.2109	3.9434	major	446.0972	4.0440	major	445.9669	4.8049	major		Failed due to not enough memory	
446.1576	76.1923	major	447.0913	29.4054	major	447.2308	79.1920	major			
472.7357	39.3081	major	469.9899	4.5378	major	477.1536	1.7802	major			
475.3082	18.8447	major	472.3189	20.8806	major	477.2097	25.1563	major			
476.7993	2.8304	major	477.7225	28.1976	major	480.1332	24.7956	major			
480.0532	10.9023	major	480.0226	3.2975	major	481.4744	0.7769	major			
506.1494	2.5103	minor	486.6518	0.8921	minor	509.7595	0.4940	minor			
506.8646	1.5891	minor	511.9071	1.1047	minor	509.8410	2.6200	minor			
557.8259	1.4172	minor	560.4898	1.0678	minor	560.3645	2.0371	minor			
558.8661	1.4306	minor	560.9102	1.4196	minor	560.5665	0.8572	minor			
615.4014	5.7298	none	614.7701	0.5441	none	615.1318	0.7191	none			
615.7967	3.7944	none	615.9454	6.5406	none	615.7908	6.3732	none			

The most important feature of the calculated data is that it can be carried forward to be used in the analysis of real polymers, in an attempt to determine their sulfur rank. In this application, it will be appropriate to average together RR and RS data, and separately cis and trans data, because statistically there should be a 50 : 50 distribution of both stereochemistries, and both regiochemistries within the polymer. Parameterisation was applied as detailed previously using the experimental spectra of real molecules. Using these parameterisation functions for Raman shifts and intensities, the

Liam James Dodd

polymer model data were parameterised and then averaged together as appropriate to give one spectrum for each sulfur rank. These spectra were then used to analyse the sulfur – sulfur band of the experimental Raman spectra of sulfur polymers.

Additionally, the computational work also elucidated the assignments of other Raman shift regions. The region of 580 cm^{-1} to 900 cm^{-1} is assigned to carbon – sulfur vibrations with contributions from the aromatic modes. What was initially hypothesized to be sulfur – oxygen modes between 1100 cm^{-1} and 1300 cm^{-1} is more likely to be carbon – hydrogen vibrations with contributions from the aromatic and carbon – sulfur bonds.

4.10. Dark Sulfur Quantification

As seen in Figure 4.15, elemental sulfur makes a contribution to the sulfur – sulfur band, as well as providing two free standing signals at about 217 and 150 cm^{-1}. The two free standing signals can be used to predict the intensity of the signals that occur within the sulfur – sulfur band, as well as allowing the quantification of dark sulfur, which is difficult by other means as most other methods can only detect crystalline elemental sulfur.

DVB50-S50 was chosen to be the first polymer to have this analysis performed upon it. In order to quantify the dark sulfur in DVB50-S50, a spectrum of elemental sulfur was necessary. This spectrum was acquired under the same laser power as DVB50-S50, to eliminate the effects of laser power upon signal intensities. Next, to make the spectra comparable, they were both divided by the integration time used to acquire the Raman spectra, which is appropriate because signal intensity varies linearly with integration time. Next, the 217 cm^{-1} elemental sulfur signal in the DVB50-S50 spectrum was made subject to a linear baseline correction, to eliminate the fluorescent background, and then integrated to find its intensity. The 217 cm^{-1} peak in the elemental sulfur spectrum was also integrated to find its intensity. According to the elemental analysis, the DVB50-S50 polymer contained 52.5 % sulfur by mass. Therefore, the elemental sulfur spectrum intensity was multiplied by 0.525 to correct for this. Comparing the intensity of the elemental sulfur signals between the polymer spectrum and the elemental sulfur spectrum, it was found that that elemental sulfur (present as S$_8$) in the DVB50-S50 polymer gave signals that were 0.43 % as intense as the elemental sulfur spectrum itself, indicating that 0.43 % of the sulfur in the polymer was in fact not polymerised, but elemental. This analysis was repeated for DVB30-S70 and DVB70-S30, revealing that DVB30-S70 had an elemental sulfur content of 4.46 % of its total sulfur content, and that DVB70-S30 had too little elemental sulfur present to quantify accurately. Using the same method, it was determined that DIB30-S70 had 11.6 % of its total sulfur content unpolymerised, and that the analogous value for DIB50-S50 was 1.7 %. The elemental sulfur signals in DIB70-S30 were too weak for accurate analysis.

What follows is a step-by-step guide on how to quantify dark sulfur in an inverse vulcanised polymer by Raman spectroscopy. Firstly, acquire a polymer spectrum and divide the intensity by the integration time. Second, identify the elemental sulfur signal at 220 cm^{-1} and then use a linear baseline correction to eliminate the contribution of the fluorescent background. Third, acquire the spectrum of elemental sulfur using the same laser power as was used for the polymer; the integration time can be different in order to prevent issues with saturating the signal detector. Divide the intensity of this spectrum by the integration time. Fourth, determine the mass percentage of sulfur in the polymer by another method, such as combustion microanalysis. Fifth, multiply the elemental sulfur spectrum intensity by the determined mass percentage of sulfur over 100. Sixth, calculate the following ratio: intensity of the 220 cm^{-1} peak in the elemental sulfur spectrum divided by intensity of the 220 cm^{-1} peak in the polymer spectrum. Multiply the result by 100 to get the percentage of sulfur in the polymer that is not polymerised. Even if the mass percentage of sulfur in the polymer cannot be obtained confidently, this

Liam James Dodd

method can still be used to qualitatively compare the content of elemental sulfur between different polymers. The aforementioned process should simply be carried out until the point at which the mass percentage of sulfur is needed. Instead of proceeding further, the signal intensity of the 220 cm^{-1} peak can then be directly compared to the equivalent peak in other polymers. Note that in order for this qualitative method to be valid, all polymer spectra must be obtained at the same laser power, and then the intensities of the spectra must be corrected for any differences in integration time.

4.11. Measuring the Sulfur Rank

One of the most valuable pieces of information that Raman spectroscopy has the potential to provide, is the proportion of different sulfur ranks within inverse vulcanised polymers. This information should be contained within the sulfur – sulfur band; specifically, it should be made up by the smaller bands which contribute to the sulfur – sulfur band. Before this analysis can be attempted, the elemental sulfur contribution to the sulfur – sulfur band must be taken into account. This is done by the same method as before: the baseline corrected intensity of the elemental sulfur peak at roughly 217 cm^{-1} in the polymer spectrum must first be measured, though in this scenario, there is no need to divide by the integration time. Separately the spectrum of elemental sulfur must be acquired, though in this scenario, the conditions under which it is measured do not need to match that of the polymer spectrum. In the elemental sulfur spectrum, the intensities of the 434 cm^{-1} and 471 cm^{-1} peaks, must be measured in comparison to the intensity of the 217 cm^{-1} peak. In this example, the intensity ratios were as follows: intensity$_{434}$/intensity$_{217}$ = 0.0891 and intensity$_{471}$/intensity$_{217}$ = 0.7492.

Returning to the polymer spectrum, in this case DVB50-S50 will be used as the example, the intensity of the 217 cm^{-1} peak must be multiplied by the aforementioned ratios in order to obtain the intensities of the 434 cm^{-1} and 471 cm^{-1} peaks in the polymer spectrum. The baseline corrected intensity of the 217 cm^{-1} peak in DVB50-S50 was 1675.96 counts. Therefore, by multiplying 1675.96 counts by 0.0891 and 0.7492 separately, the intensity of the 434 cm^{-1} and 471 cm^{-1} peaks were found to be 149.33 counts and 1255.63 respectively. With the intensity of these elemental sulfur peaks in the polymer spectrum known, their contributions in the later stages of the analysis can be accounted for.

The first attempt to extract the sulfur rank from the sulfur – sulfur band was performed on DVB50-S50, with the initial method being to use the computational data to explicitly fit the bands. The first attempt used the strategy of applying every explicit peak of the computational data set to the experimental sulfur region, and then varying the proportions of the intensities of the different sulfur ranks. Unfortunately, this method was unsuccessful due to several reasons. Trying to fit the peak data explicitly resulted in as many as thirty different contributor peaks in the band deconvolution process, which was very difficult to manage. Secondly, there were multiple different combinations of contributor peaks that would yield a mathematically acceptable fit, and it was impossible to decide which one was correct. Thirdly, this method was very vulnerable to inaccuracies in the computational data.

As such, a new, simpler strategy, less constrained by parameters was necessary. Firstly, the sulfur – sulfur band of DVB50-S50 was analysed by band deconvolution without the computational data, using the minimum number of Gaussian peaks necessary to get a mathematically acceptable fit, whilst also incorporating the peaks of elemental sulfur (Figure 4.21). In the case of DVB50-S50, besides the elemental sulfur peaks, five Gaussian peaks were needed to complete band deconvolution, though Group 1 and Group 2 will be treated as a single group, Group 1,2, since Group 2 is much larger than Group 1, and Group 1 occurs almost entirely inside Group 2. It was found later that for other polymers, this was treatment not appropriate. Therefore, the sulfur – sulfur band of DVB50-S50 was described in terms of four peaks, which will be referred to as groups (Figure 4.21).

Liam James Dodd

Peak Name	Centre / cm^{-1}	FWHM / cm^{-1}	FWHM Range / cm^{-1}	Integration
Group 1	399	23	387 to 451	5.17
Group 2	434	38	387 to 451	188.97
Group 3	463	24	451 to 475	139.95
Group 4	491	30	475 to 505	265.94
Group 5	517	25	505 to 530	27.27
Elemental Sulfur 474	472	15	N/A	11.72
Elemental Sulfur 434	433	13	N/A	1.39

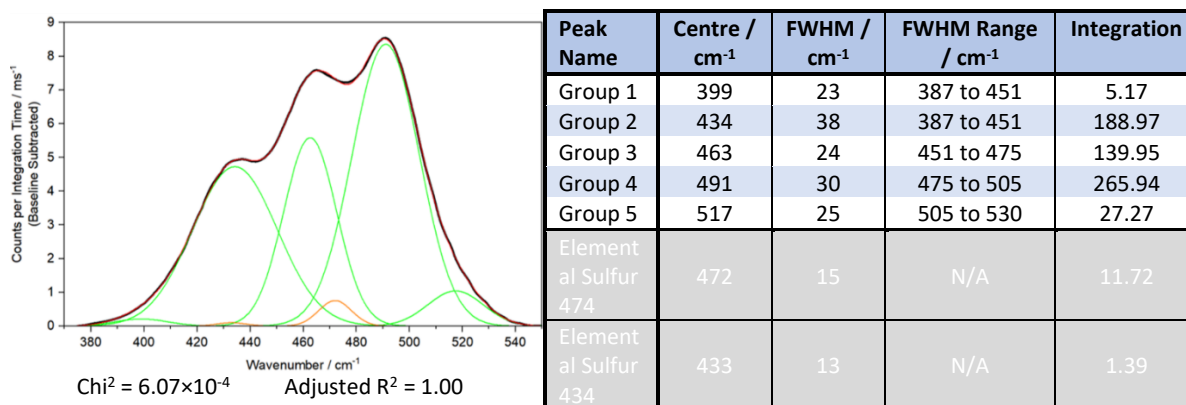Chi^2 = 6.07×10^{-4} Adjusted R^2 = 1.00

Figure 4.21: Band deconvolution of the sulfur – sulfur band of DVB50-S50, with selected peak information. Peaks resulting from elemental sulfur are coloured in orange, while peaks in green are the Gaussians assigned to polymer sulfur – sulfur vibrational modes. The black line is the linear baseline corrected experimental spectrum, while the red line is the sum of the green and orange Gaussians.

The next step was to use the computational data to determine how much intensity each sulfur rank would contribute to each group. To do this, the peak data shown in Table 4.5 was sorted by the following protocol: the Raman peak data would be sorted into a group if its parameterised harmonic frequency fell within the FWHM Range of that group (Figure 4.21). The FWHM Range was simply the Centre value ± half the FWHM. In the case that a peak occurred within 5 cm^{-1} of a boundary between two groups, the parameterised intensity of that peak would be halved, and it would be placed into both groups. This was done separately for each sulfur rank, yielding series of peak data for each group by sulfur rank. Finally, the intensities contained within each group by each sulfur rank were summed together to give a total intensity value. Thus, the intensity that each sulfur rank would contribute to each group was then known, as shown in Figure 4.22.

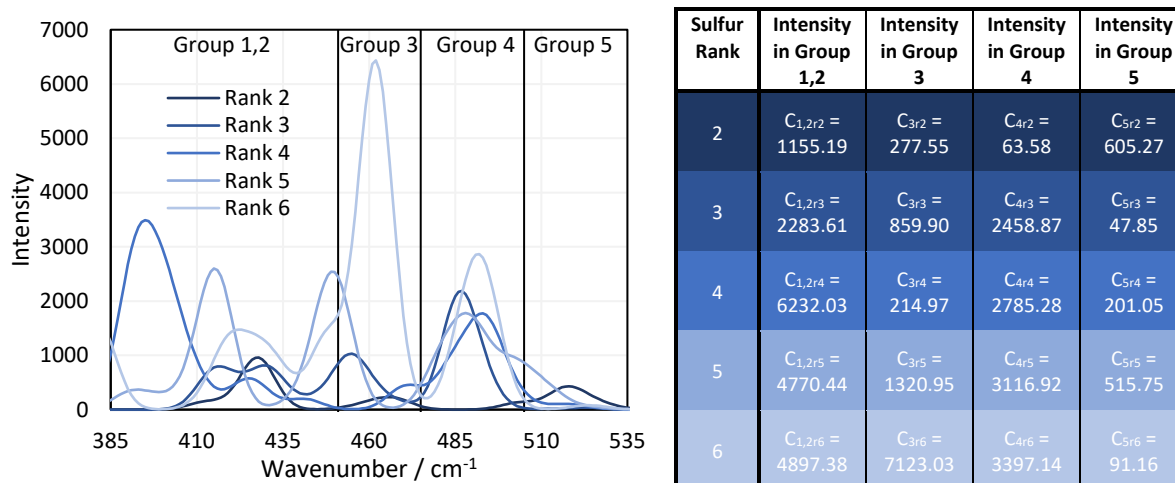| Sulfur Rank	Intensity in Group 1,2	Intensity in Group 3	Intensity in Group 4	Intensity in Group 5
2	C$_{1,2r2}$ = 1155.19	C$_{3r2}$ = 277.55	C$_{4r2}$ = 63.58	C$_{5r2}$ = 605.27
3	C$_{1,2r3}$ = 2283.61	C$_{3r3}$ = 859.90	C$_{4r3}$ = 2458.87	C$_{5r3}$ = 47.85
4	C$_{1,2r4}$ = 6232.03	C$_{3r4}$ = 214.97	C$_{4r4}$ = 2785.28	C$_{5r4}$ = 201.05
5	C$_{1,2r5}$ = 4770.44	C$_{3r5}$ = 1320.95	C$_{4r5}$ = 3116.92	C$_{5r5}$ = 515.75
6	C$_{1,2r6}$ = 4897.38	C$_{3r6}$ = 7123.03	C$_{4r6}$ = 3397.14	C$_{5r6}$ = 91.16

Figure 4.22: The sulfur – sulfur region of the calculated Raman Spectra for each sulfur rank when the Cis, Trans, RR, and RS components are average together to give one spectrum for each sulfur rank, and the intensities per mole that each sulfur rank should contribute to each group in the spectrum of DVB50-S50, according to the computational chemistry and the sorting method.

This approach is more resilient to errors in the computational data, because the band deconvolution becomes less dependent on the harmonic frequency being completely correct. The next step was to apply the theoretical group data to the real group data, in order to determine the contribution of each

Liam James Dodd

sulfur rank to each group, and therefore determine the proportional population of each sulfur rank. The initial approach was to solve the following set of simultaneous equations:

$$G_1 = r_2C_{1r2} + r_3C_{1r3} + r_4C_{1r4} + r_5C_{1r5} + r_6C_{1r6}$$
$$G_2 = r_2C_{2r2} + r_3C_{2r3} + r_4C_{2r4} + r_5C_{2r5} + r_6C_{2r6}$$
$$G_3 = r_2C_{3r2} + r_3C_{3r3} + r_4C_{3r4} + r_5C_{3r5} + r_6C_{3r6}$$
$$G_4 = r_2C_{4r2} + r_3C_{4r3} + r_4C_{4r4} + r_5C_{4r5} + r_6C_{4r6}$$
$$G_5 = r_2C_{5r2} + r_3C_{5r3} + r_4C_{5r4} + r_5C_{5r5} + r_6C_{5r6}$$

where G_n is the intensity of the group from the experimental data, $C_{n,rm}$ is the intensity that sulfur rank m should contribute to group n (Figure 4.22), and r_m are the populations of sulfur ranks 2, 3, 4, 5, and 6 respectively. For DVB50-S50, because two of its peaks were treated as one, G_1 and G_2 were combined into $G_{1,2}$, with constant $C_{1,2rm}$. To simplify solving these equations, r_5 and r_6 were considered to be negligible, therefore eliminating the last two terms from the equations. Note that where this analysis was performed here, the experimental G_n values were normalised, and then arbitrarily multiplied by a thousand to make the numbers easier to work with.

If the computational data were flawless, then solving these simultaneous equations for r_2, r_3, r_4, and r_5, would explicitly yield the correct proportions of the sulfur ranks. However this is not the case, and when the equations were solved for r_2, r_3, and r_4, the results were r_2 = 0.18, r_3 = 0.60, and r_4 = −0.17. This implies that sulfur rank 4 would have a population of less than zero, which is of course, impossible. Therefore, explicitly solving these simultaneous equations cannot yield the populations of the sulfur ranks until more accurate computational methods for this analysis are developed. This does not however mean, that a good measure of the populations cannot be obtained.

The values for r_2, r_3, and r_4 were used as starting points in an iterative trial and error approach to determine the sulfur rank proportions. To do this, the values of r_2, r_3, r_4, and r_5 were varied manually, until a minimum difference between the experimental G_n values and the calculated G_n values was achieved. This process revealed why explicitly solving the simultaneous equations failed: the computational data overestimates the intensity of peaks in Group 1,2, forcing one of the sulfur ranks to have a negative population in order to bring the intensity of $G_{1,2}$ down (Figure 4.22). Therefore, when performing the iterative approach, the difference between the experimental $G_{1,2}$ and the calculated $G_{1,2}$ was not considered when trying to achieve a minimum error scenario. From this approach, it was determined that for DVB50-S50, r_2 = 0.134, r_3 = 0.357, r_4 = 0.030, r_5 = 0.010. In other words, the proportional populations were 25.2 % sulfur rank 2, 67.2 % sulfur rank 3, 5.6 % sulfur rank 4, and 1.9 % sulfur rank 5, with the average sulfur rank being 2.84 (Figure 4.23). For DVB50-S50, based only on its sulfur content (taking into account the evaporation of DVB during synthesis and the presence of unpolymerised sulfur) the expected sulfur rank is 2.24. See Section 4.15.4 for the details of how the expected sulfur rank is calculated.

The difference between the extracted sulfur rank of 2.84 and the expected sulfur rank of 2.24 is that the expected sulfur rank cannot take into account a biased distribution of sulfur ranks, which is entirely expected from Boltzmann theory. Even still, the extracted and expected values for the average sulfur rank are not vastly different and this provides confidence that the Raman spectroscopic analysis has provided a sensible number for the average sulfur rank. What provides further confidence in the conclusion given by the Raman spectroscopy analysis is that the populations of each sulfur rank that have been obtained roughly follows the Boltzmann distribution, giving a theoretical basis for the results. To further demonstrate the success of this analysis, the process was repeated for DVB70-S30. Analysis found five distinct peaks within the sulfur band, which could not be combined into fewer

Liam James Dodd

peaks as was the case for DVB50-S50. Processing of the data revealed that DVB70-S30 had an average sulfur rank of 2.66, with the following populations: 56.8 % rank 2, 21.4 % rank 3, and 21.8 % rank 4. In this case the population of rank 4 is slightly higher than rank 3, which is difficult to rationalize with theory, and so it is likely the result of error in the computational and analysis method (Figure 4.23). However, given that the population of rank 4 is only 0.4 % higher than rank 3, it seems this error is quite small. The predicted average sulfur rank for DVB70-S30 is 1.00 based on the theory in Section 4.15.4, significantly lower than the calculated value of 2.66. This suggests that sulfur rank 1 does not occur, and that incomplete consumption or crosslinking of the double bonds may be the case in the DVB70-S30 polymer, which would explain its lower T_g value. What is very interesting in these data, is that the average sulfur rank for DVB50-S50 was found to be 2.86, and the average sulfur rank for DVB70-S30 was found to be 2.66, only marginally lower. Yet, the Raman analysis indicates that despite the similarity in the average sulfur rank values, the individual populations of the sulfur ranks in these two polymers differs significantly.
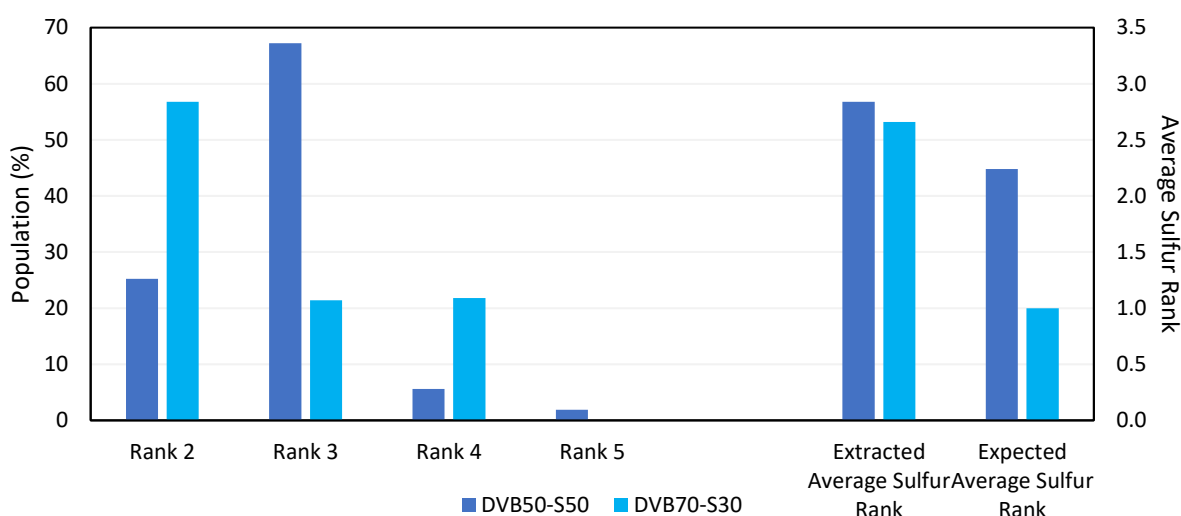

Figure 4.23: The percentage populations of different sulfur ranks of two polymers, and the expected and extracted average sulfur of those polymers.

DVB70-S30 was found to contain no rank 5 chains at all, in comparison to DVB50-S50 which contained a small population. Additionally, DVB50-S50 contained less rank 2 than rank 3 chains, whereas the opposite is true for DVB70-S30. This insight into the distribution of sulfur ranks is unobservable from the average sulfur rank which would suggest these polymers are very similar, however Raman analysis shows clearly how different these two polymers are by elucidating the individual proportions of sulfur ranks, not just the average value. This makes clear, the advantages of Raman analysis in comparison to other methods which can only indicate the average sulfur rank, and so do not provide this fascinating in depth scrutiny of the polymers' molecular structure. The ability to distinguish between sulfur ranks has tremendous importance in the characteristics of inverse vulcanised polymers. One such example is in the field of recyclability of inverse vulcanised polymers, where it was found that disulfide bridges and trisulfide bridges behaved vastly differently in their polymer, with trisulfide bridges promoting recyclability, and disulfide bridges hindering recyclability.[4.23]

This however, is just one example, and the distribution of sulfur ranks has almost ubiquitous importance throughout the different applications of inverse vulcanised polymers, with another example being lithium sulfur batteries. Unfortunately, accurate results for DVB30-S70 could not be obtained. The expected average sulfur rank was 5.11, which would suggest that the majority of chain

Liam James Dodd

lengths were sulfur rank 5 or higher. This made it impossible to analyse the sulfur rank for this polymer, because the greatest sulfur rank predicted in the quantum calculations, was sulfur rank 6. It is likely that sulfur ranks as high as 10 might need to be calculated for the accurate analysis of polymers with such high sulfur loadings, which therefore makes their analysis impossible here, though with further calculations this would be possible. These calculations were not performed here because the supercomputer used did not have sufficient resources to calculate sulfur rank 7 in a reasonable amount of time (72 hours) and at such a high level of theory. A decrease in the level of theory would be required, which would require all of the calculations to be redone. As such, fine tuning of the computational model for higher sulfur ranks will be left to future work.

An additional limitation to be addressed in future work, was that since the computational simulations were centred on a DVB system, the computational data were not transferrable to the analysis of DIB polymers. This could be solved by performing calculations on model systems for each polymer to be analysed, in whichever specific example is of study. It would be convenient for future applications of this analysis, if a generalised calculation method could be produced that was insensitive to the molecular system under scrutiny.

However, even in the absence of calculated data, the sulfur ranks can be qualitatively analysed by the form of their sulfur – sulfur band. It is suggested here that researchers wishing to apply this analysis have two options: they can generate their own computational data to analyse their polymers with, which is time consuming and challenging, but will provide the most accurate results; or they can use a more qualitative approach to analyse the sulfur band, which will be presented shortly. Provided first, is a step-by-step guide for determining the sulfur rank by Raman spectroscopy.

Firstly, a polymer spectrum must be acquired, and if it is present, the 218 cm^{-1} elemental sulfur band must be integrated to find its intensity. This should be done by using a linear baseline to remove the fluorescent background. Second, the obtained area of the 218 cm^{-1} peak must be multiplied by 0.0891 to find the area of the 434 cm^{-1} elemental sulfur peak. The value of 0.0891 was determined from the intensity ratio of the 218 cm^{-1} peak versus the 434 cm^{-1} peak in a pure elemental sulfur spectrum. Third, the obtained area of the 218 cm^{-1} peak must be multiplied by 0.7492 to find the area of the 474 cm^{-1} elemental sulfur peak. The value of 0.7492 was determined from the intensity ratio of the 218 cm^{-1} peak versus the 474 cm^{-1} peak in a pure elemental sulfur spectrum. Fourth, the upper and lower limits of the sulfur – sulfur band in the polymer spectrum must be identified, which in this work, were usually around 350 cm^{-1} and 550 cm^{-1}. From these limits, a linear baseline must be subtracted. Fifth, band deconvolution on the sulfur – sulfur band must be performed using the minimum number of bands, plus two peaks for elemental sulfur: one at 434 cm^{-1} and one at 474 cm^{-1}, the areas of which are now known from step two and three respectively. Typically, an error of ± 1 cm^{-1} on the band centre of the 434 cm^{-1} and the 474 cm^{-1} peaks was permitted in this work, and an error of ± 10 % in their areas was permitted. Sixth, once band deconvolution gives rise to a good mathematical fit with the minimum number of Gaussian bands, the area (the G$_{n,real}$ value), band centre, and FWHM value of each deconvoluted band must be noted. The deconvoluted peaks for elemental sulfur are disregarded. Seventh, a range of Raman shifts for each band must be calculated, where the upper limit of the range is the band centre + (FWHM / 2), and the lower limit is the band centre - (FWHM / 2). Each range should be labelled as Group n, so that each deconvoluted peak has its own distinct group. Note that if one group's band centre occurs within the range of another group, these two groups can be combined into a single group. Eighth, for sulfur rank 2, the computational data in Table 4.5 (which must first be parameterised) must be organised into the groups created in step seven, based on whether the calculated peak's band centre falls within the range of Raman shifts for that group. Where a calculated peak's band centre falls with 5 cm^{-1} of a boundary between two groups, that peak's intensity should

Liam James Dodd

be halved and placed into both groups. Once this sorting process is complete, the intensities contained within each group are summed together, yielding the intensity that sulfur rank 2 provides to each group. Ninth, step eight must be repeated for each sulfur rank, thus obtaining a series of $C_{n,rm}$ values, where C is the summed in intensity of all computationally predicted peaks that occur within group n, for sulfur rank m. Tenth, the following equation must be assembled for each group: $G_{n,real} = r_2C_{n,r2} + r_3C_{n,r3} + r_4C_{n,r4} + r_5C_{n,r5} + r_6C_{n,r6}$ where $G_{n,real}$ is the intensity of the group from the experimental data (step six), $C_{n,rm}$ is the intensity that sulfur rank m should contribute to group n (steps eight and nine), and r_m are the proportional populations of sulfur ranks 2, 3, 4, 5, and 6 respectively. This should lead to several simultaneous equations, where the number of equations is equal to the number of groups. The r_m value for a given sulfur rank is the same in each equation. Eleventh, the simultaneous equations created in step ten must be solved to obtain preliminary r_m values. To simplify this process, one can consider r_5 and r_6 to be negligible, such that only three simultaneous equations need be solved. If the computational data used in this study were completely accurate, then these simultaneous equations would give accurate r_m values. Since this is not the case, they give preliminary r_m values that can be improved in the next step. Twelfth, the following equation for each group must be assembled: $G_{n,predicted} = r_2C_{n,r2} + r_3C_{n,r3} + r_4C_{n,r4} + r_5C_{n,r5} + r_6C_{n,r6}$ where $G_{n,predicted}$ is the intensity of the group calculated from the equation, $C_{n,rm}$ is the intensity that sulfur rank m should contribute to group n (steps eight and nine), and r_m are the proportional populations of sulfur ranks 2, 3, 4, 5, and 6 respectively. This should lead to several simultaneous equations, where the number of equations is equal to the number of groups. The r_m value for a given sulfur rank is the same in each equation. Thirteenth, the r_m values must be adjusted in a trial and error iterative fashion until the values for $G_{n,predicted}$ are as close as possible to the corresponding $G_{n,real}$ values. This process is complete when a minimum difference between the $G_{n,real}$ values and the $G_{n,predicted}$ values is achieved, and none of the r_m values are negative, nor nonsensical (for example r2 > r3 < r4 implies that sulfur rank 3 has a lower population than sulfur rank 2 and sulfur rank 4, which makes no logical sense). Fourteenth, the r_m values should be expressed as percentages of the sum of all r_m values. The percentages obtained indicate what percentage each sulfur rank makes of the whole population. If desired, the average sulfur rank can easily be calculated from these percentage populations.

Admittedly, the in-depth analysis of the sulfur rank is time consuming and difficult, however, this Raman analysis has also opened up the possibility of an extremely rapid and convenient qualitative analysis of the sulfur rank. Observing Figure 4.21, Figure 4.22 and Figure 4.24, several general conclusions can be made about the sulfur – sulfur band. According to Figure 4.22, the different groups in the band do roughly correspond to different sulfur ranks. Group 5 mostly receives contributions from rank 2, with some smaller contributions from rank 5. Group 4 receives significant contributions from all sulfur ranks except rank 2. Group 3 receives strong contributions from rank 6, however rank 6 should be proportionally uncommon according to Boltzmann theory, so intensity in the group 3 region can be assigned to rank 3 and 5, with lesser contributions from rank 2 and rank 4. Group 1,2 receives strongest contributions from rank 4, with rank 5 and 6 contributing significantly as well, and rank 2 and 3 providing only small contributions.

To summarise, intensity in the group 5 region can be assigned to the presence of sulfur rank 2, whereas intensity in the group 1,2 region can be assigned to longer sulfur ranks of 4 and upward, whilst intensity in the group 4 region can be assigned to all sulfur ranks besides rank 2, which makes group 4 a useful comparison to group 1,2 and group 5. These assignments can be used to qualitatively compare the sulfur ranks of the polymers, as shown in Figure 4.24. Since this qualitative analysis does not require calculated data, it is adaptable to systems other than polymers based upon DVB. Observing Figure 4.24, the aforementioned assignments can be used to make qualitative statements about the sulfur ranks. Comparing across DVB30-S70 to DVB50-S50 to DVB70-S30, it can be seen that as the

Liam James Dodd

proportion of crosslinker increases, the intensity of group 5 (centred at roughly 520 cm^{-1}) increases, suggesting a greater population of rank 2 sulfur chains. Meanwhile, as the proportion of crosslinker in the polymer increases, the intensity of groups 1 (centred at roughly 415 cm^{-1}) and 2 (centred at roughly 435 cm^{-1}) falls in comparison to group 4, indicating that sulfur ranks of 4 and higher make up a smaller proportion of the population as the proportion of crosslinker is increased. Thus, Raman analysis gives an extremely simple and convenient way of qualitatively analysing which sulfur ranks are present in a polymer.
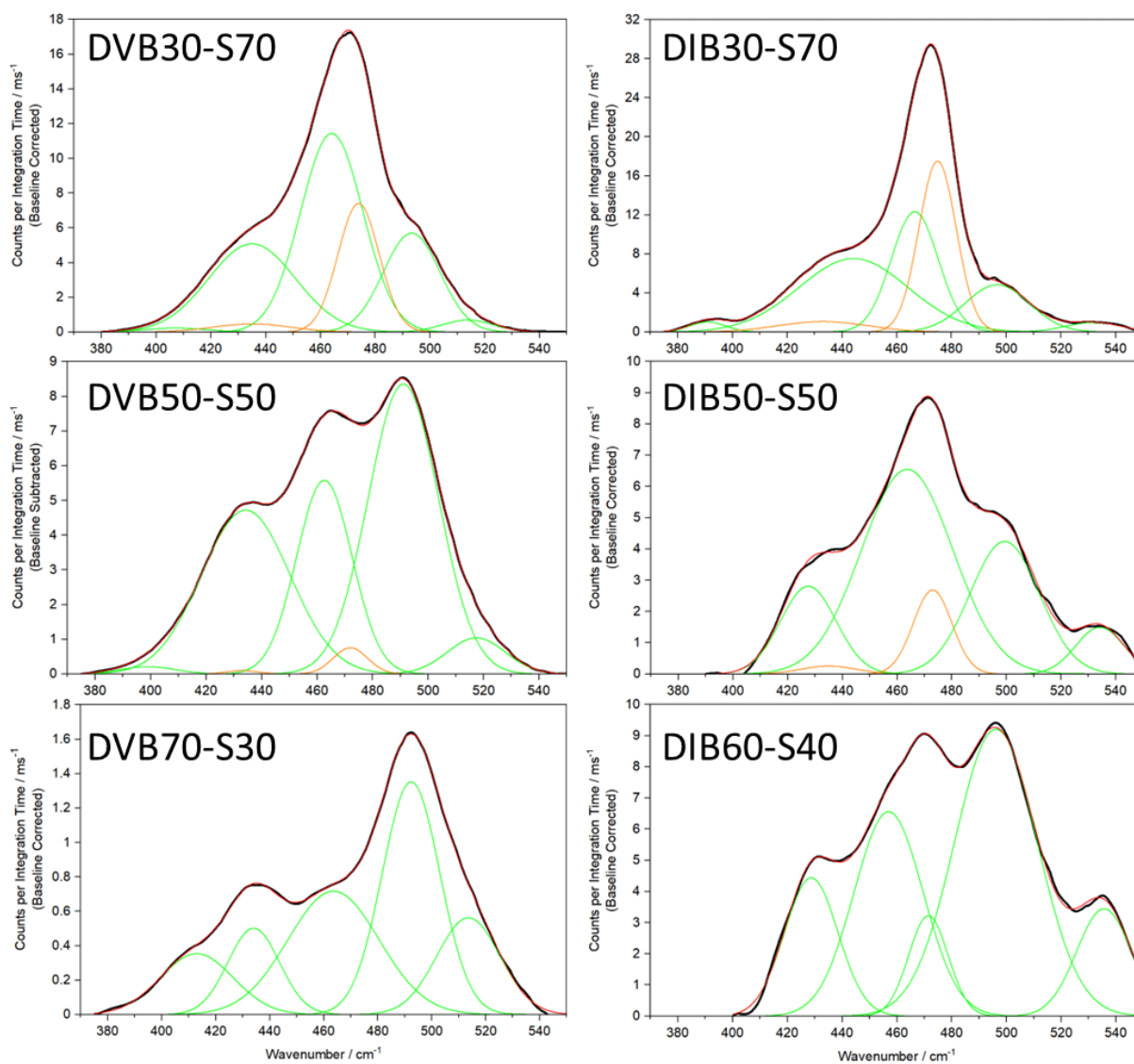

Figure 4.24: Band deconvolutions of the Raman spectra of the sulfur – sulfur band region for different inverse vulcanised polymers. Note that DIB60-S40 was obtained in place of DIB70-S30 because the sulfur – sulfur band of DIB70-S30 did not appear clearly through the fluorescent baseline. Peaks resulting from elemental sulfur are coloured in orange, while peaks in green are the Gaussians assigned to polymer sulfur – sulfur vibrational modes. The black line is the linear baseline corrected experimental spectrum, while the red line is the sum of the green and orange Gaussians.

Besides the ease of application, this qualitative analysis has one further advantage over the explicit method: it is not limited to polymers of DVB. As can be seen in Figure 4.24, the same general trends that were observed for DVB polymers, also hold true for DIB polymers, though the Raman shift ranges of the groups are shifted in comparison to DVB, a potential reason why the in-depth analysis failed.

Liam James Dodd

Regardless, it can be seen in the DIB spectra, that as the proportion of crosslinker is increased, the groups in the lower Raman shift end of the spectra (below 450 cm^{-1}), decrease in intensity compared to the higher Raman shift end of the spectrum (above 490 cm^{-1}). According to the aforementioned principles of qualitative analysis, this indicates an increasing presence of rank 2 chains in comparison to rank 4 and higher chains as the proportion of crosslinker is increased, which holds true to both theory and the basis of this analysis. Thus, even though Raman analysis cannot yet provide explicit information on the sulfur rank of polymers other than those of DVB, it appears that Raman analysis can offer qualitative insight into any polymer's sulfur ranks, provided a sulfur – sulfur band can be isolated.

4.12. Homogeneity Analysis

One very rapid, simple, and valuable application that Raman spectroscopy may see in the field of inverse vulcanisation, is assessment of the homogeneity of polymers, which is not easily observed by other bulk analysis techniques. This is because Raman analysis focuses its probe on a very small spot size (60 µm in the case of the i-Raman EX), and so can be used for analysing different locales. By comparing the different spectra obtained in different regions of the polymer, the homogeneity of the sample can be assessed. To this end, DIB30-S70 and DVB50-S50 were synthesized by the aforementioned standard method, but this time they received only 200 rpm stirring, and a few minutes after the reaction mixture became a single phase, stirring was ceased entirely. This allowed the denser phases to sink toward the bottom of the polymer, creating an intentional inhomogeneity, that was analysed by Raman analysis, wherein the spectrum of the top and the bottom of the polymers was acquired (Figure 4.25).

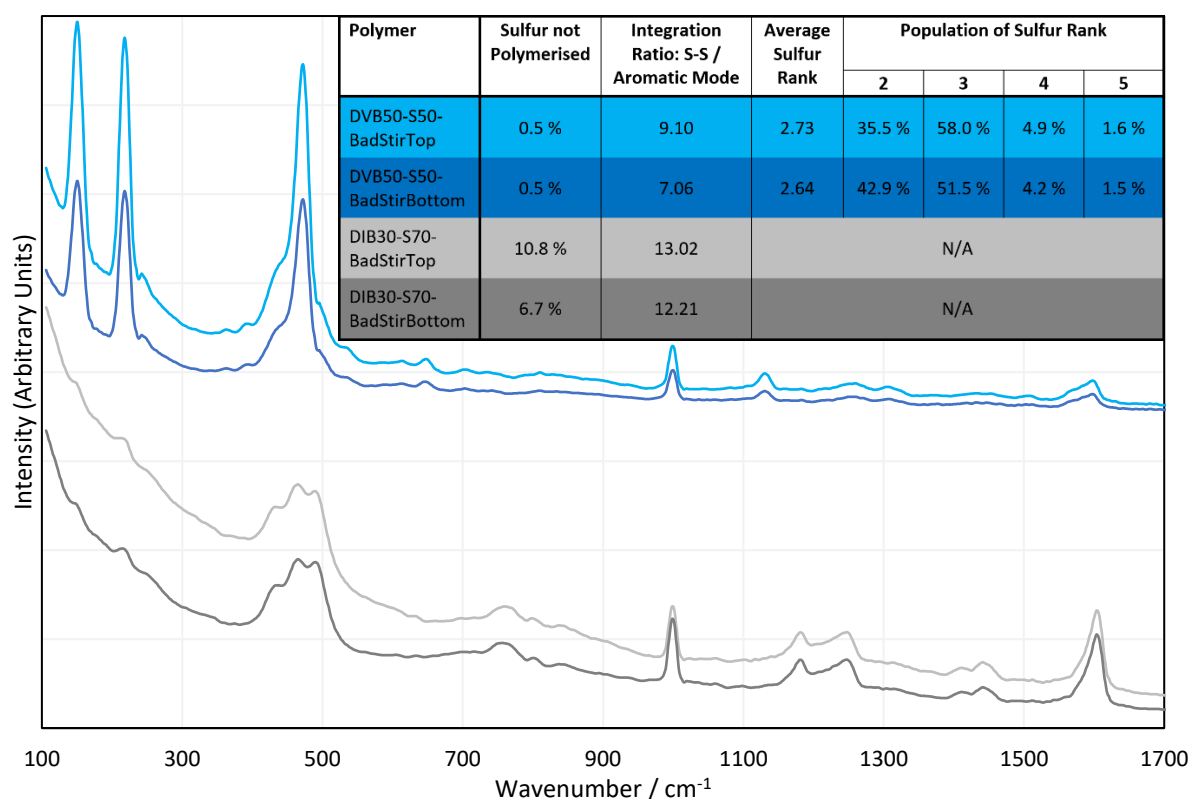| Polymer	Sulfur not Polymerised	Integration Ratio: S-S / Aromatic Mode	Average Sulfur Rank	Population of Sulfur Rank			
				2	3	4	5
DVB50-S50-BadStirTop	0.5 %	9.10	2.73	35.5 %	58.0 %	4.9 %	1.6 %
DVB50-S50-BadStirBottom	0.5 %	7.06	2.64	42.9 %	51.5 %	4.2 %	1.5 %
DIB30-S70-BadStirTop	10.8 %	13.02	N/A				
DIB30-S70-BadStirBottom	6.7 %	12.21	N/A				

Figure 4.25: The 1064 nm Raman spectra of the top and bottom faces of inhomogeneous polymers of DVB (700 ms integration time) and DIB (500 ms integration time) collected at 430 mW laser power, as well as information about the different faces of the polymers, derived from their spectra. Offsets have been applied to the intensities.

Liam James Dodd

As can be seen in Figure 4.25, there are clear differences between the spectra of the top and bottom faces of the polymers, even though there was no visibly distinguishable difference. For both the DVB polymer and the DIB polymer, there is a greater fluorescent background in the top face spectra, which suggests Raman analysis can easily give a pass-fail assessment of whether the different regions of the same polymer are homogeneous. This inhomogeneity analysis can be taken further: it is easy to analyse the percentages of dark sulfur in these top and bottom spectra, allowing for the determination of whether there are different amounts of elemental sulfur in the different regions of the polymer. Another easy analysis that can be performed, is to integrate the sulfur – sulfur band in comparison to the aromatic modes, which can give a more quantitative estimate of how much organic versus sulfurous component exists in each region of the polymer. Note that when integrating the sulfur – sulfur region, contributions from elemental sulfur were not counted. The 1000 cm^{-1} aromatic peak was chosen to represent the integration of the aromatic component. Finally, it is possible for the DVB polymer, to extract the sulfur rank from the top and bottom spectra, to indicate if the sulfur rank varies by region. The results of these analyses can be seen in Figure 4.25.

These results suggest that the top of both polymers contained more sulfur than the bottoms. Though there is no statistical difference between the dark sulfur content of the top and bottom of the DVB polymer, all other data supports the conclusion that the top of these polymers are richer in sulfur. The DIB polymer indicated a greater presence of elemental sulfur in its top face compared to its bottom, and both polymers showed that the integration of their sulfur – sulfur band compared to that of their 1000 cm^{-1} aromatic band was greater on the top face than the bottom face. Additionally, the sulfur rank data supports this conclusion that the top face of the polymer is more sulfur rich than the bottom, as the average sulfur rank is higher for the top face of the DVB polymer, and shows higher populations of sulfur ranks 3, 4 and 5, whilst showing less sulfur rank 2 in comparison to the bottom face. Therefore, these data suggest that Raman spectroscopy is effective in showing the differences in homogeneity between different regions of inverse vulcanised polymers.

It is not recommended that the integration ratio of the sulfur – sulfur band vs the aromatic region is used as a quantitative measure of the sulfur content of the polymers. This is because the intensities of each different sulfur rank's peaks are not equal, so changes in the population of sulfur ranks that come naturally with varying sulfur content will cause non-linear changes in the overall intensity of the sulfur – sulfur band. Qualitative analysis of the sulfur content by this method of comparing the integration ratio should be acceptable however; a conclusion which is supported by Figure 4.15a, which demonstrates that the sulfur – sulfur band intensity increases in comparison to the aromatic band, as the content of sulfur in the polymer is increased. Theoretically it would be possible to create a calibration curve that relates the integration ratio of the sulfur – sulfur and aromatic bands to the sulfur content, and then use this to determine the sulfur content of new inverse vulcanised polymers, but this method has two drawbacks. Firstly, the polymer would have to be of the same crosslinker as the one used in the creation of the calibration curve, which means a new calibration curve would need to be created for every polymer formed from a different crosslinker or combination of crosslinkers. Secondly, the creation of this calibration curve requires some other means of determining the sulfur content, such as combustion microanalysis, at which point, it would be more sensible to use combustion microanalysis to determine the sulfur content of the analyte polymer, and circumvent the calibration curve, cutting out the accumulated error from the additional step of data manipulation.

4.13. Reaction Tracking

Another way in which Raman Spectroscopy may be applied in the field of inverse vulcanisation is in tracking the progression of reactions. Many Raman spectrometers can be fitted with long lens attachments that allow the Raman probe to collect spectral data while positioned at a sizeable

Liam James Dodd

distance from a sample of interest. This would allow the sampling of real time data from a reaction that is in progress. Although this equipment was not available here, it was still possible to track the progress of the curing step of inverse vulcanisation. Six batches of DVB50-S50 were synthesized by the aforementioned method used for the second batch of polymers, but this time, the duration of the curing step was controlled. DVB polymers, cured for different amounts of time were then analysed by 1064 nm Raman spectroscopy, the results of which are given in Figure 4.26.
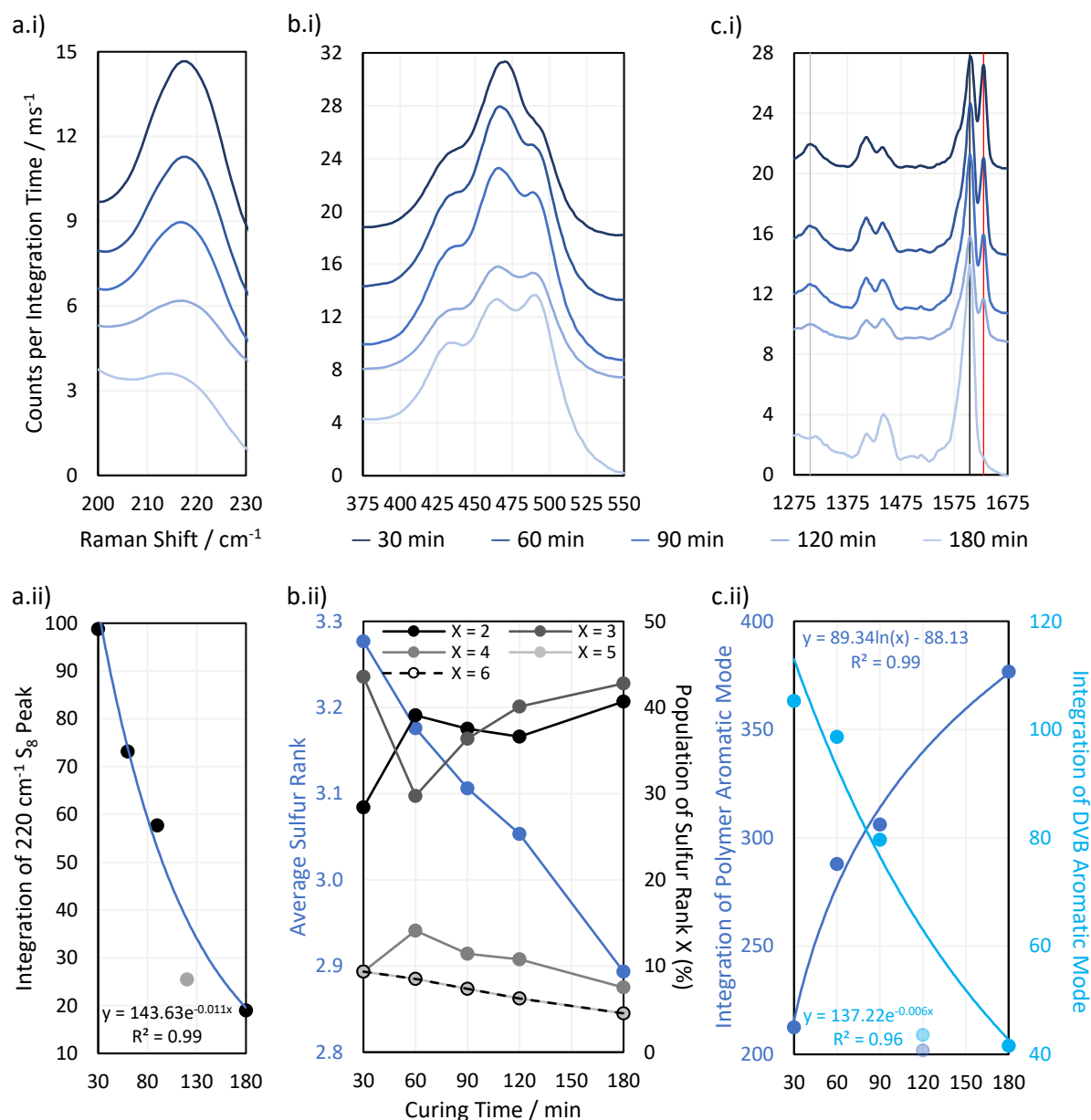

Figure 4.26: Regions of interest from the 1064 nm Raman spectra of DVB50-S50-τ polymers, where τ is the time in minutes that the polymers were left to cure, as well as accompanying analyses of the spectral regions of interest. a.i shows an elemental sulfur peak, b.i shows the sulfur – sulfur band, and c.i shows the aromatic region. a.ii shows the integration of the 220 cm⁻¹ sulfur peak with curing time with an exponential fit, b.ii shows the changes in sulfur rank with curing time, and c.ii shows the integration of the polymer and DVB aromatic modes with curing time, with a logarithmic and exponential fit, respectively. Samples were measured soon after removing them from the heat source, but long enough afterward that they had cooled to room temperature. Note that for a.i, b.i, and c.i, the intensities have been offset by arbitrary values for clarity.

Liam James Dodd

Figure 4.26 indicates that as predicted, the polymers show several changes in their spectra as the curing step proceeds. Firstly, a peak at 1630 cm^{-1} decreases in intensity as curing proceeds, to the point where it is no longer present in the fully cured polymer (Figure 4.26c.i). This peak is assigned to the aromatic signal of unreacted DVB. Therefore, the intensity of this peak decreases as DVB is consumed, whilst the aromatic signal of reacted DVB (1605 cm^{-1}) increases over the course of the reaction. Thus, the intensities of peaks associated with reacted DVB and unreacted DVB can be used a measure The 1305 cm^{-1} peak which decreases in intensity is also assigned to unreacted DVB, though its lower initial intensity makes it a less attractive candidate for reaction monitoring.

The depletion of elemental sulfur signals seen at Raman shifts below 300 cm^{-1} can also be used to track the reaction (Figure 4.26a.i). However, since the low Raman shift end of the spectrum seems to be the most prone to suffering a fluorescent background, there could be an additional error in measuring the intensity of these signals, thus, it may be more accurate to use higher Raman shift signals. It has been identified previously in this work that many polymers do still contain elemental sulfur in their fully cured state, so it cannot always be expected that the elemental sulfur signals will disappear in their entirety, but they can still be a useful measure of the reaction's progress. The elemental sulfur signals can also provide a measure of how much elemental sulfur remains as curing time progresses, which in itself is a point of interest.

Most importantly, Figure 4.26b.i shows that the sulfur – sulfur region of the polymers changes significantly as the curing step progresses. As previously mentioned, intensity at about 495 cm^{-1} is indicative of sulfur rank 2, and intensity at Raman shifts below 450 cm^{-1} is indicative of longer sulfur ranks. Thus, Figure 4.26b.i indicates that as the curing step progresses, there is a loss of longer sulfur chains, and an increase in the proportion of shorter sulfur chains.

This may be explained by the fact that when elemental sulfur is heated to higher temperatures in its molten state, longer sulfur homopolymer chains will form, much longer than two sulfur atoms. These homopolymers are what initially react with crosslinker units, forming an early-stage structure where crosslinking units are connected by longer chains of sulfur atoms. Then during the curing step, the polymer structure progresses toward its thermodynamic minimum, which entails rearranging the structure and fully crosslinking by reacting any leftover vinyl bonds (Figure 4.26c.i). This can be done by breaking longer sulfur chains and using some of their sulfur atoms to form new crosslinks, such that longer sulfur chains are sacrificed in order to form more shorter chains, which can be as short as rank 2. Thus, as the curing step proceeds, the initially present longer chains decrease in population as the shorter chains increase in population.

This conclusion is supported by Figure 4.26b.ii which, shows how the average sulfur rank and the populations of the different sulfur ranks, obtained by the aforementioned analysis method, change with time. Figure 4.26b.ii shows that as the curing time increases, the average sulfur rank decreases, as expected. Figure 4.26b.ii also shows a steady decline in the populations of sulfur ranks 4, 5, and 6, while sulfur ranks 2 and 3 increase in population, particularly sulfur rank 3, in line with the Boltzmann distribution. Initially sulfur rank 2 increases rapidly from 30 min to 60 min of curing, but then decreases, which may be due to sulfur atoms being added to rank 2 chains to convert them into rank 3, the population of which was simultaneously increasing.

It is worth noting that the data in Figure 4.26b.ii may be less accurate at the shorter curing times, because sulfur ranks longer than 6 may have been present, and the current computational data cannot take into account sulfur ranks longer than this. Such an inaccuracy might explain why the data in Figure 4.26b.ii for curing time 30 min shows difficult to explain changes in the populations of the sulfur ranks.

Liam James Dodd

4.14. DIB Case Study

In order to prove that Raman spectroscopy can have useful applications outside of the proof-of-concept examples already mentioned, Raman analysis was used to analyse inverse vulcanised polymers of DIB. DIB polymers have been observed to have different properties depending on the reaction temperature and curing time. For example, when DIB polymers are synthesized at high temperature (180 °C), they rapidly vitrify into a hard, high T_g glass. However, if they are cured for longer, the T_g reduces, and the DIB polymers can become more like a viscous, sticky liquid.

As such, Raman spectroscopy was employed to explore the reasons for these observations. DIB50-S50 polymers were synthesized by the general method described before, but this time they were reacted at either 135 °C or 180 °C, and then either not cured at all, or cured at 135 °C for 2 hour or overnight. This gave the following notation: DIB50- S50-TγΔ, where γ is the temperature of reaction in °C, and Δ is the curing time of either 0 hours, 2 hours, or overnight. These polymers were subsequently analysed by Raman spectroscopy, the results of which can be seen in Figure 4.27.
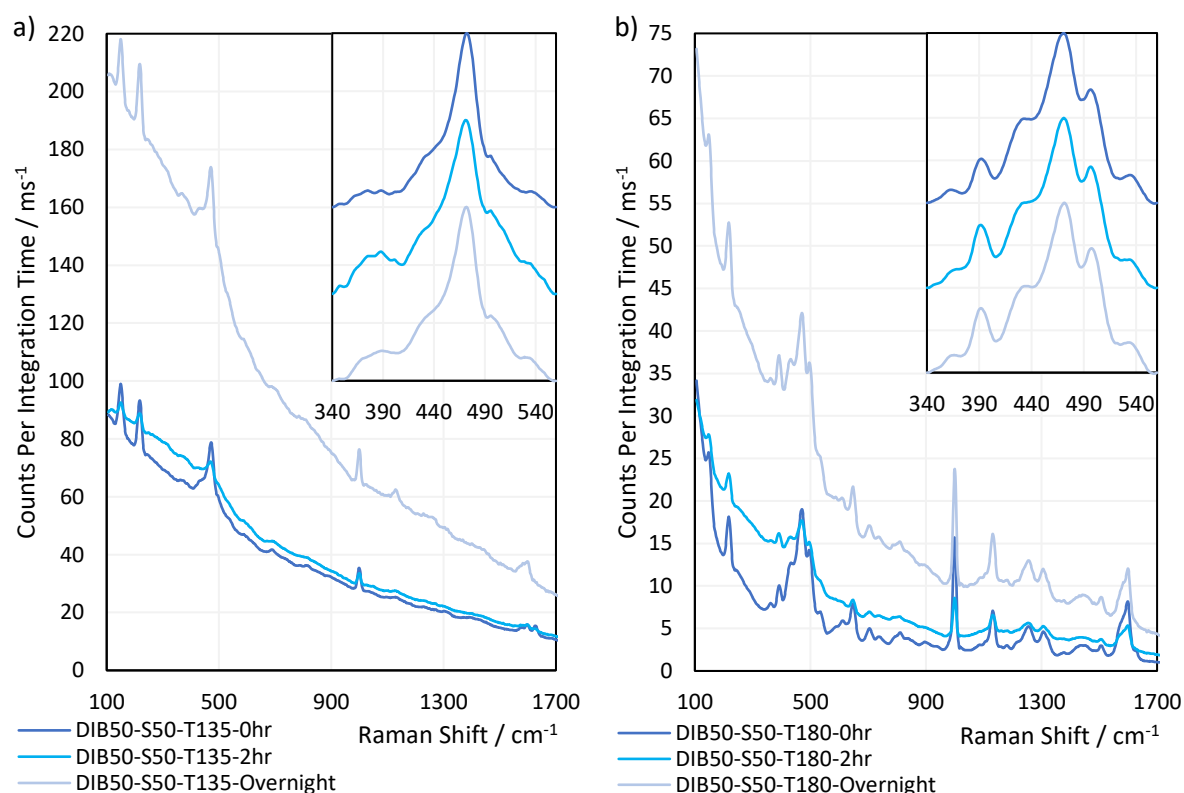

Figure 4.27: The Raman spectra of DIB polymers, synthesized and cured under different conditions. All spectra were obtained under a laser power of 430 mW (100%), with the following integration times: DIB50-S50-T135-0hr 500 ms; DIB50-S50-T135-2hr 500 ms; DIB50-S50-T135-Overnight 200 ms; DIB50-S50-T180-0hr 1500 ms; DIB50-S50-T180-2hr 1500 ms; DIB50-S50-T180-Overnight 650 ms. The inset figures show the sulfur – sulfur bands of the spectra, which have had their intensities linearly baseline corrected and normalised with offsets.

As can be seen in Figure 4.27, there is a marked difference between the spectra of DIB polymers synthesized at 135 °C and 180 °C. One of the most noticeable differences is that polymers synthesized at 180 °C show much less fluorescence than polymers synthesized at 135 °C. This influenced the integration times used to obtain the spectra, as the polymers synthesized at 180 °C were obtained with much longer integration times, as there was less concern of the signal swamping out the detector

Liam James Dodd

with the fluorescent background. One study suggested that the colour of some polymers may result from the formation of DT rings as terminal functionalities. Their work suggested that exo-olefins like DIB can be prone to the formation of these terminal functionalities, and that prolonged heating of such polymers, such as that experienced during the curing step, can result in greater populations of 1,2-dithiole-3-thione termination products.[4.24] Since these DT rings structures absorb visible light, they could be responsible for polymer fluorescence, and so could explain why DIB polymers that are cured for longer, show greater fluorescent backgrounds. This would also suggest that when DIB polymers are synthesized at high temperature, the reaction pathway that produces 1,2-dithiole-3-thione products, is suppressed or outcompeted. Thus, in the future, the behaviour of 1,2-dithiole-dithiones in relation to this Raman analysis should be investigated through a combination of experimental and computational methods.

Interestingly, for both the polymers synthesized at 135 °C and 180 °C, a two-hour curing time results in a significant reduction in Raman signal through the fluorescent background. This is surprising, as it suggests that fluorescence increases and then decreases as the curing step proceeds, though it is difficult to explain this without detailed understanding of the origin of the fluorescence. The intensity of the aromatic signals in comparison to the sulfur – sulfur band does not change much over the course of the reaction, which suggests that the proportion of crosslinker does not change much as curing proceeds, though this conclusion is complicated by the fact that different sulfur ranks give different intensities to the sulfur – sulfur band, meaning the intensity of the sulfur – sulfur band will change as a function of sulfur rank and not just the crosslinker proportion. For this reason, Raman analysis is not recommended for quantitatively assessing the proportion of crosslinker in a polymer.

Observing Figure 4.27 the intensity at about 500 cm^{-1} increases as the curing process proceeds, which indicates an increase in the proportion of rank 2 chains. This conclusion agrees with previous conclusions from the DVB curing experiments. These data suggest that as the curing step proceeds, longer sulfur rank chains are consumed and broken down, and the sulfur atoms are distributed into more shorter sulfur rank chains. Note that the band deconvolution data shown in Table 4.6 does not at first glance, seem to support this conclusion, but this is because the Gaussians are not centred on 500 cm^{-1} and also have varying FWHM values. This conclusion is also supported by the fact that Figure 4.27 shows that the intensity at about 380 cm^{-1} goes up as the curing time increases, and this may be due to an increase in the number of rank 3 chains, in accordance with Figure 4.22. Overall, the data in Figure 4.27 suggests that the sulfur rank decreases as expected as curing proceeds.

Figure 4.27b shows that DIB polymers synthesized at 180 °C are drastically different to analogous polymers synthesized at 135 °C. For instance, band deconvolution of the sulfur – sulfur band indicated that DIB polymers synthesized at 135 °C could have the sulfur – sulfur band accurately fitted by only five Gaussian peaks (excluding those for elemental sulfur) whereas polymers synthesized at 180 °C needed six Gaussian peaks to accurately describe their sulfur – sulfur band (again, excluding the peaks for elemental sulfur). It seems that in Figure 4.27b, the peaks at about 460 cm^{-1} are weaker than the 460 cm^{-1} peaks in Figure 4.27a, and so the other peaks in Figure 4.27b seem stronger in comparison to the 460 cm^{-1} peak, than the analogous peaks do in the Figure S54A spectra. The 460 cm^{-1} peak may receive contributions from all sulfur ranks, much like Group 4 in Figure 4.22, and if this is the case, it suggests that there may be a higher proportion of longer sulfur ranks present. Figure 4.22 helps to explain this justification, as it suggests that most sulfur ranks contribute very similar intensities to Group 4, but progressively longer sulfur ranks contribute progressively greater intensities outside of Group 4. According to Figure 4.22, the 392 cm^{-1} peak may correspond to sulfur rank 3, and according to the band deconvolution data in Table 4.6, this peak gains intensity as the curing proceeds, again supporting the previous conclusion that he sulfur rank shortens with increasing curing. Additional

Liam James Dodd

evidence to this is the gain in intensity at 498 cm^{-1} and the gain in intensity at 532 cm^{-1} as curing proceeds. Thus, it can be concluded that the longer the curing time, the shorter the sulfur rank becomes, and that, the higher the initial reaction temperature, the higher the sulfur rank, which is in line with the well-established theory that elemental sulfur forms longer homopolymer chains at higher temperatures, and since it is these homopolymers that initially connect the crosslinkers together, a higher sulfur rank results. Further computational studies may be required to fully understand why the sulfur – sulfur band of DIB polymers synthesized at low and high temperature are so different.

Table 4.6: Band deconvolution data for DIB polymers synthesized under different conditions. Values in light blue text are for elemental sulfur.

Polymer	Centre Gravity / cm^{-1}	Normalised Area	FWHM / cm^{-1}
DIB50-S50-T135-0hr	378.45	0.2460	38.54
	441.09	1.0000	45.27
	464.90	0.6329	22.70
	493.72	0.7515	39.65
	535.39	0.1317	24.10
	433.00	0.0789	66.78
	474.41	0.6371	16.45
DIB50-S50-T135-2hr	383.73	0.4285	44.06
	428.88	0.3276	29.03
	462.28	1.0000	36.38
	500.25	0.6316	37.12
	536.08	0.1328	24.01
	433.00	0.0321	57.21
	473.18	0.2684	16.96
DIB50-S50-T135-Overnight	384.78	0.4249	39.91
	436.13	0.9077	40.59
	465.89	1.0000	28.18
	499.13	0.7110	32.37
	534.01	0.1717	23.03
	433.00	0.0592	57.93
	474.09	0.4880	17.05
DIB50-S50-T180-0hr	363.89	0.0688	20.68
	391.64	0.1903	17.56
	431.25	0.6908	34.42
	465.42	1.0000	29.01
	497.92	0.6920	25.13
	532.90	0.1645	23.09
	435.00	0.0247	36.62
	474.85	0.2073	16.30
DIB50-S50-T180-2hr	367.91	0.1115	23.29
	391.66	0.2742	17.61
	431.03	0.7371	36.59
	465.52	1.0000	30.30
	498.30	0.7382	24.83
	531.42	0.1873	25.15
	435.00	0.0299	25.07
	474.55	0.2478	17.05
DIB50-S50-T180-Overnight	365.86	0.1029	22.00
	391.59	0.3026	18.26
	431.19	0.7514	36.02
	465.36	1.0000	29.66
	498.64	0.7776	24.30
	532.09	0.1936	23.41
	433.00	0.0325	24.55
	474.93	0.2652	16.55

Liam James Dodd

4.15. Conclusions

Raman spectroscopy has been shown to be a valuable technique in the analysis of inverse vulcanised polymers. It was found that inverse vulcanised polymers fluoresce, and this fluorescence must be avoided in order to obtain a Raman signal. Even stray ambient light may be sufficient to incite fluorescence so Raman analyses must be carried out in the dark. Several Raman techniques were found to be capable of providing well-defined polymer signals, including 1064 nm Raman spectroscopy, FT-Raman spectroscopy, and Kerr-Gated Raman spectroscopy for the most highly fluorescent samples. UV Raman was unsuitable due to the polymers' high UV absorption, which could make them useful as UV blocking materials. 488 nm Raman spectroscopy showed promise but needed optimisation to avoid laser damage.

Raman spectroscopy was shown to easily quantify unpolymerized elemental sulfur in the polymers in a rapid, convenient, and non-destructive way, even if the sulfur is amorphous and therefore undetectable by DSC and PXRD. Thus, Raman spectroscopy suggests that polymers which were otherwise expected not to contain elemental sulfur, do in fact have this impurity. Raman spectroscopy was also able to assess the homogeneity of polymers, which is not so readily accessible by other techniques. Raman spectroscopy also successfully tracked the progress of a reaction, though in the future this process could be improved by the use of long lens attachments, allowing for easy, real-time, *in situ* measurements. Most importantly, Raman spectroscopy was able to determine not only the average sulfur rank of a polymer, but also the distribution of the population of different sulfur ranks present, an insight that cannot be obtained by any other means at this time, and one that has tremendous impacts on the polymer properties. Quantitative analysis of the sulfur rank was possible, but needs further work to become applicable to a wider variety of polymers. This stems from the limitations of the quantum calculations used to assign the spectra. These calculations need to be performed for longer sulfur ranks and a broader range of crosslinker molecules in the future. Even so, a broadly applicable qualitative analysis method was developed for drawing conclusions about the sulfur rank of any inverse vulcanised polymer, which is faster and more convenient than the quantitative analysis method.

Future work may look toward finding more techniques that can circumvent the fluorescence of inverse vulcanised polymers, as although Kerr-gated Raman spectroscopy was capable of obtaining fluorescence free spectra for polymers of sulfur and dicyclopentadiene or squalene where other techniques could not, it is not a widespread nor easily accessible technique. Nevertheless, Kerr-gated Raman should receive more attention in the future, as it is the only technique that this work found to be capable of providing Raman spectra of highly fluorescent inverse vulcanised polymers, a merit that cannot be overlooked. The core focus of the future work should be placed upon the computational aspect of this analysis. Because the computations performed here focused solely on divinylbenzene, the results were not entirely applicable to other polymer systems, preventing quantitative analysis of the sulfur rank in polymers other than divinylbenzene. If such calculations could be performed for more model systems, or even better, a generally applicable system, then all polymers would be subject to quantitative analysis of their sulfur rank, rather than just qualitative analysis. Further aspects for computational chemistry to observe, would be calculations for higher sulfur ranks, allowing quantitative analysis of polymers with greater sulfur contents. To this end, it would also likely be worthwhile investigating more reliable methods of parameterisation, as it is recognised here that the strategy used in this work may limit how well the parameterisation extends to molecules that were not used to generate the parameterisation model. Finally, something that was not considered here, is whether computational chemistry could provide insights on the carbon–sulfur bonds: the connection point of organic and inorganic in these polymers, and what information this could hold. It is advocated

Liam James Dodd

here that Raman spectroscopy should become a widespread analysis technique for inverse vulcanised polymers, which may become preferred for publication of novel inverse vulcanised.
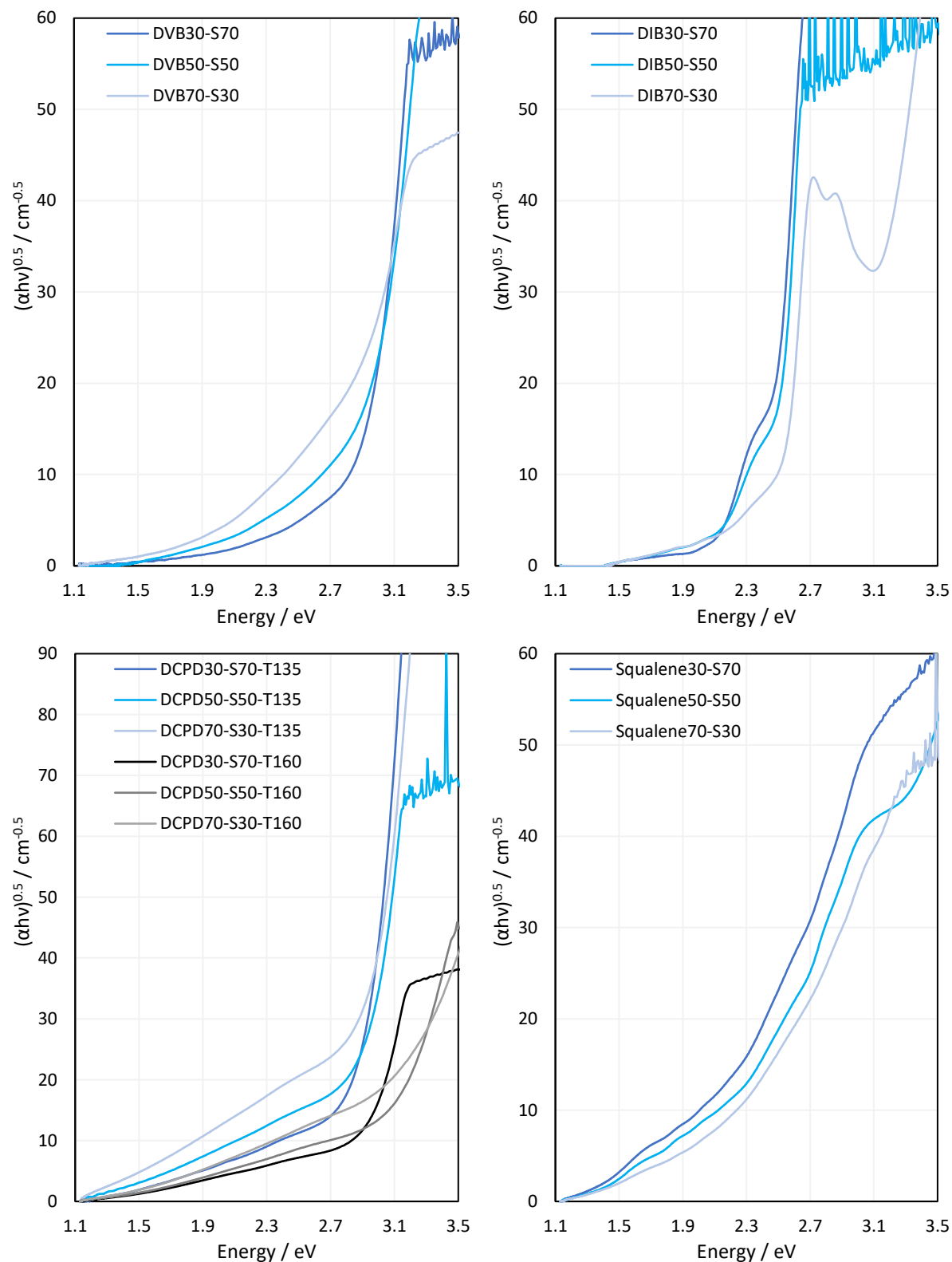
4.16. Appendices

4.16.1. Tauc Plots

Figure 4.28: Tauc plots for inverse vulcanised polymers in the form of thin films.

Liam James Dodd

4.16.2. Fluorescence Spectra

Figure 4.29: Fluorescence emission scans at different excitation wavelengths for different DVB inverse vulcanised polymers.
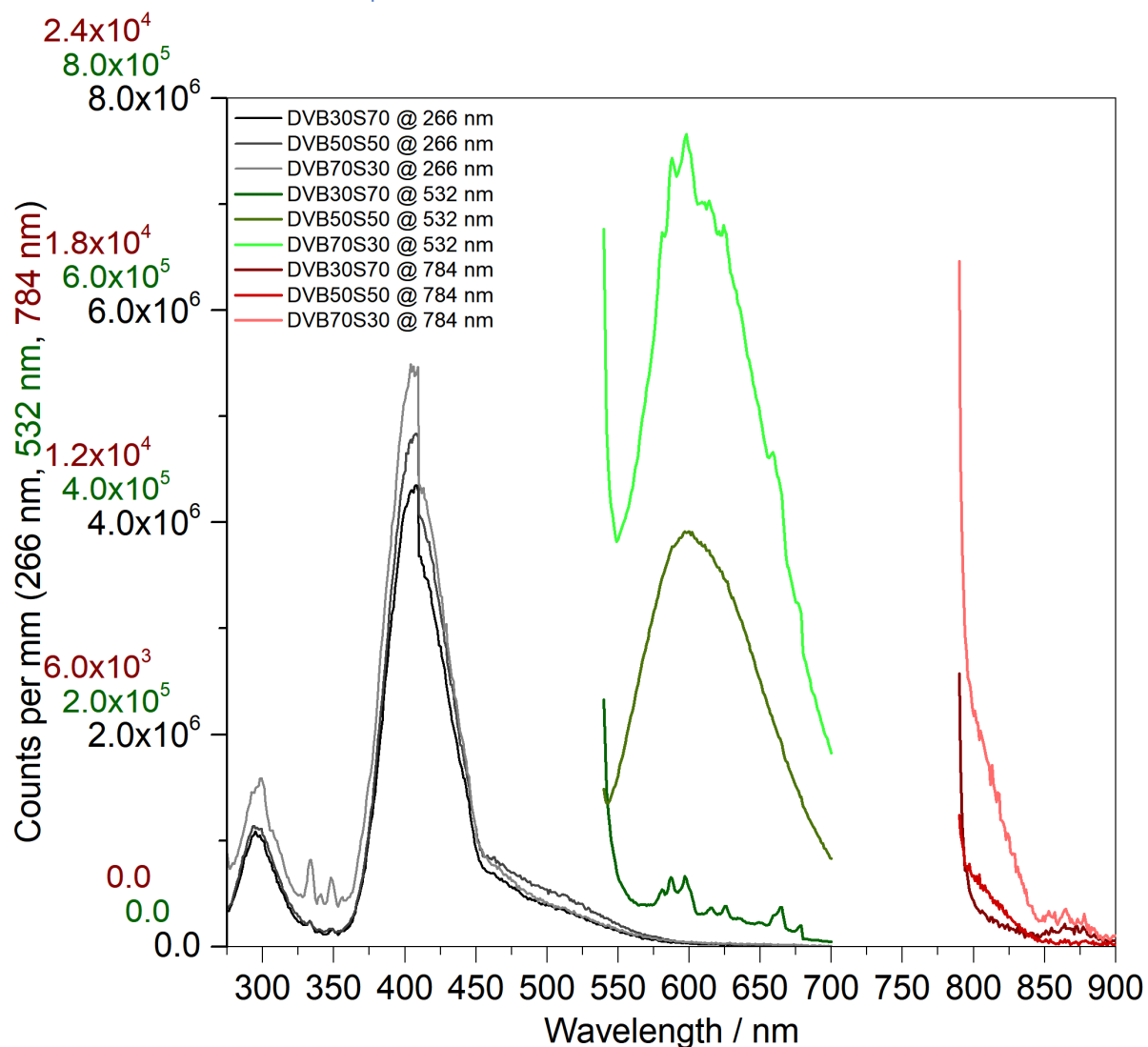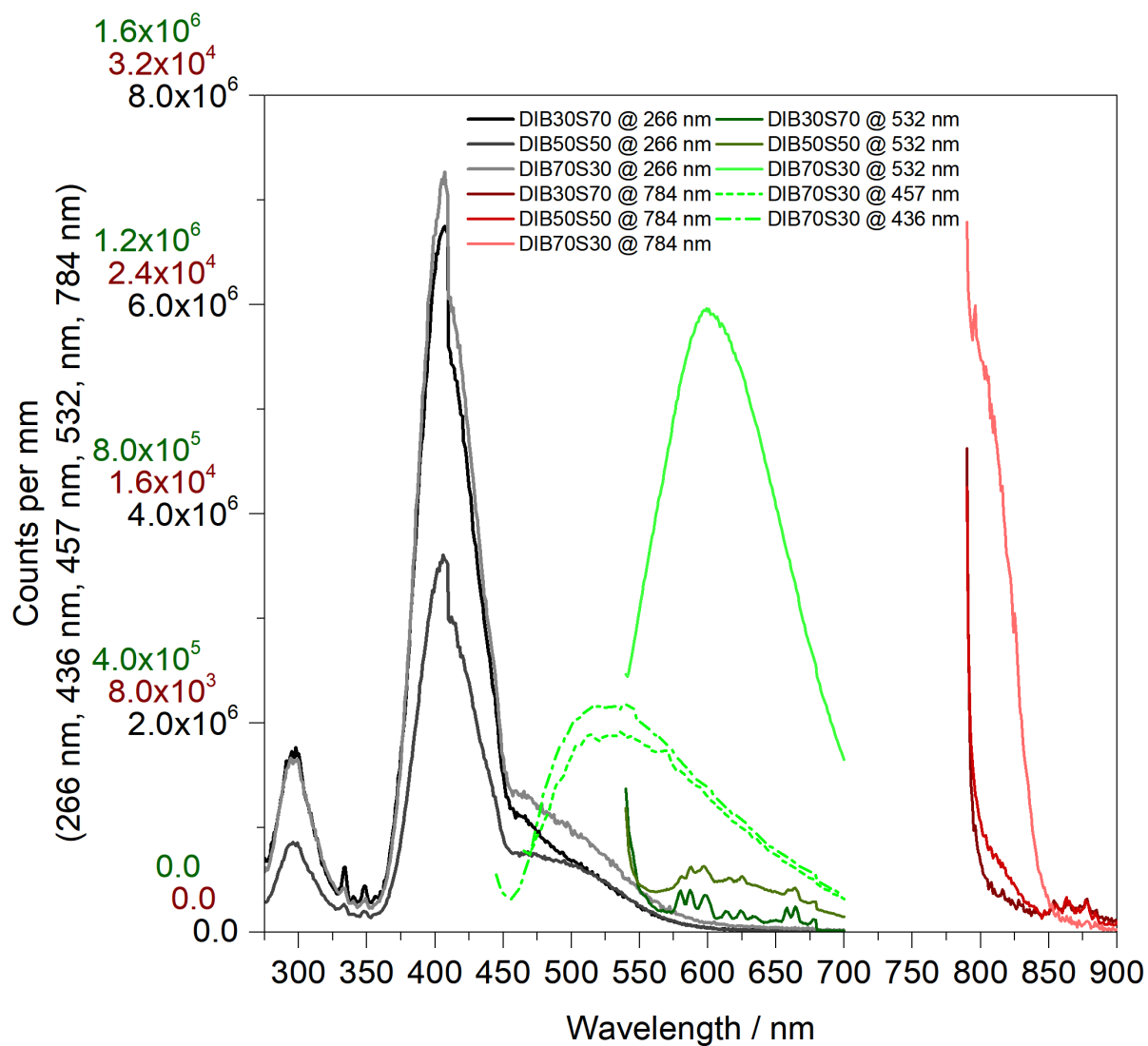
Liam James Dodd

Figure 4.30: Fluorescence emission scans at different excitation wavelengths for different DIB inverse vulcanised polymers.
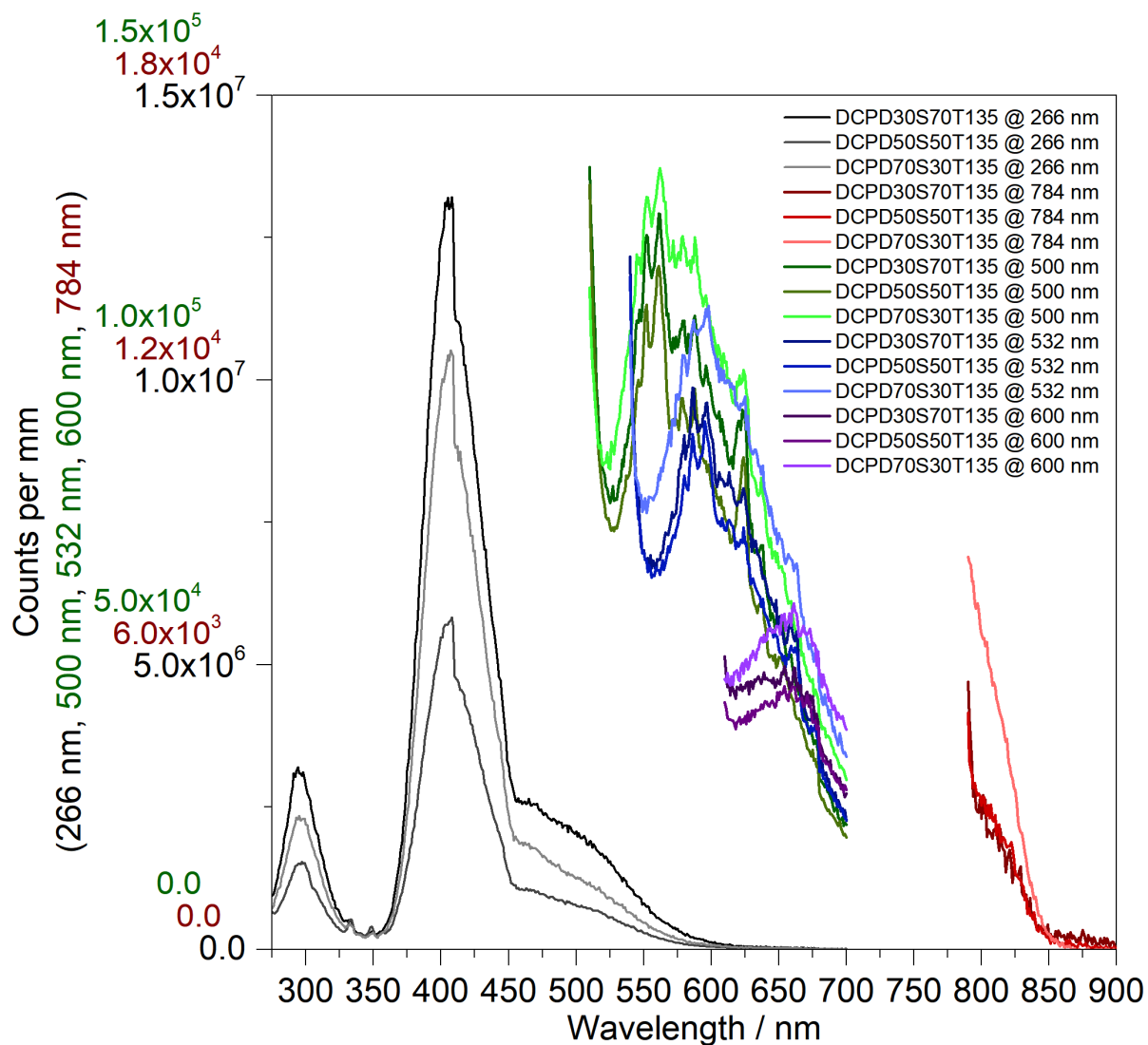
Figure 4.31: Fluorescence emission scans at different excitation wavelengths for different DCPD inverse vulcanised polymers, which were synthesized at 135 °C.
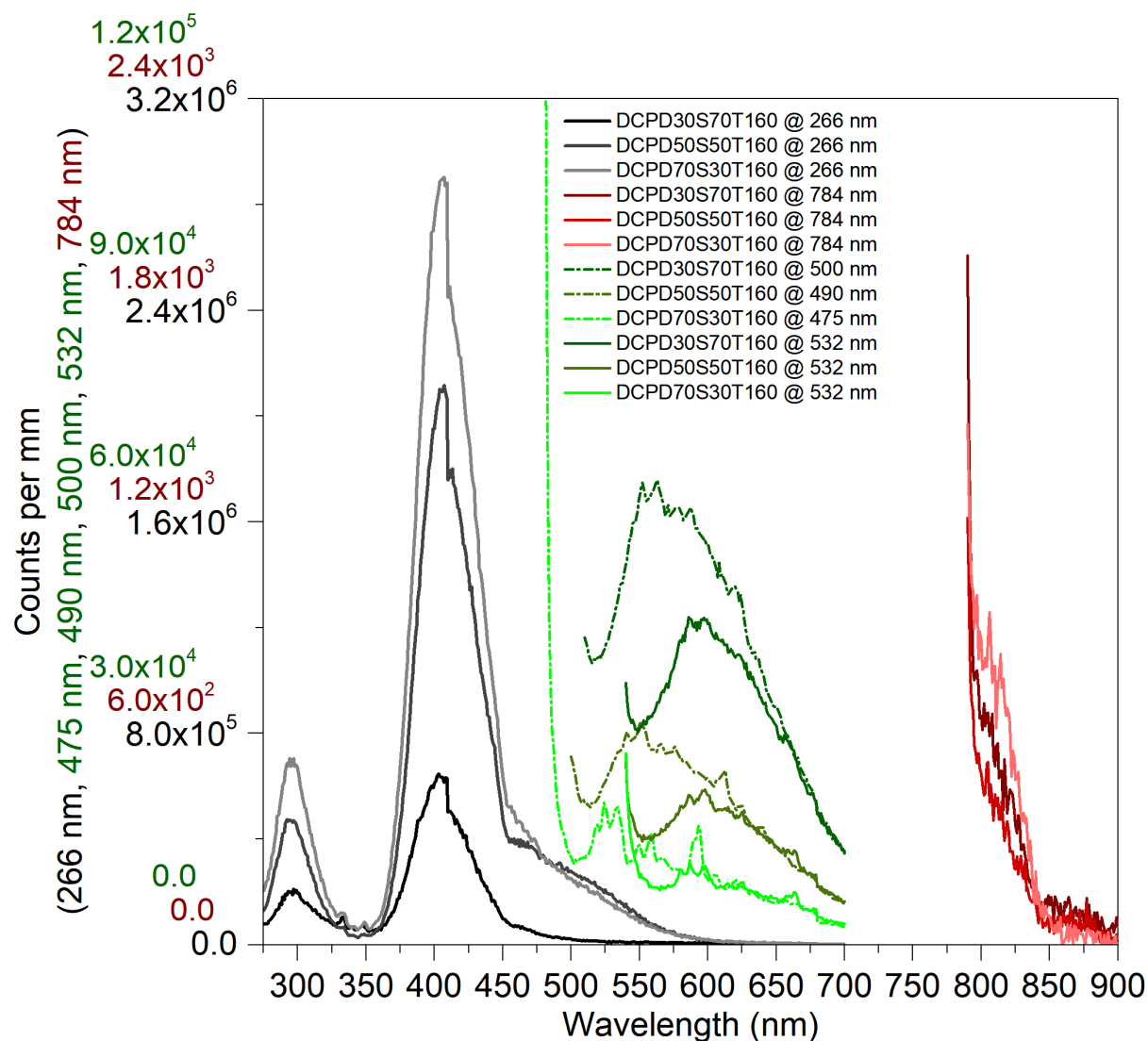
Liam James Dodd

Figure 4.32: Fluorescence emission scans at different excitation wavelengths for different DCPD inverse vulcanised polymers, which were synthesized at 160 °C.
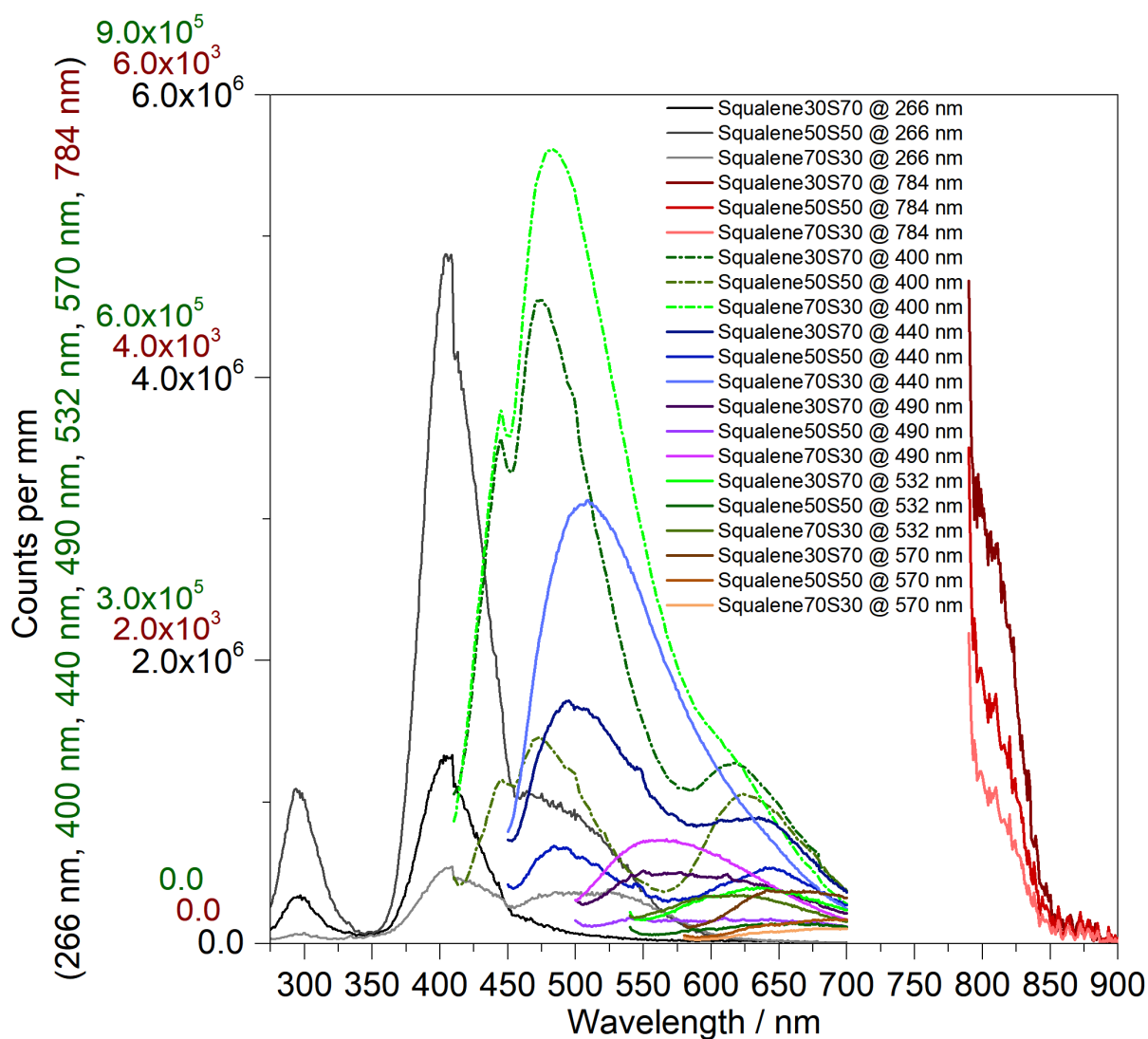
Figure 4.33: Fluorescence emission scans at different excitation wavelengths for different squalene inverse vulcanised polymers.

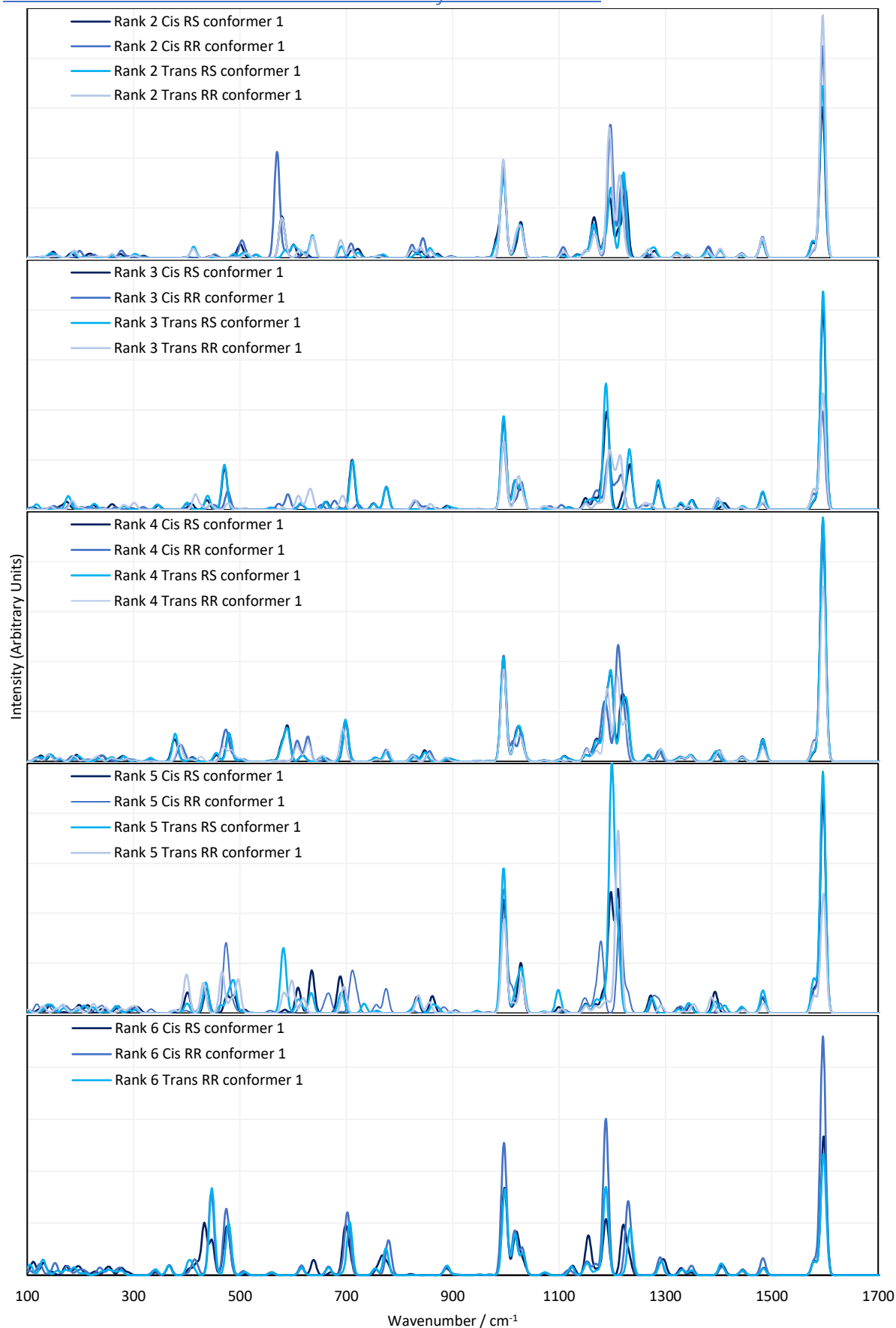## 4.16.3. Calculated Data for the Polymer Models

Figure 4.34: Calculated Raman spectra for the lowest energy conformers of the polymer models.

Liam James Dodd

4.16.4. Expected Sulfur Rank Calculation

If it is assumed that all double bonds react and that there are no sulfur loops in the polymer, then it can be deduced that the number of double bonds equals the number of sulfur bridges. This is because it does not actually matter how the sulfur bridges interconnect the organic units, the number of sulfur bridges is theoretically the same in every scenario. Figure 4.35 illustrates this conclusion.
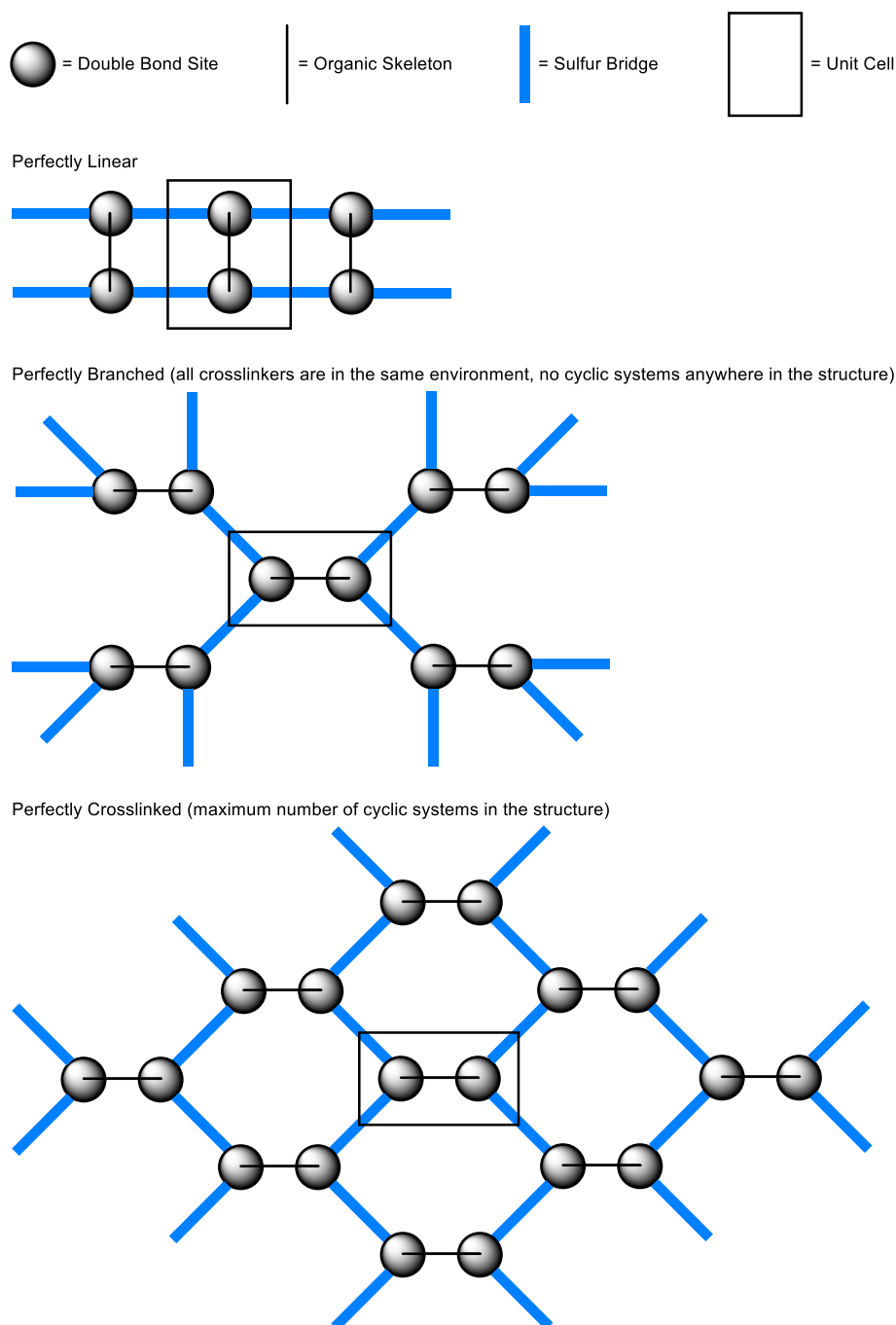
Figure 4.35: Schematic connectivity diagrams.

Inside every unit cell, regardless of the connectivity of the structure, there are two double bond sites and four halves of a sulfur bridge. In other words, there is a one to one ratio of double bonds to sulfur bridges. Similar models can be generated for crosslinkers containing three, four, or more double bond sites. One way to rationalise the justification of why the connectivity does not affect the ratio of

Liam James Dodd

double bonds to sulfur bridges is to consider a large cyclic chain of sulfur atoms. This chain can be crosslinked by inserting a carbon skeleton with two double bonds. This would divide the cyclic sulfur chain into two sulfur bridges with two double bond sites inserted into it. If a second crosslinker is added, the sulfur chains are divided again to yield four sulfur bridges, with four double bond sites. Figure 4.36 illustrates how it does not matter where the crosslinkers are inserted; the result is always the same.

Single sulfur loop

Add a crosslinker

Two double bond sites,
two sulfur bridges
1:1 ratio

Add a crosslinker

Four double bond sites,
four sulfur bridges
1:1 ratio

Add a crosslinker

Add a crosslinker

Six double bond sites,
six sulfur bridges
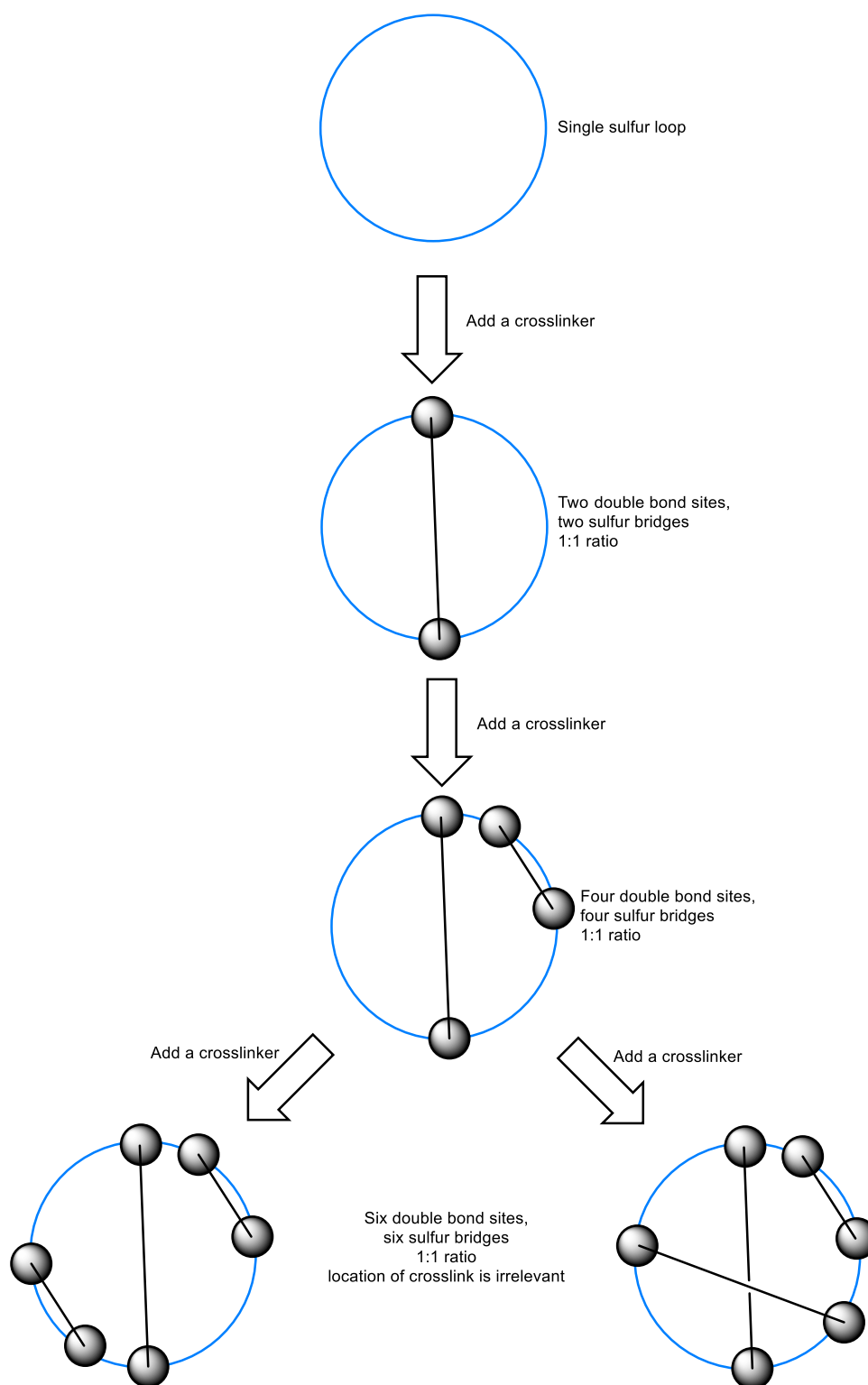1:1 ratio
location of crosslink is irrelevant

Figure 4.36: Crosslinking Diagram.

Liam James Dodd

With this fact in mind, that for all ideal structures there is one sulfur bridge for every double bond, it is simple to calculate the average expected sulfur rank. The number of sulfur atoms should be calculated from the sulfur mass that was input into the polymer. The number of sulfur atoms constituting elemental sulfur (sulfur that is not part of the polymer network) should be deducted from this total. This number of sulfur atoms should then be divided by the number of double bonds that were successfully polymerised. This number of double bonds can be calculated if the molecular mass of the crosslinker, the number of double bonds in each molecule of crosslinker, and the mass of crosslinker that actually polymerised is known. The latter of these three can be determined from the elemental analysis by the following equation, rearranged for "mass of crosslinker":

$$\frac{Mass\ percentage\ of\ sulfur}{100} = \frac{input\ mass\ of\ sulfur}{input\ mass\ of\ sulfur\ +\ mass\ of\ crosslinker}$$

It is worth noting however, that this theory does not account for the formation of by-products like DT-rings, not does it make account of alternate reaction mechanisms, such as the one proposed by Pyun *et al.* where one double bond actually results in a single sulfur bridge, though it is worth remembering that such a mechanism may not be possible in all crosslinkers.[4.24,4.25]

4.17. References

4.1 The use of elemental sulfur as an alternative feedstock for polymeric materials; W. J. Chung, J. J. Griebel, E. T. Kim, H. Yoon, A. G. Simmonds, H. J. Ji, P. T. Dirlam, R. S. Glass, J. J. Wie, N. A. Nguyen, B. W. Guralnick, J. Park, A. Somogyi, P. Theato, M. E. Mackay, Y. E. Sung, K. Char, J. Pyun; Nature Chemistry, 2013, 5, 518-524.

4.2 100th Anniversary of Macromolecular Science Viewpoint: High Refractive Index Polymers from Elemental Sulfur for Infrared Thermal Imaging and Optics; T. S. Kleine, R. S. Glass, D. L. Lichtenberger, M. E. Mackay, K. Char, R. A. Norwood, J. Pyun; ACS Macro Letters, 2020, 9, 245–259.

4.3 Dynamic Covalent Polymers via Inverse Vulcanisation of Elemental Sulfur for Healable Infrared Optical Materials; J. J. Griebel, N. A. Nguyen, S. Namnabat, L. E. Anderson, R. S. Glass, R. A. Norwood, M. E. Mackay, K. Char, J. Pyun, ACS Macro Letters, 2015, 4, 862–866.

4.4 Perfluoroaryl-Elemental Sulfur SNAr Chemistry in Covalent Triazine Frameworks with High Sulfur Contents for Lithium–Sulfur Batteries; S. H. Je, H. J. Kim, J. Kim, J. W. Choi, A. Coskun; Advanced Functional Materials, 2017, 27, 1703947.

4.5 Sulfur and Its Role In Modern Materials Science; D. A. Boyd; Angewandte Chemie International Edition, 2016, 55, 15486-15502.

4.6 Modelling mercury sorption of a polysulfide coating made from sulfur and limonene; M. J. H. Worthington, M. Mann, I. Y. Muhti, A. D. Tikoalu, C. T. Gibson, Z. Jia, A. D. Miller, J. M. Chalker; Physical Chemistry Chemical Physics, 2022, 24, 12363–12373.

4.7 Atkins' Physical Chemistry, 10th edition; P. W. Atkins, J. De Paula; Oxford University Press, Oxford, 2014.

4.8 Functionalized polysulfide copolymers with 4-vinylpyridine via inverse vulcanization; H. Berk, B. Balci, S. Ertan, M. Kaya, A. Cihaner; Materials Today Communications, 2019, 19, 336–341.

4.9 Insulating Composites Made from Sulfur, Canola Oil, and Wool; I. B. Najmah, N. A. Lundquist, M. K. Stanfield, F. Stojcevski, J. A. Campbell, L. J. Esdaile, C. T. Gibson, D. A. Lewis, L. C. Henderson, T. Hasell, J. M. Chalker; ChemSusChem, 2021, 14, 2352–2359.

4.10 Inverse Vulcanization of Styrylethyltrimethoxysilane-Coated Surfaces, Particles, and Crosslinked Materials; J. M. Scheiger, C. Direksilp, P. Falkenstein, A. Welle, M. Koenig, S. Heissler, J. Matysik, P. A. Levkin, P. Theato; Angewandte Chemie International Edition, 2020, 59, 18639–18645.

4.11 Investigating the Role and Scope of Catalysts in Inverse Vulcanization; L. J. Dodd, Ö. Omar, X. Wu, T. Hasell; ACS Catalysis, 2021, 11, 4441-4455.

Liam James Dodd

4.12 Tailoring Polysulfide Properties through Variations of Inverse Vulcanization; K. Orme, A. H. Fistrovich, C. L. Jenkins; Macromolecules, 2020, 53, 9353–9361.

4.13 Crosslinker Copolymerization for Property Control in Inverse Vulcanization; J. A. Smith, S. J. Green, S. Petcher, D. J. Parker, B. Zhang, M. J. H. Worthington, X. F. Wu, C. A. Kelly, T. Baker, C. T. Gibson, J. A. Campbell, D. A. Lewis, M. J. Jenkins, H. Willcock, J. M. Chalker, T. Hasell; Chemistry - A European Journal, 2019, 25, 10433 –10440.

4.14 Catalytic Inverse Vulcanization; X. Wu, J. A. Smith, S. Petcher, B. Zhang, D. J. Parker, J. M. Griffin, T. Hasell; Nature Communications, 2019, 10, 647.

4.15 Squalene-derived sulfur-rich copolymer@ 3D graphene-carbon nanotube network cathode for high-performance lithium-sulfur batteries; T. S. Sahu, S. Choi, P. Jaumaux, J. Zhang, C. Wang, D. Zhou, G. Wang; Polyhedron, 2019, 162, 147–154.

4.16 Laying Waste to Mercury: Inexpensive Sorbents Made from Sulfur and Recycled Cooking Oils; M. J. H. Worthington, R. L. Kucera, I. Albuquerque, C. T. Gibson, A. Sibley, A. D. Slattery, J. A. Campbell, S. F. K. Alboaiji, K. A. Muller, J. Young, N. Adamson, J. R. Gascooke, D. Jampaiah, Y. M. Sabri, S. K. Bhargava, S. J. Ippolito, D. A. Lewis, J. S. Quinton, A. V. Ellis, A. Johs, G. J. L. Bernardes, J. M. Chalker; Chemistry a European Journal, 2017, 23, 16219–16230.

4.17 All-optical nanoscale pH meter; S. W. Bishnoi, C. J. Rozell, C. S. Levin, M. K. Gheith, B. R. Johnson, D. H. Johnson, N. J. Halas; Nano Letters, 2006, 6, 1687-1692.

4.18 Fourier Transform Raman Spectroscopy; B. Chase, Analytical Chemistry, 1987, 59, 881A.

4.19 Kerr gated Raman spectroscopy of LiPF6 salt and LiPF6-based organic carbonate electrolyte for Li-ion batteries; L. Cabo-Fernandez, A. R. Neale, F. Braga, I. V. Sazanovich, R. Kosteckic, L. J. Hardwick; Physical Chemistry Chemical Physics, 2019, 21, 23833–23842.

4.20 Polysulfides as Biologically Active Ingredients of Garlic; U. Münchberg, A. Anwar, S. Mecklenburg, C. Jacob; Organic and Biomolecular Chemistry, 2007, 5, 1505−1518.

4.21 Dark Sulfur: Quantifying Unpolymerized Sulfur in Inverse Vulcanized Polymers; J. J. Dale, S. Petcher, T. Hasell; ACS Applied Polymer Materials, 2022, 4, 3169-3173.

4.22 High-Yield Synthesis of Gold Nanorods with Longitudinal SPR Peak Greater than 1200 nm Using Hydroquinone as a Reducing Agent; L. Vigderman, E. R. Zubarev; Chemistry of Materials, 2013, 25, 1450-1457.

4.23 Stretchable and Durable Inverse Vulcanized Polymers with Chemical and Thermal Recycling; P. Yan, W. Zhao, S. J. Tonkin, J. M. Chalker, T. L. Schiller, T. Hasell; Chemistry of Materials, 2022, 34, 1167–1178.

4.24 Tracking side reactions of the inverse vulcanization process and developing monomer selection guidelines; Y. Onose, Y. Ito, J. Kuwabara, T. Kanbara; Polymer Chemistry, 2022, 13, 5486–5493.

4.25 On the Mechanism of the Inverse Vulcanization of Elemental Sulfur: Structural Characterization of Poly(sulfur-random-(1,3-diisopropenylbenzene)); J. Bao, K. P. Martin, E. Cho, K. Kang, R. S. Glass, V. Coropceanu, J. Bredas, W. Parker, J. T. Njardarson, J. Pyun; Journal of the American Chemical Society, 2023, 145, 12386–12397.

Liam James Dodd

Chapter 5: Conclusions and Outlook

This chapter will summarise the main conclusions of the work performed in contribution to this thesis, and then speculate on directions the field of inverse vulcanisation could take next, both in the context of the work performed here, and in the wider field.

5.1. Conclusions

The work performed in contribution to this thesis primarily focused on the more fundamental aspects of inverse vulcanisation, rather than the end applications. In doing so, the discoveries made can lay a sturdy foundation of understanding so that others may use these findings to better access the applications they target with their research. Firstly, this work focused on catalysis of inverse vulcanisation, both on the benefits it can bring and how best to apply it for maximum benefit, as well as building some measure of understanding as to how the catalysts work, so that themselves could be rationally optimised. Secondly, this work carried forward the catalyst studies to organic activators, which were found to have many of the advantages of the traditional metal complex catalysts, but avoided concerns about contaminating the environment by remaining as a residue in the polymers, and of course, these organic activators do not contribute to the demand on limited supplies of non-renewable metal resources. In the course of studying these amine activators, the under-investigated alkyne family of comonomers were examined as a natural branch to the research, which led to the development of a dispersion polymerisation methodology to compensate for the reactions' extreme rate. Finally, this work drove forward and explored Raman spectroscopy as an analytical technique for inverse vulcanised polymers; overcoming the obstacles to the analysis, and pioneering methods to extract otherwise near-impossible to obtain but crucial information about the polymers. Among the successes of this project was a method to quantify the homogeneity of the polymers, analyse the content of unpolymerized elemental sulfur that cannot be detected by mainstream techniques that rely on sulfur crystallinity, and a method to analyse the length of sulfur chains which information of importance several applications of inverse vulcanised polymers.

In regards to the catalysis study in Chapter 2, the results reinforced the previous publication in that they demonstrated that catalytic inverse vulcanisation enhances the rate of reaction, increases the reaction yield, suppresses the formation of the toxic hydrogen sulfide by-product, raises the T_g of the product polymers, and allows otherwise unreactive comonomers to be polymerised. This work also built upon the previous publication by adding three new elements of understanding: what makes a good catalyst, how the catalysts work in terms of a potential mechanism, and developing a way to compare catalysts so that other researchers can apply the one most applicable to their work. The main mechanistic findings were that catalyst binding of the sulfur species in the reaction is likely an important step, though no evidence of binding of the organic comonomer could be found. Based on the results from catalysts with different alkyl chain lengths, phase transfer catalysis could be a relevant step, where the catalyst draws the bound sulfur species from the sulfur phase of the reaction to the organic phase where it more readily react with comonomer. This would promote a more uniform reaction as the reaction is no longer constrained to the phase boundaries. In terms the binding of sulfur monomer, it was found that soft metal cations were likely more effective, and from this, a likely catalytic intermediate was identified: metal polysulfide complexes. Some evidence for catalysts with greater nucleophilicity having greater rate enhancements was found. A range of organic catalysts was also studied and added to the comparative library of catalysts, both laying the foundation the third chapter of this thesis, and giving more than twenty-five catalysts for researchers compare and select between. Of this library of catalysts, Zn(DMDC)$_2$ was recommended for its better than average rate enhancements and improvements to the yield and T_g, whilst also being remarkably affordable and

Liam James Dodd

consistently effective amongst a range of different comonomers in inverse vulcanisation. Finally, this Chapter demonstrated the need for due care and diligence in applying catalysis to inverse vulcanisation, as it was reliably shown that the TNE was an underlying risk to excessive acceleration of the reaction rates.

In regards to Chapter 3 of this thesis, use of organic catalysts was taken further. It was shown that amines were effective in enhancing the rate of inverse vulcanisation, which circumvents any concerns about the product polymers having a residual metal content that could be leached into the environment and cause detrimental effects. As part of this project, amines with alkene and alkyne moieties included as part of the molecule were tested, as this results in them becoming intentionally incorporated into the polymer structure, preventing leaching, and bypassing any question about whether the catalyst can or should be extracted from the polymer, which could be an energy intensive step that detracts from the sustainable low-cost draw of these polymers whilst also adding complications such as whether the polymer is detrimentally affected by the extraction step. A dispersion polymerisation method was developed to manage the high rate enhancements from using such amine activators as the sole comonomer, which resulted in two separate products of different properties that could have different applications. This dispersion polymerisation avoided the TNE and in some cases yielded polymers with T_g's higher than their T_d, which could not be said of any other inverse vulcanised polymer at the time of publication. Through this dispersion polymerisation, amine containing crosslinkers were successfully polymerised at temperatures lower than the melting point of sulfur, which is a two-fold benefit: it allows polymerisation of comonomers of low boiling point, and it points to the fact that amines bring a new route of activation to inverse vulcanisation, since these reactions were occurring at temperatures where homolytic cleavage of sulfur – sulfur bonds was unfeasible. This suggests that the amines were inducing cleavage of sulfur – sulfur bonds, perhaps by nucleophilic attack to generate reactive anionic sulfur species, a conclusion that is supported by the fact that without amine activation, no reaction occurred below the melting temperature of sulfur. In this project, alkynes were also polymerised which is of note because they have thus far been under-investigated in inverse vulcanisation, with only two publications. These alkynes were found to likely react to form alkenes and then react further to form saturated carbon – carbon bonds sporting four sulfur chains, though there was evidence of competing reactions that formed aromatic by-products. The phosphorus analogues of the amine containing crosslinkers were found to give no rate enhancement due to deactivation of the phosphine by reaction to form a phosphorus – sulfur double bond. Finally, it was shown that amine containing crosslinkers can be used as a secondary crosslinker, present in catalytic quantities, in an inverse vulcanisation of a primary comonomer, and this brings several benefits, such as improved yield, decreased reaction time, and increased T_g.

In regards to the Raman analysis approach detailed in Chapter 4, several techniques capable of avoiding the fluorescent background that has previously precluded Raman analysis, were found, with the most accessible of which being Raman spectroscopy with a 1064 nm excitation laser, which was carried forward for the rest of the study. On the matter of the fluorescent background, it was found that it does not stem from leftover unreacted crosslinker, but does seem to originate from the organic component of the polymers. Although 1064 nm Raman analysis still encountered issues with darker coloured, more fluorescent polymers, it was possible with relatively little effort to quantify the amount of unpolymerized elemental sulfur within the polymer. This discovery is of note because this Raman approach can detect the presence of elemental sulfur even when other techniques cannot, as the Raman analysis approach can detect elemental sulfur which is not crystalline, whereas techniques like DSC and PXRD rely on the crystallinity of elemental sulfur to detect it. This new capability has shown that polymers otherwise assumed to have no elemental sulfur content, do in fact contain this impurity and because of the high Raman scatter cross section of elemental sulfur, Raman analysis is

Liam James Dodd

exceptionally sensitive to the impurity. Also possible with relatively little effort is an analysis of the homogeneity of inverse vulcanised polymers, which is not trivial by other means, but is simple with Raman spectroscopy as it analyses a small point upon the polymer. Kinetic studies by reaction tracking with Raman spectroscopy is also quite easy to implement, especially with the capability of Raman spectrometers to utilise long range lenses that allow the probe to avoid being in the reaction. The most profound development of Raman spectroscopy is that with albeit work intensive computational studies, not only can the average sulfur rank be quantified, but the populations of the individual sulfur ranks can be quantified, which is information extremely relevant to several applications of inverse vulcanised polymers. Granted this sulfur rank determination is in its infancy and has its limitations, such as working only for inverse vulcanised polymers of DVB and being limited in accuracy to sulfur rank 6, but these limitations can be circumvented by moving to a qualitative approach which is much easier and quicker to apply, and could work for all polymers that a spectrum can be obtained for. This project developed methods and step by step guides for applying the Raman analysis approach, as well as examining the effects of sample morphology, and so forms a comprehensive guide to the application of Raman spectroscopy to inverse vulcanised polymers, ready for use by other researchers in the field.

5.2. Outlook

Where the work performed in contribution to this thesis is concerned, each chapter has several ways in which the work could be extended to future projects and avenues of research. First of all, Chapter 2 presented metal polysulfide complexes as potential key intermediates in catalytic inverse vulcanisation, but struggled to find evidence for their existence. According to the literature, these metal polysulfides should be able to form at inverse vulcanisation temperatures from only elemental sulfur and metal DEDC precursors, and they should be stable enough to readily form, yet reactive enough to act as catalytic intermediates. As such they warrant further research attention to determine if they are present in inverse vulcanisation. An initial DFT reaction pathway study may shed initial light on whether these complexes could form and participate in a catalytic reaction pathway. From these results, DFT may be able to suggest ways in which these complexes could be detected *in situ*, by either simulating their spectra, suggesting ways to trap the intermediates, or other ways of finding indirect evidence of their existence. This could provide exciting ways to modify catalysts and exploit the catalytic mechanism toward a desired end, and so it is a research avenue worth considering.

Whilst the work in Chapter 3 was somewhat modular and came to a logical end, there are still opportunities for further research that stem from it. It could be worthwhile to examine in more detail, exactly what by-product structures are forming from the alkyne reactions, those that were only hinted at by NMR. This could point to analogous intermediates in other reactions, though it is worth considering the impact of this research versus the potential difficulty and chance for unsuccessful outcomes, which seems an unfavourable risk. More promising was the potential for XRF to added the analysis techniques in inverse vulcanisation. While it is true that XRF was not successfully applied in this project, a dedicated study could yield success, and the impact of this advancement would be much more profound for the field. Combustion microanalysis has thus far been the only way to identify the sulfur content of inverse vulcanised polymers, but comes under criticism due to the fact its calibration curve for sulfur can usually only be established between zero and ten percent sulfur, leading to a disconcerting extrapolation error when the sulfur content of inverse vulcanised polymers are concerned, which have much higher sulfur contents. If XRF could provide a way to more confidently give a measure of the sulfur content of inverse vulcanised polymers, then this could be a huge boon to the field of inverse vulcanisation.

Liam James Dodd

Finally, Chapter 4 is by far the most open ended and exciting in terms of future research opportunities. Raman analysis was shown to be of exceptional value in characterising inverse vulcanised polymers, but the analysis technique is still in its infancy and has the potential to do significantly more, for which research proposals have already been submitted. The proposed study would target the improvement of the computational aspect of the Raman analysis approach by using a new, automated strategy to generate models of the polymer in connectivities far more diverse than a human could make in a reasonable time frame. This would overcome all three limitations of the analysis to determine the sulfur rank of inverse vulcanised polymers: the strategy would be expanded to more polymers besides those formed from just DVB; the analysis would be able to analyse sulfur ranks much longer than the limiting rank six that arose from the current technique; and it would accelerate the analysis whilst making it more accessible, as the tedious, long-winded computational aspect would be automated, thus not excluding non-computational chemists from applying it. The parameterisation model also stands to be improved, expanding from just two compounds to seventy-seven, the spectra of which have already been acquired. This wider library of relevant compounds contains well defined sulfide of sulfur ranks up to five, which makes the parameterisation model far more robust, whilst also allowing better benchmarking of computational levels of theory. There are also plans to extend the Raman analysis approach to the mercury and gold capture applications of inverse vulcanised polymers. Raman spectrometer lenses for the model used in Chapter 4 for 1064 nm Raman analysis, can have ranges of up to six metres, allowing the measurement of potentially heavy metal contaminated polymers at a safe distance, where there is no chance of the analyst coming into contact with highly toxic heavy metal residues upon the polymer. If computational chemistry could identify metal – sulfur resonances within a Raman spectrum, then the adsorption of heavy metal ions by inverse vulcanised polymers could be identified by Raman spectroscopy. Even further, it may identify chemisorption versus physisorption, as chemisorption creates new chemical bond which should result in entirely new resonances in the spectrum, while physisorption does not create new chemical bonds but does perturb already existing ones with new intermolecular interactions, which should result in perturbation of already existing Raman modes. There is also the possibility for the automation of long-winded mercury uptake kinetics experiments, wherein a Raman spectrometer could be set up to automatically and periodically measure the Raman spectrum of an *in situ* sample that is in the process of absorbing mercury in a mercury kinetics experiment, and with a proper calibration curve, this could be related to the mercury concentrations based on the intensity of the Raman signals.

Further included in this aforementioned research proposal, but also extending more systemically in terms of the outlook of the field of inverse vulcanisation, it is suggested that inverse vulcanisation should see greater uptake of computational chemistry methods. Thus far, inverse vulcanisation has only seen a sparse application of computational chemistry, and has never seen a dedicated computational study. Publications have occasionally included computational components, and to fantastic effect, but only ever to answer concentrated questions that arose from a largely experimental project. It is likely that complexity and ambiguity in the structure of inverse vulcanised polymers has dissuaded computational studies, as well as a high skill barrier for entry, as a researcher would have to be well versed in both computational chemistry, which is hardly straightforward, but also inverse vulcanisation, which is far from a typical polymerisation reaction, and is riddled with nuances and pitfalls. Nevertheless, the insights that stand to be gained from integrating a hand in hand approach of computational chemistry and experimental chemistry could revolutionise the field in terms of understanding. Proposed by the author is a joint computational – experimental strategy to build structure – property relationships that can be used to understand how to rationally design inverse vulcanised polymers. The properties of inverse vulcanised polymers would be measured experimentally, while their structure and properties would be simulated computationally, searching

Liam James Dodd

for matches between reality and prediction, which can used to both corroborate the exact structure of an inverse vulcanised polymers, and create tools to understand how and why properties arise, and how to manipulate this towards certain end goals. A DFT study of the potential reaction mechanisms of inverse vulcanisation is warranted, as well as the application of time dependent DFT to identify where the colour of inverse vulcanised polymers comes from: a long standing mystery in the field. The DT rings mentioned in Chapter 1 are a likely candidate for the source of this colour, supported by the fact that preliminary calculations suggest that inverse vulcanised polymer units themselves should be colourless, as well as the advent of an electrochemically synthesized DCPD polymer that is white. This suggests that the colour of inverse vulcanised polymers does indeed stem from a coloured by-product that occurs during thermal synthesis, and not during an electrochemical one.

In terms of the broader scope of the field, it the opinion of the author that inverse vulcanisation is now at a turning point. In its early stages, inverse vulcanisation received a "gold rush" of publications, because of the versatility of the reaction and its capacity to accept a wide variety of comonomers. This led to numerous publications where research groups would identify a new comonomer, polymerise it, perform some analyses, and then publish their findings. This was valuable in the early stages as it broadened the library of possible comonomers, inherently led to discoveries about the reaction itself, and set a baseline for what properties could be expected from inverse vulcanised polymers. But it is the opinion of the author that inverse vulcanisation needs to move away from this style of publication, as it is becoming increasingly less valuable focus on producing publications with the goal of polymerising every vinyl compound that is accessible. Fewer and fewer discoveries can be made through polymerising anything with a carbon – carbon double bond, and nowhere is this more evident than the large number of research papers that report the polymerisation of a new kind of bio-renewable triglyceride oil, leading to numerous publications that all report very similar polymers, largely because many of these triglyceride oils are in fact not that different; many are just different ratio mixtures of the same or inter-related triglycerides. Instead, the author suggests that the field of inverse vulcanisation needs to take on a new direction with a two-point approach.

The first element of this approach is to finally derive a comprehensive understanding of what is actually being made when an inverse vulcanised polymer is synthesized. This would require the investigation of new analysis techniques, but also a through investigation of how to apply those techniques and what can be gained from them. This is task is challenging and likely will meet failures in many avenues, which is likely why such publications have been less favoured in comparison to polymerising new comonomers, which has a much higher chance of successful research output. But inverse vulcanisation is reaching the stage where such publications are becoming less valuable in terms of what they add to the knowledge pool, and so the increased value of more challenging projects focused upon the analysis of inverse vulcanised polymers become more worthwhile in comparison to their risk of failure. But with successful research into the analysis and understanding of inverse vulcanised polymers, many new avenues become available, especially rational design approaches, which would allow the synthesis of new polymers with superior properties, or optimisation of already existing polymers based on design principles.

The second element to this new direction for inverse vulcanisation would include a more concentrated attempt to control the synthesis and post-processing of inverse vulcanised polymers towards optimisation for specific target applications. This can reduce batch to batch variability in inverse vulcanised polymers, priming them for industrial uptake, where they can begin making a societal impact, but it also drives them toward being fit for application. Understanding what makes the optimum polymer with the best possible properties for a particular application is crucial for the successful uptake if inverse vulcanised polymers in roles where they benefit society. As part of this, a

Liam James Dodd

thorough study of how inverse vulcanised polymers change with time is required. Studies have shown that inverse vulcanised polymers age, and their properties change during this process. It is important to know the lifetime of inverse vulcanised polymers, as this could limit the operational lives of products derived from them. This is especially crucial for the suggested application of using inverse vulcanised polymers as cement substitutes and other building infrastructure applications, as ignorance of the changing properties of inverse vulcanised polymers in these applications could have potentially disastrous implications, such as a solid structure upon construction, that weakens over time toward structural failure or collapse.

Ultimately, the field of inverse vulcanisation is a small but rapidly growing field, and there is incredible potential for exciting future research and applications. Inverse vulcanisation has had an excellent start as a research field, and with the growing interest, it is hard to imagine that the field's momentum will do anything but grow and diversify. This leads to an outlook of optimism and excitement for all the discoveries yet to be made.

Liam James Dodd